

LOCKHEED MARTIN ENERGY RESEARCH LIBRARIES

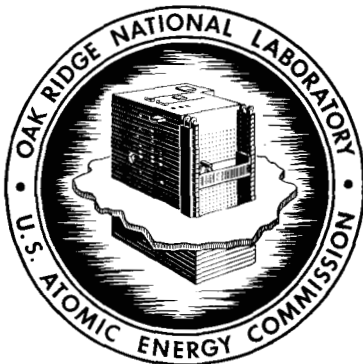


3 4456 0515720 0

CENTRAL RESEARCH LIBRARY  
DOCUMENT COLLECTION

ORNL-4570 *Cey 1*  
UC-25 – Metals, Ceramics, and Materials

METALS AND CERAMICS DIVISION  
ANNUAL PROGRESS REPORT  
FOR PERIOD ENDING JUNE 30, 1970



**OAK RIDGE NATIONAL LABORATORY**

operated by

UNION CARBIDE CORPORATION

for the

U.S. ATOMIC ENERGY COMMISSION

Printed in the United States of America. Available from Clearinghouse for Federal  
Scientific and Technical Information, National Bureau of Standards,  
U.S. Department of Commerce, Springfield, Virginia 22151  
Price: Printed Copy \$3.00; Microfiche \$0.65

**LEGAL NOTICE**

This report was prepared as an account of Government sponsored work. Neither the United States, nor the Commission, nor any person acting on behalf of the Commission:

- A. Makes any warranty or representation, expressed or implied, with respect to the accuracy, completeness, or usefulness of the information contained in this report, or that the use of any information, apparatus, method, or process disclosed in this report may not infringe privately owned rights; or
- B. Assumes any liabilities with respect to the use of, or for damages resulting from the use of any information, apparatus, method, or process disclosed in this report.

As used in the above, "person acting on behalf of the Commission" includes any employee or contractor of the Commission, or employee of such contractor, to the extent that such employee or contractor of the Commission, or employee of such contractor prepares, disseminates, or provides access to, any information pursuant to his employment or contract with the Commission, or his employment with such contractor.

Contract No. W-7405-eng-26

**METALS AND CERAMICS DIVISION ANNUAL PROGRESS REPORT**  
for Period Ending June 30, 1970

J. H. Frye, Jr., Director  
J. E. Cunningham, Associate Director

**Section Heads**

G. M. Adamson, Jr.  
B. S. Borie  
W. O. Harms  
C. J. McHargue  
P. Patriarca  
J. R. Weir, Jr.

Compiled and Edited by Sigfred Peterson

OCTOBER 1970

LOCKHEED MARTIN ENERGY RESEARCH LIBRARIES



3 4456 0515720 0

OAK RIDGE NATIONAL LABORATORY  
Oak Ridge, Tennessee  
operated by  
UNION CARBIDE CORPORATION  
for the  
U. S. ATOMIC ENERGY COMMISSION

Reports previously issued in this series are as follows:

ORNL-28	Period Ending March 1, 1948
ORNL-69	Period Ending May 31, 1948
ORNL-407	Period Ending July 31, 1949
ORNL-511	Period Ending October 31, 1949
ORNL-583	Period Ending January 31, 1950
ORNL-754	Period Ending April 30, 1950
ORNL-827	Period Ending July 31, 1950
ORNL-910	Period Ending October 31, 1950
ORNL-987	Period Ending January 31, 1951
ORNL-1033	Period Ending April 30, 1951
ORNL-1108	Period Ending July 31, 1951
ORNL-1161	Period Ending October 31, 1951
ORNL-1267	Period Ending January 31, 1952
ORNL-1302	Period Ending April 30, 1952
ORNL-1366	Period Ending July 31, 1952
ORNL-1437	Period Ending October 31, 1952
ORNL-1503	Period Ending January 31, 1953
ORNL-1551	Period Ending April 10, 1953
ORNL-1625	Period Ending October 10, 1953
ORNL-1727	Period Ending April 10, 1954
ORNL-1875	Period Ending October 10, 1954
ORNL-1911	Period Ending April 10, 1955
ORNL-1988	Period Ending October 10, 1955
ORNL-2080	Period Ending April 10, 1956
ORNL-2217	Period Ending October 10, 1956
ORNL-2422	Period Ending October 10, 1957
ORNL-2632	Period Ending October 10, 1958
ORNL-2839	Period Ending September 1, 1959
ORNL-2988	Period Ending July 1, 1960
ORNL-3160	Period Ending May 31, 1961
ORNL-3313	Period Ending May 31, 1962
ORNL-3470	Period Ending May 31, 1963
ORNL-3670	Period Ending June 30, 1964
ORNL-3870	Period Ending June 30, 1965
ORNL-3970	Period Ending June 30, 1966
ORNL-4170	Period Ending June 30, 1967
ORNL-4370	Period Ending June 30, 1968
ORNL-4470	Period Ending June 30, 1969

# Contents

SUMMARY .....	xv
---------------	----

## PART I. FUNDAMENTAL PROGRAMS

1. CRYSTAL PHYSICS .....	1
Substructure and Perfection in $\text{UO}_2$ Single Crystals .....	1
Refractory Oxide–Metal Composites: Scanning Electron Microscopy and X-Ray Diffraction of Uranium Dioxide–Tungsten .....	1
$\text{UO}_2$ -W Cermets Produced by Unidirectional Solidification .....	2
$\text{UO}_2$ -W and (U,Th) $\text{O}_2$ -W Eutectics .....	2
Growth of Thorium Oxide Crystals .....	2
Melt Growth of Pure and Neodymium-Doped $\text{CaWO}_4$ .....	2
Melt Growth of Single-Crystal $\text{Mg}_2\text{SiO}_4$ (Forsterite) .....	3
Melt Growth of $\text{KMgF}_3$ and of $\text{KMgF}_3$ Doped with Lanthanides .....	3
High-Temperature Solution Growth of Single-Crystal $\text{XSiO}_4:\text{Ln}$ (X = Zr, Hf, Th; Ln = Gd, Er, Yb) .....	3
High-Temperature Solution Growth of Single-Crystal $\text{ThO}_2$ Doped with $^{239}\text{PuO}_2$ and with ( $^{244}\text{CmO}_2 + \text{Tm}_2\text{O}_3$ ) .....	3
Hydrothermal Synthesis .....	4
Hydrothermal System $\text{SiO}_2$ -RbOH- $\text{H}_2\text{O}$ -Fe Under Dynamic Conditions .....	4
Characterization of RbOH-Grown Quartz by Infrared and Mass Spectroscopy .....	4
2. DEFORMATION, ANNEALING, AND INTERFACES IN METALLURGICAL PHENOMENA .....	5
The Recrystallization Characteristics of Moderately Deformed Aluminum .....	5
Impurities and the Power-Law Dependence of Grain-Boundary Migration Rate on Driving Force .....	5
Rolling Textures in Ordered and Disordered $\text{Cu}_3\text{Au}$ .....	6
The Recovery Characteristics of Niobium and Nb–40% V .....	7
Effect of Internal Stresses on the Apparent Stress Dependence of Dislocation Velocities .....	8
Contributions to the Theory of Jogged Screw Dislocation Glide .....	9
High-Temperature Glide in LiF Single Crystals .....	9
A Constant Stress–Continuous Load Compression Creep Machine for Small Single Crystals .....	9

3. DEFORMATION OF CRYSTALLINE SOLIDS .....	10
Precipitation and Hardening in Body-Centered Cubic Alloys .....	10
Structural and Elastic Properties of Zonal Twin Dislocations in Anisotropic Crystals .....	11
Characteristics of Stress and Dilatation Fields of Straight Dislocations in Anisotropic Crystals .....	11
Numerical Calculation of Elastic Solutions for Straight Dislocations in Anisotropic Crystals .....	11
Series Representation of Thermodynamic Functions of Binary Solutions .....	12
Configurational Changes in Nonrandom Solid Solutions .....	12
Computer Simulation of Solid Solutions .....	12
4. DIFFUSION IN SOLIDS .....	13
Invariants of Multicomponent Diffusion .....	13
Cation Self-Diffusion in Uranium Mononitride .....	13
Comparison of Penetration Plots Obtained from Alpha-Energy Degradation and Electrochemical Sectioning .....	13
Sectioning of Diffusion Specimens by Radio-Frequency Sputtering .....	14
Cation Self-Diffusion in Oxides of Titanium .....	14
Diffusion Under High Pressures .....	14
5. ELECTRON MICROSCOPY .....	16
Heterogeneous Distribution of Irradiation Voids in Iron .....	16
Supervoids in Irradiated Aluminum .....	16
Effect of Preinjected Gases on Irradiation-Produced Voids in Aluminum .....	16
Effects of Preinjected Gases on Void Formation in Quenched Aluminum .....	17
Electron Displacement Damage in Aluminum .....	17
Transmutation-Produced Silicon Precipitates in Irradiated Aluminum .....	17
Comments on "Stability of the Gas Bubbles in Solids" .....	18
Stress Concentration and Cavity Growth .....	18
Application of Electron Fractography to the Study of High-Temperature Processes .....	18
The Ratio of Stored to Expended Energy During the Room-Temperature Deformation of Copper Single Crystals .....	18
Comments on the Stored Energy in FCC Metals .....	18
Cathodic Hydrogen Absorption and Severe Embrittlement in a High-Strength Steel .....	19
6. FUNDAMENTAL CERAMICS RESEARCH .....	20
Electronic Band Structure Calculations for Uranium Compounds Having NaCl-Type Structure .....	20
Optical Properties of Paramagnetic UN .....	21
Thermal Conductivity, Electrical Resistivity, and Seebeck Coefficient of Uranium Mononitride .....	21
Low-Temperature Specific Heat of UN .....	22

7. MÖSSBAUER STUDIES OF ALLOYS .....	23
Magnetic Hyperfine Fields at $^{61}\text{Ni}$ Nuclei in Ni-Pd Alloys .....	23
8. PHYSICAL CERAMICS STUDIES .....	24
Deformation of Uranium Dioxide Single Crystals .....	24
Compressive Creep of Uranium Mononitride .....	24
Some Fundamental Ideas in Topology and Their Application to Problems in Metallography .....	25
Mechanistic Interpretation of Non-Steady-State Sintering .....	25
Desintering .....	26
9. PHYSICAL PROPERTY RESEARCH .....	27
Apparatus Development .....	27
Intercomparison of Thermal Conductivity Results .....	27
Thermal Conductivity Apparatus .....	27
Computer Data Acquisition .....	27
Electronic Heat Transport .....	28
Chromium .....	28
Tantalum .....	28
Ordered and Disordered $\text{Ni}_3\text{Fe}$ .....	29
Lattice Heat Transport .....	29
Uranium Dioxide .....	29
Lithium Fluoride .....	29
Calorimetric Studies of $\text{Ni}_3\text{Fe}$ Between 1.2 and 4.4°K .....	29
UN, ThN, and Their Alloys .....	29
10. SPECTROSCOPY OF IONIC MEDIA .....	31
Spectroscopic Behavior and Coordination of Nickel(II) in Liquid Mixtures of Zinc and Cesium Chlorides .....	31
Evidence for a Three-Coordinate Complex of Nickel(II) .....	31
Nickel(II) Tetrachloroaluminate .....	32
Preliminary Report on Titanium(II) Tetrachloroaluminate .....	32
Electrical Conductivity of Aluminum Chloride Liquid and Supercritical Vapor .....	32
Electrical Conductivities of Molten Aluminum Chloride–Potassium Chloride Mixtures .....	32
Electrical Conductivities of Molten $\text{AlBr}_3$ -NaBr Mixtures .....	33
Structural Studies in the $\text{AlI}_3$ -CsI System .....	33
Unusual Oxidation States of Posttransition Element Ions .....	33
Spectra of Dilute Solutions of Bismuth Metal in Molten Bismuth Tribromide .....	33
Densities of Molten NaBr- $\text{AlBr}_3$ Mixtures .....	33
Polarized Electronic Absorption Spectrum of Tetragonal $\text{NiCl}_4^{2-}$ in $\text{Cs}_3(\text{MgCl}_4)\text{Cl}$ .....	34
11. SUPERCONDUCTING MATERIALS .....	35
High Q Resonators in Higher dc Magnetic Fields .....	35
Superconductivity in Technetium-Base Alloys .....	35

The Critical State in Hysteretic Superconductors .....	35
Losses Due to Moving Fluxoids in Superconductors .....	36
An Elevated-Temperature X-Ray Diffraction and an Electron Microscopy Study of the Transformations to the Samarium-Type Structure in Gadolinium-Cerium Alloys .....	36
12. SURFACE REACTIONS OF METALS .....	37
Oxidation of Uranium-Base Alloys .....	37
Refractory Metals Studies .....	38
Flexure Measurements During Oxidation .....	38
The Estimation of Bending Stresses from Flexure Measurements .....	39
Oxidation of Tantalum-Tungsten Alloys .....	39
Anodic-Film Sectioning .....	39
13. THEORETICAL RESEARCH .....	40
Calculation of Constant-Energy Surfaces for Aluminum by the Korringa-Kohn-Rostoker Method .....	40
KKR Structure Constants for Complex Crystals .....	40
The Electronic States in Copper and Aluminum .....	40
Two-Particle Scattering Terms in Perturbation Theory of Electronic States in Disordered Systems .....	40
Electronic States of a Liquid Metal from the Coherent-Potential Approximation .....	41
Electronic States in Liquid Metals: A Generalization of the Coherent-Potential Approximation for a System with Short Range Order .....	41
Adjustment of Calculated Band Structures for Calcium by Use of Low-Temperature Specific Heat Data .....	41
Magnetic Properties of Terbium-Holmium Single-Crystal Alloys. I. Magnetization Measurements .....	41
Crystal Field $3d^1$ Energy Levels in a Distorted Octahedral Point Charge Environment .....	42
Discrete Variational Method for the Energy Band Problem with General Crystal Potentials .....	42
Crystal Potential and Electronic Structure of Diamond .....	42
Crystal Potential and Electronic Structure of Lithium Metal .....	42
Electronic Band Structure and Optical Properties of Graphite from a Variational Approach .....	42
Discrete Variational Method for the Energy Band Problem with LCAO Basis and Nonspherical Local Potential .....	43
Alkali Solute Knight Shifts in Alkali Matrices .....	43
Knight Shifts of the Alkali Metals .....	43
14. X-RAY DIFFRACTION .....	44
Routine Analyses .....	44
On the Interpretation of Temperature Diffuse Scattering .....	44
The Interpretation of Intensity Distributions from Disordered Binary Alloys .....	44
X-Ray Diffraction Study of Highly Oriented Graphite .....	44
Thermal Motion .....	44
Neutron Irradiation .....	45

Uranium-Niobium-Zirconium Alloys . . . . .	45
Structural Changes in Samarium Metal at Elevated Temperatures . . . . .	45
Two Modifications of the Kratky Small-Angle X-Ray Camera . . . . .	45
The Gas Amplification Factor in Xenon-Filled Proportional Counters . . . . .	46
Absolute Intensity Measurements in Small-Angle X-Ray Scattering I. Theory . . . . .	46
X-Ray Diffraction Data on Liquid Trimethylamine Decahydrate at 5°C . . . . .	46
<b>PART II. FAST REACTOR TECHNOLOGY</b>	
<b>15. FAST REACTOR OXIDE FUELS . . . . .</b>	<b>47</b>
Development of Fabrication Processes . . . . .	47
Sphere-Pac Development . . . . .	47
Pellet Development and Fabrication . . . . .	48
Fuel Pin Fabrication . . . . .	49
Characterization of (U,Pu)O <sub>2</sub> Fuels . . . . .	50
Analytical Chemistry . . . . .	50
Homogeneity of (U,Pu)O <sub>2</sub> . . . . .	50
Gas Release from (U,Pu)O <sub>2</sub> Fuels . . . . .	50
Microstructure of Unirradiated Sol-Gel (U,Pu)O <sub>2</sub> . . . . .	51
Thermal Conductivity . . . . .	52
Irradiation Behavior . . . . .	53
Uninstrumented Thermal-Flux Irradiation Tests . . . . .	53
Instrumented ETR Tests . . . . .	56
ORR Instrumented Tests . . . . .	56
Fast Flux Irradiation Tests . . . . .	57
Transient Irradiation Tests . . . . .	58
Fuel-Cladding Mechanical Interaction Tests . . . . .	60
Actinide Redistribution in Irradiated (U,Pu)O <sub>2</sub> . . . . .	60
<b>16. ADVANCED LMFBR FUELS DEVELOPMENT . . . . .</b>	<b>62</b>
Irradiation Testing . . . . .	62
Fabrication of (U,Pu)N Pellets . . . . .	63
Fabrication of Advanced Fuels by Carbothermic Reduction . . . . .	64
Characterization of (U,Pu)N . . . . .	64
Process For Producing Metal-Free Nitride Powders from U-Pu Alloy . . . . .	64
The X-Ray Lattice Parameter of U <sub>0.81</sub> Pu <sub>0.19</sub> N Pellets . . . . .	64
Chemical Analysis Results for Specimens of U <sub>0.81</sub> Pu <sub>0.19</sub> N . . . . .	65
Compatibility of Cladding with Nitride Fuels . . . . .	65
Tailoring Nitride Fuels . . . . .	65
Thermodynamic Studies . . . . .	66
The Lattice Parameter of U(C,N) as a Function of Composition . . . . .	66
Phase Behavior of the U-V-N System and Properties of UVN <sub>2</sub> . . . . .	66
Phase Behavior of the U-V-C System and the Thermodynamic Properties and Crystal Structure of UVC <sub>2</sub> . . . . .	66
Phase Investigations in the U-Cr-N System . . . . .	67
Equilibrium Investigations of Carbon-Rich V(C,N) Solutions . . . . .	67
Thermodynamic Investigations in the Uranium-Plutonium-Nitrogen System . . . . .	67
Thermal Contact Resistance . . . . .	67

17. LMFBR FUEL ELEMENT DESIGN AND MODEL DEVELOPMENT .....	68
Model Integration .....	68
Fuel Performance .....	68
Electron Microscopy and Electron Microprobe Analysis .....	68
Pressure Sintering .....	70
Normalization of Swelling and Fission Gas Release Models .....	70
Cladding Performance .....	71
Mechanical Properties of Type 316 Stainless Steel .....	71
Discrete Element Analysis of the Creep of Stainless Steel	
Tubing for LMFBR Application .....	73
Transient Stress Analysis .....	73
Failure Analysis .....	73
Power Cycling .....	75
18. CLADDING AND STRUCTURAL MATERIALS .....	76
Radiation Damage to Fast Reactor Cladding and Structural Materials .....	76
Biaxial Stress-Rupture Properties of Titanium-Modified Stainless Steel Tubing .....	81
Incoloy 800 .....	82
Electron Microscopy of Irradiated Vanadium .....	84
19. FABRICATION OF FAST BREEDER REACTOR CLADDING .....	85
Evaluation of Planetary Swaging as a Process to Produce High	
Quality Cladding .....	85
Fabrication of Ultrafine Grain Size Stainless Steel Tubing .....	86
Biaxial Stress-Rupture Properties of Ultrafine Grain Size Type 316	
Stainless Steel Tubing .....	86
Origin and Significance of Natural Defects Generated During	
Tubing Fabrication .....	87
Generation and Evaluation of Artificial Defects .....	87
20. STAINLESS STEEL WELDING DEVELOPMENT .....	88
Shielded Metal-Arc Process .....	88
Submerged-Arc Process .....	89
Metallographic Analyses .....	90
21. SODIUM CORROSION IN LMFBR SYSTEMS .....	92
Mass Transfer of Interstitial Impurities Between Vanadium Alloys	
and Sodium .....	92
Effect of Oxygen in Sodium on the Corrosion of Vanadium	
and Vanadium Alloys .....	92
Effect of Oxygen on the Mechanical Properties of Vanadium Alloys .....	93
Mass Transport Between 300 Series Stainless Steels and	
Vanadium Alloys .....	93
Compatibility of Stainless Steels and Thermal Insulation Materials .....	95

22. NONDESTRUCTIVE TESTING TECHNIQUES FOR LMFBR .....	96
Development of Advanced Nondestructive Testing .....	96
Eddy-Current Instrument .....	96
Ultrasonic Schlieren Techniques for Inspection of Welds .....	96
Measurement of Cold Work in Stainless Steel Tubing .....	97
23. FAST BREEDER REACTOR NEUTRON ABSORBER MATERIALS .....	98
Void Formation in Boron Carbide Powder During Heat Treatment .....	98
Transmission Electron Microscopy of Boron Carbide .....	99
Crystallography of Unirradiated Boron Carbide .....	99
Gas Release From Boron Carbide Powders During Irradiation in a Thermal Reactor .....	99
X-Ray Diffraction of Irradiated and Unirradiated Boron Carbide Powders .....	99
Scanning Electron Microscopy of Irradiated and Unirradiated Boron Carbide .....	101
Fast Reactor Irradiation Testing of Boron Carbide .....	102
<b>PART III. SPACE POWER TECHNOLOGY</b>	
24. ALKALI-METAL CORROSION OF REFRACTORY METALS .....	103
Lithium Corrosion Studies .....	103
Thermal-Convection Loop Tests .....	103
Forced-Circulation Lithium Loop .....	103
Effect of Oxygen on the Compatibility of Refractory Metals with Alkali Metals .....	104
Alkali Metal Penetration .....	104
Effect of Oxygen on Dissolution of Refractory Metals in Alkali Metals .....	105
25. MATERIALS DEVELOPMENT FOR ISOTOPIC POWER PROGRAMS .....	106
Curium Program .....	106
Fabrication of Tungsten Capsules for the Thermionic Generator Mockup .....	106
Capsule Welding .....	106
Nondestructive Testing .....	107
Compatibility .....	107
Chemical Vapor Deposited Tungsten Capsules for Radioisotope Sources .....	108
Cladding Materials Program .....	109
Evaporation of Cobalt- and Nickel-Base Alloys .....	109
New Platinum-Base Capsule Alloys for Space Isotopic Heat Sources .....	110
The Influence of Various Ordered States on the Mechanical Properties of Ni-Co-V Ternary Alloys .....	110
Back Extrusion of Refractory Metal Fuel Capsules .....	110
Strontium Program Compatibility Studies .....	111
SNAP-23 Nondestructive Testing .....	111
Isotope Kilowatt Program .....	111

26. METALLURGY OF REFRACTORY ALLOYS .....	112
Basic Physical Metallurgy Studies .....	112
Development of Age-Hardening Refractory Alloys .....	112
Quasichemical Models and Cahn's Spinodal Decomposition .....	112
Mechanical Properties of Commercial Refractory Alloys .....	113
Molybdenum-Base Alloys .....	113
Tantalum-Base Alloys .....	113
Niobium-Base Alloys .....	113
Bonding Refractory Alloys to Noble Metals .....	114
Thermal Conductivity of Tantalum .....	115
27. NITRIDE FUELS DEVELOPMENT .....	116
Synthesis and Characterization of Uranium Nitride .....	116
Irradiation Testing of Uranium Mononitride .....	116
28. TUNGSTEN METALLURGY .....	118
Extrusion of Tungsten Alloys .....	118
Chemical Vapor Deposition Development .....	118
Deposition of Tungsten with a Low Fluorine Content .....	118
Tungsten Alloy Deposition .....	119
Chemical Vapor Deposition of Vanadium and Vanadium Alloys .....	119
Development of Improved Methods for Joining Tungsten Alloys .....	120
Creep Properties of Tungsten Alloys .....	120
Long-Time Creep-Rupture Properties of Arc-Melted and CVD Tungsten Alloys .....	121
Correlation of Creep Properties for Tungsten .....	121
Anomalous Creep Behavior of Powder-Metallurgy W-25% Re .....	122
Electron Microscopic Study of Creep Mechanisms .....	123
Effect of Low-Pressure Oxygen on the Creep Properties of Tungsten and Its Alloys .....	123
<b>PART IV. GENERAL FUELS AND MATERIALS RESEARCH</b>	
29. CORROSION OF ADVANCED STEAM GENERATOR ALLOYS .....	124
30. FUEL ELEMENT FABRICATION DEVELOPMENT .....	127
Irradiation Studies .....	127
Postirradiation Examination of High-Temperature Refractory Metal Cermets .....	127
Irradiation Performance of a Nickel Phosphide Coating .....	127
Effect of Void Volume on the Swelling Behavior of Aluminum-Base Dispersion Fuels .....	128
HFIR Fuel Element Support .....	128
HFIR Fuel Element Manufacture .....	128
Modifications and Improvements to HFIR Fuel Plates .....	130

Fabrication Development of Aluminum Dispersion Fuel Plates . . . . .	130
Deformation Behavior of Shaped Fuel Cores During Rolling . . . . .	130
Parametric Study of $U_3O_8$ -Al and $UAl_x$ -Al Dispersion Fuel Plates . . . . .	131
Effect of Dispersoid Concentration on Void Volume of Composite Plates . . . . .	132
Chemical Preparation of Aluminum Surfaces for Roll Bonding . . . . .	132
Nondestructive Testing . . . . .	133
Radiographic Densitometry . . . . .	133
Scanner Calibration Studies . . . . .	133
Physical Properties of Two-Phase Materials Used in Fuel Plate Cores . . . . .	134
Electron-Beam Welding of Fuel Plates to Side Plates . . . . .	134
 31. HASTELLOY N IMPROVEMENT . . . . .	 136
Electron Microscope Studies of Hastelloy N . . . . .	136
Effect of Irradiation Temperature on the Creep Properties of Hastelloy N . . . . .	138
Effect of Titanium on the High-Temperature Deformation and Fracture Behavior of Some Nickel-Base Alloys . . . . .	139
Effect of Composition on the Postirradiation Mechanical Properties of Modified Hastelloy N . . . . .	140
 32. JOINING RESEARCH ON NUCLEAR MATERIALS . . . . .	 143
The Effect on Weldability of Minor Variations in Chemical Composition . . . . .	143
Ductility of Heat-Affected Zones at High Temperatures . . . . .	143
Studies on Incoloy 800 Weld Metal . . . . .	145
Austenitic Stainless Steels . . . . .	147
 33. NONDESTRUCTIVE TEST DEVELOPMENT . . . . .	 149
Electromagnetic Inspection Methods (Eddy Currents) . . . . .	149
Theoretical Solutions . . . . .	149
Development of Computer Programs . . . . .	149
Application of Computer Programs . . . . .	149
Development of Inspection Systems . . . . .	150
Ultrasonic Test Methods . . . . .	150
Fabrication of Reference Standards . . . . .	150
Optical Visualization of Ultrasound . . . . .	150
Frequency Analysis . . . . .	150
Penetrating Radiation Inspection Methods . . . . .	151
Radiation Attenuation . . . . .	151
Radiation Scattering . . . . .	151
Infrared Holographic Inspection . . . . .	151

## PART V. REACTOR DEVELOPMENT SUPPORT

34. ALUMINUM IRRADIATION DAMAGE .....	152
Irradiation-Induced Swelling of Aluminum Alloys .....	152
The Effect of High Fast Neutron Fluences on 6061 Aluminum .....	153
Void Formation in High-Purity Aluminum .....	154
35. DESALINATION .....	157
Experimental Fabrication of Th-20% U Alloy for the Unclad Metal Breeder Reactor Fuel Element .....	157
Corrosion Studies .....	159
36. GAS-COOLED REACTOR PROGRAM .....	161
Coated Particles from Ion Exchange Resins .....	161
Fuel Loading .....	161
Carbonization and Coating .....	162
Density and Dimensional Changes in Methane- and Propylene-Derived Pyrolytic Carbons Irradiated to $2 \times 10^{22}$ neutrons/cm <sup>2</sup> at 715°C .....	162
Coated-Particle Bonding Development for HTGR Fuels .....	162
Development of Bonded Coated-Particle Beds for HTGR Fuel Elements .....	164
Gas-Cooled Fast Breeder Reactor Fuel Element Development .....	165
Cooperative Irradiation Test Capsules .....	166
Experiments in the Oak Ridge Research Reactor .....	167
Fabrication of Capsules for EBR-II .....	168
37. HEAVY SECTION STEEL TECHNOLOGY .....	170
Characterization of Heavy Section Steel Plate .....	170
Characterization of Heavy Section Steel Weldments .....	172
Radiation Studies on HSST Plates and Welds .....	173
38. MILITARY REACTOR FUEL ELEMENT PROCUREMENT ASSISTANCE .....	174
39. MOLTEN-SALT REACTOR PROGRAM .....	175
Materials Work in Support of the MSRE .....	175
Hastelloy N Development .....	176
Development of a Modified Hastelloy N .....	176
Mechanical Properties of Commercial Heats of Modified Hastelloy N .....	176
Welding of Modified Hastelloy N .....	176
Corrosion Studies .....	177
Corrosion of Hastelloy N in Steam .....	178
Coated Bearing Specimens .....	178
Graphite Studies .....	179
Types of Graphite Being Studied .....	179
Graphite Fabrication .....	180
X-Ray Studies .....	181
Irradiation Damage in Graphite .....	181
Graphite Impregnation .....	183

Thermal Conductivity Apparatus for Graphite .....	185
Electron Microscopy of Graphite .....	186
Chemical Processing Materials .....	187
Corrosion of Structural Materials in Bismuth .....	187
Coatings for Corrosion Resistance .....	187
Construction of a Molybdenum Reductive Extraction Test Stand .....	187
Fabrication Development of Molybdenum Components .....	188
Molybdenum Welding Development .....	189
Development of Bismuth-Resistant Filler Metals for Brazing Molybdenum .....	189
40. REACTOR EVALUATION .....	
Computer Program Development for Cost Analysis .....	191
Fuel Fabrication Cost Analysis .....	191
Parametric Study of GCFR Fuel Fabrication Costs .....	192
Alternate Cladding Fabrication Analysis .....	192
Systems Analysis Study .....	192
Fuel Recycle Task Force .....	192
LMFBR Fuel Material Conversion Process .....	192
Cost Comparison of Four Alternate Routes for Fabricating (U,Pu)O <sub>2</sub> Fuel for LMFBR's .....	192
Fuel Performance Analysis .....	193
The Release of Fission Gases from Mixed Oxide Fuels .....	193
The Physical and Tensile Properties of Type 316 Stainless Steel .....	193
Nuclear Performance Feasibility of Molybdenum Fuel Cladding in an LMFBR .....	193
Metals and Ceramics Division Information Activities .....	193
41. THORIUM UTILIZATION .....	195
Thorium-Uranium Recycle Facility .....	195
Status of TURF .....	195
Initiation of HTGR Recycle Operations .....	196
Fueled-Graphite Development .....	196
Particle Handling .....	197
Particle Coating .....	197
Particle Inspection .....	197
Bonding of Fuel Particles .....	197
Fabrication of Recycle Test Elements .....	197
Coating of Recycle Test Element Fuel .....	197
Bonding of Recycle Test Element Fuel .....	198
HTGR Recycle Fuels Irradiation .....	198
Capsule Irradiations .....	198
Large-Scale Irradiation .....	199
Thorium Ceramics Data Compilation .....	200
42. TRANSURANIUM PROGRAM .....	201
Target Fabrication .....	201
HFIR Target Performance .....	202
Status of the Targets Exposed in HFIR .....	202
Analysis of Target Performance .....	202
HFIR Target Rod Irradiation Damage .....	203
Preparation of Platinum Filters for a Californium Ion Exchange Assembly .....	203

43. WATER REACTOR SAFETY .....	205
Program Coordination .....	205
Base-Line Data from Transient Temperature Rupture Tests of Zircaloy Tubing .....	206
Multirod Transient Burst Experiments .....	206
Metallurgical Support .....	209

#### PART VI. OTHER PROGRAM ACTIVITIES

44. ABSORBER MATERIALS FOR SULFUR DIOXIDE FROM FLUE GAS .....	213
Behavior of Dawsonite in Sorption-Regeneration Cycles .....	213
A High Temperature X-Ray and Thermal Analysis Study of Synthetic Dawsonite .....	213
45. ALLOY DEVELOPMENT FOR ARMY PULSED RADIATION FACILITY REACTOR .....	214
Core Alloy Development and Evaluation .....	214
46. METALLOGRAPHY .....	215
Electron Microprobe Analysis .....	215
Alpha Metallography Facility .....	220
Metallography of Radioactive Materials at Oak Ridge National Laboratory .....	221
Alpha Autoradiography .....	221
Shatterproof Coatings for Glass .....	222
Improved Metallograph Illumination System .....	222
Quantitative Television Microscopy .....	222
47. NERVA PROGRAM METALLURGICAL SUPPORT .....	224
Effects of Space Environment on NERVA Materials .....	224
Outgassing of NERVA Fuel Elements .....	224
Adhesion of NERVA Materials .....	225
Nondestructive Inspection of Coolant Channels in Beryllium Reflector Components .....	226
Thermal Fatigue of Nozzle Tubes .....	226
Physical Properties of Selected NERVA Materials .....	226
Beryllium .....	226
Graphites .....	227

#### PAPERS AND PUBLICATIONS

PAPERS AND ORAL PRESENTATIONS .....	228
PUBLICATIONS .....	237
AUTHOR INDEX .....	249
ORGANIZATION CHART .....	253

# Summary

## PART I. FUNDAMENTAL PROGRAMS

### 1. Crystal Physics

Using etch-pit patterns, electron microscopy, and x-ray topography, we studied the quality of  $\text{UO}_2$  single crystals grown by arc melting, by a modified floating-zone technique, and by vapor deposition. Eutectic-composite structures resulted from the directional solidification of melts consisting of uranium dioxide with 5 to 15 wt % W and  $(\text{U,Th})\text{O}_2$  with 10 wt % W. Results of scanning electron microscopy, x-ray diffraction, electrical conductivity, thermal conductivity, and mechanical strength studies on  $\text{UO}_2$ -W composites are summarized. The eutectic in the  $\text{UO}_2$ -W pseudo-binary system was determined to be approximately  $2640^\circ\text{C}$  and 9 wt % W. Progress is reported in efforts to grow  $\text{ThO}_2$  by our internal centrifugal zone growth technique at 26 MHz by the addition of 7 mole %  $\text{Y}_2\text{O}_3$  to reduce the resistivity. As a preliminary step in a program to produce a transuranic-based laser, the Czochralski (crystal pulling) method has been used to prepare single-crystal boules of  $\text{CaWO}_4$  and  $\text{CaWO}_4:\text{Nd}$  approximately 1 cm in diameter  $\times$  7 cm long. Melt growth of pure and doped crystals [ $\text{Mg}_2\text{SiO}_4$ ,  $\text{KMgF}_3$ ,  $\text{XSiO}_4:\text{Ln}$  ( $\text{X} = \text{Zr, Hf, Th}$ ;  $\text{Ln} = \text{Gd, Er, Yb}$ ),  $\text{ThO}_2:^{239}\text{Pu}$ ,  $\text{ThO}_2:^{244}\text{Cm} + \text{Tm}$ ] is discussed. Phase studies (under dynamic conditions) are summarized for the hydrothermal system  $\text{SiO}_2$ - $\text{RbOH}$ - $\text{H}_2\text{O}$ - $\text{Fe}$ . Growth conditions and alkali ion impurities of  $\text{RbOH}$ -grown quartz are correlated by analysis of infrared and mass spectroscopic data.

### 2. Deformation, Annealing, and Interfaces in Metallurgical Phenomena

Quantitative metallography showed isothermal recrystallization in moderately deformed aluminum to be quantitatively consistent with a proposed edge-nucleated, growth-controlled model. A power-law dependence of grain-boundary migration rate on driving

force may be related to impurities in solid solution capturing and controlling the boundary motion. The rolling texture of  $\text{Cu}_3\text{Au}$ , whether ordered or disordered, was similar to that of copper for all reductions in thickness between 20 and 96%. Ordering before rolling affected the subsequent recrystallization texture of  $\text{Cu}_3\text{Au}$  and enhanced the formation of the  $\{001\}\langle 100 \rangle$  component. Recovery of niobium occurred in three stages corresponding to point defect annealing, dislocation rearrangements within cell walls, and coalescence of subgrains. Migration of low-angle grain boundaries in Nb-40% V left behind a trail of hair-pin shaped dislocation loops. We contributed to the theory of jogged screw dislocation glide and to the measurement of high-temperature creep of LiF single crystals.

### 3. Deformation of Crystalline Solids

Progress has been made in understanding the nature of precipitation in Nb-Hf and Ta-Hf alloys. Work on dislocation theory has included extensive work on dislocations in anisotropic media. Computer programs have been written for simulating solid solutions based on x-ray measurements and for predicting the changes in such solutions on deformation.

### 4. Diffusion in Solids

A mathematical analysis showed that diffusivities relative to two different frames of reference in multi-component systems are invariant. Uranium diffusion coefficients in  $\text{UN}_{1+x}$  were shown to be markedly dependent on nitrogen gas overpressure. The alpha-energy degradation method was confirmed directly by comparison with results obtained for uranium in tantalum by the anodizing-and-stripping serial sectioning technique. Radio-frequency sputtering is being developed as a tool for determination of small diffusion coefficients. Cation self-diffusion coefficients are being determined and analyzed with regard to jump mechanism for both the monoxide and dioxide of titanium.

Experiments on diffusion in refractories under high pressures and temperatures are planned.

### 5. Electron Microscopy

Observations on voids produced in metals by irradiation and quenching are described, including the effects of cyclotron-injected gases, and preliminary experiments using electron irradiation to produce damage in aluminum are presented briefly. Metallographic observations of silicon precipitates produced in aluminum as a result of neutron irradiation are summarized. Theoretical and experimental studies of the stability and growth of bubbles and cavities in metals are reported. Measurements of the energy stored in copper single crystals by room-temperature deformation are presented along with a brief discussion of the use of stored energy measurements in evaluating work-hardening theories. Some observations on hydrogen absorption and embrittlement of steel are described.

### 6. Fundamental Ceramics Research

Results of a multidisciplinary study of the important nuclear fuel, uranium mononitride, and related rock-salt-structured actinide compounds are described. A synergistic increase in understanding of the behavior of UN is shown to derive from the interpretation of a number of different measurements. The studies reported include band structure calculations, optical constant measurements, physical property determinations, and low-temperature specific heat measurements. The program involves work in nine groups of the Metals and Ceramics Division, in three other divisions at ORNL, and at three other laboratories.

### 7. Mössbauer Studies of Alloys

Mössbauer measurements provided information on the field about  $^{61}\text{Ni}$  nuclei in nickel-palladium alloys.

### 8. Physical Ceramics Studies

The effects of stoichiometry on the deformation mechanisms of  $\text{UO}_2$  single crystals and on the creep of UN are being investigated. For  $\text{UO}_2$  the principal slip system changes from  $\{100\}$  to  $\{111\}$  for sufficiently hyperstoichiometric crystals.

A phenomenological model for sintering is being developed with topological ideas. In addition, new evidence for the role of dislocation movement in sintering was found. The interesting phenomenon of desintering, the decrease of the bulk density of a

sintered body on further heat treatment, was examined for sol-gel  $\text{ThO}_2$ .

### 9. Physical Property Research

Experimental investigations of heat transport in solids were continued. This effort included work on lattice or phonon conduction in  $\text{UO}_2$  and LiF and electronic and phonon transport in Ta, Cr, and  $(\text{Th}_x\text{U}_{1-x})\text{N}$ . In addition, we investigated the effect of configurational order on the transport properties and specific heat of  $\text{Ni}_3\text{Fe}$ .

### 10. Spectroscopy of Ionic Media

The physical chemistry of haloaluminate and chlorozincate systems was investigated, largely by absorption spectroscopy of molten mixtures. Information on structure and constitution of complex ions of Ni, Al, Zn, and Bi was derived.

### 11. Superconducting Materials

A study of niobium with gadolinium or yttrium dispersions was extended to high ac frequencies. Initial results indicate that these materials may exhibit lower ac losses than pure niobium. The Debye temperature of pure technetium has been found to be  $454^\circ\text{K}$  from ultrasonic measurements at  $4.2^\circ\text{K}$ . We constructed a phenomenological model of flux pinning in hysteretic superconductors, based on the assumption of thermally activated flux motion. Two material parameters derived from this model should facilitate intercomparison of superconducting properties and metallurgical structure. This model was extended to the case of moving fluxoids — flux flow and ac magnetization experiments. Metallurgical studies in cooperation with other groups of the Metals and Ceramics Division are listed.

### 12. Surface Reactions of Metals

We have developed a model for the oxidation of the ternary alloy U–7.5 wt % Nb–2.5 wt % Zr and the binary U–9.4 wt % Nb. Transient stresses on the order of  $10^6$  psi exist at the oxide-metal interface of these alloys, and these stresses can trigger phase transformations in the alloy and control oxide morphology. Flexure studies with tantalum at 550 to  $850^\circ\text{C}$  provided data for computing strain, strain energy, and stress levels that develop in the oxide and metal as tantalum oxidizes. Average stresses in excess of  $10^5$  psi exist in the oxide. Our flexure technique also showed

how specimen geometry and mechanical inhomogeneities may cause uniaxial bending to result from the uniform biaxial stress produced during oxidation. A study of the oxidation characteristics of the tantalum-tungsten alloys was initiated, and we used our sub-micron, anodic-film sectioning technique in investigating possible small differences in the activation energy for diffusion of various tracer elements in tungsten.

### 13. Theoretical Research

We are investigating a number of phenomena in solids with particular emphasis on those that are related to the electronic states. We are developing new techniques for treating the electronic states of ordered and disordered solids theoretically. For the most part, we use the Korringa-Kohn-Rostoker method to study the energy bands of ordered metals and alloys, the LCAO method for ionic and covalent compounds, and the coherent potential approximation for disordered systems.

### 14. X-Ray Diffraction

A mathematical method that analyzes temperature-diffuse x-ray scattering in terms of mean atom displacements rather than normal vibration modes was developed. We also successfully derived an analytic technique for separating components of diffuse x-ray scattering due to short-range order, static atom displacements, and thermal motion of atoms.

Our studies of x-ray scattering from neutron-irradiated highly oriented graphite specimens resulted in a plausible model for the damaged structure that involves condensation of interstitial carbon atoms to form new basal planes.

Aging reactions of gamma-stabilized uranium alloys have been followed by x-ray diffraction experiments at a series of aging conditions. Effects of sample deformation on the reactions are also being examined. Phase transitions in metallic samarium have been delineated by a high-temperature x-ray diffraction study.

Progress in small-angle x-ray scattering includes modifications to experimental apparatus to improve signal-to-noise ratios, a further analysis of proportional counter characteristics, and the development of techniques for the measurement of absolute intensities.

## PART II. FAST REACTOR TECHNOLOGY

### 15. Fast Reactor Oxide Fuels

This program is being conducted to advance the technology of (U,Pu)O<sub>2</sub> as a Liquid Metal Fast Breeder

Reactor fuel. The determination of the properties and performance of sol-gel-derived oxide fuels fabricated by the Sphere-Pac and pelletizing techniques is emphasized. A variety of irradiation capsules were fabricated during the year. Sol-gel-derived pellets were fabricated with controlled densities from 81 to 93% of theoretical. A Sphere-Pac method in which all of the plutonium is incorporated in the coarse fraction was developed. The Sphere-Pac process was used to load approximately 150 in. of (U-20% Pu)O<sub>2</sub> fuel for irradiation tests in the Engineering Test Reactor, the ORR, and the EBR-II. Smear densities of these beds ranged from 80 to 85% of theoretical. We demonstrated firing (U,Pu)O<sub>2</sub> pellets with considerably less sorbed gas by sintering in Ar-4% H<sub>2</sub> and cooling in pure argon to prevent resorption of hydrogen. We fabricated 19 unencapsulated fuel pins for our EBR-II Series II experiments and 8 fuel pins for testing gas-cooled breeder reactor conditions in the EBR-II. We constructed one instrumented capsule for the ORR and two each containing four fuel pins for irradiation in the ETR. We further improved our ability to characterize (U,Pu)O<sub>2</sub> fuels, including determining the oxygen-to-metal ratio, determining the homogeneity of (U,Pu)O<sub>2</sub> by both alpha autoradiography and by electron microprobe analysis, and demonstration of methods for light and replica electron microscopy.

Uninstrumented irradiations in the ETR to 9.7 at. % burnup and instrumented tests in the ORR have continued to confirm that Sphere-Pac fuels will perform in reactors comparably to pelletized fuels of similar smear density. Two capsules were placed in the ETR to test sol-gel pellet and Sphere-Pac fuel swelling and fuel-cladding mechanical and chemical interaction under peak LMFBR design operating conditions of 590 W/cm with the cladding inside surface at 650°C. In an ORR instrumented test, Sphere-Pac and pellet fuels having a smear density 82% of theoretical exhibited identical thermal performance to low burnup. Five encapsulated Series I pins containing Sphere-Pac (U,Pu)O<sub>2</sub> continued irradiation in the EBR-II, reaching a peak burnup of 6.2% FIMA; three capsules will continue to 11.8% FIMA. Six fuel pins containing unirradiated sol-gel (U,Pu)O<sub>2</sub> survived power transients in the TREAT that melted 50 to 60% of the fuel in the peak power regions of two pins. Extensive design work was done on instrumented ORR tests of interaction between fuel and cladding during power cycling. We also began to study in-reactor redistribution of uranium and plutonium by postirradiation electron microprobe analysis and alpha autoradiography.

## 16. Advanced LMFBR Fuels Development

Mixed (U,Pu)N is being developed as an advanced fuel for the LMFBR. Since the principal aim is good performance under irradiation to burnups in excess of 100,000 MWd/metric ton, emphasis has to be placed on the manufacture of fuel for irradiation testing. Ten pins containing a total of 30 linear inches of (U,Pu)N sodium-bonded to type 316 stainless steel cladding were fabricated for testing in the ETR at heat ratings of 30 kW/ft.

In fabrication development we found that homogeneous (U,Pu)N pellets could be made by two independent routes. In one the (U,Pu)N is synthesized from uranium-plutonium alloy; in the other UN is blended with PuN, calcined, ground, and sintered into pellets.

Reliable analytical techniques were developed for U, Pu, C, and O in (U,Pu)N. A consistent negative bias on nitrogen is observed with the micro-Kjeldahl method now being used.

If excess nitrogen produced by fissioning of plutonium in (U,Pu)N causes a problem, it can be alleviated by the addition of vanadium or chromium as metals,  $V_2N$ , or  $Cr_2N$ . The buffering action of these additives is due to the formation of (U,Pu)VN<sub>2</sub> or (U,Pu)CrN<sub>2</sub>.

## 17. LMFBR Fuel Element Design and Model Development

We are developing analytical methods to predict and evaluate the performance of LMFBR fuel pins and fuel elements. The program incorporates three areas: integrated fuel element performance modeling, modeling of fuel performance, and modeling of cladding performance. The work is coordinated with the related fuel and cladding development programs, providing methods for designing and interpreting irradiation tests, determining the influences of materials properties on fuel element performance, and identifying specific areas in which experimental research should be done. The integrated fuel performance model, FMØDEL, was completed and can perform calculations for fuel swelling, fission gas formation and release, and cladding mechanics. Fuel performance modeling is still in a quite empirical stage; thus, much of our effort was directed toward further refinement of the models for the various aspects of fuel behavior. The work included light and electron microscopy and electron microprobe analysis of irradiated (U,Pu)O<sub>2</sub> to improve our knowledge of fuel swelling, fission gas release, actinide and fission product redistribution, and restructuring.

We determined stresses in cladding exposed to service levels of temperature and pressure and the deformation

of the cladding under these stresses. We made exploratory tests on unirradiated type 316 stainless steel under cyclic stress and temperature, did discrete element analysis of the creep of stainless steel tubing for LMFBR application, and developed a method for failure analysis. In addition, we began to develop methods for treatment of the behavior of cladding under power cycling and reactor transients.

## 18. Cladding and Structural Materials

The nature of the defects produced in type 304 stainless steel during irradiation to fast fluences of the order of  $10^{22}$  neutrons/cm<sup>2</sup> was characterized as a function of irradiation temperature. At about 300°C small defect clusters were formed, from 370 to 630°C voids were formed, and above 770°C only helium bubbles were visible. The voids caused a density decrease, which was a maximum at about 400°C, and the ductility was reduced. Type 304 stainless steel modified with 0.2% Ti had better ductility than the standard alloy. Some of the titanium-modified alloy has been fabricated into tubing and shown to have properties unirradiated comparable with those of the standard alloy.

Incoloy 800 was irradiated to thermal fluences of the order of  $10^{21}$  neutrons/cm<sup>2</sup>; most of the <sup>10</sup>B was converted to helium. Alloys containing 0.1% Ti had the best postirradiation ductilities. Some aging was noted and was most embrittling at 550°C.

The defects produced in vanadium by irradiation to fast fluences of  $10^{21}$  to  $10^{22}$  neutrons/cm<sup>2</sup> over the range of 385 to 710°C were characterized.

## 19. Fabrication of Fast Breeder Reactor Cladding

The objective of the program is to develop methods to fabricate tubing free of defects and to relate mechanical properties at elevated temperatures to processing variables and defects.

Ultrafine-grain size type 304 stainless steel tubing was produced by controlling the degree of cold working and the temperatures at which the tubing was annealed between the cold working steps. This tubing is weaker than conventional tubing at elevated temperatures but also is considerably more ductile. Using planetary swaging equipment now available, this process is not attractive as the primary tubing fabrication process because of surface defect generation.

Defects in tubing can be generated during many stages of manufacturing. Machine marks on tube shells can produce defects in the final tubing. A method was

developed to produce artificial defects and allow a more precise relationship to be developed between mechanical properties and fabrication defects.

## 20. Stainless Steel Welding Development

We are studying the behavior of weldments in austenitic stainless steel at elevated temperatures as a function of both welding process and variables within a process for application to LMFBR vessels and components. Our primary concern is to determine reasons for the high degree of scatter reported for creep ductility and to develop optimized welding procedures for obtaining satisfactory mechanical properties.

Minor changes in weld metal composition (within the allowable range for type 308 filler metal) can produce significant variations in mechanical properties. The rupture life can be increased tenfold, for example, by increasing the carbon content of shielded metal-arc weld metal from 0.044 to 0.074 wt %. Coating differences are also important; lime-coated electrodes produced weaker but more ductile deposits than electrodes coated with titania or lime and titania. Submerged-arc welds exhibited lower creep strengths than did shielded metal-arc welds. All these studies are being correlated with metallographic interpretations, with special emphasis on scanning electron fractographs of the specimen surfaces.

## 21. Sodium Corrosion in LMFBR Systems

Various vanadium alloys were tested in capsules at 600°C to determine the effect of alloying elements on the reactivity of vanadium with impurities in sodium. Additions of both chromium and molybdenum to vanadium lower the affinity of vanadium for oxygen in sodium. The creep properties of vanadium were measured in vacuum and in low-pressure oxygen. The absorption of oxygen by vanadium during the creep test increased the creep rate at 600°C. However, the addition of 470 ppm O to the vanadium before creep testing had little effect on the creep rate at 600°C in vacuum.

The simultaneous exposure of vanadium and type 304L stainless steel to sodium resulted in the mass transport of carbon and nitrogen to the vanadium, embrittling it within 3000 hr at 800°C. However, similar exposures to type 321 stainless steel did not affect the mechanical properties of the vanadium.

The oxidation behavior of types 304 and 316 stainless steel was studied at 760°C in moist air and in a mixture of N<sub>2</sub>-1% O<sub>2</sub>-100 ppm H<sub>2</sub>O. Type 316 stainless steel

showed poorer resistance to scaling in moist air than did type 304. However, both steels underwent negligible oxidation in the nitrogen mixture. Contacting the steels with Al<sub>2</sub>O<sub>3</sub>-SiO<sub>2</sub> thermal insulation did not affect their oxidation behavior in either test environment. Sodium accelerated the oxidation of type 304 stainless steel in the nitrogen mixture when the sodium was introduced through a small crack in the stainless steel. However, increasing the sodium leak rate caused the sodium to move into surrounding thermal insulation, and the stainless steel specimen oxidized much less.

## 22. Nondestructive Testing Techniques for LMFBR

We are developing new methods, techniques and equipment for nondestructively inspecting materials for the LMFBR, with emphasis on measuring cold work in stainless steel tubing.

Design and development have begun on a prototype eddy-current instrument to identify both the size of a flaw and its depth below the surface. Since phase shift of the signal will be important we are using portions of a new modular phase-sensitive eddy-current instrument as a starting point.

We are applying ultrasonic schlieren techniques to specimens of welds containing intentional flaws in both aluminum and stainless steel and correlating them with results from other more conventional ultrasonic techniques.

We are developing techniques for measuring changes in magnetic permeability in both flat sheet and tubular specimens of type 316 stainless steel as a means of determining the degree of cold work in the materials. Because of the good results on the flat specimens using a breadboard, low-frequency bridge system, we performed a series of calculations to aid the design of a high-sensitivity prototype instrument for tubing and started building it.

## 23. Fast Breeder Reactor Neutron Absorber Materials

We are endeavoring to characterize boron carbide, study factors that affect its irradiation performance, and determine the mechanism of irradiation damage for this material, which is a prime candidate for use as a neutron absorber in fast reactors. We found methods to control the size and numbers of intragranular voids that may affect the irradiation performance of boron carbide. These voids are believed to form as a consequence of a Kirkendall effect.

Using an ion-bombardment milling technique, we obtained the first known transmission electron micrographs of boron carbide. The surfaces of intragranular voids were observed to be crystallographic faces. Boron carbide powder irradiated at 350°C in a thermal reactor released approximately 5.3% of the gas generated. Scanning electron microscopy of irradiated and un-irradiated boron carbide powder indicated no change in the appearance of the solid particle or fragmentation of the particles during irradiation. X-ray diffraction lines of these particles were more diffuse after irradiation. Irradiation led to the disappearance of a free graphite line that did not disappear in unirradiated material heat treated for equal times at the same temperature.

### PART III. SPACE POWER TECHNOLOGY

#### 24. Alkali-Metal Corrosion of Refractory Metals

We developed a model for the penetration of alkali metals into oxygen-contaminated tantalum and niobium. We established that temperature-gradient mass transfer of zirconium and hafnium in refractory-alloy systems containing lithium is controlled by solid-state diffusion.

To investigate the compatibility of materials with lithium under engineering conditions, we operated a large T-111 forced convection loop under conditions anticipated for the primary system of an advanced high-temperature space reactor. The loop was operated for 3000 hr at a 1370°C heater exit temperature. One field repair was required after 1750 hr to remove a leaking vent line.

#### 25. Materials Development for Isotopic Power Programs

Research and development on materials for encapsulation of isotopic power fuels is being carried out in support of a variety of space and terrestrial (including undersea) programs.

Capsules were machined from arc-cast tungsten extruded at 1775°C. Throughout fabrication and inspection, an electropolishing technique minimized propagation of cracks and revealed defects covered by metal smeared during machining. A CVD tungsten vent tube was welded to the capsule with W-25% Re filler metal and to a type 304 stainless steel extension tube with type 308 filler metal. The 1000-W (thermal)

<sup>244</sup>Cm<sub>2</sub>O<sub>3</sub>-fueled capsule was successfully seal welded in the hot cell with specially developed equipment and procedures. In our study of the compatibility of <sup>244</sup>Cm<sub>2</sub>O<sub>3</sub> with refractory metals, we examined specimens exposed for up to 10,000 hr at 1650 and 1850°C. Tantalum alloys were penetrated at 1650°C and formed low-melting fuel mixtures at 1850°C; W-26% Re, TZM, and Mo showed the best compatibility. The creep testing of CVD tungsten test capsules at 1650°C by programmed pressurization with helium verified rupture times predicted from uniaxial creep data and showed good rupture ductility (11 and 18% circumferential strain).

The evaporation of Hastelloy N and Haynes alloy No. 188 at 800 to 1050°C and 10<sup>-9</sup> torr resulted in void formation, solutioning of some precipitates, and formation of others due to the selective evaporation of chromium and manganese. Platinum-base solid solution (Pt-5% Mo) and ordered (Pt<sub>3</sub>Cr) alloys are being developed. The ordered alloy exhibits far superior creep strength and considerably slower evaporation than unordered alloys, and both have excellent oxidation resistance at 1000°C. The structure of a pseudobinary alloy (Ni,Co)<sub>3</sub>V could be controlled, although Ni<sub>3</sub>V and Co<sub>3</sub>V always ordered on quenching. Aging at 700 and 800°C produced the ductile cubic AuCu<sub>3</sub>-type ordered structure. However, longer aging formed a brittle hexagonal structure with a nine-layer stacking sequence. The activation energy for creep and the stress exponent were greater for the ordered alloy than for a similar disordered alloy.

We back extruded at 1200°C capsules of Nb-1% Zr, Mo, and Mo-0.5% Ti with hemispherical ends. The tantalum alloys T-111 and Ta-10% W are being back extruded at 1300 and 1350°C with a plasma-sprayed molybdenum coating to protect from contamination and provide lubrication by MoO<sub>3</sub>.

Nonradioactive SrTiO<sub>3</sub> and Sr<sub>2</sub>TiO<sub>4</sub> showed little interaction with Haynes alloy No. 25, Hastelloy C, or type 316 stainless steel in 10,000 hr at 900 and 1100°C. However, SrO reacted significantly because of the silicon content of the alloys. Potassium in SrO from one process increased the interaction.

Ultrasonic inspection measured weld penetration in pressure-tested SNAP-23 capsules within ±10 mils of metallographic measurements. For the Isotope Kilowatt Program, high-temperature thermal conductivity data on iron alloys were reviewed for radiation shield applications, and consumable-electrode vacuum remelting was recommended to obtain high-purity iron castings.

## 26. Metallurgy of Refractory Alloys

The aging characteristics of tantalum alloys containing 30, 50, and 60 wt % Hf were studied by x-ray diffraction, metallography, and hardness tests. Hardness increases to about 350 DPH resulted from clustering and the precipitation of coherent  $\alpha$ -hafnium. Thermodynamic and kinetic features of spinodal decomposition in a hypothetical binary system were studied with various quasicheical models. A model that considers atomic nonrandomness and concentration-dependent potential energies agrees qualitatively with experimental observations.

The creep strength of TZM was related to the subgrain size. Transverse welds in T-111 creep specimens failed in the weld at high stresses and outside the weld at lower stresses, as predicted from a study of the effect of heat treatment on creep properties. The creep strength of annealed C-129Y was improved by annealing; however, the rupture ductility was reduced.

A transition piece of tungsten between platinum and Ta-10 wt % W tubing extended the leaktight life from 100 hr to between 500 and 1000 hr at 1200°C. The thermal conductivity of tantalum estimated from experimentally derived low-temperature phonon conductivity and Lorenz function values are within 3% of the recommended values to 3000°K.

## 27. Nitride Fuels Development

A method of fabricating UN fuel pellets with only 150 ppm O contamination was developed. We irradiated UN clad in T-111 at a surface temperature of 1400°C to a burnup of about 1.75 at. % heavy metal. The test was terminated when cladding failure was detected. Failure is attributed to low cladding ductility under the conditions of the test.

## 28. Tungsten Metallurgy

The Tungsten Metallurgy Program provides base technology on the fabrication and properties of tungsten alloys for application in advanced reactor and isotope systems for space power. We are optimizing the variables to extrude high-quality tungsten tubing and extruding tubing of advanced high-strength tungsten alloys.

Over 800 in.<sup>2</sup> of high-purity chemically vapor-deposited tungsten sheet was produced for mechanical property and welding studies. The fluorine content was varied between 5 and 30 ppm by controlling the temperature of the deposition chamber. We overcame nodule formation in depositing alloys containing 1 to

5% Re by using metal-rich gas mixtures. A feasibility study showed that fully dense vanadium can be deposited by the hydrogen reduction of VCl<sub>4</sub> or VF<sub>5</sub> feed gas; however, elimination of interstitial impurities will require additional development.

We are developing improved methods for joining tungsten alloys with lower melting ductile filler metals. The variables for gas tungsten-arc welding of powder-metallurgy tungsten and arc-melted W-25% Re were determined both with and without molybdenum-rhenium alloy filler metal. Cracking in some of the welds of CVD tungsten was caused by high fluorine impurity contents.

Additional long-time creep-rupture data at creep rates as low as 10<sup>-5</sup>/hr were collected for arc-melted tungsten-rhenium alloys and high-purity CVD tungsten. At 1650°C the CVD material was the strongest on the basis of time to 1% creep in 1000 hr; however, W-5% Re is stronger if larger strains or 50% of the rupture stress is used as the criterion. Utilizing the correlation of creep strength developed by Sherby, we obtained excellent agreement of our data for arc-melted tungsten with data from three other sources. The creep rate varied with the hyperbolic sine of the stress. At very low stresses powder-metallurgy W-25% Re had a lower creep rate at 2200°C than at 1650°C. This anomalous behavior was attributed to the larger grain boundary area available for growth of creep cavities in the material tested at 1650°C. An electron microscopic study of the nucleation and growth of creep cavities in powder-metallurgy tungsten showed that gas bubbles apparently nucleate the cracks, which grow by merging with small cavities expanded by the crack front. We determined that the creep strength of tungsten in 10<sup>-5</sup> torr O<sub>2</sub> is substantially lower than in a vacuum of 10<sup>-8</sup> torr. The W-25% Re alloy is stronger in a partial pressure of oxygen because a surface layer of the rhenium-rich sigma phase forms; however, in this environment the alloy ruptures at strains of 2 to 8%.

## PART IV. GENERAL FUELS AND MATERIALS RESEARCH

### 29. Corrosion of Advanced Steam Generator Alloys

We are continuing field corrosion tests of welds in advanced steam generator alloys in commercial steam. General corrosion is assessed by determining attack rates, characterizing scales, and calculating long-term corrosion from weight-gain data. Susceptibility to

preferential corrosion is determined by examining for knife-line attack at weld fusion lines and by conducting U-bend tests.

Inconel 625, Hastelloy X, and IN 102 as both base and filler metals, Incoloy 800 as base metal, and Inconel 82 as filler metal exhibited very good corrosion resistance at both 595 and 650°C. Welds containing Inconel 600 and austenitic stainless steel exhibited somewhat inferior behavior. No preferential or unusual attack was noted.

### 30. Fuel Element Fabrication Development

We are continuing to advance the technology of research reactor fuels to obtain improved irradiation performance, lower fuel element costs, and higher fuel element reliability.

The preirradiation characteristics and irradiation performance of aluminum cermet fuels were correlated with excellent predictability of swelling up to fission densities of  $2.2 \times 10^{21}/\text{cm}^3$ . Improvements in the bonding of nickel phosphide coatings to aluminum were insufficient for successful operation of coated fuel plates in the G-12 loop of ETR. Postirradiation examination of W-UO<sub>2</sub> cermets indicated that void volume and its deployment are important factors controlling the swelling of these high-temperature cermets. But mass transfer between the fueled cermet and its cladding may be the controlling factor for fuel element lifetime.

Some fuel plates fabricated for the HFIR fuel assembly were modified at Texas Instruments, Inc., to obtain production information. No fabrication problems were found in the manufacture of a small test lot of fueled plates containing the burned grade of oxide fuel. The use of an Al<sub>2</sub>O<sub>3</sub> dispersoid on the filler side of the complex HFIR fuel plate core was investigated to reduce fuel plate rejection due to bond defects during manufacture.

Fabrication studies on shaped cores have shown that the void left in the frame cavity by the shaping of the core is filled with aluminum from the frame and cover plate. We found that the quantity of voids in aluminum-base dispersions is affected by the hot rolling temperature and the degree of cold work in addition to the type of materials used and concentration of ceramic fuel. But other fabrication variables such as compact density had no influence on the void volume of the final fuel plate.

We completed the study of radiography and densitometry to determine the capabilities and limitations for measuring fuel inhomogeneity on aluminum fuel

dispersion plates. To control many of the variables required for precision of fuel inhomogeneity measurements using radiography was extremely difficult.

### 31. Hastelloy N Improvement

The type of carbide precipitate correlated strongly with the postirradiation creep properties of Hastelloy N. Alloys with more than 0.2% Si form coarse M<sub>6</sub>C that is very stable, but the fracture strains are very low. Alloys with low silicon contents form M<sub>2</sub>C, which is finely dispersed up to 650°C but coarsens rapidly at higher irradiation temperatures. The fracture strains are quite low for both forms of M<sub>2</sub>C but much lower for the coarse, high-temperature form. Adding Nb, Ti, or Hf produces very finely dispersed MC and results in high postirradiation fracture strains. Several compositions have been found to have good properties, but the optimum concentrations of Nb, Ti, and Hf have not been determined yet.

### 32. Joining Research on Nuclear Materials

We are determining the effects of minor quantities of such elements as C, S, P, Ti, Al, Mn, and Si on the weldability of nickel-containing alloys such as Inconel 600 and Incoloy 800. In our heat-affected-zone studies on Incoloy 800, aluminum and titanium improved hot ductility, sulfur was deleterious, but phosphorus had little effect. An alloy with 0.08% C performed better than alloys with less carbon. Additional studies were concerned with alloys containing manganese and sulfur plus phosphorus. Our heat-affected-zone studies on Inconel 600 were focused on the effect of various elemental additions on microstructures. Significant grain-size differences were observed, and gross liquation in laminations was noted in high-sulfur alloys. Manganese did not affect the microstructure of sulfur-containing alloys unless phosphorus was added also.

We also tested several filler metals for use with Incoloy 800. Inconel 82T appeared to be best, but electroslag remelted Incoloy 800 also appeared satisfactory. Also an experimental phosphorus-containing composition exhibited a high yield strength and is promising.

Our study of austenitic stainless steels has centered on the effect of composition on the amount and morphology of the ferritic phases usually found in weld deposits. These phases are body-centered cubic δ-ferrite and body-centered tetragonal martensite. Measurements are made with the Magne-Gage and the quantitative television microscope. Even though the nickel and

chromium equivalents remain the same, the actual compositions of the filler metals were very important in controlling the amount, size, and distribution of ferrite. One alloy that the Schaeffler diagram predicts to have 100% austenite actually contained about 3% ferrite.

### 33. Nondestructive Test Development

We continued analytical studies of eddy-current phenomena, deriving new equations, and both writing and applying computer programs to use the equations to study cases of interest. Phase-sensitive instrumentation was modified to improve stability and sensitivity.

Improved capabilities were developed for fabricating reference standards for ultrasonic inspection. The optical portion of the schlieren system was improved. Preliminary techniques using frequency analysis were developed to allow determination of the size and orientation of flaws without dependence upon the relative intensity of reflected signal.

Quantitative radiation attenuation measurements were sensitive to changes in density or thickness as small as 0.5% in graphite. Development began on techniques for measuring radiographs with closed-circuit television. Good sensitivity has been demonstrated on measuring thickness of aluminum on uranium, using the fluorescent radiation from uranium excited by a  $^{147}\text{Pm}$  source. Preliminary studies showed the feasibility of real-time infrared holography using liquid crystals as a display medium.

## PART V. REACTOR DEVELOPMENT SUPPORT

### 34. Aluminum Irradiation Damage

Irradiation-induced changes in the microstructure and mechanical properties of aluminum alloys are described. Loops and voids form from defects produced by displacement reactions. Transmutation-produced silicon precipitates as a new phase. Hydrogen and helium, injected by cyclotron or formed by an earlier irradiation, affect the distribution of voids and loops formed during later irradiations or quenching experiments, indicating that these transmutation-produced gases play an important role in the swelling of irradiated aluminum alloys. Void formation at about 60°C in various alloys was related to original composition and structure: voids form more rapidly in high-purity aluminum than in solid-solution alloys, while 6061 aluminum, which contains precipitated  $\text{Mg}_2\text{Si}$ , exhibits only a few tenths of a percent density change after irradiation to fluences as high as  $5 \times 10^{22}$  neutrons/cm<sup>2</sup>

( $>0.821$  MeV). In high-purity aluminum irradiated to  $1.0 \times 10^{22}$  neutrons/cm<sup>2</sup> ( $>0.821$  MeV), the presence of voids up to 1100 Å in diameter causes a 7% decrease in density.

Irradiation of 6061 aluminum to high fast neutron fluences increases the tensile strength below 150°C while the ductility is moderately reduced. However, at 150°C and above the ductility measured at low strain rates is severely reduced.

### 35. Desalination

We completed exploratory experiments on fuel fabrication methods for the Unclad Metal Breeder Reactor (UMBR). This reactor, which would use Th-20 wt % U fuel elements, is a proposed low-cost source of heat for seawater distillation and power generation. We demonstrated the basic feasibility of casting to shape, casting a billet, and forming from a billet component shapes from which the fuel element can be assembled.

The most attractive and economical production method for making fuel elements now appears to consist of some combination of rolling and forming component pieces from an ingot. The ingot may be produced by consumable electrode arc-melting or possibly from alloyed or elemental powders by compaction and extrusion.

Specimens of Th and Th-20 wt % U were taken from a loop operated to determine the compatibility of these materials with sodium in type 304 stainless steel at 800°F. We found no physical evidence of corrosion; even after 2000 hr the reaction product film was less than 0.1 mil. No intergranular attack was observed.

### 36. Gas-Cooled Reactor Program

All-ceramic fuels of  $(\text{Th,U})\text{O}_2$  or  $(\text{Th,U})\text{C}_2$  particles coated with pyrolytic carbon and SiC offer considerable advantages as fission-product-retaining fuel for high-temperature gas-cooled reactors (HTGR's). An important part of our support for the Program consisted of the preparation, characterization, and irradiation testing to high fast fluence of coating materials and simulated bonded-bed fuel elements. Bonded coated-particle beds prepared with high-density matrices containing high concentrations of stable filler materials survived irradiation to full HTGR fast fluences without loss of integrity or coating failures. Binder compositions that include large concentrations of alternate commercial filler materials were developed and are being tested. Excellent dimensional stability of high-density propylene-derived pyrolytic carbon coatings as compared to methane-derived coatings was also demon-

strated to fast fluences twice the design maximum of HTGR's. A significant new activity is the development of coated particles derived from ion exchange resins. Certain types of resin particles retain their spherical shape when carbonized slowly in a fluidized bed, and stable two-layer coatings may be applied to them. Sufficient uranium may be absorbed in such particles before carbonizing to make them an attractive substitute for the small fissile particles in the HTGR fuel cycle.

We also contributed to the development of fuel elements for a gas-cooled fast breeder reactor (GCBR). We participated in the examination and evaluation of three sealed fuel pins that performed well during irradiation in the ORR and prepared the (U,Pu)O<sub>2</sub> fuel and fuel pin for a test of a new manifolded-vented fuel element design. This instrumented, vented fuel pin began irradiation in the ORR in March and is operating satisfactorily. We also prepared the (U,Pu)O<sub>2</sub> fuel for and constructed a set of eight GCBR fuel pins to be tested in EBR-II at temperatures ranging from 600 to 800°C.

### 37. Heavy Section Steel Technology

The Metals and Ceramics Division is actively involved in the Heavy Section Steel Technology (HSST) Program as consultants and experimentalists. We are characterizing 12-in.-thick quenched-and-tempered steel plates and weldments and determining the effect of irradiation on their mechanical properties.

We found that the mechanical properties of three plates were similar and satisfied the requirements of the ASTM A533, grade B, class 1, specification. Plate material from the surface locations is superior to material from the interior locations in tensile and impact properties.

The characterization studies have permitted us to extend our knowledge of flaw-initiated failures. We are analyzing the effect of the acuity of the notch in a Charpy V-notch (C<sub>V</sub>) specimen on dynamic and static fracture toughness.

We have characterized the weld metal and heat-affected zone (HAZ) of electroslag welds. The quarter-thickness tensile and impact properties of the weld metal and base metal are similar. The weld metal is somewhat poorer than the base metal in that it does not vary in properties through the thickness (even though the weldment has been double austenitized, double quenched, and tempered). Further, the ductile shelf energy of the weld metal is 80 ft-lb compared to 140 ft-lb for the base metal. The HAZ properties approximate those of the base metal.

Changes in tensile and C<sub>V</sub> properties from radiation were shown to depend on irradiation temperature; self-annealing occurred at 550°F and up.

### 38. Military Reactor Fuel Element Procurement Assistance

Technical surveillance and specification preparation aided core procurement for the Antarctica reactor, the floating "Sturgis" nuclear power plant, and the Air Force Nuclear Engineering Test Reactor.

### 39. Molten-Salt Reactor Program

Samples of Hastelloy N and graphite were removed from the MSRE after 22,533 hr at 650°C. They were quite compatible with the fluoride salt environment; however, the Hastelloy N was embrittled by the thermal neutron irradiation. We are developing a Hastelloy N of modified composition that has improved postirradiation ductility. Additions of Ti, Hf, and Nb produced the finely dispersed MC-type carbide that we believe responsible for the improved properties. Some 50- to 100-lb commercial heats of this material have been procured, and their fabricability and weldability are excellent. Continuing corrosion tests on standard Hastelloy N show that it has excellent compatibility with salts containing LiF, BeF<sub>2</sub>, UF<sub>4</sub>, and ThF<sub>4</sub>. A higher corrosion rate was observed in the proposed new coolant salt, NaBF<sub>4</sub>-8 mole % NaF. This higher rate is at least partially attributable to the ease with which this salt picks up moisture. Hastelloy N showed good compatibility with steam in tests to 6000 hr.

Graphite test bodies from various cokes were fabricated for testing. The most isotropic bodies were produced from Robinson coke. In irradiation studies on numerous graphites, the crystallite growth rates decreased with increasing isotropy and with increasing crystallite size. Metallographic studies revealed the deterioration of the particle-particle boundaries and have emphasized the need for better binder materials. Several techniques were developed for reducing the surface permeability of graphite to gaseous fission products. The first irradiation of samples so treated showed an increase in the permeability after a fluence of about  $1 \times 10^{22}$  neutrons/cm<sup>2</sup> (>50 keV).

The chemical compatibility of several materials with bismuth has been studied. Molybdenum, TZM, and Mo-0.5% Ti exhibited excellent compatibility, but Nb and Nb-1% Zr mass transferred very badly. Methods of putting adherent coatings of W and Mo on Ni- and Fe-base alloys have been partially developed. We are

fabricating a molybdenum test stand for Chemical Technology Division experiments involving bismuth. This has involved the development of back-extrusion techniques for making 4-in.-diam vessels and welding and brazing methods.

#### 40. Reactor Evaluation

We assist the AEC in evaluating and optimizing the reactor designs by analyzing the cost of fuel fabrication and evaluating the performance of nuclear fuels. We modified the basic computer code for fabrication cost analysis to extend and refine its ability to handle various cladding and structural materials and to analyze more thoroughly cost of fuel preparation by pelletization. Also, we performed a number of cost analyses of reactor fuel elements and on various fabrication processes for fuel elements, investigated the release of fission gases from mixed oxide fuels, compiled physical and tensile properties of type 316 stainless steel, and assessed the nuclear performance feasibility of molybdenum fuel cladding in an LMFBR. In addition, we assisted the AEC by revising the report of the Fuel Recycle Task Force, which is directed at updating the *Civilian Nuclear Power, A Report to the President - 1962*.

#### 41. Thorium Utilization

The objective of the Thorium Utilization Program is to demonstrate economic techniques for conducting the Th-<sup>233</sup>U fuel cycle for the High-Temperature Gas-Cooled Reactor. Fabrication processes and equipment must be developed to handle the highly radioactive recycle fuel, and the fuels produced must be demonstrated in an irradiation test program. The activities in the program this year included the maintenance of the Thorium-Uranium Recycle Facility and improvements of certain functional components in TURF, further development of various refabrication processing steps, with primary emphasis on a prototype remote fluidized-bed furnace for deposition of pyrolytic carbons from hydrocarbon gases. A principal activity was the fabrication of prototype Recycle Test Elements for irradiation in the Peach Bottom Reactor. A number of different types of fuel particles were fabricated, coated, and bonded into fuel sticks for incorporation in these elements.

#### 42. Transuranium Program

The Transuranium Project is producing quantities of the heavier transuranium elements for research by

successive neutron captures in plutonium, americium, and curium in the High Flux Isotope Reactor. Target elements are removed periodically and reprocessed to obtain the product actinides and to recycle target actinides to the HFIR. Special target elements of the higher isotopes are fabricated and irradiated in HFIR. In addition, product actinides are encapsulated. Our activities included the fabrication of targets in TRU for HFIR, the fabrication of HFIR rabbits, the fabrication of special encapsulations for neutron and gamma sources, the evaluation of the performance of the target elements, and the improvement of the processing equipment in TRU. We fabricated 15 target elements during the year, 14 loaded with <sup>244</sup>Cu and one with <sup>242</sup>Pu. Nine hydraulic rabbits for use in the HFIR were fabricated containing <sup>244</sup>Pu, <sup>253</sup>Es, and <sup>249</sup>Bk. Seven neutron sources of <sup>252</sup>Cf and one gamma source were assembled. Our failure model for the HFIR targets had predicted that increased porosity in the actinide-containing pellets would extend the target life. This model was confirmed by the operation of six targets with lower density pellets up to 82% FIMA and fast fluences up to  $5.45 \times 10^{22}$  neutrons/cm<sup>2</sup> (>0.81 MeV). These targets contain pellets ranging in density from 75 to 80%, compared with 90%-dense pellets in targets that had failed at about 60% FIMA. We continued to seek the causes of low-ductility failures in the HFIR targets and alloys more suitable for cladding use in the targets.

#### 43. Water Reactor Safety

The deformation and rupture of Zircaloy-clad fuel rods during the thermal transient associated with a loss-of-coolant accident in a light-water reactor may play an important role in determining whether the outcome of such an accident is acceptable. Therefore, we are examining the failure of these rods in terms of their environmental history and postulated accident conditions and assessing the effect of this failure on the termination of the accident transient. We coordinate this work for the U.S. Atomic Energy Commission and study the high-temperature deformation of Zircaloy.

### PART VI. OTHER PROGRAM ACTIVITIES

#### 44. Absorber Materials for Sulfur Dioxide from Flue Gas

A comparison of the SO<sub>2</sub> absorption and H<sub>2</sub> regeneration characteristics of pure sodium aluminate and a sodium aluminate modified with kaolinite and sodium silicate indicated that the pure sodium aluminate has

serious limitations but is generally superior to the modified material as a possible flue-gas absorber. Extensive DTA, TGA, and x-ray experiments showed that formation of sodium aluminate from  $\text{NaAlCO}_3(\text{OH})_2$ , the mineral dawsonite, is complex and involves at least one noncrystalline intermediate.

#### 45. Alloy Development for Army Pulsed Radiation Facility Reactor

In seeking an improved core alloy for pulsed reactor service, we determined the toughness properties of several U-10% Mo alloys containing small additions (to 1.0%) of Al, Cr, Nb, Ta, and Ti. After aging at the maximum embrittlement temperature of 475°C, the alloy U-10% Mo-0.3% Ti showed a clear superiority in notch toughness at all aging times to 64 hr. While inferior to the alloy containing 0.3% Ti, the alloy U-10% Mo-1% Ta exhibited impact properties that were independent of aging time.

#### 46. Metallography

The electron microprobe continues to be an extremely useful analytical tool. Its utility was extended to soft biological tissue with gratifying results. Multiple elemental cathode-ray tube x-ray displays can be shown in a single photograph by use of color film. Computer-plotted graphs can be made from x-ray intensities. The alpha metallography facility is operating very well. Low-moisture-containing abrasive vehicles helped us reveal the microstructures of uranium-plutonium carbides, nitrides, and carbonitrides. A report on the

metallography of radioactive materials at ORNL was presented. Some technique developments in alpha autoradiography improved our microstructural evaluations. Reports on shatterproof coatings on glass and an improved illumination system for older research metallographs were published. The quantitative television microscope continues to be a useful quantitative tool. More accurate data are now obtained because of a better understanding of the instrument performance.

#### 47. NERVA Program Metallurgical Support

A Hall device magnetic probe has been designed, built, and tested for the nondestructive inspection of coolant channels in beryllium reactor components. This probe has demonstrated the feasibility and usefulness of the inspection technique. Outgassing of NERVA fuel elements is being measured under conditions similar to those expected in space operations; the rates for 11 different gases are determined semicontinuously during each test run, and the results are analyzed and plotted as a function of time and temperature with the aid of a computer. Adhesion studies are concentrated on the effects of shear motion in controlled vacuum environments.

Tensile data on type 347 stainless steel were obtained to aid in the analysis of thermal fatigue problems in the NERVA nozzle. Study of irradiation effects in beryllium and selected carbonaceous materials requires a knowledge of their properties unirradiated. To provide this base-line data we measured the thermal conductivity, electrical resistivity, and thermopower of several materials in the range 80 to 400°K.

# Part I. Fundamental Programs

## 1. Crystal Physics

G. W. Clark

Crystal growth of high-melting-point refractory materials is the central theme of our group. Very specific crystals (composition, phase, purity, perfection, size, etc.) are often required to characterize physical properties uniquely or are required for the operation of technical devices. Suitable crystals are often difficult to obtain; hence we are conducting a continuing program to provide crystals needed in research, to devise and improve methods of crystal growth, and to develop an increased understanding of crystal growth processes and kinetics. Crystals are being grown by several methods: by internal centrifugal zone growth, from high-temperature solutions, by temperature-gradient zone melting, from supercritical aqueous systems, and by the general Verneuil method. During this report period we shared our crystals with over 20 different researchers in such diverse investigations as electron spin resonance; optical, defect, magnetic, and elastic properties; deformation; gas bubble migration; diffusion; and radiation damage. Our ferrite crystals are being evaluated by others as possible neutron-beam chopper, monochromator, or polarizer, and the  $\text{UO}_2$ -W rod eutectic material is under study for electron-optical devices and electron and ion emitter sources. Also, we are investigating selected physical properties of these materials, including those related to crystal-growth process and those important for characterizing new compounds.

<sup>1</sup> Abstracted from *J. Am. Ceram. Soc.* 53, 46-51 (1970).

<sup>2</sup> Consultant from Georgia Institute of Technology.

<sup>3</sup> Present address, Gaseous Diffusion Plant, Union Carbide Corp., Oak Ridge, Tenn.

### SUBSTRUCTURE AND PERFECTION IN $\text{UO}_2$ SINGLE CRYSTALS<sup>1</sup>

A. T. Chapman<sup>2</sup> D. E. Hendrix<sup>3</sup>  
G. W. Clark C. S. Yust  
O. B. Cavin

The quality of  $\text{UO}_2$  single crystals grown by (1) arc-melting, (2) a modified floating-zone technique (ICZG), and (3) vapor deposition was studied by use of etch-pit patterns, electron microscopy, and x-ray topography. These techniques complemented each other and indicated significant differences among the crystals grown by the different techniques. Both types of melt-grown crystals contained extensive substructure and approximately  $10^6$  etch pits/cm<sup>2</sup>; finely dispersed inhomogeneities were found in the vapor-grown crystals. Stoichiometry control during growth permitted a major improvement in the perfection of the ICZG crystals.

### REFRACTORY OXIDE-METAL COMPOSITES: SCANNING ELECTRON MICROSCOPY AND X-RAY DIFFRACTION OF URANIUM DIOXIDE-TUNGSTEN<sup>4</sup>

R. J. Gerdes<sup>2</sup> A. T. Chapman<sup>2</sup> G. W. Clark

Unidirectional solidification of a melt consisting of uranium dioxide with 5 to 15 wt % W formed well-ordered arrangements of tungsten fibers or platelets in the uranium dioxide matrix. Fiber shape and

<sup>4</sup> Abstracted from *Science* 167, 979-80 (1970).

orientation relations of the components indicate the development of several dominant growth modes.

### UO<sub>2</sub>-W CERMETS PRODUCED BY UNIDIRECTIONAL SOLIDIFICATION<sup>5</sup>

A. T. Chapman<sup>2</sup> G. W. Clark D. E. Hendrix<sup>3</sup>

Both plate- and rod-type eutectics of tungsten can be produced by controlled unidirectional solidification of uranium oxide containing 5 to 15 wt % W. The mechanical strength of the composite material is 2 to 3 times higher than that of UO<sub>2</sub> crystals at 1150°C. The electrical and thermal conductivities of the composite material are strongly anisotropic.

### UO<sub>2</sub>-W AND (U,Th)O<sub>2</sub>-W EUTECTICS

A. T. Chapman<sup>2</sup> B. F. Oliver<sup>6</sup>  
G. W. Clark J. C. Wilson

The eutectic temperature and composition in the UO<sub>2</sub>-W pseudobinary system were determined to be approximately 2640°C and 9% W. The eutectic composition was obtained by areal analysis of the eutectic structure. Samples containing 5 to 12.5 wt % W were examined, and the eutectic composition was the same in all if measured in the center of the bar. The geometry of the ICZG process tends to produce eutectic in the center of the bar even though the overall composition may be off the eutectic value. Primary UO<sub>2</sub> or primary tungsten tends to solidify around the periphery of the molten zone near the walls because the melt must pass down the walls (surrounding the void generated in melting) on its way to the growing solid-liquid interface. The feed material coming from above the melt void is stripped of the primary UO<sub>2</sub> (or tungsten, depending upon composition) toward the outside of the molten zone. This leaves the eutectic composition to solidify in the center.

The melting temperature of the UO<sub>2</sub>-W eutectic was measured by observing the melting point of chips of eutectic composition on a resistance-heated tungsten strip under 1 atm N<sub>2</sub>. Temperatures measured on the strip were calibrated with the melting point of Al<sub>2</sub>O<sub>3</sub>. Attempts to measure the melting point of UO<sub>2</sub> in the same configuration result in the formation of a eutectic liquid upon heating. The liquid forms first at the points of contact between the UO<sub>2</sub> and tungsten.

Tungsten rods were again obtained upon directional solidification of a Th<sub>0.6</sub>U<sub>0.4</sub>O<sub>2</sub> solid solution containing 10 wt % W by use of a 26-MHz generator at Georgia Institute of Technology. Generator stability and induction coupling problems are the major deterrents to progress.

### GROWTH OF THORIUM OXIDE CRYSTALS

A. T. Chapman<sup>2</sup> G. W. Clark J. C. Wilson

Growth of ThO<sub>2</sub> crystals by the ICZG method has not been possible because the high electrical resistivity did not allow rf coupling to the oxide at the frequency (4 MHz) and maximum preheater temperature (1400°C) available to us. We were able to melt the center of an 18-mm-diam rod of thoria by doping with 7 mole % Y<sub>2</sub>O<sub>3</sub> to reduce the resistivity, using a 26-MHz generator at the Georgia Institute of Technology and a higher preheating temperature. The higher preheating temperature was reached by employing SiC susceptors and placing the bottom of the thoria rod on a pedestal of ZrO<sub>2</sub>-8% CaO. At 26 MHz power was readily coupled to the ZrO<sub>2</sub> to preheat the bottom of the thoria to a high enough temperature for direct rf coupling.

The molten zone was moved upward approximately 1 cm through the thoria in 20 min (without rotation). Crystals with maximum dimensions of several millimeters grew in the molten region. In principle, therefore, it appears possible to grow ThO<sub>2</sub> by the ICZG method if a generator of sufficiently high frequency is employed. Thoria is much less able than UO<sub>2</sub> to withstand the stresses of cooling without cracking. It will therefore be necessary to grow ThO<sub>2</sub> at much slower rates or provide a high-temperature anneal.

### MELT GROWTH OF PURE AND NEODYMIUM-DOPED CaWO<sub>4</sub>

C. B. Finch G. W. Clark

As a preliminary step in a program to produce a transuranic-based laser, the Czochralski (crystal pulling) method was used to prepare single-crystal boules (rods) of CaWO<sub>4</sub> (mp 1620°C) and CaWO<sub>4</sub> doped with 0.1 to 1.0 at. % Nd. The crystal growth apparatus included an iridium crucible-susceptor, inductively coupled under air to a 10-kW, 450-kHz generator. The temperature of the system could be controlled to an estimated ±2.0°C, using a Radiamatic pyrometer sighted at the crucible bottom.

<sup>5</sup> Abstracted from *J. Am. Ceram. Soc.* 53, 60-61 (1970).

<sup>6</sup> Consultant from the University of Tennessee, Knoxville.

Optical-quality growth was achieved under the conditions outlined in the literature:<sup>7</sup> high-purity reagents, 1.25 cm/hr pull rate, 10 to 25 rpm seed rotation, and a high degree of temperature stability. The largest optical-quality boule produced in this program is of  $\text{CaWO}_4$ -0.35 at. % Nd, and is approximately 1 cm diam  $\times$  7 cm long. Initial difficulties, which have centered about formation of inclusions and cracking during cooling, now appear to have been surmounted.

#### MELT GROWTH OF SINGLE-CRYSTAL $\text{Mg}_2\text{SiO}_4$ (FORSTERITE)

C. B. Finch

To provide larger specimens for ESR, Mössbauer, and other studies, pure and transition-ion-doped single-crystal boules of  $\text{Mg}_2\text{SiO}_4$  (orthorhombic) were grown from the melt<sup>8</sup> at approximately 1900°C. The growth system included a crystal puller and an iridium crucible-susceptor inductively coupled to a 10-kW, 450-kHz radio-frequency generator. With high-purity starting reagents (melt composition = 2  $\text{MgO}\cdot\text{SiO}_2$ ), optical quality growth was attained at a pull rate of 1.2 cm/hr and 10 to 25 rpm rotation. A polycrystalline deposit was first nucleated on a narrow iridium strip and was then necked down to a single crystal. We have grown crystals up to 1 cm in diameter  $\times$  3 cm long.

Forsterite has a Moh's hardness of 6.5 and cleaves with difficulty on {010}. It is transparent and colorless when pure but becomes violet when doped with  $\text{Cr}^{3+}$  and brown with  $\text{Fe}^{3+}$ . Boules doped with 0.1 wt %  $\text{Fe}^{3+}$ ,  $\text{Mn}^{2+}$ , or  $\text{Cr}^{3+}$  each displayed paramagnetic resonances attributable to their respective dopants. The transition ion occupies a  $\text{Mg}^{2+}$  site.

#### MELT GROWTH OF $\text{KMgF}_3$ AND OF $\text{KMgF}_3$ DOPED WITH LANTHANIDES

C. B. Finch

The Bridgman method was used to grow single crystals of the congruently melting perovskite  $\text{KMgF}_3$  (mp = 1075°C) and of  $\text{KMgF}_3$  doped with 0.1 wt % (individually) of  $\text{Gd}^{3+}$ ,  $\text{Ho}^{3+}$ ,  $\text{Tm}^{3+}$ ,  $\text{Er}^{3+}$ , and  $\text{Yb}^{3+}$ . The growth technique involved the lowering of conical-bottomed platinum ampuls (charged with high-purity reagents and sealed under vacuum) through 40 cm of

negative thermal gradient from 1125°C to room temperature. The lowering rate was approximately 0.25 cm/hr. At the end of a run, the crystal was extracted after the ampul was sawed open.

A typical run produced crystals of optical quality up to 1  $\times$  1  $\times$  1 cm; however, still larger crystals could be obtained. Although the lanthanide dopant did not usually affect the color of  $\text{KMgF}_3$ , it often produced a strong fluorescence under 2600-Å ultraviolet light (e.g., Tm = orange). The crystals cleaved readily on the {100} planes and were moderately hygroscopic. Electron spin resonance studies have detected the substitution of  $\text{Gd}^{3+}$  at a  $\text{K}^+$  site and of  $\text{Tm}^{3+}$  ( $\text{Tm}^{2+}$  after irradiation) and  $\text{Yb}^{3+}$  at  $\text{Mg}^{2+}$  sites in this host.

#### HIGH-TEMPERATURE SOLUTION GROWTH OF SINGLE-CRYSTAL $\text{XSrSiO}_4\text{:Ln}$ (X = Zr, Hf, Th; Ln = Gd, Er, Yb)

C. B. Finch

A program to provide single-crystal samples for the ESR characterization of lanthanide ions in the tetragonal zircon-structure hosts  $\text{ZrSiO}_4$ ,  $\text{HfSiO}_4$ , and  $\text{ThSiO}_4$  was continued. Well-developed single crystals (in the 3-mm size range and of optical quality) were grown of  $\text{ZrSiO}_4$ ,  $\text{HfSiO}_4$ , and  $\text{ThSiO}_4$ , each doped individually with  $\text{Gd}^{3+}$ ,  $\text{Er}^{3+}$ , or  $\text{Yb}^{3+}$ . The crystals were grown in air at 1150 to 1200°C from  $\text{Li}_2\text{O}\cdot 2\text{WO}_3$  or  $\text{Li}_2\text{O}\cdot 2\text{MoO}_3$  solvent by a described thermal gradient method.<sup>9</sup> Crystals from each run gave usable ESR data, and eight types of site symmetry for rare-earth substitution were detected in  $\text{HfSiO}_4$  and  $\text{ZrSiO}_4$  and four in  $\text{ThSiO}_4$ .

#### HIGH-TEMPERATURE SOLUTION GROWTH OF SINGLE-CRYSTAL $\text{ThO}_2$ DOPED WITH $^{239}\text{PuO}_2$ AND WITH ( $^{244}\text{CmO}_2 + \text{Tm}_2\text{O}_3$ )

C. B. Finch M. M. Abraham<sup>10</sup>

As part of a continuing program to provide single-crystal samples for the ESR characterization of lanthanide and transuranic ions,  $\text{ThO}_2$  single crystals up to 3 mm on octahedral edge were grown doped (1) with  $\text{PuO}_2$  and (2) with both  $^{244}\text{CmO}_2$  and  $\text{Tm}_2\text{O}_3$ . The crystals were grown in air by a described thermal gradient method<sup>11</sup> from  $\text{Li}_2\text{O}\cdot 2\text{WO}_3$ -2 wt %  $\text{Bi}_2\text{O}_3$  solvent at 1275 to 1350°C.

<sup>7</sup>K. Nassau and A. M. Broyer, *J. Appl. Phys.* 33, 3064 (1962).

<sup>8</sup>We had previously grown small (1 mm) but well-developed  $\text{Mg}_2\text{SiO}_4$  single crystals from the high-temperature solvents  $\text{PbO}$  and  $\text{Li}_2\text{O}\cdot\text{MoO}_3$  at 1000-1350°C.

<sup>9</sup>M. M. Abraham, G. W. Clark, C. B. Finch, R. W. Reynolds, and H. Zeldes, *J. Chem. Phys.* 50, 2057-62 (1969).

<sup>10</sup>Solid State Division.

<sup>11</sup>C. B. Finch and G. W. Clark, *J. Appl. Phys.* 36, 2143-45 (1965).

Subsequent ESR examination identified the two lines of  $^{239}\text{Pu}^{3+}$  and measured the  $g$  value. This  $g$  value corresponded to an earlier weak line observed in a  $\text{ThO}_2$  crystal doped initially with  $^{244}\text{Cm}$ . Thus this weak line is due to the daughter  $^{240}\text{Pu}$  of  $^{244}\text{Cm}$ .

In  $\text{ThO}_2$  crystals doped with  $\text{Tm}^{3+}$  and  $^{244}\text{Cm}^{3+}$  the test was to determine if the radiation from the decay of  $^{244}\text{Cm}$  at liquid helium could change the valence of  $\text{Tm}^{3+}$ . This change was not observed.

## HYDROTHERMAL SYNTHESIS

### Hydrothermal System $\text{SiO}_2$ - $\text{RbOH}$ - $\text{H}_2\text{O}$ - $\text{Fe}$ Under Dynamic Conditions<sup>12</sup>

O. C. Kopp<sup>6</sup> L. A. Harris

Rubidium iron micas, feldspars, and a "zeolite" have been synthesized under hydrothermal conditions in the system  $\text{SiO}_2$ - $\text{RbOH}$ - $\text{H}_2\text{O}$ - $\text{Fe}$  studied in the range 300 to 500°C and 1 to 2 kbar. A boundary curve appears to separate the field of micas plus "zeolite" from the field of "zeolite" alone when the only source of iron is the liner of the vessel. The addition of  $\text{Fe}_2\text{O}_3$  to the system raises the temperature of the boundary curve by as much as 60°C. The position of the boundary curve is determined by oxygen fugacity, availability of iron, growth temperature, and pressure.

A green mica is formed under low-temperature reducing conditions, while a more typical black mica is produced over a wide range of conditions, below the boundary curve. The "zeolite" phase is favored by high temperatures and more oxidizing conditions. The feld-

spar phases (primarily the "sanidine" form, but with minor "microcline") are produced only at the highest temperatures and when  $\text{Fe}_2\text{O}_3$  has been added to the system. Feldspar crystals up to 2 mm were obtained in 4 days.

### Characterization of $\text{RbOH}$ -Grown Quartz by Infrared and Mass Spectroscopy<sup>13</sup>

O. C. Kopp<sup>6</sup> P. A. Staats<sup>14</sup>

Infrared frequencies of  $\text{RbOH}$ -grown quartz include bands at 3200, 3300, 3350, 3396, 3438, 3500, 3515, 3555, and 3580  $\text{cm}^{-1}$ . An unusual time- (or temperature-) related phenomenon causes an increase in absorbance in the region 2900 to 3550  $\text{cm}^{-1}$  when crystals are examined over intervals up to several hours while held in a liquid nitrogen cell. The band at 3580  $\text{cm}^{-1}$  is not affected. A linear relationship exists between the average growth rate and extinction coefficient at 3580  $\text{cm}^{-1}$  and is influenced by the temperature of the growth zone. Typically, the extinction coefficient decreases (and presumably the crystal quality improves) as the growth temperature increases for a given growth rate. Impurity ions such as  $\text{Li}^+$ ,  $\text{Na}^+$ , and  $\text{K}^+$  present in the  $\text{RbOH}$  solvent are taken preferentially into the quartz structure because of their smaller sizes. Aluminum and iron present are derived from the nutrient and vessel liner respectively. The ratio of  $\text{Fe}^{3+}$  and  $\text{Al}^{3+}$  to total alkalis is close to but slightly greater than 1.

<sup>12</sup>Abstract of paper accepted for publication by the *Journal of the Tennessee Academy of Science*.

<sup>13</sup>Abstract of paper accepted for publication by the *Journal of the Physics and Chemistry of Solids*.

<sup>14</sup>Physics Division.

## 2. Deformation, Annealing, and Interfaces in Metallurgical Phenomena

R. A. Vandermeer

Interfaces such as grain and subgrain boundaries, dislocation cell walls, twin boundaries, antiphase ordered domain walls, and external surfaces play important roles in metallurgical phenomena. We seek to understand the interaction of solid-solution impurities with migrating grain boundaries, the importance of matrix grain edges as the source of nucleation sites in recrystallization, and the recovery mechanisms whereby dislocations rearrange into cell walls, subgrains coalesce, and high-angle boundaries are formed.

In recent years our deformation studies have focused on texture development in body-centered cubic metals and alloys and in ordered face-centered cubic alloys. The fundamentals governing the deformation behavior of these classes of materials are much less understood than for face-centered cubic metals. In attempting to broaden our deformation studies, we initiated theoretical studies on dislocation behavior during plastic deformation and annealing. High-speed computing procedures are being developed and employed to simulate dislocations and dislocation interactions in crystals.

### THE RECRYSTALLIZATION CHARACTERISTICS OF MODERATELY DEFORMED ALUMINUM<sup>1</sup>

R. A. Vandermeer

The early stages of isothermal recrystallization of moderately deformed, polycrystalline alloys of zone-refined aluminum containing 20 and 45 at. ppm Au were studied by quantitative metallography. The basic structural parameters  $X_v$ , the volume fraction recrystallized, and  $S_v$ , the grain-boundary area per unit volume, were measured on specimens annealed for different

times at specific temperatures in the range 80 to 187°C. Both the maximum,  $G_m$ , and the average,  $\bar{G}$ , growth rates of the recrystallizing grains were also determined. All results could be interpreted in terms of a site-saturated, matrix grain edge nucleation followed by two-dimensional growth perpendicular to the nucleated edge controlling recrystallization kinetics. An equation relating  $S_v$  to  $X_v$  was derived and described the experimental data quite well. Experimentally,  $G_m/\bar{G}$  was 2.6 and the activation energy for growth was 25,700 cal/mole.

### IMPURITIES AND THE POWER-LAW DEPENDENCE OF GRAIN-BOUNDARY MIGRATION RATE ON DRIVING FORCE<sup>2</sup>

R. A. Vandermeer

The impurity drag theory of grain-boundary migration, specifically the transition from a high impurity-independent velocity to a low impurity-controlled one is examined. A rationalization of the behavior expected from a "discontinuous" transition explains the power-law dependence of velocity on driving force recently observed by Rath and Hu for zone-refined aluminum bicrystals. A calculation is outlined in which, as a consequence of this rationalization, the power-law exponent can be related to impurity and intrinsic drag parameters and composition. A correlation of these ideas with experiment suggests that residual transition metal impurities (iron, for example), but not non-transition impurities, may be responsible for the sharp dependence of velocity on driving force in zone-refined aluminum.

<sup>1</sup>Abstracted from R. A. Vandermeer, *Met. Trans.* 1, 819-26 (1970).

<sup>2</sup>Paper presented at the AIME Spring Meeting, May 11, 1970, Las Vegas, Nev.

## ROLLING TEXTURES IN ORDERED AND DISORDERED $\text{Cu}_3\text{Au}$ (REF. 3)

J. C. Ogle

Preferred orientation developed by rolling and by subsequent recrystallization for fully ordered, partially ordered, and disordered  $\text{Cu}_3\text{Au}$  alloy were studied. The effects of rolling variables, rolling temperature, degree of order, and recrystallization after rolling were examined. For comparison the textures of pure copper and 70/30 brass rolled under the same conditions were also determined. No effect of order, rolling temperature, or strain rate on rolling texture formation was noted for  $\text{Cu}_3\text{Au}$ ; the texture was always similar to that of copper for reductions in thickness of 20 to 96%. The final texture may be qualitatively described as an orientation spread about  $\langle 110 \rangle$  directions located at  $0^\circ$  and  $\pm 60^\circ$  from the normal direction on the diameter of

the pole figure from the normal direction to the rolling direction. The spreads extend  $70^\circ$  from one  $\{110\}\langle 112 \rangle$  ideal orientation to another. Brass on the other hand developed its own characteristic texture at deformations as low as 30%. It differed from  $\text{Cu}_3\text{Au}$  and copper in that the orientations tended to concentrate at the end points of the above mentioned spreads – that is, at  $\{110\}\langle 112 \rangle$  orientations.

Figure 2.1 shows the recrystallization textures of  $\text{Cu}_3\text{Au}$  after a 5-min anneal at  $500^\circ\text{C}$  for different initial degrees of long range order. These  $\{111\}$  pole figures indicate that the disordered alloy recrystallizes to a texture similar to the deformation texture but the ordered alloy recrystallizes to the cube texture – that is,  $\{001\}\langle 100 \rangle$  plus other components.

<sup>3</sup>Manuscript in preparation and presented at the AIME Spring Meeting, May 1970, Las Vegas, Nev.

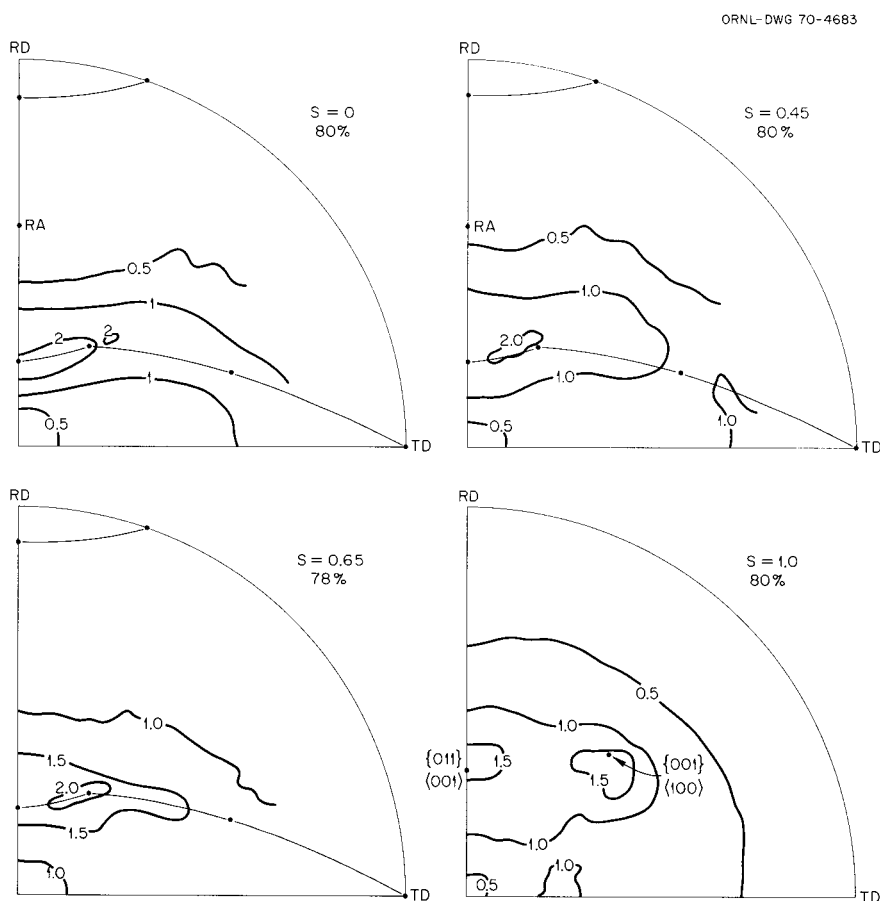


Fig. 2.1. The  $\{111\}$  Pole Figures of Rolled  $\text{Cu}_3\text{Au}$  Annealed 5 min at  $500^\circ\text{C}$ . The long range order parameter,  $S$ , indicates the initial degree of order.

**THE RECOVERY CHARACTERISTICS OF NIOBIUM  
AND Nb-40% V (REF. 4)**

P. V. Guthrie<sup>5</sup>

Isothermal recovery of heavily cold-rolled niobium and a Nb-40% V alloy was studied with x-ray diffraction techniques, transmission electron microscopy, and hardness measurements. Before the onset of

<sup>4</sup>Summary of thesis dissertation presented to University of Cincinnati in partial fulfillment of the requirements for Ph.D. degree, June 1970; to be published as ORNL TM report.

<sup>5</sup>ORAU Fellow.

recrystallization in niobium the particle size, rms strain, integral breadth, and hardness all recovered linearly with the logarithm of annealing time, and the recovery could be divided into three stages:

1. 25 to 340°C – annealing out of point defects with possible strain aging effects;
2. 340 to 700°C – dislocation rearrangement within the heavily tangled dislocation cell walls to form lower energy, sharply delineated, often high-angle subgrain boundaries;
3. above 700°C – the formation of recrystallization nuclei by coalescence of subgrains.

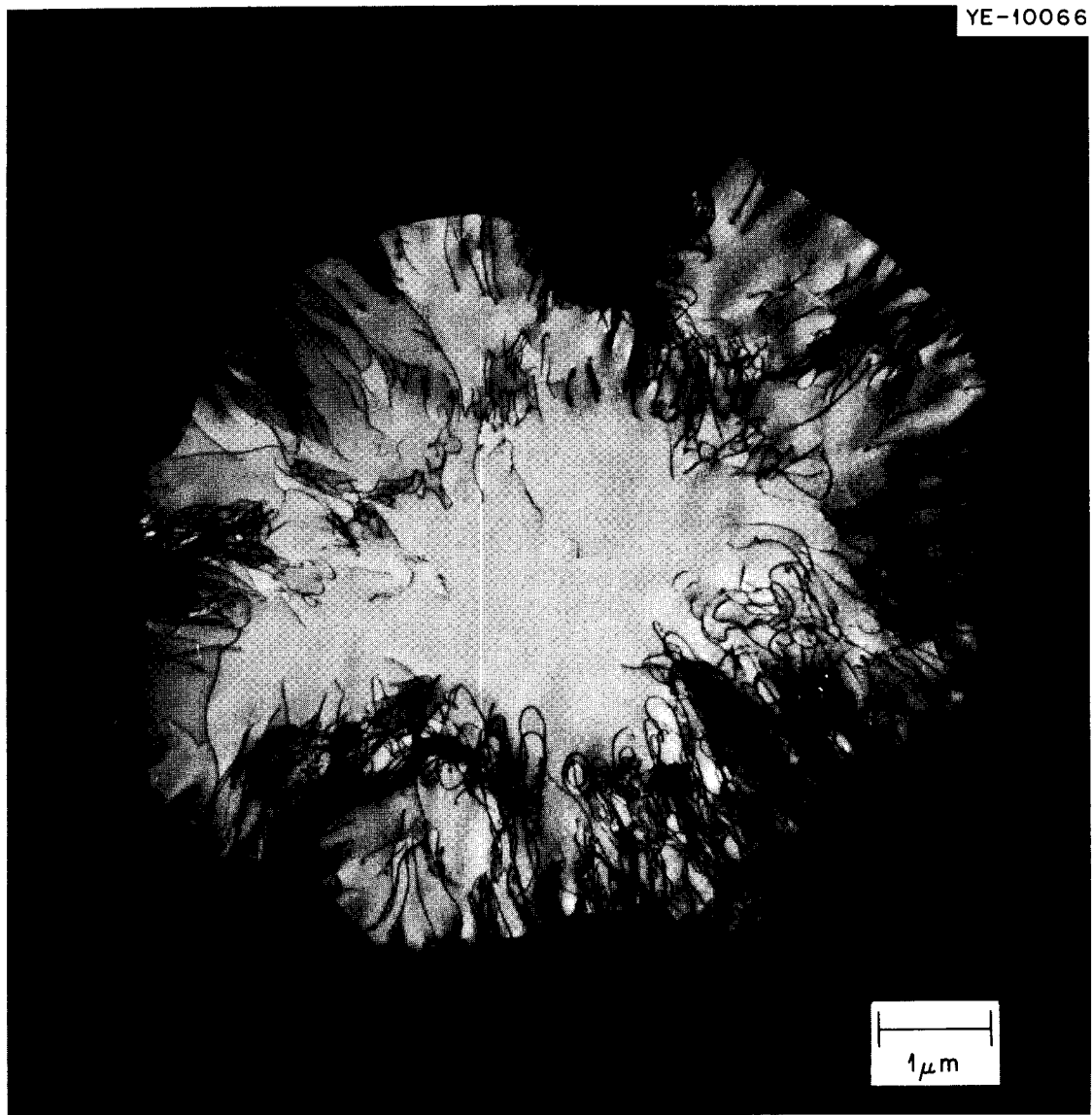


Fig. 2.2. Hair-Pin Shaped Dislocations Left Behind by Migrating Boundary in Nb-40% V.

Vacancy and interstitial migration are thought to be the rate controlling processes in stage 1. Thermally activated dislocation glide under the action of the internal stress is proposed as the rate-controlling step in stage 2, whereas diffusion-controlled dislocation climb appears to dominate stage 3 recovery. In agreement with these, the activation energy increased with increasing recovery and increasing temperature from a value below the predicted migration energy of a single vacancy up to that for self-diffusion in niobium.

The alloy recovered in a different manner. The initially dense, random dislocation array annealed out uniformly — that is, the nature of the dislocation distribution tended to remain unchanged with no large-scale regrouping of dislocations into distinct subgrains. Occasionally at the higher temperatures small regions would become sufficiently clear of dislocations and surrounded by low- to medium-angle boundaries to become viable nuclei for recrystallization. Subsequent migration of these boundaries left a trail of hair-pin shaped dislocation loops extending radially into each of these recrystallization nuclei (see Fig. 2.2). On a homologous temperature basis, the alloy was more resistant to recovery than was pure niobium.

In niobium no simple correlation was found between the effective particle size determined from x-ray dif-

fraction profile analysis and the average cell or subgrain size determined by transmission electron microscopy. As Fig. 2.3 shows, where different annealing conditions developed the same effective particle size, different subgrain sizes were noted. Such observations suggest that these two parameters do not represent the same structural features.

### EFFECT OF INTERNAL STRESSES ON THE APPARENT STRESS DEPENDENCE OF DISLOCATION VELOCITIES<sup>6,7</sup>

W. D. Nix<sup>8</sup> W. A. Coghlan C. R. Barrett<sup>8</sup>

The effects of sinusoidal internal stresses on average dislocation velocities are examined for the power-law stress dependence,  $v = v_1 \tau_e^{m*}$ ; the exponential stress dependence,  $v = v_2 \exp(-D/\tau_e)$ ; and the hyperbolic sine stress dependence,  $v = v_3 \sinh B\tau_e$ . When the magnitude

<sup>6</sup>Abstracted from W. D. Nix, W. A. Coghlan, and C. R. Barrett, *Mater. Sci. Engr.* 4, 98–105 (1969).

<sup>7</sup>Experimental work was done at Stanford University, but part of the analysis and the manuscript preparation were done at ORNL.

<sup>8</sup>Department of Materials Science, Stanford University, Stanford, Calif.

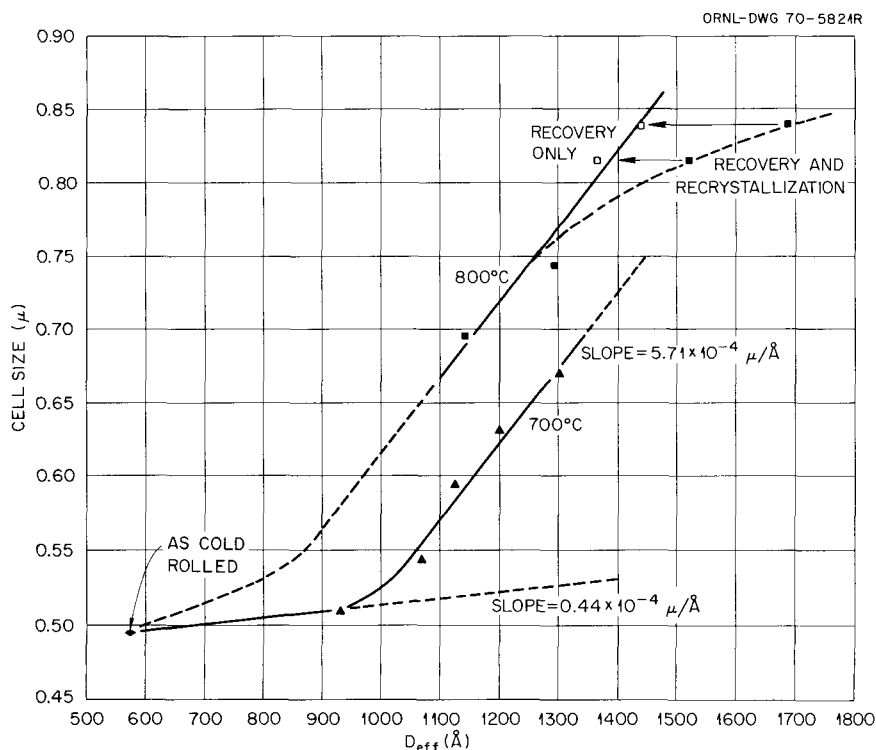


Fig. 2.3. Relation Between Dislocation Cell Size and Effective Particle Size for Niobium.

of the internal stresses was comparable with the applied stress, the stress dependence of the velocity became anomalously high. We suggest that neither the mechanism controlling dislocation motion nor the mechanisms of yielding may be decided on the basis of stress dependence unless care is taken to account for the effective stresses that act on the dislocations. Further, we suggest that the stress dependence of plastic flow as obtained from stress relaxation and strain rate sensitivity tests can be misleading if the internal stresses are not taken into account.

### CONTRIBUTIONS TO THE THEORY OF JOGGED SCREW DISLOCATION GLIDE<sup>9,7</sup>

W. A. Coghlan W. D. Nix<sup>8</sup>

The velocity of screw dislocations limited by the nonconservative motion of jogs was investigated. We calculated the vacancy concentration profile near a moving screw dislocation containing alternately signed jogs separated by a distance  $\lambda b$ , where  $b$  is the magnitude of the Burgers vector. For  $\lambda > 20$  the vacancy profile is essentially the same as that found previously for a moving screw dislocation containing isolated jogs. The jog-jog diffusion interaction did not change the stress dependence of the glide velocity, as has been suggested. The steady-state velocity of a gliding jogged screw dislocation responding to an effective stress  $\tau_e$  was calculated by the quasi-equilibrium approach to dislocation climb and the steady-state vacancy concentration profile. The glide velocity exhibited hyperbolic-tangent stress dependence if the average vacancy concentration in the crystal equalled the equilibrium vacancy concentration,  $C_0$ . However, if the average vacancy concentration in the crystal follows the relation  $C_0 \cosh(\lambda b^3 \tau_e / kT)$  during deformation, the glide velocity can be expressed as  $v = \pi D_v b^2 C_0 \sinh(\lambda b^3 \tau_e / kT)$ , where  $D_v$  is the diffusion coefficient for vacancies in the crystal. We presented a model that suggests that the equilibrium vacancy concentration follows a relation similar to the hyperbolic cosine dependence.

<sup>9</sup>Paper accepted for publication in *Metallurgical Transactions* and presented at the 1970 AIME Spring Meeting, Las Vegas, Nev.

### HIGH-TEMPERATURE GLIDE IN LiF SINGLE CRYSTALS<sup>10,7</sup>

W. A. Coghlan W. D. Nix<sup>8</sup>

From analyses of low-stress sigmoidal creep curves, we determined the glide velocities of dislocations in lithium fluoride single crystals having high purity and low dislocation density. The glide velocity had a very high stress dependence and also a very high activation energy. Within the limits of experimental error, the average glide velocity in centimeters per second may be expressed as  $v = 7 \times 10^{23} \exp(-4.19/kT) \exp(-291/\tau_e)$  where  $\tau_e$  (in g/mm<sup>2</sup>) is the effective stress acting on the dislocation and  $kT$  is in electron-volts. Although more measurements are needed to determine the exact form of the effective stress and temperature dependence, these values indicate that commonly proposed mechanisms for dislocation glide at high temperatures are not responsible for high-temperature glide in pure lithium fluoride.

### A CONSTANT STRESS—CONTINUOUS LOAD COMPRESSIVE CREEP MACHINE FOR SINGLE CRYSTALS<sup>11</sup>

W. A. Coghlan

To learn more about the fundamental aspects of high-temperature deformation, we designed and built a machine that can be used to study compressive creep of small samples at constant stress and temperature. Constant stress is maintained in the deforming sample through the use of a specially curved arm, which increases the applied load to compensate for the increasing cross section area. The temperature is maintained by enclosing the sample area in a tube furnace. A sample of polycrystalline aluminum was tested in the machine, and the resulting creep rate and activation energy agreed very well with previously published data.

<sup>10</sup>Abstracted from paper submitted to *The Philosophical Magazine* and presented at the 1970 AIME Spring Meeting, Las Vegas, Nev.

<sup>11</sup>Abstracted from paper to be submitted to the *Review of Scientific Instruments*.

### 3. Deformation of Crystalline Solids

R. O. Williams

The single most important property of metals and alloys is their ability to undergo extensive deformation yet be able to exhibit useful strengths in service. The methods by which this flow strength may be influenced include alloying, prior deformation, and precipitation hardening. Our interests are primarily concerned with understanding such factors.

#### PRECIPITATION AND HARDENING IN BODY-CENTERED CUBIC ALLOYS

R. W. Carpenter C. T. Liu P. G. Mardon<sup>1</sup>

Phase relations in concentrated alloys of the Ta-Hf, Nb-Hf, and Nb-Zr alloy systems were investigated by x-ray diffraction to determine the stability of body-centered cubic miscibility gaps at elevated temperature. The only stable precipitate in both the Nb-Hf and Ta-Hf alloy systems was the hafnium-rich hexagonal close-packed alpha phase; thus the correct phase diagram type for each system is beta-isomorphous, in agreement with results of Taylor and Doyle<sup>2</sup> and Babitzke *et al.*<sup>3</sup> for niobium-hafnium alloys and in disagreement with other investigators of both systems, whose results predicted a monotectoid-miscibility gap phase diagram in each system.<sup>4-6</sup> Results of similar work on several

niobium-zirconium alloys prepared by other investigators<sup>7</sup> confirmed the existence of a stable body-centered cubic miscibility gap, in good agreement with the results of Rogers and Atkins.<sup>8</sup> Our results show that all three alloy systems exhibit a positive deviation from ideality; the beta-isomorphous diagram exists for the hafnium alloys, but the miscibility gap-monotectoid type diagram is correct for niobium-zirconium alloys. This difference results from the relatively high stability of the hexagonal close-packed allotrope of hafnium compared to that of zirconium. This conclusion is in good agreement with theoretical calculations of these phase diagrams,<sup>9</sup> which show in addition that the metastable body-centered cubic miscibility gap in the hafnium alloys is very close to the  $\alpha + \beta$  phase field boundary, also in qualitative agreement with the experimentally observed slope of that boundary. This leads to the supposition that the hafnium alloys may undergo a phase separation analogous to spinodal decomposition before alpha precipitation. Transmission electron microscopy of a Nb-38 at. % Hf alloy showed that the transformation is nucleated homogeneously and remains homogeneous during initial growth. However, the morphology is not modulated, as in other spinodal systems,<sup>10</sup> but is discrete GP zones. The composition of this alloy places it near the chemical spinodal in the niobium-hafnium system (i.e., the "no theory" region<sup>11</sup>), where homogeneous nucleation is

<sup>1</sup>On attachment from AERE, Harwell.

<sup>2</sup>A. Taylor and N. J. Doyle, *J. Less-Common Metals* 7, 37-53 (1964).

<sup>3</sup>H. R. Babitzke, G. Asai, and H. Kato, *Columbium-Hafnium Binary Alloys for Elevated-Temperature Service*, BM-RI-6101 (February 1962).

<sup>4</sup>M. A. Tylkina, L. A. Tsyganova, and E. M. Savitskii, *Russian J. Inorg. Chem.* 9, 893 (1964).

<sup>5</sup>L. L. Oden *et al.*, *The Hafnium-Tantalum Equilibrium Diagram*, BM-RI-6521 (February 1964).

<sup>6</sup>V. N. Svechnikov *et al.*, *Compilation of Scientific Work of the Metal Physics Institute* 19, 206-11 (1964), Ukrainian Academy of Science, Kiev, U.S.S.R.

<sup>7</sup>G. R. Love and M. L. Picklesimer, *Trans. Met. Soc. AIME* 236, 430-35 (1966).

<sup>8</sup>B. A. Rogers and D. F. Atkins, *Trans. AIME* 203, 1034-41 (1955).

<sup>9</sup>L. Kaufman and H. Bernstein, *Development and Application of Methods for Predicting the Temperature-Composition Stability of Refractory Compounds*, AFML-TR-67-108 (April 1967).

<sup>10</sup>E. P. Butler and G. Thomas, *Acta Met.* 18, 347-65 (1970).

<sup>11</sup>J. E. Hilliard, to be published in *Phase Transformations*, ed. by H. I. Aaronson, American Society for Metals.

possible but morphological features are presently undefined. We are investigating further the precipitate morphology in alloys of higher hafnium content to remove this complication. In the late stages of the reaction, when incoherent alpha is present, its morphology is rod type, and the crystallographic relationship with the body-centered cubic beta lattice is  $\langle 0001 \rangle \parallel \langle 110 \rangle$ ,  $\langle 11\bar{2}0 \rangle \parallel \langle 111 \rangle$  within  $5^\circ$ .

Mechanical property tests showed that the maximum increases in yield strength and hardness occur during the coherent stage of the reaction, before well-defined sharp diffraction patterns characteristic of incoherent alpha are observed.

This work will be continued, with the primary effort devoted to structural analysis of the precipitation reaction in hafnium-rich alloys with niobium and a preliminary investigation (by transmission microscopy) of the precipitation reactions in the Nb-Zr and Ta-Hf alloy systems.

### STRUCTURAL AND ELASTIC PROPERTIES OF ZONAL TWIN DISLOCATIONS IN ANISOTROPIC CRYSTALS<sup>1,2</sup>

M. H. Yoo B. T. M. Loh

A descriptive definition of zonal twin dislocations for compound twin systems is given based on the well-established rational crystallographic elements. Geometric characteristics of zonal twin dislocations in double lattice structures are thoroughly discussed. Equilibrium shapes of an incoherent twin boundary were analyzed by use of the anisotropic elastic properties of edge dislocations. Short-ranged structural properties of zonal twin dislocations are discussed in terms of a Peierls-Nabarro model. We found that the "anisotropic parameter,"  $K_e S_{66}$ , correctly predicts the active mode of crystallographically nonequivalent conjugate twin systems.

### CHARACTERISTICS OF STRESS AND DILATATION FIELDS OF STRAIGHT DISLOCATIONS IN ANISOTROPIC CRYSTALS<sup>1,3</sup>

M. H. Yoo B. T. M. Loh

The stress fields,  $\sigma_{ij}$ , and the dilatation field,  $\Delta$ , have been obtained in contour plots for a straight disloca-

tion perpendicular to a reflection plane in an anisotropic crystal. A common characteristic feature of the results obtained for various metals at room temperature is that no twofold symmetry exists in any of  $\sigma_{ij}$  or in  $\Delta$  with respect to any axis normal to the dislocation line. For certain values of the modified elastic compliances  $S_{16}$  and  $S_{26}$ , anomalous patterns have been found in the elastic fields such that each of the  $\sigma_{11}$ ,  $\sigma_{33}$ , and  $\Delta$  fields is divided into six sectors as compared to the usual case of two sectors, and either of the fields  $\sigma_{12}$  and  $\sigma_{22}$  is divided into two sectors in contrast to the normal pattern of six sectors. Some direct effects of the asymmetries and certain anomalies of these elastic fields on deformation processes are discussed.

### NUMERICAL CALCULATION OF ELASTIC SOLUTIONS FOR STRAIGHT DISLOCATIONS IN ANISOTROPIC CRYSTALS

M. H. Yoo B. T. M. Loh

An efficient method of numerically calculating the elastic solutions for a straight dislocation of any arbitrary orientation in the most general anisotropic medium was developed by extending the earlier work (see preceding section). The symmetry condition that the dislocation line lies normal to a reflection plane — the only restriction in the earlier work — is eliminated. Various dislocations of  $\frac{1}{2}\langle 111 \rangle$  Burgers vector with  $(1\bar{1}0)$ ,  $(11\bar{2})$ , and  $(12\bar{3})$  slip planes in body-centered cubic crystal are considered for numerical computation. Numerical results are obtained for Group VA and VIA transition metals, the alkali metals,  $\alpha$ -Fe, Fe<sub>3</sub>Al, and  $\beta$ -brass at various temperatures.

Both  $(1\bar{1}0)$  and  $(12\bar{3})$  edge dislocations possess  $\sigma_{23}^e$  and  $\sigma_{13}^e$ , minor stress components, in addition to their major stress components,  $\sigma_{11}^e$ ,  $\sigma_{22}^e$ ,  $\sigma_{33}^e$ , and  $\sigma_{12}^e$ . Four minor stress components,  $\sigma_{11}^s$ ,  $\sigma_{22}^s$ ,  $\sigma_{33}^s$ , and  $\sigma_{12}^s$ , are associated with a  $[111]$  screw dislocation in addition to its major components,  $\sigma_{23}^s$  and  $\sigma_{13}^s$ . The major stress components of a  $(1\bar{1}0)$  edge dislocation are symmetric with respect to the dislocation coordinate axes, whereas those of  $(11\bar{2})$  and  $(12\bar{3})$  edge dislocations are asymmetric. While the major stress components of edge and screw dislocations show their normal appearances, anomalous patterns appear in most minor stress components — namely, three zero lines for  $\sigma_{22}^s$ ,  $\sigma_{33}^s$ ,  $\sigma_{23}^s$ , and  $\sigma_{13}^e$  and four zero lines for  $\sigma_{11}^s$  and  $\sigma_{12}^s$ .

Based on the present results the following are under study: (1) effects of asymmetries and anomalies of the stress fields upon elastic interaction between dislocations, (2) the characteristics of dilatation fields and their influences on interaction between point defects

<sup>1,2</sup>To be published in *Fundamental Aspects of Dislocation Theory*, 1970, ed. by J. A. Simmons, R. DeWit, and R. Bullough, National Bureau of Standards, Washington, D.C.

<sup>1,3</sup>Abstract of *J. Appl. Phys.* 41, 2805–14 (1970).

and a dislocation, and (3) the relationships between the elastic displacement fields and body-centered cubic crystal structures.

### SERIES REPRESENTATION OF THERMODYNAMIC FUNCTIONS OF BINARY SOLUTIONS

R. O. Williams

In this investigation a new series, based upon statistical considerations, was proposed for representing the thermodynamics of binary solutions. The work has now been published.<sup>14</sup>

### CONFIGURATIONAL CHANGES IN NONRANDOM SOLID SOLUTIONS

R. O. Williams

The investigation has shown that the changes brought about by deformation are described exactly in terms of the Warren short-range order parameters by differential equations provided that known slip systems operate macroscopically homogeneously.<sup>15</sup> Actual calculations are awkward since the coefficients in the equations depend on the specific combinations of operating slip

systems, and a numerical evaluation in terms of increasing strain is required. A computer program was written for solving both these problems.<sup>16</sup>

### COMPUTER SIMULATION OF SOLID SOLUTIONS

R. O. Williams

One obtains information about the arrangements of the different kinds of atoms in a solid solution from diffuse x-ray measurements. However, having obtained such measurements one has no direct method to generate some kind of statistical model which will reproduce the observed intensities. Perhaps the most powerful method presently available, due to Gehlen and Cohen,<sup>17</sup> is a computer simulation in which the two kinds of atoms are shifted between sites until the populations in three or more shells agree with the experimental measurements. From statistical considerations a fairly large model, not less than about 10,000 sites, is desirable, so having an efficient program is important. We wrote and reported<sup>18</sup> a program 100 times more efficient than that of Gehlen and Cohen.

---

<sup>16</sup>R. O. Williams, *Computer Program for Calculating the Configurational Changes in Nonrandom Alloys Due to Deformation*, ORNL-TM-2855 (February 1970).

<sup>17</sup>P. C. Gehlen and J. B. Cohen, *Phys. Rev.* 139A, 844-55 (1965).

<sup>18</sup>R. O. Williams, *A Computer Program for the Simulation of Solid Solutions from X-Ray Data*, ORNL-TM-2866 (March 1970).

---

<sup>14</sup>R. O. Williams, *Trans. Met. Soc. AIME* 245, 2565-70 (1969).

<sup>15</sup>R. O. Williams, "Calculation of Configurational Changes in Nonrandom Solid Solutions Due to Deformation," *Acta Met.* 18, 457-61 (1970).

## 4. Diffusion in Solids

T. S. Lundy

Our interest encompasses the entire subject of atomic migration in metals and ceramics, including the relationships that exist between diffusion and nearly all high-temperature solid-state processes. During this reporting period we concentrated our research efforts on the topics reported below.

### INVARIANTS OF MULTICOMPONENT DIFFUSION<sup>1</sup>

J. P. Stark<sup>2</sup>

The mathematical equivalence of diffusion coefficients with invariants of diffusive motion is extended to multicomponent systems. In particular, diffusivities relative to a solvent and center of volume are developed as invariant. Consequently, these two frames of reference can be linked to the intrinsic coordinate system for evaluation of marker movement in multicomponent systems or to any other reference system of physical or mathematical interest.

### CATION SELF-DIFFUSION IN URANIUM MONONITRIDE

D. K. Reimann<sup>3</sup> D. M. Kroeger

Tracer diffusion of  $^{233}\text{U}$  into large-grained polycrystalline UN has been investigated by the alpha-energy degradation method. This is a nondestructive technique in which the diffusion coefficient is deduced from the energy spectrum of the  $^{233}\text{U}$  alpha particles emitted from the surface of the sample after diffusion. In the ranges of 1600 to 1850°C and 0.1 to 200 torr  $\text{N}_2$  overpressure, the diffusion coefficient is a strong

function of nitrogen pressure and almost independent of temperature at a given nitrogen pressure. These results and those of Holt and Almassy<sup>4</sup> for nitrogen diffusion in UN are in qualitative but not quantitative accord with a simple defect chemistry calculation.

### COMPARISON OF PENETRATION PLOTS OBTAINED FROM ALPHA-ENERGY DEGRADATION AND ELECTROCHEMICAL SECTIONING

D. M. Kroeger

The alpha-energy degradation method<sup>5</sup> as usually employed for determining diffusion coefficients of alpha-emitting tracers does not provide penetration plots of tracer concentration as functions of depth. Thus, little indication of the importance of side effects such as short-circuiting is obtained. An expression has been derived, which allows calculation of penetration plots from the energy spectrum of alpha particles emitted after diffusion for the case of tracers, such as  $^{233}\text{U}$  and  $^{230}\text{Th}$ , that emit alpha particles in significant quantities at more than one energy. Results of such a calculation using the energy spectra from  $^{233}\text{U}$  tracer for diffusion in tantalum single crystals were in good agreement with penetration plots obtained from the same samples by the highly precise electrochemical sectioning technique known as anodizing-and-stripping.<sup>6</sup> Therefore, the validity of the alpha-energy degradation method for determination of diffusion coefficients has now been verified directly.

<sup>4</sup>J. B. Holt and M. Y. Almassy, *J. Am. Ceram. Soc.* 52, 631 (1969).

<sup>5</sup>F. Schmitz and M. Fock, "Diffusion of Thorium, Protactinium and Uranium in Face-Centered Cubic Thorium," *J. Nucl. Mater.* 21, 317-22 (1967).

<sup>6</sup>R. E. Pawel and T. S. Lundy, *J. Appl. Phys.* 35, 435-38 (1964).

<sup>1</sup>Abstract of paper submitted for publication.

<sup>2</sup>Summer employee (1969) from the faculty of the Department of Mechanical Engineering, University of Texas at Austin.

<sup>3</sup>Temporary noncitizen employee from Germany.

## SECTIONING OF DIFFUSION SPECIMENS BY RADIO-FREQUENCY SPUTTERING

D. M. Kroeger E. W. Chandler<sup>7</sup>

Preliminary experiments have indicated that very small controlled amounts of material can be removed uniformly from the surface of a diffusion specimen by radio-frequency sputtering. A reproducible fraction of the material removed can be collected on a substrate and assayed to indicate the amount of radioactive tracer in that section. We have designed a turntable to hold up to 18 substrates and position them in turn below the specimen during sputtering. We are optimistic that this addition to our sputtering unit will allow the serial sectioning of diffusion samples of virtually any material of interest and the subsequent rapid and convenient determination of very small diffusion coefficients.

## CATION SELF-DIFFUSION IN OXIDES OF TITANIUM

T. S. Lundy R. A. Padgett L C Manley, Jr.

We are using the radioactive isotope <sup>44</sup>Ti as a tracer for measurement of cation self-diffusion rates in both TiO<sub>2</sub> (rutile) and the high-temperature NaCl-type phase of TiO. Most of the data to date have been for the former system.

The titanium atoms in rutile are arranged in a body-centered tetragonal configuration with  $a_0 = 4.58 \text{ \AA}$  and  $c_0 = 2.95 \text{ \AA}$ , as illustrated in Fig. 4.1. Two diffusion coefficients,  $D_c$  and  $D_a$ , are needed to completely describe diffusion in this anisotropic lattice. The diffusion coefficient at any arbitrary angle  $\theta$  relative to the  $z$  axis is then given<sup>8</sup> by:

$$D = D_a \sin^2 \theta + D_c \cos^2 \theta .$$

For diffusion via vacancies in this system, three types of jumps may be important – 1-2, 1-3, and 1-4 in Fig. 4.1. One might suppose upon comparing the jump distances –  $d_{12} = 2.95 \text{ \AA}$ ,  $d_{13} = 3.57 \text{ \AA}$ , and  $d_{14} = 4.58 \text{ \AA}$  – that the 1-2 jump would be preferred. However, in the extreme case of only 1-2 jumps, we would be confronted with a zero  $D$  value in all directions because of the zero correlation factor in a linear chain. If the 1-3 jump were the sole jump of importance, the ratio of the two diffusion coefficients,

ORNL-DWG 70-10075

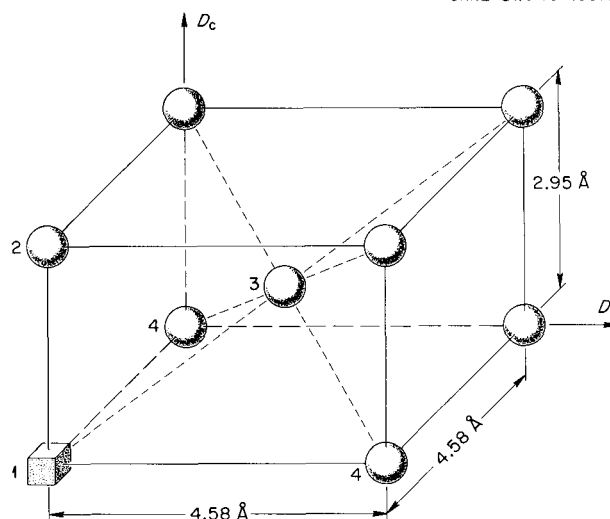


Fig. 4.1. The Body-Centered Tetragonal Cation Sublattice of Rutile. The vacancy at position 1 can migrate by 1-2, 1-3, or 1-4 jumps.

$D_c/D_a$ , could be found from x-ray information as  $D_c/D_a = (c_0/a_0)^2 = 0.414$ . Allowance of only 1-4 jumps would, of course, result in a zero diffusion coefficient along the  $c$  axis and a coefficient  $D_a$  with a correlation factor of 0.467 corresponding to two-dimensional diffusion in a square array.<sup>9</sup> For the case of a mixture of different jumps, the effective correlation factor would depend upon their relative frequency of occurrence. To date, our experiments support the 1-3 diagonal jump as the prime diffusive jump.

## DIFFUSION UNDER HIGH PRESSURES

T. S. Lundy O. A. Kelly<sup>10</sup>

A high-pressure, high-temperature gas system for performing diffusion experiments is being purchased, and delivery, installation, and debugging are expected to be completed during the next reporting period. Hydrostatic pressures in the range of 1 to 14 kilobars and temperatures up to 1500°C will be automatically controlled for prolonged diffusion anneals of specimens contained within a cylindrical cavity 0.56 in. in diameter × 2.5 in. long.

<sup>7</sup>Plant and Equipment Division.

<sup>8</sup>J. R. Manning, p. 26 in *Diffusion Kinetics for Atoms in Crystals*, D. Van Nostrand, Princeton, N.J., 1968.

<sup>9</sup>J. R. Manning, p. 95 in *Diffusion Kinetics for Atoms in Crystals*, D. Van Nostrand, Princeton, N.J., 1968.

<sup>10</sup>General Engineering Division.

For a defect mechanism of self-diffusion in cubic crystalline solids, the diffusion coefficient is given by

$$D = fa_0^2 \nu \exp[-(\Delta G_f + \Delta G_m)/RT],$$

where  $f$  is the correlation factor,  $a_0$  the lattice parameter,  $\nu$  the vibration frequency,  $\Delta G_f$  the change in Gibbs free energy for formation of the defect, and  $\Delta G_m$  the change in Gibbs free energy for migration of the defect. Therefore

$$\left[ \frac{\partial \ln(D/fa_0^2 \nu)}{\partial P} \right]_T = -\frac{1}{RT} \left[ \left( \frac{\partial \Delta G_f}{\partial P} \right)_T + \left( \frac{\partial \Delta G_m}{\partial P} \right)_T \right] = -\frac{\Delta V_f + \Delta V_m}{RT} = -\frac{\Delta V_a}{RT},$$

where  $\Delta V_f$ ,  $\Delta V_m$ , and  $\Delta V_a$  are the formation, migration, and total activation volumes for the jump process.

The activation volume,  $\Delta V_a$ , as determined experimentally, represents the increase in volume relative to that of the perfect crystal upon the formation and migration of the defect responsible for the diffusion process. Its determination and comparison with theory therefore constitute a useful tool in studying the mechanism of atomic diffusion in solids.

## 5. Electron Microscopy

J. O. Stiegler

The activities of the Electron Microscopy Group emphasize the relationship between the microstructure of a metal and its properties. Attention is focused currently on the holes that form in metals under service conditions: voids and gas bubbles produced by neutron irradiation, and cracks and cavities that develop during creep deformation. We are also interested in the precipitation reactions that occur at elevated temperatures in Hastelloy N and type 316 stainless steel. In the low temperature range we are investigating the relationships between the energy stored by a metal during plastic deformation and its corresponding microstructure.

In this section we describe briefly some of the more important aspects of our work completed during the past year. Since many of the microstructural changes of interest to us also occur in reactor structural components during irradiation, we are working closely with the LMFBR, Aluminum Irradiation Damage, Tungsten Metallurgy, and Molten-Salt Reactor Programs. Other contributions by members of the Electron Microscopy Group appear in Chapters 3, 18, 26, 28, and 39 of this report.

### HETEROGENEOUS DISTRIBUTION OF IRRADIATION VOIDS IN IRON<sup>1</sup>

K. Farrell J. T. Houston

Warm-worked, spectrographically pure iron was irradiated to a fast neutron fluence of  $1.5 \times 10^{21}$  neutrons/cm<sup>2</sup> (>0.1 MeV) at 415°C. Partial recrystallization occurred at this temperature, giving a microstructure of islands of recrystallized grains in a matrix of recovered subgrains. Voids in the recrystallized regions were arranged in "walls" comprising a network similar to a grain-boundary network but on a smaller

<sup>1</sup>Abstract of paper to be published in *Journal of Nuclear Materials*.

scale than that of the recrystallized grains. We suggest that these voids are nucleated at preexisting impurities on the sites of former grain boundaries. The void concentration in the recrystallized regions was triple that in the recovered regions; the maximum and most frequent void sizes in the recrystallized regions were, respectively, double and triple those in the recovered regions. A recovered substructure, therefore, appears to be effective in reducing swelling.

### SUPERVOIDS IN IRRADIATED ALUMINUM<sup>2</sup>

K. Farrell R. T. King

High-purity aluminum was irradiated to a fast neutron fluence of  $4 \times 10^{20}$  neutrons/cm<sup>2</sup> (>1 MeV) at 125 and 150°C. Grain boundaries were denuded of voids, but very large voids were formed adjacent to the denuded regions; the size of the voids decreased toward the grain interiors. The voids took the form of ribbons, faceted cylinders, plates, and equiaxed polyhedra. Most of the voids were associated with small solid particles, probably transmutation-produced silicon. At 125°C the largest voids were about 0.3 μm long × 0.05 μm wide. At 150°C the voids were fewer and larger, the longest being at least 3.0 μm long with length-to-width ratios as high as 20.

### EFFECT OF PREINJECTED GASES ON IRRADIATION-PRODUCED VOIDS IN ALUMINUM<sup>3</sup>

K. Farrell R. T. King A. Wolfenden

Aluminum sheets of nominal 99.9999% purity were cyclotron injected with 3 at. ppm He, 3 at. ppm H, or 9

<sup>2</sup>Abstract of paper to be published in *Physica Status Solidi*.

<sup>3</sup>Abstract of a paper presented at the 1970 Spring Meeting of AIME, Las Vegas, Nev., May 1970.

at. ppm H in a uniform distribution and were then irradiated at 125 and 150°C to a fast neutron fluence of about  $4 \times 10^{20}$  neutrons/cm<sup>2</sup> (>1 MeV). The pre-injected gases had little or no effect on the size, number, shape, and location of the voids produced during the 125°C irradiation. Uninjected specimens irradiated at 150°C had very large voids; preinjection with hydrogen or helium significantly reduced the average size of these voids and increased their number. This effect was more pronounced for helium than for either hydrogen concentration. Despite these changes, the total void volume appeared to be unaffected by the preinjected gases. No voids were found in commercially pure aluminum (99.0%) at this neutron fluence, whether preinjected with gases or not.

### EFFECTS OF PREINJECTED GASES ON VOID FORMATION IN QUENCHED ALUMINUM

A. Wolfenden

High-purity aluminum foils 0.005 mm thick were given one of the following treatments: (1) proton bombardment to introduce 1.5 at. ppm H uniformly distributed through the foil, (2) alpha-particle bombardment to introduce 6 at. ppm He, or (3) prolonged annealing in air to cause more general contamination. The foils were then quenched from 655°C into water at room temperature. Subsequent examination of the foils revealed that the alpha-particle-bombarded material contained about  $4 \times 10^{13}$  voids/cm<sup>3</sup>, only one tenth the concentration in the other foils. But the average size of the voids in the alpha-bombarded foils was 130 Å, triple that in the other foils. Any effects of the proton bombardment are believed to have been swamped by the 7 to 10 at. ppm H already present in the aluminum. This effect of helium on void formation during quenching is contrary to the observed effect of helium on irradiation void nucleation. The difference is explained by a reduction in the number of void nuclei by agglomeration of helium during the prequench anneal.

### ELECTRON DISPLACEMENT DAMAGE IN ALUMINUM

A. Wolfenden

As a result of the recent increasing metallurgical interest in high-voltage electron microscopy, a few papers on the electron displacement damage of metals in the Cambridge 750-kV electron microscope have been published.<sup>4-6</sup> Specifically, Makin<sup>4,5</sup> reported the observation of defect clusters (loops) formed in copper and aluminum in the microscope above about 500 kV.

Iphorski and Spring<sup>6</sup> investigated the factors affecting the nucleation and growth of electron displacement damage at 600 kV in copper and observed loops as large as about 1 μm. All these authors interpreted their results in terms of interstitial loops and submicroscopic vacancy clusters.

The present work, being concerned with electron displacement damage in both high-purity (99.9999%) and commercial-purity (1100) aluminum at 200 kV, is an extension to lower operating voltages of the above investigations. Small defect clusters formed in about 20 min at 200 kV, although none was seen in specimens irradiated at 175 kV for about 1 hr. The clusters formed homogeneously in the high-purity aluminum, even on and near the grain boundaries. However, in the 1100 aluminum the clusters formed nonuniformly; they were first observed near the grain boundaries and later also within the grains. We think this difference is due to differences in impurity behavior in the two materials. The clusters grow to form loops observed throughout the thickness of the specimen foil. A Burgers vector analysis of these loops was attempted, but difficulties in interpretation were encountered because of the cube texture of the aluminum foils. We plan to pursue these experiments more intensely using the 650-kV electron microscope and hope to elucidate the effects of gases on irradiation-produced voids and loops in metals.

### TRANSMUTATION-PRODUCED SILICON PRECIPITATES IN IRRADIATED ALUMINUM<sup>7</sup>

K. Farrell J. O. Stiegler R. E. Gehlbach

Commercially pure aluminum and Al-1% Ni exposed to high-fluence neutron irradiation contain a finely divided precipitate phase. This precipitate coarsens markedly during postirradiation annealing. Chemical analyses, electron diffraction, and electron probe microanalyses were used to identify the precipitate as silicon, produced by the transmutation reaction with thermal neutrons  $^{27}\text{Al}(n,\gamma)^{28}\text{Al}$ ,  $^{28}\text{Al} \rightarrow ^{28}\text{Si} + \beta$ .

<sup>4</sup>M. J. Makin, *Electron Displacement Damage in Copper and Aluminum in a High Voltage Electron Microscope*, AERE-R-5821 (1968).

<sup>5</sup>M. J. Makin, *Phil. Mag.* 18, 637 (1968).

<sup>6</sup>M. Iphorski and M. S. Spring, *Phil. Mag.* 20, 937 (1969).

<sup>7</sup>Abstract of a paper to be published in *Metallography*.

### COMMENTS ON "STABILITY OF THE GAS BUBBLES IN SOLIDS"<sup>8</sup>

B. T. M. Loh K. Farrell

Tiwari<sup>9</sup> has discussed the stability of gas bubbles in solids in terms of surface curvature and has concluded that the bubbles should grow spontaneously. This is incorrect, because of the use of an incorrect sign for the radius of curvature of a hole in a solid. We point out his error and also outline the correct stability conditions for gas bubbles in solids.

### STRESS CONCENTRATION AND CAVITY GROWTH<sup>10</sup>

B. T. M. Loh

Grain-boundary cavity growth by stress-induced vacancy condensation from the boundary is modified by including the interaction of vacancies with the stress concentration around the cavity. The critical stress for a given cavity size above which the cavity would grow depends strongly on the value of dilatation,  $\lambda$ , associated with a vacancy in the crystal. The critical tensile stress increases with increasing dilatation to infinity at some critical value,  $\lambda_c$ . For  $\lambda > \lambda_c$ , compressive stress should induce cavity growth.

### APPLICATION OF ELECTRON FRACTOGRAPHY TO THE STUDY OF HIGH-TEMPERATURE PROCESSES<sup>11</sup>

K. Farrell J. O. Stiegler

Many high-temperature phenomena in solids involve the development or elimination of small holes, which significantly affect the mechanical and physical properties of the materials. Examples of such holes are sintering pores, creep cavities, and gas bubbles. If the matrix is brittle at low temperatures the holes can be exposed for detailed examination by snapping the specimen and using electron fractographic techniques. This requirement is satisfied in tungsten, and we have studied the crystallography and the growth rates of gas bubbles, the morphologies and distributions of creep cavities, and the mechanism of hot cracking in fusion welds.

<sup>8</sup> Abstract of a paper to be published in *Journal of Nuclear Science Technology (Tokyo)*, June 1970.

<sup>9</sup> G. P. Tiwari, *J. Nucl. Sci. Technol. (Tokyo)* 5, 648 (1968).

<sup>10</sup> Summary of *Scripta Met.* 4, 299–303 (1970).

<sup>11</sup> Abstract of a paper presented at the ASTM Annual Meeting, June 1970, Toronto, Canada; to be published in the proceedings.

### THE RATIO OF STORED TO EXPENDED ENERGY DURING THE ROOM-TEMPERATURE DEFORMATION OF COPPER SINGLE CRYSTALS<sup>12</sup>

A. Wolfenden

A single-step deformation calorimeter has been used to measure the ratio of stored to expended energy at room temperature in copper single crystals as a function of tensile strain and orientation. Most values of the ratio were in the range 0.15 to 0.25. The data are compared with those from previous pertinent investigations and are discussed in terms of two work-hardening theories.

### COMMENTS ON THE STORED ENERGY IN FCC METALS<sup>13</sup>

D. Kuhlmann-Wilsdorf<sup>14</sup> A. Wolfenden

The statement<sup>15</sup> that stored energy measurements are of limited usefulness for testing theories of work hardening was recently opposed by Kronmüller and Wilkens.<sup>16</sup> They argued that the recent stored energy data of Wolfenden<sup>17</sup> are in conflict with all theories based on individually moving dislocations<sup>18</sup> but are properly explained on the basis of Seeger's theory,<sup>19</sup> which is based on the assumption of pileups. We have examined in detail the equations of the two theories and the relevant experimental detail. From detailed examination of the various parameters used by Kronmüller and Wilkens, we conclude that with such a flexible theory,<sup>16,19-24</sup> any data can be explained.

<sup>12</sup> Summary of *Scripta Met.* 4, 327–32 (1970).

<sup>13</sup> Summary of two papers: *Scripta Met.* 3, 503–6 (1969); 4, 3–4 (1970).

<sup>14</sup> Department of Physics, University of Virginia, Charlottesville, Va.

<sup>15</sup> D. Kuhlmann-Wilsdorf, *Scripta Met.* 2, 643 (1968).

<sup>16</sup> H. Kronmüller and M. Wilkens, *Scripta Met.* 3, 495 (1969).

<sup>17</sup> A. Wolfenden, *Scripta Met.* 2, 621–24 (1968).

<sup>18</sup> H. Kronmüller and M. Wilkens, *Scripta Met.* 4, 1 (1970).

<sup>19</sup> D. Kuhlmann-Wilsdorf, p. 97 in *Work Hardening*, ed. by J. P. Hirth and J. Weertman, Gordon & Breach, New York, 1968.

<sup>20</sup> A. Seeger, p. 243 in *Dislocations and Mechanical Properties of Crystals*, Wiley, New York, 1957.

<sup>21</sup> A. Seeger and H. Kronmüller, *Phil. Mag.* 7, 897 (1962).

<sup>22</sup> H. Kronmüller, *Can. J. Phys.* 45, 631 (1967).

<sup>23</sup> U. Dehlinger, H. Kronmüller, and A. Seeger, *Z. Metallk.* 59, 240 (1968).

<sup>24</sup> H. Rieger, H. Kronmüller, and A. Seeger, *Z. Metallk.* 54, 553 (1963).

However, the obvious question arises to what extent such flexible agreements (obtained by Kronmüller and Wilkens) between theory and experiment can be adduced in support of the theory.

**CATHODIC HYDROGEN ABSORPTION  
AND SEVERE EMBRITTLEMENT IN A  
HIGH-STRENGTH STEEL<sup>25</sup>**

K. Farrell

Hydrogen absorption and consequent embrittlement are studied in hardened low-alloy steel tensile specimens

---

<sup>25</sup>Summary of a paper published in *Corrosion* 26, 105 (1970).

after electrolytic hydrogenation in an aqueous solution of 4% H<sub>2</sub>SO<sub>4</sub> containing arsenic. A critical arsenic content greater than 0.5 mg/liter is needed to cause poisoning. Saturation with hydrogen at a level of 5 to 6 wt ppm is readily achieved but reduces the true fracture stress from 385,000 psi to as low as 35,000 psi. Much of this embrittlement is recovered when the specimens are degassed, but some permanent damage remains in the form of near-surface cracks, many of which are associated with inclusions. These cracks develop during cathodic electrolysis. Hydrogen absorption is much more rapid than is degassing at room temperature. These effects are consistent with a picture of hydrogen migration and embrittlement involving entrapment of hydrogen gas at internal interfaces.

## 6. Fundamental Ceramics Research

W. Fulkerson

We have continued our multidisciplinary investigation of uranium mononitride. During the year work was in progress in nine groups of the Metals and Ceramics Division as well as in the Solid State Division, the Health Physics Division, the Physics Division, and three outside laboratories — Argonne National Laboratory, Florida State University, and the Research Institute for Advanced Studies of the Martin Marietta Corporation. Besides the research achievements reported below, this report includes diffusion of  $^{233}\text{U}$  in UN in Chapter 4, stoichiometry relations in UN in Chapter 8, and physical properties of (Th,U)N alloys in Chapter 9. Development of UN for reactor use is reported in Chapters 16 and 27.

We might ask whether these diverse studies have produced more than just the sum of the results of the independent investigations. Indeed, there have been significant examples of synergism. Below are given extended low-temperature specific heat data, which agree well with our previous results.<sup>1</sup> We obtained a specific heat Debye temperature in the range 320 to 334°K, considerably below that calculated<sup>2</sup> from elastic moduli (364°K). This indicates a significant  $T^3$ -dependent magnetic contribution to the specific heat as would be predicted by theory<sup>3</sup> providing there is no significant energy gap between the ground state of the solid and the lowest magnon state. Further evidence supporting this conclusion that the gap energy is small derives from a significant temperature-dependent magnetic contribution to electrical resistivity found even at 4.2°K and lower.<sup>4</sup> Thus three different measurements

give us an interpretation of the magnetic structure of the solid that would not have been apparent from any one separately. The ultimate proof of the argument will be the direct measurement of the gap energy by inelastic neutron scattering, an experiment that will await the availability of large single crystals, for which we are striving.

Sometimes the results of several studies pose riddles. For example, the volume self-diffusion coefficient of uranium in UN is several orders of magnitude smaller than that of nitrogen (see Chapter 4 of this report), so if the sintering in UN is controlled by volume diffusion, uranium diffusion should be the rate limiting process. The uranium self-diffusion coefficient increases with increasing nitrogen pressure; however, the sintering rate has the opposite pressure dependence (see Chapter 27 of this report). What is happening here? We don't know yet.

With respect to the band structure calculations discussed below, we have the problem of experimental verification of the calculations and ultimately of experimental feedback into the calculations. The low-temperature specific heat indicates a high density of states at the Fermi energy in qualitative agreement with band structure calculations. Potentially a more crucial test may be comparison of the calculations with the optical properties shown in Fig. 6.1 below.

### ELECTRONIC BAND STRUCTURE CALCULATIONS FOR URANIUM COMPOUNDS HAVING NaCl-TYPE STRUCTURE

H. L. Davis<sup>5</sup>

To correlate calculated band structures with the many unusual physical properties of metallic actinide com-

<sup>1</sup>J. O. Scarbrough, H. L. Davis, W. Fulkerson, and J. O. Betterton, Jr., "Specific Heat of Uranium Mononitride from 1.3 to 4.6°K," *Phys. Rev.* **176**, 66-71 (1968).

<sup>2</sup>H. L. Whaley, W. Fulkerson, and R. A. Potter, "Elastic Moduli and Debye Temperature of Polycrystalline Uranium Nitride by Ultrasonic Velocity Measurements," *J. Nucl. Mater.* **31**, 345-50 (1969).

<sup>3</sup>F. Keffer, "Spin Waves," Chapter I in *Encyclopedia of Physics*, chief editor S. Flügge, Springer-Verlag, Berlin, 1966.

<sup>4</sup>W. Fulkerson, J. P. Moore, and D. L. McElroy, *Metals and Ceramics Div. Ann. Progr. Rept. June 30, 1969*, ORNL-4470, p. 33.

<sup>5</sup>Solid State Division.

pounds, preliminary band structure calculations have now been completed for UC, UN, UP, UAs, US, and USE. The calculations correspond to the paramagnetic states of the compounds and were done using our existing library of computer codes for performing nonrelativistic Korringa-Kohn-Rostoker band structure calculations. The necessary one-electron potentials were of the "muffin-tin" form and were constructed by lattice superposition of free-atom charge densities, using the Slater approximation for the exchange potential. Some of the features of our calculations that correlate reasonably with available experimental evidence follow. (1) All the investigated compounds had sufficient band overlap in the vicinity of their Fermi energies to account for their observed metallic behaviors. (2) The calculations for all the compounds predict a completely occupied "p band," whose electron density distribution resembles a covalent chemical bond. This feature correlates nicely with the hardness and brittleness of the compounds. Furthermore, this "p band" being predominantly responsible for the bonding energy then provides a plausible explanation of why these compounds solidify with the NaCl-type structure. (3) The calculated Fermi energies intersect a narrow hybridized "f-d" band, which gives a high density of states at each of the Fermi energies and correlates with the observed anomalously high low-temperature electronic specific heat coefficient. (4) The conduction electrons are "f-d" in character and predominantly localized on the uranium site, with 1 to 3% overlap to the negative atom site. This feature correlates with neutron diffraction evidence on ferromagnetic US, which implies that only 1 to 2% of the magnetic electrons are on the sulfur site.

#### OPTICAL PROPERTIES OF PARAMAGNETIC UN

E. T. Arakawa<sup>6</sup> M. W. Williams<sup>6</sup>

Preliminary measurements of the reflectance at near-normal incidence of a polished arc-melted 100%-dense polycrystalline UN specimen<sup>7</sup> have been obtained from 2 to 75 eV. In addition, reflectance as a function of the angle of incidence has been measured for 11 strong lines between 16 and 73 eV. For each of these lines the real and imaginary parts,  $n$  and  $k$ , of the complex refractive index have been obtained by a least-squares fit to

<sup>6</sup>Health Physics Division.

<sup>7</sup>The specimen was heat treated at 2300°C for 1 hr in 1 atm N<sub>2</sub> to bring it to a nearly stoichiometric composition and to clean the surface. To minimize exposure to air the specimen was bottled in argon and transferred from the bottle to the reflectivity apparatus in an argon-filled bag.

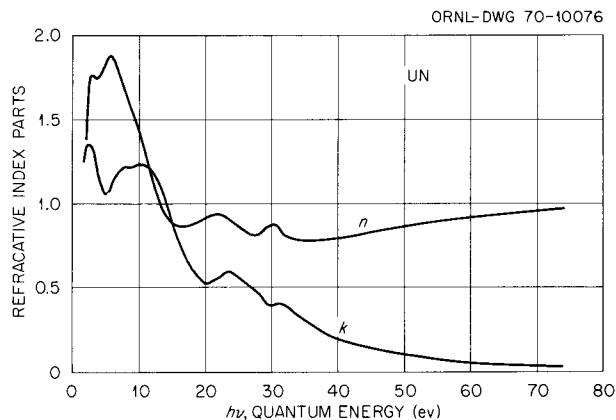


Fig. 6.1. The Refractive Index of UN Showing the Energy Dependence of  $n$  and  $k$ , the Real and Imaginary Parts, Respectively.

Fresnel's equations. A modified Kramers-Kronig analysis<sup>8</sup> was then performed using these  $n$  and  $k$  values and the reflectance at near-normal incidence. The resulting  $n$  and  $k$  as functions of photon energy are shown in Fig. 6.1. Analysis of the conductivity calculated from these data indicates strong optical absorption in the regions of 10, 22, and 32 eV and weaker absorption in the region from 2 to 10 eV. The absorption will be correlated with band structure calculations and x-ray spectra. Analysis of the data in Fig. 6.1 also indicates strong plasma resonances at about 17 and 29 eV.

#### THERMAL CONDUCTIVITY, ELECTRICAL RESISTIVITY, AND SEEBECK COEFFICIENT OF URANIUM MONONITRIDE<sup>9</sup>

J. P. Moore W. Fulkerson D. L. McElroy

Measurements are reported for the thermal conductivity,  $\lambda$  (80 to 400°K), electrical resistivity,  $\rho$  (4.2 to 400°K), and absolute Seebeck coefficient,  $Q$  (6 to 400°K), of pressed and sintered uranium mononitride. The measurements between 77 and 400°K were made with an absolute longitudinal heat flow apparatus. These data and literature values for the thermal conductivity and electrical resistivity at higher temperatures were used to separate the electronic and lattice portions of the thermal conductivity. The results

<sup>8</sup>E. T. Arakawa and M. W. Williams, *J. Phys. Chem. Solids* **29**, 735 (1968).

<sup>9</sup>Abstract of *J. Am. Ceram. Soc.* **53**, 76-82 (1970).

indicate that the lattice conductivity peaks in the range 250 to 300°K and that the high-temperature limit of the Lorenz function may be greater than the Sommerfeld value of  $2.443 \times 10^{-8} \text{ V}^2/(\text{°K})^2$ . The electrical resistivity and the absolute Seebeck coefficient exhibit sharp slope changes near the Néel temperature,  $T_N \approx 50$  to 60°K. The Seebeck coefficient has a minimum at 34°K and then rises to a local maximum at 10°K. This low-temperature peak is probably due to magnon drag. The temperature dependence of the electrical resistivity is dominated by the magnetic contribution, which increases as  $T^{2.38 \pm 0.08}$  between 10 and 52°K. The magnetic contribution is constant at high temperatures at an estimated value of  $142 \mu\Omega\text{-cm}$ .

### LOW-TEMPERATURE SPECIFIC HEAT OF UN

J. O. Scarbrough

The low-temperature calorimeter has been modified to permit measurements above 4.6°K by the use of a heated shield in which the specimen is suspended and by the use of a calibrated germanium resistance thermometer. Measurements from 1.6 to 10°K on a 92.8%-dense pressed-and-sintered UN specimen are shown in Fig. 6.2 along with our previous measurements<sup>1</sup> on another specimen. The specimen used in this study contained no second-phase  $\text{UO}_2$ . There is excellent agreement between the measurements. The data could be fitted to a linear function with a maximum deviation of about 1.5%, discounting one point, which deviated 3%. The fit to the data yielded a  $\gamma$  value of  $49.04 \text{ mJ mole}^{-1} (\text{°K})^{-2}$  and a Debye temperature of 320.4°K, compared to  $49.52 \text{ mJ mole}^{-1} (\text{°K})^{-2}$  and 324°K obtained previously<sup>1</sup> over the range 1.3 to 4.6°K. A Debye temperature of 333.7°K is calculated from the data for the range  $5 < T^2 < 30$ , and this is about the maximum value that can be obtained from the data. This is still considerably less than a value of 364°K obtained<sup>2</sup> from elastic moduli. The discrepancy is probably due to a  $T^3$  magnetic contribution to the specific heat. Subtracting the lattice plus electronic

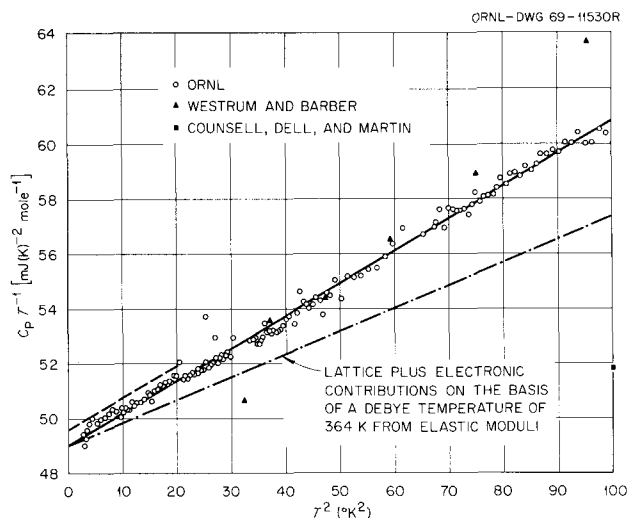


Fig. 6.2. The Low-Temperature Specific Heat of UN. The dot-dash curve represents an estimate of the electronic plus lattice portions of the specific heat. The dashed curve indicates previous ORNL data to 4.6°K obtained on another specimen. The references cited are: E. F. Westrum, Jr., and C. M. Barber, *J. Chem. Phys.* **45**, 635 (1966) and J. F. Counsell, R. M. Dell, and J. F. Martin, *Trans. Faraday Soc.* **62**, 1736 (1966).

contributions indicated in Fig. 6.2 leaves a magnetic contribution of  $3.55 \times 10^{-2} T^3 \text{ mJ mole}^{-1} (\text{°K})^{-1}$ .

The calibration of the germanium resistance thermometer used the helium vapor pressure scale below 4.2°K and the manufacturer's NBS-referred calibration above that temperature. This agreed with the specific heat of pure copper below 10°K to within 0.5% of the values recommended by Osborne, Flotow, and Schriener.<sup>10</sup>

<sup>10</sup>D. W. Osborne, H. E. Flotow, and F. Schriener, "Calibration and Use of Germanium Resistance Thermometers for Precise Heat Capacity Measurements from 1 to 25°K. High Purity Copper for Interlaboratory Heat Capacity Comparisons," *Rev. Sci. Instr.* **38**, 159 (1967).

## 7. Mössbauer Studies of Alloys

C. J. McHargue

Measurements of hyperfine interactions at  $^{61}\text{Ni}$  nuclei in transition metal alloys are used to obtain information on magnetic and other properties related to the electronic structure of these alloys.

### MAGNETIC HYPERFINE FIELDS AT $^{61}\text{Ni}$ NUCLEI IN Ni-Pd ALLOYS<sup>1</sup>

F. E. Obenshain<sup>2</sup>    G. Czjzek  
W. Glaeser<sup>3</sup>        J. E. Tansil<sup>4</sup>

We have obtained nuclear gamma resonance absorption spectra of  $^{61}\text{Ni}$  in Ni-Pd alloys over the entire composition range with a source of  $^{61}\text{Co}$  embedded in a nonmagnetic  $^{64}\text{Ni}$ -14 at. % V foil. Source and absorber were held at 4.2°K. The magnetic hyperfine field at  $^{61}\text{Ni}$  in pure nickel is  $H_{hf} = (-75 \pm 1)$  kOe. Spectra taken with the alloy absorbers show at every palladium concentration a distribution of hyperfine fields. First and second moments [ $\langle |H_{hf}| \rangle$ ,  $M_2(|H_{hf}|)$ ] of the distribution of absolute values of the field have

been deduced. The first moment,  $\langle |H_{hf}| \rangle$ , has a minimum of approximately 30 kOe near 50 at. % Pd, and a maximum of  $170 \pm 3$  kOe near 90 at. % Pd. The concentration dependence of  $\langle |H_{hf}| \rangle$  and  $M_2(|H_{hf}|)$  can be explained if we assume (1) that the hyperfine field at any  $^{61}\text{Ni}$  nucleus is determined by the distribution of nickel and palladium atoms on neighboring lattice sites and (2) that the palladium atoms give a strong positive contribution to the field. Our results have been correlated with magnetic moments of nickel atoms in this alloy system<sup>5</sup> in the framework of the same model.

---

<sup>1</sup> Abstract of paper submitted to the International Conference on Magnetism in Grenoble, France, September 1970.

<sup>2</sup> Physics Division.

<sup>3</sup> Guest scientist, Kernforschungszentrum Karlsruhe.

<sup>4</sup> ORAU Fellow from the University of Tennessee.

<sup>5</sup> J. W. Cable and H. R. Child, *Bull. Am. Phys. Soc.* **14**, 320 (1969).

## 8. Physical Ceramics Studies

C. S. Morgan    W. Fulkerson

Very much less is known about the mechanisms of deformation in ceramic materials than in metals, and this can also be said for other processes that involve mass transfer in the solid state, such as sintering and diffusion. In this program we are trying to determine systematically the variables that are important in controlling such processes in ceramics. Specifically, we are looking at deformation mechanisms in the actinide compound and important nuclear fuel  $\text{UO}_2$ , a semiconductor with the fluorite structure. As is discussed below, stoichiometry may play a pronounced role in determining the preferred slip system for this material. Similar investigations have been initiated for UN, which is also an important fuel but is an electrical conductor with the sodium chloride lattice structure.

We have continued to seek more explicit proof of the role of dislocation motion in the sintering process. However, because sintering is so complex we are also following a phenomenological approach by evoking ideas of topology to describe the pore structure of a sintering solid.

As a spinoff of our growing facility with electron microscopy of ceramic materials we have aided other groups and projects. The work includes the characterization of  $\text{UO}_2$  single crystals described in Chapter 1 and the examination of irradiated and unirradiated hot pressed pyrolytic graphite and polycrystalline graphite reported in Chapter 39 of this report.

### DEFORMATION OF URANIUM DIOXIDE SINGLE CRYSTALS

C. S. Yust

Deformation of hyperstoichiometric uranium dioxide single crystals is being studied. Room-temperature examination of the two-phase hyperstoichiometric crystals by transmission electron microscopy reveals that the formation of the second phase on cooling does not introduce dislocations into the lattice. However, a cycle

of oxidation and reduction does create small voids in the lattice on or near dislocations, as is shown in Fig. 8.1. Specimens having an oxygen-to-uranium ratio of 2.10 when deformed in compression show evidence of slip on  $\{111\}$  planes, while at 2.05 or less the active slip plane appears to be  $\{100\}$ . Transmission electron microscopy of deformed specimens shows that, at least in the room-temperature state, the excess oxygen segregates to the dislocations. The critical resolved shear stress values measured for the hyperstoichiometric crystals are about the same as that previously measured for stoichiometric  $\text{UO}_2$  single crystals,<sup>1</sup> although a minimum in this quantity has not been observed in the hyperstoichiometric specimens as had been for stoichiometric crystals.

### COMPRESSIVE CREEP OF URANIUM MONONITRIDE

C. S. Yust

A necessary preliminary step in the study of creep of uranium mononitride is to consider the effect of possible stoichiometric variations in this material. Related experiments in this material, such as the sintering and self-diffusion experiments described in Chapters 27 and 4 of this report, respectively, suggest that such variations are significant at high temperatures. Experiments have been performed, therefore, to determine the effect on UN specimens of exposure at elevated temperatures to atmospheres containing varying concentrations of nitrogen. The results suggest that the nitrogen content of the specimens does vary enough with the pressure of nitrogen in the surrounding atmosphere to be detectable by weighing, but further work is required to measure the stoichiometric changes.

---

<sup>1</sup>C. S. Yust and C. J. McHargue, "Dislocation Substructures in Deformed Uranium Dioxide Single Crystals," *J. Nucl. Mater.* 31, 121-37 (1969).

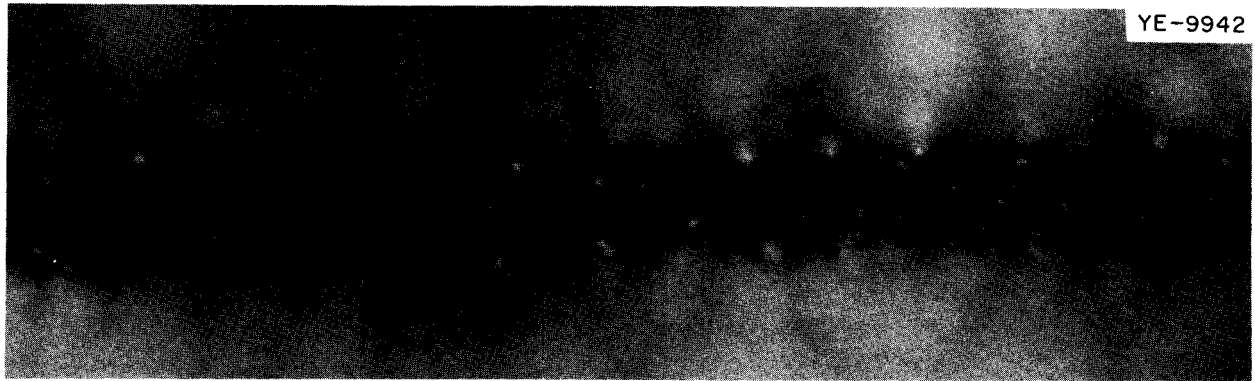


Fig. 8.1. Voids Produced at a Subgrain Boundary in  $\text{UO}_2$  that was Oxidized to an Oxygen-to-Uranium Ratio of 2.03, Deformed 7%, and Subsequently Reduced. 65,000X.

### SOME FUNDAMENTAL IDEAS IN TOPOLOGY AND THEIR APPLICATION TO PROBLEMS IN METALLOGRAPHY<sup>2</sup>

Lida K. Barrett<sup>3</sup> C. S. Yust

The topological ideas and results that have been used by metallurgists, together with several results not previously presented in the metallurgical literature, are developed in a systematic manner. Based on this presentation, the use of topology in metallurgy is reviewed. The additional topology that is introduced is used to establish interrelationships among the results of several papers and to clarify the mathematical treatment.

The new ideas introduced include the Alexander duality theorem, the Euler-Poincaré formula, and the concept of deformation retract. The Euler-Poincaré formula is used to relate results of F. N. Rhines to those of J. W. Cahn. The topological model of sintering of F. N. Rhines is discussed as a deformation retract. Deformation retract properties, together with the Alexander duality theorem, are used to mathematically validate a formula of Kronsbein, Buteau, and DeHoff and to establish in a new mathematical manner a formula of Kronsbein and Steele.

### MECHANISTIC INTERPRETATION OF NON-STEADY-STATE SINTERING<sup>4</sup>

C. S. Morgan L. L. Hall

Sintering model studies developed by Kuczynski and refined by others usually have indicated the sintering of crystalline substances to be a volume diffusion process. However certain types of sintering studies indicate that material transport by dislocation motion may be

important. The nonisothermal densification kinetics of highly sinterable powder compacts are reviewed and the implications of the striking behavior are considered. The initial nonisothermal densification kinetics are not compatible with a diffusion-controlled process — that is, the densification rate does not respond to temperature changes in the manner expected of a diffusion-controlled process. This indicates that an alternative material transport mechanism is operating, and it is assumed to be dislocation slip. The possible role of dislocations in sintering is strengthened by an examination of dislocation arrangements in partially sintered powder compacts by electron transmission microscopy.

Partially sintered MgO powder compacts were thinned and examined after various heat treatments. Cold-pressed MgO powder compacts brought directly to high temperatures densified extensively but had very small grains, and dislocations were difficult to distinguish because of moiré patterns and thickness fringes. If the MgO powder compacts were presintered several days at 1450°C, the resulting partially sintered compacts had large grains and were satisfactory for nonisothermal sintering tests and observation of dislocations. The specimens sintered for long times at 1450°C had such a low dislocation density that dislocations were rarely observed at high magnification in the electron microscope. If presintered specimens were heated to only 1800°C large numbers of dislocations were not seen and the specimen density did not increase. Specimens

<sup>2</sup> Abstract of a paper appearing in *Metallography* 3, 1–33 (1970).

<sup>3</sup> Consultant from the University of Tennessee.

<sup>4</sup> Abstract of a paper submitted for the 1970 International Powder Metallurgy Conference, New York, July 12–16.

presintered at 1450°C and resintered by heating to 2450°C showed a 1 to 3% density increase. These specimens contained many areas thickly populated with dislocations if they were not held at temperature but were cooled rapidly. In presintered specimens taken to 2450°C and held 10 min at temperature, the dislocation concentration increased only insignificantly. Specimens held only 1 min at temperature increased moderately in dislocation concentration. If specimens were heated to 2450°C at 2°/sec or slower only a few additional dislocations were observed. Extremely rapid cooling of specimens from 2450°C showed that thermal stresses did not play a part in dislocation generation.

The dislocations appear to result from sintering forces and cause material transport, which contributes to densification. Material transport by dislocation motion is evidenced in initial sintering, as previously reported, by densification kinetics. This study indicates that dislocation motion also occurs late in the sintering process. Although evidence of dislocation participation in the form of high concentrations is produced only by strong heat treatment, there may be a slow flux of dislocations during all densification. The relative amount of the accompanying contribution to densification by volume and grain-boundary diffusion is not determinable.

### DESINTERING

K. H. McCorkle<sup>5</sup> C. S. Morgan

Ceramic powder compacts will sometimes decrease in density and become more porous if held at high temperature for a sufficient time. This phenomenon is observable in sintered ThO<sub>2</sub> specimens. Figure 8.2 shows the pores of a sol-gel ThO<sub>2</sub> specimen sintered to about 99% of theoretical density at 1400°C and the larger pores in a similar specimen after holding 16 hr at 1800°C (0.58 times absolute melting point). The density of the specimen held at 1800°C had decreased to 89%. The dedensification of material is customarily attributed to pressure of gases trapped in the pores. Mercury porosimetry on several partially desintered specimens showed that all porosity in some specimens was accessible at 15,000 psi. Most of the voidage is in pores accessible only near the maximum pressure, which suggests that the inaccessible voids found in some samples are in pore sizes below the range of the porosimeter rather than truly closed. Figure 8.3 is a scanning electron micrograph of the fractured surface of a ThO<sub>2</sub> specimen in which the density had changed from 99% to 94% during 1.5 hr at 1800°C. Pores are

primarily between grains and have faceted surfaces. It is difficult to reconcile these observations with a pore growth mechanism dependent on trapped gas pressure.

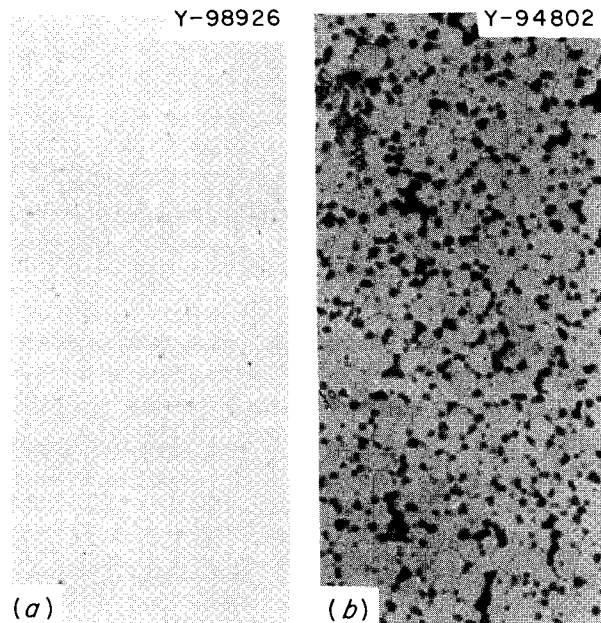


Fig. 8.2. Sol-Gel ThO<sub>2</sub> Specimens (a) Sintered at 1400°C (b) Sintered at 1400°C and then Annealed at 1800°C for 16 hr. 500X.

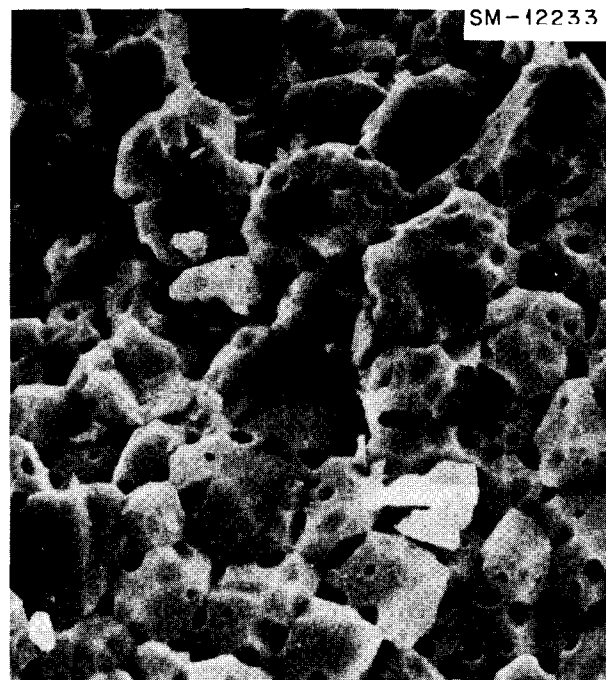


Fig. 8.3. Scanning Electron Micrograph of a Fractured Surface of a Sol-Gel ThO<sub>2</sub> Specimen Sintered to 99% of Theoretical Density and then Desintered by Annealing 1.5 hr at 1800°C. 3000X.

<sup>5</sup>Chemical Technology Division.

## 9. Physical Property Research

D. L. McElroy

Current work includes experimental investigation of electron, phonon, and photon conduction in solids. The importance of such variables as static imperfections, lattice vibrations, and magnetic structure is being studied in detail. Comparison of the results of these studies with existing theories has revealed many cases where the theories are inadequate. Our work also produces heat and electrical transport information useful to other projects. Coordinated efforts with these projects are reported in Chapters 6, 15, 16, 26, 30, 39, and 47 of this report.

### APPARATUS DEVELOPMENT

Our program requires accurate thermophysical property measurements over as wide a temperature range as possible. This requirement has led to improvement of techniques and efforts to extend our measurement range.

#### Intercomparison of Thermal Conductivity Results

"Comparison of results from eight different apparatus located at three laboratories (ORNL, National Bureau of Standards, and National Research Council of Canada) on ten metals indicated that various absolute steady-state methods for measuring thermal conductivity,  $\lambda$ , can yield experimental results accurate to within  $\pm 2\%$  from 100 to 1200°K for  $\lambda$  values from 0.1 to 5 W cm<sup>-1</sup>(°K)<sup>-1</sup>" (ref 1). We completed an extensive review of radial heat flow methods for measurement of the  $\lambda$  solids.<sup>2</sup> Although such methods offer no panacea

<sup>1</sup>M. J. Laubitz and D. L. McElroy, modified abstract of a paper prepared for submission to *Metrologia* and for presentation at the 1970 *Thermal Conductivity Conference*, Boston, Mass., Sept. 28-30, 1970.

<sup>2</sup>D. L. McElroy and J. P. Moore, "Radial Heat Flow Methods for the Measurement of the Thermal Conductivity of Solids," Chapter 4, pp. 185-239, in *Thermal Conductivity Volume I*, ed. by R. P. Tye, Academic Press, London and New York, 1969.

for measuring  $\lambda$ , they do provide unique theoretical and practical advantages over wide ranges of  $\lambda$  and temperature, and this reinforces our advocacy of such methods.

### Thermal Conductivity Apparatus

We designed and constructed a guarded-longitudinal apparatus for measurements of the electrical resistivity,  $\rho$ ,  $\lambda$ , and the thermoelectric power,  $S$ , on small rods from 300 to 1000°K. This device has been successfully tested to 800°K with an Armco iron standard.

Using an Nb-10% W specimen, we tested an electrical heating method for obtaining  $\lambda$ ,  $\rho$ , and  $S$ ; however, the  $\lambda$  results indicate that further development of this technique is required.

### Computer Data Acquisition

Determinations of specific heat capacity,  $C_p$ , and  $\rho$  by the pulse calorimetry method require measurements of the temperature, power-dissipation  $P_i$  within a specimen, and power loss  $P_l$  from a specimen during a pulse.<sup>3</sup> A technique is reported in which a direct current heats a rod specimen suspended in a vacuum furnace. The joulean heat is  $P_i$ , and  $P_l$  is evaluated from the free-cooling rate of the specimen after a pulse.

During a pulse, 100 readings/sec are recorded by a computer-operated data acquisition system (CODAS). During cooling the temperature is read once each second, heating data are retrieved from the data disk, and  $C_p$  and  $\rho$  values are calculated and printed out. The raw data are then transferred to a magnetic tape for detailed processing on an IBM 360/91 computer.<sup>4</sup>

<sup>3</sup>T. G. Kollie, M. Barisoni, and D. L. McElroy, "Pulse-Calorimetry Using a Digital Voltmeter for Transient Data Acquisition," *High Temperatures-High Pressures* 1(2), 167-84 (1969).

<sup>4</sup>T. G. Kollie, abstract of paper to be presented at the 25th Calorimetry Conference, NBS, Washington, D.C., Oct. 19-22, 1970.

The heart of CODAS is a DEC PDP-8 computer with 4K core and two 32K magnetic disk memories. Peripheral devices include an analog input multiplexer, an analog-to-digital converter, external contact relays, a real-time clock, a teletypewriter, and a magnetic tape. Resolution of input analog signals is  $1 \pm 0.5$  part in 8190.

Salient features of the technique are data acquisition at heating rates up to  $60^\circ\text{C}/\text{sec}$  and at intervals of  $0.1^\circ\text{C}$ . The calculated uncertainties are  $\pm 1\%$  for  $C_p$  and  $\pm 0.5\%$  for  $\rho$ , which are confirmed by measurements<sup>5</sup> on  $\text{Ni}_3\text{Fe}$ .

## ELECTRONIC HEAT TRANSPORT

### Chromium<sup>6</sup>

J. P. Moore R. K. Williams D. L. McElroy

A peak has been reported in the thermal conductivity (and hence the Lorenz function) of chromium at the Néel temperature.<sup>7</sup> The investigators reporting this

<sup>5</sup>T. G. Kollie, J. O. Scarbrough, and D. L. McElroy, "Effects of Configurational Order on the Specific Heat Capacity of  $\text{Ni}_3\text{Fe}$  between 1.2 and  $4.4^\circ\text{K}$ ," abstract of paper submitted to *The Physical Review*.

<sup>6</sup>Abstract of "Comments on 'Lorenz Function Enhancement Due to Inelastic Processes Near the Néel Point of Chromium,'" *Phys. Rev. Letters* **24**, 587-88 (1970).

<sup>7</sup>G. T. Meaden, K. V. Rao, and H. Y. Loo, *Phys. Rev. Letters* **23**, 475 (1969).

effect have ignored a considerable body of previous results on several chromium specimens. Figure 9.1 shows that the previous results do not indicate a peak in the thermal conductivity. We feel that the effect is suspect and may be associated with defects in experimental technique. Similar conclusions were reached by Laubitz and Matsumura.<sup>8</sup>

### Tantalum<sup>9</sup>

R. K. Williams J. P. Moore D. L. McElroy

We have accurately measured  $\rho$  of high-purity tantalum ( $\rho_{300}/\rho_{4.5} = 5 \times 10^2$ ) from 4.5 to  $2600^\circ\text{K}$  and  $\lambda$  and  $S$  from 80 to  $400^\circ\text{K}$ . These same properties were determined for Ta-5% W and Ta-10% W from 80 to  $400^\circ\text{K}$ . Analysis of the  $\rho$  and  $\lambda$  data for these three materials yielded the Lorenz function and lattice component of  $\lambda$  for pure tantalum. The Lorenz function approaches the Sommerfeld value above  $250^\circ$ , and the lattice component to  $\lambda$  is between 10 and 20% of  $\lambda$  at  $100^\circ\text{K}$ . Use of these results in estimating high-temperature  $\lambda$  values is discussed in Chapter 26.

<sup>8</sup>M. J. Laubitz and T. Matsumura, "The Transport Properties of Chromium Through the Néel Point," *Phys. Rev. Letters* **24**, 727-30 (1970).

<sup>9</sup>Abstracted from "Transport Properties of Tantalum and Tantalum-Tungsten Alloys," accepted for presentation at the International Conference on Transport Properties of Solids, Sydney, Australia, Aug. 27-29, 1970.

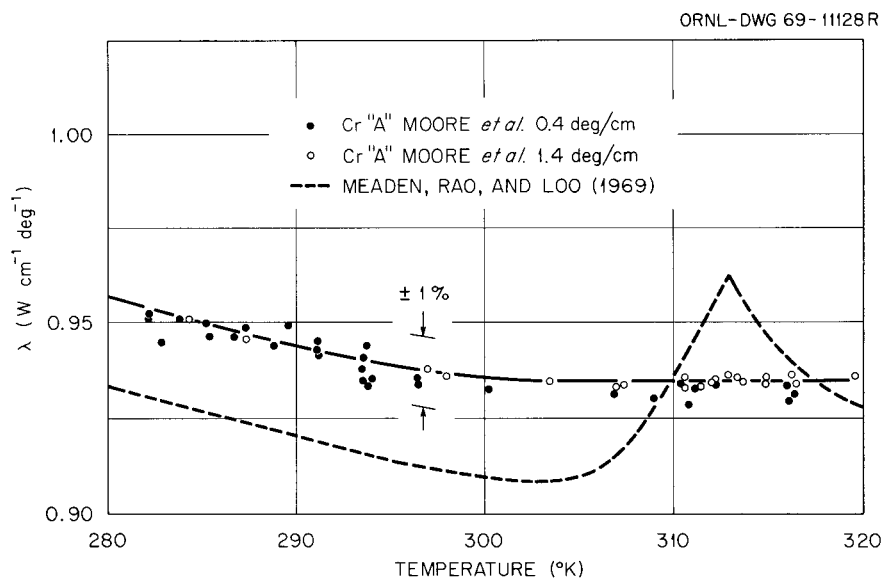


Fig. 9.1. Thermal Conductivity of Chromium from One Sample Studied by Moore *et al.*<sup>6</sup> and from Results Reported by Meaden *et al.*<sup>7</sup>

### Ordered and Disordered Ni<sub>3</sub>Fe

J. P. Moore T. G. Kollie R. S. Graves

Transport property data on disordered and ordered Ni<sub>3</sub>Fe, which we reported previously,<sup>10</sup> showed a significant lattice component of  $\lambda$  below 300°K. Above 300°K, the Wiedemann-Franz ratio ( $\lambda\rho/T$ ) was equal to the Sommerfeld value for the ordered sample but was 2.5% higher for the disordered sample. To check this result, measurements were made on Ni<sub>3</sub>Fe in an intermediate state of disorder ( $\rho_{4.2} = 4.00 \mu\Omega\text{-cm}$ ). These later results indicate that  $\lambda\rho/T$  is near the Sommerfeld value for all states in Ni<sub>3</sub>Fe at temperatures above 300°K. All three states studied have maximum values of  $\lambda$  between 140 and 175°K. These peaks are caused by peaks in the electronic component of  $\lambda$ , and their unusual relative positions are due to marked deviations from electrical resistivities predicted by Matthiessen's rule.

### LATTICE HEAT TRANSPORT

#### Uranium Dioxide<sup>11</sup>

J. P. Moore D. L. McElroy

The thermal conductivities of mono- and polycrystalline UO<sub>2</sub> were measured from 80 to 420°K. The results indicate no observable difference in  $\lambda$  between the two types of UO<sub>2</sub>, with both materials having broad peaks in  $\lambda$  at about 220°K. The results were used with some literature values to determine the effect of closed porosity on  $\lambda$ . The thermal conductivity of theoretically dense UO<sub>2</sub> is described phenomenologically from 80 to 1400°K.

Over this temperature range, conduction is dominated by the phonon component. The phonon conduction is analyzed through a comparison with ThO<sub>2</sub>. The analysis indicates that the high-temperature  $\lambda$  is limited by 3-phonon Umklapp scattering processes. Scattering by the disordered spins associated with the paramagnetic uranium ion contributes a large temperature-independent phonon scattering term. This mechanism has a mean free path of about 51 Å, which implies that grain boundaries and impurities have a relatively insignificant effect on the phonon conduction above the

<sup>10</sup>J. P. Moore and R. S. Graves, *Metals and Ceramics Div. Ann. Progr. Rept. June 30, 1969*, ORNL-4470, p. 33.

<sup>11</sup>Abstracted from "The Thermal Conductivity of Near Stoichiometric Single Crystal and Polycrystal UO<sub>2</sub>," paper submitted to the *Journal of the American Ceramic Society*.

antiferromagnetic-paramagnetic transition near 30°K. This implication is in agreement with the new experimental results.

### Lithium Fluoride

P. H. Spindler<sup>12</sup> J. P. Moore R. S. Graves

Thermal conductivity measurements from 80 to 1100°K on mono- and polycrystalline LiF specimens indicated that the thermal resistance,  $\lambda^{-1}$ , does not increase linearly with increasing temperature. Two approaches were used to calculate a possible infrared conduction (photon) component. For each material the depth of transmittance of thermal radiation emitted by a central heater into a cylindrical solid was calculated from known values of the spectral absorption coefficient. This analysis indicated that the polycrystalline LiF was optically thick, thus permitting a calculation of the photon component. The depth of transmittance calculation indicated that the single crystal LiF was optically thin, and the magnitude of the photon component was estimated assuming no absorption within the material and various emittance values for the cylindrical boundary surfaces.

### CALORIMETRIC STUDIES OF Ni<sub>3</sub>Fe BETWEEN 1.2 AND 4.4°K (REF. 13)

T. G. Kollie J. O. Scarbrough D. L. McElroy

Measurements of the specific heat capacity of configurationally ordered and disordered Ni<sub>3</sub>Fe between 1.2 and 4.4°K are presented. Coefficients of the electronic, magnetic, and harmonic phonon contributions decreased significantly on ordering (21.5, 8.5, and 4.8% respectively). These results are justified theoretically and compared where possible with other measurements in the literature.

### UN, ThN, AND THEIR ALLOYS

S. C. Weaver T. G. Kollie

An analysis of our  $\lambda$ ,  $\rho$ , and  $S$  data for UN below 400°K has been reported.<sup>14</sup> Measurements of  $\rho$  and  $S$  from 295 to 1700°K were completed on polycrystalline

<sup>12</sup>Present Address: Siemens Company, Munich, Germany.

<sup>13</sup>Abstracted from "Effects of Configurational Order on the Specific Heat Capacity of Ni<sub>3</sub>Fe between 1.2 and 4.4°K," paper submitted to *The Physical Review*.

<sup>14</sup>J. P. Moore, W. Fulkerson, and D. L. McElroy, *J. Am. Ceram. Soc.* 53, 76-82 (1970).

UN using a standard four-probe technique with CODAS providing on-line data acquisition and reduction. Above 400°K our  $\rho$  of UN increases nearly linearly with temperature, suggesting resistance control by electron-phonon interactions. Thermal contact resistance results on UN-metal interfaces are reported in Chapter 16.

We measured  $\lambda$ ,  $\rho$ , and  $S$  from 80 to 400°K on specimens ranging in composition from ThN to  $(\text{Th}_{0.95}\text{U}_{0.05})\text{N}$ . Results indicate that  $\lambda$  of ThN is 4 times that of UN at 100°K and more than twice that of UN at 400°K. Alloying reduces the  $\lambda$  of ThN, but the alloy containing 5% UN still has a  $\lambda$  twice that of UN at 400°K.

## 10. Spectroscopy of Ionic Media

G. P. Smith

The physical chemistry of chloroaluminate systems was investigated along a wide front. Work on the complexes formed by Ni(II) in molten CsAlCl<sub>4</sub> led to the discovery of a very unusual ion, NiCl<sub>3</sub><sup>-</sup>, which is described in a letter communication summarized here. Similar work on the complexes of Pt(II) in the same medium is still too preliminary to report. A compound that defied previous attempts by others at preparation, Ni(AlCl<sub>4</sub>)<sub>2</sub>, was discovered in a phase relation study and its structure was determined. A terminal report is summarized. We prepared a compound, Ti(AlCl<sub>4</sub>)<sub>2</sub>, in which titanium has the well-defined oxidation state II and measured some of its properties. Most compounds attributed to this state are actually mixtures of states. A preliminary report is given. Research on the electrical conductivities of liquid AlCl<sub>3</sub> and the liquid systems AlCl<sub>3</sub>-KCl and AlBr<sub>3</sub>-NaBr was completed and abstracts of the terminal papers are reported. Research on halopolyaluminate ions continues with studies of compounds in the AlI<sub>3</sub>-CsI system. Finally, we are trying to prepare new homopolynuclear ions of posttransition elements in chloroaluminate melts as described in a progress report. Studies of related entities in the molten Bi-BiBr<sub>3</sub> system were completed, and the terminal paper is summarized.

Our investigation of the coordination of Ni(II) in ZnCl<sub>2</sub>-CsCl melts is now completed and the final paper is abstracted.

Solid state spectroscopy was confined to the energy states associated with Ni(II) in a Cs<sub>3</sub>(MgCl<sub>4</sub>)Cl host lattice, and a comprehensive paper is abstracted.

### SPECTROSCOPIC BEHAVIOR AND COORDINATION OF NICKEL(II) IN LIQUID MIXTURES OF ZINC AND CESIUM CHLORIDES<sup>1</sup>

W. E. Smith<sup>2</sup> J. Brynestad G. P. Smith

Optical absorption spectra of dilute solutions of NiCl<sub>2</sub> in molten ZnCl<sub>2</sub>-CsCl mixtures were measured

over the complete range of solvent compositions. The temperature extremes investigated were 260°C for melts containing 38 mole % CsCl and 1000°C for 75 mole % CsCl. Within 100 to 300°C of the liquidus (depending on melt composition) the spectra were highly dependent on composition and temperature and consisted of relatively narrow absorption bands. Analysis of these spectra showed the presence under different conditions of six kinds of nickel(II) centers with well-defined coordination geometries. An equilibrium between octahedral and tetrahedral centers occurred in 0 to 8 mole % CsCl such that the octahedral form was favored with increasing CsCl content. A different octahedral-tetrahedral pair occurred in 20 to 50 mole % CsCl, with the tetrahedral form favored by increasing CsCl content and temperature. In CsCl-rich melts tetrahedrally coordinated Cl<sub>3</sub>NiClZnCl<sub>3</sub><sup>3-</sup> and NiCl<sub>4</sub><sup>2-</sup> were found. In ZnCl<sub>2</sub>-rich melts at high temperatures the absorptions became broad and only mildly dependent on solvent composition. Suggestions are made regarding the relationships between these coordination effects and structure in the solvent.

### EVIDENCE FOR A THREE-COORDINATE COMPLEX OF NICKEL(II)<sup>3</sup>

J. Brynestad G. P. Smith

We showed that Ni(II) dissolved in liquid CsAlCl<sub>4</sub> containing small amounts of CsCl is present as an equilibrium mixture of two complexes, the well-known NiCl<sub>4</sub><sup>2-</sup> and the previously unknown NiCl<sub>3</sub><sup>-</sup>. The thermochemical and spectroscopic properties of the latter indicate that it is unsolvated and has a *D*<sub>3h</sub> geometry. Hence, it is a three-coordinate complex in

<sup>1</sup> Abstract of *J. Chem. Phys.* 52, 3890-3903 (1970).

<sup>2</sup> Visitor from the United Kingdom.

<sup>3</sup> Summary of *J. Am. Chem. Soc.* 92, 3198-99 (1970).

which a nickel atom centers an equilateral triangle of chlorine atoms. Three-coordinate complexes are very unusual, having previously been observed only for Cu(I), Ag(I), Ag(II), and Au(I) bonded to phosphorous or sulfur.

#### NICKEL(II) TETRACHLOROALUMINATE<sup>4</sup>

J. Brynestad H. L. Yakel G. P. Smith

The binary system NiCl<sub>2</sub>-AlCl<sub>3</sub> has an invariant phase equilibrium at a temperature in the range 205 to 215°C among the four phases gas, liquid, solid Ni(AlCl<sub>4</sub>)<sub>2</sub>, and a second solid nickel-containing compound. Below this invariant point the stable solid phase is Ni(AlCl<sub>4</sub>)<sub>2</sub>, while above it the other solid phase is stable. The compound Ni(AlCl<sub>4</sub>)<sub>2</sub>, previously believed not to exist, is isostructural with Co(AlCl<sub>4</sub>)<sub>2</sub>.

#### PRELIMINARY REPORT ON TITANIUM(II) TETRACHLOROALUMINATE

J. Brynestad S. von Winbush<sup>5</sup> G. P. Smith

The compound Ti(AlCl<sub>4</sub>)<sub>2</sub> was prepared via four routes, namely: (1) reduction of liquid AlCl<sub>3</sub> by titanium metal, (2) reduction of TiCl<sub>3</sub> or TiCl<sub>4</sub> by titanium metal in liquid AlCl<sub>3</sub>, (3) reduction of TiCl<sub>3</sub> or TiCl<sub>4</sub> by aluminum metal with or without AlCl<sub>3</sub>, and (4) reaction of TiCl<sub>2</sub> with liquid AlCl<sub>3</sub>. The latter reaction, which would appear to be the most direct, is in fact not direct and gives much the poorest yield of the four types of reactions. All of these reactions are very slow and produce numerous unidentified products in addition to Ti(AlCl<sub>4</sub>)<sub>2</sub>. The latter occurs in two or possibly three crystalline modifications depending on the preparative conditions. The optical spectrum indicates the well-defined oxidation state Ti(II) with a triplet ground state. Research continues.

#### ELECTRICAL CONDUCTIVITY OF ALUMINUM CHLORIDE LIQUID AND SUPERCRITICAL VAPOR<sup>6</sup>

C. R. Boston S. J. Yosim<sup>7</sup> L. F. Grantham<sup>7</sup>

The electrical conductivity of aluminum chloride was measured for the liquid from the melting point (192°C)

<sup>4</sup>Summary of J. Brynestad, H. L. Yakel, and G. P. Smith, *Inorg. Chem.* **9**, 686 (1970).

<sup>5</sup>Visitor from Fisk University.

<sup>6</sup>Summary of *J. Chem. Phys.* **51**, 1669-71 (1969).

<sup>7</sup>Atomics International Division of North American Rockwell Corporation, Canoga Park, Calif.

to the critical point (350 ± 2°C) and for the supercritical fluid from the critical point to 500°C. The specific conductivities were less than 3 × 10<sup>-7</sup> ohm<sup>-1</sup> cm<sup>-1</sup> at all temperatures (distilled water is about 10<sup>-5</sup> ohm<sup>-1</sup> cm<sup>-1</sup> at these temperatures) and in general were considerably lower than the literature values, presumably because of the extreme purity of the aluminum chloride used. Liquid conductivities increased almost linearly with increasing temperature for the first 70°, and then the conductivity-temperature slope decreased, resulting in a conductivity maximum near 300°C. Above this temperature the conductivity decreased until the critical temperature was reached, at which point a sharp break occurred. With further heating the conductivity of the supercritical fluid increased. The conductivity maximum for the liquid was attributed to the opposing effects of, first, an increase in fluidity and ionic mobility at low temperatures causing an increase in conductivity, and, second, an increase in ionic association, which becomes the dominant effect at higher temperatures causing the conductivity to decrease. In the supercritical region an increase in temperature apparently causes an increase in dissociation and thereby an increase in conductivity.

#### ELECTRICAL CONDUCTIVITIES OF MOLTEN ALUMINUM CHLORIDE-POTASSIUM CHLORIDE MIXTURES<sup>8</sup>

C. R. Boston L. F. Grantham<sup>7</sup> S. J. Yosim<sup>7</sup>

The electrical conductivities of AlCl<sub>3</sub>-KCl mixtures were measured over the range 15 to 80 mole % AlCl<sub>3</sub> and 180 to 1080°C. A minimum at 33 mole % AlCl<sub>3</sub> and a maximum at 50 mole % were observed in the equivalent conductivity as a function of composition. The system was considered as consisting of the two binary systems, KCl-KAlCl<sub>4</sub> and KAlCl<sub>4</sub>-Al<sub>2</sub>Cl<sub>6</sub>, since the compound KAlCl<sub>4</sub> is extremely stable in the liquid. The compound KAlCl<sub>4</sub> had a maximum specific conductance with temperature near 1000°C. The negative deviations of conductivity isotherms for the KCl-KAlCl<sub>4</sub> system are apparently due to large differences in anion polarizabilities, whereas the positive deviations for the KAlCl<sub>4</sub>-Al<sub>2</sub>Cl<sub>6</sub> system are attributed to basic changes in melt structure.

<sup>8</sup>Abstract of *J. Electrochem. Soc.* **117**, 28-31 (1970).

## ELECTRICAL CONDUCTIVITIES OF MOLTEN AlBr<sub>3</sub>-NaBr MIXTURES<sup>9</sup>

C. R. Boston

The electrical conductivities of AlBr<sub>3</sub>-NaBr mixtures have been measured from 25 to 98 mole % AlBr<sub>3</sub> and 140 to 1000°C. A minimum in the equivalent conductance as a function of composition was observed near 33 mole % AlBr<sub>3</sub> and a maximum near 50 mole % AlBr<sub>3</sub>. With increasing temperature, conductivities increased linearly at low temperatures and gradually went through a maximum at high temperatures. The maximum was actually reached for only one composition — namely, that corresponding to the compound NaAlBr<sub>4</sub> at a temperature of 800 to 900°C. "Activation energies" were lower than those observed for the AlCl<sub>3</sub>-KCl mixtures but showed a similar pattern of behavior with composition.

## STRUCTURAL STUDIES IN THE AlI<sub>3</sub>-CsI SYSTEM

C. R. Boston H. L. Yakel G. M. Begun<sup>10</sup>

Attempts to determine the crystal structure of CsAl<sub>2</sub>I<sub>7</sub> by x-ray diffraction have met with limited success since the Cs<sup>+</sup> and I<sup>-</sup> ions have the same number of electrons and hence are virtually indistinguishable in their x-ray scattering ability. Other approaches are being explored. These include neutron diffraction and Raman measurements. The neutron scattering cross section for Cs, Al, and I differ sufficiently to make this approach seem promising. Preliminary Raman measurements have been carried out on solid and liquid CsAl<sub>2</sub>I<sub>7</sub> and CsAlI<sub>4</sub> with encouraging results.

## UNUSUAL OXIDATION STATES OF POSTTRANSITION ELEMENT IONS

C. R. Boston G. P. Smith

Earlier measurements<sup>11,12</sup> on the lower oxidation states of bismuth showed the existence of Bi<sup>+</sup>, Bi<sub>5</sub><sup>3+</sup> and Bi<sub>8</sub><sup>2+</sup>. The absorption spectrum of Bi<sup>+</sup> was explained<sup>13</sup> in terms of electronic transitions within the partially filled *p* shell. To determine if other elements

<sup>9</sup>Abstract of paper being prepared for publication.

<sup>10</sup>Chemistry Division.

<sup>11</sup>N. J. Bjerrum, C. R. Boston, and G. P. Smith, *Inorg. Chem.* **6**, 1162–72 (1967).

<sup>12</sup>N. J. Bjerrum and G. P. Smith, *Inorg. Chem.* **6**, 1968–72 (1967).

<sup>13</sup>H. L. Davis, N. J. Bjerrum, and G. P. Smith, *Inorg. Chem.* **6**, 1172–78 (1967).

exhibit this type of behavior, exploratory measurements have been carried out on Pb, Sb, Se, and I. Measurable spectra were obtained for unidentified, lower oxidation state species of both lead and antimony. In both cases, low solubility is a major problem. The selenium system also appears promising. The spectrum of Se-SeCl<sub>4</sub> in AlCl<sub>3</sub>-NaCl eutectic at 137°C shows bands at 725 and 1410 nm, which may be due to the cluster ion Se<sub>8</sub><sup>2+</sup> reported by Barr *et al.*<sup>14</sup> The iodine system is the least promising. The compound ICl was prepared and its spectrum measured in the gas phase and dissolved in molten AlCl<sub>3</sub>, AlBr<sub>3</sub>, AlCl<sub>3</sub>-NaCl eutectic, and carbon tetrachloride. In all cases the spectrum appears to be that of molecular ICl and in no way resembles what one would expect for the *p*<sup>4</sup> cation I<sup>+</sup> or what has been observed by Gillespie and Milne<sup>15</sup> for I<sub>2</sub><sup>+</sup>.

## SPECTRA OF DILUTE SOLUTIONS OF BISMUTH METAL IN MOLTEN BISMUTH TRIBROMIDE<sup>16</sup>

C. R. Boston

Previous studies indicated two subvalent bismuth species in dilute solutions of bismuth in molten BiCl<sub>3</sub>. Rather convincing evidence indicates that the Bi<sup>+</sup> ion is a dominant species in very dilute solutions of subvalent bismuth in both molten BiX<sub>3</sub> and AlX<sub>3</sub>-NaX solvents. Mass action constants for equilibria involving Bi<sup>+</sup> and the cluster ion Bi<sub>4</sub><sup>4+</sup> are in good agreement with values obtained electrochemically<sup>17,18</sup> for both BiCl<sub>3</sub> and BiBr<sub>3</sub> solvents. Band intensities for what is presumed to be Bi<sup>+</sup> are ten times greater in BiX<sub>3</sub> than in NaX-AlX<sub>3</sub> solvents; this may be due to a Bi(I)-Bi(III) intervalence-transfer absorption.

## DENSITIES OF MOLTEN NaBr-AlBr<sub>3</sub> MIXTURES<sup>19</sup>

C. R. Boston W. M. Ewing

Liquid densities of NaBr-AlBr<sub>3</sub> mixtures were measured with the float method. Compositions of 33.3,

<sup>14</sup>J. Barr *et al.*, *Can. J. Chem.* **46**, 149 (1968).

<sup>15</sup>R. J. Gillespie and J. B. Milne, *Inorg. Chem.* **5**, 1577 (1966).

<sup>16</sup>Summary of C. R. Boston, *Inorg. Chem.* **9**, 389–90 (1970).

<sup>17</sup>L. E. Topol, S. J. Yosim, and R. A. Osteryoung, *J. Phys. Chem.* **65**, 1511 (1961).

<sup>18</sup>L. E. Topol and R. A. Osteryoung, *J. Phys. Chem.* **66**, 1587 (1962).

<sup>19</sup>Abstract of a paper submitted to *Journal of Chemical and Engineering Data*.

50.0, 66.7, and 80.0 mole %  $\text{AlBr}_3$  were measured over a range of temperatures and the data fitted to equations of the form  $\rho = \alpha - \beta t$  by a least-squares analysis. Molar volumes showed negative deviations from additivity of about 10% at 220°C and 50% at 600°C.

**POLARIZED ELECTRONIC ABSORPTION  
SPECTRUM OF TETRAGONAL  $\text{NiCl}_4^{2-}$  IN  
 $\text{Cs}_3(\text{MgCl}_4)\text{Cl}$  (REF.20)**

T. W. Couch<sup>21</sup> G. P. Smith

The optical absorption spectrum (4000 to 17,000 Å) of crystals of  $\text{Cs}_3(\text{Mg}_{0.996}\text{Ni}_{0.004}\text{Cl}_4)\text{Cl}$  was measured at approximately 5 and 80°K. The host material was found by x-ray diffraction to have the  $\text{Cs}_3(\text{CoCl}_4)\text{Cl}$  structure ( $I4/mcm$ ) at temperatures down to at least

10°K. In the solid solution the spectra showed that nickel(II) substituted for magnesium, which lies at sites of  $D_{2d}$  symmetry with the principal axis aligned with the c axis of the tetragonal crystal. Spectra were measured in both  $\text{E} \perp \text{c}$  and  $\text{E} \parallel \text{c}$  polarizations, and the results were in accord with a ligand-field model having  $B$ ,  $C$ ,  $\zeta$ ,  $B_0^2$ ,  $B_0^4$ , and  $B_4^4$  as parameters. Numerous phonon creation bands were observed and provided information about excited state potential wells and nuclear motions. In some band systems the individual bands were unusually narrow and well-resolved.

---

<sup>20</sup>Abstract of paper accepted for publication in *The Journal of Chemical Physics*.

<sup>21</sup>Graduate student from the University of Tennessee.

## 11. Superconducting Materials

C. C. Koch G. R. Love<sup>1</sup>

We are studying the effects of metallurgical variables on the properties of superconducting materials. The most highly structure-sensitive superconducting property appears to be current carrying capacity in an applied magnetic field; it is sensitive to mechanical strain, preferred orientation, fabrication, and heat-treatment procedures, grain size, and the morphology, composition, and volume fraction of second-phase particles. Meaningful correlation of structure and properties requires detailed knowledge of both. Consequently, much of our effort is devoted to obtaining basic metallurgical information on phase diagrams, transformation kinetics and products, and the microstructures that result from them in systems based upon superconducting materials. The alloy systems of primary interest are those based on niobium and technetium.

We have also contributed to other studies in cooperation with other groups. Work on structural changes in samarium,<sup>2</sup> specific heat of UN, and specific heat of nickel-iron intermetallic<sup>3</sup> is reported in Chapters 14, 6, and 9, respectively. A study of transformations in gadolinium-cerium alloys is summarized below.

### HIGH Q RESONATORS IN HIGHER dc MAGNETIC FIELDS<sup>4</sup>

G. R. Love<sup>1</sup> J. M. Victor<sup>5</sup>  
C. C. Koch G. A. Persyn<sup>5</sup>  
W. L. Rollwitz<sup>5</sup>

Superconducting circuits will exhibit negligible ac losses until magnetic flux penetration occurs. Niobium with a lower critical field of about 1400 gauss is the most promising material for ac applications. Recently, we found that niobium with dispersed gadolinium or yttrium particles tested at a frequency of 520 MHz excludes flux to higher dc fields than those attained with pure niobium. These initial results indicate that the niobium dispersions are promising materials for ac applications.

### SUPERCONDUCTIVITY IN TECHNETIUM-BASE ALLOYS

C. C. Koch

Technetium, which has the second highest superconducting transition temperature for an element, is the base for promising superconducting alloys and compounds. Many of the physical properties of technetium related to its superconductivity have not been measured previously. Recently we measured the elastic moduli of pure technetium by ultrasonic techniques at 4.2, 77, and 298°K in cooperation with the Nondestructive Testing Group<sup>6</sup> and found the Debye temperature to be 454°K at 4.2°K.

### THE CRITICAL STATE IN HYSTERETIC SUPERCONDUCTORS<sup>7</sup>

G. R. Love<sup>1</sup>

A model description is proposed for the transport properties of type II superconductors. It proceeds from the general concepts of a critical state resulting from thermally activated motion of current vortices (fluxoids) past barriers (pins) due to forces resembling

<sup>1</sup>Now at Union Carbide Corporation, P.O. Box 5928, Greenville, South Carolina.

<sup>2</sup>P. G. Mardon and C. C. Koch, "Structural Changes in Samarium Metal at Elevated Temperatures," *Scripta Met.* 4, 477-83 (1970).

<sup>3</sup>T. G. Kollie, J. O. Scarbrough, and D. L. McElroy, "Effects of Configurational Order on the Specific Heat Capacity of Ni<sub>3</sub>Fe Between 1.2 and 4.4°K." submitted to *The Physical Review* for publication.

<sup>4</sup>Abstracted from *Cryogenics* 9, 392 (1969).

<sup>5</sup>Southwest Research Institute, San Antonio, Texas.

<sup>6</sup>G. R. Love, C. C. Koch, H. L. Whaley, and Z. R. McNutt, "Elastic Moduli and Debye Temperature of Polycrystalline Technetium by Ultrasonic Velocity Measurements," *J. Less-Common Metals* 20, 73-75 (1970).

<sup>7</sup>Abstracted from *Phil. Mag.* 21, 1003-26 (1970).

Lorentz forces. The variations in strength of the fluxoid-pin interaction is formally described as a function of local field and temperature. We derived expressions that describe the variation in sample critical current density with applied field and temperature and contain two material parameters, the spacing  $r_0$  and the effectiveness  $p$  of pinning sites. Empirical determinations of these parameters, for example from the grain size dependence of critical current density, yield plausible values, and the values determined in a single experiment (for example, current density as a function of field) allow successful prediction of the outcome of other experiments (for example, current density as a function of temperature at constant field).

### LOSSES DUE TO MOVING FLUXOIDS IN SUPERCONDUCTORS<sup>8</sup>

G. R. Love<sup>1</sup> D. M. Kroeger

A macroscopic description of the intermediate state in hysteretic superconductors, previously applied to the case of near-static fluxoid distributions, has now been extended to the case of fluxoids constrained to move at definable average velocities. The model allows semi-quantitative analytic prediction of the results of flux-flow experiments, and it establishes an analytic correlation between those results and measurements of the frequency dependence of the apparent critical current density determined by ac magnetization. Since a number of physical parameters of the superconductors are incorporated into the model, a variety of checks on the validity of the model description are available.

<sup>8</sup>Abstracted from paper submitted to *The Philosophical Magazine*.

Samples having a single composition and metallurgical history were tested extensively both in the flux-flow geometry and in ac magnetization under a variety of test conditions. Analysis of these experimental results in terms of the model constitutes both a test of the model and a quantitative correlation between metallurgical structure and superconducting properties for this system.

### AN ELEVATED-TEMPERATURE X-RAY DIFFRACTION AND AN ELECTRON MICROSCOPY STUDY OF THE TRANSFORMATIONS TO THE SAMARIUM-TYPE STRUCTURE IN GADOLINIUM-CERIUM ALLOYS<sup>9</sup>

C. C. Koch P. G. Mardon<sup>10</sup> C. J. McHargue

Further results of a study of the phase transformations to the samarium-type structure in gadolinium-cerium alloys are presented. More complete data on the critical temperatures determined by electrical resistance measurements are given. Elevated-temperature x-ray diffraction experiments establish that the higher temperature set of critical temperatures reflect the structural change to and from the samarium-type phase, while the lower critical temperatures coincide with a discontinuous dimensional change in the samarium-type unit cell.

Transmission electron microscopy reveals a heavily faulted structure with the presence of twins, dislocation loops, and nonmetallic second-phase precipitate particles.

<sup>9</sup>Abstracted from paper presented at The 8th Rare Earth Research Conference, Reno, Nev., April 19–22, 1970.

<sup>10</sup>On temporary assignment from AERE, Harwell, England.

## 12. Surface Reactions of Metals

J. V. Cathcart

The objective of this research is a better understanding of the fundamental mechanisms of the oxidation of metals and alloys. Specific research projects include a study of the oxidation of uranium-base alloys and an investigation of the high-temperature oxidation of tantalum and a tantalum-tungsten alloy. A study of diffusion in refractory metals is also in progress in cooperation with the Diffusion in Solids Group.

The common feature of all this work is the evaluation of the role of stress in the oxidation process. In our previous research on the oxidation of pure metals, we demonstrated that stresses generated during oxidation could influence the rate of oxidation through a gross rupturing of an otherwise protective film or, more subtly, through the development of paths of easy diffusion in the oxide. As the emphasis in our research has shifted more and more to studies of alloy oxidation, we have found that oxidation-induced stress can, in addition, trigger phase transformations and control oxide morphology to a marked degree. Stress obviously has far-reaching consequences in oxidation processes generally.

### OXIDATION OF URANIUM-BASE ALLOYS

J. V. Cathcart   G. F. Petersen   R. E. Pawel

We have continued our studies of the oxidation of uranium-base alloys, especially the ternary alloy U-7.5 wt % Nb-2.5 wt % Zr and the binary U-9.4 wt % Nb. A variety of techniques ranging from oxidation rate measurements to electron microprobe studies were used to investigate the oxidation characteristics of these materials, and the following conclusions were reached.

The stress level developed during oxidation is very high. At 800°C the surface layers of sheet specimens were extended laterally during oxidation, increasing the gross surface area of the ternary alloy by 100% in 6 hr.

The flexure behavior of specimens oxidized on one side only suggested the existence of transient stresses at the oxide-metal interface on the order of  $10^6$  psi. Also, the presence of an oxide scale tended to trigger low-temperature phase transformations in the alloys.

Two and sometimes three phases could be detected in the oxide scale. The oxide matrix is  $UO_2$  with a highly columnar structure (see Fig. 12.1) and contains stringers of a metallic-appearing phase (Fig. 12.2), which is either niobium or one of the lower oxides of niobium. Oxidation at 900 and 1000°C results in the



Fig. 12.1. Fracture Surface of the Oxide Formed in 6 hr at 800°C and 0.05 torr O on U-9.4 wt % Nb. Note columnar structure of oxide. The columns run perpendicular to the oxide-metal interface. 6000X. Reduced 51%.

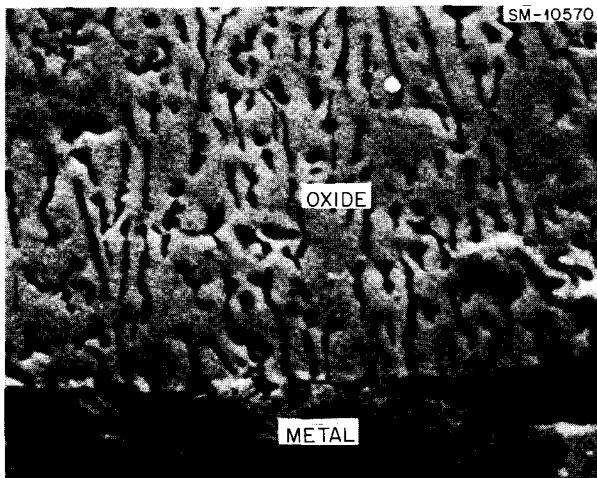


Fig. 12.2. Scanning Electron Micrograph of the Cross Section through the Oxide-Metal Interface of a U-9.4 wt % Nb Specimen Oxidized 6 hr at 800°C and 0.05 torr O. The specimen was polished metallographically and etched lightly. The dark regions in the oxide are the metallic stringers. 6000X. Reduced 56%.



Fig. 12.3. Scanning Electron Micrograph of Nb<sub>2</sub>O<sub>5</sub> Whisker Cluster Formed on the Surface of a U-9.4 wt % Nb Specimen Oxidized 200 min at 1000°C and 0.050 torr O. 6000X. Reduced 56.5%.

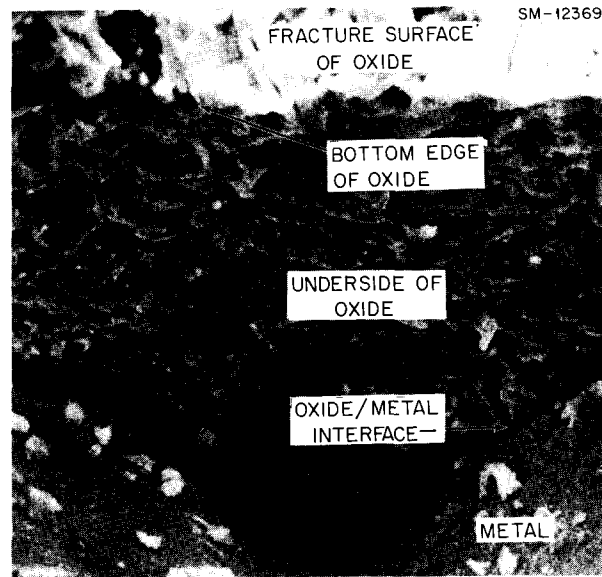


Fig. 12.4. Scanning Electron Micrograph Showing the Underside of the Oxide Scale Formed on U-9.4 wt % Nb Oxidized 6 hr at 800°C and 0.050 torr O. This view was obtained by fracturing the original specimen and observing the oxide at a point where a metal grain was missing from the oxide-metal interface. 10,000X. Reduced 40.5%.

growth of Nb<sub>2</sub>O<sub>5</sub> needles at the gas-oxide interface, as shown in Fig. 12.3.

The oxidation rate curves for these alloys are approximately parabolic, and an activation energy of 18 kcal/mole was obtained between 700 and 1000°C. This small value for the activation energy suggests the importance of short-circuit diffusion in the oxidation process and is consistent with the fine columnar structure of the oxide.

The large stresses generated during oxidation arise as a consequence of the large oxide-to-metal volume ratio ( $V_{UO_2}/V_U = 1.95$ ) and the occurrence of anion diffusion in the oxide. The lateral extension of the metal surface is achieved through a "keying" on a very fine scale of the oxide to the metal, as is illustrated in the view of the underside of the oxide in Fig. 12.4.

## REFRACTORY METAL STUDIES

R. E. Pawel

### Flexure Measurements During Oxidation

We completed a set of flexure measurements on polycrystalline tantalum specimens as they oxidized at temperatures from 550 to 850°C in dry oxygen at atmospheric pressure. At each temperature the flexure

behavior of several specimens having thicknesses from about 10 to 45 mils was studied. We then used machine computations based on certain simple models for stress generation to obtain pertinent strain, strain energy, and stress values from these data. The results are being analyzed to find a self-consistent model and to see if a correlation exists between the stress characteristics and the oxidation kinetics, particularly in the temperature range of the oxidation-rate reversal, for this metal. Over the whole temperature range, the data indicate that in the early stages of oxidation there are significant contributions to the total strain from both oxide film and oxygen solution effects. The latter source has been discussed in some detail.<sup>1</sup> Average stresses in excess of  $10^5$  psi appear to exist in the oxide, although as the films thicken stress relief is probable, resulting in stress gradients through the oxide. While we have not yet incorporated such effects into our mathematical model relating stresses to the measured strain, the qualitative results have reemphasized the large stress-generating potential of an oxidation process involving a combination of anion diffusion with a large oxide-to-metal volume ratio.

#### The Estimation of Bending Stresses from Flexure Measurements<sup>2</sup>

Experiments in which thin disks of tantalum were oxidized on one side were used to illustrate the fact that specimen geometry and mechanical inhomogeneities may promote the condition where essentially uniaxial bending results from a uniform biaxial stress source. We were thus able to support our use of the simpler flexure formulae in obtaining bending stress values from our strain measurements.

#### Oxidation of Tantalum-Tungsten Alloys

Oxidation rate measurements, principally at 600°C, on plain and anodized T-111 (Ta-10 wt % W-2 wt % Hf) have indicated that this alloy exhibits a catastrophic increase in the oxidation rate, which is due to local breakdown of an otherwise protective oxide film. Anodized T-111 specimens did not show a dramatic enhancement of the oxidation resistance such as that observed in the case of plain tantalum.

<sup>1</sup>R. E. Pawel and J. J. Campbell, "Stress Generation During High-Temperature Oxidation. I. Oxygen Solution Effects," *J. Electrochem. Soc.* **116**, 828-32 (1969).

<sup>2</sup>Abstracted from *J. Electrochem. Soc.* **116**, 1144-46 (1969).

We are also investigating the characteristics of anodic oxide film formation on T-111 as well as on tantalum alloys containing 25 and 50% W. As we found for pure tantalum and niobium, anodizing these alloys in dilute fluoride solutions results in films that are easily stripped from the surface. We intend to use this property to prepare alloy-oxide specimens for subsequent heat treatment and examination in the electron microscope. In principle, this procedure will furnish a unique method for the study of phase equilibria in these oxide films.

#### Anodic-Film Sectioning

In cooperation with the Diffusion in Solids Group, we have continued our studies of diffusion phenomena in the refractory metals using our very sensitive anodic-film sectioning technique. Recent data for the diffusion of Ta, Nb, and W isotopes in tungsten over a wide temperature range<sup>3,4</sup> have shown that each of these processes may be adequately described by a single activation energy and, furthermore, that only small differences exist between these energies.

By means of a series of "double-isotope" experiments, we attempted to add a higher degree of statistical confidence to the answer to the question of whether or not these activation energy differences actually exist. Tantalum and niobium isotopes were diffused simultaneously into tungsten specimens at a series of temperatures, and the concentration profile of each was determined by appropriate isotopic discrimination. In principle, the ratio of the diffusivities determined in this way should not be influenced by several possible experimental errors. Thus, a statistical confidence interval for the slope of the graph of the logarithm of diffusivity ratio against reciprocal temperature should be quite narrow and permit a more sensitive inquiry into the question of the reality of small differences in activation energy.

The results so far have tended to favor the hypothesis that there is no difference in the activation energy for tantalum and niobium diffusing in tungsten. However, 90% confidence intervals are still too wide to preclude the possibility of 1% or so difference.

<sup>3</sup>T. S. Lundy and R. E. Pawel, "Effect of Short-Circuiting Paths on Diffusion Coefficient Measurements," *Trans. Met. Soc. AIME* **245**, 283-86 (1969).

<sup>4</sup>R. E. Pawel and T. S. Lundy, "Tracer Diffusion in Tungsten," *Acta Met.* **17**, 979-88 (1969).

## 13. Theoretical Research

J. S. Faulkner

We are investigating a number of phenomena in solids with particular emphasis on those that are related to the electronic states. We are developing new techniques for treating the electronic states of ordered and disordered solids theoretically. For the most part we use the Korringa-Kohn-Rostoker method to study the energy bands of ordered metals and alloys, the LCAO method for ionic and covalent compounds, and the coherent-potential approximation for disordered systems.

### **CALCULATION OF CONSTANT-ENERGY SURFACES FOR ALUMINUM BY THE KORRINGA-KOHN-ROSTOKER METHOD<sup>1</sup>**

J. S. Faulkner

Radii for constant-energy surfaces corresponding to 561 directions in 1/48 of the Brillouin zone are calculated for a number of energy values for each of four different potential functions that were generated by different methods to describe the electronic states of aluminum. The radii are all calculated by the Korringa-Kohn-Rostoker method for first-principles band-theory calculations. These surfaces are used to find the Fermi energies for the potentials very accurately and to compare the predicted Fermi surfaces.

### **KKR STRUCTURE CONSTANTS FOR COMPLEX CRYSTALS<sup>2</sup>**

J. S. Faulkner

We showed how all of the structure constants for complex crystals can be expressed as linear combinations of quantities that can be calculated as for crystals with one atom per unit cell.

### **THE ELECTRONIC STATES IN COPPER AND ALUMINUM<sup>3</sup>**

J. S. Faulkner

During the past decade a number of experimental methods that can be interpreted unambiguously to give

a rather precise description of the electronic states in a metal have been developed. For technical reasons, the first material investigated by many of these methods was copper. Partly as a reflection of this experimental interest there have been a number of band-theory calculations for copper. There have also been many experimental and theoretical studies on aluminum. In view of this previous work a new theoretical investigation of these materials must have some distinguishing features to make it worthwhile. The major feature of this work is that accurate and detailed numerical representations of constant-energy surfaces are obtained entirely from a convergent first-principles band-theory calculation. Most first-principles calculations are time-consuming, especially for k-vectors that do not lie on symmetry axes where group theory can be used for simplification. Our experience with the Korringa-Kohn-Rostoker (KKR) band-theory method has been that by a careful treatment of computational problems involved it can be used to obtain accurate results in all regions of the Brillouin zone with an expenditure of computer time that is quite modest by band-theory standards.

### **TWO-PARTICLE SCATTERING TERMS IN PERTURBATION THEORY OF ELECTRONIC STATES IN DISORDERED SYSTEMS<sup>4</sup>**

J. S. Faulkner

When applied to liquid metals the coherent-potential approximation leads to the same results as certain

<sup>1</sup> Abstracted from *Phys. Rev.* 178, 914–18 (1969).

<sup>2</sup> Abstracted from *Phys. Letters* 31A, 227–28 (1970).

<sup>3</sup> Summary of an invited paper presented at the Fall Meeting of the Metallurgical Society of the American Institute of Mining, Metallurgical and Petroleum Engineers, Philadelphia, Oct. 13–16, 1969.

<sup>4</sup> Abstract of a paper presented at the March Meeting of the American Physical Society, Dallas, March 23–26, 1970.

diagram summation techniques that arise in a perturbation treatment of this problem. Efforts to sum diagrams corresponding to scattering from clusters have so far been unsuccessful, but we show a simple model for which the summation can be carried out. We use the results to comment on the general problem.

### ELECTRONIC STATES OF A LIQUID METAL FROM THE COHERENT-POTENTIAL APPROXIMATION<sup>5</sup>

J. S. Faulkner

A treatment of the electronic states in a liquid metal based on the coherent-potential method is given. The equations for the coherent potential and the average Green's function obtained from the requirement that the average  $T$  matrix is zero are shown to have as solutions certain expressions that were previously derived by Klauder from a different point of view. Connections with other work are mentioned.

### ELECTRONIC STATES IN LIQUID METALS: A GENERALIZATION OF THE COHERENT-POTENTIAL APPROXIMATION FOR A SYSTEM WITH SHORT RANGE ORDER<sup>6</sup>

B. L. Gyorffy<sup>7</sup>

The problem of finding the ensemble averaged Green's function  $\langle G \rangle$  that describes an electron moving in the potential field of  $N$  stationary scatterers is formulated in terms of multiple scattering theory. The correlations between the positions of the scatterers are explicitly taken into account. By making use of the quasicrystalline approximation and a generalization of the coherent potential prescription, a procedure for calculating  $\langle G \rangle$  is proposed. Because of the use of the quasicrystalline approximation it involves only the radial distribution function of the scatterers in addition to the scatterer-electron interaction potential. The procedure reduces to the coherent potential approximation for randomly distributed scatterers — namely, no short range order — and to Korringa's band-structure calculation for an ordered lattice. The method is applicable to the problems of electronic states in random alloys and of vibrational spectra of imperfect crystals.

<sup>5</sup> Abstract of *Phys. Rev.* **B1**, 934–36 (1970).

<sup>6</sup> Abstract of an article accepted for publication in the *Physical Review*.

<sup>7</sup> Consultant during the summer of 1969. Permanent address is Department of Physics, The University, Sheffield, United Kingdom.

### ADJUSTMENT OF CALCULATED BAND STRUCTURES FOR CALCIUM BY USE OF LOW-TEMPERATURE SPECIFIC HEAT DATA<sup>8</sup>

R. W. Williams H. L. Davis<sup>9</sup>

The electronic band structure of calcium has been studied theoretically by employing the Korringa-Kohn-Rostoker method. The crystal potentials used in our calculation were obtained by a standard superposition of free-atom charge densities. Curves of  $E_k$  vs  $k$  and the density of states at the Fermi energy were calculated for various potentials, with the measured low-temperature electronic specific heat coefficient,  $\gamma$ , being used as an empirical aid to adjust the exchange portion of the crystal potential. The important feature of the potentials used is that they all give band structures which have definite  $d$ -band character in the vicinity of the Fermi surface. These  $d$  bands or their corresponding  $d$  scattering resonances vary rapidly in energy for small changes in the exchange, resulting in values of  $\gamma$  that are extremely sensitive to exchange.

### MAGNETIC PROPERTIES OF TERBIUM-HOLMIUM SINGLE-CRYSTAL ALLOYS. I. MAGNETIZATION MEASUREMENTS<sup>10</sup>

F. H. Spedding<sup>11</sup> R. G. Jordan<sup>11</sup> R. W. Williams

We have investigated the magnetic properties of three single crystals of the terbium-holmium alloy system containing 10, 50, and 90% Ho from 4.2 to 300°K in applied fields up to 28 kOe. Magnetic-moment measurements were made along the  $a(11\bar{2}0)$ ,  $b(10\bar{1}0)$ , and  $c(0001)$  directions of the close-packed hexagonal structures. Within the limitations of such measurements we find that the alloys exhibit similar characteristics to the pure metals. The trend upon increasing the concentration of holmium in terbium is to enhance and widen the antiferromagnetic region at the expense of the ferromagnetic region. The Néel temperatures and polycrystalline paramagnetic Curie temperatures decrease approximately linearly with holmium content to the values for pure holmium. The absolute saturation moments in the basal plane and effective number of

<sup>8</sup> Abstracted from a paper presented at the 3rd IMR Symposium on Electronic Density of States, Washington, D.C., Nov. 3–6, 1969, and to be published in the proceedings.

<sup>9</sup> Solid State Division.

<sup>10</sup> Abstract of *J. Chem. Phys.* **51**, 509 (1969).

<sup>11</sup> Institute for Atomic Research and Department of Physics, Iowa State University, Ames, Iowa; this paper is based on work done there.

Bohr magnetons in the paramagnetic region increase linearly with holmium content. Anisotropy between the  $a$  and  $b$  directions is observed at low temperatures in all the alloys, with the  $b$  preferred. The  $c$  direction is the hard direction in all cases, although there is some evidence for a small amount of ordering along the  $c$  direction in the alloy containing 90% Ho.

### CRYSTAL FIELD $3d^1$ ENERGY LEVELS IN A DISTORTED OCTAHEDRAL POINT CHARGE ENVIRONMENT<sup>1,2</sup>

G. S. Painter C. P. Poole, Jr.<sup>1,3</sup>

Crystal field  $3d^1$  orbital energy levels in an octahedral complex have been calculated as functions of tetragonal and trigonal distortion parameters. In this work, symmetry correct angular solutions are generated by projection operators, and the radial part of the  $3d$  wave function is approximated by a hydrogen-like function in which flexibility is introduced through a variable orbital parameter,  $Z$ . The problem is formulated by applying the variational principle to  $Z$  to minimize the total energy. We compared results obtained using both the effective charge model of the central metal ion core and a diffuse inner shell electron core described by a Hartree product wave function of Slater-type orbitals.

### DISCRETE VARIATIONAL METHOD FOR THE ENERGY BAND PROBLEM WITH GENERAL CRYSTAL POTENTIALS<sup>1,4</sup>

D. E. Ellis<sup>1,5</sup> G. S. Painter

A general variational method for efficiently calculating energy bands and charge densities in solids is presented; the method can be viewed alternately as a weighted local energy procedure and as a numerical integration scheme. This rapidly convergent procedure circumvents many of the difficulties associated with evaluation of matrix elements of the Hamiltonian in an arbitrary basis and treats the general nonspherical potential with no more complication than the usual "muffin-tin" approximation. Thus the band structure of ionic and covalent materials can be calculated with realistic crystal potentials. As an example, the method

<sup>1,2</sup> Abstract of an article submitted for publication in the *Journal of Physics and Chemistry of Solids*.

<sup>1,3</sup> Department of Physics, University of South Carolina, Columbia, S.C.

<sup>1,4</sup> Abstract of an article submitted for publication in the *Physical Review*.

<sup>1,5</sup> Department of Physics, Northwestern University, Evanston, Ill.

is applied to the one-electron-model Hamiltonian with a nonspherical local potential, using a linear combination of atomic orbitals basis. Matrix elements of the Hamiltonian are evaluated directly without decomposition into atomic basis integrals; no "tight binding" approximations are made. Various prescriptions for the construction of crystal potentials are considered, and convenient least-squares expansions are described. The extension of these methods to nonlocal potentials such as are encountered in the Hartree-Fock SCF procedure is discussed.

### CRYSTAL POTENTIAL AND ELECTRONIC STRUCTURE OF DIAMOND<sup>1,4</sup>

G. S. Painter D. E. Ellis<sup>1,5</sup>

The crystal potential, energy bands, and wave functions of diamond are calculated by numerical-variational methods developed in a previous article. Nonspherical terms in the potential significantly affect the valence band width and the gap between the valence and conduction bands. The band structure is only slightly affected by scaling the  $\rho^{1/3}$  Slater exchange potential. Component charge densities are obtained for comparison with x-ray data.

### CRYSTAL POTENTIAL AND ELECTRONIC STRUCTURE OF LITHIUM METAL<sup>1,4</sup>

G. S. Painter D. E. Ellis<sup>1,5</sup>

The Seitz empirical potential for lithium metal is compared with the *a priori* superposition of atomic potentials. Nonspherical components of the superposed atomic potential lead to deviations of 1.5% from a "muffin-tin" average over part of the unit cell. The discrete variational method outlined in a previous paper has been applied to determine the band structure, using an LCAO basis set. Matrix elements of the Hamiltonian are evaluated by direct numerical integration, and no "tight binding" approximations are made. Changes in the band structure due to different potentials are studied, and results are compared with those of previous calculations. The bonding charge density is displayed.

### ELECTRONIC BAND STRUCTURE AND OPTICAL PROPERTIES OF GRAPHITE FROM A VARIATIONAL APPROACH<sup>1,4</sup>

G. S. Painter D. E. Ellis<sup>1,5</sup>

The electronic band structure of graphite has been calculated from an *ab initio* variational approach using

an LCAO basis of Bloch states, including nonspherical terms in the one-electron crystal potential. Matrix elements of the Hamiltonian are evaluated directly without any "tight binding" approximations. The optical transitions deduced from the energy bands calculated with a single-layer crystal model agree nicely with recent polarized light reflectance measurements. Details of the band structure are calculated for the three-dimensional Brillouin zone and related to the results obtained using the single-layer crystal structure. The results are encouraging, not only from the standpoint that the method employed is an *ab initio* approach with no special *a priori* assumptions, but also because the band structure is quite insensitive to the particulars of the crystal potential function.

#### DISCRETE VARIATIONAL METHOD FOR THE ENERGY BAND PROBLEM WITH LCAO BASIS AND NONSPHERICAL LOCAL POTENTIAL<sup>16</sup>

G. S. Painter

The discrete variational method described previously by D. E. Ellis is unrestricted with regard to the form of the variational basis set. Here we discuss the accuracy and efficiency of this technique as implemented with an LCAO basis to illustrate the advantages that our approach offers in avoiding the difficulties of the LCAO tight-binding scheme. The convergence properties of this method with respect to the basis size and the number of integration points are investigated for metallic, semiconducting, and insulating solids with a one-electron-model Hamiltonian with nonspherical local potentials. We demonstrate that this method provides an efficient approach to a variety of band theory problems, particularly for systems in which nonspherical potentials are important.

#### ALKALI SOLUTE KNIGHT SHIFTS IN ALKALI MATRICES<sup>17</sup>

G. M. Stocks   W. H. Young<sup>18</sup>   A. Meyer<sup>19</sup>

We calculated solute Knight shifts in binary alkali systems. The results agree semiquantitatively with experiment. The crucial parameter seems to be the

effective mass of valence electrons at the Fermi level. If we observe the resonance of a given ion A in two matrices B and C, then the Knight shift is greater in B if the effective mass in B is greater than in C.

#### KNIGHT SHIFTS OF THE ALKALI METALS<sup>8</sup>

A. Meyer<sup>19</sup>   G. M. Stocks   W. H. Young<sup>18</sup>

Being leading members of transition series, K, Rb, and Cs have pseudoatoms with virtual bound *d* states; lithium has a somewhat analogous *p* state. By contrast, sodium has no such states. Evidence is offered as to how the associated scattering accounts for the following observed electron transport properties. (1) Under pressure, the resistance of lithium rises, and eventually so do those of Cs, Rb, and K. (2) The thermopower of lithium is anomalous (positive) and stays so under pressure, while that of cesium very quickly becomes positive when pressure is applied.

The same features can now be used in the theory of Knight shifts to explain the following observations. (3) The conduction electron susceptibility for lithium is enhanced very significantly above that for free (and even interacting) electrons. (4) The nuclear contact density in lithium is much lower than that predicted by one-orthogonal-plane-wave theory. (5) The Knight shifts of lithium and sodium decrease and those for rubidium and cesium increase when pressure is applied. (6) The Knight shift for a given ion increases when it is successively resonated in Na, K, Rb, and Cs matrices. The key to the interpretation of (5) and (6) is the variation in the density of states (and therefore susceptibility) under conditions of pressure change and alloying.

<sup>16</sup> Abstract of a paper presented at and to be published in the proceedings of the Conference on Computational Methods in Band Theory, May 14–15, Yorktown Heights, New York.

<sup>17</sup> Abstract of an article published in *J. Phys. Ser. C*, 3, 40 (1970).

<sup>18</sup> Department of Physics, The University, Sheffield, United Kingdom.

<sup>19</sup> Department of Physics, Northern Illinois University, DeKalb, Ill.

## 14. X-Ray Diffraction

Bernard Borie    H. L. Yakel

Applications of x-ray diffraction methods in studies of the structure of matter play a vital role in metallurgical and ceramic research. To bring these techniques to bear on problems of interest to other groups, as well as on problems of basic interest generated within our group, constitutes a brief description of our mission in the Metals and Ceramics Division.

We made significant progress in the interpretation of diffuse x-ray scattering due to thermal motion of atoms and that due to disorder in binary alloys. We have continued our work on the imperfect structures of unirradiated and neutron-irradiated graphite and on the aging transformations of gamma-stabilized uranium alloys. Progress was also made in several experimental and theoretical areas of small-angle x-ray scattering.

### ROUTINE ANALYSES

L. A. Harris    R. M. Steele  
P. G. Mardon<sup>1</sup>    H. L. Yakel

We completed required diffraction analyses on over 900 samples submitted to our laboratory by other groups during the reporting period. Results may be found in the reports of those groups and will not be presented separately here.

### ON THE INTERPRETATION OF TEMPERATURE DIFFUSE SCATTERING<sup>2</sup>

Bernard Borie

An alternative formulation of temperature diffuse scattering theory is described. The result is in terms of the mean atomic displacements rather than the usual normal mode representation. The theory leads to a

<sup>1</sup> On temporary assignment from AERE, Harwell, England.

<sup>2</sup> Abstracted from paper accepted for publication in *Acta Crystallographica*.

direct relation between first- and second-order diffuse intensity, which, by iteration, allows for a correction for the second-order contribution without approximation. It seems likely that this theory should be useful for highly anharmonic thermal motion.

### THE INTERPRETATION OF INTENSITY DISTRIBUTIONS FROM DISORDERED BINARY ALLOYS<sup>3</sup>

Bernard Borie    Cullie J. Sparks, Jr.

X-ray diffuse scattering from disordered alloys is the primary direct source of information concerning the Warren parameters, which describe the existing state of order. However, the short range order diffuse intensity is obscured by other contributions to the diffraction pattern resulting from static atomic displacements from the average lattice and from effects related to thermal motion. Described here is a method to separate the diffraction pattern into its various components so that each may be interpreted independently. We assume only that the atomic displacements,  $\delta$ , are sufficiently small and that the diffraction vector,  $k/2\pi$ , is sufficiently small that terms beyond the term quadratic in  $k \cdot \delta$  may be neglected in the series expansion of  $\exp[ik \cdot \delta]$ .

### X-RAY DIFFRACTION STUDY OF HIGHLY ORIENTED GRAPHITE

#### Thermal Motion

Cullie J. Sparks, Jr.    J. E. Epperson

X-ray measurements of the thermal vibrations in hexagonal graphite with all basal plane normals within

<sup>3</sup> Abstracted from paper submitted for publication to *Acta Crystallographica*.

0.3° of the mean direction were undertaken to determine the frequency spectrum. This will lead to a better understanding of thermal properties such as thermal expansion, specific heat, and thermal conductivity. We found that graphite behaves as rigid plates with the basal planes having a high resistance to bending but a low resistance to shearing over each other. Graphite basal planes vibrate in thermal motion as rigid plates, with the amplitudes being large perpendicular to these basal planes and coupled over distances of about 12 basal planes. The vibrations within the basal plane are smaller and coupled over distances in excess of 1000 Å.

#### Neutron Irradiation

Cullie J. Sparks, Jr. Wen Lin<sup>4</sup> C. R. Kennedy

Neutron irradiation at 715°C to  $1.1 \times 10^{22}$  neutrons/cm<sup>2</sup> on the same highly oriented hexagonal graphite as used for the thermal motion study resulted in an 8.9% expansion in the *c* direction (normal to the basal planes) and a 1.2% contraction in the *a* direction. The unit cell dimensions increased 0.17% in the *c* direction and decreased slightly in the *a* direction. The major change in the x-ray diffraction pattern occurred for reflections  $H - K \neq 3n$  where *n* is an integer. Little change occurred for reflections of the type  $H - K = 3n$ . This result is explained by a random stacking of the three possible positions *A*, *B*, and *C* with the limitation of no *A* on *A*, *B* on *B*, or *C* on *C* as first-neighbor planes and with the *a* axes remaining parallel.

The most plausible model of irradiation damage in graphite is the condensation of interstitial carbon atoms between basal planes such that the new plane is unlike the two neighboring planes. We conclude from our data that the stacking sequence has become almost random. This model explains why isotropic graphite is needed for dimensional stability in reactor application.

#### URANIUM-NIOBIUM-ZIRCONIUM ALLOYS

H. L. Yakel L. A. Harris

Single crystals of nominal composition U-16.60 at. % Nb-5.64 at. % Zr were rapidly quenched from a soaking temperature in the body-centered cubic gamma phase field and then aged at 150, 350, 450, and 550°C in dry and moist argon. X-ray diffraction patterns of the aged crystals suggested a retarding effect of the moist atmosphere on the aging reactions below 400°C. An indication of reversion on high-temperature aging of

a crystal previously aged below 400°C was seen in one specimen.

Recent work on crystals cut from a better characterized sample shows that the structure obtained on gamma-quenching may be sensitive to composition. Only  $\gamma^{\circ}$  phases were retained in an alloy with just slightly lower solute content than other alloys<sup>5</sup> in which a  $\gamma^s$  phase was found. The structural features of aging these crystals in a salt bath at 350°C are being followed as a function of time. We are also investigating effects of deformation on the structures of crystals and polycrystalline materials.

Thermal expansion of the gamma phase in a polycrystalline wire of composition U-(8.0 ± 0.2) wt % Nb-(2.9 ± 0.1) wt % Zr was examined by high-temperature x-ray diffraction. A least-squares fit of the measured lattice parameters in the interval 700 to 970°C gave a linear thermal expansion coefficient of  $(19.9 \pm 0.7) \times 10^{-6}/^{\circ}\text{C}$  for this phase.

#### STRUCTURAL CHANGES IN SAMARIUM METAL AT ELEVATED TEMPERATURES<sup>6</sup>

P. G. Mardon<sup>1</sup> C. C. Koch

Samarium metal has been studied by x-ray diffraction, dilatometric, and electrical resistance methods as a function of temperature from 25 to 600°C. Diffraction data show abnormal changes in the samarium-type unit cell dimensions near 300°C; at higher temperatures the axial ratio becomes essentially constant. This effect is also reflected in the dilatometry and resistance data. A transformation from the nine-layered samarium structure to a two-layered hexagonal close packed structure is observed at higher temperatures. The stability of the hexagonal close packed phase is sensitive to atmospheric contamination; the phase is believed to be stable in pure samarium metal above 600°C.

#### TWO MODIFICATIONS OF THE KRATKY SMALL-ANGLE X-RAY CAMERA<sup>7</sup>

Robert W. Hendricks

A Kratky small-angle x-ray camera has been modified in two respects to provide increased sensitivity and performance. (1) Flexible metal bellows seals have been mounted between the collimation system vacuum cover

<sup>4</sup>Postdoctoral fellow from The University of Tennessee.

<sup>5</sup>H. L. Yakel, *J. Nucl. Mater.* 33, 286-95 (1969).

<sup>6</sup>Summary of *Scripta Met.* 4, 477-83 (1970).

<sup>7</sup>Abstracted from paper accepted for publication in the *Journal of Applied Crystallography*.

and the specimen chamber and between the specimen chamber and the tank that provides a vacuum path to the detector. The consequent elimination of four Mylar windows in the x-ray path near the sample significantly reduced the background scattering. The degree of improvement depends on several variables including the collimation system geometry, the x-ray tube power, and the electronic noise of the counting system. (2) A flat piece of hot-pressed pyrolytic graphite has been mounted as a diffracted beam monochromator. Experimental results show the diffracting efficiency of the graphite to be about 25%. This is sufficiently high that for the same total counting time, the detector will record the same net number of x-ray photons as with balanced filters but with much improved statistics.

### THE GAS AMPLIFICATION FACTOR IN XENON-FILLED PROPORTIONAL COUNTERS<sup>8</sup>

Robert W. Hendricks

The gas amplification factor in a variety of commercial xenon-filled proportional counters has been found to obey the Diethorn equation

$$M = \exp \left\{ \frac{V \ln 2}{\Delta V \ln(b/a)} \ln \left[ \frac{V}{Kpa \ln(b/a)} \right] \right\}.$$

For fill gases containing 10% CH<sub>4</sub> as a quench gas, the parameter  $K$  is  $3.65 \times 10^{-4} \text{ V atm}^{-1} \text{ cm}^{-1}$ , while for fill gases containing 5% CO<sub>2</sub> as a quench gas,  $K$  is  $3.50 \times 10^{-4} \text{ V atm}^{-1} \text{ cm}^{-1}$ . The parameter  $\Delta V$  was found to be 32.3 V in both cases.

### ABSOLUTE INTENSITY MEASUREMENTS IN SMALL-ANGLE X-RAY SCATTERING.

#### I. THEORY

Robert W. Hendricks

Following a discussion of the definition of absolute intensity units, a general procedure is developed for

relating the absolute intensity scattered by a sample to the power detected in an x-ray counting system. The effects of a nonuniform incident beam are treated rigorously. The theoretical basis of various methods for measurements of the intensity of the incident are discussed in detail. These include attenuation by multiple foils and measurement of the scattering from a calculable standard such as gases or quartz. The use of secondary standards, such as Kratky's standardization of polyethylene with a high-speed rotating disk and Patel and Schmidt's use of Ludox spheres are also considered.

### X-RAY DIFFRACTION DATA ON LIQUID TRIMETHYLAMINE DECAHYDRATE AT 5°C<sup>9</sup>

C. Folzer<sup>10</sup> R. W. Hendricks A. H. Narten<sup>11</sup>

Trimethylamine is one of many compounds known to form a clathrate hydrate [ideal composition 4(CH<sub>3</sub>)<sub>3</sub>N·41H<sub>2</sub>O]. The scattering of x-rays from a solution of trimethylamine in water having the same composition as the clathrate crystal has been measured and analyzed at the melting point of the solid hydrate (5°C). In this report both the raw data and the intensity and radial distribution functions derived from them are tabulated. The radial distribution function of the solution is very similar to that of pure water at the same temperature, and the absence of interference maxima in the small-angle portion of the intensity function precludes any significant deviation of the pair density from the uniform bulk density beyond approximately 8 Å.

<sup>8</sup> Abstracted from paper to be submitted for publication in the *Review of Scientific Instruments*.

<sup>9</sup> Abstract of work to be published as an ORNL Report.

<sup>10</sup> Crystallography Laboratory, University of Pittsburgh, Pittsburgh, Pa.

<sup>11</sup> Chemistry Division.

## Part II. Fast Reactor Technology

### 15. Fast Reactor Oxide Fuels

A. L. Lotts

This program is being conducted to advance the technology of (U,Pu)O<sub>2</sub> as an LMFBR fuel, but the results are applicable to other advanced reactors such as the Gas-Cooled Fast Breeder Reactor. Determination of the properties and performance of sol-gel-derived oxide fuels fabricated by Sphere-Pac and pelletizing techniques is emphasized, but these fuels are also compared with other fuels, such as pellets from mechanically blended or coprecipitated oxide. The main objectives of our program are:

1. to establish the performance characteristics and limitations of (U,Pu)O<sub>2</sub> fuels fabricated by different processes,
2. to obtain a fundamental understanding of the mechanisms involved in the irradiation behavior of fuel elements incorporating these fuels, and
3. to develop fabrication techniques that provide both economy and a product with optimized performance.

These objectives are being met through a program that includes fabrication of fuel with different structures, characterization of these by out-of-reactor methods, and irradiation under a variety of conditions. The emphasis in the program is on irradiation testing and postirradiation examination of the various fuel structures. We are utilizing such facilities as the Oak Ridge Research Reactor, the Transient Reactor Test Facility, the Experimental Breeder Reactor II, and the Engineering Test Reactor. The program includes instrumented and noninstrumented tests under steady-state, power cycling, and transient conditions. The interpreta-

tion of the results depends heavily upon the preirradiation characterization and quality assurance program on the fuels and upon correlations with the theoretical fuel modeling work, which is reported in Chapter 17.

This program also provides technology that applies to the Gas-Cooled Breeder Reactor, development for which is reported in Chapter 36. This is a joint program with the Chemical Technology Division, which prepares the sol-gel-derived fuel, and the Reactor Division, which conducts the irradiation tests in the ORR.

#### DEVELOPMENT OF FABRICATION PROCESSES

J. D. Sease

The objective of our (U,Pu)O<sub>2</sub> program is to develop fabrication techniques that provide both economy and a product with optimized performance. A large portion of this program has been the development of Sphere-Pac and sol-gel pellet fabrication techniques and the fabrication of irradiation test specimens by these processes. We completed initial engineering evaluation of the Sphere-Pac process and introduced a new Sphere-Pac process. The Sphere-Pac process was used to load approximately 150 in. of fuel for irradiation tests. Sol-gel-derived pellets with controlled densities from 81 to 93% of theoretical were fabricated for a number of irradiation tests.

#### Sphere-Pac Development

C. R. Reese    J. D. Sease

The Sphere-Pac process involves the sequential loading of sol-gel microspheres into cladding. This year

most of our work involved the engineering evaluation of the process.<sup>1-4</sup> Sufficient engineering data were collected to evaluate the Sphere-Pac process as an economically feasible method for loading LMFBR fuel pins. Based on these studies, an alternate method of loading (U,Pu)O<sub>2</sub> microspheres was proposed.<sup>4,5</sup> By incorporating all of the plutonium in the coarse fraction and working with UO<sub>2</sub> fines, the alternate method offers several significant advantages.

For irradiation tests the Sphere-Pac process was used to load approximately 150 in. of (U-20% Pu)O<sub>2</sub> fuel for irradiation tests in the ETR, ORR, and EBR-II. All these pins were loaded with a binary mixture composed of a 420 to 595- $\mu$ m coarse fraction and fines smaller than 44  $\mu$ m. Smear densities ranged from 80 to 85% of theoretical. Details of the irradiation tests are discussed later in this chapter.

<sup>1</sup>R. A. Bradley, *Fuels and Materials Development Program Quart. Progr. Rept. March 31, 1970*, ORNL-4560, pp. 6-7.

<sup>2</sup>C. R. Reese, *Fuels and Materials Development Program Quart. Progr. Rept. Dec. 31, 1969*, ORNL-4520, pp. 5-6.

<sup>3</sup>W. L. Moore, *Fuels and Materials Development Program Quart. Progr. Rept. Sept. 30, 1969*, ORNL-4480, pp. 4-6.

<sup>4</sup>F. E. Harrington, R. W. Horton, R. B. Pratt, and J. D. Sease, *Cost Study of Four Alternate Routes for LMFBR Fuel Material Preparation and Element Fabrication*, ORNL-TM-2813 (February 1970).

<sup>5</sup>J. D. Sease, C. R. Reese, R. A. Bradley, W. H. Pechin, and A. L. Lotts, "Sphere-Pac and Pelletization of (U,Pu)O<sub>2</sub>," pp. 323-41 in *Proceedings on Sol-Gel Processes and Reactor Fuel Cycles*, CONF-700502.

## Pellet Development and Fabrication

R. A. Bradley

The objective of this work is to develop methods of fabricating sol-gel (U,Pu)O<sub>2</sub> pellets and to produce pellets of controlled density and stoichiometry for irradiation tests. The experiments for which we fabricated pellets during the past year and the pellet properties are summarized in Table 15.1. The (U,Pu)O<sub>2</sub> powder was prepared by blending UO<sub>2</sub> and PuO<sub>2</sub> sols, drying to a gel, and grinding to a fine powder. This method has been described in more detail previously.<sup>6,7</sup>

By mercury porosimetry and B.E.T. surface area measurements, we determined the physical characteristics of the (U,Pu)O<sub>2</sub> gel particles.<sup>7</sup> The effects of thermal treatments on gel particles have been studied thermogravimetrically. These studies, along with ceramographic examination of gel particles and sintered pellets, have provided an insight into the densification of sol-gel (U,Pu)O<sub>2</sub>. The typical sol-gel (U,Pu)O<sub>2</sub> particle is a tightly bonded porous agglomerate of crystallites, and it resists consolidation during pellet pressing. This porous particle shrinks away from neighboring particles during sintering, creating a macroporosity and hence a low density. Having this understanding of the behavior of sol-gel (U,Pu)O<sub>2</sub>, we altered

<sup>6</sup>R. A. Bradley, *Metals and Ceramics Div. Ann. Progr. Rept. June 30, 1969*, ORNL-4470, p. 128.

<sup>7</sup>R. A. Bradley and W. H. Pechin, *Fuels and Materials Development Program Quart. Progr. Rept. Dec. 31, 1969*, ORNL-4520, pp. 7-16.

Table 15.1. (U,Pu)O<sub>2</sub> Pellets Fabricated for Irradiation Experiments

Reactor	Irradiation Capsule	Pellet Configuration	Density (% of theoretical)	Oxygen-to-Metal Ratio
ORR	GCFR P-9	Dished end, annular	91	1.98
ORR	SG-3	Annular	83	1.98
ETR	43-120 43-121	Solid	84	1.98
EBR-II	ORNL Series II 8 pins for 37-pin subassembly	Solid	83 88 93	1.94 1.94, 1.98 1.98
EBR-II	GGA G-1-G-8 <sup>a</sup>	Dished end, annular	91	1.98

<sup>a</sup>Irradiation experiment described in Chapter 36.

our process to produce pellets with various densities ranging from 80 to 95% of theoretical.

Low-density pellets (80 to 85%) have been made directly from powder calcined in argon or Ar-4% H<sub>2</sub> by taking advantage of the agglomerated nature of sol-gel material.<sup>7-9</sup> High-density pellets (93 to 95%) have been produced from powder that has been oxidized and reduced and then ball milled to break up the agglomerates.<sup>9</sup> Three different techniques have been used to make pellets in the intermediate density range (88 to 91%). One involved an oxidation-reduction calcination to partially break up the agglomerates.<sup>8</sup> The other two methods employed ball milling to break up the agglomerates so the powder would sinter to high-density pellets. The desired density was then obtained by sintering in a slightly oxidizing atmosphere to incorporate porosity in the structure<sup>9</sup> or by prepressing and granulating.<sup>10</sup> Other than density, the fuel specifications most difficult to meet have been sorbed gas content and oxygen-to-metal ratio. An extensive investigation of the source of sorbed gas led to a process change that has reduced the sorbed gas content to meet the specification (<0.05 cm<sup>3</sup>/g) routinely.<sup>7</sup> We sinter in Ar-4% H<sub>2</sub> and cool in argon to prevent hydrogen reabsorption. By monitoring the moisture in the effluent furnace gas, we have been able to achieve an oxygen-to-metal ratio of 1.98 in most cases.<sup>7,9</sup> We have not been able to achieve a ratio of 1.94 reproducibly in flowing Ar-4% H<sub>2</sub> but have in some batches obtained 1.94 to 1.95. Our inability to achieve the low ratio reproducibly appears to be due to residual moisture in the Al<sub>2</sub>O<sub>3</sub> tube furnace. We are continuing our efforts to find a technique for controlling this process. Another approach to obtaining low oxygen-to-metal ratio employs a titanium getter in static Ar-4% H<sub>2</sub>; however, this process is also difficult to control.<sup>11</sup>

#### Fuel Pin Fabrication

R. A. Bradley      W. J. Leonard  
M. K. Preston<sup>12</sup>    R. B. Pratt<sup>13</sup>

Fuel pins for irradiation testing in the ETR, ORR, and EBR-II were fabricated this year. Most of this effort was in making 19 unencapsulated pins for our EBR-II Series II experiments and in making eight fuel pins for irradiation capsules in conjunction with Gulf General Atomic (GGA) for testing GCBR conditions in the EBR-II. The fuel preparation for these pins is summarized above.

The ORNL EBR-II Series II fast flux irradiation test consists of irradiating 19 unencapsulated pins in a 37-pin subassembly shared with Babcock and Wilcox

Company. These pins use type 316 stainless steel cladding 0.250 in. OD × 0.015 in. wall and are about 40 in. long. The 13.5-in.-long fuel column, which is either pellets or Sphere-Pac, is nominally U<sub>0.8</sub>Pu<sub>0.2</sub>O<sub>2</sub> with an adjusted oxygen-to-metal ratio of either 1.98 or 1.94. The experiment is described later in this chapter under "Fast Flux Irradiation Tests." During this year we prepared the design, procured all necessary material, fabricated all component parts, and performed many detailed inspections required by our quality and process control procedures. For the first loading, seven Sphere-Pac and four pellet pins have been completed, with the remainder scheduled for completion in mid-July. Major development areas have been the gas content of the fuel, density control in pelletizations, homogeneity of plutonium in the spheres, obtaining 1.94 oxygen-to-metal ratio in the fuel, and xenon tagging of the fuel pins. More details of this fabrication effort are contained in the Fuels and Materials Development Program Quarterly Progress Reports.<sup>11,14-16</sup>

In cooperation with GGA eight fuel pins to test GCBR conditions in the EBR-II were fabricated. These fuel pins contain sol-gel U<sub>0.85</sub>Pu<sub>0.15</sub>O<sub>1.98</sub> encapsulated in type 316 stainless steel tubing 0.300 in. OD × 0.263 in. ID and consist of either four or five separate sections for charcoal traps, spider spacers, plenums, and fuel, all welded together. The fuel for these pins consisted of approximately 400 dished-end, 91%-dense annular pellets. The major problem in fabricating these

<sup>8</sup>R. A. Bradley, *Fuels and Materials Development Program Quart. Progr. Rept. Sept. 30, 1969*, ORNL-4480, pp. 6-8.

<sup>9</sup>R. A. Bradley, *Fuels and Materials Development Program Quart. Progr. Rept. March 31, 1970*, ORNL-4560, pp. 7-11.

<sup>10</sup>L. J. Ferrell, *Fabrication of Plutonia-Urania Pellet, Shard, and Sphere Irradiation Specimens*, BAW-3714-11, p. 13 (September 1969).

<sup>11</sup>R. A. Bradley, W. J. Leonard, T. B. Lindemer, R. B. Pratt, and W. H. Pechin, "Series II Unencapsulated Fuel Pins for Irradiation in the Experimental Breeder Reactor-II," *Fuels and Materials Development Program Quart. Progr. Rept. June 30, 1970*, ORNL-4600, in preparation.

<sup>12</sup>On loan from General Engineering Division.

<sup>13</sup>Present address: Autoclave Engineers, Inc., Erie, Pa. 16512.

<sup>14</sup>R. B. Pratt, M. K. Preston, and R. A. Bradley, *Fuels and Materials Development Program Quart. Progr. Rept. Sept. 30, 1969*, ORNL-4480, pp. 8-10.

<sup>15</sup>M. K. Preston and R. B. Pratt, *Fuels and Materials Development Program Quart. Progr. Rept. Dec. 31, 1969*, ORNL-4520, pp. 16-20.

<sup>16</sup>R. B. Pratt and R. A. Bradley, *Fuels and Materials Development Program Quart. Progr. Rept. March 31, 1970*, ORNL-4560, pp. 11-14.

fuel pins was meeting the extremely tight time schedule. The irradiation experiment is described in Chapter 36.

Two fuel pins of the ORR instrumented capsule SG-3 were fabricated without difficulty and sent to the Reactor Division for insertion into the irradiation capsule. Each pin was clad with  $\frac{3}{8}$ -in.-OD titanium-modified type 304 stainless steel and was loaded with either Sphere-Pac or pellet  $U_{0.8}Pu_{0.2}O_{2.0}$  with smear densities of 82% of theoretical. More details are reported elsewhere.<sup>17</sup>

For thermal-flux irradiation tests in the ETR, ten fuel pins were fabricated for the first of a series of instrumented capsules. These pins were clad with type 316 stainless steel 0.250 in. OD  $\times$  0.015 in. wall thickness and were approximately 8 in. long with 3-in. fueled sections. Five pins were loaded with pellets and five by the Sphere-Pac process. The densities of the pellets were  $84 \pm 1\%$  of theoretical, which is equivalent to a smear density of  $81 \pm 1\%$ . The smear density of the Sphere-Pac pins was 83 to 84%.

## CHARACTERIZATION OF (U,Pu)O<sub>2</sub> FUELS

W. H. Pechin

The preirradiation characterization of a fuel material is necessary for understanding the fabrication processes and for the interpretation of irradiation test results. Characterization includes both the examination of the fuel material as produced and the determination of basic properties of the fuel.

### Analytical Chemistry

W. H. Pechin R. A. Bradley W. J. Lackey

We have continued the investigation of the gravimetric determination of oxygen-to-metal ratio in (U,Pu)O<sub>2</sub>. A drying step that preceded the oxidation-reduction cycle of the analysis biased the results.<sup>18</sup> After the drying step was eliminated, the ratio determination was studied statistically.<sup>19</sup> The precision was

<sup>17</sup>R. B. Fitts, V. A. DeCarlo, K. R. Thoms, and D. R. Cuneo, *Fuels and Materials Development Program Quart. Progr. Rept. Dec. 31, 1969*, ORNL-4520, pp. 44–45.

<sup>18</sup>W. H. Pechin, W. J. Lackey, and R. A. Bradley, *Fuels and Materials Development Program Quart. Progr. Rept. March 31, 1970*, ORNL-4560, pp. 14–15.

<sup>19</sup>W. J. Lackey, R. A. Bradley, W. H. Pechin, and T. L. Hebble, "Precision and Source of Variation of Oxygen-to-Metal Analyses for (U,Pu)O<sub>2</sub>," *Fuels and Materials Development Program Quart. Progr. Rept. June 30, 1970*, ORNL-4600, in preparation.

satisfactory within a single day, but the day-to-day variation was unacceptable. However, the day-to-day variation was caused by certain "bad" days for which all results were biased in the same direction. Samples are now being submitted in a manner to detect large day-to-day variations. In addition, the analytical equipment has been changed to avoid several suspected sources of error.

## Homogeneity of (U,Pu)O<sub>2</sub>

W. J. Lackey R. A. Bradley W. H. Pechin

We have investigated three methods for determining the homogeneity of (U,Pu)O<sub>2</sub> with respect to Pu:U ratio.<sup>20</sup> The first method is alpha autoradiography. Figure 15.1 compares a photomicrograph and an alpha autoradiograph of the same field of view of a batch of (U,Pu)O<sub>2</sub> microspheres. The sphere-to-sphere variation in contrast in Fig. 15.1(b) is caused by variation in plutonium content. The Pu/(Pu + U) ratios in the numbered microspheres in Fig. 15.1, determined by electron microprobe analysis, are shown in Table 15.2. In addition, six microspheres from the same batch as the metallographic sample were analyzed by gamma ray spectroscopy and found to contain 13.2, 23.5, 2.7, 21.0, 21.0, and 25.1% Pu in the heavy metal. Thus, the three methods were in agreement as to the range of plutonium concentrations in this batch of microspheres.

## Gas Release from (U,Pu)O<sub>2</sub> Fuels

R. A. Bradley W. H. Pechin J. D. Sease

Gas release from the mixed oxide fuels was a major problem for us this year. Tentative fast reactor fuel specifications<sup>21</sup> require that the fuel release not more than 0.05 cm<sup>3</sup>/g of gas to vacuum at 1600°C. We found that the actual gas release figure could be as high as 1.0 to 2.0 cm<sup>3</sup>/g. Our first impression was that the gas released was due to water adsorbed by the fuel during storage.<sup>22</sup> A more careful examination showed that the gas was being adsorbed by the fuel during heat treatment, and the problem was eliminated by changing the furnace atmosphere from Ar–4% H<sub>2</sub> to argon at

<sup>20</sup>R. A. Bradley, R. S. Crouse, W. J. Lackey, and W. H. Pechin, *Fuels and Materials Development Program Quart. Progr. Rept. March 31, 1970*, ORNL-4560, pp. 15–22.

<sup>21</sup>C. A. Strand and C. A. Burgess, *Provisional Product Description No. PNL 35.0 UO<sub>2</sub>–PuO<sub>2</sub> Fuel Pellets*, PNL Report AA-0080-A (September 1968).

<sup>22</sup>W. H. Pechin, *Fuels and Materials Development Program Quart. Progr. Rept. Sept. 30, 1969*, ORNL-4480, pp. 11–15.

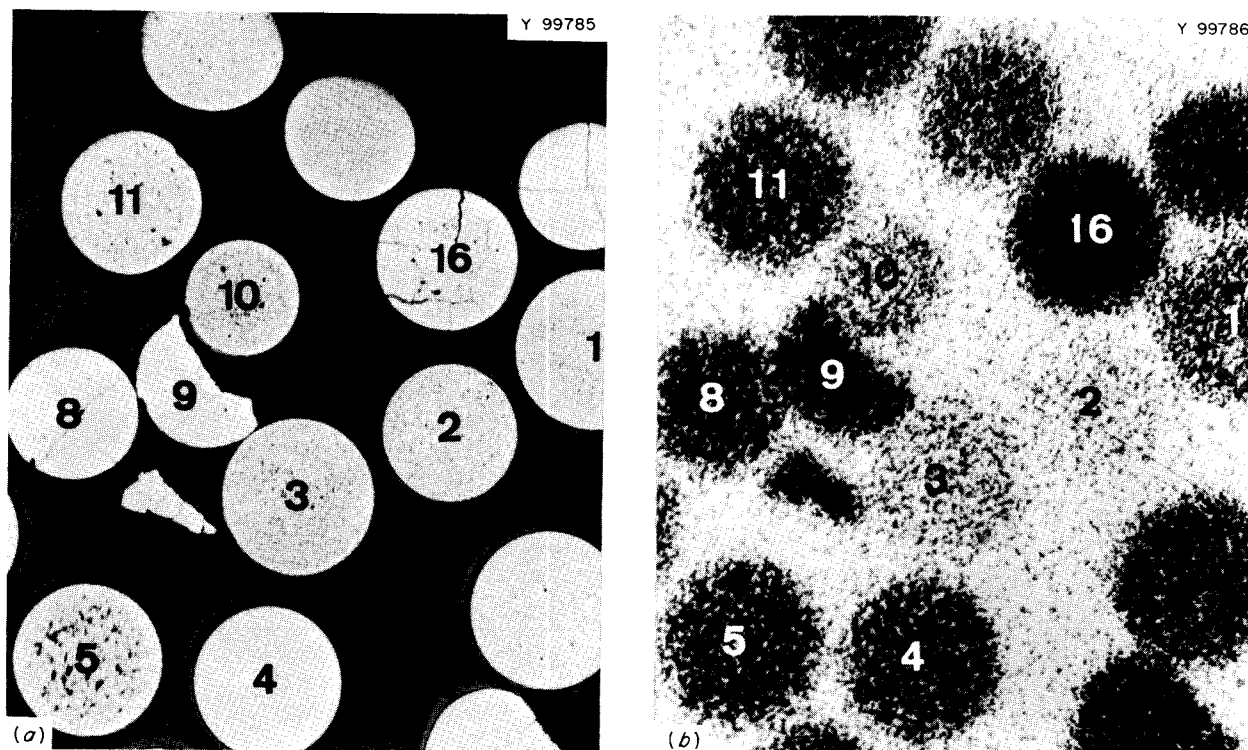


Fig. 15.1. Microspheres of  $U_{0.80}Pu_{0.20}O_2$ . 29X. (a) Photomicrograph. (b) Alpha autoradiograph of same field.

Table 15.2. Plutonium Content of Mixed Oxide Microspheres

Sphere <sup>a</sup>	Pu/(U + Pu) (at. %)
1	15.0
2	4.7
3	7.3
4	19.3
5	20.3
8	22.6
9	29.5
10	10.7
11	22.7
16	33.9
	Average 18.6

<sup>a</sup>In Fig. 15.1.

800°C while the pellets were cooling from the heat treating or sintering temperature.<sup>23</sup>

<sup>23</sup>R. A. Bradley and W. H. Pechin, *Fuels and Materials Development Program Quart. Progr. Rept. Dec. 31, 1969*, ORNL-4520, pp. 20-27.

### Microstructure of Unirradiated Sol-Gel $(U,Pu)O_2$

W. J. Lackey R. A. Bradley

Light and replica electron microscopy, alpha autoradiography, and electron microprobe analysis were used to characterize the microstructure of the sol-gel  $U_{0.8}Pu_{0.2}O_2$  fabricated for the ETR instrumented tests.<sup>24,25</sup> Briefly, all these tests showed the fuel to be of excellent quality. The fuel examined was in the form of coarse microspheres 420 to 597  $\mu m$  in diameter, fine microspheres less than 44  $\mu m$  in diameter, and a cold-pressed and sintered pellet. During fabrication all of the fuel was sintered at 1450°C for 4 hr or longer.

The density and grain size of the most dense coarse microspheres were 99.1% of theoretical and 3.2  $\mu m$  as determined from electron micrographs like that shown in Fig. 15.2. For the most porous coarse microsphere

<sup>24</sup>W. J. Lackey and R. A. Bradley, "Microstructure of Unirradiated  $(U,Pu)O_2$  Fuel for the ETR Instrumented Tests," *Fuels and Materials Development Program Quart. Progr. Rept. June 30, 1970*, ORNL-4600, in preparation.

<sup>25</sup>C. F. Sanders, "Instrumented ETR Tests," this chapter.

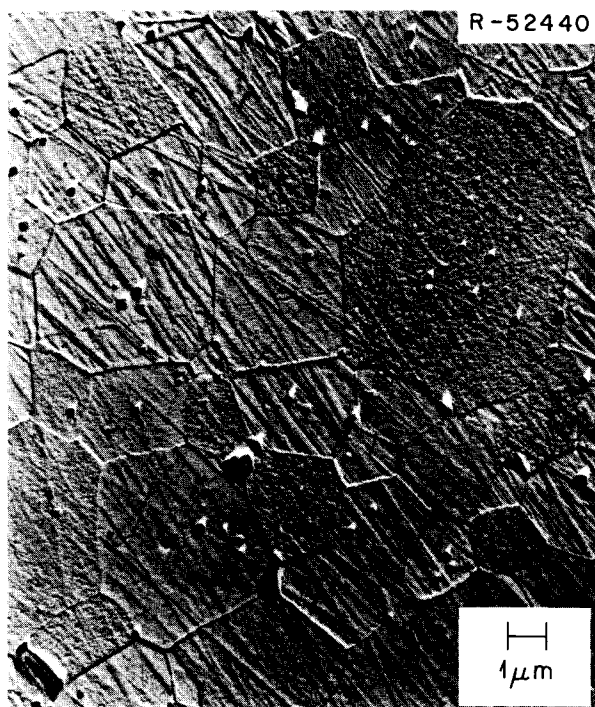


Fig. 15.2. Electron Micrograph of a Dense Coarse  $U_{0.8}Pu_{0.2}O_2$  Microsphere. Pores appear as dark areas and cast white shadows. 4800X.

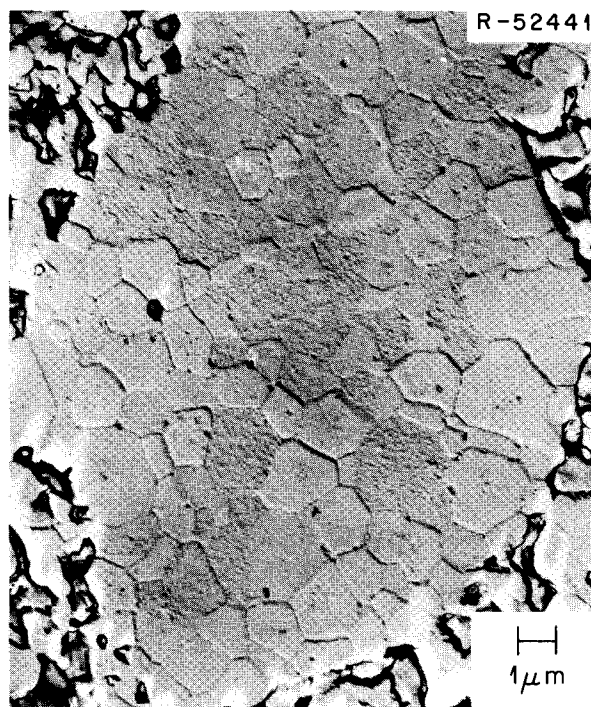


Fig. 15.3. Electron Micrograph of an 84%-Dense Sol-Gel  $U_{0.8}Pu_{0.2}O_2$  Pellet. A dense region and the porous matrix are shown. 3320X.

the corresponding values were 95.4% and 1.7  $\mu\text{m}$ . The pores were inside the grains in the dense microspheres but at grain boundaries in the porous spheres. The fine microspheres were very dense and had a grain size of  $1.2 \pm 0.2 \mu\text{m}$ . The microstructure of the pellets consisted of a very porous matrix with open porosity, regions of almost theoretical density dispersed throughout the matrix (Fig. 15.3), and regions with an intermediate amount of closed porosity. This triplex microstructure can be traced to the processes used to prepare powder for pelletizing.

#### Thermal Conductivity

D. L. McElroy J. P. Moore P. H. Spindler<sup>26</sup>

We constructed and tested a radial heat flow apparatus for thermal conductivity measurements to 10 atm and 1400°K on powders and solids. Glove boxes were obtained for this apparatus and for other equipment including an electrical resistivity apparatus, an absolute

heat flow apparatus, and a comparative heat flow apparatus. This equipment will be used on plutonium-bearing nuclear fuels to define their high-temperature thermal conductivity  $\lambda$ . The effect of infrared radiation conduction on  $\lambda$  of  $UO_2$  and  $(U,Pu)O_2$  is unknown at high temperatures. In fact high-temperature  $\lambda$  data do not exist on any material that demonstrates this effect. Consequently we obtained experimental confirmation of a large infrared effect in LiF. We derived and applied to LiF a computer calculation that uses spectral absorption measurements to describe properly infrared radiation conduction as a function of temperature.<sup>27</sup> This calculation requires knowledge of the absorption coefficient as a function of wavelength and temperature. Unfortunately this information is known for  $UO_2$  only at room temperature.<sup>28</sup>

<sup>27</sup>P. H. Spindler and J. P. Moore, *Fuels and Materials Development Program Quart. Progr. Rept. Dec. 31, 1969*, ORNL-4520, pp. 32–38.

<sup>28</sup>J. L. Bates, *Visible and Infrared Absorption Spectra of Uranium Dioxide*, HW-79033 (September 1963).

<sup>26</sup>Present address: Siemens Company, Munich, West Germany.

## IRRADIATION BEHAVIOR

C. M. Cox

We are conducting an irradiation test program to determine the in-reactor properties and performance of (U,Pu)O<sub>2</sub> fuels as functions of fabrication form, porosity distribution, stoichiometry, and irradiation conditions. This program includes both fast and thermal flux irradiations and both steady-state and transient power conditions. To obtain a fundamental understanding of the irradiation behavior of these fuels, we concentrate on well-characterized operating conditions, detailed postirradiation examinations, and analysis in terms of fuel performance models.

## Uninstrumented Thermal-Flux Irradiation Tests

A. R. Olsen D. R. Cuneo<sup>29</sup>

A series of uninstrumented capsules is being irradiated in the X-basket facilities of the ETR. Each capsule contains four test pins arranged in tandem. We first

<sup>29</sup>On loan from Reactor Chemistry Division.

sought the effects of fabrication form with extended burnup on the release of fission gas, migration of fission products, and fuel swelling. Some capsules are now being irradiated specifically to provide short-cooled irradiated fuel for LMFBR reprocessing studies. The status of the first ten capsules in this series is described in Table 15.3. The results of the three capsules irradiated to low burnup have been presented.<sup>30</sup>

Capsule 43-113 was removed from the reactor at a calculated burnup of 7% FIMA to obtain a neutron radiograph. All fuel pins were intact, and there was no evidence of fuel penetration of the ThO<sub>2</sub> insulators, which would indicate overpowering as reported for earlier capsules in this series.<sup>31</sup> The capsule was reinserted to complete its scheduled irradiation to 10% FIMA. This capsule has now reached 9.7% FIMA and will be removed for examination early next year.

<sup>30</sup>A. R. Olsen, C. M. Cox, and R. B. Fitts, *Trans. Am. Nucl. Soc.* 12(2), 605-6 (November 1969).

<sup>31</sup>A. R. Olsen, R. B. Fitts, J. Komatsu, and C. M. Cox, *Metals and Ceramics Div. Ann. Progr. Rept. June 30, 1969*, ORNL-4470, pp. 134-36.

Table 15.3. Noninstrumented Thermal Flux Tests of (U,Pu)O<sub>2</sub> Fuels

Experiment	Fuel		Number of Rods	Peak Burnup (% FIMA) <sup>a</sup>	Peak Linear Heat Rate (W/cm)	Peak Cladding Inner Surface Temperature (°C)	Status June 1970
	Form	Composition					
43-99	Sphere-Pac	<sup>235</sup> U <sub>0.80</sub> Pu <sub>0.20</sub> O <sub>2.00</sub>	2	1.5 <sup>b</sup>	1640 <sup>b</sup>	1000	Examined
43-100	Sphere-Pac	<sup>235</sup> U <sub>0.80</sub> Pu <sub>0.20</sub> O <sub>2.00</sub>	2	1.4 <sup>b</sup>	1470 <sup>b</sup>	900	Examined
43-103	Sphere-Pac	UO <sub>2.02</sub> (20% <sup>235</sup> U)	3	5	690	530	Examined
	Pellet	UO <sub>2.00</sub> (20% <sup>235</sup> U)	1				
43-112	Sphere-Pac	<sup>238</sup> U <sub>0.85</sub> Pu <sub>0.15</sub> O <sub>1.97</sub>	3	0.7	500	360	Examined
		UO <sub>2.02</sub> (20% <sup>235</sup> U)	1				
43-115	Sphere-Pac	<sup>238</sup> U <sub>0.85</sub> Pu <sub>0.15</sub> O <sub>1.97</sub>	3	10 <sup>c</sup>	500 <sup>c</sup>	380 <sup>c</sup>	In-reactor, ≈9.7% FIMA
		UO <sub>2.02</sub> (20% <sup>235</sup> U)	1				
43-115	Sphere-Pac	<sup>238</sup> U <sub>0.85</sub> Pu <sub>0.15</sub> O <sub>1.97</sub>	3	6.5	600	460	Examined
		UO <sub>2.02</sub> (20% <sup>235</sup> U)	1				
43-116	Sphere-Pac	<sup>238</sup> U <sub>0.85</sub> Pu <sub>0.15</sub> O <sub>1.97</sub>	4	1.5 <sup>c</sup>	600 <sup>c</sup>	460 <sup>c</sup>	Processed
43-117	FTR Pellets	<sup>238</sup> U <sub>0.75</sub> Pu <sub>0.25</sub> O <sub>1.98</sub>	4	1.5	430 <sup>c</sup>	360 <sup>c</sup>	In preparation
43-118	FTR Pellets	<sup>238</sup> U <sub>0.75</sub> Pu <sub>0.25</sub> O <sub>1.98</sub>	4	4.0	430 <sup>c</sup>	360 <sup>c</sup>	In preparation
43-119	FTR Pellets	<sup>238</sup> U <sub>0.75</sub> Pu <sub>0.25</sub> O <sub>1.98</sub>	4	8.0	430 <sup>c</sup>	360 <sup>c</sup>	In preparation
43-123	FTR Pellets	<sup>238</sup> U <sub>0.75</sub> Pu <sub>0.25</sub> O <sub>1.98</sub>	4	4.0	350 <sup>c</sup>	310 <sup>c</sup>	In preparation

<sup>a</sup>Fissions per initial actinide metal atom.

<sup>b</sup>Pins failed in reactor from overpowering.

<sup>c</sup>Target design values.

The routine postirradiation examination of all eight pins from capsules 43-103 and 43-115 was completed.<sup>32</sup> The data on these pins are given in Table 15.4. Both capsules operated with higher linear heat rates than expected because the fluxes in the test locations were 15 to 30% higher than advertised. This overpower led to some central fuel melting and redistribution of fuel for the center pins in each capsule. The postirradiation examination showed that the molten center did not persist during the entire irradiation. Concentric rings of varying fission product activity are normally associated with molten fuel.<sup>33,34</sup> The vague nature of the rings shown in the beta-gamma autoradiograph of Fig. 15.4 indicates that even the most overpowered pin had no molten fuel during the later stages of irradiation. Even these vague gamma activity differences could not be seen in the beta-gamma autoradiographs of the other seven pins.

One of the most striking features of the autoradiographs was the spherical islands of higher plutonium content in the cooler peripheral areas of the columnar grains of all three (U,Pu)O<sub>2</sub> pins, as shown in the alpha autoradiograph of Fig. 15.5. The appearance of the alpha autoradiographs supports the vaporization-condensation theory of restructuring without melting in the columnar grain growth region. The various modes of restructuring have been discussed in detail elsewhere.<sup>35</sup> Briefly, for the (U,Pu)O<sub>2</sub> fuels the vapor is more concentrated in uranium.<sup>36</sup> The movement of this vapor down the radial temperature gradient in the fuel leaves a higher concentration of plutonium near the central void and reduces the relative concentration of

plutonium in the condensing area near the columnar grain periphery. These variations are shown by the relative alpha activities in the postirradiation autoradiograph. The radiographs from these test pins also indicate that fuel homogenizes at the intermediate temperature near the central void. However, at the temperatures near the periphery of the columnar grains, even during 4000 hr of operation at power, the diffusion rates are too slow to homogenize the fuel in the large-diameter spheres with the surrounding condensate and fine microspheres. This phenomenon will be investigated more thoroughly with electron microscopy and microprobe analysis.

All hardware and fuel for capsules 43-117, 43-118, 43-119, and 43-123 are on hand. The capsule fabrication is approximately 50% complete, the performance and safety analyses have been finished, and irradiation will start during the first quarter of next fiscal year.

<sup>32</sup>A. R. Olsen, *Trans. Am Nucl. Soc.* 13(1), 32 (June 1970).

<sup>33</sup>J. A. L. Robertson *et al.*, *J. Nucl. Mater.* 7, 225-62 (1962).

<sup>34</sup>J. A. Christensen, *Stoichiometry Effects in Oxide Fuels - I. Power Rating Required for Melting and Oxygen Redistribution in Molten Center UO<sub>2±x</sub> Fuels*, BNWL-536 (December 1967).

<sup>35</sup>A. R. Olsen, R. B. Fitts, and J. Komatsu, *Fuels and Materials Development Program Quart. Progr. Rept. Sept. 30, 1968*, ORNL-4350, pp. 22-25.

<sup>36</sup>M. H. Rand and T. L. Markin, "Some Thermodynamic Aspects of (U,Pu)O<sub>2</sub> Solid Solutions and Their Use as Nuclear Fuels," pp. 637-50 in *Thermodynamics of Nuclear Materials, 1967*, International Atomic Energy Agency, Vienna, 1968.

Table 15.4. Fabrication and Operating Data for Intermediate Burnup Tests

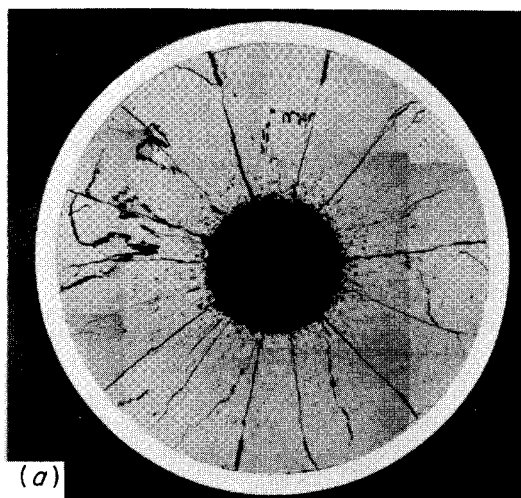
Test Pin	Smear Density (% of theoretical)	Fuel		Peak Linear Heat Rate <sup>b</sup> (W/cm)	Peak Cladding Inside Temperature (°C)	Fuel Center $\int_{400^{\circ}\text{C}} k dt$ (W/cm)	Peak Burnup (% FIMA)	Equivalent Full-Power Days	Fission Gas Release (% <sup>85</sup> Kr)
		Form <sup>a</sup>	Composition						
103-1	74	SP	UO <sub>2.02</sub>	540	380	34	4.2	126.3	30
103-2	84	P <sup>c</sup>	UO <sub>2.02</sub>	850	540	64	4.9	126.3	47
103-3	73	SP	UO <sub>2.02</sub>	710	470	44	5.5	126.3	44
103-4	74	SP	UO <sub>2.02</sub>	590	400	38	4.5	126.3	41
115-1	80	SP	U <sub>0.85</sub> Pu <sub>0.15</sub> O <sub>1.97</sub>	590	400	40	5.6	174.2	36
115-2	74	SP	UO <sub>2.02</sub>	560	390	31	5.9	174.2	47
115-3	82	SP	U <sub>0.85</sub> Pu <sub>0.15</sub> O <sub>1.97</sub>	680	460	46	6.5	174.2	44
115-4	81	SP	U <sub>0.85</sub> Pu <sub>0.15</sub> O <sub>1.97</sub>	440	370	32	4.2	174.2	38

<sup>a</sup>SP = Sphere-Pac; P = solid pellet.

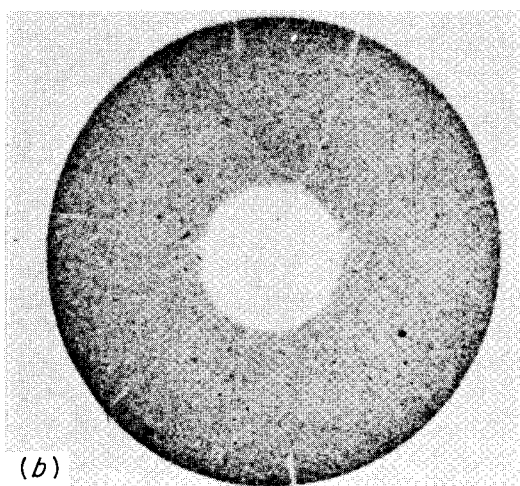
<sup>b</sup>Time averaged values based on the total exposure in equivalent full-power days.

<sup>c</sup>4-mil average cold diametral gap between fuel and cladding.

R-52146

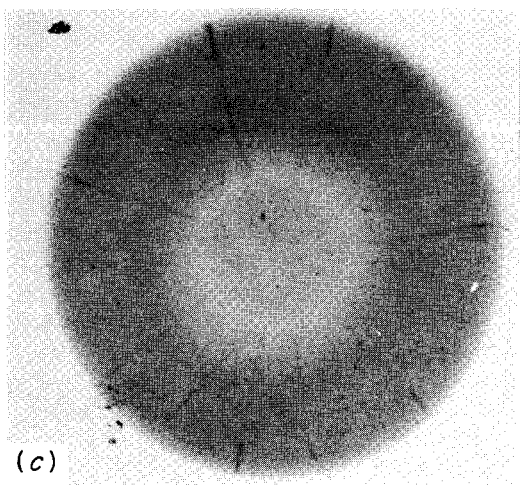


(a)



(b)

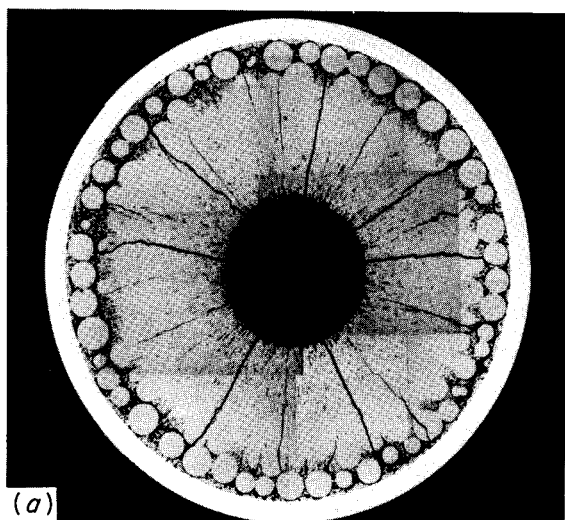
0.25 in.



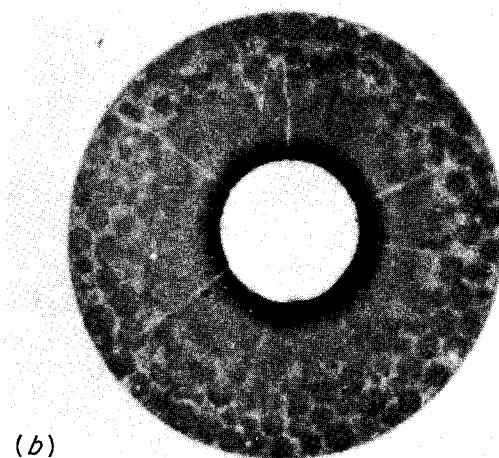
(c)

Fig. 15.4. Pelletized  $\text{UO}_2$  (20% Enriched) Irradiated at 850 W/cm to 4.9% FIMA. Smear density 84% of theoretical. (a) Photograph. (b) Alpha autoradiograph. (c) Beta-gamma autoradiograph.

R-52144

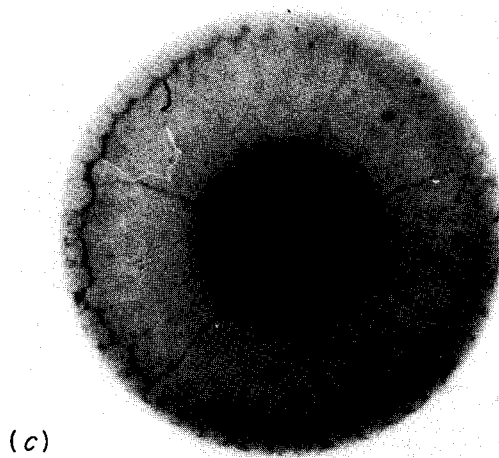


(a)



(b)

0.25 in.



(c)

Fig. 15.5. Sphere-Pac  $(\text{U}-15\% \text{Pu})\text{O}_{1.97}$  Irradiated at 460 W/cm to 4.2% FIMA. Smear density 81% of theoretical. (a) Photograph. (b) Alpha autoradiograph. (c) Beta-gamma autoradiograph.

Table 15.5. ETR Instrumented Oxide Fuel Pins

Pin	Smear Density (% of theoretical)	Oxygen-to-Metal Ratio	Heat Rate (W/cm)		Cladding Temperature (°C)	
			Design Peak	Measured <sup>a</sup>	Design Peak	Measured <sup>a</sup>
43-120-1	81.1	1.985	490	525	560	595
43-120-2	81.5	1.985	590	560	650	630
43-120-3	84.8	1.977	560	525	620	595
43-120-4	84.6	1.977	380	360	460	440
43-121-1	81.0	1.985	490	480	560	545
43-121-2	81.2	1.985	590	540	650	610
43-121-3	83.9	1.977	560	400	620	475
43-121-4	85.5	1.977	380	330	460	407

<sup>a</sup>June 16, 1970.

### Instrumented ETR Tests

C. F. Sanders

Two capsules containing cladding thermocouples have been fabricated and inserted in the Engineering Test Reactor (ETR). These capsules are designed to investigate sol-gel pellet and Sphere-Pac fuel swelling and fuel-cladding mechanical and chemical interaction under current peak LMFBR design operating conditions. These are simulated by a peak heat rate of 590 W/cm with cladding inside surface temperatures of 650°C. Each capsule contains four test pins arranged in tandem with two thermocouples in the NaK annulus located at the midplane of each of the four 3-in.-long fuel columns. Details of the capsule loading and operating conditions are given in Table 15.5. The capsules will be moved periodically during the planned exposures, 5% FIMA and 10% FIMA.

### ORR Instrumented Tests

R. B. Fitts V. A. DeCarlo<sup>37</sup> D. R. Cuneo<sup>38</sup>

The ORR instrumented capsule tests are being used to investigate the basic in-reactor characteristics of (U,Pu)O<sub>2</sub> fuels. Since a knowledge of the fuel temperatures is fundamental to the analysis and understanding of fuel behavior, the capsule has been designed<sup>39</sup> to monitor fuel-central and cladding-surface temperatures and fuel pin heat generation rates. The primary fuel properties to be investigated are the in-reactor thermal conductivity and the characteristic temperatures for fuel microstructural changes. With the first series of

capsules, we are examining these properties for sol-gel (U-20% Pu)O<sub>1.98</sub> Sphere-Pac<sup>40</sup> and pellet<sup>41</sup> fuels at a smear density of about 82%. The influence of such variables as fuel composition, stoichiometry, density, fabrication history, and burnup may be investigated later.

The results<sup>39</sup> of the first capsule in this series, SG-1, verified the capsule design and showed that the Sphere-Pac fuels had thermal characteristics similar to pellet fuels of the same overall density.

The second capsule, SG-2, contained two fuel pins of Sphere-Pac U<sub>0.80</sub>Pu<sub>0.20</sub>O<sub>1.98</sub> from the batch used in the first series of Transient Irradiation Tests (see below). This experiment was designed and operated<sup>42</sup> to study the thermal conductance and restructuring of the Sphere-Pac fuel below 1500°C. The test was terminated after operation at increasing power levels until the fuel central temperature reached the desired 1500°C. The measured fuel pin thermal conductance agreed with that from the first capsule and was within 10% of that predicted from pellet fuel thermal conductivity.<sup>43</sup> Postirradiation examination to correlate fuel structure and temperature is in progress.

<sup>40</sup>R. B. Fitts, A. R. Olsen, and J. Komatsu, "Sphere-Pac Fabrication of Sol-Gel Nuclear Fuels," *Am. Ceram. Soc. Bull.* 47, 844 (1968).

<sup>41</sup>R. A. Bradley, *Fuels and Materials Development Program Quart. Progr. Rept. Sept. 30, 1969*, ORNL-4480, pp. 6-8.

<sup>42</sup>R. B. Fitts, D. R. Cuneo, V. A. DeCarlo, and K. R. Thoms, *Fuels and Materials Development Program Quart. Progr. Rept. Sept. 30, 1969*, ORNL-4480, pp. 26-27.

<sup>43</sup>W. E. Baily *et al.*, "Thermal Conductivity of Uranium-Plutonium Oxide Fuels," pp. 293-308 in *Intern. Symp. Plutonium Fuels Technol., Scottsdale, Ariz., 1967*, *Nucl. Met.* 13, ed. by K. E. Horton, R. E. Macherrey, and R. J. Allio, American Institute of Mining, Metallurgical, and Petroleum Engineers, New York, 1968.

<sup>37</sup>Reactor Division.

<sup>38</sup>On loan from the Reactor Chemistry Division.

<sup>39</sup>R. B. Fitts and V. A. DeCarlo, *Metals and Ceramics Div. Ann. Progr. Rept. June 30, 1968*, ORNL-4370, pp. 145-49.

The third capsule in this series, SG-3, contained two  $U_{0.80}Pu_{0.20}O_{1.98}$  fuel pins at a smear density 82% of theoretical in the annulus between the inner fuel surface and the cladding. One pin was Sphere-Pac and the second contained 83.5%-dense sol-gel pellet fuel. This experiment was operated at fuel central temperatures up to  $2000^{\circ}C$  to directly compare the in-reactor thermal conductance and restructuring of pellet and Sphere-Pac fuels. The operating temperatures of the cladding, coolant, and fuel center line are shown as a function of heat generation in Fig. 15.6. Also shown is the predicted fuel center-line temperature based upon the measured cladding temperature and heat generation, a fuel-to-cladding gap conductance of  $1 W/cm^2$ , and the Baily *et al.* data correlation<sup>43</sup> for the thermal conductivity of  $(U,Pu)O_2$  pellet fuels of this smear density. The measured temperatures are within  $\pm 8\%$  of the predicted values. We feel that this is an insignificant difference in view of the accuracy obtainable with in-reactor instrumentation. For all practical purposes, pellet and Sphere-Pac fuels of this density exhibit identical thermal performance during in-reactor operation to low burnup.

Capsule SG-3 was removed from the ORR test facility after 1763 hr of operation and is being examined.

### Fast Flux Irradiation Tests

A. R. Olsen

The ORNL fuels irradiation program in the EBR-II currently involves two series of tests. During the past year the five encapsulated Series I pins, all containing Sphere-Pac ( $^{235}U-20\% Pu$ ) $O_2$ , were removed from the reactor. The initial irradiation period was extended so that a calculated peak burnup of 6.2% FIMA was achieved rather than the 4% FIMA reported last year.<sup>44</sup> The status of these pins is given in Table 15.6. Two of

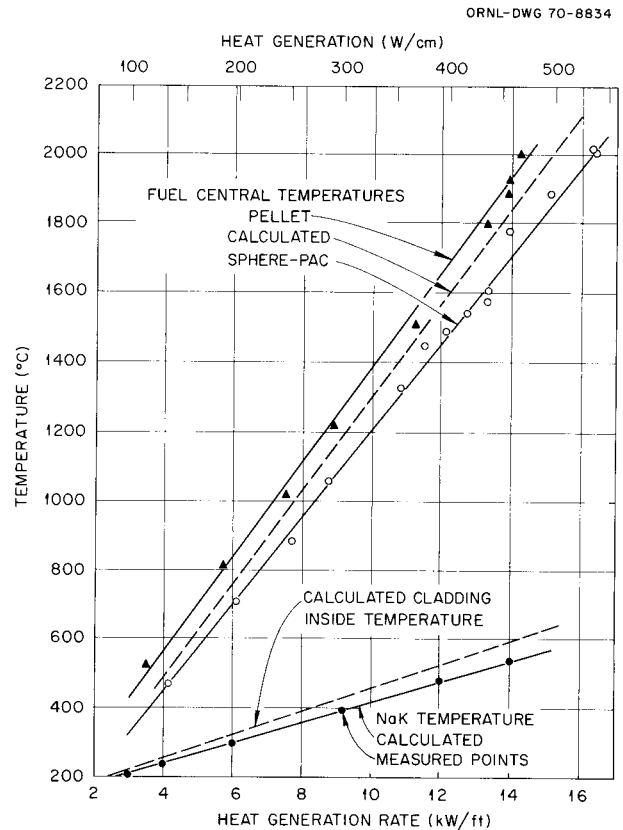


Fig. 15.6. Variation of Calculated and Measured Fuel and Capsule Temperatures with Heat Generation Rate in Capsule SG-3.

these pins will be returned to ORNL after neutron radiographs have been taken. The other three are scheduled to be reinserted in a new subassembly for continued irradiation to a peak burnup of 11.8% FIMA.

<sup>44</sup> A. R. Olsen and C. M. Cox, *Metals and Ceramics Div. Ann. Progr. Rept. June 30, 1969*, ORNL-4470, pp. 137-38.

Table 15.6. ORNL Series I Sphere-Pac  $U_{0.8}Pu_{0.2}O_{1.98}$  Capsules in EBR-II

Capsule Identity	Cladding Stainless Steel Type	Fuel Smear Density (% of theoretical)	Peak Linear <sup>a</sup> Heat Rate (W/cm)	Peak Cladding Inside Temperature ( $^{\circ}C$ )	Peak Burnup (% FIMA)	
					Current <sup>a</sup>	Target
S-1-A	304	83	400	500	4.6	4.6
S-1-B	304	86	490	580	5.6	5.6
S-1-C	316	83	490	580	6.2	11.8
S-1-D	316	80	460	540	5.7	11.8
S-1-E	316	82	460	540	5.6	11.8

<sup>a</sup>Calculated with EBR-II fission rates.

This additional burnup has been approved so that these pins can serve as lead experiments for the Series II tests.

The Series II tests are unencapsulated pins to be irradiated in a 37-pin subassembly to be shared with pins fabricated by Babcock and Wilcox Company. Both Sphere-Pac and pellet fuel derived from the sol-gel process are included in this ORNL test series. These tests have been coordinated with the Babcock and Wilcox Company tests to provide comparative tests of a variety of fuel forms, densities, and oxygen-to-metal ratios. A preliminary subassembly layout and reactor test location have been established. The preparation of a data package to define the total operating conditions and safety of the proposed subassembly has started and is scheduled for completion by August 1970.

#### Transient Irradiation Tests

C. M. Cox      D. R. Cuneo<sup>38</sup>  
E. J. Manthos   R. E. Adams

Six fuel pins containing unirradiated sol-gel  $U_{0.80}Pu_{0.20}O_2$  were subjected to power transients at the Transient Reactor Test Facility (TREAT). These experiments were aimed at establishing the behavior of sol-gel-derived (U,Pu) $O_2$  fuel pins during severe power transients that cause various amounts of fuel melting. No failures occurred even though 50 to 60% of the fuel melted in the peak power regions of two Sphere-Pac pins.

We tested two capsules, each containing three fuel pins in tandem. Each fuel pin had an 8-in.-long fuel column and was clad with 0.254-in.-OD  $\times$  0.016-in.-wall type 304 stainless steel tubing. The principal fuel variables were smear density (81 and 88% of theoretical) and fabrication form (pellets and Sphere-Pac). The fuel columns were partially restrained axially with a spring-loaded extensometer that allowed up to  $\frac{3}{16}$ -in. increase in fuel length. The first capsule, TR-1, was initially subjected to a calibration transient to verify the design techniques. The experiments were continued with test transients designed to melt about 25% of the 81%-dense fuel in the peak power region of the first capsule and 50% for the second capsule, TR-2. Table 15.7 briefly summarizes the results. More complete information has been reported on fabrication and operating data, postirradiation neutron radiography, profilometry, plenum gas analyses, and fuel burnup analyses.<sup>45-47</sup>

<sup>45</sup>E. J. Manthos and D. R. Cuneo, *Fuels and Materials Development Program Quart. Progr. Rept. Dec. 31, 1969*, ORNL-4520, pp. 45-50.

<sup>46</sup>C. M. Cox, E. J. Manthos, and D. R. Cuneo, *Fuels and Materials Development Program Quart. Progr. Rept. March 31, 1970*, ORNL-4560, pp. 30-34.

<sup>47</sup>C. M. Cox, E. J. Manthos, and D. R. Cuneo, "Transient Tests," *Fuels and Materials Development Program Quart. Progr. Rept. June 30, 1970*, ORNL-4600, in preparation.

Table 15.7. Transient Test Data

Fuel Pin	TR-1A	TR-1B	TR-1C	TR-2A	TR-2B	TR-2C
Fabrication Data						
Fuel fabrication form <sup>a</sup>	P	S	P	S	S	P
Fuel smear density, % of theoretical	88.9	80.9	79.7	82.0	80.9	80.2
Fuel-cladding diametral gap, mils	5		5			5
Transient Data						
Reactor integrated power, MWsec	140	140	140	487	487	487
Peak instantaneous linear power, kW/cm <sup>b</sup>	5.8	5.1	3.9	5.7	5.3	3.4
Energy release, cal/g <sup>b</sup>	390	375	291	518	487	316
Postirradiation Examination						
Cladding maximum ovality, max diam - min diam, mils <sup>c</sup>	<0.5	<0.5	1.5	<0.5	<0.5	1.8
Number of fuel column separations <sup>d</sup>	2	3	0	0	2	1
Total width of fuel column separations, mils <sup>d</sup>	140	160-250			120	60
Fuel column length decrease, mils <sup>d,e</sup>	50	180-270	30	60	150	20

<sup>a</sup>P = solid pellets; S = Sphere-Pac.

<sup>b</sup>At fuel column midplane.

<sup>c</sup>Maximum diametral increase < 0.5 mil.

<sup>d</sup>Based on neutron radiographs; estimated accuracy  $\pm 20$  mils.

<sup>e</sup>Corrected for fuel column separations.

Metallography was completed for the three fuel pins in capsule TR-2, and typical results are shown in Figs. 15.7 and 15.8. Figure 15.7 is a transverse cross section  $\frac{3}{4}$  in. below the fuel column midplane. We believe the columnar grains formed during cooling from a molten state that included about 50 vol % of the fuel at this cross section. The gap between fuel and cladding is formed by a combination of sintering and shrinkage during cooling from the melt. Figure 15.8 is a longitudinal section taken  $1\frac{1}{2}$  to  $2\frac{1}{2}$  in. above the fuel column midplane. In addition to the central void formed on restructuring, there are spherical surfaces from gas bubbles arising from the release of adsorbed gases. These bubbles apparently propagate both upward and downward.

The results indicate that unirradiated sol-gel Sphere-Pac and pellet (U,Pu)O<sub>2</sub> fuel pins behave similarly to axially unrestrained coprecipitated pellets of the same smear density during TREAT-type transients.<sup>48,49</sup> That is, the fuel pins can accommodate severe transients causing fuel volume melts of 50 to 60% without failing.

<sup>48</sup>J. E. Hanson, J. H. Field, and S. A. Rabin, *Experimental Studies of Transient Effects in Fast Reactor Fuels, Series II - Mixed Oxide (PuO<sub>2</sub>-UO<sub>2</sub>) Irradiations*, GEAP-4804 (June 1965).

<sup>49</sup>G. R. Thomas and J. H. Field, "Response of Axially Restrained Pellet Fuel to Transient Overpower," *Trans. Am. Nucl. Soc.* 10(2), 707-9 (1967).

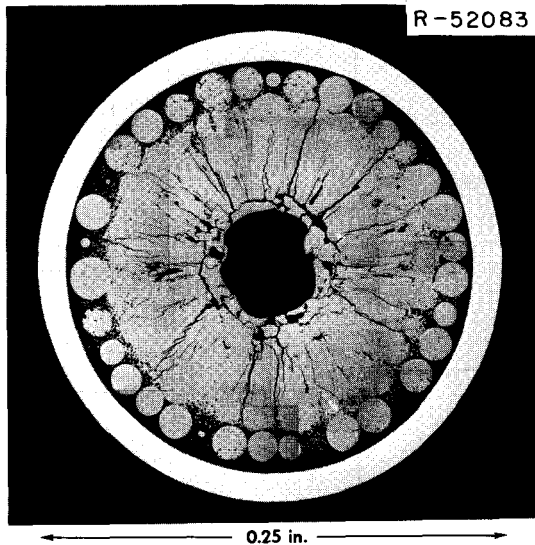


Fig. 15.7. Transverse Cross Section of Sphere-Pac Fuel Pin TR-2B.



Fig. 15.8. Longitudinal Section of Sphere-Pac Fuel Pin TR-2B.

### Fuel-Cladding Mechanical Interaction Tests

R. B. Fitts      J. G. Morgan<sup>50</sup>  
J.D. Jenkins<sup>37</sup>   R. L. Senn<sup>37</sup>

The first two power cycling capsules to test fuel-cladding mechanical interaction behavior will contain fuel pins designed to be prototypical of those to be used in the Fast Test Reactor (FTR). These tests will be conducted in the ORR poolside facility<sup>51</sup> where thermal conditions typical of fast reactor operation can be achieved.<sup>52</sup>

The first test capsule (MINT-1) will contain a fuel pin made from fuel and cladding material having nominal or average FTR dimensions and clearances. It will operate to about 2.5% FIMA at 330 W/cm and then at 525 W/cm to a peak burnup of about 7% FIMA. Superimposed on these heat rates will be a daily power transient and an occasional 20% overpower transient. The second experiment (MINT-2) will be operated to 5% burnup at nominally 525 W/cm with a small fuel-cladding gap and a 90% fuel smear density. This represents the upper density range of the FTR fuel element specifications.

From these experiments we expect an indication of whether it is practical to manage the FTR fuel by moving the peripheral fuel into the center of the core to obtain a higher average burnup. Also, with the second capsule we intend to aggravate mechanical interaction and hence to find out whether or not this is indeed a problem.

The design effort on MINT-1 is progressing satisfactorily. It is scheduled for reactor insertion during September or November 1970. The fuel pin is to be fabricated from mechanically blended  $U_{0.75}Pu_{0.25}O_{1.97}$  solid pellets having dished ends and a density  $89.4 \pm 0.5\%$  of theoretical. The cladding is 20%-cold-worked type 316 stainless steel. The fuel pin will be immersed in NaK, which is used as a heat transfer medium in the capsule. The capsule is instrumented with 12 thermocouples, a transducer to measure the internal pressure, and magnetic length-measuring devices to measure mechanical interaction between fuel and cladding.

The mechanical interaction irradiation tests will be used as one of the benchmark cases for the working

<sup>50</sup>Reactor Chemistry Division.

<sup>51</sup>D. B. Trauger, *Some Major Fuel Irradiation Test Facilities of the Oak Ridge National Laboratory*, ORNL-3574 (April 1968).

<sup>52</sup>C. M. Cox, R. B. Fitts, and A. R. Olsen, "Analysis of the Validity of Fast Reactor Fuel Tests in Existing Test Reactors," pp. 127-50 in *National Symposium on Developments in Irradiation Testing Technology*, CONF-690910 (September 1969).

group on LMFBR fuel element modeling (see Chapter 17). For the first round of calculations, steady-state operation of the MINT-2 capsule at the overpower heat rate of 620 W/cm will be assumed. The principal differences between operation of this fuel pin in the ORR and in an LMFBR are the low cladding flux,  $1.71 \times 10^{13}$  neutrons  $cm^{-2} sec^{-1}$  ( $>0.1$  MeV) at 10% FIMA, and the flux depression in the fuel. A very large power depression follows from the high  $^{239}Pu$  concentration in the 0.198-in.-diam, 92%-dense  $U_{0.75}Pu_{0.25}O_{1.98}$  fuel pellets. The temperature distribution in the MINT capsule, compared with that for the peak FTR fuel pins in Fig. 15.9, is reasonably prototypic of FTR conditions.

### Actinide Redistribution in Irradiated (U,Pu)O<sub>2</sub>

W. J. Lackey    J. L. Miller, Jr.    A. R. Olsen

In-reactor redistribution of uranium and plutonium is being studied<sup>53</sup> by electron microprobe analysis and

<sup>53</sup>W. J. Lackey and J. L. Miller, Jr., "Fuel Performance," *Fuels and Materials Development Program Quart. Progr. Rept. June 30, 1970*, ORNL-4600, in preparation.

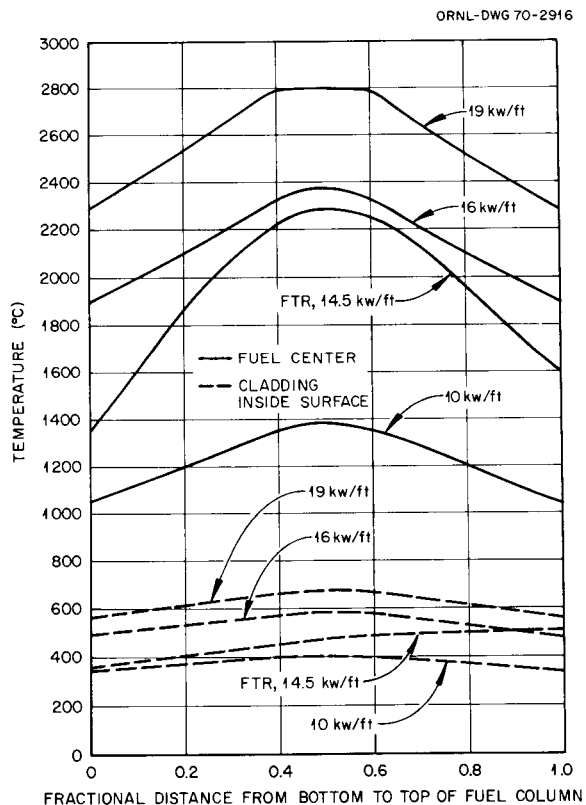


Fig. 15.9. Fuel Center-Line and Cladding Inside Surface Temperatures for 0.230-in.-OD Fuel Pins. The FTR fuel pin at 475 W/cm is compared with the MINT capsules at 330 to 620 W/cm.

alpha autoradiography because of its potential influence on the performance of  $(U,Pu)O_2$  fuels. The microprobe analysis was conducted by simultaneously determining the uranium and plutonium contents as functions of radial position on a transverse section of a Sphere-Pac  $U_{0.85}Pu_{0.15}O_2$  fuel pin previously irradiated in the ETR at a linear heat rate of 460 W/cm to 0.7% FIMA. Although the microprobe results are preliminary, two interesting trends are indicated. First, near the central void the ratio  $Pu/(U + Pu)$  increased to about 21%, compared to a preirradiation value of 15%. The second region of interest occurs near the interface between the columnar and equiaxed grains, where fuel had been

vapor deposited on the surface of the microspheres. Both electron microprobe analysis and alpha autoradiography indicate less plutonium in the deposited material than the preirradiation value. An alpha autoradiograph, shown in Fig. 15.5, of another Sphere-Pac pin, which received considerably higher burnup, revealed the initial location of the coarse microspheres in the cooler regions of the columnar grains as high-alpha-activity areas compared to the surrounding material. These observations appear to be in agreement with transport of a uranium-rich gas phase down the temperature gradient.

## 16. Advanced LMFBR Fuels Development

J. L. Scott    P. Patriarca

The goals of this program are to investigate the properties and behavior of those uranium- and plutonium-based ceramic fuels that we term conductors — such as the mononitrides, carbonitrides, and monocarbides — and to compare their potential as liquid-metal fast breeder reactor (LMFBR) fuel with that of (U,Pu)O<sub>2</sub>, which by comparison is an insulator. Since the thermal conductivity of the ceramic conductors is about ten times that of (U,Pu)O<sub>2</sub>, one could theoretically operate a conductor at ten times the power density with the same temperature at the center of the fuel. In practice, heat transfer limitations, thermal stresses in the cladding, and high rates of swelling at high temperatures limit the power density that can be achieved with conducting fuels to about two or three times that of (U,Pu)O<sub>2</sub> — still a challenging improvement. Additionally, the margins for transient overpower in the ceramic conductors are much higher than those for (U,Pu)O<sub>2</sub>.

We seek to provide the information necessary for evaluating the true potential of nitrides, carbonitrides, and carbides in comparison to each other and to mixed oxides. We need to define the structures, composition, and quality control required to achieve 150,000 MWd/metric ton at peak linear heat ratings of 30 to 50 kW/ft. We must also demonstrate the possibility of a low-cost fuel cycle for manufacturing fuel with the needed properties. Our work is oriented primarily toward demonstrating the irradiation performance of (U,Pu)N at high burnups and high heat ratings. Therefore, much of our effort is devoted to fabricating and characterizing fuel for irradiation testing.

Other work on nitride fuels is reported in Chapters 6 and 27.

### IRRADIATION TESTING

T. N. Washburn

The initial series of irradiation tests comprises two capsules (43-N1 and 43-N2) of four fuel pins each,

noninstrumented and conducted in the ETR. These tests are of the “screening” type to test the performance of (U,Pu)N fuel synthesized from metal.

The ratio of the fuel column length to pellet diameter ( $L/D$ ) is 10 or greater in the test. With this  $L/D$  we can use one-dimensional analyses for heat transfer and heat generation rate calculations. With  $L/D$  ratios significantly less than 10, the value of temperatures calculated from mathematical models becomes questionable. The fuel pins operate at a peak linear heat rating of 30 kW/ft to burnups of 30,000 and 60,000 MWd/metric ton.

The fuel is cold-pressed and sintered (U,Pu)N pellets with densities from 86 to 91% of theoretical. The fuel pin will have a 0.010-in. radial gap between the fuel pellet and inside surface of the type 316 stainless steel cladding. The gap will be filled with NaK-19 to enhance

Table 16.1. Design Parameters for Mixed Nitride Capsules 43-N1 and 43-N2

Fuel	U <sub>0.80</sub> Pu <sub>0.20</sub> N
Fuel diameter, in.	0.245
Fuel density, % of theoretical	85 to 90
Fuel length, in.	3
Cladding material	Type 316 stainless steel
Cladding diameter, in.	0.3
Cladding wall thickness, in.	0.0175
Fuel-to-cladding bond	NaK-19
Fuel-to-cladding gap, in.	0.010
Capsule material	Type 304 stainless steel
Capsule diameter, in.	0.501
Capsule wall thickness, in.	0.025
Instrumentation	None
Heat rating, kW/ft	30
Maximum burnup, % FIMA	3 and 6
Temperature, °C	
Fuel center	925
Fuel surface	610
Inner cladding	585
Outer cladding	495
Pins per capsule	4

heat transfer. These capsules are being fabricated and will be inserted in the ETR as soon as flux mapping of the position is completed. Design parameters are shown in Table 16.1.

We are designing an instrumented capsule for irradiation testing in the ETR. We are also designing an encapsulated pin capsule for testing in the EBR-II.

#### FABRICATION OF (U,Pu)N PELLETS

E. S. Bomar V. J. Tennery

Fabrication of (U,Pu)N from mechanical mixtures of UN and PuN powders results in a considerable cost savings in the synthesis and fabrication. We established a powder treatment procedure that permits prototype reactor fuel pellets to be sintered to densities approximately 90% of theoretical from mechanically mixed starting materials. The microstructure of a sintered specimen of  $U_{0.8}Pu_{0.2}N$  derived from mechanically mixed powders is shown in Fig. 16.1. This microstructure is identical with that of sintered pellets derived from nitride powders formed from uranium-plutonium alloy.

The mononitride phase exhibits cubic crystal symmetry. The lattice parameter was determined precisely for  $U_{0.8}Pu_{0.2}N$  specimens derived from both mechanically mixed powders and a uranium-plutonium alloy. That of the nitride derived from the alloy was  $a_0 = 4.89040 \pm 0.00035 \text{ \AA}$ , whereas that of the sample shown in Fig. 16.1 was  $a_0 = 4.89049 \pm 0.00020 \text{ \AA}$ . Therefore, these two materials are essentially identical.

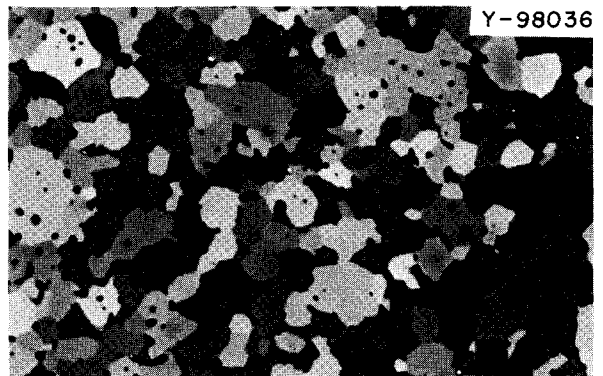


Fig. 16.1. Microstructure of  $U_{0.8}Pu_{0.2}N$  Fabricated From Mechanically Mixed UN and PuN Powders.

We completed a campaign to synthesize and fabricate the pellets required for loading capsules 43-N1 and 43-N2 for irradiation of mixed nitride fuel in the ETR. Five batches of the (U,Pu)N totaling about 400 g were made from uranium-plutonium alloy by successive hydriding and nitriding steps. We cold pressed and sintered 185 pellets weighing approximately 360 g in 13 lots. These will provide three pellets from each lot for chemical analysis, metallographic examination, x-ray diffraction, and archival purposes and 146 pellets for loading of irradiation pins. With an average pellet length of about 0.205 in., we have 29.93 in. of  $1/4$ -in.-diam fuel, sufficient for ten fuel pins.

Table 16.2. Sintering Results for  $U_{0.815}Pu_{0.185}N$  Pellets

Powder Code	Sintering Lot	Number of 2-g Pellets	Average Measured Values for Sintered <sup>a</sup> Pellets			
			Diameter (in.)	Height (in.)	Density (g/cm <sup>3</sup> )	(%) <sup>b</sup>
A-4-C	1	13	0.243	0.210	12.48	87.3
A-5-C	2	13	0.242	0.216	12.29	85.8
	3	13	0.242	0.215	12.25	85.8
	4	13	0.242	0.215	12.33	86.1
A-6-C	5	13	0.246	0.203	12.58	87.8
	6	13	0.247	0.204	12.49	87.2
	7	13	0.248	0.204	12.43	86.8
A-7-C	8	13	0.242	0.207	12.77	89.2
	9	13	0.242	0.206	12.91	90.2
	10	9	0.243	0.205	12.79	89.3
A-8-C	11	13	0.243	0.208	12.64	88.3
	12	13	0.242	0.210	12.62	88.1
	13	7	0.243	0.208	12.61	88.1

<sup>a</sup>Sintered in  $N_2$  176 min at  $2100^\circ C$ , then 15 min at  $2250^\circ C$ .

<sup>b</sup>Based on a theoretical density of  $14.32 \text{ g/cm}^3$ .

Dimensions and densities measured for 159 mixed nitride pellets containing 18.5 at. % Pu in the metal are summarized in Table 16.2. Since sintered density depends on powder batch, subsequent sintering behavior is related to some variation in the synthesis process. The A-5-C powder gave the least dense pellets and also showed less longitudinal shrinkage than the other powders. Pellets pressed from the A-6-C powder sintered more longitudinally and less transversely than did pellets made from four other powders.

Samples representative of the first five lots of pellets were found to be fine-grained and to have a single-phase microstructure. A partial chemical analysis of one pellet made from A-4-C powder showed 720 ppm O, 460 ppm C, and 100 ppm Fe. The iron content is essentially unchanged from that found in the uranium-plutonium alloy used to prepare the nitride powder.

### FABRICATION OF ADVANCED FUELS BY CARBOTHERMIC REDUCTION<sup>1</sup>

T. B. Lindemer

Considerable effort has been expended to synthesize the carbides, nitrides, and carbonitrides of uranium, plutonium, and their solid solutions by the carbothermic reduction of oxide-carbon mixtures produced by the sol-gel process. This process appears to be economically attractive compared with our present process. Many factors affect the time required to accomplish the synthesis by carbothermic reduction. These factors are directly related to the thermodynamics of the reactions, the diffusional mechanisms in the system, and the particular processes used for the conversion.

A fundamental approach was taken to the analysis of a fluidized-bed process for the carbothermic conversion of oxides. First, the quite dissimilar techniques used by Lindemer *et al.*,<sup>2</sup> and Ainsley *et al.*<sup>3</sup> gave a consistent prediction for the diffusion-controlled reaction of  $\text{UO}_2$  with carbon. Second, a derivation was made to predict the conditions for control of the carbothermic process by the rate of removal of carbon monoxide. Third,

<sup>1</sup>Abstracted from "Factors that Control the Carbothermic Reduction of Fuels," pp. 423-33 in *Symposium on Sol-Gel Processes and Reactor Fuel Cycles*, Gatlinburg, Tennessee, May 4-7, 1970, CONF-700502.

<sup>2</sup>T. B. Lindemer, M. D. Allen, and J. M. Leitnaker, *J. Am. Ceram. Soc.* 52, 233-37 (1969).

<sup>3</sup>R. Ainsley *et al.*, pp. 349-76 in *New Nuclear Materials Including Non-Metallic Fuels*, vol. 1, International Atomic Energy Agency, Vienna, 1963.

these developments were used to analyze the conversion parameters studied by Holmes *et al.*<sup>4</sup> to show how the operation of a fluidized bed could be optimized.

### CHARACTERIZATION OF (U,Pu)N

E. S. Bomar V. J. Tennery J. P. DeLuca

#### Process for Producing Metal-Free Nitride Powders from Uranium-Plutonium Alloy

While developing techniques for producing pellets of  $\text{U}_{0.80}\text{Pu}_{0.20}\text{N}$  for irradiation studies we observed that considerable care must be exercised in making metal-free nitride powders from arc-melted alloy. The powders were produced by the hydride-dehydride-nitride process. We established that the tube furnaces being used for making these powders required at least three hydride-dehydride-nitride cycles. Employment of fewer cycles led to the presence in the powders of free metal, which was not evident by x-ray powder diffraction but was evident in the microstructure and x-ray diffraction patterns of pellets sintered from these powders.

Apparently incomplete nitriding of the metal particles generated by the hydriding reactions leads to powders consisting of metal cores surrounded by nominal  $\text{U}_{0.80}\text{Pu}_{0.20}\text{N}$ , and the nitride screens the cores from the x-ray beam and thus prevents detection of the metal phases.

#### The X-Ray Lattice Parameter of $\text{U}_{0.81}\text{Pu}_{0.19}\text{N}$ Pellets

Considerable data are now being accumulated on the precision lattice parameter observed in specimens being prepared for use in irradiation experiments. The irradiation specimens have all been prepared from the same lot of uranium-plutonium alloy, and we have documented the compositions of the sintered nitride pellets by chemical analysis. Some of the lattice parameters observed for various specimens are given in Table 16.3. The age of the samples from the time they were last at high temperature until the x-ray pattern was run varied from 39 days for sample 5 to 48 days for sample 1; thus any radiation damage effects (from plutonium alpha-particles) should be essentially the same for all samples. The parameter of a sample made from a mechanical mixture of UN and PuN is also given for comparison.

<sup>4</sup>J. T. Holmes *et al.*, *A High-Temperature, Fluidized-Bed Process for Converting Uranium Dioxide to Uranium Monocarbide*, ANL-7482 (November 1968).

Table 16.3. Lattice Parameter of  $U_{0.81}Pu_{0.19}N$  Samples

Sintering Run	Powder Lot	Age of Sample <sup>a</sup> (days)	$a_0$ , Lattice Parameter (Å)
1	A-4-C	48	$4.89093 \pm 0.00034$
2	A-5-C	42	$4.89095 \pm 0.00032$
3	A-5-C	43	$4.89149 \pm 0.00033$
4	A-5-C	42	$4.89086 \pm 0.00037$
5	A-6-C	39	$4.89103 \pm 0.00026$
M1 <sup>b</sup>		55	$4.89049 \pm 0.00020$

<sup>a</sup>Time since last at sintering temperature.

<sup>b</sup>Specimen made from mechanically mixed UN and PuN.

The values in Table 16.3 are lower than the value of  $a_0 = 4.8930$  Å published by Anselin<sup>5</sup> for synthesized powders and considerably lower than the value of  $a_0 = 4.8960$  Å given by Anselin for  $U_{0.80}Pu_{0.20}N$  sintered at 1650°C. The reason for Anselin's values being higher than those given in Table 16.3 is probably that his specimens were contaminated with oxygen or some other impurity. The explanation of these differences is now being determined.

#### Chemical Analysis Results for Specimens of $U_{0.81}Pu_{0.19}N$

Considerable effort has been expended in resolving the problems associated with the various techniques required to produce reliable routine quantitative analyses of the major elements in sintered pellets of (U,Pu)N. Coulometric methods have now been developed to determine the uranium and plutonium concentrations to about  $\pm 0.3$  and  $\pm 0.7\%$ , respectively. The nitrogen content when determined by the Kjeldahl method presently gives results having a scatter band of about  $\pm 2\%$  of the nitrogen present for an average of three determinations, and the results generally are slightly below the expected theoretical value. The oxygen results obtained by inert-gas fusion usually provide a scatter band of about  $\pm 30\%$  of the average value for three analyses on a given sample containing 500 to 800 ppm O.

Analytical results obtained on two typical pellets of (U,Pu)N made from a uranium-plutonium alloy source were transformed into molecular compositions and are given in Table 16.4. The compositions were computed two ways. One method assumes that the theoretical

Table 16.4. Molecular Compositions of Nominal  $U_{0.80}Pu_{0.20}N$  Specimens Calculated from Analytical Results

Specimen	Calculation Basis	Molar Composition
S-147	Mol. wt = 252.2 <sup>a</sup>	$U_{0.806}Pu_{0.193}N_{0.993}$
	Per atom N	$U_{0.809}Pu_{0.194}N$
S-153	Mol. wt = 252.2 <sup>a</sup>	$U_{0.806}Pu_{0.196}N_{0.986}$
	Per atom N	$U_{0.815}Pu_{0.198}N$

<sup>a</sup>Molecular weight = 252.2 g when U is <sup>238</sup>U, Pu is <sup>239</sup>Pu, and N is <sup>14</sup>N.

molecular weight of 252.2 g is applicable, in the other the mole ratios of the elements present are computed, and then the atom fractions are normalized relative to the nitrogen. In both methods the oxygen and carbon contents of 0.1% were assumed to be nitrogen for calculation. Total mass balances between 99.85 and 100.05% are typical for the analysis of a given sample.

#### COMPATIBILITY OF CLADDING WITH NITRIDE FUELS

J. P. DeLuca K. E. Spear<sup>6</sup> J. M. Leitnaker

The compatibility of nitride fuels with candidate cladding alloys must be thoroughly investigated and understood if these fuel materials are to be considered seriously for use in LMFBR systems. The problem is complicated because of the several multicomponent cladding alloys under consideration and the important effects of burnup on the composition, constitution, and nitrogen activity of the fuel. Our approach is to investigate systematically the thermodynamics and kinetics of those interactions that are pertinent to the compatibility problem. Such interactions involve components of the fuel and cladding.

#### Tailoring Nitride Fuels<sup>7</sup>

J. M. Leitnaker K. E. Spear<sup>6</sup>

Nitride nuclear fuels increase in nitrogen activity during operation in a reactor. This increase during

<sup>6</sup>Present address, Department of Materials Science, Pennsylvania State University.

<sup>7</sup>Based on *Stabilized Uranium or Uranium-Plutonium Nitride Fuel and Nitrogen Buffer for Nitride Reactor Fuels*, patents applied for.

<sup>5</sup>F. Anselin, *Preparation and Study of the Nitrides and Mixed Carbide-Nitrides of Uranium and Plutonium*, CEA-R-2988 (June 1966).

burnup has been reported previously<sup>8</sup> and occurs because not enough of the fission products form nitrides that are more stable than (U,Pu)N or (U,Pu)<sub>2</sub>N<sub>3</sub>. This nitrogen may embrittle the cladding material and cause other compatibility problems. We have discovered two methods for providing a nitrogen sink for nitride fuels. Fuels are chemically tailored so that they can add excess nitrogen and still maintain a nitrogen pressure below that needed for nitriding the chromium in stainless steel. We previously reported one method, the stabilization of nitride fuels by oxygen.<sup>9</sup> Excess nitrogen in this fuel forms an as-yet uncharacterized phase containing the fuel metals and both nitrogen and oxygen. Uranium nitride fuels may be tailored with additions of vanadium, chromium, or V<sub>2</sub>N. Fuels containing vanadium take up excess nitrogen by forming first V<sub>2</sub>N and then newly discovered UVN<sub>2</sub>. Fuels containing chromium take up excess nitrogen by forming another new nitride, UCrN<sub>2±x</sub>. Similarly tailored (U,Pu)N fuels probably take up excess nitrogen by forming (U,Pu)VN<sub>2</sub> or (U,Pu)CrN<sub>2±x</sub>.

### Thermodynamic Studies

K. E. Spear<sup>6</sup> J. M. Leitnaker

The thermodynamic properties of advanced LMFBR fuels are studied on a continuing basis to help define and solve problems that might arise in advanced concepts of space and civilian power breeder reactor systems. Thermodynamic analyses of questions concerning stability at high temperatures and compatibility with cladding alloys not only guide the experimental program but also help interpret experimental results.

#### The Lattice Parameter of U(C,N) as a Function of Composition<sup>10</sup>

J. M. Leitnaker K. E. Spear<sup>6</sup>  
R. A. Potter W. R. Laing<sup>11</sup>

The UC-UN solid solution shows significant variation from Vegard's law. The single-phase region is narrow. The equation

$$N/(N + C) = 1.00 - 12.6057 (a_0 - 4.8892) \\ + 55.8264 (a_0 - 4.8892)^2 - 3.38174 \\ \times 10^2 (a_0 - 4.8892)^3 - 1.04432 \\ \times 10^4 (a_0 - 4.8892)^4,$$

where  $a_0$  is in angstroms, best expresses the relationship between lattice parameter and mole fraction.

To obtain these results, equilibrium was approached from two directions, and two sides of the single-phase solid solution region have been examined. Obtaining true equilibrium between UC and N<sub>2</sub> was very difficult even at temperatures as high as 1900°C. The lack of complete equilibrium is probably responsible for much of the scatter in lattice parameter versus composition data for U(C,N) in the literature. We carefully characterized the samples chemically.

### Phase Behavior of the U-V-N System and Properties of UVN<sub>2</sub> (Ref. 12)

K. E. Spear<sup>6</sup> J. M. Leitnaker

The phase behavior of the ternary U-V-N system was investigated by annealing ternary compositions at constant temperatures from 1400 to 2000°C and constant pressures from vacuum to 650 torr N<sub>2</sub>. The products were examined by x-ray diffraction, and the equilibrium tie lines in the ternary system were established. Qualitative data indicated that ternary solid solubilities were small. A ternary phase UVN<sub>2</sub> was discovered and found to be isomorphous with UMoC<sub>2</sub> by x-ray powder diffraction data and intensity calculations. The ternary compound appears to be stable with respect to decomposition to the binary nitrides over the entire temperature range studied. Thermodynamic properties of UVN<sub>2</sub> were calculated with the use of reactions deduced from the ternary phase behavior.

### Phase Behavior of the U-V-C System and the Thermodynamic Properties and Crystal Structure of UVC<sub>2</sub> (Ref. 13)

K. E. Spear<sup>6</sup> J. M. Leitnaker T. B. Lindemer

The solid-state phase behavior and melting characteristics of the ternary U-V-C system were investigated by x-ray and metallographic techniques. The equilibrium tie lines were established; the lattice parameter indicated that ternary solid solubilities involving UC and VC were slight. The existence of a ternary phase

<sup>8</sup>K. E. Spear and J. M. Leitnaker, *Metals and Ceramics Div. Ann. Progr. Rept. June 30, 1969*, ORNL-4470, p. 81.

<sup>9</sup>K. E. Spear and J. M. Leitnaker, *Metals and Ceramics Div. Ann. Progr. Rept. June 30, 1969*, ORNL-4470, p. 80.

<sup>10</sup>Abstracted from *High Temp. Sci.* **1**, 389-400 (1969).

<sup>11</sup>Analytical Chemistry Division.

<sup>12</sup>Abstracted from paper submitted for publication to *High Temperature Science*.

<sup>13</sup>Abstracted from paper accepted for publication in *High Temperature Science*.

UVC<sub>2</sub> was confirmed, and it was determined to be isomorphous with UMoC<sub>2</sub> by x-ray powder diffraction data and intensity calculations. The ternary compound is unstable with respect to the binary phases above 1900 ± 100°C. The decomposition reaction and ternary reactions at lower temperatures were used to determine the free energy, enthalpy, and entropy of formation of UVC<sub>2</sub>.

#### Phase Investigations in the U-Cr-N System<sup>1 2</sup>

K. E. Spear<sup>6</sup> J. M. Leitnaker

A portion of the U-Cr-N system was studied as part of a program for investigating the chemical and thermodynamic properties of systems of interest for nuclear reactors. We determined a tentative ternary phase diagram for 1600°C and 1 atm, and we obtained x-ray diffraction data for a new ternary compound UC<sub>r</sub>N<sub>2±x</sub>. This ternary compound can exist in equilibrium with both chromium and Cr<sub>2</sub>N. The crystal symmetry or the structure of the ternary phase was not established; however, its diffraction pattern is not similar to that for UVC<sub>2</sub> (see above).

#### Equilibrium Investigations of Carbon-Rich V(C,N) Solutions<sup>1 4</sup>

K. E. Spear<sup>6</sup> J. M. Leitnaker

Relationships of temperature, pressure, lattice constant, and composition are reported for V(C,N) solutions in equilibrium with carbon and nitrogen. In accordance with previous results, the lattice constant depended on starting material; we attribute this to the formation of a thermodynamically active form of carbon as a product of the reaction of VC with nitrogen to form carbonitride solutions. The molar ratio of (N + C)/V is constant at 0.89 ± 0.02 for N/(N + C) ratios less than about 0.2 and increases to a value of 1 at the VN boundary. Superstructure lines similar to those caused by the ordering of carbon vacancies in the carbon-rich monocarbide were observed in diffraction patterns of carbonitrides with N/(N + C) ratios less than 0.1.

#### Thermodynamic Investigations in the Uranium-Plutonium-Nitrogen System

J. P. DeLuca J. M. Leitnaker

As a part of our study of the compatibility of mixed nitride fuels a system was built for measuring nitrogen pressures over nitrides that contain plutonium. We are trying to define the factors that affect fuel performance and behavior toward cladding materials. The system constructed is similar to one described by Inouye and Leitnaker,<sup>15</sup> except that extensive modifications were

necessary to safely contain the plutonium. The heater is made of tungsten mesh, and the crucible is suspended inside it from a Cahn microbalance. Also included in the system is a residual gas analyzer.

#### THERMAL CONTACT RESISTANCE

R. K. Williams

Thermal contact resistance ( $R_c$ ) associated with fuel-cladding interfaces is an important quantity for design of advanced LMFBR fuel elements. Our studies of UN-metal interfaces have shown that many factors can influence the portion of  $R_c$  due to heat flow across solid-solid contacts. The effects of most of the variables can be described by a modified form of a correlation proposed by Tien:<sup>1 6</sup>

$$R_c = A\gamma(B + H)/\lambda_h m^n \sigma,$$

where

$A$ ,  $B$ , and  $n$  are constants,

$\gamma$  is rms surface roughness,

$H$  is hardness of softer interface material,

$$\lambda_h^{-1} = \sum \lambda_i^{-1} / N,$$

$\lambda_i$  = thermal conductivity of  $i$ th material,

$N$  = number of materials,

$\sigma$  = compressive stress,

$m$  = rms slope as defined by Tien.<sup>1 6</sup>

Surface effects are contained in the factor  $\gamma/m^n$ , which is related to both the surface roughness and the distances between surface asperities. This factor shows that  $R_c$  depends on both the height of the asperities and the number of asperities per unit area. Short-term surface deformation characteristics are described by the dimensionless quantity  $(B + H)/\sigma$ , but long-term (creep) effects were also found to be important for some softer materials such as copper and aluminum. Finally, the variation of the thermal resistance of individual contacts is given by the factor of  $\lambda_h$ . Data for the UN-metal interfaces indicate that stress and surface topography changes can produce larger  $R_c$  reductions than alteration of the material properties,  $\lambda$  and  $H$ .

<sup>1 4</sup> Abstracted from *High Temp. Sci.* 1, 401–11 (1969).

<sup>1 5</sup> H. Inouye and J. M. Leitnaker, "Equilibrium Nitrogen Pressures and Thermodynamic Properties of UN," *J. Am. Ceram. Soc.* 51, 6–9 (1968).

<sup>1 6</sup> C. L. Tien, "A Correlation for Thermal Contact Conductance of Nominally Flat Surfaces in Vacuum," pp. 755–60 in *Thermal Conductivity, Proceedings of the Seventh Conference*, ed. D. R. Flynn and B. A. Peary, Jr., N.B.S. Special Publication 302, September 1968.

## 17. LMFBR Fuel Element Design and Model Development

C. M. Cox    A. L. Lotts    P. Patriarca

We are developing analytical methods for predicting and evaluating the performance of LMFBR fuel pins and fuel elements. This work is closely coordinated with the related fuel and cladding development programs, providing methods for designing and systematically evaluating irradiation tests, determining the influences of materials properties on fuel element performance, and identifying specific areas in which experimental research needs to be intensified.

The program is divided into three areas: model integration, fuel performance, and cladding performance. The fuel and cladding performance tasks are oriented toward mathematical description of the various phenomena of the fuel and cladding under irradiation such as swelling, gas formation, and mechanical, thermal, and chemical behavior. These individual models are incorporated into a generalized computer program that simulates the performance of an operating fuel pin. The program is oriented to emphasize fission gas behavior and fuel-cladding mechanical interactions.

### MODEL INTEGRATION

F. J. Homan

The FMØDEL computer code was sufficiently completed to perform calculations. Included are models for fuel swelling, fission gas formation and release, and cladding mechanics. The code can calculate temperature distributions and cladding stress-strain distributions as functions of axial position and elapsed time. At present the code covers essentially only steady-state operation but is being modified to apply to power cycling.

The code has been in continual use during its development.<sup>1,2</sup> It is being continually improved as additional phenomenological models are added and existing models are updated and improved.

FMØDEL is composed of essentially three main units — heat transfer, cladding mechanics, and fuel perform-

ance. These three components have been separated to provide simplified design tools for use in planning irradiation experiments. Of course the integrated model is still available for more sophisticated work but requires much more computer time and input effort.

### FUEL PERFORMANCE

C. M. Cox

This aspect of the modeling effort is concerned with describing fuel behavior during irradiation. Of particular importance are fission gas formation and release, swelling, porosity changes, grain growth, and chemical changes. The sections below contain some of the recent work aimed at providing better models of these phenomena for use in the FMØDEL code.

### Electron Microscopy and Electron Microprobe Analysis

W. J. Lackey

Light and electron microscopy and electron microprobe analyses of irradiated (U,Pu)O<sub>2</sub> are being conducted to improve our knowledge of fuel swelling, fission gas release, actinide and fission product redistribution, and restructuring. A Sphere-Pac U<sub>0.85</sub>Pu<sub>0.15</sub>O<sub>2</sub> fuel pin, 43-112-3, was extensively examined by light and electron microscopy.<sup>3</sup> Numerous fission gas bubbles (Fig. 17.1) were observed at columnar grain boundaries. Occasionally, fission gas bubbles 0.1 and 0.2 μm in diameter were observed at equiaxed

<sup>1</sup>C. M. Cox and F. J. Homan, *Trans. Am. Nucl. Soc.* 12(2), 536–37 (November 1969).

<sup>2</sup>A. R. Olsen and F. J. Homan, *Experiment Description and Hazards Evaluation for the Series I ORNL Oxide Fuels Irradiation in EBR-II*, ORNL-TM-2635 (Supplement) (June 1970).

<sup>3</sup>W. J. Lackey, *Fuels and Materials Development Program Quart. Progr. Rept. March 31, 1970*, ORNL-4560, pp. 71–74.

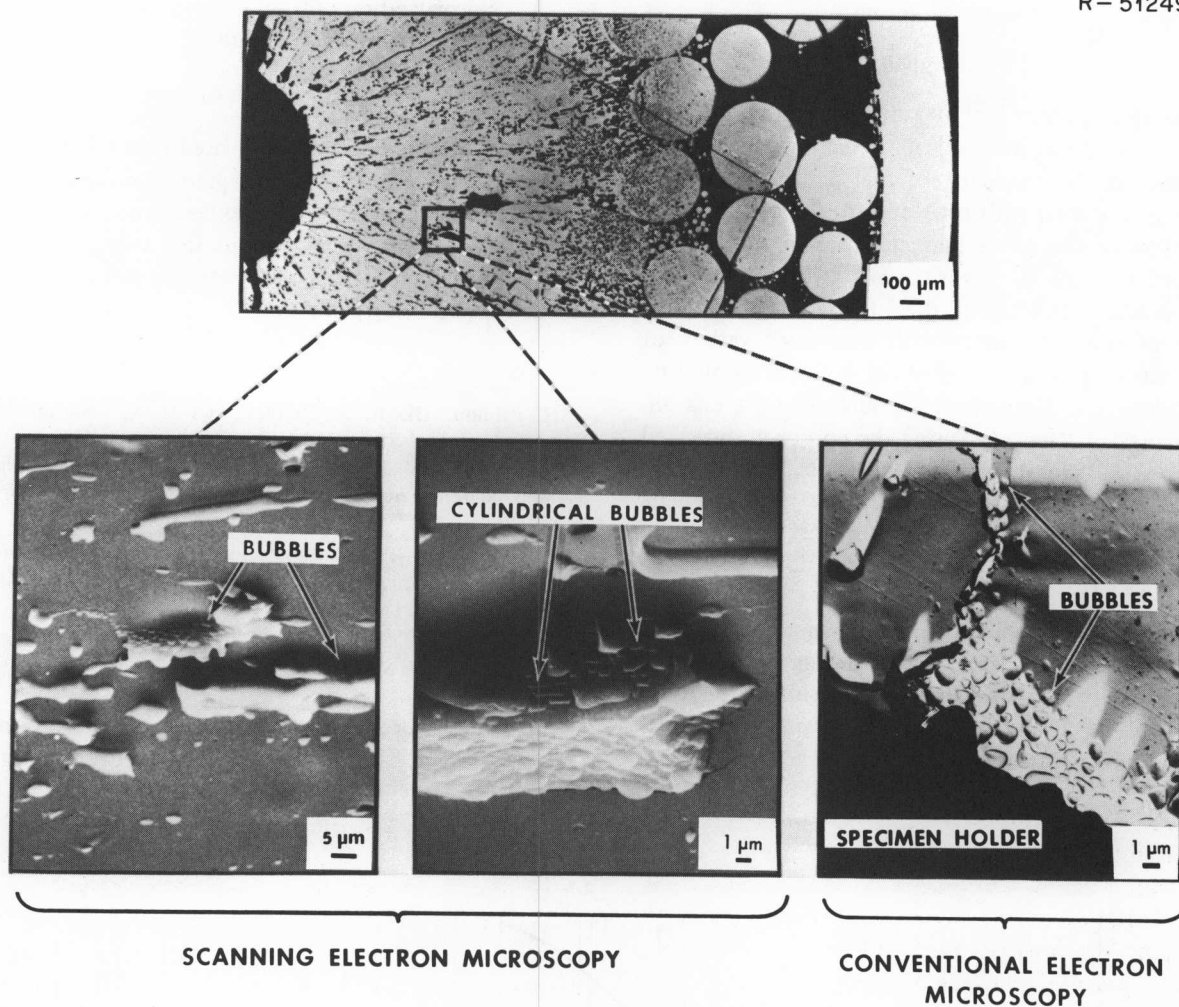


Fig. 17.1. Fission Gas Bubbles on Columnar Grain Boundaries of  $(U,Pu)O_2$  Irradiated to 0.7% Burnup at a Linear Heat Rate of 13.6 kW/ft.

grain boundaries. Any bubbles formed at temperatures below about  $1450^\circ\text{C}$  were less than  $0.1\ \mu\text{m}$  in diameter. A preliminary observation is that many  $0.1\text{-}\mu\text{m}$ -diam fabrication pores were eliminated during irradiation between  $450$  and  $1200^\circ\text{C}$ . The radial plutonium distribution, determined by electron microprobe examination,<sup>4</sup> was consistent with transport of uranium-rich vapor down the temperature gradient with deposition at the region of transition from columnar to equiaxed grains.

The variation in equiaxed grain size with irradiation temperature was determined<sup>5</sup> for another Sphere-Pac sol-gel  $U_{0.85}Pu_{0.15}O_2$  fuel pin after irradiation at a linear heat rate of  $10.5\ \text{kW/ft}$  to 0.5% FIMA. Grain growth occurred at temperatures at least as low as  $1100^\circ\text{C}$ . The observed growth was described by Eq. (1):

$$D^2 - D_0^2 = 12.4t \exp(-16,900/RT), \quad (1)$$

where

$D$  = final grain size,  $\mu\text{m}$ ,

$D_0$  = initial grain size,  $\mu\text{m}$ , and

$t$  = time, hr.

The low activation energy observed indicates that in-reactor grain growth is not nearly as temperature dependent as out-of-reactor grain growth of  $UO_2$  and  $ThO_2$ .

<sup>4</sup>W. J. Lackey, *LMFBR Fuel Cycle Studies Progr. Rept. for May 1970*, No. 15, ORNL-TM-3018, pp. 80-84.

<sup>5</sup>W. J. Lackey, *LMFBR Fuel Cycle Studies Progr. Rept. for April 1970*, No. 14, ORNL-TM-2996, pp. 71-74.

### Pressure Sintering

F. J. Homan

Sintering of porous fuel by radial pressures developed during fuel-cladding mechanical interaction may be very important in the modeling of fuel pin behavior. The change in porosity with time due to pressure sintering will influence the creep characteristics of the fuel; in addition, the loss of porosity will affect the rate of radial pressure buildup at the fuel-cladding interface. Curves of porosity change with time for a variety of temperatures, pressures, and initial porosities would be highly desirable. Unfortunately, such data are unavailable at present. However, using the approach suggested by Palmour,<sup>6</sup> we have generated such curves from uniaxial creep data for  $UO_2$ . Figure 17.2 presents several examples from creep equations published by Bohaboy.<sup>7</sup> The details of the calculations have been published.<sup>8</sup>

An advantage to curves generated in this fashion is that a much greater variety of time, temperature, and initial porosity conditions can be considered than are likely to be available soon from direct pressure sintering experiments.

### Normalization of Swelling and Fission Gas Release Models

C. M. Cox W. H. Bridges

Many of the models currently used in the FMØDEL code are semiempirical, and their predictions need to be normalized and verified with experimental data. We have reported our justification for the adjustable parameters used to describe fuel swelling and fission gas release for  $(U,Pu)O_2$  pellet fuels.<sup>9</sup>

<sup>6</sup>H. Palmour III, R. A. Bradley, and D. R. Johnson, "A Reconsideration of Stress and Other Factors in the Kinetics of Densification," p. 392 in *Kinetics of Reactions in Ionic Systems*, Materials Science Research, Vol. 4, Plenum Press, New York, 1969.

<sup>7</sup>P. E. Bohaboy, R. R. Asamoto, A. E. Conti, *Compressive Creep Characteristics of Stoichiometric Uranium Dioxide*, GEAP-10054 (May 1969).

<sup>8</sup>F. J. Homan, "Modeling of Fuel-Cladding Interaction," *LMFBR Fuel Cycle Studies Progr. Rept. for June 1970*, No. 16, in preparation.

<sup>9</sup>C. M. Cox, *Fuels and Materials Development Program Quart. Progr. Rept. March 31, 1970*, ORNL-4560, pp. 67-71.

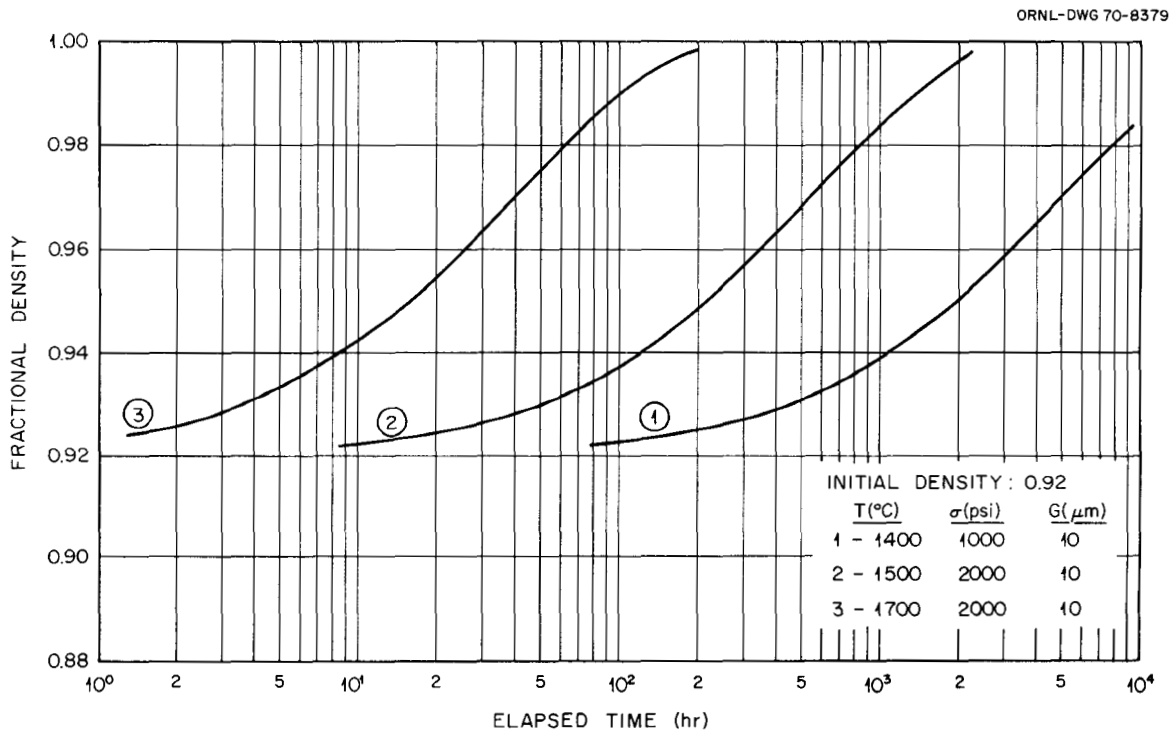


Fig. 17.2. Derived Pressure Sintering Curves for  $UO_2$ .

The basic cause of fuel swelling is the buildup of solid fission products and fission gas bubbles. Based on the calculations of Anselin and Baily<sup>10</sup> and high burnup irradiation experiments with high-density (U,Pu)O<sub>2</sub> fuel,<sup>11</sup> we have assumed that the solid fission product swelling can be estimated as 0.32 vol % per percent FIMA.

For gaseous fission product swelling we have used the Greenwood-Speight model<sup>12</sup> with modifications similar to those of Goldberg *et al.*<sup>13</sup> Since this model does not account for the effects of large temperature gradients and such defects as grain boundaries, its use for oxide fuels is primarily as a pseudoempirical fit to data. The gas swelling model is strongly influenced by fission gas release. Fast reactor irradiation tests of (U,Pu)O<sub>2</sub> fuel have typically shown gas releases of 50 to 80%, as shown previously.<sup>14</sup> Although fission gas release seems to depend on burnup, fuel fabrication form, and power cycling, measured gas releases can be correlated, to a first approximation, with the temperature distribution.<sup>9,14</sup> We assumed a 3-zone model, similar to our empirical restructuring model, in which 98% of the gas is released from fuel above 1800°C, 50% from fuel between 1400 and 1800°C, and 30% at lower temperatures. These values arise from our analysis of microstructural and gas release data of irradiated fuel. We started to statistically analyze irradiation test data to improve this correlation.

The incubation period during which swelling is accommodated in some of the fabricated porosity depends on the fuel porosity after restructuring, temperature, stress, and time. Karsten *et al.*<sup>15</sup> have summarized data that indicate that about 80% of the

porosity of fuel above 1700°C, 50% at 1300 and 1700°C, and up to 30% below 1300°C should be available to accommodate swelling. Fuel swelling is assumed to be accommodated in the porosity left after initial restructuring until these minimum values are reached.

## CLADDING PERFORMANCE

F. J. Homan

The cladding performance work is directed at determining stresses in cladding exposed to levels of temperature and pressure loadings present in service and the response of the cladding to these stresses in terms of deformations. Such evaluations require tensile and creep data measured in environments approximating service conditions and, in addition, descriptions of such phenomena as density loss due to neutron irradiation and stress-induced void growth. Much of our work during the past year has been published,<sup>16-19</sup> but the sections below are a representative cross section of this work.

### Mechanical Properties of Type 316 Stainless Steel

R. W. Swindeman

In support for the LMFBR Fuel Element Model Development Program, we are conducting exploratory tests on unirradiated type 316 stainless steel under cyclic stress and temperature. Such tests will assist in evaluation of fuel pin performance under power cycling.

First we selected a relatively "low-strength" heat material comparable in properties to two heats studied by Garofalo.<sup>20,21</sup> This material had a 0.2% yield strength of 16,300 psi at 650°C. Since step loading tests established that the initial creep rate depended on the amount of instantaneous plastic strain, we chose to begin tests at 14,500 psi, just below the knee of the yield curve at 650°C. Once a significant strain had been

<sup>10</sup>F. Anselin and W. E. Baily, "The Role of Fission Products in the Swelling of Irradiated UO<sub>2</sub> and (U,Pu)O<sub>2</sub> Fuels," *Trans. Am. Nucl. Soc.* 10(1), 103-4 (1967).

<sup>11</sup>E. L. Zebroski, H. Kittel, and D. Moss, "Reviews of Status of Technology of Fast Reactor Fuels," pp. 2-63-2-80 in *Fast Reactors National Topical Meeting, San Francisco, April 1967*, Report ANS-101, American Nuclear Society.

<sup>12</sup>G. W. Greenwood and M. V. Speight, "An Analysis of the Diffusion of Fission Gas Bubbles and Its Effect on the Behavior of Reactor Fuel," *J. Nucl. Mater.* 10, 140-44 (1963).

<sup>13</sup>I. Goldberg, L. L. Lynn, and C. D. Sphar, *FIGRØ - Fortran IV Digital Computer Program for the Analysis of Fuel Swelling and Calculation of Temperatures in Bulk Oxide Cylindrical Fuel Elements*, WAPD-TM-618 (December 1966).

<sup>14</sup>C. M. Cox, R. B. Fitts, and F. J. Homan, *Fuels and Materials Development Program Quart. Progr. Rept. March 31, 1969*, ORNL-4420, pp. 33-39.

<sup>15</sup>G. Karsten, T. Dippel, and H. J. Lane, *Fabrication of Fast Reactor Fuel Pins for Test Irradiations*, KFK-577 (April 1967).

<sup>16</sup>F. J. Homan, B. R. Dewey, and W. E. Stillman, *Fuels and Materials Development Program Quart. Progr. Rept. Sept. 30, 1969*, ORNL-4480, pp. 63-68.

<sup>17</sup>F. J. Homan, *Fuels and Materials Development Program Quart. Progr. Rept. March 31, 1970*, ORNL-4560, pp. 75-81.

<sup>18</sup>F. J. Homan, *LMFBR Fuel Cycle Studies Progr. Rept. for March 1970*, No. 13, ORNL-TM-2949, pp. 79-85.

<sup>19</sup>F. J. Homan, *LMFBR Fuel Cycle Studies Progr. Rept. for April 1970*, No. 14, ORNL-TM-2996, pp. 70-71.

<sup>20</sup>F. Garofalo *et al.*, *Trans. Met. Soc. AIME* 221, 310 (1961).

<sup>21</sup>F. Garofalo *et al.*, *Trans. Am. Soc. Metals* 54, 430 (1961).

introduced by creep, the threshold for instantaneous flow increased, permitting stress cycles to in excess of 20,000 psi. Creep rate data collected under cyclic conditions over the time interval 100 to 1000 hr are summarized for three temperatures in Fig. 17.3. These data are compared to constant-load data reported in the literature. Above 10,000 psi there appeared to be no more than a factor of 2 variation in the creep rate for any given temperature or stress.

Within  $\pm 0.005\%$  extension and  $\pm 2^\circ\text{C}$ , we found no significant short-time history effects under either load or thermal cycling. Creep rates generally returned to their values before the interruption. However, we observed a long-time hardening effect, especially at lower temperatures and stresses. We believe this is a strain hardening effect, but it may be a time hardening

effect or a combination of both. Some data supporting our belief are shown in Fig. 17.4. Here the creep rates are plotted for five temperatures as a function of strain. Included are two data sets obtained from specimens annealed for 0.5 hr at  $1050^\circ\text{C}$ , one set for a specimen aged 2000 hr at  $650^\circ\text{C}$ , another set loaded to 8000 psi over 2000 hr at  $650^\circ\text{C}$ , and a fifth set for a specimen crept at 8000 psi and  $650^\circ\text{C}$  for 2000 hr. The curves on the left of the figure correspond to the first 140 hr of test at 14,500 psi at  $650^\circ\text{C}$ . All specimens showed similar behavior with the exception of the specimen crept at 8000 psi to 0.25%. In this case the initial creep rate was well below that of annealed material but was comparable at strains exceeding 0.5%. Data at 625 and  $600^\circ\text{C}$  show more strain hardening than at higher temperatures.

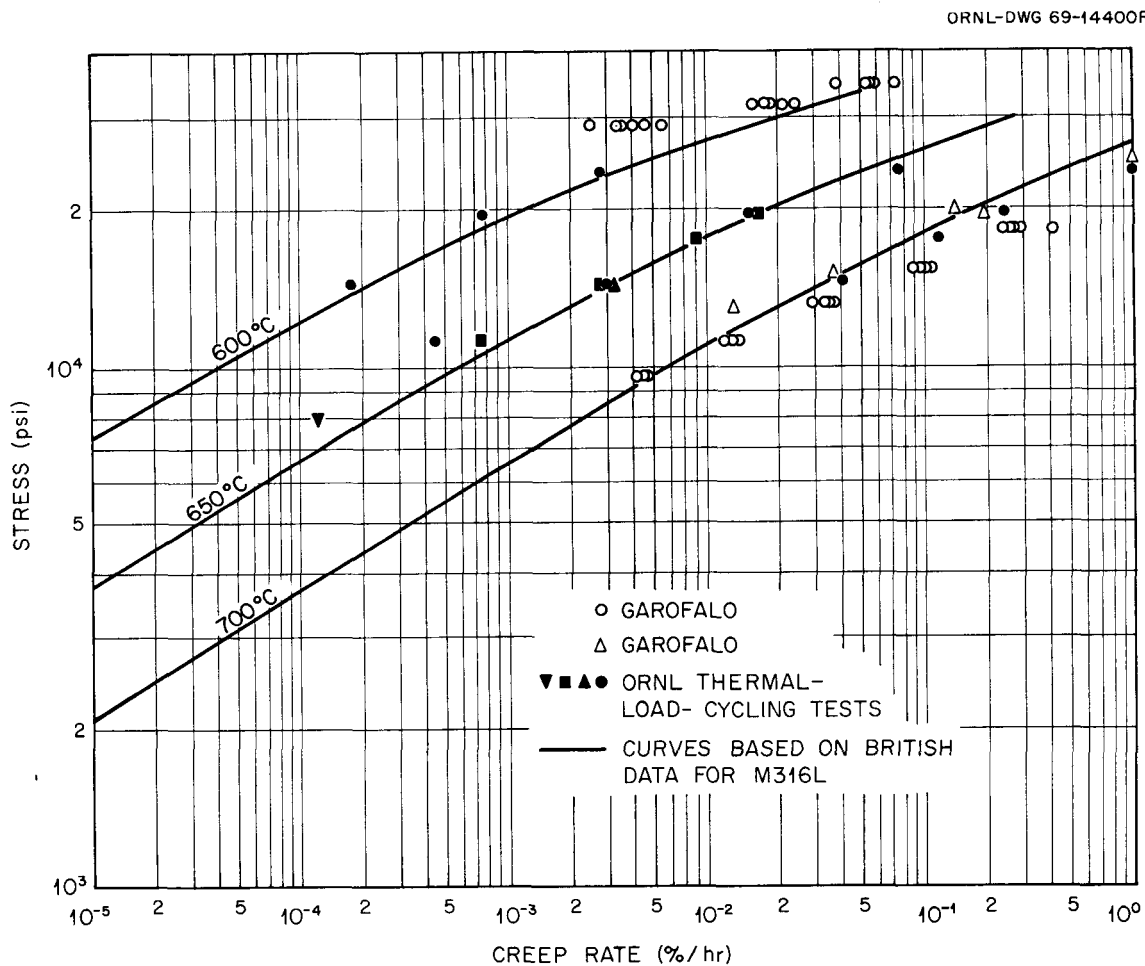


Fig. 17.3. Creep Rate vs Stress for "Low-Strength" Type 316 Stainless Steel. [Refs. F. Garofalo *et al.*, *Trans. Met. Soc. AIME* 221, 310 (1961); *Trans. Am. Soc. Metals* 54, 430 (1961).]

## Discrete Element Analysis of the Creep of Stainless Steel Tubing for LMFBR Application

B. R. Dewey<sup>22</sup>

The discrete element approach to stress and displacement analysis consists of: (1) subdividing the continuum into concentric cylinders (discrete elements), (2) using known solutions for the analysis of the cylinders, and (3) creating an assemblage by conditions of equilibrium and compatibility. This method permits arbitrary radial variation of material properties and allows any pressure and thermal loading. The approach differs from the usual finite element methods in that far fewer of the sophisticated discrete elements are needed and that creep and plastic action are treated in a much simpler way.

At the present time, the discrete element analysis handles the same class of problems as does FMØDEL,<sup>23</sup> a finite difference approach. However, the simpler discrete elements are more amenable to extension to problems with axial effects and to those with bowing.

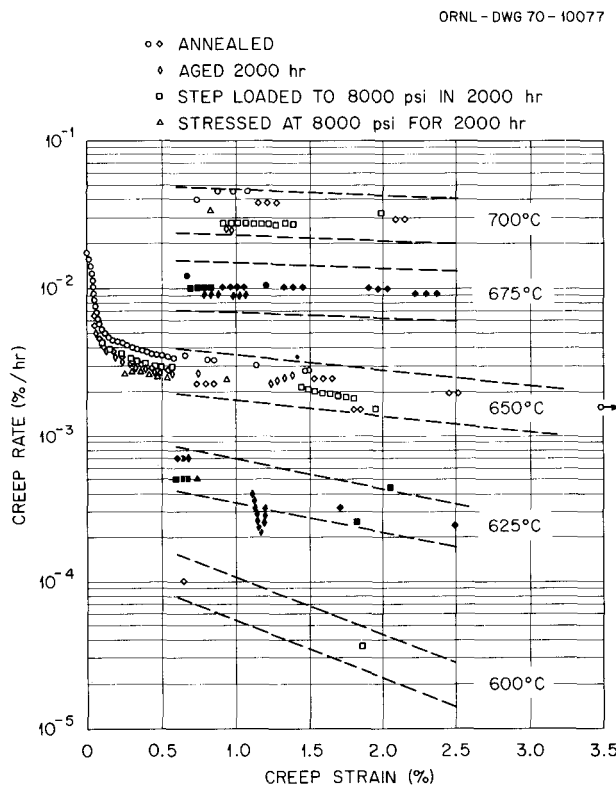


Fig. 17.4. Dependence of Creep Rate on Creep Strain for Type 316 Stainless Steel at 14,400 psi. Data were taken during thermal cycling of five specimens.

In a limited comparison with experimental data,<sup>24</sup> the code appears to satisfactorily predict strain as a function of time. Two types of problems have been considered: (1) biaxial steady-state creep of internally pressurized stainless steel tubing at a uniform, elevated temperature, and (2) stress rupture of similar tubing, internally pressurized and with a radial temperature gradient. An important result from the analysis is that the thermal variation of material properties significantly affects the stress distribution; hence, the typical simplified "thin wall" theories should be used with caution in such application.

## Transient Stress Analysis

W. E. Stillman<sup>22</sup>

The TRANS computer code was developed to predict stress in a plastically loaded thick-walled cylinder subjected to load cycling. Equilibrium and compatibility equations are solved for a discrete number of points in the wall by a finite difference procedure as described by Puthoff.<sup>25</sup> When the equivalent stress at a point exceeds the yield stress, plastic strain increments are computed by the Prandtl-Reuss incremental theory shown by Mendelson.<sup>26</sup> This is the main difference from the FMØDEL code,<sup>23</sup> in which computations proceed based on the total strain or deformation theory of Hencky. Several results cited by Smith and Sidebottom<sup>27</sup> indicate better accuracy for the incremental theory.

## Failure Analysis

F. J. Homan

We developed a failure model in which the pressure that builds up at the cladding inner surface is compared with constant-pressure biaxial stress-rupture data. The "life fraction" concept is used - calculated internal

<sup>22</sup>Consultant from University of Tennessee.

<sup>23</sup>F. J. Homan, *Fuels and Materials Development Program Quart. Progr. Rept. Sept. 30, 1969*, ORNL-4480, pp. 59-61.

<sup>24</sup>J. H. Shively and M. W. Mahoney, *Thermal Gradient Effects on Stress-Rupture Behavior of Thin-Walled Tubing*, AI-AEC-12896 (January 1970).

<sup>25</sup>R. L. Puthoff, *A Digital Computer Program for Determining the Elastic-Plastic Deformation and Creep Strains in Cylindrical Rods, Tubes, and Vessels*, NASA-TM-X-1723 (January 1969).

<sup>26</sup>A. Mendelson, *Plasticity: Theory and Application*, MacMillan, New York, 1968.

<sup>27</sup>J. O. Smith and O. M. Sidebottom, *Inelastic Behavior of Load-Carrying Members*, Wiley, New York, 1965.

pressures for a given time interval are compared to measured rupture lifetimes for that pressure, and the lifetime fraction is calculated. These fractions are summed over all time intervals, and when the sum reaches unity, failure is assumed.

Constant-pressure stress-rupture data are influenced by neutron exposure, temperature gradients, prior working, and thermal cycling. For this reason the biaxial data most closely approximating the fuel pin

cladding and reactor conditions should be used. Figure 17.5 is a plot of internal pressure against Larson-Miller parameter<sup>28</sup> calculated from the data of several experiments. The effects of different initial conditions and operating environment are evident from this figure.

<sup>28</sup>J. B. Conway, *Stress-Rupture Parameters, Origin, Calculation and Use*, Gordon & Breach Science Publishers, New York, 1969.

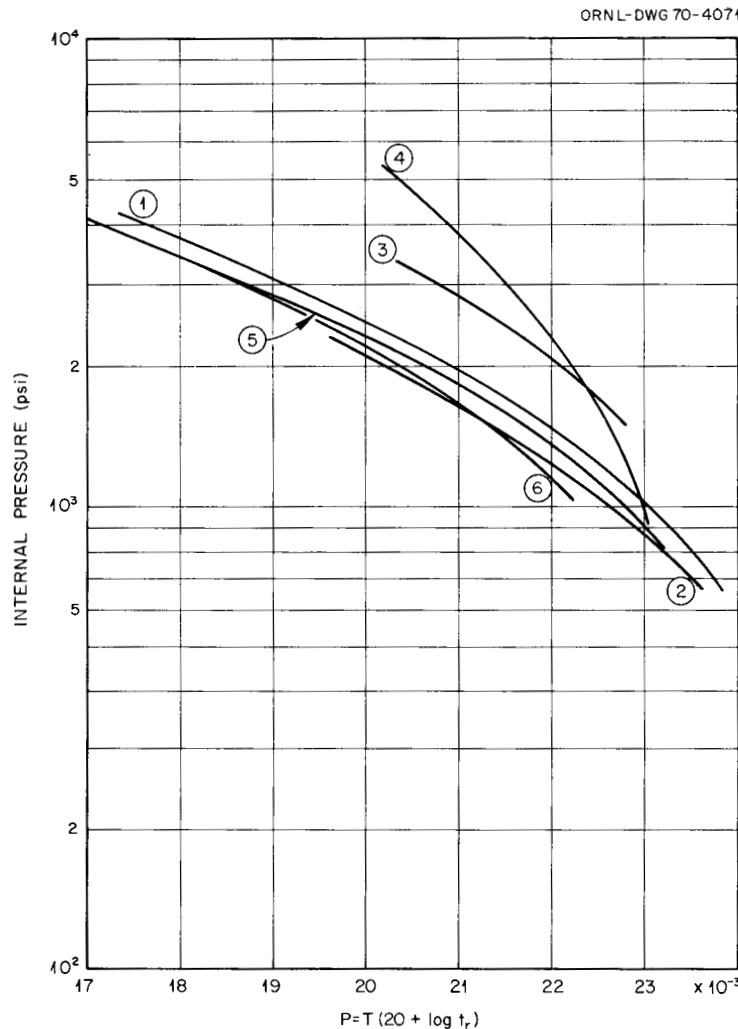


**Fig. 17.5. Larson-Miller Parameter Curves for Type 316 Stainless Steel.** Curves 1 and 2 from data of W. T. Lee, *Biaxial Stress-Rupture Properties of Austenitic Stainless Steels in Static Sodium*, AI-AEC-12694 (June 1968), for 10–15% cold worked and annealed type 316 stainless steel, respectively. Curves 3 and 4 from data of H. K. Richardson and R. McDowell, *Elevated Temperature Stress Rupture Properties of M316, FV548 and Nimonic PE16 P.F.R. Type Tube*, TRG-Report-1482 (1967), for annealed and 20% cold worked type 316 stainless steel, respectively. Curves 5 and 6 from data of R. W. Barker, *Quarterly Progress Report for July, August, September 1969, Reactor Fuels and Materials Development Programs for Fuels and Materials Branch of USAEC Division of Reactor Development and Technology*, BNWL-1223, p. 4.53 (November 1969), for unirradiated and irradiated ( $8 \times 10^{21}$  neutrons/cm<sup>2</sup>, >0.1 MeV) annealed type 316 stainless steel tubing.

### Power Cycling

F. J. Homan

The accuracy of fuel performance models will be measured in part by their success in predicting actual data from irradiation experiments. Except for the most highly instrumented experiments, the data most commonly available for comparison are fission gas release and diametral expansion measurements. Both these events are heavily influenced by the cycling history

experienced by the fuel pin, and thus the performance model should be able to duplicate the power cycling history of the pin. Accordingly, we are modifying our steady state models to account for power cycling. The first results of the modification effort are reported.<sup>29</sup>

---

<sup>29</sup>F. J. Homan, "Power Cycling," *Fuels and Materials Development Program Quart. Progr. Rept. June 30, 1970*, ORNL-4600, in preparation.

## 18. Cladding and Structural Materials

J. R. Weir, Jr.    H. E. McCoy, Jr.

Nuclear reactors expose fuel cladding and structural materials to neutrons. These neutrons can alter the properties of the materials through transmutations or through atomic displacements. The most common transmutation in a low-energy neutron spectrum is the production of helium from  $^{10}\text{B}$ . This results in reduced fracture strains at high temperatures. When the spectrum becomes harder, helium and hydrogen can be produced from nickel, nitrogen, and other elements contained in structural alloys. These more energetic neutrons also displace atoms from their normal sites, thus producing vacancy-interstitial pairs. Many interstitial atoms migrate back to the vacancies, but many of the defects combine to form voids and various dislocation structures. These result in some decrease in density. These atomic rearrangements are very temperature sensitive, and the specific defect configuration that forms depends markedly upon the irradiation temperature.

Much of our work is in direct support of the LMFBR program — particularly the first demonstration reactors and the FFTF. The temperature range of interest is 400 to 650°C. The fuel element cladding and some of the core structural members will be exposed to high fluences of fast neutrons and will suffer property changes due to transmutations and displacements. The reactor vessel will be exposed to a lower fluence, where the changes will be due mostly to helium from transmutation.

Cold worked type 316 stainless steel has been chosen for the FFTF, but other austenitic stainless steels such as type 304 and our titanium-modified steels may be used in later systems. Incoloy 800 and vanadium were both included as candidate materials early in the program conception but have since been dropped. Our continued work with these materials involves only samples that were already being irradiated.

### RADIATION DAMAGE TO FAST REACTOR CLADDING AND STRUCTURAL MATERIALS

E. E. Bloom    J. O. Stiegler

Radiation damage to fast reactor cladding and structural materials, primarily austenitic stainless steels, is being investigated by a study of the changes in density, tensile properties, and creep rupture properties that occur as a result of neutron irradiation in the range 370 to 800°C. The observed changes in properties are then related to the irradiation-produced defects as characterized by electron microscopy.

Type 304 stainless steel irradiated to  $1.4 \times 10^{20}$  neutrons/cm<sup>2</sup> (>0.1 MeV) at 370°C contained small defect clusters, which appeared as black dots under suitable diffraction conditions. Most of these small defect clusters were dislocation loops with Burgers vectors of the type  $\frac{a}{3}\langle 111 \rangle$ . A small fraction of the dots exhibited diffraction contrast consistent with either that expected from  $\frac{a}{2}\langle 110 \rangle$  dislocation loops or from defect clusters having spherically symmetric strain fields. The concentration of the small defect clusters decreased as the irradiation temperature was increased above 370°C. After irradiation at 524°C, no defect clusters were observed by transmission electron microscopy, indicating the concentration to be less than about  $10^{12}$  defects/cm<sup>3</sup>.

Specimens irradiated to fast (>0.1 MeV) neutron fluences in the range  $2 \times 10^{21}$  to  $5 \times 10^{22}$  neutrons/cm<sup>2</sup> at 370 to 470°C contained voids and faulted interstitial dislocation loops. After irradiation to the lower fluences in this range the damage was heterogeneously distributed. Specimens of type 304 stainless steel irradiated to fluences of 2 to  $4 \times 10^{22}$  neutrons/cm<sup>2</sup> (>0.1 MeV) contained dislocation loops clustered around dislocation lines and voids located on

dislocation lines. The void concentration was proportional to the 0.66 and 1.66 powers of fluence for specimens irradiated at 370 to 380 and 460 to 470°C, respectively. Void concentration as a function of fluence is shown in Fig. 18.1. After irradiation at 570 to 630°C, the damage structure consisted of a dislocation network, a few unfaulted dislocation loops, and voids that were nearly always associated with the dislocation lines or precipitate particles. The only damage observed after irradiation at 770 to 840°C was helium bubbles, which were present both at grain boundaries and within the matrix. The changes in void structure with increasing irradiation temperature in specimens irradiated to  $3.7 \times 10^{22}$  neutrons/cm<sup>2</sup> (>0.1 MeV) are shown in Fig. 18.2.

Measurement of maximum void diameter as a function of fast neutron fluence<sup>1</sup> in specimens irradiated at

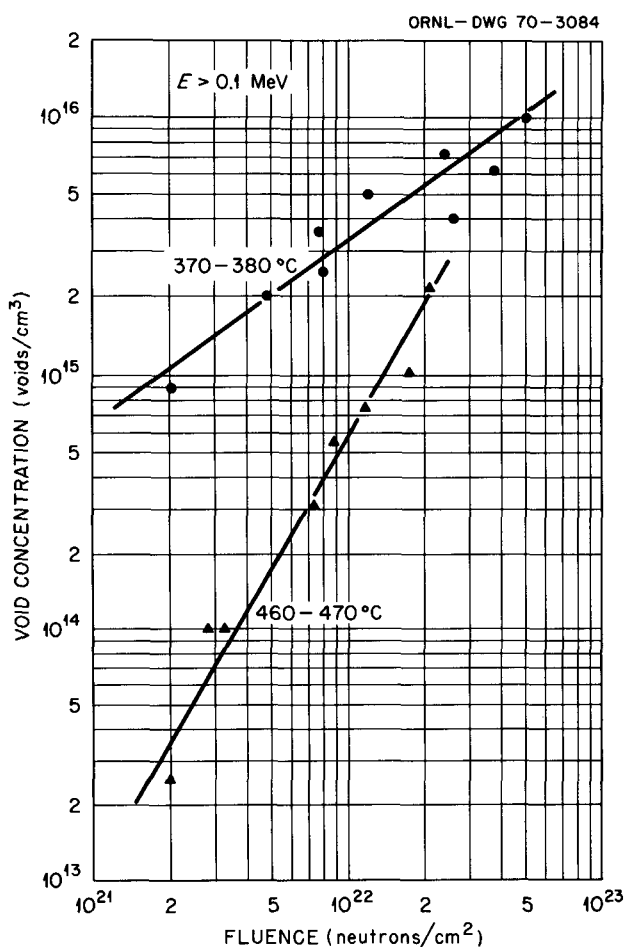


Fig. 18.1. Variation of Void Concentration with Fast Neutron Fluence in Type 304 Stainless Steel Irradiated at 370 to 380 and 460 to 470°C.

either 370 to 380 or 460 to 470°C showed that a given void grew rapidly early in its life when it was small. A short time after its formation the void growth rate decreased sharply. This void growth behavior leads to a density decrease, which is shown as a function of fluence for two irradiation temperatures in Fig. 18.3 and as a function of irradiation temperature for one fluence in Fig. 18.4. The density decrease is closely related to the void nucleation rate.

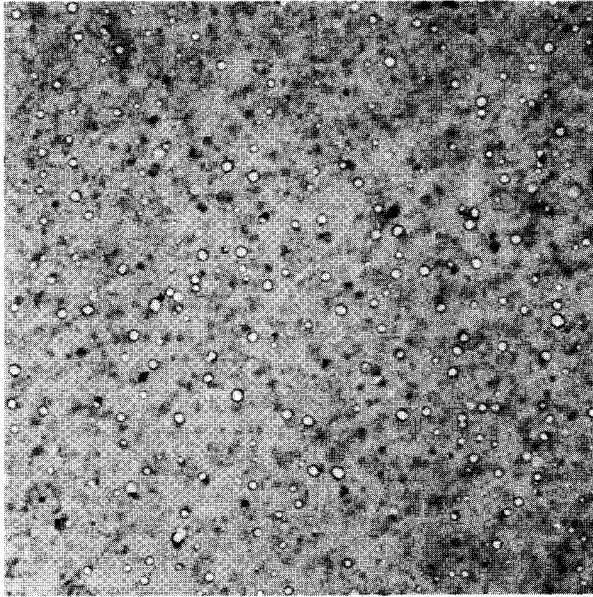
Specimens of type 304 stainless steel that had been injected with  $20 \times 10^{-6}$  atom fraction helium before irradiation at 390°C to  $7.6 \times 10^{21}$  neutrons/cm<sup>2</sup> (>0.1 MeV) contained a higher concentration of smaller voids than specimens without injected helium but irradiated under identical conditions.<sup>2</sup> These results indicate that helium, which is produced during fast neutron irradiation by  $(n, \alpha)$  reactions, will play an important role in the void nucleation step. The actual nucleation step may be the formation of helium bubbles of a critical size for the existing vacancy supersaturation; these then grow as voids by adding vacancies. At low fluences and thus low helium concentrations, helium collects on dislocations, and the first voids appear at these defects. As the helium concentration increases, stable nuclei form in the matrix and give a more uniform void distribution. Helium stabilization of void nuclei gives a void nucleation rate that is initially low and increases until the void concentration saturates. We attribute the decrease in void growth rate to the buildup of a shell around the void within which the vacancy diffusivity is lower than in the homogeneous alloy.

The effect of irradiation at 450°C (void and faulted dislocation loop structure), 600°C (void and dislocation network), and 800°C (helium bubbles) on the tensile properties of type 304 stainless steel is shown in Fig. 18.5. Irradiation at 450°C produced an increase in the ultimate tensile strength and a large increase in yield stress. Specimens irradiated and tested at 450°C exhibited little work hardening and uniform strains below 0.1%. For these irradiation and test conditions the deformation was confined to narrow bands or channels, as shown in Fig. 18.6. The voids and dislocation loops act as barriers to dislocation motion, causing an increased flow stress. When the stress does become high enough to move dislocations through the lattice, the first dislocations soften the matrix, and subsequent

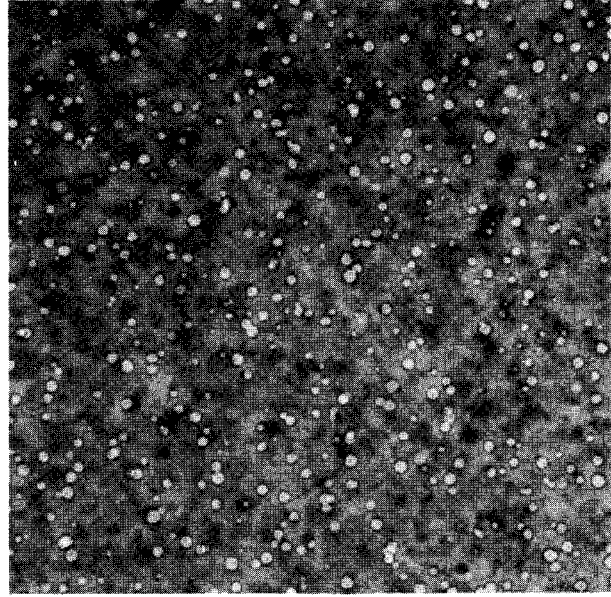
<sup>1</sup>E. E. Bloom, *An Investigation of Fast Neutron Irradiation Damage in an Austenitic Stainless Steel*, ORNL-4580, in press.

<sup>2</sup>E. E. Bloom and J. O. Stiegler, "The Effect of Helium on Void Formation in Irradiated Stainless Steel," accepted for publication in *Journal of Nuclear Materials*.

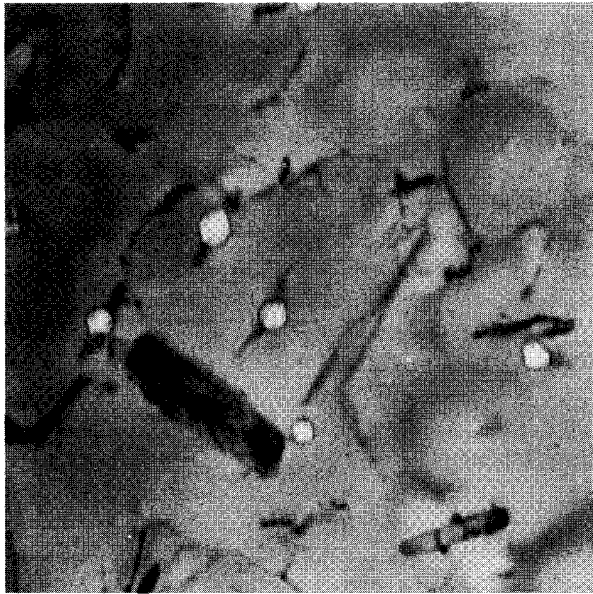
Y-99441



370-380°C



430-440°C



570-630°C



770-840°C

0.1  $\mu\text{m}$   
|-----|

Fig. 18.2. Effect of Irradiation Temperature on the Void Concentration and Size in Type 304 Stainless Steel Irradiated to  $3.7 \times 10^{22}$  neutrons/cm<sup>2</sup> (>0.1 MeV).

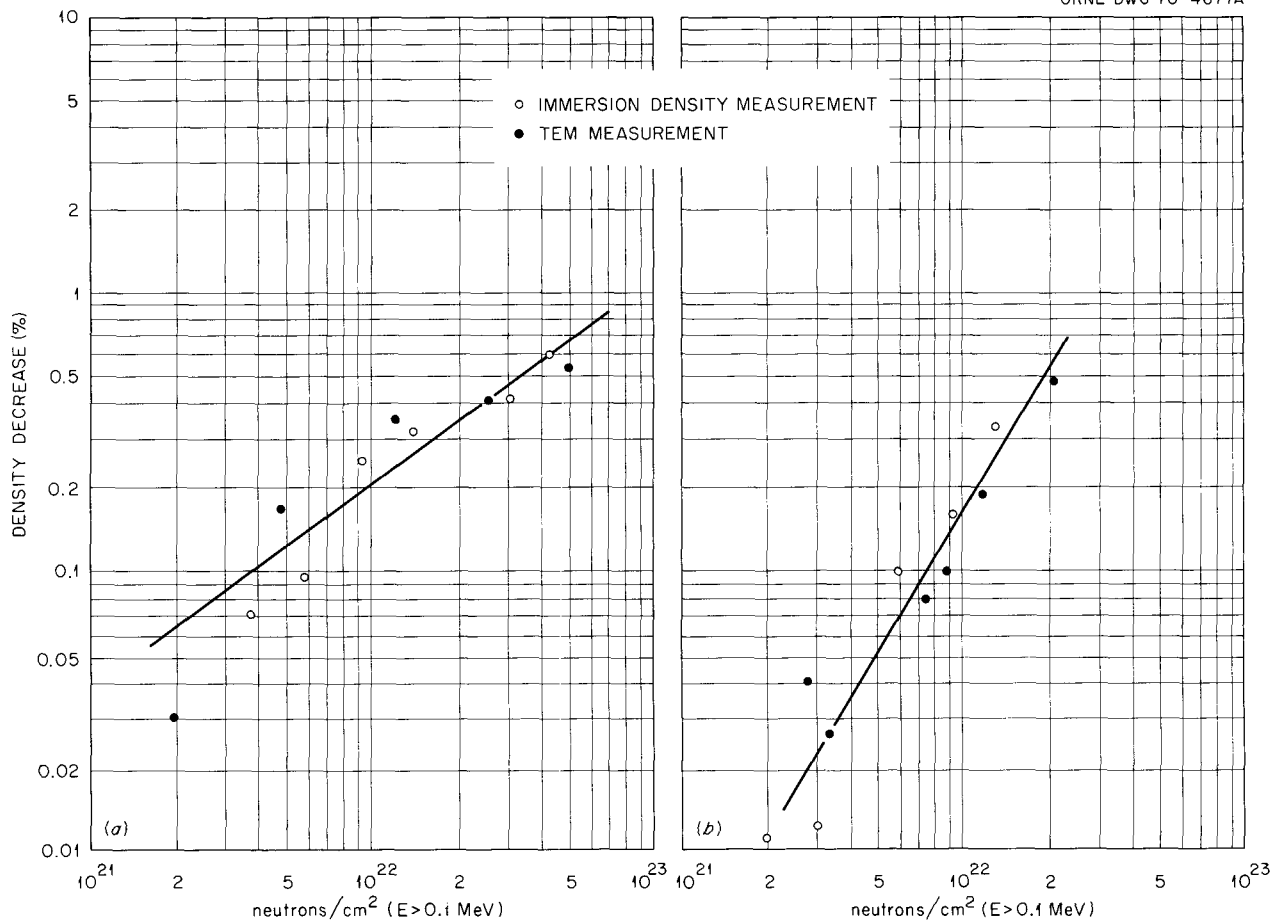


Fig. 18.3. Density Decrease as a Function of Fast Neutron Fluence for Specimens Irradiated at (a) 370 to 380°C and (b) 460 to 470°C.

deformation occurs on the same planes, giving rise to the observed channels. Specimens irradiated at 600°C exhibited a smaller increase in yield stress due to the lower concentration of irradiation-produced voids and dislocations. The deformation of specimens irradiated and tested at about 600°C was much more homogeneous than in specimens irradiated and tested at 450°C. In specimens irradiated at 600°C the reduction in area decreased rapidly with increasing test temperature; in contrast, in the unirradiated alloy the reduction in area was essentially independent of temperature. Fractures of irradiated specimens were primarily intergranular. This behavior is consistent with previous observations of the effect of helium upon elevated-temperature ductility and fracture.<sup>3,4</sup>

The strength properties were not affected in the specimens that were irradiated and tested above 650°C; in them the only visible damage was in the form of

helium bubbles. However, the ductility was reduced and the fractures were entirely intergranular.

Specimens of titanium-modified types 304 and 304L stainless steel have been irradiated in the EBR-II to fast neutron fluences of  $3.0 \times 10^{22}$  neutrons/cm<sup>2</sup> (>0.1 MeV) at 600 and 800°C. Limited results from immersion density and electron microscopy measurements suggest that the temperature dependence of the void formation may be shifted to higher temperatures in the modified types 304 and 304L stainless steel as compared to the standard types. A specimen of modified type 304 stainless steel irradiated to  $3.0 \times 10^{22}$

<sup>3</sup>J. R. Weir, Jr., "Radiation Damage at High Temperatures," *Science* 156, 1689-95 (1967).

<sup>4</sup>D. R. Harries, "Neutron Irradiation Embrittlement of Austenitic Stainless Steels and Nickel Base Alloys," *J. Brit. Nucl. Energy Soc.* 5, 74 (1966).

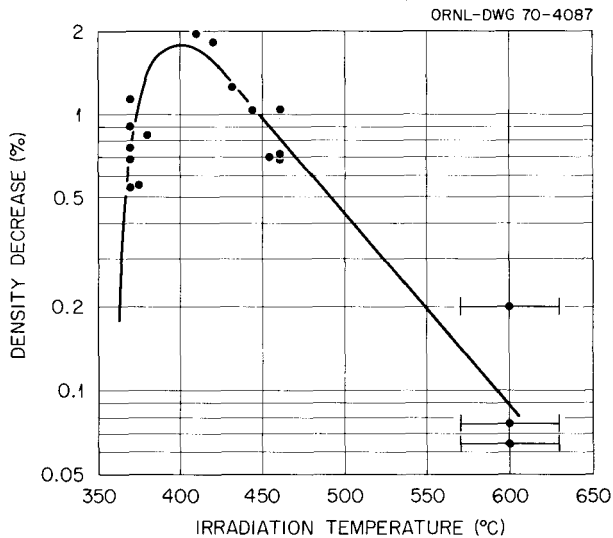


Fig. 18.4. Density Decrease as a Function of Irradiation Temperature for Type 304 Stainless Steel. Data normalized to fluence of  $4 \times 10^{22}$  neutrons/cm<sup>2</sup> (>0.1 MeV) by  $\Delta\rho/\rho_0 \propto \phi t$ .

neutrons/cm<sup>2</sup> (>0.1 MeV) decreased 1.6% in density. Figure 18.7 shows the microstructure of this specimen. Nearly all of the voids are associated with precipitate particles. Regions that had the largest precipitate particles also contained the largest voids, and regions with few precipitate particles had few voids. In contrast, in type 304 stainless steel irradiated at approximately the same conditions (see Fig. 18.4 and ref.5) density decreases ranging from 0.10 to 0.88% were measured. A specimen of the modified alloy irradiated at 450°C decreased less in density than the standard alloy,<sup>6</sup> and at 800°C irradiation temperature the only damage present in either alloy was helium bubbles.

The postirradiation tensile ductilities of standard and titanium-modified type 304 stainless steels are compared in Fig. 18.8. Specimens of these two alloys irradiated and tested at 450°C exhibited about the same

<sup>5</sup>J. L. Straalsund *et al.*, *Quarterly Progress Report October, November, December, 1969 Reactor Fuels and Materials Programs of Fuel and Materials Branch of USAEC Division of Reactor Development and Technology*, BNWL-1279, p. 4.45.

<sup>6</sup>E. E. Bloom and J. O. Stiegler, "A Comparison of Irradiation-Induced Swelling and Void Formation in Two Austenitic Stainless Steels," *J. Nucl. Mater.* 35, 244-46 (1970).

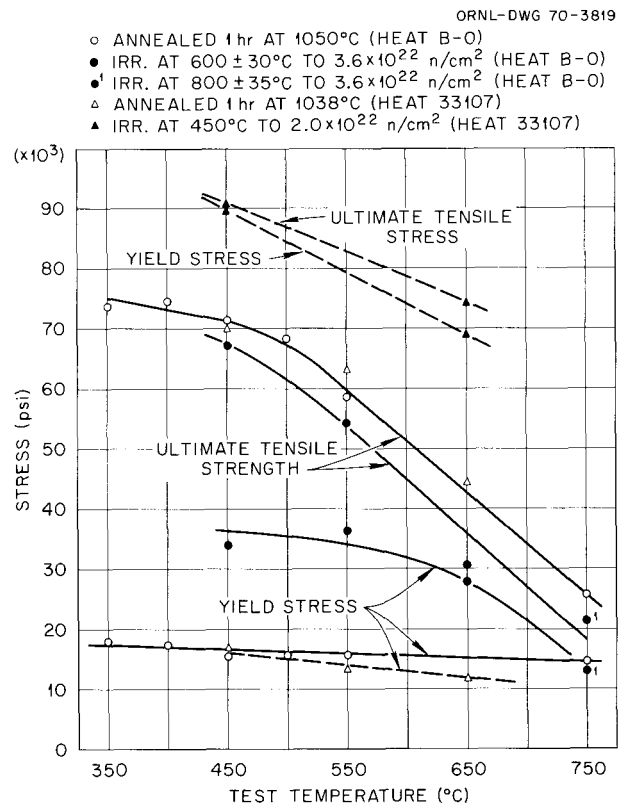


Fig. 18.5. Effect of Fast Neutron Irradiation on the Tensile Properties of Type 304 Stainless Steel. Strain rate 0.002/min.

total elongation. Specimens of the modified alloy irradiated at 600°C and tested at 550, 650, and 760°C exhibited significantly higher tensile elongations than did the standard alloy, even though the irradiation-produced damage was much more severe in the modified alloy, as shown by a comparison of Figs. 18.2 and 18.7. The improved ductility above about 550°C is consistent with previous observations of the improved resistance of the modified type 304 stainless steel to intergranular fracture and helium embrittlement.<sup>7</sup>

Specimens of titanium-modified types 304, 304L, and 316 stainless steel are being irradiated in EBR-II and HFIR. Results of these irradiations will help define the swelling behavior as a function of temperature and

<sup>7</sup>E. E. Bloom and J. R. Weir, Jr., "Development of Austenitic Stainless Steels with Improved Resistance to Elevated-Temperature Irradiation Embrittlement," pp. 261-89 in *Irradiation Effects in Structural Alloys for Thermal and Fast Reactors*, Spec. Tech. Publ. 457, American Society for Testing and Materials, Philadelphia, 1969.

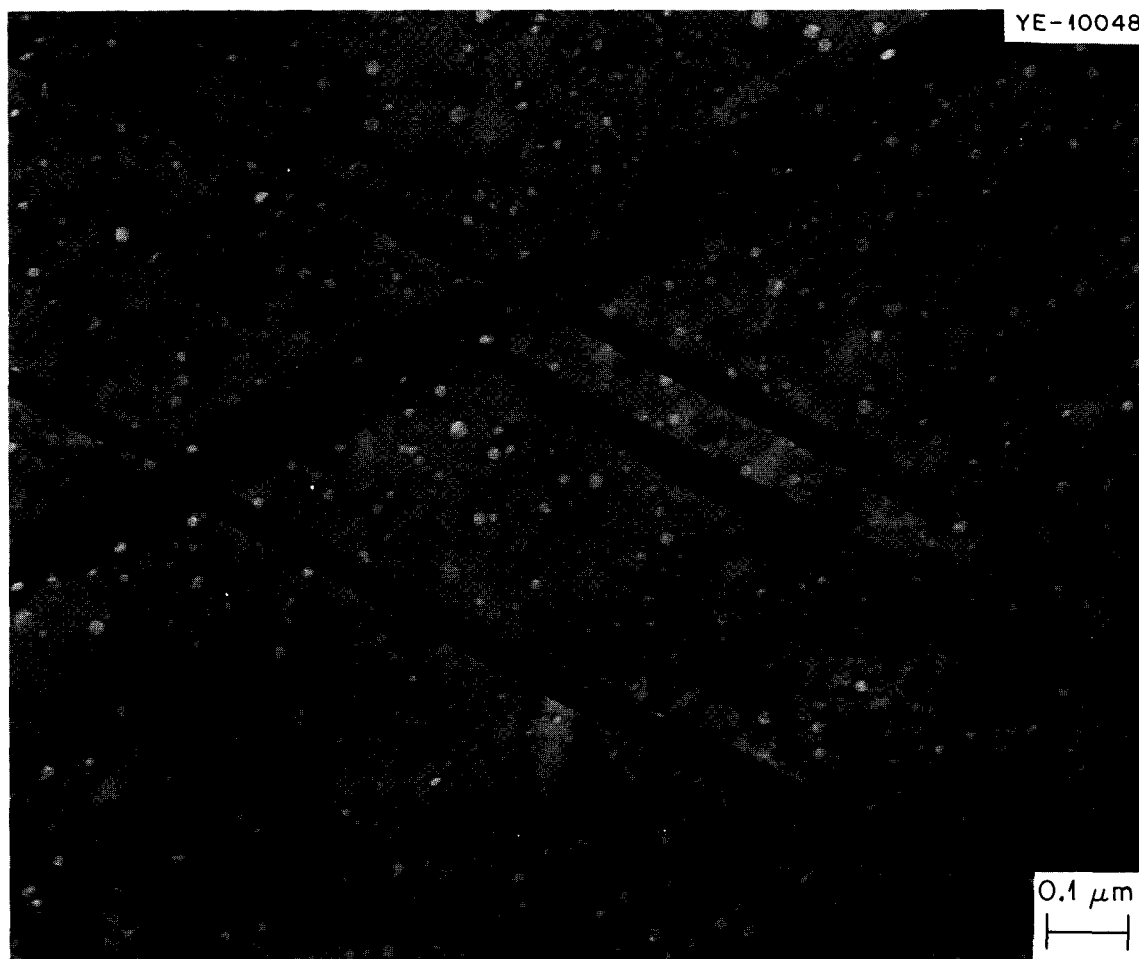


Fig. 18.6. Type 304 Stainless Steel Irradiated at 450°C to  $2.0 \times 10^{22}$  neutrons/cm<sup>2</sup> and Tensile Tested at 450°C. Deformation was confined to narrow bands or channels.

fluence. Specimens of these alloys having variations in the preirradiation microstructure (cold work, grain size, precipitate structure, etc.) are also being irradiated. Through these irradiations we hope to take advantage of both those microstructural modifications that minimize swelling and the improved mechanical properties of the titanium-modified alloys.

#### BIAXIAL STRESS-RUPTURE PROPERTIES OF TITANIUM-MODIFIED STAINLESS STEEL TUBING

R. T. King

As discussed previously, the titanium-modified alloys have attractive properties, and a further step in their development is to demonstrate that they can be made into tubing sufficiently strong and ductile to be useful

as fuel cladding. Tubing of 0.2% Ti-type 304L stainless steel was either planetary swaged or drawn in a final cold reduction of 6.5/1 to 0.25-in. OD  $\times$  0.016-in. wall thickness and solution annealed for 1 hr at 925 or 1038°C. It was tested unirradiated under biaxial stress-rupture conditions in He-1% O<sub>2</sub> at 550 and 650°C. Stresses for these tests produced rupture times ranging up to 200 hr.

Because earlier studies on this tubing indicated that ultrasonically detectable discontinuities could reduce both ductility and rupture life, we selected for this study specimens that showed no discontinuities and inspected on a 0.002-in.-deep  $\times$  0.030-in.-long reference notch basis.

The rupture life of this tubing was not affected by the fabrication histories or annealing temperatures employed. Where comparable data existed for rod speci-

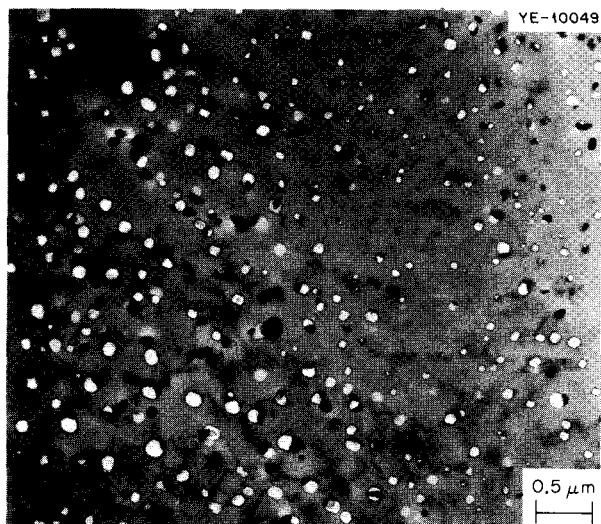


Fig. 18.7. Titanium-Modified Type 304 Stainless Steel Irradiated at 600°C to  $3.0 \times 10^{22}$  neutrons/cm<sup>2</sup> (>0.1 MeV). Note that most of the voids are associated with precipitate particles.

mens from the same heat, the minimum creep rates of tubing and rods agreed well at the same maximum principal stress. Consistent total circumferential elongations between 18 and 35% at 650°C and between 10 and 25% at 550°C were observed, compared with strains of 10 to 20% at 650°C and 6 to 20% at 600°C for unmodified type 304 stainless steel. Furthermore, the uniform strains represented a significant fraction of the total strain and were always greater than 13% at 650°C and 10% at 550°C. The fact that planetary swaged tubing was slightly more ductile than drawn tubing offers the possibility of producing improved properties by controlling fabrication techniques.

### INCOLOY 800

D. G. Harman

We studied various commercial and experimental heats of Incoloy 800 to assess the effects of composition on this alloy's susceptibility to thermal aging and neutron irradiation damage. We investigated three carbon levels – 0.006, 0.03, and 0.12% – and a range of titanium contents from less than 0.002 to 0.6%. Our irradiation experiments were conducted in the Oak Ridge Research Reactor at controlled temperatures ranging from ambient to 760°C. Neutron fluences for the various experiments were from 0.2 to  $1.6 \times 10^{21}$  neutrons/cm<sup>2</sup> thermal and 0.1 to  $1.6 \times 10^{21}$  neutrons/cm<sup>2</sup> fast (>1 MeV).

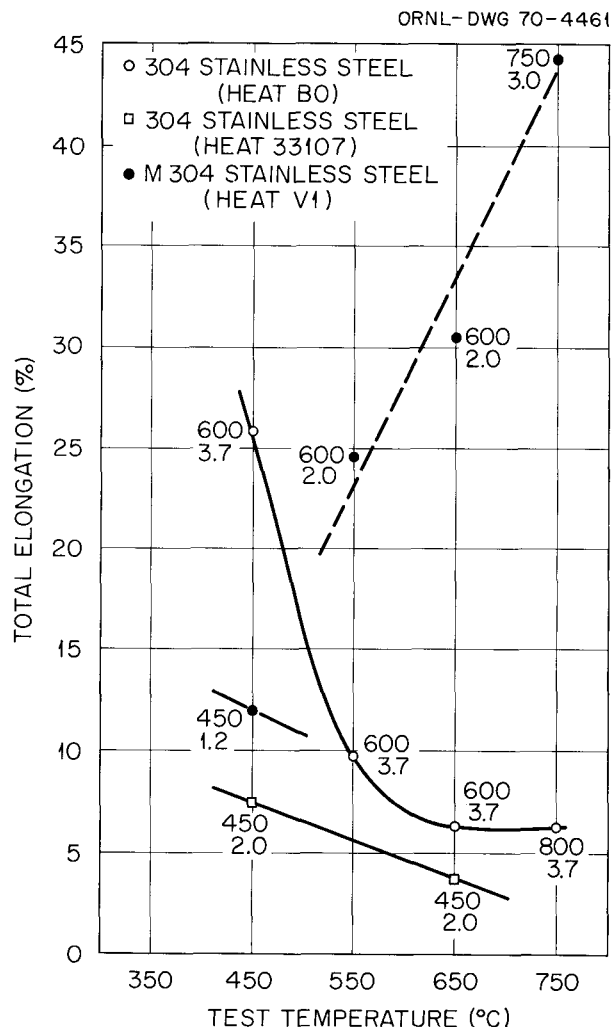


Fig. 18.8. Ductility of Standard and Titanium-Modified Type 304 Stainless Steel After Irradiation in EBR-II. Numbers associated with data points are irradiation temperatures in °C and fluences in (neutrons/cm<sup>2</sup> × 10<sup>22</sup>) (>0.1 MeV). All samples tested at a strain rate of 0.002/min.

Heats containing 0.1% Ti at each of the three carbon levels showed enhanced postirradiation ductility, which could be further improved by selected preirradiation treatments. The 0.12% C, 0.1% Ti heat of Incoloy 800 was less ductile after irradiation at 500°C than after irradiation at 700°C (refs. 8, 9). Test results from the

<sup>8</sup>D. G. Harman, *Metals and Ceramics Div. Ann. Progr. Rept. June 30, 1969*, ORNL-4470, pp. 177–78.

<sup>9</sup>D. G. Harman, "Effects of Thermal Aging and Neutron Irradiation on Incoloy 800," to be presented at the Second International Conference on the Strength of Metals and Alloys, Aug. 30–Sept. 4, 1970, Asilomar, Calif.

thermal control specimens showed this embrittlement to be a combined effect of thermal and neutron exposure. The loss of ductility was prevented by heat treating to a finer grain size before irradiation or by aging to agglomerate the carbide particles.

We continued our investigations of this composition, using specimens irradiated to  $1.6 \times 10^{21}$  neutrons/cm<sup>2</sup> (thermal and >1 MeV) at 350, 450, 550, and 650°C. The specimens were at temperature for 4400 hr during the irradiation. The results listed in Table 18.1 show a significant effect of irradiation temperature on rupture time, total elongation, and minimum creep rate. The largest irradiation effect was shown for the material irradiated at 550°C; it had a creep elongation of only 1.3% and a rupture time of 8 hr. The minimum creep rate was also significantly affected and varied nearly two orders of magnitude with irradiation temperature.

Figure 18.9 shows creep curves for the specimen irradiated at 350°C to  $1.6 \times 10^{21}$  neutrons/cm<sup>2</sup>

**Table 18.1. Effect of Irradiation on the Creep-Rupture Properties at 30,000 psi Stress and 650°C of Incoloy 800 with 0.1% Ti and 0.12% C<sup>a</sup>**

Irradiation Temperature (°C)	Rupture Time (hr)	Total Elongation (%)	Minimum Creep Rate (%/hr)
350	238	3.9	0.0057
450	191	2.8	0.0065
550	8	1.3	0.122
650	10	3.5	0.255

<sup>a</sup>All specimens were cold worked >50%, annealed 0.5 hr at 1150°C, and then irradiated at the indicated temperatures for four cycles in a core position in the Oak Ridge Research Reactor to about  $1.6 \times 10^{21}$  neutrons/cm<sup>2</sup> (thermal and >1 MeV).

(thermal and fast) over a period of 4400 hr and for the control specimen, which was held in a laboratory furnace for 4400 hr at 350°C and tested at 650°C at a

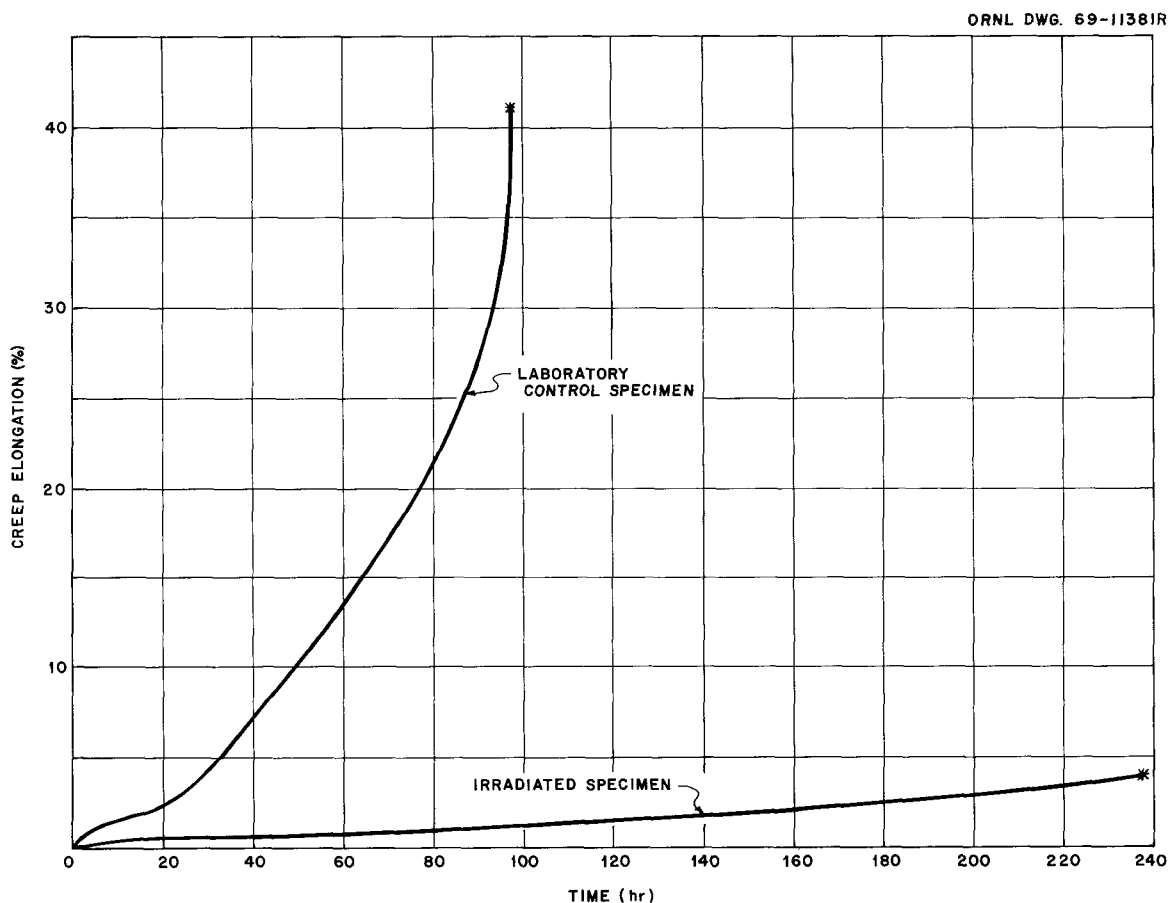


**Fig. 18.9. Creep Curves for Irradiated and Control Specimens of Incoloy 800, Tested in Air at 30,000 psi and 650°C.** Irradiation was conducted in the Oak Ridge Research Reactor at 350°C to a fluence of  $1.6 \times 10^{21}$  neutrons/cm<sup>2</sup> (thermal and fast). The control specimen was held in a laboratory furnace in air for an equivalent time (about 4400 hr).

stress of 30,000 psi. The creep curve for the control specimen shows that the aged structure is not stable at the test conditions; that is, a discontinuity occurs after about 20 hr and the creep rate increases. On the other hand, the creep curve for the irradiated specimen shows no discontinuity, indicating a stable structure, and retains the very low creep rate throughout the test. This results in a longer rupture life for the irradiated sample than for the unirradiated sample. This is contrary to our observations at higher irradiation temperatures.

Aging studies now under way should lead to a better understanding of the aging observed for this heat of material and may possibly explain the significantly lesser effects for the alloys that contained 0.03 and 0.006% C. These alloys showed better postirradiation ductility after irradiation at 500°C than at higher temperatures, and the alloys with 0.03% C were relatively unaffected by aging before irradiation.

### ELECTRON MICROSCOPY OF IRRADIATED VANADIUM

F. W. Wiffen

Unalloyed vanadium irradiated in the range 385 to 710°C was examined extensively by transmission electron microscopy, with the main emphasis on a complete characterization of the voids. As in other metals, the irradiation temperature strongly influenced the size and number of voids formed in vanadium. Table 18.2 summarizes void formation data for a number of irradiation temperatures. The very small void size and the very high number density suggest that 385°C may be near the lower temperature limit for void formation at this fluence.

The material purity had a very strong influence on the density of voids produced by irradiation at 385°C. Although the fluence varied only 20%, the material with about 1800 ppm interstitial impurities contained

an order of magnitude more voids than that with about 240 ppm. The size of the voids was similar in the two materials, and there was little range in the sizes in either condition. The impurity content also affected the microstructure viewed in diffraction contrast. The impure material contained a regular, faceted precipitate, while the purer vanadium did not, but did contain some dislocation loops.

For irradiation temperatures between about 475 and 630°C the void density ranged from  $10^{15}$  to  $10^{16}/\text{cm}^3$ , with the higher void densities at the lower irradiation temperatures. The diameters of the voids increased with irradiation temperature. The data in Table 18.2 at 475, 550, 575, and 600°C were taken from a single segment of vanadium fuel cladding. Positive identification of the reactor position of this segment and, hence, of temperature and fluence was possible. The three highest temperatures of this set are all for the same fluence and were obtained by thinning to examine material near the inner surface, center of the wall, and outer surface of the tube. These three data points show clearly that at constant fluence the void number density and void volume fraction decrease with increasing temperature, while the average void diameter increases with increasing temperature. Precipitate platelets seen in diffraction contrast were much larger at the higher irradiation temperatures. No voids were found in the general matrix of samples irradiated to  $2.5 \times 10^{21}$  neutrons/cm<sup>2</sup> (>0.1 MeV) at 600 and 710°C. A few isolated regions were found in the impure material in which classical helium recoil damage was seen. These regions contained precipitate particles of  $\text{V}_3\text{B}_2$  at their centers. The damage in these shells was in the form of bubbles or cavities, with a dislocation structure in the region that may have resulted from growth of loops to the point where they intersected to form a connected network.

Table 18.2. Void Data for Irradiated Vanadium<sup>a</sup>

Irradiation Temperature (°C)	Interstitial Impurities (ppm)	Reactor	Fluence [neutrons/cm <sup>2</sup> (>0.1 MeV)]	Void Density (voids/cm <sup>3</sup> )	Average Void Diameter (Å)	Void Volume Fraction (%)
			$\times 10^{21}$	$\times 10^{15}$		
385	240	EBR-II	4.9	11.9	50 ± 10	0.08
385	1800	EBR-II	5.7	118.0	45 ± 10	0.56
475	1000	EBR-II	9.7	10.6	82	0.34
550	1000	EBR-II	14.0	5.94	168	1.77
575	1000	EBR-II	14.0	3.54	194	1.58
600	1000	EBR-II	14.0	2.03	226	1.47
660	240	ORR	2.5	0		
660	1800	ORR	2.5	0 <sup>b</sup>		
710	1800	ORR	2.5	0 <sup>b</sup>		

<sup>a</sup>All material annealed before irradiation.

<sup>b</sup> Helium-stabilized cavities formed surrounding boride particles. No cavities were found in the matrix away from precipitate particles.

## 19. Fabrication of Fast Breeder Reactor Cladding

W. R. Martin

Successful performance of Fast Breeder Reactor (FBR) fuel pins demands high-quality tubing for proper containment of fuel. Our goal is to develop methods of fabrication that produce tubing free of harmful defects and that has elevated-temperature mechanical properties tailored to meet the needs of FBR. We have continued to work primarily on type 316 stainless steel to show the relationships among mechanical properties at elevated temperatures, processing variables, and defects.

### EVALUATION OF PLANETARY SWAGING AS A PROCESS TO PRODUCE HIGH- QUALITY CLADDING

G. A. Reimann

A new more rigid ORNL planetary swager has been constructed, with a capability for a wide range of tubing sizes.<sup>1</sup> Several modifications were made in the power train, the most recent being the installation of a more powerful drive motor (7.5 hp), to widen the available range of process variables.

Several samples of types 304 and 316 stainless steel tubing were subjected to planetary swaging. Initial efforts indicated that planetary swaging heavily works the outside tube surface. The mode of tube deformation should be restricted to ironing rather than sinking to avoid surface cracking as shown in Fig. 19.1. Greater total deformation may be obtained by many light passes than by few heavy passes, and the ratio of wall thickness to tube diameter appears critical, since poor results were obtained with thicker walled tubes.

Studies to date indicate that planetary swaging is best suited to light passes to achieve final size, and this

process does not seem practical now as a means of primary fabrication.

Y-96514A



Fig. 19.1. Transverse Section of Type 304L Stainless Steel Tubing Subjected to Sinking During Deformation. Note development of cracks on both surfaces and heavily worked outer surface.

<sup>1</sup>G. A. Reimann, *Fuels and Materials Development Program Quart. Progr. Rept. Sept. 30, 1969*, ORNL-4480, pp. 99-103.

## FABRICATION OF ULTRAFINE GRAIN SIZE TYPE 316 STAINLESS STEEL TUBING

G. A. Reimann

As part of the overall program to improve the mechanical properties of cladding, a process was devised to produce an ultrafine grain size and a fine carbide precipitate in type 316 stainless steel tubing intended for use as fuel element cladding.

Figure 19.2 is a transmission electron micrograph showing the ultrafine grain size and the fine carbide precipitate in a section of the tube wall. The grain size averages 0.003  $\mu\text{m}$  or less, which is about one-tenth that obtained by commercial tube drawing practice. This ultrafine grained structure with the carbide precipitate was obtained in two different heats of type 316 stainless steel by using a conventional drawing schedule but modifying the interpass annealing schedule.<sup>2</sup> Stainless steel will recrystallize below 800°C when cold worked 40 to 45%, and carbon will precipitate as metal carbides at these temperatures. Repetitive cold working and annealing at 760°C are required to develop the fine grain size and the precipitate.

<sup>2</sup>G. A. Reimann, *Development of an Ultrafine Grain Size Type 316 Stainless Steel Cladding*, ORNL-TM-2937 (May 1970).

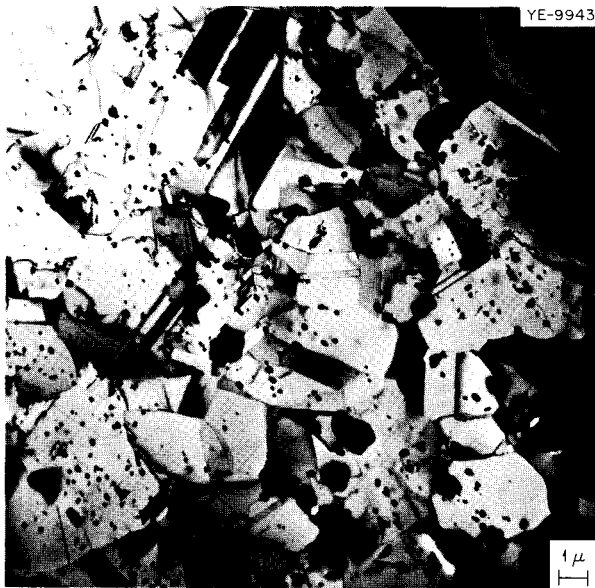


Fig. 19.2. Structure of Ultrafine-Grained Type 316 Stainless Steel Tubing Containing 0.06% C. Normal processing of stainless steel to produce a grain size of ASTM 8 would show only a single grain in the area of this figure.

## BIAXIAL STRESS-RUPTURE PROPERTIES OF ULTRAFINE GRAIN SIZE TYPE 316 STAINLESS STEEL TUBING

R. T. King H. E. McCoy, Jr.

Ultrafine grain size (UFG) type 316 stainless steel tubing containing a dense carbide dispersion was developed at ORNL. The biaxial stress-rupture properties of the material (ASTM grain size 13 to 14) and conventional tubing (ASTM grain size 7) from the same material heat were determined in He-1% O<sub>2</sub> at 650°C. Tube burst specimens used in these tests were ultrasonically inspected and found free from discontinuity responses greater than those of 0.002-in.-deep  $\times$  0.030-in.-long standard spark-machined notches; the specimens were of the standard LMFBR cladding geometry — 0.25 in. OD  $\times$  0.016 in. wall thickness.

The stress-rupture lives of the unirradiated ultrafine-grain tubing<sup>3</sup> in the 20% cold worked and stress relieved conditions are compared with those of conventional tubing in Fig. 19.3. In short-time tests at high stresses, the rupture times are all comparable; however, at lower stresses the UFG tubing ruptures after much shorter time than the conventional material. The presence of dissolved carbon in the conventional tubing, which causes dynamic strain aging by the precipitation of (Fe,Cr)<sub>23</sub>C<sub>6</sub> on dislocations,<sup>4</sup> accounts for the

<sup>3</sup>R. T. King and G. A. Reimann, "Effect of Fabrication Variables on the Biaxial Creep Rupture Properties of Stainless Steel Tubing." Presented at the 16th Annual Meeting of American Nuclear Society, Los Angeles, Calif., June 28–July 2, 1970 (to be published).

<sup>4</sup>J. T. Bamby, *J. Iron Steel Inst. (London)* 204, 23 (1966).

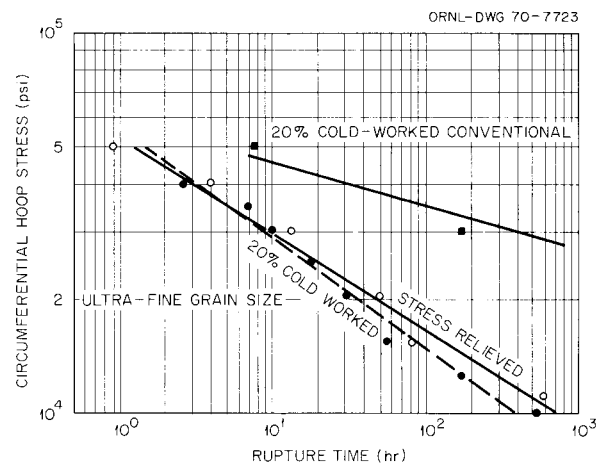


Fig. 19.3. Comparison of Stress-Rupture Strength at 650°C of Type 316 Stainless Steel with Ultrafine Grains and More Conventional Grains.

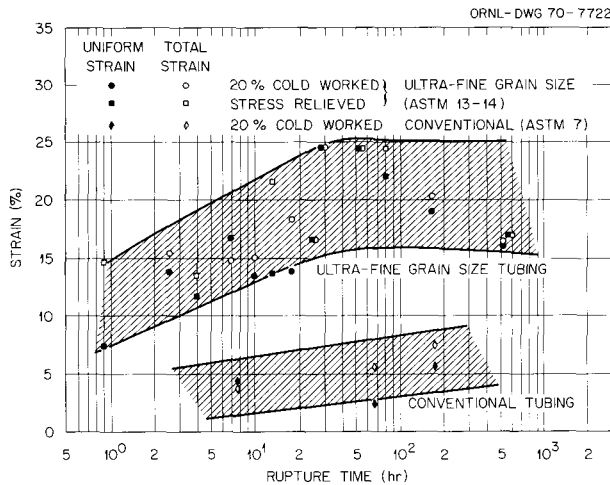


Fig. 19.4. Ductility of Ultrafine-Grain and Conventional-Grain Type 316 Stainless Steel in Biaxial Tube Tests at 650°C.

difference in behavior. Most of the carbon in the UFG material is in the form of carbide precipitated during fabrication. However, both the maximum circumferential strain at the point of fracture and the maximum uniform strains exhibited by the UFG tubing are higher than those for the conventional tubing (Fig. 19.4). (Occasional uniform strains larger than total strains reflect lack of measuring precision.) It is particularly noteworthy that the cold-worked UFG tubing exhibits uniform and total strains above 15% in tests lasting over 100 hr.

#### ORIGIN AND SIGNIFICANCE OF NATURAL DEFECTS GENERATED DURING TUBING FABRICATION

G. A. Reimann

The object of this work is to detect and characterize defects in conventionally drawn tubing so as to determine their origin and their influence on the me-

chanical properties of the tubing. Several defect sources have been identified. These are: surface discontinuities in starting material (i.e., machining marks); mechanical damage during handling; adhering particulate matter; and nonmetallic inclusions.

In nearly all specimens of type 316 stainless steel tubing subjected to room-temperature burst testing, close examination of the fracture site disclosed that a tube wall defect either caused the failure or was a contributing factor. Frequently, the defects in question were less than 0.0005 in. deep and were below the threshold of ultrasonic detection.<sup>5</sup> Burst properties would be improved if these "subthreshold" flaws were minimized or eliminated.

#### GENERATION AND EVALUATION OF ARTIFICIAL DEFECTS

R. W. McClung K. V. Cook

The influence of fabrication defects on the elevated-temperature properties of tubing could be better determined if a method was available to produce simulated fabrication defects of specific sizes at specific locations on tubing. To make simulated defects that more nearly resemble naturally occurring discontinuities, such as cracks, we have electrical-discharge machined notches at various up-stream times within the tube fabrication schedule. Our studies indicate that we can predict the effect of a drawing schedule on the configuration of the defect. A sinking pass (with no significant wall change) reduces the notch width; however, a multipass drawing schedule involving both sinking and ironing changes the notch length, depth, and width.

<sup>5</sup>G. A. Reimann, *Fuels and Materials Development Program Quart. Progr. Rept. Dec. 31, 1969*, ORNL-4520, pp. 146-50.

## 20. Stainless Steel Welding Development

G. M. Slaughter    N. C. Binkley  
G. M. Goodwin    D. G. Harman  
N. C. Cole

We are studying the behavior of weldments in austenitic stainless steel at 370 to 650°C as a function of both welding process and variables within a process for application to LMFBR vessels and components. The solidification substructure (the structure in its finest microscopically resolvable detail) markedly influences the mechanical properties of a weldment at elevated temperatures. Since the size and type of substructure in a weldment are significantly influenced by factors that the welding operator can control, we determine the effects of composition, individual welding process, and the welding variables (current, voltage, travel speed, etc.) on the observed microstructure and, subsequently, on elevated-temperature mechanical properties. In all instances, highly pedigreed materials are used, and all of the variations in composition are within allowable specifications.

We reviewed the published data concerning the elevated-temperature mechanical properties of austenitic stainless steel weldments. Little information was available, and it showed a high degree of scatter, particularly in ductility.<sup>1</sup> For type 347 stainless steel weld metal, for example, the total elongation values from stress-rupture tests at 650°C plotted as a function of rupture life show an essentially random pattern. Most of the total elongation values are less than 10%, and many are 1% or less. Thus, our welding programs were undertaken to augment the meager literature data and to determine the individual effects of some of the variables that we feel are responsible for the above situation, such as changes in welding input parameters and minor composition variations.

### SHIELDED METAL-ARC PROCESS

Our objective is to determine the effects of electrode coating variables on the shielded metal-arc (stick electrode) welding process. We are comparing the substructures and elevated-temperature mechanical properties of several shielded metal-arc weldments made with type 308 electrodes.<sup>2</sup> Included are the three most popular electrode coatings; lime, titania, and lime-titania. The last mentioned is the most widely used, and we are studying the effects of minor changes in C, Si, P, S, and B contents of the electrode coating and subsequent deposited weld metal (deposit composition is within the allowable type 308 composition limits in all cases). Significant variations in creep strength and ductility were observed. For example, the rupture life at 650°C increased tenfold by increasing carbon content from 0.044 to 0.074 wt %, all other compositional variables being maintained constant. All of the shielded metal-arc welds show total creep elongations decreasing markedly with increasing rupture times, but some compositions are better than others.

Figure 20.1 shows the microstructures of weldments prepared from lime, lime-titania, and titania coated electrodes. Each was prepared by the same operator using the same equipment and identical welding parameters, and each showed the same bulk chemical analysis. The microstructures are essentially indistinguishable and contain the same measured amounts of  $\delta$ -ferrite, yet weld-metal specimens from the lime-coated electrode weld were consistently weaker than those from the other two. This is illustrated in Fig. 20.2, which shows creep curves at 650°C with a stress of 18,000 psi.

<sup>1</sup>G. M. Goodwin, *Fuels and Materials Development Program Quart. Progr. Rept. Sept. 30, 1969*, ORNL-4480, pp. 105-8.

<sup>2</sup>N. C. Binkley, G. M. Goodwin, and D. G. Harman, *Fuels and Materials Development Program Quart. Progr. Rept. Dec. 31, 1969*, ORNL-4520, pp. 165-72.

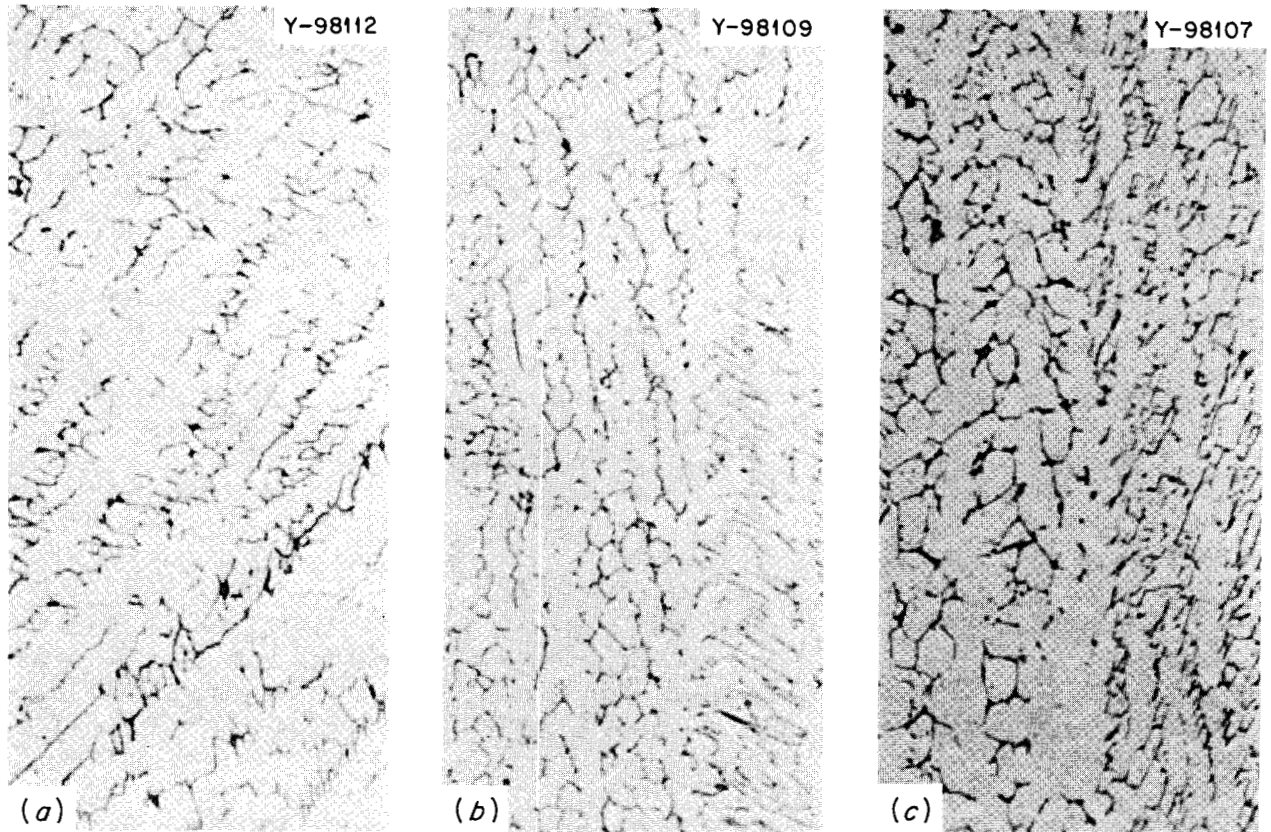


Fig. 20.1. Microstructures of Welds Made with (a) Lime-Coated, (b) Lime-Titania-Coated, and (c) Titania-Coated Electrodes. Etch:  $H_2O$ ,  $KOH$ ,  $K_3Fe(CN)_6$ . 500X.

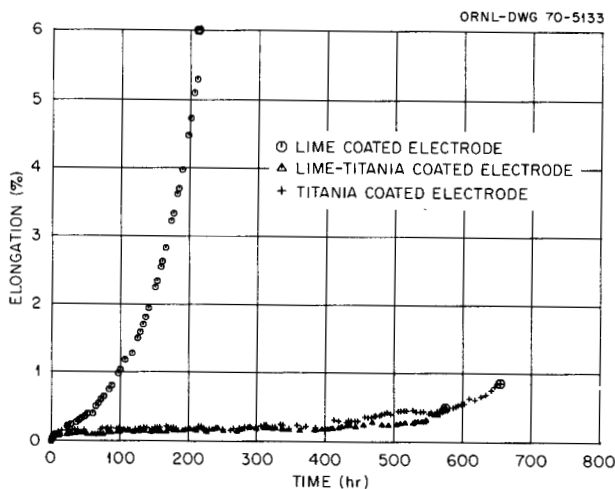


Fig. 20.2. Creep Curves of Stainless Steel Welds Made at  $1200^{\circ}F$  and 18,000 psi. The weld made with the lime-coated electrode is weaker but more ductile than welds made with titania-coated and lime-titania-coated electrodes.

These variations, as yet unresolved, are thought to result from minor differences in trace element composition and/or from differences in the distribution of solute elements.

### SUBMERGED-ARC PROCESS

We are investigating the effects of variations in welding parameters and minor compositional changes due to flux composition variations for the submerged-arc process. Based on the analysis of a bead-on-plate study,<sup>3</sup> we prepared weldments in 1-in.-thick type 304 plate at the practically attainable extremes of energy input, ranging from 40 to 270 kJ/in., using commercially available submerged-arc fluxes.

<sup>3</sup>G. M. Goodwin, D. G. Harman, and N. C. Cole, *Fuels and Materials Development Program Quart. Progr. Rept. March 31, 1970*, ORNL-4560, pp. 111-18.

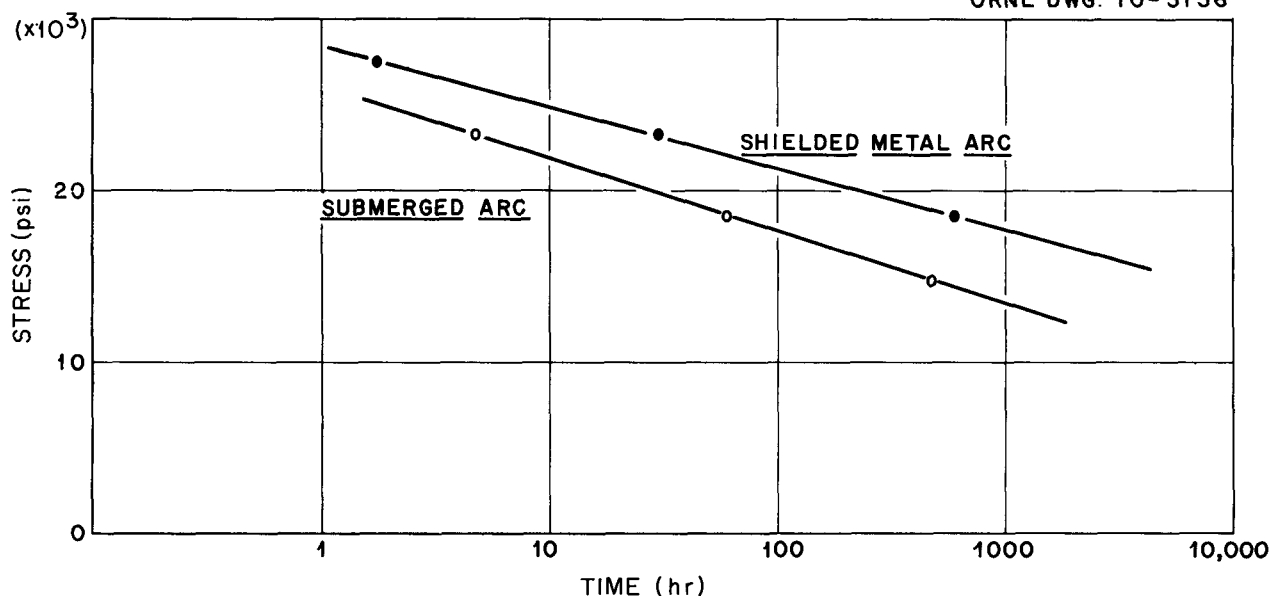


Fig. 20.3. Comparison of Stress-Rupture Properties of Shielded Metal-Arc and Submerged-Arc Stainless Steel Welds. The base metal is type 304 stainless steel, the filler metal is type 308 stainless steel, and the testing temperature is 650°C.

Submerged-arc welds made with typical industrial parameters for stainless steel vessels show elevated-temperature strengths much lower than those obtained from shielded metal-arc welds. Figure 20.3 compares the as-welded stress-rupture properties at 650°C. The shielded metal-arc data are from the weld made with commercial lime-titania-coated electrodes.

#### METALLOGRAPHIC ANALYSES

Since the object of the program is to determine the link between the various welding variables, the solidification substructures, and the elevated-temperature mechanical properties, metallographic analyses are obviously important. We have used extensively the electron microprobe, quantitative television microscope, scanning electron microscope, and optical metallography to correlate the structures observed with the mechanical properties. The measurement of  $\delta$ -ferrite in austenitic stainless steel weld metal is in itself an area of

great uncertainty;<sup>4</sup> we found that the actual ferrite content may vary up to threefold from that determined by usual nondestructive techniques. Also, the distribution of that ferrite is critical in determining the strength of the weld metal and the fracture mechanisms.

Figure 20.4 shows a typical scanning electron fractograph of the surface of the specimen tested at the lowest stress level. Note that the fracture path follows the austenite-ferrite boundaries, revealing the solidification substructure on the fracture surface. Although the fracture mechanism is, to an extent, dependent upon the test temperature and the imposed stress, the amount and distribution of  $\delta$ -ferrite obviously determines to a great extent the elevated-temperature mechanical properties of the material.

<sup>4</sup>R. B. Gunia and G. A. Ratz, *The Measurement of Delta Ferrite in Austenite Stainless Steels*, Bulletin 132, Welding Research Council, New York, August 1968.

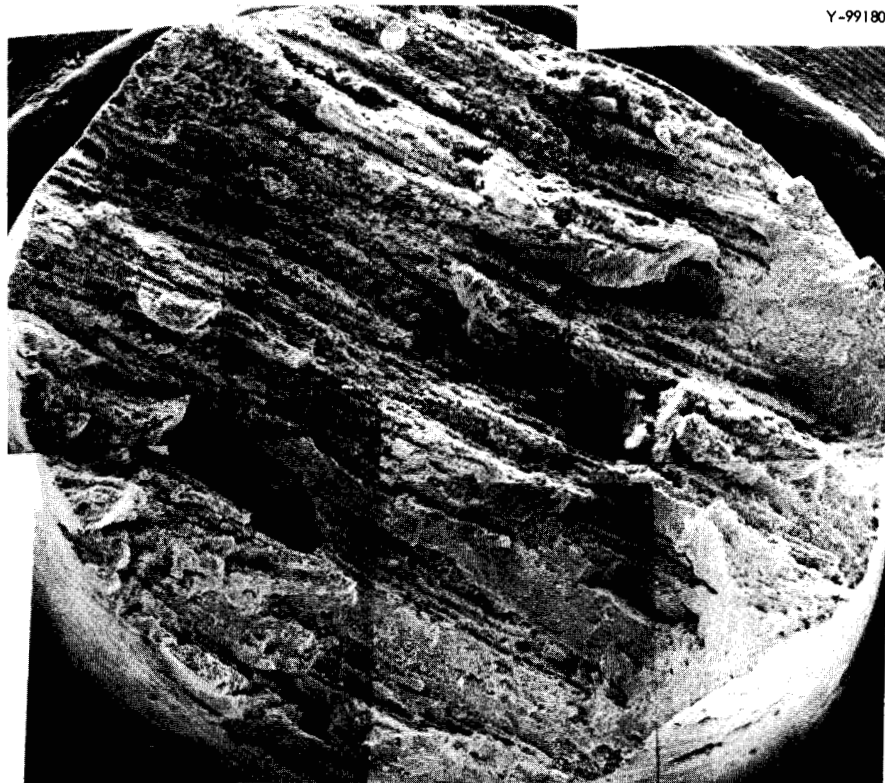


Fig. 20.4. Fracture Surface of Submerged-Arc Weld Tested Transverse to Weld Direction at 1200°F in the As-Welded Condition. Specimen diameter is  $\frac{1}{8}$  in.

## 21. Sodium Corrosion in LMFBR Systems

J. H. DeVan W. O. Harms

The purpose of this program is to determine the corrosion properties of fuel-cladding and structural materials for liquid-metal fast breeder reactor (LMFBR) systems. Our studies are concerned with (1) the effects of interstitial impurities in sodium on the mechanical and corrosion properties of vanadium alloys and (2) the interaction of 300 series stainless steels, thermal insulation, and sodium in air at 600 to 800°C.

Corrosion of refractory metals by other alkali metals is reported in Chapter 24.

### MASS TRANSFER OF INTERSTITIAL IMPURITIES BETWEEN VANADIUM ALLOYS AND SODIUM

While vanadium alloys strongly resist dissolution by sodium, they are adversely affected by reaction with the interstitial impurities O, C, and N, which are carried by the sodium. We have studied the partitioning of these elements between vanadium alloys and sodium and the attendant effect of this partitioning on the mechanical properties of vanadium alloys.

#### Effect of Oxygen in Sodium on the Corrosion of Vanadium and Vanadium Alloys

R. L. Klueh

Various vanadium alloys were tested in static capsules at 600°C to determine the effect of alloying elements on the reactivity of vanadium with oxygen in sodium.<sup>1,2</sup> The alloys tested: V-5% Cr, V-10% Cr, V-15% Cr, V-1.3% Zr, V-5% Zr, V-20% Mo, V-20% Ti, V-15% Cr-5% Ti, Vanstar 7 (V-9% Cr-3% Fe-1.3% Zr-0.05% C), Vanstar 8 (V-8% Cr-10% Ta-1.3% Zr-0.05% C), and Vanstar 9 (V-6% Fe-5%

Nb-1.3% Zr-0.05% C). The results of these tests are summarized below.

1. The distribution coefficient for oxygen between sodium and vanadium-chromium alloys, as shown in Fig. 21.1, decreases with increasing chromium content (i.e., chromium decreases the solubility of oxygen in vanadium). The addition of molybdenum to vanadium produced a similar result.
2. Vanadium alloys containing zirconium and titanium form internal oxides, and the saturated alloys contain more oxygen – both dissolved and combined as precipitated oxides – than similarly exposed unalloyed vanadium.
3. Vanstar 7 acquires less oxygen from sodium at a given oxygen level than either Vanstar 8 or 9.

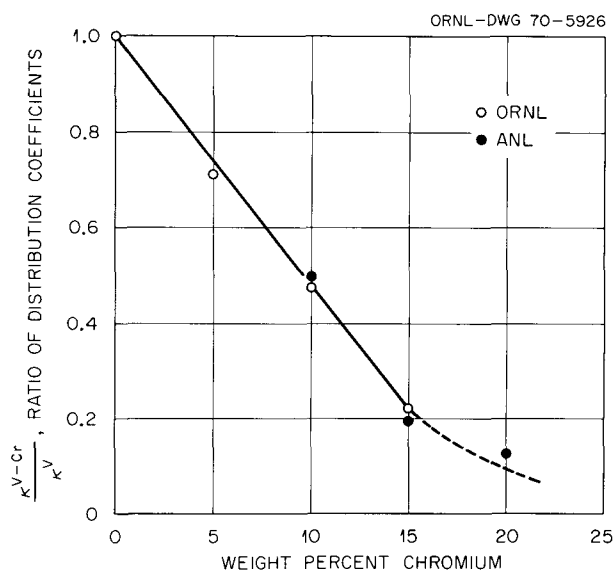


Fig. 21.1. The Effect of Chromium Concentration in Vanadium on the Distribution Coefficient for Oxygen Between Sodium and Vanadium. ANL results appear in *Reactor Development Program Progress Report December 1969*, ANL-7655, p. 53.

<sup>1</sup>R. L. Klueh, *Fuels and Materials Development Program Quart. Progr. Rept. Dec. 31, 1969*, ORNL-4520, pp. 176-77.

<sup>2</sup>R. L. Klueh, *Fuels and Materials Development Program Quart. Progr. Rept. March 31, 1970*, ORNL-4560, pp. 129-33.

### Effect of Oxygen on the Mechanical Properties of Vanadium Alloys

H. Inouye R. L. Wagner<sup>3</sup>

We creep tested unalloyed vanadium in ultrahigh vacuum and in oxygen at low pressure to determine the effects of oxygen absorption by vanadium on its creep behavior. Before the creep tests, we determined the effects of oxygen pressure and temperature on the oxidation of vanadium and its alloys.

The contamination rates of vanadium, V-5% Cr, V-10% Cr, V-15% Cr, and the Vanstar alloys (see previous section for compositions) were determined<sup>4</sup> between 500 and 700°C in oxygen at pressures of  $10^{-6}$  to  $10^{-7}$  torr. Increasing the chromium content decreased the rate of contamination by oxygen. Decreasing the oxygen pressure from  $5 \times 10^{-6}$  to  $1 \times 10^{-7}$  torr at 600°C reduced the contamination rate by more than a factor of ten.

We found that the creep properties of vanadium precontaminated with oxygen are quite different than those that develop during contamination to the same

end-of-test oxygen concentration.<sup>5</sup> As shown in Fig. 21.2, the creep properties of vanadium stressed to 11,000 psi in vacuum at 600°C are the same uncontaminated and precontaminated with 470 ppm O. However, when oxygen was introduced into the vanadium by maintaining an oxygen overpressure of  $3 \times 10^{-7}$  torr during the creep test, the creep rate was five times that of the precontaminated specimen. Moreover, the time to produce 1% strain was lower by a factor of 30. The fact that creep strains greater than 24% can be achieved without fracture indicates that an oxygen content of about 0.05% does not impair the ductility of vanadium.

### Mass Transport Between 300 Series Stainless Steels and Vanadium Alloys

D. H. Jansen

The transfer of carbon and nitrogen from austenitic stainless steels to vanadium alloys is predicted thermodynamically when these alloys coexist in sodium. We are studying the kinetics of this transport process in bimetallic thermal convection loops of the design

<sup>3</sup>Present address, Cabot Corp., Kokomo, Ind.

<sup>4</sup>R. L. Wagner, *Fuels and Materials Development Program Quart. Progr. Rept. Dec. 31, 1969, ORNL-4520, pp. 179-80.*

<sup>5</sup>H. Inouye, *Fuels and Materials Development Program Quart. Progr. Rept. March 31, 1970, ORNL-4560, pp. 133-34.*

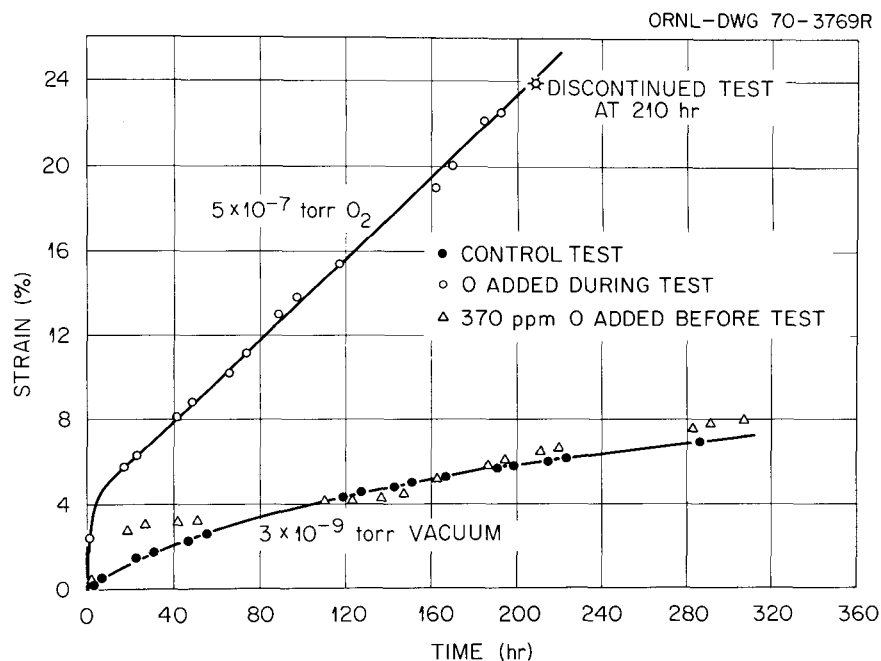


Fig. 21.2. Creep Behavior of 0.021-in.-thick Vanadium Sheet Specimens in Vacuum and in Low-Pressure Oxygen. Specimens were creep tested at 600°C at a stress of 11,000 psi.

ORNL-DWG 68-10751A

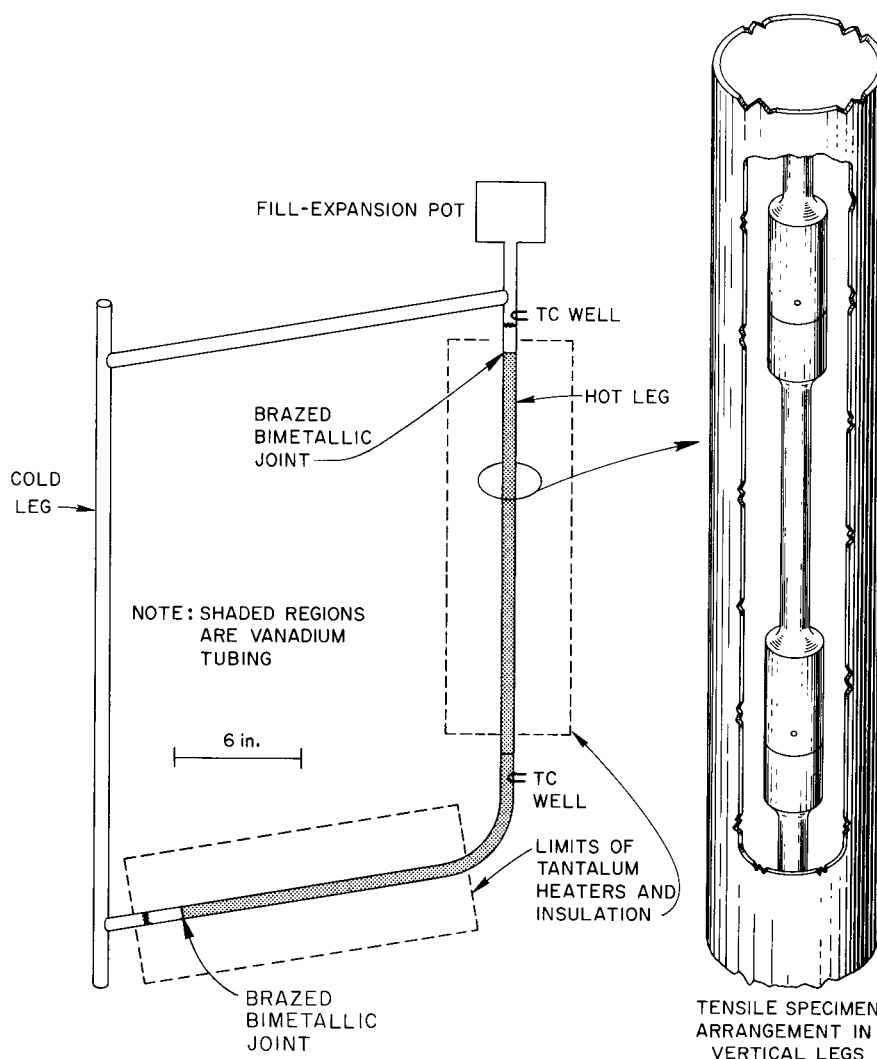


Fig. 21.3. Schematic Drawing of Sodium Thermal Convection Loop for Studying Mass Transfer Between Austenitic Stainless Steels and Vanadium Alloys.

shown in Fig. 21.3. In loops operated for 3000 hr at a hot-leg temperature of  $700^{\circ}\text{C}$ , we observed<sup>6,7</sup> that carbon and nitrogen migrated from the stainless steel to the vanadium, the rate increasing as the surface temperature of the vanadium increased. At a given loop temperature, the transport rate was the same, irrespective of loop position. Interstitial transfer was greater in a type 304L stainless steel loop than in a type

321 stainless steel loop of similar design. Vanadium specimens exposed at 650 to  $700^{\circ}\text{C}$  in a type 304L stainless steel loop showed a decrease in room-temperature ductility and an increase in tensile strength. In contrast, the room-temperature mechanical properties of vanadium specimens exposed in a type 321 stainless steel loop were comparable to those of control specimens exposed to argon for a similar time and temperature.

The transport of carbon and nitrogen between vanadium and austenitic stainless steels in sodium was also studied in a series of static pots.<sup>6</sup> In these tests, stainless steel and vanadium-base tensile specimens were

<sup>6</sup>D. H. Jansen, *Fuels and Materials Development Program Quart. Progr. Rept. Sept. 30, 1969*, ORNL-4560, pp. 118-22.

<sup>7</sup>D. H. Jansen, *Fuels and Materials Development Program Quart. Progr. Rept. Sept. 30, 1970*, ORNL-4560, pp. 134-38.

immersed in sodium in stainless steel vessels for 500 hr at 700 and 800°C. The surface area of vanadium was one-fourth that of stainless steel. Equal numbers of tests used type 304L and type 321 stainless steel. The vanadium-base materials included purified and commercial grades of unalloyed vanadium, V-5% Cr, V-10% Cr, and V-15% Cr.

The extent of movement of carbon and nitrogen in the tests at 700°C closely paralleled the results from the thermal-convection loops described above. Interstitial transport between type 304L stainless steel and vanadium was about ten times greater at 800°C than at 700°C. In contrast, transport between type 321 stainless steel and vanadium-base alloys was only 50% greater at 800°C than at 700°C. Transport of interstitial impurities significantly decreased the ductility of vanadium-base specimens exposed to type 304L but not type 321 stainless steel at 800°C.

#### COMPATIBILITY OF STAINLESS STEELS AND THERMAL INSULATION MATERIALS

C. D. Bopp<sup>8</sup> J. H. DeVan

We studied the reactions that occur between commercial thermal-insulation materials and austenitic stainless steel of the type under consideration for LMFBR primary circuit piping. In a supplemental study, we studied the effect of sodium leakage on the oxidation behavior of austenitic stainless steels and on the reaction of these steels with thermal-insulation materials.

In the first phase of this task we investigated the compatibility of Al<sub>2</sub>O<sub>3</sub>-SiO<sub>2</sub> blanket insulations with types 304L and 316 stainless steel between 370 and 760°C in the absence of sodium oxidation products.<sup>9</sup> Initial tests were conducted in moist air under cyclic temperature conditions. From both metallographic and kinetic measurements, we concluded that there is little effect of contact with insulation on the oxidation of either of these stainless steels, even at 760°C. Although there was metallographic evidence of breakaway oxidation at 760°C, the scaling rate was still very low after 3000 hr. In agreement with other investigators, we found that the resistance of type 316 stainless steel to scaling at 760°C was noticeably poorer than that of type 304 stainless steel under comparable conditions.

<sup>8</sup>On loan from Reactor Chemistry Division.

<sup>9</sup>A. P. Litman, *Fuels and Materials Development Program Quart. Progr. Rept. Dec. 31, 1969*, ORNL-4520, pp. 181-86.

We attribute this to a difference in the sensitization properties of the two alloys.<sup>10</sup>

Additional oxidation tests were conducted<sup>9,10</sup> on types 304, 304L, 304H, 316, and 316L stainless steels at 760°C in an atmosphere of N<sub>2</sub>-1% O<sub>2</sub>-100 ppm H<sub>2</sub>O. All steels formed a highly protective scale within a few hours, and the amount of metal consumed by oxidation was no more than 1.7 mg/cm<sup>2</sup> after 2700 hr. Here again, contact with commercially available thermal-insulation materials had little effect on oxidation.

In our studies of the effect of a small sodium leak on the oxidation behavior of austenitic stainless steels in and out of contact with thermal insulation,<sup>9,10</sup> the test variables included (1) the effect of moisture in the atmosphere, (2) the temperature of the sodium, and (3) the size and shape of the leak. The tests were conducted on type 304 stainless steel tubing 0.5 in. OD × 0.35 in. wall thickness partially surrounded by insulation. A defect of controlled size was put into the tube wall, and sodium was forced through the hole from the inside to the outside of the tube. Tests conducted in an atmosphere of N<sub>2</sub>-1% O<sub>2</sub>-100 ppm H<sub>2</sub>O at 760°C gave the following results.

1. Injection of sodium through a large hole (about 0.001 in. in diameter and larger) resulted in complete loss of sodium from inside the tube with no plugging of the hole.<sup>9</sup> As a consequence of oxidation, the diameter of the hole increased slightly, and the insulation reacted with sodium to a depth of about 0.5 in. to produce a brittle, black, charcoal-like substance. Some yellow sodium peroxide was also evident. Except for enlargement of the hole, the leaking sodium did not affect the stainless steel. Alumina blanket-type insulation (Kaowool, a product of Babcock & Wilcox) and colloidal silica insulation (MIN-K 2000, a product of Johns-Manville) gave the same results.
2. Injection of sodium through a small crack (air leak rate less than 10<sup>-4</sup> atm cm<sup>3</sup> sec<sup>-1</sup>) was prevented by the formation of sodium oxide; a slight seepage of sodium was effected by establishing a 250 psig pressure difference across the crack, but then the crack closed permanently. Oxidation around the crack was more extensive than around the larger leaks, suggesting that in the latter case sodium is forced more quickly into the insulation. In none of the tests did the products of the sodium-insulation reaction appear to be reactive with stainless steel.<sup>10</sup>

<sup>10</sup>J. H. DeVan, *Fuels and Materials Development Program Quart. Progr. Rept. March 31, 1969*, ORNL-4560, pp. 138-41.

## 22. Nondestructive Testing Techniques for LMFBR

W. O. Harms    R. W. McClung

We are developing new methods, techniques, and equipment for nondestructively inspecting materials or components related to the liquid-metal fast breeder reactor (LMFBR). Among the methods studied are electromagnetic induction, ultrasonics, and penetrating radiation. Special emphasis is being given to developing techniques for measuring the degree of cold work in stainless steel tubing with a small diameter.

### DEVELOPMENT OF ADVANCED NONDESTRUCTIVE TESTING

#### Eddy-Current Instrument

C. V. Dodd

One of the major problems with detection of defects by means of eddy currents is properly identifying signals from defects. Defects near the surface and other surface irregularities produce signals that obscure internal defects that may be in a more critical region in terms of failure of a component. Our analytical studies indicate that by measuring the phase shift of the signal we can determine the depth of the defect below the surface. We should then be able to use this information to correct the amplitude of the signal so that all defects of the same size have the same amplitude. In addition, defect signals from a noncritical region could be ignored.

We have begun design of a prototype instrument to investigate these potential benefits. Since the proposed instrument will measure phase shift, we had a modular phase-sensitive eddy-current instrument constructed, and we plan to use many of the modules in the prototype. We have constructed a scaled-up experiment consisting of a large driver coil with two pickup coils encircling a column of mercury. Various simulated defects can be placed in the mercury and moved about to selected locations. We shall use these to measure the phase and amplitude response that would be related to different depths in a solid rod.

### Ultrasonic Schlieren Techniques for Inspection of Welds

H. L. Whaley, Jr.    K. V. Cook

We are studying the response of ultrasound to various types of weld defects in a series of stainless steel and aluminum samples. The samples are consumable-electrode butt welds in 1-in.-thick plate. The welds contain intentional defects such as porosity, inclusions, incomplete fusion, and incomplete penetration. Initial tests<sup>1</sup> performed with our optical schlieren system on the series of aluminum samples confirmed the existence of defects in the intended areas of the welds and determined optimum transducer placement for detection by the schlieren technique of defects in the root and interface.

Each sample is being examined by three independent ultrasonic techniques: (1) schlieren, (2) pulse-echo, (3) delta technique. These have been described in detail elsewhere.<sup>2</sup>

Each technique has certain advantages that can help us to learn more about interactions between ultrasound and flaws in welds and thus, hopefully, suggest improvements in weld inspection techniques. The results from each examination are being correlated with those from the other two techniques and with radiographs of the samples. Some samples will ultimately be analyzed destructively to determine directly the exact nature of the defects.

---

<sup>1</sup>H. L. Whaley and K. V. Cook, *Fuels and Materials Development Program Quart. Progr. Rept. Sept. 30, 1969*, ORNL-4480, pp. 114-15.

<sup>2</sup>H. L. Whaley and K. V. Cook, "Ultrasonic Schlieren Techniques for Evaluation of Welds," *Fuels and Materials Development Program Quart. Progr. Rept. June 30, 1970*, ORNL-4600, in preparation.

## MEASUREMENT OF COLD WORK IN STAINLESS STEEL TUBING

C. V. Dodd    W. A. Simpson, Jr.

We are investigating methods for nondestructively measuring the degree of cold work in small-diameter stainless steel tubing. We emphasize the use of electromagnetic induction for detecting the changes in magnetic permeability produced by cold work.

We prepared two sets of samples of type 316 stainless steel, each containing known amounts of cold work ranging from none to 50%. One set is a series of tubes 0.250 in. in diameter  $\times$  0.015 in. in wall thickness; the other is a series of sheets 0.015 in. thick. Our first efforts, with the flat sheet, were to establish quantitative instrument response relative to cold work without the problems that might be caused by the small radius of curvature on the tubes.

Cold work has been correlated with the magnetic permeability in some austenitic stainless steels.<sup>3</sup> An increase in relative permeability from 1.003 to 1.01 in the normal ranges of cold work and values as high as 10 for severe cold work are reported. Using the relationship we previously developed,<sup>4</sup> we calculated the response from a low-frequency inductance bridge circuit and determined that we could measure permeability changes between 1.003 and 1.01. We constructed on a breadboard a system for making these measurements and operated it in a "bridge unbalanced" mode, similar to many eddy-current tests, to separate the conductivity variations from the permeability variations. The permeability correlated very well with the

degree of cold work. Although these preliminary measurements were very encouraging, considerable refinement is needed in both the circuitry and the technique to optimize this method.

Because of the excellent response of the eddy-current bridge system to cold-rolled flat sheets, we designed a prototype system that uses encircling coils for tubes. As part of the design study, we used our recent computer program that is a mathematical model for an impedance bridge and allows studies of variations in the components of the circuit.<sup>5</sup> The system finally selected was determined to be the best of a number that we analyzed on the computer. The calculations indicate that we can measure the relative permeability in the tubes to within  $\pm 50$  ppm. Our work thus far indicates that a change from 19 to 21% cold work increases permeability by 150 ppm. With our computer program we determined how much variance we could allow in the components of the impedance bridge and still achieve this accuracy. While this places a rather stringent requirement on the components, the required quality is commercially available. We have obtained all the components and begun construction on the instrument.

<sup>3</sup>Taylor Lyman (ed.), *Metals Handbook*, 8th ed., pp. 423, 793, vol. I, American Society for Metals, Metals Park, Novelty, Ohio, 1961.

<sup>4</sup>J. W. Luquire, W. E. Deeds, C. V. Dodd, and W. G. Spoeri, *Computer Programs for Some Eddy Current Problems*, ORNL-TM-2501 (August 1969).

<sup>5</sup>C. V. Dodd, W. G. Spoeri, W. E. Deeds and W. A. Simpson, *Fuels and Materials Development Program Quart. Progr. Rept. Dec. 31, 1969*, ORNL-4520, pp. 308-9.

## 23. Fast Breeder Neutron Absorber Materials

W. R. Martin

One of the most popular neutron absorber materials for thermal reactors is boron carbide. For the Fast Breeder Reactor (FBR), boron carbide and tantalum were selected as the prime candidate materials. But little is known about the irradiation behavior of these materials or alternate absorber materials at the temperature and fluence anticipated for FBR's. The purpose of this program over the last year has been to characterize boron carbide, study its basic irradiation behavior, and use this information to improve its projected performance in FBR service.

### VOID FORMATION IN BORON CARBIDE POWDER DURING HEAT TREATMENT

G. L. Copeland R. S. Mateer<sup>1</sup>

Heating of some commercial crushed boron carbide powders to high temperatures produces polyhedral pores in the center of some particles. These appear to be Kirkendall porosity formed as boron diffuses from the center to the edge of the particle as homogenization occurs. The voids appear in hot-pressed boron carbide as shown in Fig. 23.1, which is an electron micrograph of a fracture surface. These voids may influence the irradiation behavior of boron carbide.

We have proposed a mechanism for the formation of these voids. The solidification of boron carbide during manufacture yields a cored structure with a boron-rich boron carbide in the center of the grains and a eutectic of stoichiometric boron carbide and graphite in the grain boundaries. During crushing, fracture occurs predominantly through or around the grain boundaries, which contain the carbon-rich eutectic, resulting in many particles containing graphite on the surface and excess boron in the center. During subsequent heat treatment, the excess boron diffuses to the edge of the particle and reacts with the graphite to form boron carbide.

The size of the voids can be varied by temperature and duration of heat treatment. After 1 hr at 2000 and 1500°C, typical void sizes are 3 and 1  $\mu\text{m}$ , respectively. The volume of voids produced can be varied by adjusting the chemical composition. Blending boron powder with the crushed boron carbide powder before heat treating decreases the void volume produced, whereas blending carbon with the crushed powders increases the void volume. Pycnometer measurements indicate a maximum of 5% decrease in density during heat treatment.

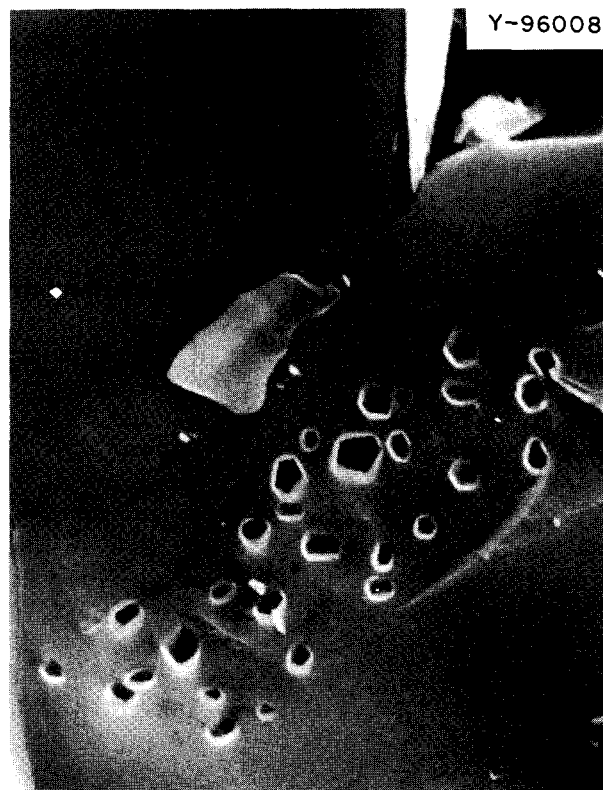


Fig. 23.1. Scanning Electron Micrograph of Voids Observed on the Fracture Surface of Hot Pressed Boron Carbide, 3000X.

<sup>1</sup>Consultant from University of Kentucky.

## TRANSMISSION ELECTRON MICROSCOPY OF BORON CARBIDE

C. K. H. DuBose D. N. Braski<sup>2</sup> G. L. Copeland

To allow better characterization of boron carbide, we developed a technique for preparing thin films of boron carbide for transmission electron microscopy. Boron carbide has resisted successful thinning by conventional techniques because of its hardness, brittleness, and chemical inertness combined with the presence of voids, which are attacked preferentially as the film is thinned. These difficulties have been overcome through use of an ion-bombardment milling machine. A high-quality thin film has been produced from a high-density boron carbide pellet hot pressed from Norbide 325F powder. The electron transmission micrograph, Fig. 23.2, shows that the film was uniformly thinned in the area of the voids. The edges of the voids are parallel to crystal planes, as shown by comparison to dislocations in the film. The twins and grain boundaries are revealed clearly. Transmission electron microscopy should prove to be a valuable tool in the study of irradiated materials.

## CRYSTALLOGRAPHY OF UNIRRADIATED BORON CARBIDE

L. A. Harris H. L. Yakel

A single-crystal x-ray diffraction study of boron carbide was undertaken to characterize crystals before irradiation. Most of these crystals can be described as elongated or needle-like in shape.

X-ray diffraction data for the crystals were obtained from rotation and Weissenberg photographs recorded with Cu K $\alpha$  ( $\lambda = 1.5418 \text{ \AA}$ ) radiation. The crystals were rhombohedral with unit cell dimensions  $a_0 = 5.17 \text{ \AA}$  and  $\alpha = 65^\circ 40'$ . The dimensions may be compared with those given by Clark and Hoard<sup>3</sup> ( $a_0 = 5.19 \text{ \AA}$ ,  $\alpha = 65^\circ 15'$ ); and Zhdanov and Sevastyanov<sup>4</sup> ( $a_0 = 5.18 \text{ \AA}$ ,  $\alpha = 65^\circ 45'$ ) for B<sub>4</sub>C crystals.

Our crystals had their long axes parallel to a rhombohedral  $a$ -axis, whereas the crystals described by Clark and Hoard were elongated parallel to a hexagonal  $a$ -axis. Though the crystal habits for these two sets of crystals differed, they are both twinned on rhombohedral faces,

<sup>2</sup>Isotopes Division.

<sup>3</sup>H. K. Clark and J. L. Hoard, *J. Am. Chem. Soc.* **65**, 2115 (1943).

<sup>4</sup>G. S. Zhdanov and N. G. Sevastyanov, *Compt. Rend. Acad. Sci. URSS*, **32**, 432 (1941) as cited by F. W. Glaser, D. Moskowitz, and B. Post, *J. Appl. Phys.* **24**, 731-33 (1953).

(10 $\bar{1}1$ ) hexagonal. We found no untwinned crystals. Many had repeated twinning, so the crystals appear serrated when viewed down the long axis.

## GAS RELEASE FROM BORON CARBIDE POWDERS DURING IRRADIATION IN A THERMAL REACTOR

G. L. Copeland

We irradiated boron carbide powder in the Oak Ridge Research Reactor in sealed capsules insulated from the cooling water to increase the temperature of the experiment by gamma heating. The Norbide 325F powder was irradiated as received and after annealing in vacuum for 1 hr at 1500 and 2000°C. Pycnometer measurements of density indicated that 2.6 and 4.9% voids were formed by 1500 and 2000°C anneals. The results are summarized in Table 23.1. The powders all released about 5.3% of the gas generated, indicating that the void volumes had no effect on the gas release at these low irradiation temperatures. This is not unexpected, since the major factor in gas release is recoil from the small particle during the three-week irradiation at 350°C. Longer tests at higher temperatures are now in progress.

Table 23.1. Summary of Irradiation Tests of Norbide 325F Boron Carbide<sup>a</sup> in the ORR

	Capsule		
	0-1	0-2	0-3
Heat treatment	1500°C, 1 hr	2000°C, 1 hr	None
Irradiation temperature, °C	340		360
Burnup, % of <sup>10</sup> B	8.8	9.4	6.6
Helium release, %	5.8	5.2	5.0

<sup>a</sup>B:C ratio 3.62.

## X-RAY DIFFRACTION OF IRRADIATED AND UNIRRADIATED BORON CARBIDE POWDERS

V. J. Tennery R. S. Mateer<sup>1</sup> G. L. Copeland

Several changes were observed in the Debye-Scherrer x-ray diffraction patterns of boron carbide powders after heat treatment and after irradiation. Some of these changes are not presently understood and will be studied further.

After heat treatment for 1 hr at 1500°C and higher, the free graphite lines are not observed, although they are generally present in as-crushed material. We observed some line shifts, which are probably related to

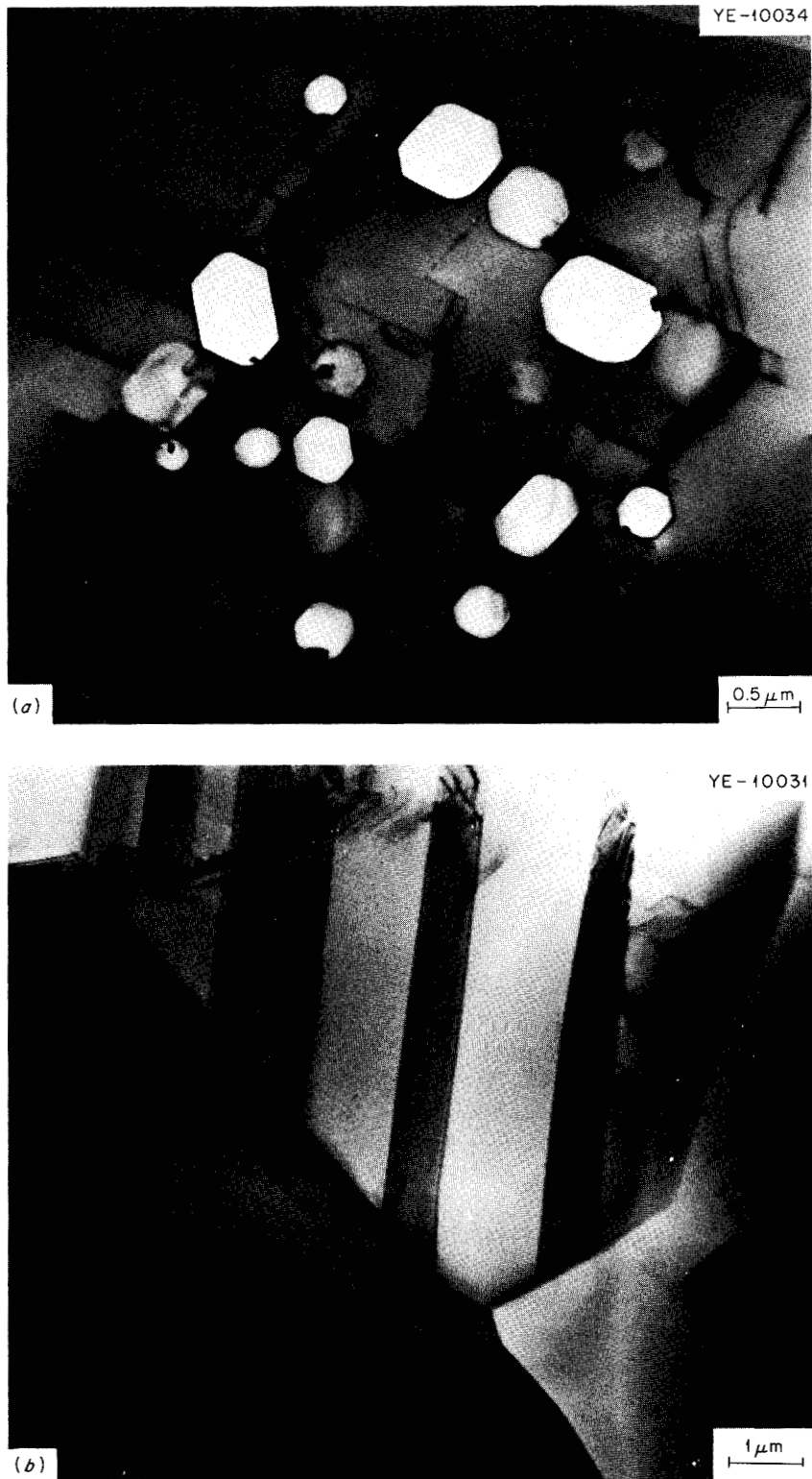


Fig. 23.2. Transmission Electron Micrographs Showing (a) Voids and Dislocations and (b) Grain Boundary and Twins.

lattice parameter changes due to homogenization of the material. In several instances, extraneous lines that could not be attributed to contamination appeared in the patterns of heat treated material.

After irradiation, the residual gamma level necessitates careful tailoring of the x-ray beam intensity to produce the diffraction lines on the film before the low residual activity darkens the film and obscures weak lines. Powder patterns of the three powders irradiated to about 9% depletion of  $^{10}\text{B}$  [ $19 \times 10^{20}$  ( $n, \alpha$ ) reactions/cm $^3$ ] at 350°C were compared with patterns taken before irradiation. The diffraction lines were more diffuse in the patterns of the irradiated material. Irradiation led to the disappearance of the extraneous lines in the heat treated sample and the disappearance of the free graphite line. Heat treatment at comparable time and temperature did not remove free graphite from unirradiated material. Another change observed in the pattern made after irradiation was a sizable increase in the relative intensity of the (006) boron carbide line. This could possibly correspond to a displacement of the carbon atoms during irradiation, as observed by Tucker

and Senio.<sup>5</sup> No lines attributable to any proposed lithium compounds were observed; however, new low-intensity lines appeared at  $d$  spacings of 1.763 and 1.242 Å.

### SCANNING ELECTRON MICROSCOPY OF IRRADIATED AND UNIRRADIATED BORON CARBIDE

G. L. Copeland

We examined crushed boron carbide powders using the scanning electron microscope. The as-received powders shown in Fig. 23.3(a) show many small irregular specks on the larger particles. We believe that most of these are free graphite. Lines indicating free graphite are observed on the x-ray diffraction powder patterns of this material. After heat treatment at 2000°C in vacuum for 1 hr, the powders appear as in Fig. 23.3(b). The irregular specks have rounded and

<sup>5</sup>C. W. Tucker and P. P. Senio, *Acta Cryst.* 8, 371-78 (1955).

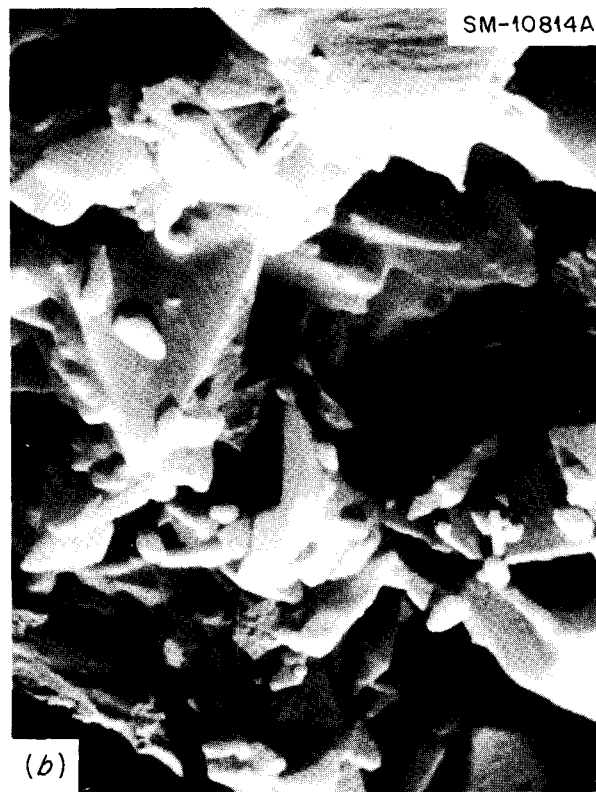


Fig. 23.3. Scanning Electron Micrographs of Boron Carbide Particles. 3000X. (a) As crushed. (b) After vacuum heat treatment for 1 hr at 2000°C.

their appearance has changed. We believe the free graphite has reacted with boron to form boron carbide. This heat treatment produces voids in the center of some of these particles, and the free graphite lines are not observed on x-ray diffraction powder patterns after the 2000°C heat treatment.

The powders irradiated at 350°C to 7 to 9% depletion of  $^{10}\text{B}$  [ $15$  to  $19 \times 10^{20}$  ( $n, \alpha$ ) reactions/cm $^3$ ] were examined in the scanning electron microscope. The powders appeared exactly the same after irradiation as before. The heat treated powders were scanned carefully after irradiation for evidence of voids such as shown in Fig. 23.1. The fact that no voids were observed indicates that there was no significant fracturing of the particles during irradiation.

### FAST REACTOR IRRADIATION TESTING OF BORON CARBIDE

G. L. Copeland G. W. Keilholtz<sup>6</sup>

Irradiation tests in a fast reactor are necessary to correlate basic test results to expected performance in a

fast reactor. We are preparing a test of six capsules in row 7 of the Experimental Breeder Reactor-II (EBR-II). Each capsule consists of two pellet pins. The variables included in the 12 pellet pins are summarized in Table 23.2. The test is designed to determine the effects on performance of (1) irradiation temperature, (2) pellet density, (3) boron-to-carbon ratio, (4) size and volume of intraparticle voids, (5) particle size of the powder used for the pellets, and (6) hot-pressing temperature. The capsules have been designed and are being fabricated for insertion in the reactor.

<sup>6</sup>Reactor Chemistry Division.

Table 23.2. Summary of Planned Tests of Boron Carbide in Experimental Breeder Reactor-II

Pellet Pin	Irradiation Temperature (°C)	Atom Ratio B:C	Particle Size (U.S. Standard Mesh)	Density (% of Theoretical)	Hot-Pressing Temperature (°C)	Notes
1-T	427	3.62	-325	>98	2300	a
1-B	427	3.62	-325	90	2300	a
2-T	427	4.50	-325	>98	2300	b
2-B	427	4.50	-325	90	2300	b
3-T	427	4.50	-325	90	2300	c
3-B	427	4.50	-80 +325	90	2300	c
4-T	427	3.62	-325	90	1800	d
4-B	427	3.62	-325	90	1800	e
5-T	700	3.62	-325	>98	2300	a
5-B	700	3.62	-325	90	2300	a
6-T	700	4.50	-325	>98	2300	b
6-B	700	4.50	-325	90	2300	b

<sup>a</sup>Intraparticle voids held constant, but more interparticle voids in B pins. Powder is -325 mesh fraction of a commercial boron carbide.

<sup>b</sup>Boron powder blended with powder from the same batch used for pins 1 and 5 to decrease the amount of intraparticle voids.

<sup>c</sup>Boron-to-carbon ratio is obtained by selecting a size fraction of a crushed ingot that contains proeutectic boron carbide rich in boron with no free carbon. The selected size fraction will then be ground to different sizes for 3-T and 3-B. Pellets hot pressed from this powder should contain no intraparticle voids.

<sup>d</sup>Powder from the same batch used in pins 1 and 5. Hot pressing in vacuum at a lower temperature will result in decreased intraparticle void size.

<sup>e</sup>Powder from the same batch used in pins 1 and 5. The powder will be vacuum annealed at 2300°C to provide the same intraparticle void size as in pins 1 and 5. The pellet will then be hot pressed in vacuum at 1800°C.

## Part III. Space Power Technology

### 24. Alkali-Metal Corrosion of Refractory Metals

J. H. DeVan    W. O. Harms

The purpose of this program is to investigate the chemical and metallurgical effects produced in refractory metals during exposure to alkali metals for primary and secondary circuits of space nuclear power systems. Principal emphasis during this report period was on studies of mass-transfer reactions in both primary lithium circuits and secondary (Rankine-cycle) power-conversion circuits involving boiling potassium.

Work on corrosion by sodium, aimed primarily at fast breeder reactor applications, is reported in Chapter 21.

#### LITHIUM CORROSION STUDIES

Lithium is of interest as a coolant for high-performance nuclear reactor systems.<sup>1</sup> Refractory alloys based on Nb, Ta, W, and Mo are ideally suited as container materials for these applications because of their low solubilities in lithium and their superior high-temperature strengths. We have investigated the corrosion behavior of refractory metals in lithium with respect to thermal-gradient mass transfer and the effects of oxygen on grain-boundary penetration.

#### Thermal-Convection Loop Tests

J. H. DeVan

We continued our study of the mechanisms that control the mass transfer of oxygen, nitrogen, and carbon in lithium-refractory metal systems. The results

---

<sup>1</sup>W. O. Harms and A. P. Litman, "Compatibility of Materials with Alkali Metals for Space Nuclear Power Systems," *Nucl. Appl.* 5, 156-72 (1968).

of thermal convection loop tests on niobium-base alloys that have been conducted over the past four years point to a link between the transfer of nitrogen and zirconium from hot to cold regions. We have now shown that the rate of transport of these two elements is limited by the solid-state diffusion of zirconium to surfaces of the loop where zirconium is being depleted.<sup>2</sup>

We procured sheet and tubing for the construction of thermal convection loops of unalloyed tungsten and of W-25% Re. A brazing procedure was developed to connect various sections of the loops to avoid the recrystallization problem associated with fusion welding of tungsten and its alloys. All connections were designed as socket joints to provide tight, overlapping fits between adjacent loop sections. For this application, the gas tungsten-arc process with Mo-50% Re filler alloy was determined to be superior to the electron-beam process using the same filler alloy.

#### Forced-Circulation Lithium Loop

B. Fleischer

A lithium outlet temperature of 1370°C and a temperature difference of 165°C were achieved<sup>3,4</sup> in

---

<sup>2</sup>C. E. Sessions and J. H. DeVan, "Thermal Convection Loop Tests of Nb-1% Zr Alloy in Lithium at 1200 and 1300°C," *Nuclear Applications & Technology*, to be published.

<sup>3</sup>J. H. DeVan and W. R. Huntley, *Fuels and Materials Development Program Quart. Progr. Rept. March 31, 1970*, ORNL-4560, pp. 200-12.

<sup>4</sup>J. H. DeVan and A. P. Litman, *Fuels and Materials Development Program Quart. Progr. Rept. Dec. 31, 1969*, ORNL-4520, pp. 254-56.

an engineering-scale, forced-circulation loop constructed of the tantalum-base alloy T-111 (Ta-8% W-2% Hf). Specimens of the T-111 alloy were placed in the system to measure the effects of mass transfer, including mechanical properties. Pertinent test parameters are presented below.

Temperature, °C	
Maximum	1370
Minimum	1205
Flow rate, gal/min	5.2
Maximum velocity of lithium, ft/sec	18
Maximum Reynolds number	89,000
Total system pressure drop, psi	36
Resistance heater power, kW	30
Volume of circulated lithium, in. <sup>3</sup>	300
Number of Corrosion Specimens	
Flat	84
Annular	9

The loop was operated at design conditions for the scheduled test period of 3000 hr. However, the test was interrupted after 1735 hr when a lithium leak occurred in an auxiliary line leading from the hot leg to a surge tank.<sup>3</sup> Since the line was not essential, we removed it and sealed the opening where it adjoined the loop. This successful field repair constituted an important milestone in the application of tantalum-base alloys in high-temperature piping systems for space nuclear systems. Although we have not pinpointed the cause of the vent line leak, it appears to have been associated with the original condition of the vent line rather than to effects induced by the lithium.

The loop was instrumented with various types of thermocouples<sup>5</sup> to provide information on cost, reliability, and accuracy of high-temperature thermometry techniques. Thermocouples of W-3% Re vs W-25% Re showed no drift even when welded directly to the loop.<sup>3</sup> This experiment also demonstrated that the helical induction<sup>2</sup> pump affords a satisfactory means for circulating lithium at 1200°C.

The loop was designed so that the sections containing test specimens could be removed and new specimens substituted. We completed the fabrication of replacement specimens<sup>4</sup> of arc-cast tungsten, chemically vapor deposited tungsten, wrought chemically vapor deposited tungsten, W-25% Re, ASTAR 811C (Ta-8% W-1% Re-1% Hf-0.025% C), and T-111. In preparation for installing the second test section, we developed welding techniques for cutting into a tube filled with lithium and making a new field weld with automatic equipment.

<sup>5</sup> J. H. DeVan and A. P. Litman, *Fuels and Materials Development Program Quart. Progr. Rept. Sept. 30, 1969*, ORNL-4480, pp. 196-200.

## EFFECT OF OXYGEN ON THE COMPATIBILITY OF REFRACTORY METALS WITH ALKALI METALS

R. L. Klueh

We continued our study of the effect of oxygen on the compatibility of niobium and tantalum with the alkali metals potassium, sodium, and lithium. Reactions with oxygen in these systems depend upon whether the oxygen is present in the refractory metal or alkali metal. Oxygen added to the refractory metal above a threshold concentration renders the metal subject to penetration by the alkali metal. Oxygen added to the alkali metal promotes dissolution of the refractory metal.

### Alkali Metal Penetration

We showed that the rate of penetration of a refractory metal by an alkali metal was too rapid for a diffusion mechanism to apply and proposed a "wedging" mechanism to explain the observed penetration kinetics.<sup>6</sup> Wedging is caused by the formation of a corrosion product — presumably a ternary oxide — having a larger volume than the metal from which it forms.

<sup>6</sup> R. L. Klueh, paper presented at Symposium on Corrosion by Liquid Metals, Philadelphia, October 13-15, 1969, to be published by Plenum Press.

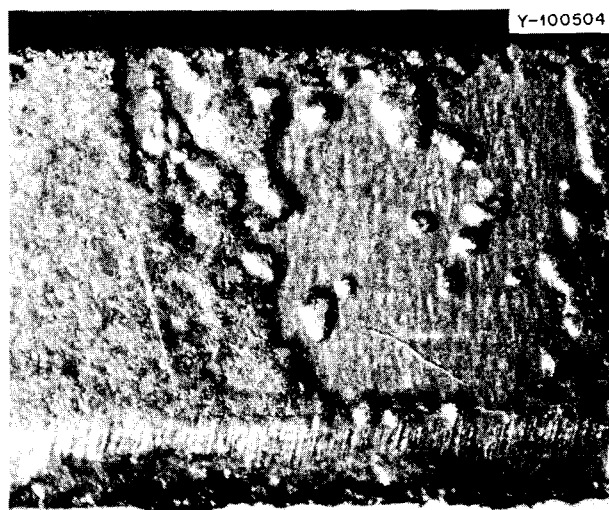


Fig. 24.1. Protuberances Observed on the Outside of a Tantalum Specimen Exposed to Potassium for 50 hr at 1000°C. The specimen contained 2000 ppm O before exposure. 25X. Reduced 28.5%.

We found evidence in the Ta-O-K and Nb-O-K systems that the formation of corrosion product does produce a volume expansion. Figure 24.1 shows protuberances on the external surface of a tantalum specimen that contained 2000 ppm O and was exposed to potassium at 1000°C. Sectioning this specimen (Fig. 24.2) revealed that the position of the subsurface corrosion products matched the locations of the surface protuberances. That is, the corrosion products distorted the external surface of the specimens when the stresses generated by the larger volume material could not be restrained by the surrounding material. We propose that penetration occurs when the pressure generated by the formation of corrosion products causes a crack and that subsequently liquid metal is drawn to the crack tip by both capillary action and the low-pressure region of the newly formed crack.

#### Effect of Oxygen on Dissolution of Refractory Metals in Alkali Metals

The effect of oxygen in potassium on the compatibility of tantalum and potassium was studied at 600, 800, and 1000°C in static capsules to which various amounts of K<sub>2</sub>O had been added. Increases in the oxygen concentration of the potassium were accompanied by increased amounts of tantalum found in the potassium after test. Unlike the Nb-O-K and Nb-O-Na systems,<sup>7,8</sup> the oxygen content of the refractory metal did not depend on changes in the oxygen concentration of the potassium. This observation suggests that a ternary oxide phase was formed.

<sup>7</sup>R. L. Klueh, *Corrosion* 25, 416-22 (1969).

<sup>8</sup>R. L. Klueh, pp. 171-76 in *Proceedings of the International Conference on Sodium Technology and Large Fast Reactor Design*, November 7-9, 1968, ANL-7520, Part I.

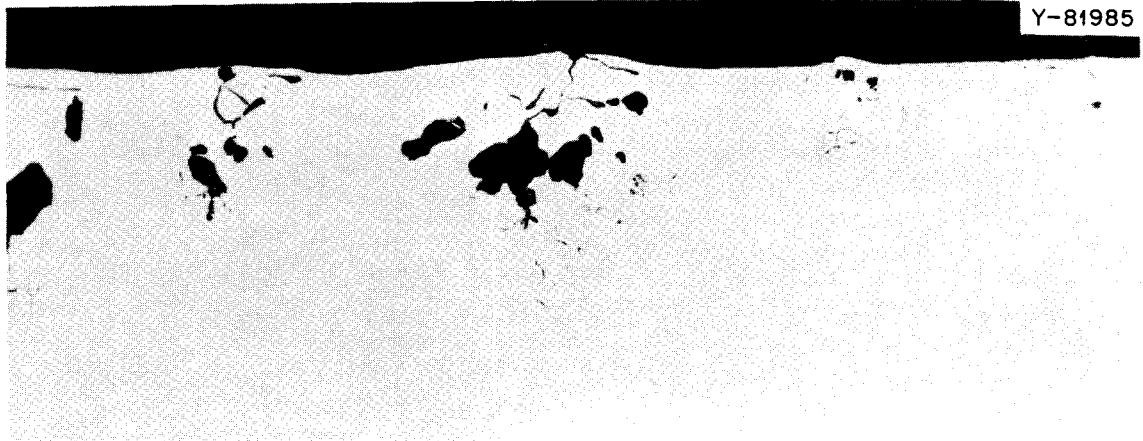


Fig. 24.2. Cross Section of Specimen Shown in Fig. 24.1. Note how protuberances are formed by stresses generated by subsurface corrosion products. 100X. Unetched.

## 25. Materials Development for Isotopic Power Programs

R. G. Donnelly    P. Patriarca

Materials studies were conducted on five separate programs concerned with power application of radioisotopes. The Curium-244 and the Cladding Materials Programs are space-oriented, while the Strontium-90, SNAP-23, and Isotope Kilowatt Programs are terrestrially oriented.

On the Curium Program we have been concerned with the fabrication of a tungsten capsule assembly for a 1000-W thermionic test and basic fuel-material compatibility.

On the Cladding Materials Program we completed studies on the effects of vacuum on superalloys, investigated the disorder-order transformation in alloys, and developed strong, noble-metal-base alloys. We are also investigating back extrusion for the fabrication of refractory metal capsules.

We completed our compatibility studies using non-radioactive strontium compounds for the Strontium-90 Program and our ultrasonic inspection of strontium-fueled capsules for the SNAP-23 Program. On the Kilowatt Program we provided consultation on the thermal conductivity and fabricability of iron alloys for a high-temperature radiation shield.

### CURIUM PROGRAM

#### Fabrication of Tungsten Capsules for the Thermionic Generator Mockup

R. E. McDonald    A. C. Schaffhauser

The isotope fuel capsule for the thermionic generator mockup experiment required intricate machining of 2 $\frac{1}{8}$ -in.-diam arc-melted tungsten bar. We developed the procedures and conditions to extrude this large-diameter bar with the microstructure and properties needed for successful machining of the capsule. Sufficient hot deformation was needed to break up the cast grain structure and produce a fine recrystallized or wrought grain structure.

Extrusion billets, nominally 8 in. in diameter  $\times$  18 in. long and weighing approximately 500 lb, were machined from 10-in.-diam castings procured from Climax Molybdenum Company. They were extruded under our supervision on the 2750-ton press leased from the Fansteel Metals Center, Baltimore. The first two billets were extruded at a reduction ratio of 3.7 at 1650 and 1725°C to provide 4-in.-diam billets for reextrusion on our 1250-ton press. However, the first extrusions had rough surfaces and radial cracks and did not yield sufficient sound material for successful reextrusion. Some of this material was used for end caps and welding studies.

Further investigation of this material indicated that the radial cracks may have been initiated from cracks in the casting. These cracks were not detected by dye penetrant inspection because of metal smearing during machining. We developed an electropolishing procedure to expose cracks and blunt the tips of the cracks so they would not propagate during machining. This procedure provided sound billets. The next extrusion, performed at 1775°C and a reduction ratio of 6.1 to break up the cast structure better, had an excellent surface and provided material for nine capsule blanks. The capsule was also electropolished at various steps during machining to ensure a crack-free surface. The completed capsule is shown in Fig. 25.1.

#### Capsule Welding

G. M. Goodwin

The need for highly reliable welding procedures during the assembly of the  $^{244}\text{Cm}_2\text{O}_3$ -fueled thermionic generator mockup dictated extensive pretest development. Optimum techniques were developed for welding each joint in the assembly, and aging studies were conducted to determine any possible deleterious effects. We tested welding atmospheres to determine



Fig. 25.1. Completed Capsule and Cap Machined from Extruded Arc-Melted Tungsten with Welded CVD Tungsten Vent Tube and Stainless Steel "S" Extension.

the tolerable impurity level in the final cell atmosphere during welding. A Lucite model of the test assembly was used to rehearse the assembly sequence and make necessary design modifications. With a resistance-heated mockup of the test assembly we determined the approximate temperature of the fueled capsule to be welded. Development was concentrated on three critical welds.

**1. Tungsten to Stainless Steel Vent Tube.** — The CVD tungsten vent tube was joined to an S-shaped type 304 stainless steel tube by gas tungsten-arc (GTA) braze welding in an inert atmosphere with type 308 stainless steel filler metal. Aging of such joints 1000 hr at the expected service temperature of 700°C showed no deleterious effects.

**2. Tungsten Vent Tube to Capsule.** — The CVD tungsten tube was joined to the arc-cast tungsten capsule by GTA braze welding in an inert atmosphere with W-25% Re filler metal.

**3. Tungsten Cap to Capsule Seal.** — The arc-cast tungsten cap was GTA fusion welded to the arc-cast tungsten capsule in the inert atmosphere of the hot cell. Tests in purposely contaminated atmospheres showed that the weld could be successfully completed if the atmosphere contained less than 100 ppm O<sub>2</sub>. A

supplementary purge chamber was constructed for use if the cell atmosphere could not reach this purity. The self-heating of the as-fueled capsule was simulated on test rings with the welding torch, bracketing the expected capsule preheat of 1000°C. Several test rings cracked until proper adjustment of the welding conditions prevented cracking. An independently rotating torch holder was developed to eliminate the need for rotation of the entire assembly. All components were leak tested before and after assembly in the hot cell.

The device was fueled and welded without need for the auxiliary purge chamber. Test rings were welded in-cell before fueling as an additional visual test of cell atmosphere. Seal welding was performed without incident, and visual observation showed the weld to be sound and exceptionally free of oxide contamination. The vent tube welds are shown in Fig. 25.1.

### Nondestructive Testing

K. V. Cook

Machining has smeared tungsten capsule material to cover discontinuities that would otherwise open to the surface. We had previously noted this on a number of materials and had found it necessary, as in this situation, to lightly etch before a valid penetrant examination. Thus, an electropolishing step was incorporated into the fabrication method to remove the smeared metal. An additional benefit was gained in that the polishing and penetrant test revealed defective stock before being committed to costly machining. Since insufficient smeared material might be removed to ensure an adequate penetrant test and since some discontinuities might not open to the surface, we employed an ultrasonic pulse-echo technique to select the best capsule for fueling. The capsule configuration required the use of a secondary transducer to supply a reference reflection to trigger an electronic gate for processing of flaw signals. The test was sufficiently sensitive to detect electrical-discharge-machined reference notches on both inner and outer surfaces with depths 3% of the wall thickness.

### Compatibility

J. R. DiStefano

We continued to study the compatibility of <sup>244</sup>Cm<sub>2</sub>O<sub>3</sub> fuel with refractory metals and alloys at 1650 and 1850°C for thermionic applications.<sup>1</sup> We

<sup>1</sup>J. R. DiStefano, *Metals and Ceramics Div. Ann. Progr. Rept. June 30, 1969, ORNL-4470, pp. 86-87.*

exposed Ta, Ta-10% W, T-111, Mo, TZM, W, and W-26% Re to  $^{244}\text{Cm}_2\text{O}_3$  for 1000 and 10,000 hr at 1650°C, and 1000, 5000, and 10,000 hr at 1850°C.

At 1650°C we found extensive penetration of the tantalum-base materials, but attack on Mo, TZM, W, and W-26% Re was limited to depths of 0.001 to 0.002 in. and occurred primarily as subsurface voids. However, in some cases  $^{244}\text{Cm}$  was detected in these areas.

Although the melting temperature of pure  $^{244}\text{Cm}_2\text{O}_3$  is approximately 2100°C, it showed evidence of liquefaction when exposed to tantalum or tantalum alloys at 1850°C. However, neither  $^{244}\text{Cm}$  nor  $^{244}\text{Cm}_2\text{O}_3$  penetrated these materials as at 1650°C.

Our conclusions are that W-26% Re, TZM, and Mo, in that order, showed the best compatibility with  $^{244}\text{Cm}_2\text{O}_3$ , especially at 1850°C, and all three would be acceptable container materials for up to 10,000 hr. We recently obtained unalloyed rhenium components for testing with  $^{244}\text{Cm}_2\text{O}_3$ , and from our results with W-26% Re we feel that it may also be a good containment material.

We tested some of the potential container materials for  $^{244}\text{Cm}_2\text{O}_3$  at the lower temperatures that are applicable for thermoelectric or Brayton-cycle devices. After 1000 hr at 750°C, no attack of Ni, Ni-10% Cr, Ni-20% Cr, Co-10% Cr, Hastelloy C, Hastelloy N, or Haynes alloy No. 25 was found. In a second series, Nb, Nb-1% Zr, Ta, Ta-10% W, Mo, V, and Zr were tested for 1000 hr at 1200°C, but the capsules have not yet been examined.

#### Chemical Vapor Deposited Tungsten Capsules for Radioisotope Sources<sup>2</sup>

K. W. Haff<sup>3</sup>    W. R. Martin  
J. I. Federer    D. W. Ramey<sup>3</sup>

Tungsten is a prime candidate for encapsulating isotope heat sources in power-generating devices because it has high strength and good thermal conductivity at high temperatures. Since tungsten is difficult to fabricate by conventional methods, we are studying its fabrication by chemical vapor deposition (CVD). Three tungsten capsules were prepared by CVD and are being tested to failure by internal pressurization at 1650°C.

The capsules are about 2.23 in. long X 0.8 in. ID X 0.028 in. wall with a small integrally deposited tube

extending about 2 in. from one of the ellipsoidal ends. A 16-in.-long tungsten tube welded to the integrally deposited tube allows the capsule to be pressurized with helium for testing. The capsule is heated to 1650°C in vacuum, internally pressurized with helium to 25 psig, then subjected to step increases in pressure of 2.5 psig/day until it fails. If the capsules behave similarly to CVD tungsten tested in uniaxial tension, a rupture life of about 90 days can be predicted from the life-fraction rule and the above stress-temperature history.

The first capsule failed<sup>4</sup> in only 44 days because of strain induced during a pretest leak check of 250 psig for 68 hr at 1650°C. The tangential stress at rupture was 1800 psi, and the circumferential strain was about 11%. The second capsule was not leak checked at 1650°C before test. It ruptured in the 88th day at a stress of about 3370 psi. The circumferential strain was about 18%. The third capsule has not yet been tested.

The ductility observed for the first two capsules implies that CVD tungsten might be especially useful in the containment of alpha-emitting (helium-generating) radioisotopes.

### CLADDING MATERIALS PROGRAM

#### Evaporation of Cobalt- and Nickel-Base Alloys<sup>5</sup>

D. T. Bourgette

Evaporation rates of Hastelloy N (Ni-17% Mo-7% Cr-4% Fe) and Haynes alloy No. 188 (Co-22% Cr-22% Ni-14% W-0.08% La) were measured at 800 to 1050°C and  $10^{-9}$  torr to determine the alloys' suitability for use in high vacuum. Evaporation rates increased with concentration of the more volatile elements (chromium and manganese) but decreased with time at constant temperature. The time-dependent decrease in evaporation is slower, the thicker the specimen, at least to times of 1500 hr. This is because a greater proportion of the evaporating elements can diffuse to the surface in thinner specimens. Material losses resulted in microstructural damage such as void formation and solutioning of precipitates. Void formation was confined in alloy 188 to grain matrices and in Hastelloy N principally to the grain boundaries. Scanning electron microscopy of as-evaporated surfaces indicated that evaporative losses result in precipitation on the surface as shown in Fig. 25.2. The phase MoNi

<sup>4</sup>W. C. Robinson, Jr., *Metals and Ceramics Div. Ann. Progr. Rept. June 30, 1969*, ORNL-4470, pp.87-88.

<sup>5</sup>Paper presented at AIME Meeting, Las Vegas, Nev., May 15, 1970.

<sup>2</sup>Paper presented at the American Nuclear Society Meeting in Los Angeles, June 28-July 2, 1970.

<sup>3</sup>Isotopes Division.

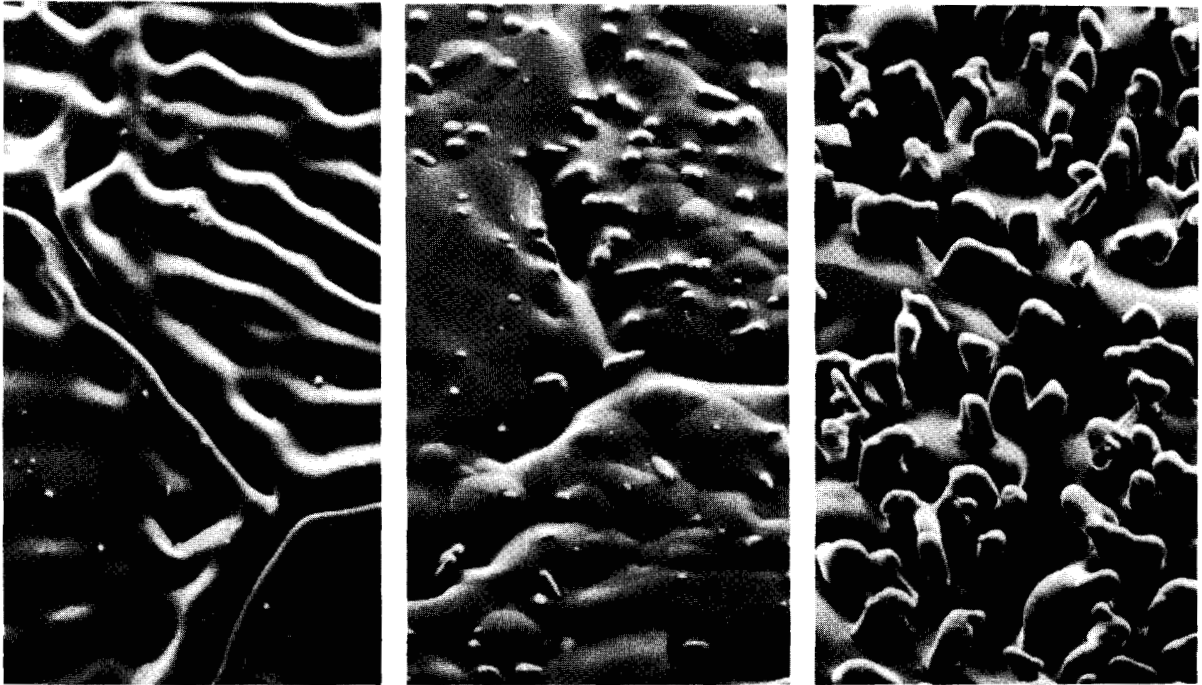


Fig. 25.2. The Effect of Temperature and Evaporation Losses on the Surface Morphology of 0.007-in.-Thick Hastelloy N, as Viewed with the Scanning Electron Microscope. 1000X. (a) After  $0.45 \text{ mg/cm}^2$  evaporation loss in 1520 hr at  $900^\circ\text{C}$ . (b) After  $1.44 \text{ mg/cm}^2$  in 1514 hr at  $950^\circ\text{C}$ . (c) After  $9.61 \text{ mg/cm}^2$  in 1400 hr at  $1000^\circ\text{C}$ .

precipitates above  $900^\circ\text{C}$  and  $\text{MoNi}_2$  below  $900^\circ\text{C}$  in Hastelloy N, but only after a sufficient loss of chromium and nickel over a long exposure.

#### New Platinum-Base Capsule Alloys for Space Isotopic Heat Sources<sup>6</sup>

H. Inouye C. T. Liu

The launching of radioisotope-fueled thermoelectric generators into space requires a highly reliable cladding, not only to contain the fuel during its normal operation of several years, but also to survive launch-pad fires, severe aerodynamic heating on reentry, and high-velocity earth impact. Because no single alloy of current manufacture can meet the severe service and safety requirements, multiple layers of refractory alloys clad with a platinum alloy are now being considered so that one alloy compensates for the shortcomings of another.

<sup>6</sup>Paper presented at Sixteenth Annual ANS Meeting, June 28, 1970, Los Angeles; summary to be published in *Transactions of the American Nuclear Society*.

Although the multilayered structure offers improvement, its reliability could be greatly increased by substituting for the refractory metal alloys, alloys that are more oxidation resistant. The available platinum-base alloys possess adequate oxidation resistance and fabricability, but they lack mechanical strength. Our objective is to improve the strength without sacrificing the other desirable properties.

The basic characteristics of long-range ordered alloys are being exploited because the disorder-to-order transformation significantly improves the mechanical properties that are critical in this application. As an example, the steady-state creep rate,  $\dot{\epsilon}$ , of  $\text{Pt}_3\text{Cr}$  shows a sharp discontinuous change around its critical temperature of  $1070^\circ\text{C}$ . The ordering reaction, which produces an  $\text{AuCu}_3$ -type superlattice below  $1070^\circ\text{C}$ , reduces the creep rate by a factor of 42.

The data further show the  $\dot{\epsilon}$  of  $\text{Pt}_3\text{Cr}$  is proportional to the third power of stress ( $\dot{\epsilon} \propto \sigma^3$ ) as opposed to the fifth power of stress ( $\dot{\epsilon} \propto \sigma^5$ ) dependency in a disordered Pt-5 wt % Mo alloy. Stress transients, therefore, result in lower creep strains in ordered alloys.

And finally, ordered alloys exhibit an "inverse" primary creep stage during which the creep rate is a minimum rather than the maximum observed in disordered alloys. This property is a critical factor in applications requiring low creep strains in a given period. As a comparison, the creep rate of Pt-10% Rh is 1000 times that of Pt<sub>3</sub>Cr.

The ordering reaction decreases the rate of transport processes such as diffusion. Thus, in this application, the evaporation rate in vacuum also decreases. For example, the conventional cobalt-base Haynes alloy No. 25 containing about 20 at. % Cr evaporates at 1000°C in vacuum at  $2.3 \times 10^{-2}$  mg cm<sup>-2</sup> hr<sup>-1</sup>; however, when 25 at. % Cr is alloyed with platinum to form the ordered phase Pt<sub>3</sub>Cr, the evaporation rate is immeasurably low.

Platinum oxidizes in air at a constant rate<sup>7</sup> of  $7 \times 10^{-4}$  mg cm<sup>-2</sup> hr<sup>-1</sup> at 1000°C. By comparison Pt-5 wt % Mo oxidizes at an average rate<sup>8</sup> of  $1.1 \times 10^{-3}$  mg cm<sup>-2</sup> hr<sup>-1</sup> and Pt<sub>3</sub>Cr at  $1.3 \times 10^{-3}$  mg cm<sup>-2</sup> hr<sup>-1</sup>. The corresponding rates are 10 mg cm<sup>-2</sup> hr<sup>-1</sup> for the tantalum-base alloy selected for this application and 400 mg cm<sup>-2</sup> hr<sup>-1</sup> for its back-up molybdenum-base alloy.

#### The Influence of Various Ordered States on the Mechanical Properties of Ni-Co-V Ternary Alloys<sup>9</sup>

C. T. Liu H. Inouye

Our objective is to study the effect of the ordered state on the mechanical properties of Ni-Co-V ternary alloys. Two compositions were prepared: one is the ordered S-4, (Ni,Co)<sub>3</sub>V, Ni-32% Co-25% V; the other disordered S-3, Ni-45% Co-10% V. Alloy S-4 is a pseudobinary solid solution whose two ordered components are face-centered tetragonal Ni<sub>3</sub>V and hexagonal close-packed Co<sub>3</sub>V. The ordering reaction in these binary alloys is so fast that the disordered state cannot be retained even by severe quenching.<sup>10</sup> However, the rate of ordering in S-4 is much slower, and the disordered structure is readily retained on quenching.

Neutron and x-ray diffraction show that atomic ordering and structural transformation take place sepa-

rately. After long-time aging below 700°C or short-time aging above 800°C, the arrangement of the vanadium atoms among nickel and cobalt atoms gives the cubic AuCu<sub>3</sub>-type ordered structure characterized by three close-packed layers with the stacking sequence ABC. As a consequence of atomic order, the hardness increases from 10 (the quenched value) to 35 R<sub>c</sub>. Further aging causes the transformation of the cubic structure to a hexagonal structure characterized by nine layers with stacking sequence ABCBCACAB. This change of stacking character is due to the influence of the atomic radius ratio and was first recognized by Van Vucht and Buschow.<sup>11</sup> Transmission electron micrographs show that the last transformation produces a tremendous amount of substructure consisting of microtwins, dislocations, and stacking faults, which further increases the hardness to 49 R<sub>c</sub>.

Typical heat treatments required to produce various ordered states in alloys S-4 and S-3 and their corresponding room-temperature tensile properties are indicated in Table 25.1.

The steady-state creep rate ( $\dot{\epsilon}$ ) of both alloys can be described by the equation,  $\dot{\epsilon} = (k\sigma^n/T) \exp(-Q/RT)$ , where  $k$  is a materials constant,  $n$  the stress exponent, and  $Q$  the activation energy for creep. The formation of long-range order increases the  $Q$  values from 58 for disordered S-3 to 84 kcal/mole for ordered S-4. The plot of  $\ln(\dot{\epsilon}T)$  against  $1/T$  shows a discontinuous change in creep rate around 1020°C, the critical ordering temperature of S-4. The stress exponent,  $n$ , of S-3 and S-4 is 5 in the disordered state but 2 in the long-range ordered state.

#### Back Extrusion of Refractory Metal Fuel Capsules

R. E. McDonald A. C. Schaffhauser

We are developing a back extrusion process for fabricating isotope fuel capsules up to 4 in. OD with hemispherical ends from alloys of Nb, Mo, Ta, and W. This process involves the extrusion of a solid blank into a closed die and back over an advancing plunger. The advantages of this process are that large-diameter capsules with closed ends can be fabricated from a simple blank, the geometry can be changed by relatively simple changes in die and plunger design, and a large amount of deformation can be accomplished below the recrystallization temperature to produce a wrought structure and good mechanical properties. This process is described further in Chapter 39 as applied to molybdenum components for service in bismuth.

<sup>11</sup>J. H. N. Van Vucht and K. H. J. Buschow, *J. Less-Common Metals* 10, 98 (1965).

<sup>7</sup>W. L. Phillips, Jr., *Trans. Am. Soc. Metals* 57, 33-37 (1964).

<sup>8</sup>H. Nishimura and H. Kimura, *Nippon Kinzoku Gakkaishi* 23, 616-20 (1959).

<sup>9</sup>Summary of paper accepted for oral presentation at Second International Conference on Metals and Alloys, Asilomar, Calif., August 1970; to be published in conference proceedings.

<sup>10</sup>L. E. Tanner *et al.*, *Mechanical Behavior of Intermetallic Compounds*, ASD-TDR-62-1087, Parts I, II, and III (January 1963-December 1964).

Table 25.1. Heat Treatment, Alloy State, and Tensile Properties of Alloys S-3 and S-4

Alloy	Heat Treatment	State	Yield Strength (psi)	Ultimate Strength (psi)	Elongation (%)
S-3	Quenched from 1150°C 5 hr aging at 800°C	Disordered	$\times 10^3$ 22	$\times 10^3$ 83	55
		Short-range ordered	32	84	40
S-4	Quenched from 1150°C 5 hr aging at 600°C 5 hr aging at 700°C 5 hr aging at 800°C	Disordered	67	134	63
		Short-range ordered	83	143	60
		Cubic ordered	117	183	13.7
		Hexagonal ordered	125	131	0.8

We have fabricated a number of capsules of Nb-1% Zr, Mo, and Mo-0.5% Ti having nominal dimensions of 2.5 in. OD  $\times$  5 in. long  $\times$  0.25 in. wall thickness with hemispherical ends. They were back extruded at loads of 150 to 300 tons on starting blanks cut from extruded-and-rolled bar stock heated to 1200°C in a salt bath.

We are also investigating back extrusion as a more economical method for fabricating the T-111 strength member and Ta-10% W liner for the isotope capsule to be used in the Transit Satellite thermoelectric generator. The present deep drawing process requires many fabrication steps and intermediate anneals. Our initial experiments show that back extrusion of the 6-in.-long capsule body is a two-step process for blank preheat temperatures of 1300 and 1350°C. The tantalum alloys are protected from contamination with a plasma-sprayed molybdenum coating, which also provides lubrication by MoO<sub>3</sub> during extrusion. Machining less than 0.020 in. from the extruded surface provides a capsule free of defects and contamination.

#### STRONTIUM PROGRAM COMPATIBILITY STUDIES

J. R. DiStefano

We have completed a study of the compatibility of nonradioactive SrTiO<sub>3</sub>, Sr<sub>2</sub>TiO<sub>4</sub>, and SrO with Haynes alloy No. 25, Hastelloy C, and type 316 stainless steel. In 10,000-hr tests at 900 and 1100°C, SrTiO<sub>3</sub> and Sr<sub>2</sub>TiO<sub>4</sub> had little effect on these alloys. However, a reaction zone up to 0.010 in. deep was found<sup>12</sup> in the alloys exposed to SrO. The reaction product was high in silicon, and subsequently we related the reaction process to the initial concentration of silicon present in the alloys.

<sup>12</sup>J. R. DiStefano, *Metals and Ceramics Div. Ann. Progr. Rept. June 30, 1969*, ORNL-4470, p. 92.

The SrO pellets used in these studies were prepared by two different processes. In one process potassium was left as a residual impurity in the SrO, and we noted more extensive attack in Hastelloy C exposed to these pellets than for pellets prepared by the alternate process.

#### SNAP-23 NONDESTRUCTIVE TESTING

K. V. Cook

We used the weld inspection technique developed<sup>13</sup> for SNAP-21 to evaluate welds before and after pressure testing of mockup SNAP-23 capsules. The weld condition changed little although the capsule wall had deformed. Metallographic sectioning correlated with the ultrasonic data within  $\pm 0.010$  in. Even though the inspection is reliable, it was much more difficult than for the SNAP-21 capsule because of the lack of a built-in reference step.

#### ISOTOPE KILOWATT PROGRAM

D. L. McElroy G. M. Goodwin

Iron appears to possess the most attractive combination of high melting point, high thermal conductivity, and low cost desired for the radiation shield-heat transfer block to be used on this program. We have reviewed the data on the thermal conductivity of iron and iron alloys as a function of temperature and found adequate information to design such a device.

If a high-purity iron (such as Armco iron) is necessary to obtain higher thermal conductivity and to avoid the transformation to austenite, the fabrication of the 3-ft-diam  $\times$  5-ft-high shield block will be more difficult than with steel or conventional iron castings. We have suggested the consumable electrode vacuum remelting process if the high purity is necessary.

<sup>13</sup>K. V. Cook, *Metals and Ceramics Div. Ann. Progr. Rept. June 30, 1969*, ORNL-4470, pp. 92-93.

## 26. Metallurgy of Refractory Alloys

P. Patriarca R. G. Donnelly

The purpose of this program is to provide a broad, base-technology evaluation of high-temperature alloys for use in high-performance nuclear reactors and isotopic heat sources for advanced space, terrestrial, and civilian power applications. Principal emphasis is placed on tantalum-, niobium-, and molybdenum-base alloys. We emphasize the systematic development and characterization of high-temperature alloys that are adequately resistant to creep, fabricable, weldable, and structurally stable under the designated service conditions. Our work on tungsten and its alloys is reported in Chapter 28.

### BASIC PHYSICAL METALLURGY STUDIES

H. Inouye

#### Development of Age-Hardening Refractory Alloys

C. T. Liu

The development of age-hardening refractory alloys for use at elevated temperatures focused on compositions within the tantalum-hafnium system. Alloys of tantalum with 30, 50, and 65 wt % Hf were studied by x-ray diffraction, metallography, and hardness tests. Our newly determined phase diagram (see Chapter 3 of this report) of this system shows a wide two-phase region within which the high-temperature body-centered cubic beta phase precipitates nearly pure hexagonal close-packed  $\alpha$ -hafnium at lower temperatures. The phase relation also indicates the possible existence of a metastable body-centered cubic miscibility gap below the two-phase boundary with the critical temperature around 1400°C.

Optical metallography showed that the precipitate morphology is related to both the hafnium concentration in the alloy and the quenching rate from the homogenization temperature. The fine, uniformly distributed precipitate throughout the grains can be

obtained by aging rapidly quenched specimens. Discontinuous precipitates appear as pearlitic patches starting on the grain boundary in slowly quenched alloys and in severely quenched alloys containing less hafnium, for example, Ta-30% Hf.

The age-hardening response in these three alloys is very similar. Representative data are shown in Fig. 26.1, where the microhardness of Ta-50% Hf is plotted as a function of time of aging in the range 850 to 1300°C. The specimens aged at and below 1030°C respond with a sharp increase in hardness in the early stage of precipitation, while those aged at higher temperatures show an initial drop of hardness. Both x-ray diffraction and metallography indicate that the features of hardness curves shown in Fig. 26.1 resulted from the various stages of decomposition, which involve the clustering of hafnium atoms on the beta lattices (G. P. zones), precipitation of coherent and noncoherent  $\alpha$ -hafnium, and coarsening of particles. The crystallographic relation between the phases is  $(0002)_\alpha \parallel (110)_\beta$ .

### Quasichemical Models and Cahn's Spinodal Decomposition<sup>1</sup>

C. T. Liu B.T.M. Loh

The thermodynamic and kinetic features of spinodal decomposition in a binary system have been studied with various quasichemical models. The models based on the first approximation to the quasichemical theory have demonstrated some unique features due to atomic clustering. The most distinctive ones are that the curves of both the driving force for decomposition and the fastest growing wavelength of structural modulations as functions of concentration both bow upward at low temperatures, which creates a maximum around the

<sup>1</sup>Paper presented at AIME Meeting, Las Vegas, Nev., May 1970.

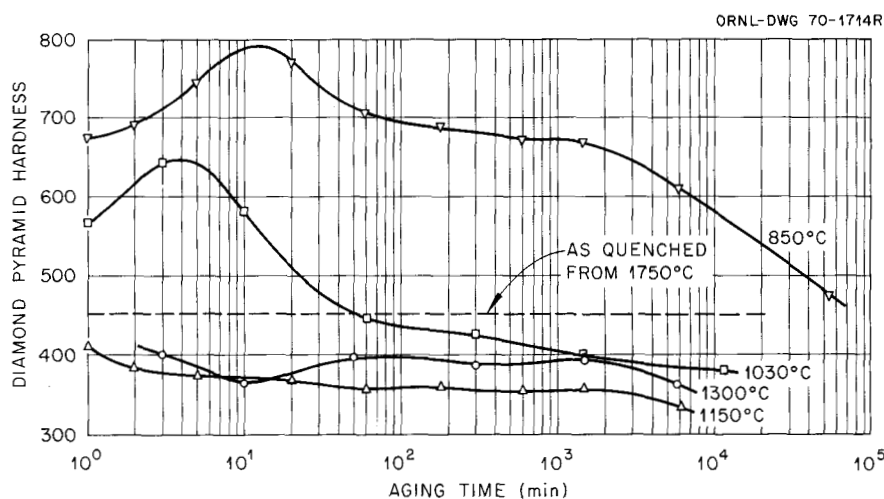


Fig. 26.1. Effect of Aging on Hardness of Ta-50% Hf.

critical composition of the miscibility gap. Models that do not consider atomic nonrandomness fail to show such features. The existing experimental observations on spinodal decomposition appear to agree qualitatively with the predicted features due to clustering.

Nonsymmetrical miscibility gaps are generally observed in the real solutions. To explain this, a conceptual view of the concentration dependence of the pairwise potential energies was introduced into the quasichemical theory.

#### MECHANICAL PROPERTIES OF COMMERCIAL REFRACTORY ALLOYS

H. E. McCoy, Jr. R. L. Stephenson  
K. Farrell

##### Molybdenum-Base Alloys

We recently published a study of the effects of fabrication variables on the long-time creep properties of molybdenum alloys.<sup>2</sup> Fabrication variables affected the creep properties of TZM profoundly. We are now examining this alloy by transmission electron microscopy in the hope of discovering the mechanism responsible for the observed changes. Specifically, we have studied the relation of subgrain size to creep behavior. Fine subgrain sizes are associated with high

strengths while coarse subgrain sizes are associated with low strengths.

Such a correlation is found for several materials, and it is often speculated that, if a fine subgrain size could be stabilized as by a precipitate, then a high stress might be required to produce a given creep rate. We fabricated three batches of TZM with different subgrain sizes, and these materials were compared to recrystallized materials. The subgrain sizes, before and after test, are plotted in Fig. 26.2 as a function of the stress to produce a creep rate of 0.001/hr. For these three materials, the subgrain sizes are seen to be stable during test and the stress required to produce this creep rate is inversely proportional to the subgrain size.

##### Tantalum-Base Alloys

The results of our study of the response to heat treatment of the creep-rupture properties of T-111 alloy were reported previously.<sup>3</sup> At high stresses material annealed at 1650°C showed shorter rupture times than material annealed at 1200°C. At low stresses the reverse is true. Since weld heat-affected zones are exposed to high temperatures it seemed likely that welds would show a similar effect. We creep tested specimens of T-111 containing transverse welds. At a test temperature of 1200°C, for example, specimens tested at high stresses (35,000 psi) failed in the weld at

<sup>2</sup>R. L. Stephenson, "The Effect of Fabrication Variables on the Creep-Rupture Properties of Molybdenum-Base Alloys," *Trans. Met. Soc. AIME* 245, 997-1001 (1969).

<sup>3</sup>H. E. McCoy, Jr., and R. L. Stephenson, *Metals and Ceramics Div. Ann. Progr. Rept. June 30, 1969*, ORNL-4470, pp. 59-60.

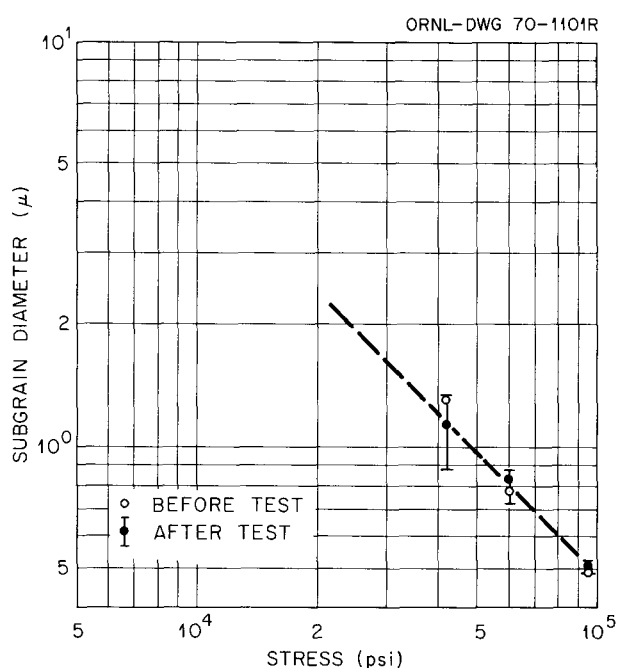


Fig. 26.2. Stress to Produce a Secondary Creep Rate of  $10^{-3}$ /hr in TZM at  $980^{\circ}\text{C}$  as a Function of Subgrain Diameter.

times shorter than did control specimens. At lower stresses (16,000 psi), specimens failed outside the weld and at times in agreement with those of control specimens.

### Niobium-Base Alloys

We also studied the creep rupture properties of C-129Y (Nb-10% W-10% Hf-0.1% Y) and their response to heat treatment.<sup>4</sup> The creep-rupture properties were determined to 1000 hr at 980, 1095, and  $1205^{\circ}\text{C}$  for cold worked material. Annealing at  $1425^{\circ}\text{C}$

$1650^{\circ}\text{C}$  improved rupture time and time to low creep strains but only at the expense of reduced rupture ductility. Microstructures show extensive intergranular cracking.

### BONDING REFRACTORY ALLOYS TO NOBLE METALS

D. A. Canonico G. M. Goodwin

For certain high-temperature applications, such as the Large Radioisotope Heat Source Capsule (LRHSC), a combination of strong refractory metal such as Ta-10% W and oxidation-resistant precious metal such as platinum is desirable. The problem of joining these materials presented a challenge, in that very little is known concerning the compatibility of these combinations. The anticipated service conditions for such a combination are high temperature (above  $1000^{\circ}\text{C}$ ) and vacuum ( $<10^{-5}$  torr). The requirement for the joint was that it be "leaktight" (leak rate  $<10^{-10}$   $\text{cm}^3/\text{sec}$ ) and serviceable for extended periods of time under the anticipated service conditions.

We attempted the six methods for accomplishing the union listed in Table 26.1. Five of these successfully satisfied the "leaktight" criterion as joined. The joints that satisfied the initial leak test were again tested after exposures at  $1200^{\circ}\text{C}$  for various intervals. Specimens that failed the leak test after extended exposure were investigated metallographically.

Table 26.1 synthesizes the results. Coextruded joints were unacceptable as joined. Brazing with filler metals specially developed at ORNL successfully joined the

<sup>4</sup>R. L. Stephenson, "Creep-Rupture Properties of C-129Y in Vacuum," paper presented at International Vacuum Metallurgy Conference, June 15-19, 1970, Anaheim, Calif.

Table 26.1. Results of Platinum-to-Tantalum Alloy Joining Program

Joining Technique	As Joined	After Aging <sup>a</sup>		
		100 hr	500 hr	1000 hr
Coextrusion	Not acceptable <sup>b</sup>			
Brazing	Acceptable <sup>c</sup>	NA <sup>b</sup>		
Swagelok	Acceptable	NA		
Electron-beam welds	Acceptable	A <sup>c</sup>	NA	
Pressure bonding	Acceptable	NA		
Brax weld (three-tube transition)	Acceptable	A	A	NA

<sup>a</sup>Aging at  $1200^{\circ}\text{C}$  in vacuum.

<sup>b</sup>Not acceptable - excessive leak rate.

<sup>c</sup>Acceptable - leak rate less than  $1 \times 10^{-10}$   $\text{cm}^3/\text{sec}$ .

platinum to Ta-10% W; however, the joints developed leaks after the 100-hr exposure. The mechanical Swagelok joint and the pressure bonded joint also leaked after the 100-hr exposure. The electron-beam weld satisfied the initial requirements and remained acceptable after 100 hr at the operating conditions but failed during the 500-hr interval. Using pure tungsten as a transition metal between the platinum and Ta-10% W extended the life of the joint to between 500 and 1000 hr.

The cause of the failures is evident in Fig. 26.3. Kirkendall voids form in platinum in juxtaposition with refractory metals. These voids, in turn, provide a leak path and, hence, unsatisfactory performance. The rate at which the voids form depends on time, temperature, and material. Tungsten proved to be more favorable than Ta-10% W alloy in combination with platinum. Other transition materials are under study.

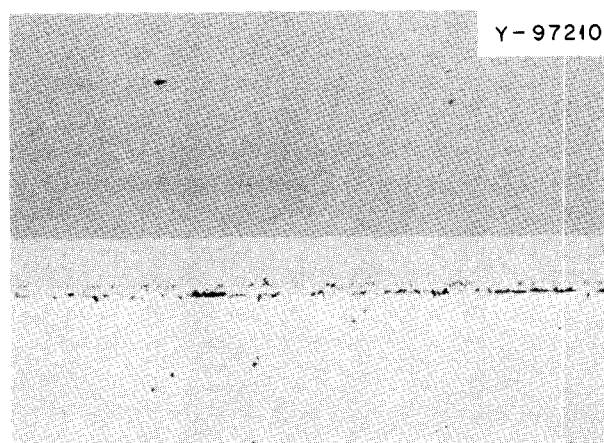


Fig. 26.3. Platinum (Bottom) to Ta-10% W (Top) Pressure-Bonded Joint After Exposure to 1200°C for 100 hr. The dark areas in the platinum are Kirkendall voids. 100X.

## THERMAL CONDUCTIVITY OF TANTALUM

R. K. Williams J. P. Moore  
D. L. McElroy

Good high-temperature thermal conductivity ( $\lambda$ ) estimates for metals and alloys can frequently be obtained by combining high-temperature electrical resistivity ( $\rho$ ) data with low-temperature  $\rho$  and  $\lambda$  data. In fact, for temperatures above 1300°K the  $\lambda$  estimates are usually more reliable than available measurements. We believe that experimentally derived phonon conductivity and Lorenz function ( $L$ ) values form the best available basis for these  $\lambda$  estimates, and we previously<sup>5</sup> reported a comparison for tungsten and several tungsten base alloys. New  $\lambda$  and  $\rho$  measurements (80 to 400°K) on tantalum, Ta-5% W and Ta-10% W and our previously reported<sup>6</sup> high-temperature  $\rho$  data for pure tantalum allow a similar comparison for tantalum. Data for the tantalum-tungsten alloys were used to substantiate the  $\lambda$  and  $L$  values obtained by fitting  $\lambda$  and  $\rho$  data (80 to 400°K) to a theoretically based equation. The results of this comparison are shown in Table 26.2. The excellent agreement between the estimated and recommended  $\lambda$  values shows that the thermal conductivity of tantalum behaves about as expected from transport theory.

<sup>5</sup>R. K. Williams, J. P. Moore, W. P. Murray, and D. L. McElroy, *Metals and Ceramics Div. Ann. Progr. Rept. June 30, 1969*, ORNL-4470, pp. 61-62.

<sup>6</sup>R. K. Williams, *Metals and Ceramics Div. Ann. Progr. Rept. June 30, 1969*, ORNL-4470, pp. 30-31.

Table 26.2. Comparison of Thermal Conductivity Estimates for Tantalum

Temperature (°K)	Electrical Resistivity ( $\mu\Omega$ -cm)	Thermal Conductivity [W cm <sup>-1</sup> (°K) <sup>-1</sup> ]		Deviation from Recommended Value (%)	
		Recommended Value <sup>a</sup>	ORNL <sup>b</sup> Estimate	Reported <sup>a</sup> Range	ORNL Estimate
500	22.55	0.582	0.570	+4.3 to -17.7	-2.1
1000	43.17	0.602	0.583	+21.1 to -2.7	-3.2
1500	61.75	0.622	0.606	+22.8 to -27.7	-2.6
2000	78.85	0.640	0.631	+26.1 to -39.7	-1.4
2500	94.85	0.656	0.654	+6.7 to -53.2	-0.3
3000	110.22 <sup>c</sup>	0.665	0.674	-22.7 to -32.3	+1.3

<sup>a</sup>C. Y. Ho, R. W. Powell, and P. E. Liley, *Thermal Conductivity of Selected Materials Part 2*, NSRDS-NBS 16 (February 1968).

<sup>b</sup> $\lambda = 2.462 \times 10^{-8} [1 - \exp(T/75.0 + 0.214)] T/\rho + 12.25/T$ .

<sup>c</sup>Extrapolated.

## 27. Nitride Fuels Development

J. L. Scott    P. Patriarca

Uranium mononitride is of interest as a fuel material for space-nuclear reactors because of its high thermal conductivity, high melting point of 2800°C, and good irradiation stability. Because space reactors reject heat by radiation, fuel pin cladding temperatures of interest are 1000°C or greater. The objective of our program is to establish the rate of swelling and fission-gas release of UN irradiated in refractory metal cladding at surface temperatures above 1000°C. The program also includes development of fabrication of very high purity UN, because impurities such as carbon or oxygen may adversely affect performance.

Development of nitride fuels for fast breeders is reported in Chapter 16 of this report and fundamental studies of nitrides are in Chapter 6 and others.

### SYNTHESIS AND CHARACTERIZATION OF URANIUM NITRIDE<sup>1,2</sup>

V. J. Tennery    R. A. Potter    T. G. Godfrey

Techniques have been developed for producing uranium nitride powders containing as little as 150 ppm O by the hydride-dehydride-nitride process. Methods for measuring the particle size distributions of these powders were evaluated, and a nitrogen gas sedimentation technique was found to be suitable. Morphology of the nitride powder particles was determined by scanning electron microscopy and transmission electron microscopy.

The fabrication technique of isostatic pressing of uranium nitride outside a glove box has been developed. This step can be accomplished with the nitride powder protected from oxidation. During this process the oxygen content of the surface of a fabricated UN part

typically reaches 1000 ppm, but upon sintering the oxygen content of the bulk drops to values from 100 to 300 ppm. The sintering activity of UN depends strongly upon the nitrogen pressure maintained over it during sintering. Nitrogen pressures just above that in equilibrium with UN and molten uranium lead to higher sintered densities for a given temperature than do nitrogen pressures of about 1 atm, and this effect is very marked below 2000°C.

### IRRADIATION TESTING OF URANIUM MONONITRIDE<sup>3</sup>

T. N. Washburn    S. C. Weaver  
K. R. Thoms<sup>4</sup>    D. R. Cuneo  
E. L. Long, Jr.

The objective of the ORNL program for irradiation testing of uranium mononitride (UN) is to obtain basic information on fuel swelling, fission-gas release, and compatibility with cladding materials at fuel temperatures from 1000 to 1500°C, cladding outside surface temperatures of 900 to 1400°C, and linear heat ratings of 5 to 10 kW/ft. Detailed descriptions of our capsule design<sup>5</sup> and previous test results<sup>6</sup> have been reported.

A current irradiation test (Capsule UN-3) was designed to investigate fuel pin performance at the highest temperatures in our program. The capsule contained three fuel pins loaded in tandem in a NaK heat transfer medium with a 450-psi gas overpressure to suppress

<sup>3</sup> Abstracted from "Examination of UN Fueled Pins Irradiated at 1400°C Cladding Temperature," paper presented at the American Nuclear Society 16th Annual Meeting, Los Angeles, Calif., June 1970.

<sup>4</sup> Reactor Division.

<sup>5</sup> V. A. DeCarlo, F. R. McQuilkin, R. L. Senn, K. R. Thoms, and S. C. Weaver, *Design of a Capsule for Irradiation Testing of Uranium Nitride Fuel*, ORNL-TM-2363 (February 1969).

<sup>6</sup> S. C. Weaver, K. R. Thoms, and V. A. DeCarlo, "Irradiation Testing of UN in ORR," *Trans. Am. Nucl. Soc.* 12, 547 (1969).

<sup>1</sup> This work was supported in part by NASA-Lewis Research Center, Cleveland, Ohio.

<sup>2</sup> Abstracted from a paper presented at the American Ceramic Society 72nd Annual Meeting, Washington, D. C., May 1970.

boiling of the NaK. The bottom and middle fuel pins contained 0.300-in.-diam solid UN pellets, 95.5% of theoretical density (T.D.), clad in T-111 (Ta-8% W-2% Hf) tubes of 0.365 in. OD  $\times$  0.027 in. wall thickness. A 0.003-in. tungsten barrier was formed on the inner surface of the tube by chemical vapor deposition.<sup>7</sup> The top fuel pin contained 0.300-in.-OD  $\times$  0.105-in.-ID annular UN pellets, 94% of T.D., clad in a W-25% Re tube of 0.365 in. OD  $\times$  0.030 in. wall thickness.

This test operated for 5800 hr to a burnup of about 1.75 at. % and was terminated when fission gas was detected in the capsule. Visual examination and Zygo penetrant testing revealed several cracks in the cladding of the middle fuel pin but none in the other two fuel pins. No abnormalities in fission product distribution or significant changes in the fuel column lengths were detected by gamma scanning.

After longitudinal slitting of the failed fuel pin, we observed that minute scratches on the honed inner surface of the cladding were replicated on the fuel surfaces, suggesting that significant restraining force had been exerted by the cladding on the fuel. The pin

increased 0.8% (0.003 in.) in diameter in the region of failure; the increase at the exact point of failure, including local deformation, was 2.5% (0.009 in.). Grain size in the cladding in the fueled region was about four times that in both the unfueled region of the pin and in the unirradiated control.

The postirradiation microhardness values of the cladding over the fueled region were higher than those of the preirradiation control specimens, with the increase ranging from 22% at the outer surface to 35% near the tungsten liner interface at the tube inner surface. Metallographic examination of the cladding showed that the failure was intergranular. Numerous cracks in the tungsten liner and in the T-111 cladding did not extend through the full thickness of either material. The appearance of the cladding, as shown in Fig. 27.1, and its increase in hardness reflect its decrease in ductility that led to failure.

<sup>7</sup>R. L. Heestand, J. I. Federer, and C. F. Leitten, Jr., *Preparation and Evaluation of Vapor-Deposited Tungsten*, ORNL-3662 (August 1964).

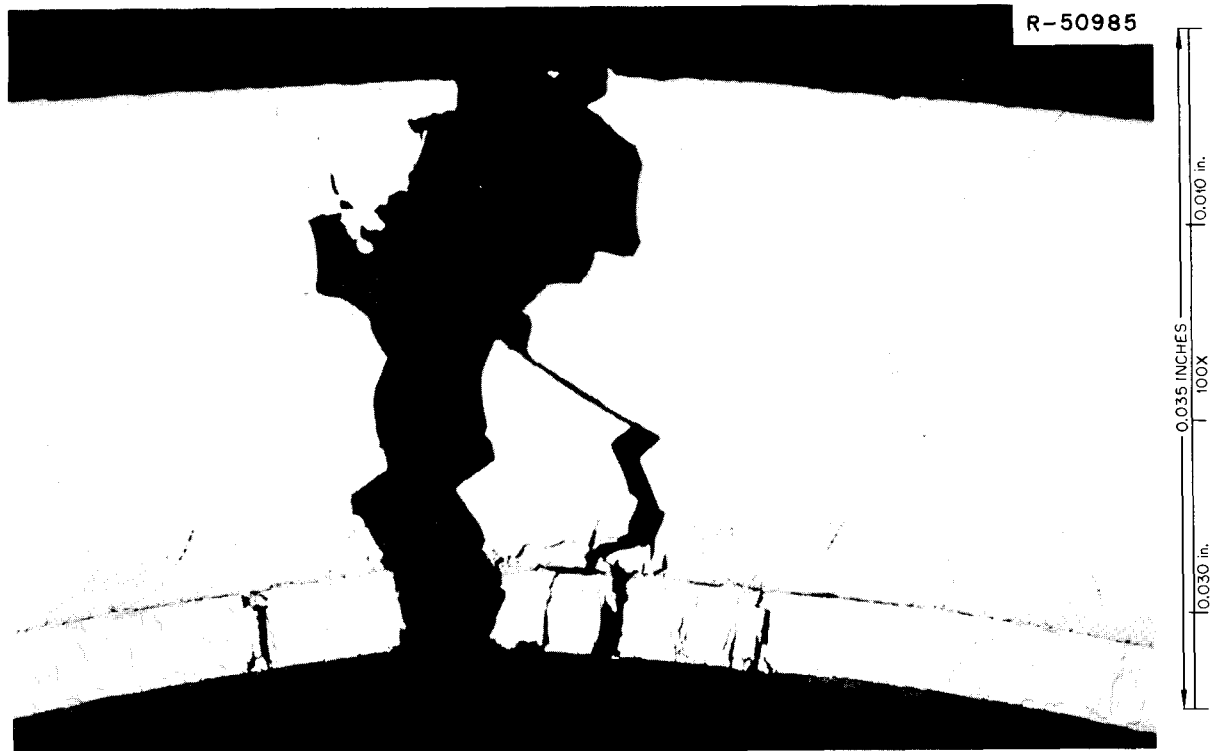


Fig. 27.1. Appearance of a Transverse Section Through a Failed Region in the T-111 Cladding and Tungsten Liner. As polished.

## 28. Tungsten Metallurgy

P. Patriarca A. C. Schaffhauser

The objective of this program is to provide the base technology on tungsten alloys for advanced power applications in space. We are developing fabrication processes for tungsten alloys based on modification of conventional extrusion and warm-drawing techniques, direct chemical vapor deposition, and welding. Since the primary criterion for the use of tungsten alloys for these applications is based on the creep-rupture properties, we are conducting extensive long-time tests at the temperatures of interest. We are also determining the mechanisms that control the creep behavior and the effect of interactions with the vapor species from a radioisotope or reactor fuel.

More detailed descriptions of the work presented in this chapter are given in the Tungsten Metallurgy Chapter of the Fuels and Materials Development Program Quarterly Progress Reports.<sup>1-3</sup>

### EXTRUSION OF TUNGSTEN ALLOYS

R. E. McDonald A. C. Schaffhauser

We determined the mechanical properties of powder-metallurgy tungsten tubing duplex extruded at 1150 to 1760°C. Ring specimens were cut from the tubing, and the tensile properties at 20 to 400°C were determined by applying a tangential load at opposite locations on the circumference of the rings.<sup>1</sup> Tests at 300°C showed that the largest reductions in area (up to 50%) were obtained for tubing extruded at 1150 and 1250°C; such

<sup>1</sup>P. Patriarca and A. C. Schaffhauser, *Fuels and Materials Development Program Quart. Progr. Rept. Sept. 30, 1969*, ORNL-4480, pp. 167-87.

<sup>2</sup>P. Patriarca and A. C. Schaffhauser, *Fuels and Materials Development Program Quart. Progr. Rept. Dec. 31, 1969*, ORNL-4520, pp. 227-44.

<sup>3</sup>P. Patriarca and A. C. Schaffhauser, *Fuels and Materials Development Program Quart. Progr. Rept. March 31, 1970*, ORNL-4560, pp. 186-97.

tubing had a wrought microstructure. Further tests showed that the tubing extruded at 1250°C had the lowest ductile-to-brittle transition temperature, approximately 100°C.

Similar extrusion experiments are under way for arc-melted tungsten alloys. A 10-in.-diam ingot of unalloyed arc-melted tungsten was procured from the Climax Molybdenum Company. Billets machined from this ingot were successfully extruded at 1775°C under our supervision at the Fansteel Metal Center to 3.25 in. in diameter. This extrusion development work is described in more detail in Chapter 25 of this report. Billets for the extrusion of tube shells are being machined from the primary extrusion. Ingots of arc-melted W-5 wt % Re from Wah Chang Corporation, Albany, Oregon, and W-4 at. % Re-0.35 at. % Hf-0.35 at. % C from the Lewis Research Center of the National Aeronautics and Space Administration are also being prepared for extrusion to tube shells.

### CHEMICAL VAPOR DEPOSITION DEVELOPMENT

J. I. Federer

#### Deposition of Tungsten with a Low Fluorine Content

Tungsten sheet stock was deposited for mechanical testing and welding studies. We prepared 15 deposits on resistance-heated Mo-0.5% Ti substrates at 600 to 650°C, 5 torr, 2000 cm<sup>3</sup>/min H<sub>2</sub>, and 200 cm<sup>3</sup>/min WF<sub>6</sub>. The deposition efficiency was about 65%, and the deposition rate was about 0.0035 in./hr. Each deposit provides about 55 in.<sup>2</sup> of sheet material from which 12 tensile or welding specimens can be obtained. The substrate can be dissolved in acid at any stage of the process of specimen machining.

Mechanical testing is most conveniently conducted with 0.06-in.-thick material, while 0.03- and 0.06-in.-thick material was desired for welding studies. The deposits were made oversize, then ground and electro-

polished to the required thickness. Metallographic examination of the deposits revealed a typically columnar grain structure with a small amount of grown-in porosity in a few areas.

The temperature of the deposition chamber wall affects the fluorine content of these large sheet deposits, as was previously observed for small tubular deposits.<sup>4</sup> The chamber wall was cooled with water at about either 20 or 75°C. Without cooling water the wall would reach about 150°C. Deposits prepared with the wall at 75°C contained 20 to 30 ppm F, while the wall at 25°C led to only 5 to 10 ppm F. The reason for the difference is uncertain, but the cooler wall may lower the partial pressure of some fluorine-bearing gas that contaminates by reaction or entrapment.

### Tungsten Alloy Deposition

We have continued to study the deposition of W-5% Re alloys to prepare sheet material for mechanical testing. The alloys are being deposited on resistance-heated substrates by hydrogen reduction of WF<sub>6</sub> and ReF<sub>6</sub> at about 750°C, the minimum temperature for compositional uniformity.<sup>5</sup> During the past year we have attempted to minimize nodules and grown-in porosity because such defects limit the amount of useful material in a deposit. Nodules usually appear after layers of dense fine-grained and columnar material have been deposited. We have attempted to keep the deposition process in the early stages, characterized by a fine-grained structure, by interrupting deposition by such techniques as pulsing the WF<sub>6</sub> and ReF<sub>6</sub> flows, pulsing the H<sub>2</sub>-WF<sub>6</sub>-ReF<sub>6</sub> flow, simultaneously pulsing the gas flows and thermally cycling to room temperature, alternating the WF<sub>6</sub> and ReF<sub>6</sub> flows, and periodically reversing the direction of gas flow through the reaction chamber. These techniques were intended to cause periodic nucleation of new growth to avoid the condition that causes nodules. None of these methods has been successful because none causes complete renucleation. Grains frequently grow through laminations caused by pulsing or interrupting gas flows and eventually develop nodules. However, we found that

deposits containing about 1 and 3% Re have fewer nodules than those containing 5% Re.

Recently we began to study the effect of gas composition on morphology at 750°C and 5 torr. The smoothest deposits occurred at H<sub>2</sub>/(WF<sub>6</sub> + ReF<sub>6</sub>) ratios of 1 and 3, the latter representing a stoichiometric mixture of H<sub>2</sub>, WF<sub>6</sub>, and ReF<sub>6</sub>. The deposits had a few nodules with no associated porosity. As the ratio increased to 20 the number of nodules increased and porosity formed at their interface with the matrix. These results indicate that smooth deposits are favored by a gas mixture that is rich in WF<sub>6</sub> and ReF<sub>6</sub>, and that nodules occur in mixtures that are lean or depleted in WF<sub>6</sub> and ReF<sub>6</sub>.

### Chemical Vapor Deposition of Vanadium and Vanadium Alloys<sup>6</sup>

The purpose of this study was to determine whether chemical vapor deposition could provide a practical alternate method of fabricating vanadium tubing and complex shapes or of obtaining a product with unique properties. The reactions studied were the hydrogen reduction of halides at 900 to 1200°C and a pressure of 5 torr. We prepared VCl<sub>4</sub> and VF<sub>5</sub> by reacting vanadium metal with chlorine and fluorine at 400°C. The halide vapors were transferred into a reaction chamber heated by a furnace. The vanadium deposited on the inside of a 3/4-in.-diam steel liner.

The efficiency of vanadium deposition from VCl<sub>4</sub> was only 8% at 900°C and increased to about 50% at 1100 and 1200°C. Lower chlorides, which deposited in the relatively cool ends of the substrate, limited the amount of vanadium metal deposited. Only VF<sub>3</sub> was obtained from VF<sub>5</sub> at 900°C; however, the efficiency of vanadium deposition from VF<sub>5</sub> was about 80% at 1000 and 1100°C and increased to 100% at 1200°C. These experimental results are in qualitative agreement with physical and thermodynamic data except that vanadium metal was not deposited from VF<sub>5</sub> at 900°C.

The characteristics of deposits prepared from both VCl<sub>4</sub> and VF<sub>5</sub> were similar. The thickest deposit occurred progressively closer to the inlet end of the substrate with increasing temperature. The deposits contained up to 1.2% total impurities, principally carbon, nitrogen, and oxygen. The grain structure was columnar, but since the deposition temperatures were greater than half the absolute melting point some grain

<sup>4</sup>A. C. Schaffauser and R. L. Heestand, "Effect of Fluorine Impurities on the Grain Stability of Thermochemically Deposited Tungsten," pp. 204-11 in *IEEE Conference Record of 1966 Thermionic Conversion Specialist Conference, Nov. 3 and 4, 1966, Houston, Texas*, The Institute of Electrical and Electronics Engineers, New York, 1966.

<sup>5</sup>J. I. Federer, *Metals and Ceramics Div. Ann. Progr. Rept. June 30, 1969*, ORNL-4470, pp. 63-64.

<sup>6</sup>J. I. Federer, *Chemical Vapor Deposition of Vanadium and Vanadium Alloys - A Feasibility Study*, ORNL-TM-2923 (May 1970).

growth probably occurred during deposition. The deposits also alloyed with the steel substrates. X-ray diffraction indicated that the deposits were highly oriented with {110} planes parallel to the substrate. Efforts to codeposit alloys with chromium and titanium failed because of the stability of the lower halides of chromium and titanium.

We showed that deposition of vanadium metal is feasible, but that temperatures of 1000°C or higher are required to obtain a deposition efficiency of at least 50%. Such high temperatures cause serious difficulties including contamination with interstitial impurities and reaction with the substrate. We believe that these problems can be solved, but their solution was not included in the scope of this study.

#### DEVELOPMENT OF IMPROVED METHODS FOR JOINING TUNGSTEN ALLOYS

N. C. Cole G. M. Slaughter

The objectives of this program are to develop improved techniques for joining tungsten and its alloys and to determine the properties of the resulting joints. We have gas tungsten-arc (GTA) welded powder-metallurgy tungsten, arc-cast W-25% Re, and CVD tungsten sheet as base metals. Several powder-metallurgy molybdenum-rhenium filler metals having melting points lower than the base metal were used to make some of the welds in the first two materials.

The advantage of lower melting filler metals is the reduced overall energy required, which reduces thermal stresses, recrystallization, and grain growth in the heat-affected zone. The following lower melting filler metals were used to weld powder-metallurgy tungsten: Mo-1 wt % Re, Mo-20 wt % Re, Mo-50 wt % Re, and W-25 at. % Re-30 at. % Mo. All the welds were free of cracks except for a center-line crack in a weld made with Mo-20% Re. Slight porosity was encountered as expected, since both the base and filler metals were powder-metallurgy products.

When unalloyed tungsten is welded with or without filler metal, preheating the base metal to 150°C or higher is necessary to prevent cracking. However, we have successfully GTA welded W-25% Re without preheating, using both butt-weld and bead-on-sheet joints. Crater cracking occurred but was eliminated by gradually increasing the current at the beginning of each weld and gradually decreasing it at the end.

We have had limited success with welding CVD tungsten sheet. We were able to produce welds free of cracks in 0.030-in. sheet; however, some welds in 0.050-in. sheet resulted in cracks transverse to the weld.

Bend tests of the welded specimens at temperatures up to 550°C resulted in cracking in the base metal and heat-affected zone. However, in several tests the weld metal did not crack at test temperatures above 450°C. We believe that the high fluorine impurity content of this material (25 ppm in the 0.050-in. sheet and 19 ppm in the 0.030-in. sheet) and the associated accumulation of gas bubbles in the heat-affected zone caused the premature cracking.<sup>7</sup>

#### CREEP PROPERTIES OF TUNGSTEN ALLOYS

H. E. McCoy, Jr.

##### Long-Time Creep-Rupture Properties of Arc-Melted and CVD Tungsten Alloys

R. L. Stephenson

We have determined the creep-rupture properties of selected tungsten-base materials at 1400 to 2200°C. Our data at 1650°C are summarized in Fig. 28.1, which compares 1000-hr isochronous stress-strain curves for arc-melted W, W-5% Re, W-26% Re, and W-25% Re-30 % Mo and for CVD tungsten. At low strains CVD tungsten appears strongest at this temperature followed by W-5% Re and tungsten. On the basis of rupture, W-5% Re is strongest.<sup>8</sup>

The creep-rupture properties of CVD tungsten were studied by McCoy and Stiegler<sup>9</sup> several years ago. Since then much has been learned about the deposition process. The current values, for recently produced material, are very close to those of McCoy and Stiegler even though the fluorine content (5 to 10 ppm) is lower than in most of their material.

##### Correlation of Creep Data for Tungsten

R. L. Stephenson

Sherby<sup>10</sup> has suggested that for pure metals and dilute alloys above 0.4 times the absolute melting point

<sup>7</sup>K. Farrell, J. T. Houston, and J. W. Chumley, *Welding J.* (N. Y.) **49**, 132-s-37-s (1970).

<sup>8</sup>R. L. Stephenson, "Material Selections for Thermionic Capsules," pp. 404-10 in *IEEE Conference Record of 1969 Thermionic Conversion Specialist Conference, Carmel, Calif., Oct. 21-23, 1969*, The Institute of Electrical and Electronic Engineers, New York, 1969.

<sup>9</sup>H. E. McCoy and J. O. Stiegler, pp. 391-425 in *Proceedings of the Conference on Chemical Vapor Deposition of Refractory Metals, Alloys, and Compounds, Gatlinburg, Tennessee, September 12-14, 1967*, ed. by A. C. Schaffhauser, American Nuclear Society, Hinsdale, Ill.

<sup>10</sup>O. D. Sherby, *Acta Met.* **10**, 135 (1962).

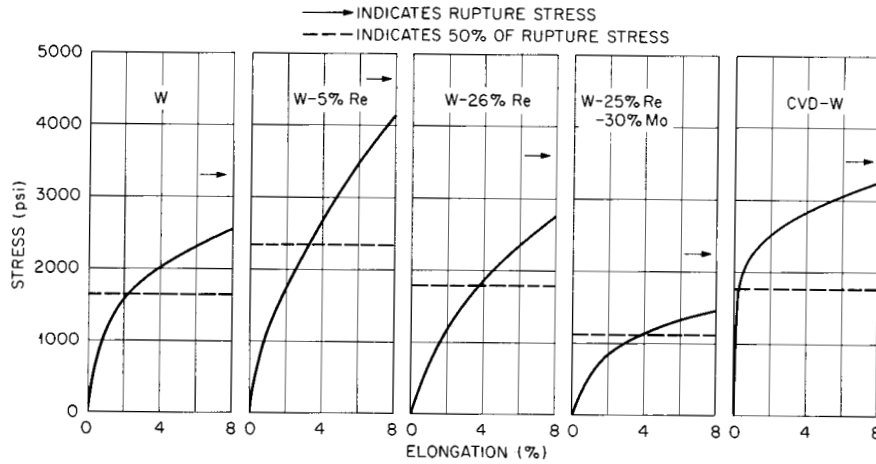


Fig. 28.1. Isochronous Stress-Strain Curves (1000 hr) for Selected Tungsten-Base Materials.

creep strength is influenced by elastic modulus ( $E$ ), diffusivity ( $D$ ), and grain or subgrain size ( $L$ ). He further suggests that the creep data can be correlated by an equation of the form:

$$\dot{\epsilon} = SL^2 D(\sigma/E)^n \quad (1)$$

where  $S$  and  $n$  are constants,  $\sigma$  is the stress, and  $\dot{\epsilon}$  is the secondary creep rate.

Plots of  $\dot{\epsilon}/D$  against  $\sigma/E$  for several materials show a change in slope, usually at values of  $\sigma/E$  between 1.5 and  $2.0 \times 10^{-4}$ . Garofalo<sup>11</sup> and others have suggested that the creep rate for many materials may vary as the hyperbolic sine of the stress. We have combined these two approaches using an equation of the form

$$\dot{\epsilon} = S'D [\sinh(\alpha'\sigma/E)]^n \quad (2)$$

where  $S'$  and  $\alpha'$  are constants.

Figure 28.2 shows  $\dot{\epsilon}/D$  plotted against  $\sigma/E$  for the tungsten data from this study and from three sources correlated by Robinson and Sherby.<sup>12</sup> Equation (2), represented by the dotted line, agrees well with all these data.

We are examining this material by transmission electron microscopy to determine if the subgrain size can be correlated with this equation.

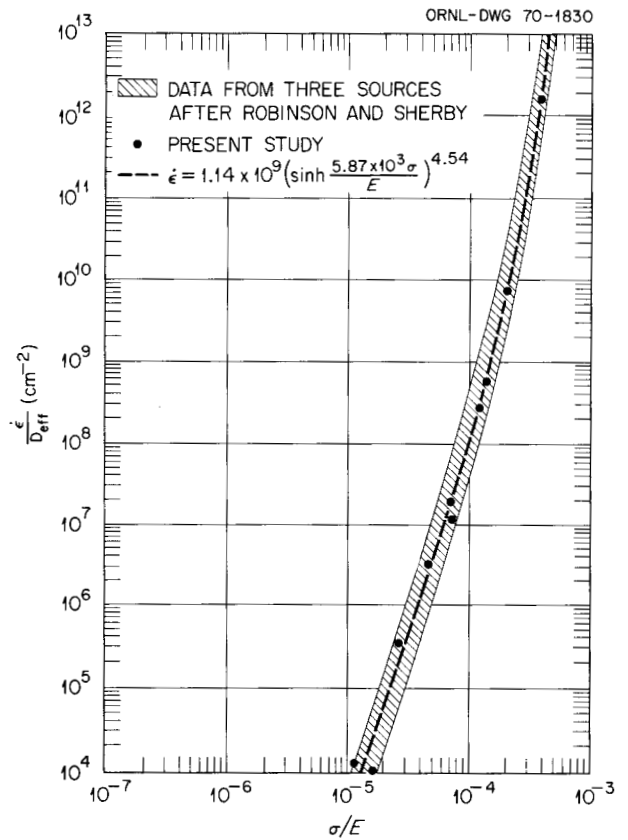


Fig. 28.2. Correlation of Creep Rate with Stress for Tungsten from 1400 Through 2200°C.

<sup>11</sup>F. Garofalo, *Trans. Met. Soc. AIME* 227, 351 (1963).

<sup>12</sup>S. L. Robinson and O. D. Sherby, *Acta Met.* 17, 109 (1969).

### Anomalous Creep Behavior of Powder-Metallurgy W-25% Re

R. L. Stephenson

Previously we compared the creep-rupture properties of arc-melted and powder-metallurgy W-25% Re sheet produced from common feed material.<sup>13</sup> The secondary creep rate and its stress dependence were greater for powder-metallurgy material than for the arc-melted material at 1650°C but less at 2200°C. Extrapolation of the data for the powder-metallurgy material indicated that at very low stresses the material would actually creep faster at 1650°C than at 2200°C. To determine whether this anomalous behavior would actually occur, we loaded a specimen to 500 psi at 1650°C and measured strain until the secondary creep rate was established. After about 50 hr, a creep rate of  $6 \times 10^{-5}$ /hr was established. Without changing the load, we abruptly changed the temperature to 2200°C. The creep rate increased by several orders of magnitude, but after approximately 10 hr it decreased to about  $3 \times 10^{-5}$ /hr. The creep rate as a function of time (i.e., the slope of the creep curve at any given time) is shown in Fig. 28.3.

In powder-metallurgy tungsten the small grain size is stable for long times at temperatures up to a critical temperature above which secondary recrystallization takes place.<sup>14</sup> If this is so for the alloy and if most of the observed deformation is due to the growth of

grain-boundary voids, then the creep rate at certain stresses could be lower at 2200 than at 1650°C. There is less total strain and a lower creep rate simply because there are fewer grain boundaries on which voids can grow. When the specimen was again cooled to 1650°C after having been exposed at 2200°C, the creep rate, of course, decreased far below that observed for the fine grain size that had prevailed before exposure to the higher temperature.

Before the temperature was raised to 2200°C, it was cycled between 1648 and 1590°C to determine the apparent activation energy for creep. The value was about 40,000 cal/mole. This value is surprisingly low; however, Vandervoort and Barmore<sup>15</sup> observed a more or less systematic decrease in apparent activation energy with decreasing stress for this alloy. If their results are plotted as a function of stress, then a value of 40,000 cal/mole at 500 psi seems to be in reasonable agreement.

<sup>13</sup>R. L. Stephenson, *Comparative Creep-Rupture Properties of W-25% Re Consolidated by Arc Melting and Powder Metallurgy Techniques*, ORNL-TM-2651 (September 1969).

<sup>14</sup>K. Farrell, A. C. Schaffhauser, and J. O. Stiegler, *J. Less-Common Metals* 13, 144-45 (1967).

<sup>15</sup>R. R. Vandervoort and W. L. Barmore, "Elevated Temperature Deformation and Electron Microscope Studies of Polycrystalline Tungsten and Tungsten-Rhenium Alloys," pp. 108-37 in *6th Plansee Seminar*, ed. by F. Benesovsky, Metallwerk Plansee AG., Reutte/Tyrol, Austria, 1969.

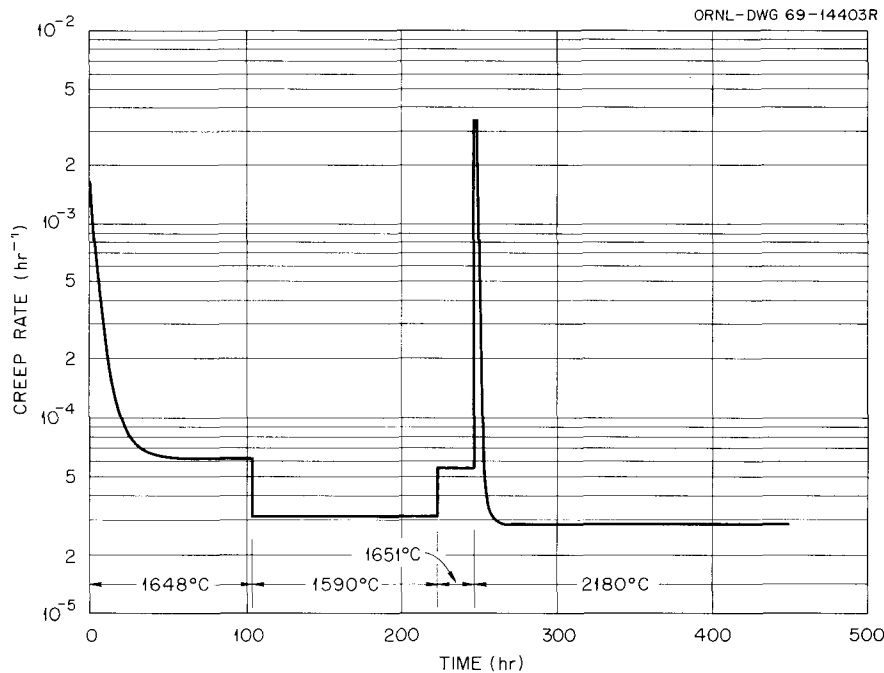


Fig. 28.3. Variation of Creep Rate with Time for Powder-Metallurgy W-25% Re at 500 psi.

## ELECTRON MICROSCOPIC STUDY OF CREEP MECHANISMS

J. O. Stiegler

We are studying in detail the microstructural changes produced in powder-metallurgy tungsten during creep deformation in order to develop an understanding of the mechanisms that control creep flow and fracture. During the past year attention has been directed at the effect of stress on the deformation process. Creep tests conducted at 1600°C at stresses between 4500 and 12,000 psi were interrupted to permit observation of the progressive evolution of the creep microstructure. Significant findings resulting from this work follow.

1. For the particular grade of tungsten used in this study annealing 1 hr at 1600°C produces a moderate concentration of cavities ( $>10^{11}/\text{cm}^3$ ), probably gas bubbles, both within the grains and on the grain boundaries. Many of the cavities are associated with particles. The concentration of such cavities in arc-melted tungsten specimens similarly deformed and annealed is below the limit of detection by transmission electron microscopy.

2. The bubbles located on grain boundaries appear to nucleate the cracks produced during creep.

3. Large cracks do not grow by uniform advancement; instead the crack merges with small cavities expanded in advance of its front.

4. Small flat cavities or cracks enlarged by stress show little tendency to become spherical or close upon annealing at the deformation temperature (1600°C). That is, only weak forces oppose crack growth for these deformation conditions.

We believe that the small cavities or bubbles present in powder-metallurgy tungsten strongly influence the fracture characteristics of the material. The variability of the powder-metallurgy product may arise in part because bubble concentrations and distributions are strongly influenced by the processing history of the material.

## EFFECT OF LOW-PRESSURE OXYGEN ON THE CREEP PROPERTIES OF TUNGSTEN AND ITS ALLOYS

H. Inouye

The creep strength of tungsten during its interaction with low-pressure oxygen at 1500 to 2000°C is significantly lower than the strength measured in a vacuum of  $10^{-8}$  torr. For example, at 1650°C and a stress of 2000 psi, the creep rate of tungsten in  $10^{-5}$  torr  $\text{O}_2$  is 4.4 times that in vacuum.<sup>16</sup> The strength loss is attributed to the sublimation of the metal as volatile oxides, to oxygen dissolving in the metal, and to oxygen increasing the rate at which creep cavities grow in tungsten.

Low-pressure oxygen also has a significant effect on the creep properties of W-25% Re at 1650 and 1850°C. The creep rates in  $8 \times 10^{-6}$  torr  $\text{O}_2$  are lower than in a vacuum of  $10^{-8}$  torr, which is opposite to the effect of oxygen on the creep rate of tungsten. Higher creep strengths are initially observed in  $7 \times 10^{-5}$  torr  $\text{O}_2$ ; however, the alloy goes into an early third-stage creep and subsequently ruptures at strains of approximately 2.8%. This behavior is due to the preferential sublimation of tungsten from the alloy as a volatile oxide, which results in the formation of the rhenium-rich sigma phase on the surface of the specimen.

<sup>16</sup>H. Inouye, "The Effect of Low-Pressure Oxygen on the Creep Properties of Tungsten and a Tungsten-Molybdenum Alloy," pp. 425-29 in *IEEE Conference Record of 1969 Thermionic Conversion Specialist Conference, Carmel, Calif., Oct. 21-23, 1969*, The Institute of Electrical and Electronic Engineers, New York, 1969.

## Part IV. General Fuels and Materials Research

### 29. Corrosion of Advanced Steam Generator Alloys

J. P. Hammond   G. M. Slaughter   P. Patriarca

Study of the corrosion behavior of weldments in conventional superheater alloys for advanced steam generator applications is continuing.<sup>1</sup> Fourteen similar- and dissimilar-metal weldments containing Incoloy 800, Inconel 625, Hastelloy X, IN 102, 2¼% Cr-1% Mo low-alloy steel, Inconel 600, and type 304 stainless steel plate, welded with various recommended filler metals including Inconel 82, Hastelloy W, and type 308 stainless steel, were exposed isothermally to superheated steam for periods to 10,000 hr at 1100 and 1200°F (595 and 650°C). These field corrosion tests were conducted under subcontract to Southern Nuclear Engineering Company at the Bartow plant of the Florida Power Corporation by flowing commercial, high-quality steam over specimens at 5 ft/sec velocity and 900 psi (63.5 kg/cm<sup>2</sup>) pressure. The specimens were longitudinal strips cut from ½-in.-thick weldments prepared by the gas tungsten-arc welding process. General corrosion is assessed by determining attack rates and by calculating long-term corrosion from weight-gain data. The scales were characterized and their thicknesses determined separately in the plate and weld metal. Susceptibility to preferential corrosion is determined by examining for knife-edge attack at fusion lines of welds and by conducting U-bend-type, stress-corrosion tests in uncontaminated steam at 595°C.

The initial results of this work have been reported,<sup>2</sup> and the highlights are summarized here. Typical corro-

sion curves are shown in Fig. 29.1, which illustrates the results on the similar-metal weldments. Table 29.1 lists corrosion rates and 20-year metal-penetration values for these weldments calculated from the equation

$$\Delta W = \Delta W_0 + K_I T,$$

where  $\Delta W$  is the weight gain in time  $T$ , and  $\Delta W_0$  and  $K_I$  are constants. Joints of Inconel 625, Hastelloy X, IN 102, and Incoloy 800 (this base metal was welded with Inconel 82 filler metal) exhibited exceedingly good corrosion resistance at both temperatures. Calculated 20-year penetration depths were all less than 0.5 mil. The scales formed on Inconel 625, Hastelloy X, and IN 102 as base metal and weld deposit and on Inconel 82 as filler metal were uniform, tenacious, and less than 5  $\mu\text{m}$  thick. Interestingly, IN 102 exhibited less corrosion at the higher temperature. Incoloy 800 displayed corrosion on a par with the foregoing alloys at 595°C and only slightly higher at 650°C. An analysis of the data for dissimilar-metal joints revealed that weldments of Inconel 625, Hastelloy X, and IN 102 joined to Incoloy 800 with themselves and with Inconel 82 as filler metals also possessed good corrosion resistance at both temperatures.

Similar-metal weldments in Inconel 600 joined with Inconel 82 and type 304 stainless steel welded with

<sup>1</sup>J. P. Hammond, *Metals and Ceramics Div. Ann. Progr. Rept.*, June 30, 1969, ORNL-4470, pp. 153-56.

<sup>2</sup>J. P. Hammond *et al.*, "Corrosion of Advanced Steam Generator Alloy Weldments in 1100 and 1200°F (595 and 650°C) Steam," paper 46 presented at the National Association of Corrosion Engineers 26th National Conference, March 2-6, 1970, Philadelphia; to be published in the proceedings.

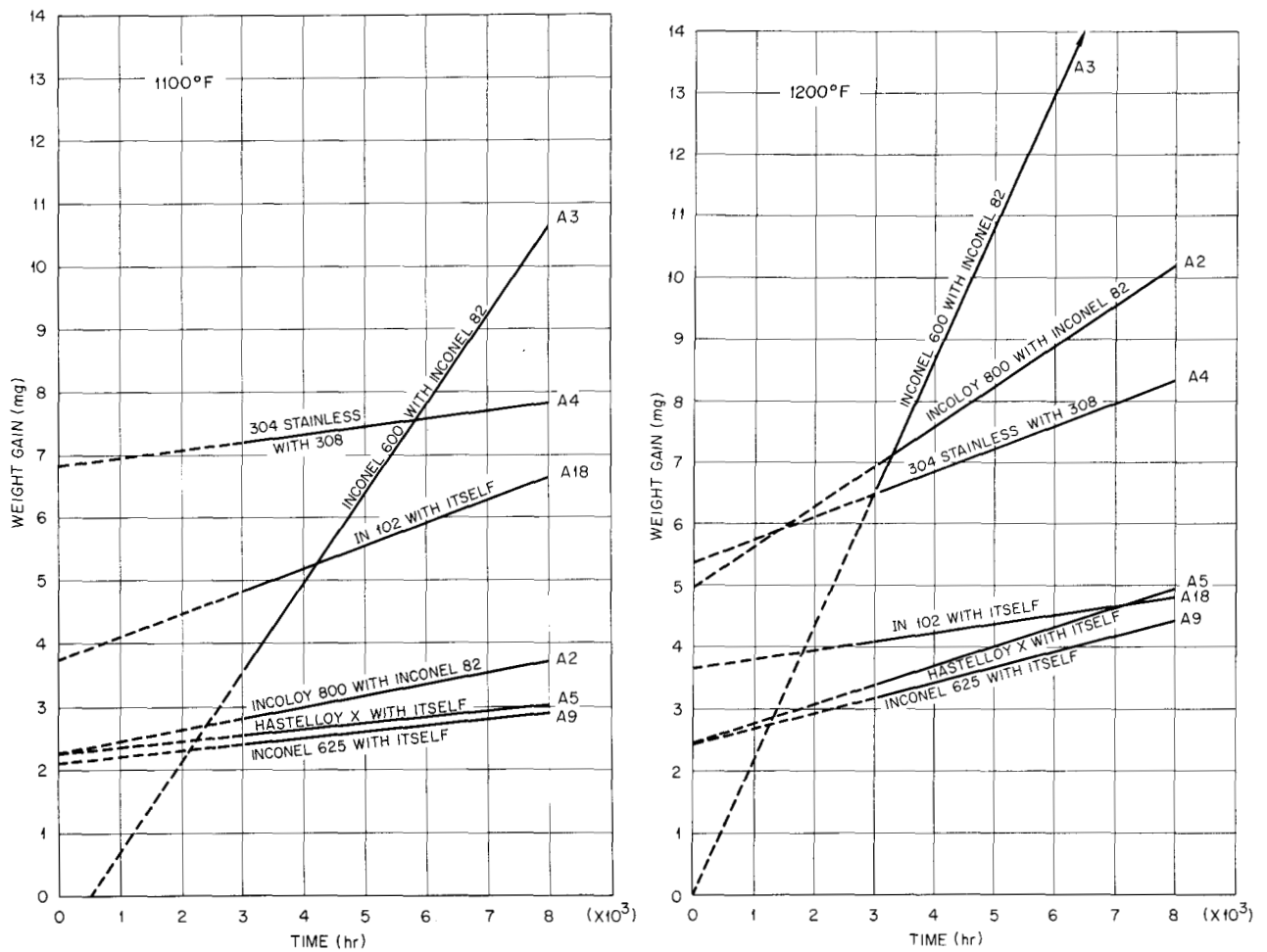


Fig. 29.1. Corrosion of Similar-Metal Weldments in Superheated Steam at 1100 and 1200°F (595 and 650°C).

type 308 (these combinations were included for baseline data) exhibited somewhat inferior behavior. Penetration of about 2 and 3 mils in 20 years at 1100 and 1200°F, respectively, were calculated for Inconel 600 weldments, and the scale formed on them was highly irregular, penetrating intergranularly two to three grain widths (approx 20  $\mu\text{m}$ ) into the substrate (Fig. 29.2). The scales formed on the stainless steel weldments spalled.

A thorough examination of fusion lines and adjacent regions of all welds failed to disclose any evidence of preferential or unusual attack. The U-bend stress-corrosion tests showed no cracking in uncontaminated steam with the prevailing amounts of moisture. A test loop for investigating stress-corrosion cracking with chloride and oxygen as contaminants has been constructed, and statically stressed U-bend specimens have been prepared and are ready for testing at 480 and 540°C.

Table 29.1. Corrosion and Metal Penetration of Similar-Metal Weldments Calculated from Weight-Gain Data<sup>a</sup>

Code	Base and Filler Alloy	Intercepts and Slopes of Weight-Gain Curves <sup>b</sup> With Standard Errors		Calculated Metal Consumed in 20 years (mg/cm <sup>2</sup> )	Calculated Penetration in 20 years	
		$\Delta W_0^c$ (mg/dm <sup>2</sup> )	$K_I$ [mg dm <sup>-2</sup> (1000 hr) <sup>-1</sup> ]		( $\mu$ m)	(mils)
Exposed at 1100°F (595°C)						
A9	Inconel 625 with itself	10.6 ± 0.53	0.50 ± 0.05	3.09	3.7	0.14
A5	Hastelloy X with itself	11.4 ± 0.67	0.47 ± 0.08	2.78	3.4	0.13
A18	IN 102 with itself	19.1 ± 0.32	1.77 ± 0.29	10.8	12.7	0.50
A2	Incoloy 800 with Inconel 82	11.4 ± 0.71	0.91 ± 0.12	4.72	5.8	0.23
A3	Inconel 600 with Inconel 82	-3.98 ± 2.19	7.18 ± 0.37	40.1	48.1	1.89
A4	Type 304 stainless steel with type 308 stainless steel	34.2 ± 0.65	0.63 ± 0.11	3.57	4.5	0.18
Exposed at 1200°F (650°C)						
A9	Inconel 625 with itself	12.2 ± 0.72	1.24 ± 0.12	7.31	8.7	0.34
A5	Hastelloy X with itself	13.3 ± 1.07	1.55 ± 0.18	8.14	9.9	0.39
A18	IN 102 with itself	18.1 ± 1.19	0.75 ± 0.20	4.90	5.7	0.23
A2	Incoloy 800 with Inconel 82	24.9 ± 2.71	3.27 ± 0.17	16.6	20.5	0.81
A3	Inconel 600 with Inconel 82	-1.19 ± 8.13	10.9 ± 0.45	60.9	73.0	2.87
A4	Type 304 stainless steel with type 308 stainless steel	26.8 ± 1.47	1.86 ± 0.25	8.77	10.9	0.43

<sup>a</sup>Amounts of corrosion do not allow for oxide flaking during test and are based on the following calculated concentrations of metal in the scales of the respective weldments: A9 - 76.1%, A5 - 74.1%, A18 - 76.7%, A2 - 73.5%, A3 - 76.2%, and A4 - 71.3%.

<sup>b</sup> $\Delta W = \Delta W_0 + K_I T$  where  $T$  is the exposure in thousands of hours and where  $\Delta W$  is weight gain.

<sup>c</sup>The standard error of the intercept is for an individual specimen.

Y-97501

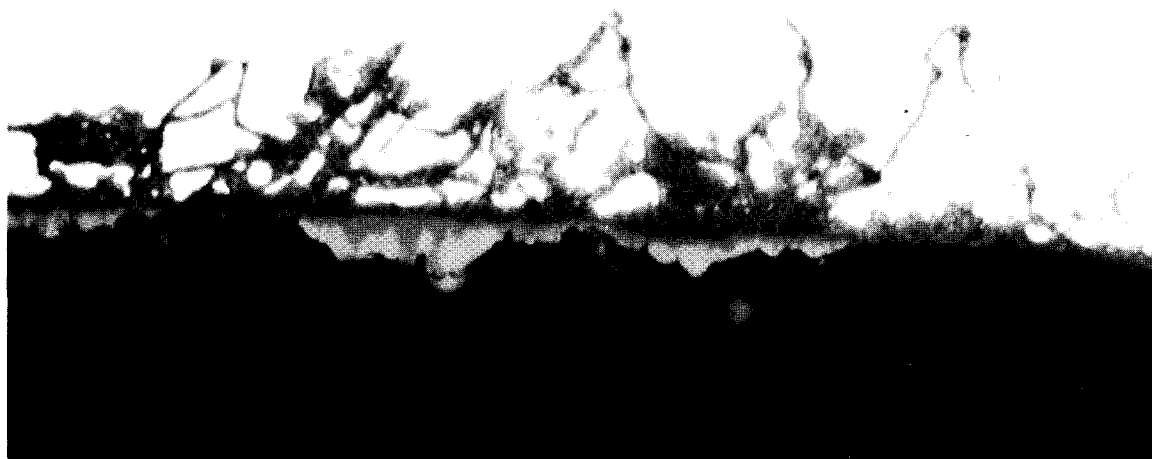


Fig. 29.2. Scale (Gray) Formed on Inconel 600 (White) in 8000 hr at 650°C. As polished, 2000X.

## 30. Fuel Element Fabrication Development

G. M. Adamson, Jr.    W. R. Martin

The goal of this program is to advance the fuel element technology for research reactors. Efforts are on the irradiation performance of cermet fuels, parametric study of fabrication processes, development of improved nondestructive techniques to aid quality control, and methods for extending the reactor lifetime of HFIR and ATR fuel elements.

### IRRADIATION STUDIES

W. R. Martin    R. G. Donnelly

The irradiation performance of cermet fuels is being studied with respect to the cermet characteristics that are altered by the mode of fabrication and choice of materials. Correlations between these characteristics and the resistance to irradiation damage are being developed to extend lifetimes and improve reliability of current operating systems. Coatings for aluminum cermets were studied to find a means of reducing fuel plate corrosion.

#### Postirradiation Examination of High-Temperature Refractory Metal Cermet Fuels

A. E. Richt    M. M. Martin

We completed the postirradiation examination of tungsten-urania and tungsten-urania-thoria dispersions irradiated in the Oak Ridge Research Reactor by the Missile and Space Division of General Electric. Eight capsules were irradiated in the range 1500 to 1730°C to a burnup of approximately  $1.4 \times 10^{20}$  fissions/cm<sup>3</sup> of the composite core. These capsules were irradiated to study the effect of type and magnitude of voids in reducing swelling of W-UO<sub>2</sub> and W-UO<sub>2</sub>-ThO<sub>2</sub> cermets clad with a W-Re-Mo alloy.

All phases of the postirradiation examination program — including burnup determination, dimensional measurements, and metallographic examination — have been

completed.<sup>1</sup> Analysis of the irradiation data indicates that the performance of the refractory metal cermets depended on their mean operating temperature in-reactor and their total as-fabricated void volume. The maximum increase in diameter of all eight pins ranged between 1.3 and 6.7%. The most dimensionally stable specimens operated at the lowest temperatures and contained the largest void volume. Greatest swelling and evidence of actual and incipient failures occurred in specimens subjected to the highest temperature and containing the least void volume. The total void space of the refractory metal cermets could have been located in the fuel dispersion, up to 14% in the end plenum chambers, or distributed between these two regions with equivalent effectiveness. Aside from a means of increasing total void volume, drilling small holes into the fueled region of the cermet (to shorten the diffusion path of the permeable fission gases) was not necessary for cermets having at least 2% porosity within the core. The maximum total void volume that appears to effectively accommodate fission products by reducing swelling is 24 to 33 vol %.

Failure of one fuel capsule during irradiation may have been premature and caused by excessive mass transfer between fuel and cladding. This serious effect may have been due to the formation of tungsten iodide from fission products and needs to be investigated further.

#### Irradiation Performance of a Nickel Phosphide Coating

A. E. Richt    M. M. Martin

Miniature fuel plates were irradiated in a pressurized water loop of the ETR to test the integrity of a nickel

<sup>1</sup>A. E. Richt, M. M. Martin, and W. R. Martin, *Postirradiation Examination and Evaluation of Tungsten-Urania Cermets*, ORNL-4569 (June 1970).

coating deposited electrolessly on types 6061 and 2219 aluminum cladding. Characterization of the unirradiated coating and a description of the test have been reported.<sup>2</sup> The nickel-coated plates were irradiated to maximum center-line core temperatures of 200 and 225°C and achieved a burnup of  $12.7 \times 10^{20}$  fissions/cm<sup>3</sup>. After the exposure, only traces of nickel remained on the plates. Analysis of the temperature histories of the two instrumented plates in this test suggested that the coatings spalled soon after the reactor reached full power at the start of the irradiation. We conclude that the nickel phosphide coating failed the test and should not be considered for use in aluminum-base research reactors.

### Effect of Void Volume on the Swelling Behavior of Aluminum-Base Dispersion Fuels

M. M. Martin    A. E. Richt

We have continued our studies of the effects of void volume and fuel fines upon the irradiation behavior of aluminum-base fuel dispersions. Early results<sup>3</sup> indicated that the void content of the as-fabricated dispersion was a major factor in the swelling of both U<sub>3</sub>O<sub>8</sub> and UAl<sub>x</sub> dispersion fuels. A subsequent review of all other available data on aluminum-based fuel dispersions not only supported this conclusion but led us to believe that we could predict within about ±1% the amount of swelling during irradiation of either type of dispersion by simply assuming that (1) the dispersion swells at a rate of 6.3 vol % per 10<sup>21</sup> fissions/cm<sup>3</sup> and (2) all voids initially present in the dispersion were available to accommodate this swelling.<sup>4</sup>

Recent irradiation results continued to support this model for UAl<sub>x</sub> fuels but indicate that an additional factor is influencing the swelling behavior of the U<sub>3</sub>O<sub>8</sub> dispersions.<sup>5</sup> As shown in Fig. 30.1, burned U<sub>3</sub>O<sub>8</sub> dispersions swelled about 1% more than would be predicted by our model, while high-fired U<sub>3</sub>O<sub>8</sub> dispersions swelled about 3% less than predicted. However, the fact that the difference between the measured and predicted swelling values appears to be a constant for

each type of U<sub>3</sub>O<sub>8</sub> suggests that the basic assumptions in our swelling model (i.e., the intrinsic swelling rate and effect of the initial void content) are correct. The difference between predicted and measured swelling of U<sub>3</sub>O<sub>8</sub> may be related to the chemical reactions between the U<sub>3</sub>O<sub>8</sub> and the aluminum matrix material. The extent of the reaction involving burned oxide is different than high-fired oxide. Thus volume change associated with the reaction may be the other factor influencing the swelling behavior of these dispersions. Additional work will be necessary to determine if the reaction can account for this discrepancy.

Increasing amounts of fuel fines appear to have little or no effect upon the swelling behavior of U<sub>3</sub>O<sub>8</sub> dispersion fuels except possibly during the early stages of irradiation, when burned U<sub>3</sub>O<sub>8</sub> dispersions appear to show an increasing tendency to shrink slightly with increasing fines content.

### HFIR FUEL ELEMENT SUPPORT

W. R. Martin    G. M. Adamson, Jr.

### HFIR Fuel Element Manufacture

R. W. Knight

Assistance to Texas Instruments, Inc., has continued throughout the past year. To date 91 fuel assemblies have been delivered. Table 30.1 shows fuel element rejections by groups. None of the 91 assemblies met all the specifications, but all have been accepted on waiver and will be operated at full power. The most trouble-

Table 30.1. Total Fuel Element Deviations by Groups

Group	Type	Numbers	Elements with Deviation	Total Deviations
1	Outer	1-12	12	88
	Inner		11	48
2	Outer	13-24	12	74
	Inner		12	35
3	Outer	25-36	12	92
	Inner		9	13
4	Outer	37-48	12	37
	Inner		7	18
5	Outer	49-60	11	35
	Inner		2	2
6	Outer	61-72	12	36
	Inner		3	3
7	Outer	73-84	12	43
	Inner		5	6

<sup>2</sup>M. M. Martin and J. H. Erwin, *Metals and Ceramics Div. Ann. Progr. Rept. June 30, 1969*, ORNL-4470, pp. 107-8.

<sup>3</sup>M. M. Martin and A. E. Richt, *Metals and Ceramics Div. Ann. Progr. Rept. June 30, 1969*, ORNL-4470, pp. 94-97.

<sup>4</sup>A. E. Richt, *Fuels and Materials Development Program Quart. Progr. Rept. Sept. 30, 1969*, ORNL-4480, pp. 218-19.

<sup>5</sup>A. E. Richt and M. M. Martin, *Fuels and Materials Development Program Quart. Progr. Rept. Dec. 31, 1969*, ORNL-4520, pp. 266-72.

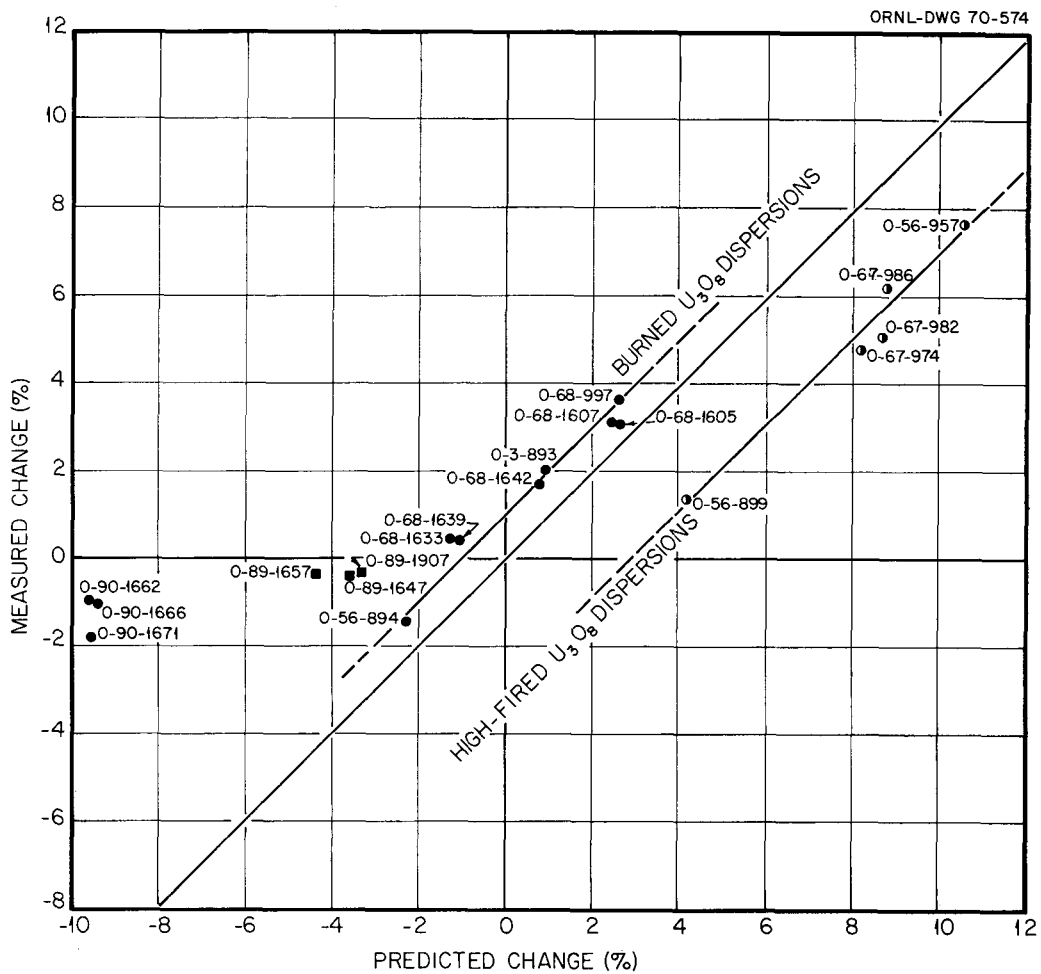


Fig. 30.1. Comparison Between Predicted and Measured Changes in Core Volume in Irradiated  $U_3O_8$  Dispersion Fuels. Point labels refer to experimental plate numbers.

some factor for all assemblies was welding. The fuel plate yields for plates in groups are presented in Table 30.2. The major type of fuel plate rejection is bond defects. These results show a 2.5% improvement in yield over last year's total and 0.80% improvement in yield for all fuel plates manufactured.

During the year 34 approval requests were submitted and processed; of these, seven were submitted for fuel plate waivers. Waivers on 190 fuel plates were requested; 159 were approved for a yield of 84%. Several requests were submitted and approved: 11 for routine process and drawing changes, four for the qualification and use in manufacturing of the new Marshall vacuum furnace, five for the manufacture of fuel plates and reporting results of the high loaded, high-fired, and burned  $U_3O_8$ , two for purchase of new equipment, two

for disposition of obsolete equipment, one reporting the results of a double-sided channel spacing probe, and one reporting on limits of surface defects for 6061 frame and cover plate raw stock. One approval request outlining a program to qualify and certify inspectors in accordance with SNTS standards was conditionally approved.

The incidence of blistered fuel plates suddenly increased. A brown discoloration on the 1100 aluminum side of the alclad aluminum was found after preheating the cover plates at 500°C. This organic material is believed to have caused the high incidence of blistering and was traced to contamination in the commercial grade nitric acid. Etching and pickling of fuel plate and assembly components with reagent grade nitric acid solved the problem.

Table 30.2. Fuel Plate Yield

Reasons for Rejections	Plates Rejected <sup>a</sup>					
	FY 1970		FY 1969		All Production to Date	
	Number of Rejections	Percent	Number of Rejections	Percent	Number of Rejections	Percent
Compacts	2	0.02	47	0.57	281	0.47
Surface	27	0.30	117	1.42	1988	3.35
Bond defects	354	3.96	483	5.85	3447	5.80
Core location	57	0.64	69	0.84	597	1.01
Homogeneity	84	0.94	165	2.00	1277	2.15
Dimensions	48	0.54	32	0.39	142	0.24
Form	1	0.01	2	0.02	36	0.06
Miscellaneous	6	0.07	22	0.26	236	0.40
Total	579	6.48	937	11.35	8004	13.48
Accepted on waiver	159	1.78	343	4.15	2516	4.24
Net Rejected	420	4.70	594	7.20	5488	9.24

<sup>a</sup>Number manufactured: 8934 in FY 1970, 8256 in FY 1969, 59,374 total.

### Modifications and Improvements to HFIR Fuel Plates

R. W. Knight

The burned grade of  $U_3O_8$  is cheaper than the high-fired grade of oxide that is currently being used in HFIR. Research at ORNL indicated that full-size HFIR fuel plates containing burned oxide could be fabricated and should perform at a level equal to or better than the high-fired oxide fuel. Eight lots of fuel plates using burned  $U_3O_8$  have been manufactured at Texas Instruments, Inc. by the HFIR reference process. As expected from ORNL tests, no problems were encountered in manufacturing these fuel plates. Permission has been granted by Reactor Operations Review Committee to use six inner and outer fuel plates in a HFIR fuel assembly during normal reactor operation to obtain irradiation damage experience.

Bond defects are a major cause of fuel plate rejection during manufacture. Most of these bond rejects are on the filler side of the fuel plate. We are attempting to reduce these bond defects. Dummy fuel plates were manufactured with the same volume percent  $Al_2O_3$  in the filler section of the fuel plate core as  $U_3O_8$  in the fuel section. The addition of the  $Al_2O_3$  introduces approximately 2% additional void volume into the filler section. If the nonbond rejections are related to gases on the filler side of the core, these fabrication voids may accommodate those gases at a much lower pressure, so the plates could bond during rolling. With composite plates containing only aluminum powder in the filler, one can expect 35 to 40% rejection due to blisters during rolling. Of the 72 plates rolled incorpo-

rating  $Al_2O_3$ , none were rejected for blisters. Further work will include fabricating samples for irradiation damage studies.

### FABRICATION DEVELOPMENT OF ALUMINUM DISPERSION FUEL PLATES

W. R. Martin R. G. Donnelly

#### Deformation Behavior of Shaped Fuel Cores During Rolling

J. H. Erwin

In a continued effort to solve the problems confronting fabricators of roll bonded fuel plates, we examined the deformation of shaped fuel cores, which are sometimes used to prevent excessive dogboning. We hot rolled, at  $490^\circ C$ , billets containing a 46 wt %  $U_3O_8$  core and a wrought 2219 aluminum core to simulate a  $UAl_x$  dispersion. A lengthwise cross section was examined after each rolling reduction. We arbitrarily selected two core shapes for comparison with rectangular cores. Leading and trailing edges were rounded to a radius of either  $1/8$  or  $1/2$  in. The cylindrical surfaces were tangent to the tops and bottoms of the cores and intersected the ends 0.070 in. from the top or bottom. Progressive thickness changes from the original core, blistering, and cracking were noted.

The 46 wt %  $U_3O_8$  dispersion is weaker than the 6061 aluminum cladding, but the 2219 wrought alloy used as a simulated core is stronger. For both core types, the void in the billet assembly as a result of the

shaped ends is filled during billet reduction by a combination of cover plate sinking and fuel core end swelling. After the void is filled by a few roll passes, all elements of the fuel core thickness, except the extreme ends, are reduced in about the same proportion. At the core end, the reduction differs with material strength. The ratio of end thickness (0.010 in. from original core end) to the average thickness for each of the fuel cores is presented as a function of reduction in Fig. 30.2. The curves for the two shaped cores of each material are parallel, differing primarily in the intercept, which is the thickness difference due to the two radii used. From our experiments we conclude that while shaping is useful to limit the dogbone formation, the necking as reported by some fabricators of ATR fuel elements is related to the uniform reduction of excessively shaped cores.

No blisters were observed on the plates containing the 46 wt %  $U_3O_8$  compacts, but all the plates containing the shaped and most of the rectangular 2219 aluminum simulated cores blistered at the core ends. The ability of powder metal cermets to accommodate trapped air to prevent blistering has been recognized previously.<sup>6</sup>

<sup>6</sup>M. M. Martin, J. H. Erwin, and W. R. Martin, *Metals and Ceramics Div. Ann. Progr. Rept. June 30, 1969, ORNL-4470*, pp. 105-6.

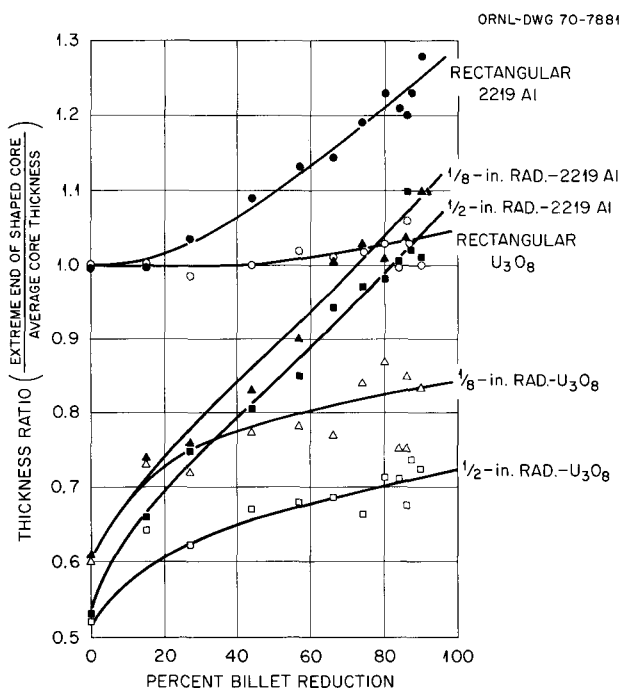


Fig. 30.2. Effect of Rolling on Ratio of Core End Thickness to Average Core Thickness.

### Parametric Study of $U_3O_8$ -Al and $UAl_x$ -Al Dispersion Fuel Plates

M. M. Martin

The introduction of fabrication voids explains the major variations in irradiation performance of many fuel dispersions for nuclear reactors. To obtain consistent and improved irradiation performance, we must understand the fabrication factors that control the amount of void volume and perhaps its deployment.

We investigated the void content of aluminum-base dispersion fuel plates at all stages of manufacture. Two grades of  $U_3O_8$  (burned and high fired) and two grades of  $UAl_x$  (arc cast and solid state reacted) have been examined at various uranium loadings up to 1.7 g/cm<sup>3</sup> of core and in full-size HFIR and miniature irradiation test core geometries. The fuel compounds differ in uranium content, density, and particle crushing strength. All dispersions were fabricated and clad with type 6061 aluminum by conventional powder metallurgy and roll bonding techniques. Miniature cores of 49 wt % burned  $U_3O_8$  were also clad with aluminum alloys 1100 from 500 to 600°C and 2219 at 500°C to investigate the effect of the cladding strength. Plates of identical materials and fabrication history showed excellent uniformity in void concentrations, within about  $\pm 0.75$  vol % about the average for a given dispersion.

The void content of the roll-clad aluminum-base dispersions depends on (1) the type and concentration of the fuel compound, (2) the type and strength of the aluminum cladding alloy, and (3) the amount of cold rolling deformation at room temperature. The quantity of voids increases with increasing dispersoid concentration, decreasing crushing strength of the dispersoid, decreasing compressive yield strength of cladding material, and increasing amount of cold rolling. For a particular material combination, the first roll-bonding reduction of as little as 15% in thickness established a constant void concentration for all subsequent hot-rolling passes. This equilibrium quantity of voids is insensitive to the initial density of fuel compact, hot bonding temperature in the range 500 to 600°C, and the proportion of -325-mesh fuel particles in the dispersions. The final void content of the completed fuel plate shows only a secondary dependency on cold deformation and heat treatment. However, even these small changes in magnitude of void volume from secondary effects could accumulate to a quantity that would significantly influence the irradiation performance of dispersion plates.

### Effect of Dispersoid Concentration on Void Volume of Composite Plates

M. M. Martin

The principal factors affecting the void volume of aluminum-base composites are the type and concentration of the fuel compounds and the degree of cold deformation after hot rolling.<sup>7</sup> (Also, see preceding section.) To provide more information in support of these findings, we investigated the effect of cold rolling for dispersoid contents over the entire concentration range. The miniature fuel plates used were dispersions in aluminum of high-fired  $U_3O_8$  and  $\alpha-Al_2O_3$  clad with aluminum alloy 6061 by conventional hot bonding techniques.

The void contents of the dispersions were determined at six stages of fabrication: after hot rolling and annealing, cold rolling to 8, 16, 25, and 31% reduction in thickness, and final annealing. In general, cold rolling increased the void content of both oxide cores, but the amount of the change depended on the type and concentration of the oxide. Figure 30.3 shows these effects for the  $U_3O_8$  dispersions. We have presented the data for only three conditions — hot rolled and annealed, cold rolled 16%, and cold rolled 31% — since the void content depends linearly on the amount of cold rolling. In the range 0 to 40 vol % oxide, the  $U_3O_8$ -Al dispersions contain more voids than  $Al_2O_3$ -Al dispersions of similar oxide concentration. Above 50 vol % oxide, the rate at which voids are produced with increasing oxide content is constant but is greater for the  $Al_2O_3$  than the  $U_3O_8$ -bearing cermet. On the basis of these observations, we conclude that the voids produced during cold rolling are physically associated with the oxide phase, and as such, they should enhance irradiation performance of dispersion fuel plates.

### Chemical Preparation of Aluminum Surfaces for Roll Bonding

J. H. Erwin

The expanded use of the Oakite 160 chemical cleaning process requires more knowledge in the latitude of operating variables to establish process sensitivity. We investigated effects on the metallurgical bond that could be accountable to control of solution strength, solution life, temperature, etching time, smut removal, storage of cleaned parts, rolling temperature,

<sup>7</sup>M. M. Martin, J. H. Erwin, and W. R. Martin, *Trans. Am. Nucl. Soc.* **11**, 107-8 (1968).

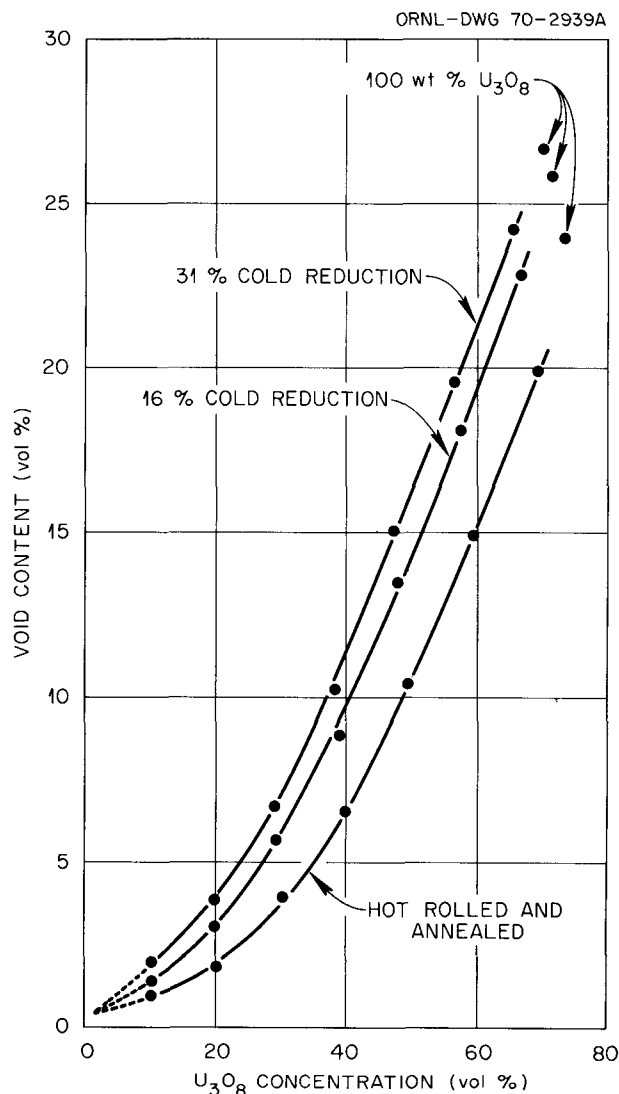


Fig. 30.3. Effect of Cold Deformation and  $U_3O_8$  Concentration on the Void Content of High-Fired  $U_3O_8$ -Al Dispersions Clad with Type 6061 Aluminum by Hot Rolling at  $500^\circ C$ .

and billet reduction rate. Simulated fuel plate billets consisting of two  $\frac{1}{8}$ -in.-thick cover plates and an unpunched  $5 \times 8 \times \frac{1}{4}$  in. frame were chemically cleaned with Oakite 160 and roll bonded. The percentage grain growth across the two interfaces was observed in both transverse and longitudinal samples 1 in. long cut from each rolled plate. The alloys 6061 and 2219 were used.

Billets cleaned with 2.5 to 10 oz/gal Oakite 160 in water in the  $54$  to  $82^\circ C$  range and rolled according to standard HFIR plate rolling conditions produced metal-

lurgical bonds that exhibited 75% or greater interfacial grain growth. Within this range, the strength of new solutions does not appear to be important, but the reaction is slowed by the dissolved aluminum. At 74°C fresh solutions remove about 0.001 in./min from the surface, but after the Oakite dissolves half its weight of aluminum, the rate of aluminum removal is reduced about 65%. At 82°C with fresh solutions, the reaction is somewhat boisterous, whereas the same solution at 54°C is quiescent and will only remove about 0.0002 in./min from the surface. Surface removal is uniform if alkali-insoluble contaminants are not present, and extended periods of etching (15 min) did not affect the plate bond. All surface contamination must be removed before the aluminum is heated.

No substantial difference was observed in the bond produced from smut removal and pacification of the surface by rinsing in 28 to 70% HNO<sub>3</sub> and then soaking 2 to 15 min after all visible smut had disappeared. However, plates rolled from parts treated with a commercial deoxidizer, Oakite 34, suffered 70% blister rejection and exhibited a 58% average grain growth, as compared with no blister rejects and 86% average grain growth for plates similarly treated with all strengths of nitric acid.

A week's storage of the cleaned parts before plate fabrication did not appear to affect the bond; however, two week's storage produced 10% blister rejection and reduced the interfacial grain growth by 10%.

Billets rolled at 400°C failed to bond in some large areas, while in other areas excellent grain growth with an average value of 87% was obtained. Similarly, at 490°C billets rolled with light reductions (8 and 12%/mill pass) generally developed extremely poor bonds (about 20% interfacial grain growth); however, some of these samples also exhibited an interfacial grain growth of about 90%. All of the samples rolled at 490°C with 25, 30, and 40% reduction per pass exhibited greater than 83% interfacial grain growth. Bonding at the lower reduction rates was not expected. That some interfacial grain growth can occur under these conditions indicates that the billet components can adhere sufficiently during the initial mill passes to prevent oxidation of portions of the interface even at low reduction rates or at the 400°C rolling temperature.

We conclude that the Oakite 160 cleaning process offers sufficient latitude in the conditions for use to allow normal production use in cleaning the aluminum alloys 2219 and 6061 preparatory to roll bonding if alkali-insoluble contamination is not present on the surface.

## NONDESTRUCTIVE TESTING

R. W. McClung

### Radiographic Densitometry

B. E. Foster S. D. Snyder

We completed the study of radiography and densitometry to determine the capabilities and limitations of standard techniques for measuring fuel inhomogeneity in aluminum fuel plates with dispersion cores. Much of the effort was devoted to considering the many variables that can affect the density of radiographic film: x-ray energy, exposure times, distance from film to focal spot, x-ray scattering, film processing, fog factor, densitometer aperture size, and repeatability.

It was extremely difficult to control these many variables and obtain reproducible film densities of the precision required for good quantitative measurement of fuel inhomogeneity. The use of an aluminum step wedge with a separate calibration on each radiograph somewhat relieves the need of close control of these variables if only relative changes within a given radiograph are to be measured. But even then, there is an inaccuracy of  $\pm 0.02$  in film density due to the inherent limitations of the densitometer. At normal operating conditions, this is equivalent to about  $\pm 5\%$  uncertainty in fuel measurements. A report is in progress covering this complete study.

### Scanner Calibration Studies

B. E. Foster S. D. Snyder

We are seeking an understanding of the effects of fuel particle size on the x-ray attenuation calibration curves for powder metallurgy fuel plates fabricated from high-fired and burned U<sub>3</sub>O<sub>8</sub>. The original HFIR calibration was used to determine the uranium content in 26 sets of flat core plates fabricated with different uranium loadings and from different mesh size powders. A general relationship was observed between the deviation of the uranium loading, as determined from the HFIR calibration, from the actual loading and powder mesh sizes over broad ranges. An even better correlation between particle or mesh size and fuel loading variation is expected when we normalize by weighting the data on particle size distribution with the particle area and/or volume.

## PHYSICAL PROPERTIES OF TWO-PHASE MATERIALS USED IN FUEL PLATE CORES

D. L. McElroy R. S. Graves  
J. P. Moore

A guarded-longitudinal heat flow apparatus<sup>8</sup> was used to measure the thermal conductivity ( $\lambda$ ) and electrical resistivity ( $\rho$ ) from 7 to 127°C of three types of plate samples: (a) type 101 aluminum, (b) nominally 12% Al<sub>2</sub>O<sub>3</sub> dispersed in type 101 aluminum, and (c) nominally 19% Al<sub>2</sub>O<sub>3</sub> dispersed in type 101 aluminum. The latter samples were machined from fuel plate material fabricated to these compositions by the picture-frame technique. The picture frame constituents were Norton Company type 38 Alundum and type 101 aluminum powder. The aluminum cladding of the fuel plates was machined away to yield cermet plates, nominally 0.5 × 0.025 × 3 in. To accommodate this sample geometry the specimen mount was modified and the specimen heaters were wrapped over an electrically insulating coating of epoxy applied to one end of the sample. Property values were obtained with heat and electron flow in the plane of the cermet, which is perpendicular to the heat flow direction during use of a fueled plate.

The  $\lambda$  and  $\rho$  values as functions of temperature are listed in Table 30.3. The results on this sample of type 101 aluminum are within 2% of our previous measurements on type 101 aluminum. The  $\lambda$  of type 101 aluminum powder exhibits a small maximum near 77°C and thus in the range 7 to 127°C is nearly independent of temperature. As expected, the Al<sub>2</sub>O<sub>3</sub> additions increase  $\rho$  and decrease  $\lambda$ . The  $\lambda$  of the cermet decreases about 2% from 7 to 127°C, reflecting the influence of Al<sub>2</sub>O<sub>3</sub>, which decreases about 40% in  $\lambda$  over this range.<sup>9</sup>

The  $\rho$  values of the samples permit the calculation of the volume fraction ( $P$ ) of electrically insulating material. Since the Al<sub>2</sub>O<sub>3</sub> particles and any porosity in the cermet are electrical insulators, one can reduce the Eucken equation to:

$$\frac{\rho_{Al}}{\rho_{cermet}} = \frac{1 - P}{1 + 0.5P}$$

This calculation yields  $P = 0.1388 \pm 0.002$  for the nominal 12% cermet and  $0.1992 \pm 0.002$  for nominal 19% cermet. These values were used to plot the measured  $\lambda$  values shown in Fig. 30.4. For this range of Al<sub>2</sub>O<sub>3</sub> the experimentally determined  $\lambda$  is nearly a linear function of composition and can be represented to within 2% by  $\lambda_{cermet} = (1 - 1.2067P)\lambda_{Al}$  to  $P = 0.3$ . Figure 30.4 illustrates calculated  $\lambda$  values using the Eucken equation, our  $\lambda$  values for type 101 aluminum, and recommended<sup>9</sup>  $\lambda$  values for 100%-dense, 99.5%-pure Al<sub>2</sub>O<sub>3</sub>. Extrapolation of these results beyond  $P = 0.3$  is not recommended.

## ELECTRON-BEAM WELDING OF FUEL PLATES TO SIDE PLATES

W. J. Werner G. M. Slaughter

We have been working toward characterization of the electron-beam process using statistical methods. Variables of primary importance are welding current, voltage, and beam focusing current. We held both gun-to-work distance and welding speed constant.

<sup>8</sup>J. P. Moore, D. L. McElroy, and R. S. Graves, *Can. J. Phys.* 45, 3849-65 (1967).

<sup>9</sup>R. W. Powell, C. Y. Ho, and P. E. Liley, *Thermal Conductivity of Selected Materials*, NSRDS-NBS-8 (Nov. 25, 1966).

Table 30.3. Smoothed Thermal Conductivity and Electrical Resistivity Values for 101 Aluminum and 12% Al<sub>2</sub>O<sub>3</sub>- and 19% Al<sub>2</sub>O<sub>3</sub>-Al Cermets

Temperature		Type 101 Aluminum		Al-12% Al <sub>2</sub> O <sub>3</sub> Cermets		Al-19% Al <sub>2</sub> O <sub>3</sub> Cermets	
(°C)	(°K)	$\lambda$ [W cm <sup>-1</sup> (°K) <sup>-1</sup> ]	$\rho$ ( $\mu\Omega$ -cm)	$\lambda$ [W cm <sup>-1</sup> (°K) <sup>-1</sup> ]	$\rho$ ( $\mu\Omega$ -cm)	$\lambda$ [W cm <sup>-1</sup> (°K) <sup>-1</sup> ]	$\rho$ ( $\mu\Omega$ -cm)
7	280	2.218	2.80	1.860	3.36	1.721	3.72
27	300	2.226	2.93	1.860	3.64	1.715	4.03
47	320	2.232	3.16	1.858	3.92	1.708	4.34
67	340	2.236	3.40	1.856	4.21	1.701	4.66
87	360	2.236	3.62	1.851	4.50	1.694	4.97
107	380	2.224	4.09	1.836	5.08	1.674	5.61
127	400	2.224	4.09	1.836	5.08	1.674	5.61

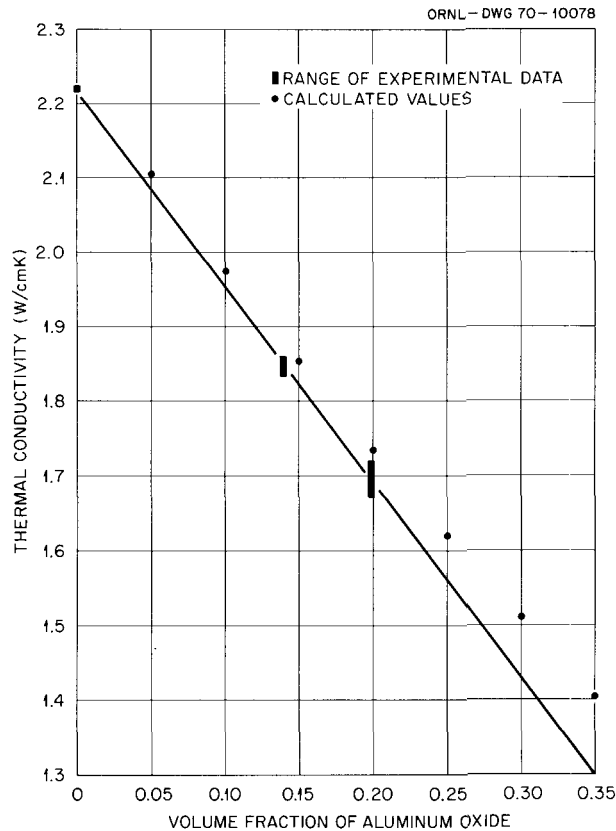


Fig. 30.4. Thermal Conductivity of Aluminum-Aluminum Oxide Cermets.

Welds were made on solid plates with the beam focused  $\frac{1}{8}$  in. below the work surface, on the work surface, and  $\frac{1}{8}$  in. above the work surface. Welding currents ranged from 65 to 85 mA and voltages ranged from 16 to 24 kV. Weld width and depth were measured metallographically. Our experimental design was such that the data for a given focus could be analyzed according to a mathematical model. The coefficients in the mathematical model were calculated from our experimental data, and curves of constant weld width, depth, and width at half depth were obtained as functions of welding current and voltage for each focus. Using these curves, we hope to choose the welding variables for a given fuel element.

Although the experimental points did not fit this model well, there was excellent reproducibility of data within any given weld. Cooldown parameters between welding cycles were not held constant in the experiment; therefore, the initial temperature of the test assembly probably varied considerably from one weld to the next. We believe that these differences in preheat between the various welds account for the rather poor fit of the experimental points to the curves.

## 31. Hastelloy N Improvement

J. R. Weir, Jr.    H. E. McCoy, Jr.

Hastelloy N is a nickel-base alloy that was developed specifically for use with fluoride salts.<sup>1</sup> It contains 16% Mo for solid solution strengthening, 7% Cr for moderate oxidation resistance, 0.04 to 0.08% C, and several other residual elements — such as Fe, Si, and Mn — whose concentrations depend upon the melting practice. This alloy is the sole metallic structural material in the MSRE, an 8-MW (thermal) demonstration reactor at Oak Ridge, and has also been used in the SNAP-8 core and for limited applications in gas turbine engines.

Our studies have shown that the alloy is embrittled by thermal neutron irradiation.<sup>2</sup> This embrittlement is associated with the production of helium by the  $^{10}\text{B}(n,\alpha)^7\text{Li}$  transmutation and is characteristic of most nickel- and iron-base alloys. The threshold level of helium (and hence boron) required to embrittle the alloy is only a few parts per billion, so it is unreasonable to solve the problem by purification. Our approach has been to modify the chemical composition to obtain a carbide precipitate that helps disperse the boron uniformly throughout the grains and makes the grain boundaries more resistant to fracture. This has involved the addition of strong carbide-forming elements such as Ti, Nb, and Hf.

Our work to date has been confined to 2-lb laboratory melts and 50- to 100-lb commercial melts. Our planned application of this alloy is for a molten-salt breeder reactor that will operate at 700°C with transients to slightly higher temperatures. The material will be exposed to a maximum fast fluence of about  $1 \times 10^{21}$  neutrons/cm<sup>2</sup> over 30 years, so the production of helium by the thermal flux will be the problem of primary concern. Thus, most of our irradiations have

been conducted at 650 to 760°C in the ORR to thermal fluences of 2 to  $5 \times 10^{20}$  neutrons/cm<sup>2</sup>.

Other work on Hastelloy N is reported in Chapter 39.

### ELECTRON MICROSCOPE STUDIES OF HASTELLOY N

R. E. Gehlbach    S. W. Cook

The electron microscopy studies of Hastelloy N are primarily devoted to characterizing the microstructures of the alloy resulting from variations in composition and heat treatment. We are investigating the role of several elements in changing the type, morphology, and distribution of carbide precipitation to generate a microstructure that will be stable and resistant to irradiation-induced embrittlement up to 760°C. During the past year we studied the effect of Si, Ti, Nb, and Hf in small laboratory melts (2 lb) and small commercial melts (50 to 100 lb).

The sole carbide formed in Hastelloy N without additions of the previously mentioned elements is  $\text{M}_2\text{C}$  (the M represents an element or combination of elements that make up the metallic constituents) having the hexagonal  $\text{Mo}_2\text{C}$  structure with chromium replacing a portion of the molybdenum. This carbide is distributed in both the matrix and grain boundaries, and its morphology depends upon the temperature of exposure. At 760°C, the highest temperature used in our studies, the precipitate existed as discrete particles. At 650°C it was finer and grew from the grain boundaries in a platelike morphology.

Small additions of silicon (0.1 to 0.5%) to the alloy promoted the formation of stable silicon-rich  $\text{M}_6\text{C}$  carbides. This type of carbide was not dissolved during normal solution treatments at about 1200°C and existed as large coarse particles throughout the material. Precipitation of  $\text{M}_2\text{C}$  also occurred when the silicon concentration was less than about 0.3%.

<sup>1</sup>H. E. McCoy, "The INOR-8 Story," *ORNL Review* 3(2), 35-49 (Fall 1969).

<sup>2</sup>H. E. McCoy, "Variation of Mechanical Properties of Irradiated Hastelloy N with Strain Rate," *J. Nucl. Mater.* 31, 67-85 (1969).

Sufficient additions of titanium or hafnium or combinations of titanium, hafnium, and niobium promoted the precipitation of MC-type carbides rather than  $M_2C$ . The amounts necessary to stabilize MC depended on the aging temperature, larger quantities being required to stabilize the monocarbides at increasingly higher temperatures. The MC carbides generally were not pure monocarbides (e.g., HfC) but contained large quantities of molybdenum, some chromium, and some of the MC-forming elements (Ti, Hf, or Nb) present in the alloys. The lattice parameters of these carbides varied with the particular MC-forming elements added and their concentrations in the alloy, thus reflecting differences in composition of the metallic portion of the monocarbides.

The size and morphology of MC depended upon the particular element(s) added to cause precipitation of MC rather than  $M_2C$ . The morphology of MC in titanium-modified alloys varied with solution annealing temperature and subsequent aging temperature and could exist as particles, platelets or films, and very fine particles on  $\{111\}$  planes. In alloys containing hafnium, MC precipitated as small particles both in the matrix and in grain boundaries, as shown in Fig. 31.1. All of the laboratory heats containing hafnium that we have examined by transmission electron microscopy have this characteristic morphology. Additions of hafnium

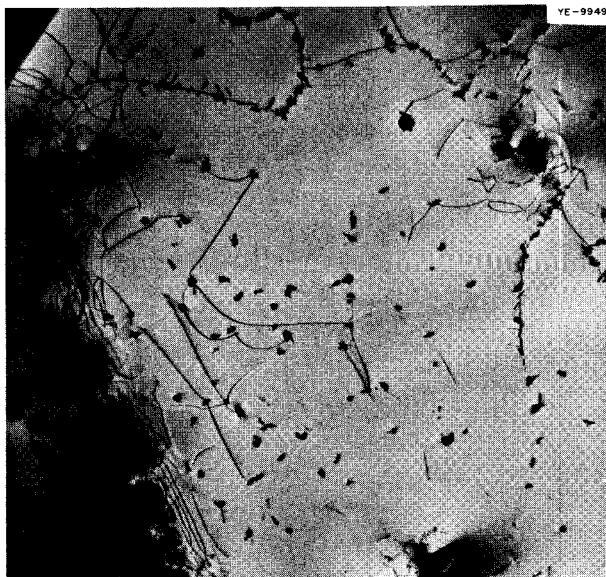


Fig. 31.1. Transmission Electron Micrograph Showing the Distribution of MC Characteristic of Hafnium-Modified Hastelloy N. The alloy contains 0.7% Hf. Aged 200 hr at 760°C. 5000X. Reduced 57%.

appeared to control the microstructure even when much larger quantities of titanium or niobium were present in the alloy.

Additions of silicon in combination with the MC-forming elements resulted in the formation of stable silicon-rich  $M_6C$ . The effect of silicon is more potent than all other elements that we have studied. The silicon is concerned in forming the coarse  $M_6C$ -type carbide, and any remaining carbon will react with the carbide-forming elements (Nb, Ti, Hf) to form MC. The microstructure of an alloy containing both hafnium and silicon is shown in Fig. 31.2. Note that both coarse  $M_6C$  and fine MC carbides were formed. We may be able to tolerate small amounts of silicon in the final alloy, particularly if hafnium is used as an addition.

Our studies have indicated that improved post-irradiation mechanical properties are associated with alloys having a relatively fine distribution of carbides. The MC carbides are generally finer than the  $M_2C$  type and much finer than the silicon-rich  $M_6C$ . This improvement may result from the effects of the precipitates in (1) strengthening the grain boundaries and decreasing the effectiveness of helium in embrittling the boundaries and (2) in tying up the boron in a stable matrix precipitate to prevent its migration to the grain boundaries.

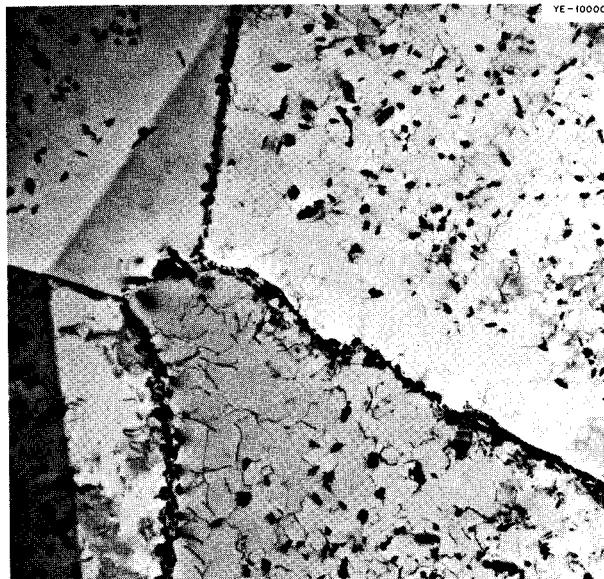


Fig. 31.2. Transmission Electron Micrograph Showing Coarse Grain Boundary  $M_6C$  and Finer Matrix MC. This modified Hastelloy N contains 0.65% Hf, 0.80% Ti, 1.3% Nb, and 0.35% Si. Aged 200 hr at 760°C. 5000X. Reduced 57%.

## EFFECT OF IRRADIATION TEMPERATURE ON THE CREEP PROPERTIES OF HASTELLOY N

H. E. McCoy, Jr. R. E. Gehlbach

Our studies have shown that the postirradiation creep properties of Hastelloy N can be very dependent upon the irradiation temperature.<sup>3</sup> Three types of alloys have been involved in this work: (1) standard Hastelloy N that was air melted and contained about 0.5% Si, (2) standard Hastelloy N that was vacuum melted and contained about 0.1% Si or less, and (3) modified alloys that generally were low in silicon and contained small additions of carbide formers such as Ti, Nb, Hf, and Zr. The range of irradiation temperatures was 50 to 800°C and the thermal fluence was 2 to  $5 \times 10^{20}$  neutrons/cm<sup>2</sup>. Numerous postirradiation test conditions were investigated, but let us confine the current discussion to creep testing at 650°C.

The air-melted standard Hastelloy N (0.5% Si) contained a carbide of the M<sub>6</sub>C type that was stable over the entire temperature range investigated. The post-irradiation properties were equivalent for samples irradiated over the entire range studied. The vacuum-

melted standard alloy (<0.1% Si) contained an M<sub>2</sub>C carbide that coarsened readily at temperatures above 700°C. Accordingly, the postirradiation properties were altered markedly by the irradiation temperature (Fig. 31.3). Irradiation at 760°C resulted in higher creep rates, shorter rupture lives, and lower fracture strains than observed after irradiation at 650°C.

The modified alloys exhibited a range of behaviors that will be discussed further. However, the general observation has been that low concentrations of carbide-forming elements (e.g., about 0.5%) caused finely dispersed MC carbides to be formed at irradiation temperatures of 650°C or lower.<sup>4</sup> At higher irradiation temperatures a coarser M<sub>2</sub>C carbide formed, and the

<sup>3</sup>H. E. McCoy and R. E. Gehlbach, "Influence of Irradiation Temperature on the Creep-Rupture Properties of Hastelloy N," submitted to *Nuclear Applications & Technology*.

<sup>4</sup>H. E. McCoy, Jr., and J. R. Weir, Jr., "Development of a Titanium-Modified Hastelloy N with Improved Resistance to Radiation Damage," pp. 290-311 in *Irradiation Effects in Structural Alloys for Thermal and Fast Reactors, Spec. Tech. Publ. 457*, American Society for Testing and Materials, Philadelphia, 1969.

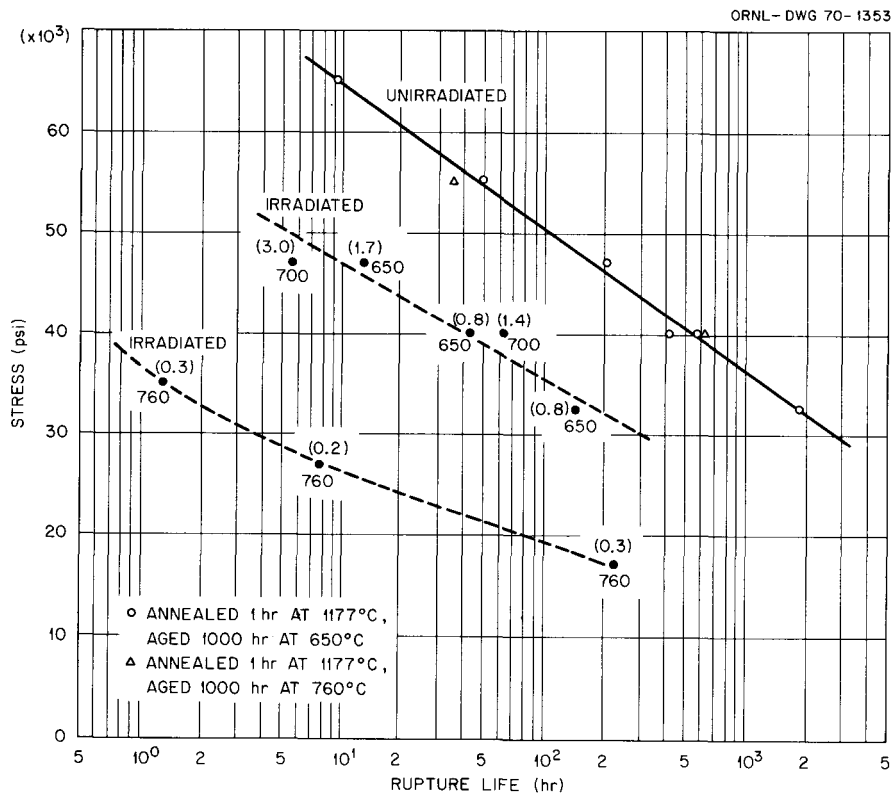


Fig. 31.3. Stress-Rupture Properties of Vacuum-Melted Hastelloy N After Irradiation at Various Temperatures, Tested at 650°C. The number in parentheses by each data point indicates the percent fracture strain, and the second number designates the irradiation temperature in degrees Centigrade.

postirradiation properties were equivalent to those of the vacuum-melted standard alloy. Higher additions of the carbide-forming elements were required to stabilize the fine MC carbide during irradiation at 760°C.

The postirradiation properties correlate qualitatively with the carbide distribution: fine dispersions give good properties and coarse dispersions give poor properties. This is because the finer precipitates provide more sites for trapping helium, and also their favorable distribution along the grain boundaries inhibits fracture.

### EFFECT OF TITANIUM ON THE HIGH-TEMPERATURE DEFORMATION AND FRACTURE BEHAVIOR OF SOME NICKEL-BASE ALLOYS<sup>5</sup>

C. E. Sessions

The influence of titanium on the elevated-temperature deformation and fracture behavior of nickel and a nickel-base alloy Hastelloy N (Ni-12% Mo-7% Cr-0.07% C) was investigated. The purpose was to relate the influence of titanium additions on the precipitate type, morphology, and distribution and their contribution to the creep and tensile behavior. The study involved (1) measuring creep-rupture properties at 650°C as a function of titanium (from 0 to 1.2%) and carbon (0.003 to 0.3%) contents for laboratory heats of a Ni-12% Mo-7% Cr alloy, (2) defining the effect of titanium on the phase equilibria of four commercial heats of Hastelloy N, and (3) correlating the carbide types, morphologies, and distributions established in these four heats with creep and tensile properties after aging at 650 or 760°C. This influence of titanium in the Ni-Mo-Cr alloy was compared with that in pure nickel alloyed with various titanium levels ranging from 0 to 1.5%.

The influence of 0.5% Ti on the creep properties of the Ni-Mo-Cr alloy was small unless the alloy was aged before mechanical testing. The addition of 0.5% Ti to the alloy resulted in an increase in the creep and stress-rupture strengths, a small increase in ductility, and no change in the intergranular fracture mode. On the other hand, when the carbon content was increased from 0.003 to 0.3% in the alloy containing 0.5% Ti, the rupture life increased by four orders of magnitude, the creep rate decreased by four orders of magnitude, and the creep ductility tripled. The fracture mode at 650°C changed from intergranular at low carbon to mixed trans- and intergranular at high carbon contents for similar heat treatments.

Extensive metallographic examinations, involving optical, electron transmission, extraction replication, and scanning electron microscopy, were made to assess the alloying behavior. The precipitate type and distribution changed when titanium was added to the alloy. Increasing the titanium concentration promoted the precipitation of MC carbides rather than the M<sub>2</sub>C type that formed when titanium was absent. For some aging conditions the MC carbides precipitated on dislocations, and certain dislocations dissociated and formed stacking faults. Growth of the stacking fault facilitated continued precipitation. The resulting precipitate distribution was that of a planar array of particles lying on the stacking faults. When titanium was absent, the M<sub>2</sub>C carbide that was precipitated did not cause growth of this stacking fault precipitate distribution.

Increasing concentrations of titanium up to 1.2% favored the formation of an MC carbide rather than an M<sub>2</sub>C type during aging at 650 and 760°C. Titanium substituted for chromium and molybdenum in the MC carbide, increasing the lattice parameter and stabilizing it to higher aging temperatures. Alloys containing a favorable distribution of MC carbides had greater ductility after aging in both creep and tensile tests than did alloys containing the M<sub>2</sub>C carbides. A heavy grain boundary distribution of MC carbides resulted in greater ductility than did the widely spaced M<sub>2</sub>C grain boundary precipitate distribution. This enhanced ductility of the higher titanium alloys was attributed to limiting the growth of grain boundary cracks by reducing grain boundary shearing.

Titanium also promoted the formation of an MC-type carbide distribution that was detrimental to ductility but beneficial to tensile strength at 650°C. The tendency to form stacking fault precipitates in the commercial alloys increased with an increase in either titanium content, solution annealing temperature, or aging temperature over the range of these variables investigated. When the commercial alloy containing 1.2% Ti was solution annealed at 1260°C and aged at 760°C, a maximum in the yield strength at 650°C occurred after 200 hr, and a minimum ductility was reached after approximately 1500 hr of aging. Stacking fault precipitate particles grew to a size resolvable in transmission electron microscopy (about 2 μm) on aging 5 hr at 760°C. Although this precipitate had a greater effect on short-time tensile tests than on creep tests, a loss of ductility was found for both testing conditions. The nucleation and growth of the precipitate and simultaneous formation of extrinsic faults in this Ni-Mo-Cr-Ti system confirms the theoretical model

<sup>5</sup> Abstracted from ORNL-4561 (in press).

proposed by Silcock and Tunstall,<sup>6</sup> which was based on observations of NbC precipitation in austenitic stainless steels. However, grain boundary denuding of this type precipitate was not extensive in our alloys, as was reported for the stainless steels.

We found that small concentrations of titanium drastically reduced the tendency for intergranular fracture in both creep and tensile tests at 600°C. Since the enhanced tensile ductility resulted from an increase in the "nonuniform" deformation, the strain rate sensitivity best reflected the influence of the titanium. It was reasonable that titanium acted as a scavenger and changed the distribution of impurities along the grain boundaries. The grain boundaries thus had a greater mobility, which allowed stress relaxation. Also, the absence of impurities from the boundaries should decrease the number of nucleation sites for intergranular cavitation.

Thus, we propose that titanium influences the mechanical behavior of the Ni-Mo-Cr alloy by controlling the type and distribution of metal carbides and that titanium enhances the elevated-temperature ductility of nickel by increasing the grain boundary mobility.

#### EFFECT OF COMPOSITION ON THE POSTIRRADIATION MECHANICAL PROPERTIES OF MODIFIED HASTELLOY N

C. E. Sessions    H. E. McCoy, Jr.

We concentrated on optimizing the composition of Hastelloy N with respect to minor additions of strong carbide-forming elements such as Ti, Hf, and Nb. We used as our "criteria of excellence" the postirradiation fracture strain and creep rupture life at 650°C following irradiation at 760°C to a thermal fluence of  $3 \times 10^{20}$  neutrons/cm<sup>2</sup>. Approximately 35 alloy compositions were tested under these conditions. The alloy additions were made to a Ni-12% Mo-7% Cr base and included various combinations of the elements Ti, Hf, Nb, Si, Zr, and C added independently or collectively. Our conclusions concerning the influence of these alloying additions on the high-temperature irradiation embrittlement of the nickel-base alloy are described.

We emphasized primarily the effects of titanium additions on the Ni-12% Mo-7% Cr alloy, and Fig. 31.4 summarizes the creep properties at 650°C following irradiation at 760°C. For tests at a relatively

high stress of 47,000 psi the rupture life varied from 0 to 1500 hr over the range of 0 to 3.0% Ti. This increased rupture life is the result of a drastic decrease in the creep rate (Fig. 31.4). Unfortunately, the superior creep resistance at the higher titanium concentrations is offset by low ductilities, which we attribute to either precipitation of intermetallic compounds or precipitation of carbides along stacking faults. Compositions near 2% seem to offer the best combination of strength and ductility under these test conditions.

The influence of other alloying additions on the postirradiation creep-rupture behavior of Hastelloy N is compared in Fig. 31.5. Each curve corresponds to the maximum rupture life attributable to either single or multiple additions of the elements Ti, Nb, and Hf to a nominal Ni-12% Mo-7% Cr-0.06% C base. Figure 31.5(a) compares the maximum rupture life achieved for alloys with additions of either Ti, Nb, or Hf. It is clear that 3% Ti produced greater postirradiation creep-rupture lives than either 1.2% Hf or 2% Nb. The alloy with 1.2% Hf was superior to the alloy with 2%

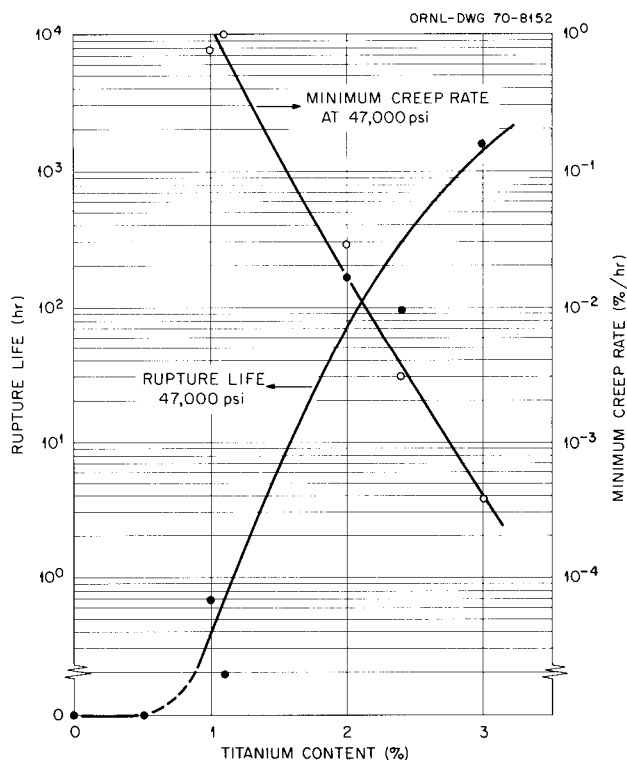


Fig. 31.4. Effect of Titanium Content in Hastelloy N on the Postirradiation Creep-Rupture Properties at 650°C and 47,000 psi Stress. Samples were solution annealed 1 hr at 1177°C and irradiated at 760°C to a thermal fluence of  $3 \times 10^{20}$  neutrons/cm<sup>2</sup>.

<sup>6</sup>J. M. Silcock and W. J. Tunstall, "Partial Dislocations Associated with NbC Precipitation in Austenitic Stainless Steels Observed by Thin Film Electron Microscopy," *J. Iron Steel Inst. (London)* 204, 409 (1963).

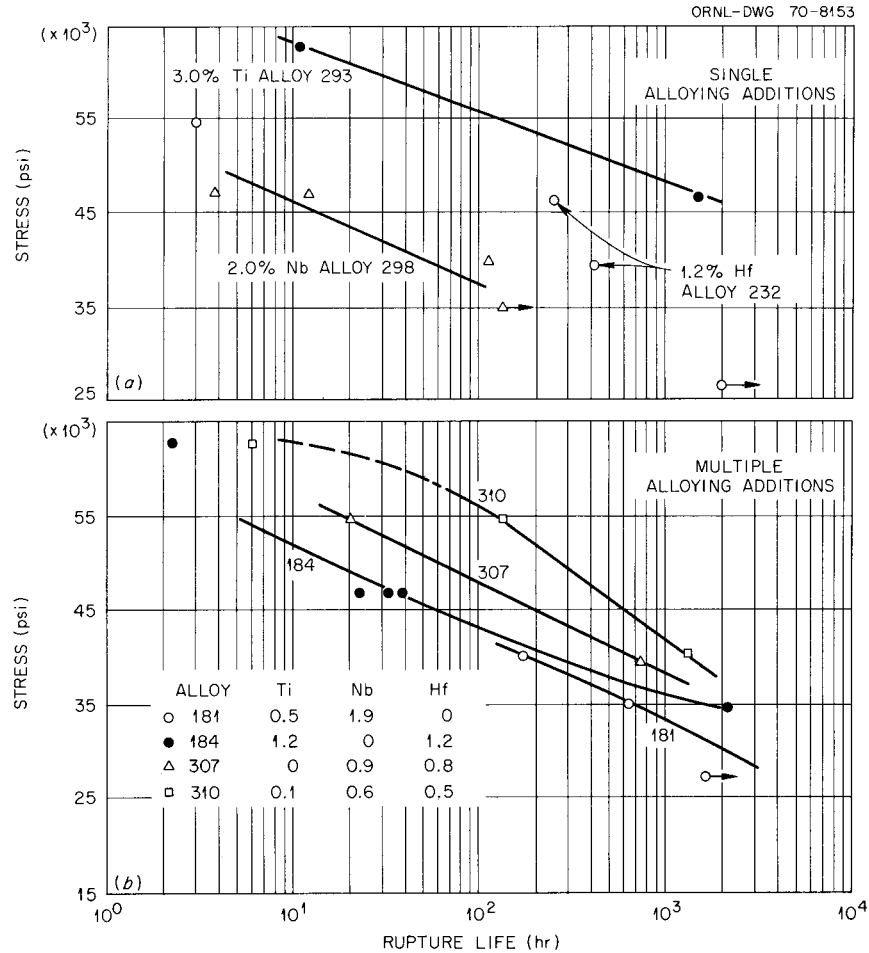


Fig. 31.5. Postirradiation Creep-Rupture Properties of Several Modified Hastelloy N Compositions at 650°C. Samples were annealed 1 hr at 1177°C, irradiated at 760°C to  $3 \times 10^{20}$  neutrons/cm<sup>2</sup>, and tested at 650°C. (a) Properties achieved with single additions of either Ti, Nb, or Hf. (b) Properties achieved with combined additions of Ti, Nb, and Hf.

Nb and, in fact, was comparable in rupture strength to an alloy with 2% Ti, which is not plotted here.

The combined effects of Ti-Hf, Ti-Nb, Hf-Nb, and Ti-Hf-Nb additions to the Ni-12% Mo-7% Cr-0.06% C base are compared in Fig. 31.5(b). The alloy with the greatest rupture life contained 0.1% Ti, 0.6% Nb, and 0.5% Hf. The addition of 0.9% Nb + 0.8% Hf was next best on the basis, and the other two alloys shown in Fig. 31.5(b) had approximately equivalent rupture lives for these test conditions.

Thus, based on a maximum of three postirradiation creep tests per alloy, we conclude that hafnium is more effective than either titanium or niobium on a weight fraction basis, and that combined additions of all three elements (Ti, Nb, and Hf) are superior to any two of these taken together.

The effects of alloying on the postirradiation ductility are more difficult to summarize, but intermediate titanium levels of approximately 2% and even a 0.5 to 1.0% Hf produced alloys with very good postirradiation creep ductility. Niobium additions alone did not enhance postirradiation ductility. Multiple additions of Ti-Hf, Nb-Hf, and Ti-Nb-Hf yielded alloys with excellent ductilities of from 5 to 25% depending on the composition and postirradiation creep stress. The Ti-Nb additions resulted in alloys with up to 5% postirradiation ductility, which is also relatively good.

For a potential reactor application at 700°C we would favor alloy compositions of modified Hastelloy N (Ni-12% Mo-7% Cr-0.06% C) containing the following additions: (1) titanium in the range of 1.5 to 2.0%, (2) titanium and hafnium both in the range of 0.5

to 1.0%, or (3) Ti-Nb-Hf each in the range of 0.2 to 0.7%. Other factors such as fabricability, corrosion resistance, or commercial availability will undoubtedly dictate which of these three modified alloy types is most practical.

Another element of importance that we have not examined fully is carbon. Since carbide precipitation reactions influence the magnitude of the radiation damage<sup>7</sup> in titanium-modified Hastelloy N, it is quite reasonable that the carbon content be important. We have investigated the effects of high and low carbon contents (0.03 and 0.08% C) for irradiations conducted from 550 to 760°C. In alloys with 1.0% Ti irradiated at

550°C, the alloy with the higher carbon content had greater rupture life and ductility in postirradiation creep tests at 650°C. For irradiations at 650 and 760°C the effects of increasing carbon content were similar, but the postirradiation properties were influenced greatly by the temperature of irradiation. Higher irradiation temperatures increased the particle size of the carbide precipitate and resulted in reduced creep strength and ductility.

---

<sup>7</sup>C. E. Sessions, H. E. McCoy, R. E. Gehlbach, and S. W. Cook, *Metals and Ceramics Div. Ann. Progr. Rept. June 30, 1969*, ORNL-4470, pp. 184-89.

## 32. Joining Research on Nuclear Materials

G. M. Slaughter

This program is concerned with obtaining a basic understanding of the weldability of materials commonly used in the fabrication of nuclear power plants. We have concentrated on nickel-containing alloys, since they have exhibited a strong tendency to crack during welding. Difficulties during welding have been encountered in weld metal and in heat-affected base metal, both at high temperatures (near the solidus) and at intermediate temperatures (about 650°C). The nickel contents under study vary from low percentages (about 10%) representative of stainless steels to high percentages (about 75%) representative of Inconel 600.

Our primary effort has been to determine the effects of minor quantities of such elements as C, S, P, Ti, Al, Mn, and Si on weldability. However, we are placing an increasing amount of attention upon the nature and morphology of the ferritic phases usually present in stainless steel weld deposits.

### THE EFFECT ON WELDABILITY OF MINOR VARIATIONS IN CHEMICAL COMPOSITION

#### Ductility of Heat-Affected Zones at High Temperatures

D. A. Canonico W. J. Werner

The Duffer's Gleeble was employed to study the effect of various elements on the heat-affected-zone properties of nickel-rich alloys. Previously, we reported<sup>1,2</sup> the effect of Ti, Al, S, and P on the hot ductility of experimental alloys of Incoloy 800 and Inconel 600. We also investigated<sup>3</sup> the effects of minor elements on Incoloy 800 in the range 650 to 870°C.

<sup>1</sup>D. A. Canonico and W. J. Werner, *Metals and Ceramics Div. Ann. Progr. Rept. June 30, 1968*, ORNL-4370, pp. 151-55.

<sup>2</sup>D. A. Canonico and W. J. Werner, *Metals and Ceramics Div. Ann. Progr. Rept. June 30, 1969*, ORNL-4470, pp. 112-13.

<sup>3</sup>W. J. Werner, *An Investigation of the Effect of Certain Minor Elements on the Elevated Temperature Ductility of Incoloy 800*, ORNL-4504 (March 1970).

The Gleeble studies showed that the effect of sulfur in Incoloy 800 was inconsequential when present in combination with titanium. We also showed that sulfur very seriously affected the hot ductility of an alloy such as Inconel 600 that did not contain titanium. This past year we have studied the effect of the elements Al, Ti, S, P, and C on the hot ductility of experimental alloys of Incoloy 800 (Figs. 32.1 and 32.2). Aluminum and titanium are beneficial; both improve the on-heating and on-cooling hot ductility of the ternary Incoloy 800 (Fe-Ni-Cr) composition.

Sulfur caused a severe loss of hot ductility when tested on heating to the peak temperature and on cooling after exposure to a thermal cycle simulating that of the heat-affected zone of a weld. Phosphorus had essentially no effect on the hot ductility of the ternary composition. Combining both elements resulted in some improvement (over the individual effects) in the on-heating and on-cooling ductilities; however, the low ductility at 1150°C (2100°F) persisted. The experimental Incoloy 800 base composition with 0.08 wt % C had better heat-affected zone properties than lower carbon alloys.

Our investigation of the experimental Inconel 600 compositions (shown in Table 32.1) focused on the effect of the various elemental additions on heat-affected-zone microstructures (from hot-ductility specimens whose mechanical properties were previously reported<sup>2</sup>). Figure 32.3 shows the microstructural differences between the ternary Ni-Cr-Fe experimental alloy (600-1) and the nominal Inconel 600 alloy (600-2). The addition of C, Si, Cu, and Mn resulted in a much finer grain size, which persists through the zero-ductility temperature (ZDT).

Increasing the sulfur content caused liquation. Some was evident in the grain boundaries of the 0.006% S alloy (600-3) at its ZDT, and the 0.012% S alloy showed gross liquation in laminations. This occurred in spite of the fact that the zero-ductility temperatures

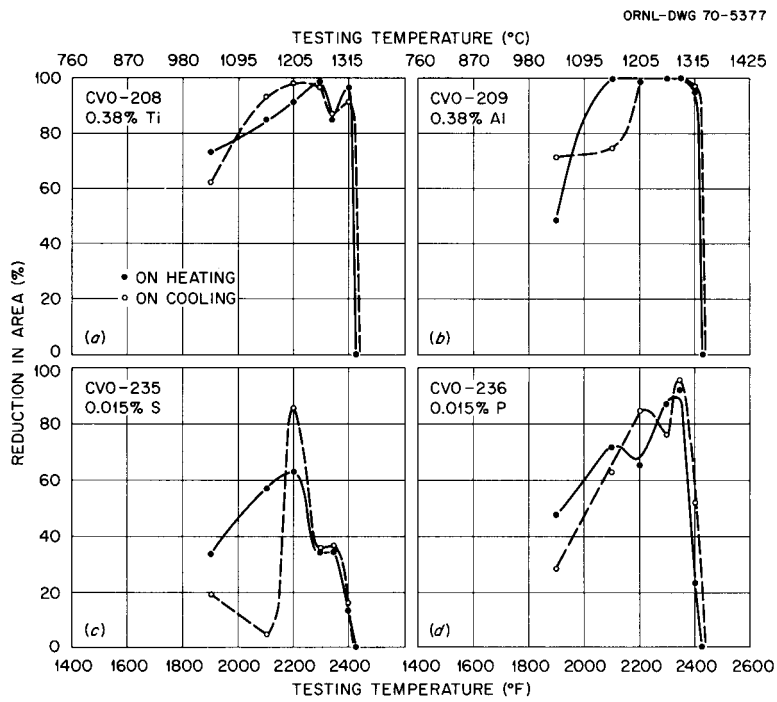


Fig. 32.1. The Effect of Ti, Al, S, and P on the Hot Ductility of Experimental Incoloy 800 Alloys. Note the detrimental effect of sulfur on both the on-heating and on-cooling ductility.

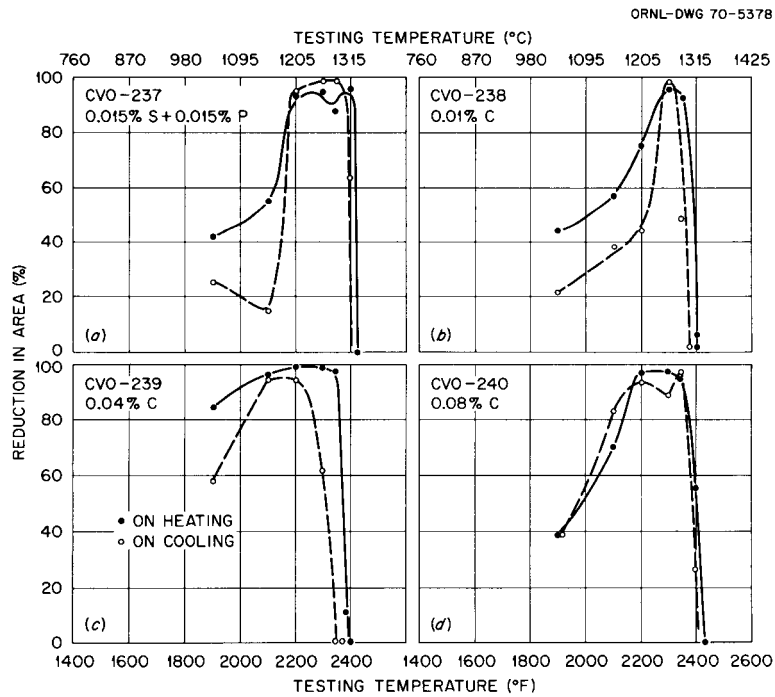


Fig. 32.2. The Effect of Sulfur Plus Phosphorus and of Carbon on the Hot Ductility of Experimental Incoloy 800 Alloys. The effect of combined sulfur plus phosphorus is not great at very high temperatures, but low ductility at 1150°C is evident. Low carbon levels have moderately detrimental effects on the on-cooling properties, but higher carbon does not appear to affect the hot ductility.

Table 32.1. Nominal and Actual Compositions of the Inconel 600 Hot-Ductility Specimens

Alloy	Composition <sup>a</sup> (wt %)												B (ppm)
	Ni	Cr	Fe	C	H	N	O	S	P	Si	Mn	Cu	
600-1	75.2	15.9	8.13	0.004	0.0011	0.0004	0.019	0.003	0.001	0.01	0.007	<0.01	1
600-2	75.6	16.1	8.55	0.028	0.0002	0.0010	0.0081	0.002	0.002	0.2	0.11	0.026	1
600-3	75.2	16.0	8.40	0.028	<0.0001	0.0004	0.0005	0.006	0.001	0.2	0.11	0.022	1
600-4	74.7	15.5	8.04	0.025	0.0002	0.0005	0.0025	0.010	0.002	0.2	0.15	0.029	2
600-5	74.5	15.7	8.32	0.026	0.0005	0.0010	0.0061	0.012	0.002	0.2	0.12	0.18	<0.2
600-6	70.9	15.9	12.1	0.027	0.0008	0.0013	0.0079	<0.002	0.006	0.2	0.23	0.021	0.3
600-7	73.7	15.8	9.33	0.026	0.0029	0.0018	0.017	<0.002	0.011	0.2	0.20	0.021	0.3
600-8	72.6	15.9	10.4	0.023	0.0025	0.0028	0.082	<0.002	0.015	0.3	0.17	0.018	0.3
600-9	72.6	16.2	11.4	0.034	0.0021	0.0016	0.0075	0.003	0.004	0.2	0.16	0.024	0.4
600-10	72.3	16.2	11.5	0.026	0.0029	0.0011	0.018	0.003	0.006	0.2	0.17	0.023	0.7
600-11	73.7	16.1	8.98	0.026	0.0019	0.0007	0.0079	0.006	0.008	0.2	0.17	0.018	0.2
600-12	75.6	16.2	8.28	0.033	0.0009	0.0015	0.0086	0.009	0.002	0.2	0.32	0.021	0.2
600-13	75.4	15.9	8.11	0.022	0.0012	0.0015	0.012	0.009	0.002	0.2	0.48	0.024	0.4
600-14	75.2	16.0	9.05	0.026	0.0002	0.0013	0.016	0.009	0.002	0.2	0.84	0.029	0.4
600-15	72.5	16.6	11.3	0.026	0.0005	0.0008	0.011	0.008	0.007	0.2	0.80	0.022	0.5

<sup>a</sup><0.05% Al, <0.01% Ti, <2 ppm Pb.

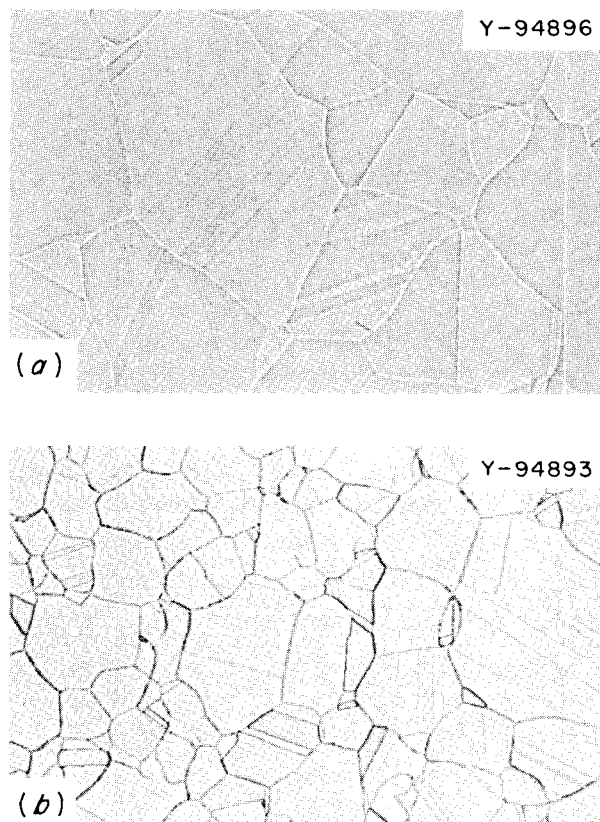


Fig. 32.3. Gross Difference in Grain Size Between (a) the Ni-Cr-Fe Ternary Composition (Alloy 600-1) and (b) the Nominal Inconel 600 Composition (Alloy 600-2). Both alloys were annealed at 1180°C. 100X.

differ by nearly 40°C (1338°C for low sulfur compared to 1300°C for the high sulfur). Figure 32.4 illustrates the effect of sulfur on the microstructure of the samples removed from the ZDT specimens. Laminations are evident in the high-sulfur base metal. Moreover, sulfur resulted in large grains similar to those in the ternary composition.

Phosphorus additions up to 0.015 wt % (alloys 600-6 through -8) did not have a deleterious effect. The fracture appearance and microstructure (at the ZDT) are similar to those of the nominal alloy (600-2) in both the heat-affected zone and the unaffected base metal. When both sulfur and phosphorus are added (600-9 through -11), sulfur appears to dominate, and the microstructures show grain coarsening and bonding.

The effect of between 0.32 and 0.84% Mn was studied when present with about 0.009% S. Increasing the manganese content did not affect the microstructure of the sulfur alloy, but adding phosphorus to the alloy containing manganese and sulfur caused grain refinement. This effect indicates an association between manganese and sulfur, thereby neutralizing the effect of sulfur and promoting that of phosphorus.

### Studies on Incoloy 800 Weld Metal

D. A. Canonico

We prepared  $1/16$ -in.-diam filler wire from the specially melted and processed experimental heats that had been

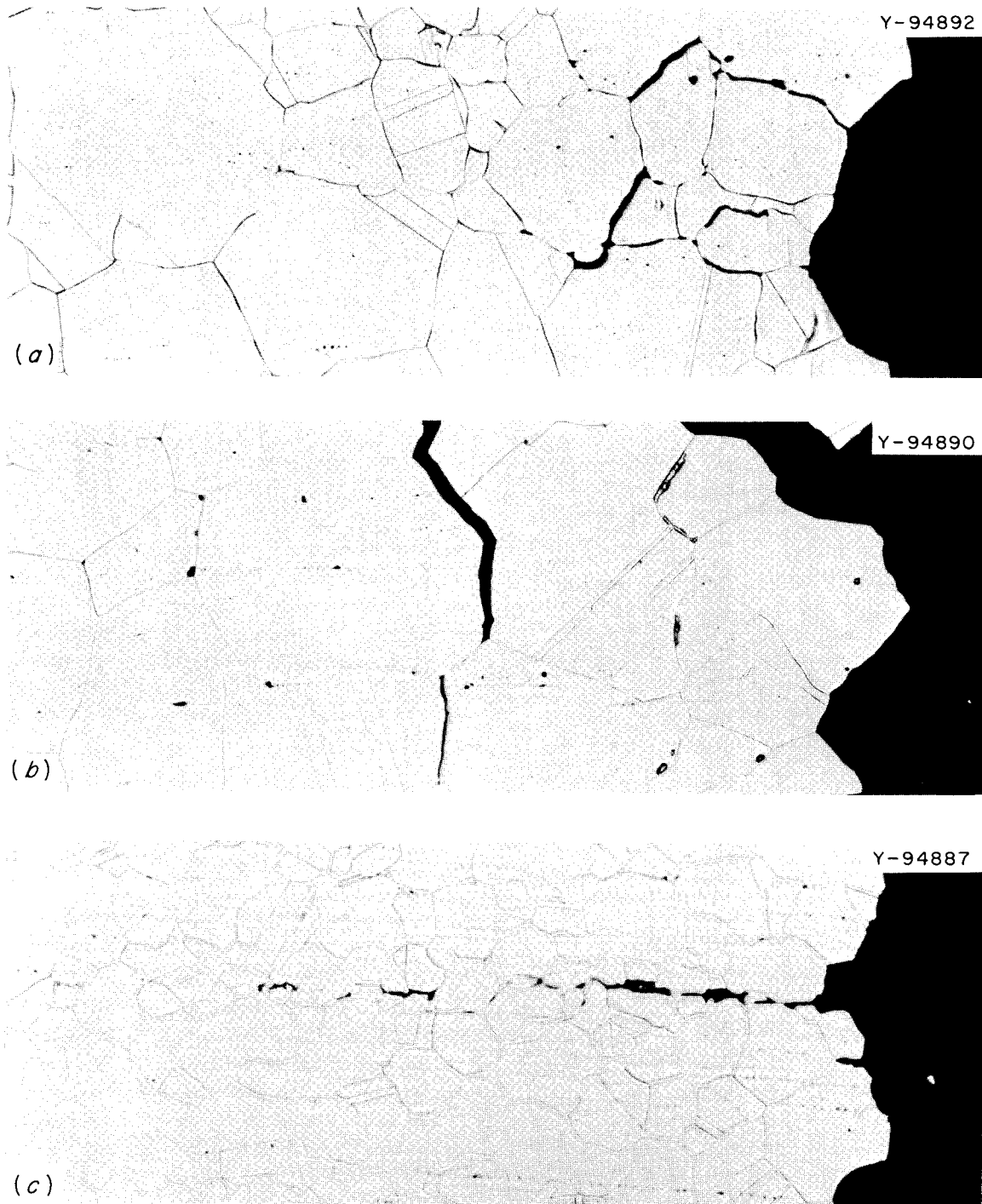


**Fig. 32.4. Fractured Regions in Specimens Tested for Zero-Ductility Temperature.** Note the tendency toward gross liquation as the sulfur content is increased. 100X. (a) Alloy 600-3: 0.006% S, ZDT = 1338°C. (b) Alloy 600-4: 0.010% S, ZDT = 1330°C. (c) Alloy 600-5: 0.012% S, ZDT = 1300°C.

used previously in tests with the Duffer's Gleeble.<sup>4</sup> Three additional filler wires were studied; two of these, Inconel 62 and Inconel 82, are commercial filler metals recommended for joining high-nickel alloys, and the third was prepared from electroslag remelted Incoloy 800 base plate. Tungsten-arc welds were deposited with all these filler metals on 1/8-in.-thick commercial Incoloy 800 plate.

The welds were all nondestructively examined and, except for those with sulfur-containing filler metals, were acceptable. The sulfur-containing welds cracked. When tensile specimens containing the welds were tested at room temperature, the weld with the Inconel 82T filler metal was strongest; it failed in the base metal at 79,500 psi. All the other tests failed in the weld metal at about 72,000 psi. Of those filler metals that failed in the weld, the electroslag remelted Incoloy 800 had the best strength (77,000 psi) and ductility (36%). Of the experimental filler metals, a phosphorus-containing alloy had the highest yield strength (38,000 psi). Nominally 0.015% S reduced ductility and strength to 17% and 66,000 psi. The fracture of the sulfur-containing filler metal revealed microfissures.

## AUSTENITIC STAINLESS STEELS

A. J. Moorhead D. A. Canonico

Our study has centered on the effect of chemical composition on the amount and morphology of the ferritic phases usually present in stainless steel weld deposits. Although the primary interest is on the body-centered phase ( $\delta$ -ferrite) believed to form early in the solidification of the weld metal, a second ferritic phase, body-centered tetragonal martensite, may also be present. Its transformation from austenite occurs at considerably lower temperatures. The transformation kinetics of the two ferritic phases (for example, to the brittle sigma phase) are different, but there may be an interaction between them. Further, the mechanical properties of a weld may be more dependent on the presence (or absence) of the martensitic phase than they are on the ferrite phase.

Using the Schaeffler diagrams as a guide,<sup>5</sup> we are determining the effectiveness of various combinations of Ni, Cr, and Fe to provide austenitic weld metals with

similar quantities of ferrite. The alloys we are using lend themselves to an investigation of the effect of temperature and strain on the transformation of austenite to martensite. Of considerable interest is the effect of the presence of the ferrite on the diffusionless transformation of austenite to martensite.

We have prepared 1-lb drop castings of each of the 13 alloys shown in Table 32.2. Their relative locations on a Schaeffler diagram are shown in Fig. 32.5. The riser and a section of the bottom were machined from each casting, producing bars  $1\frac{1}{32} \times 3\frac{1}{32} \times 4\frac{3}{4}$  in. These bars were homogenized in hydrogen at 1150°C for 1 hr and then cooled in the water-cooled zone of a tube furnace.

To detect body-centered cubic phases (ferrite or martensite) in the castings, we measured magnetic response with a Magne-Gage. The results are also reported in Table 32.2.

We have concentrated our microstructural studies on alloys 5409, 5410, 5419, and 5420. These were selected to provide three levels of ferrite, 0, 6, and 10%, and two different compositions with 10% ferrite. We measured the ferrite contents with the quantitative television

Table 32.2. The Effect of Homogenization<sup>a</sup> on Magnetic Strength

Alloy	Nominal Composition (wt %)			Magne-Gage Reading <sup>b</sup>	
	Ni	Cr	Fe	Before	After
				Homogenization	Homogenization
5408	12	19	69	111	WNA
5409 <sup>c</sup>	12	19	64	102	153
5410	10	19	71	20	139
5411	14	19	67	WNA	WNA
5412	16	19	65	WNA	WNA
5415	12	21.5	66.5	8	102
5416	14	21.5	64.5	93	155
5417	16	21.5	62.5	155	WNA
5418	18	21.5	60.5	WNA	WNA
5419	14	24	62	9	92
5420	16	24	60	89	132
5421	18	24	58	144	WNA
5422	20	24	56	WNA	WNA

<sup>a</sup>Heated at 1150°C for 1 hr in H<sub>2</sub>.

<sup>b</sup>All readings were taken with the No. 4 magnet. The higher the number, the lower the magnetic strength and ferrite content. WNA denotes that the magnet would not adhere to these specimens, so that no reading could be taken.

<sup>c</sup>This alloy contained 5% Mn.

<sup>4</sup>D. A. Canonico and W. J. Werner, *Fuels and Materials Development Program Quart. Progr. Rept. Dec. 31, 1969*, ORNL-4520, pp. 298-300.

<sup>5</sup>A. L. Schaeffler, "Selection of Austenitic Electrodes for Welding Dissimilar Metals," *Welding J. (N.Y.)* 26, 601-s-620-s (1947).

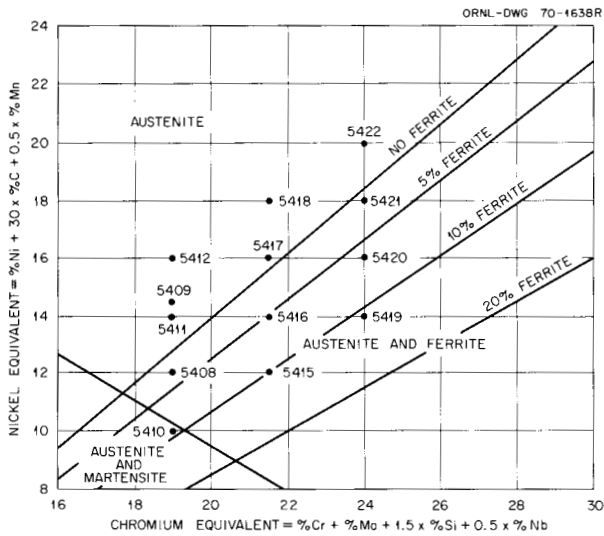


Fig. 32.5. Location of 13 Ternary Drop-Cast Alloys on the Schaeffler Diagram for Stainless Steel Weld Metal.

microscope (QTM). Although alloy 5409 had been formulated to contain 100% austenite, the QTM showed that it actually contained nearly 3% ferrite.

Two alloys with quite different chemical compositions (alloys 5410 and 5419) were designed to provide identical levels of ferrite (10%). The nickel and chromium equivalents were varied to obtain these similar microstructures. Figure 32.6 comprises photomicrographs of these two alloys as etched. The differences in the size and distribution of the ferrite (the darker phase) are striking. An electron-beam microprobe study is under way on these alloys.<sup>6</sup>

<sup>6</sup>A. J. Moorhead and D. A. Canonico, *Fuels and Materials Development Program Quart. Progr. Rept. March 31, 1970*, ORNL-4560, pp. 244-49.

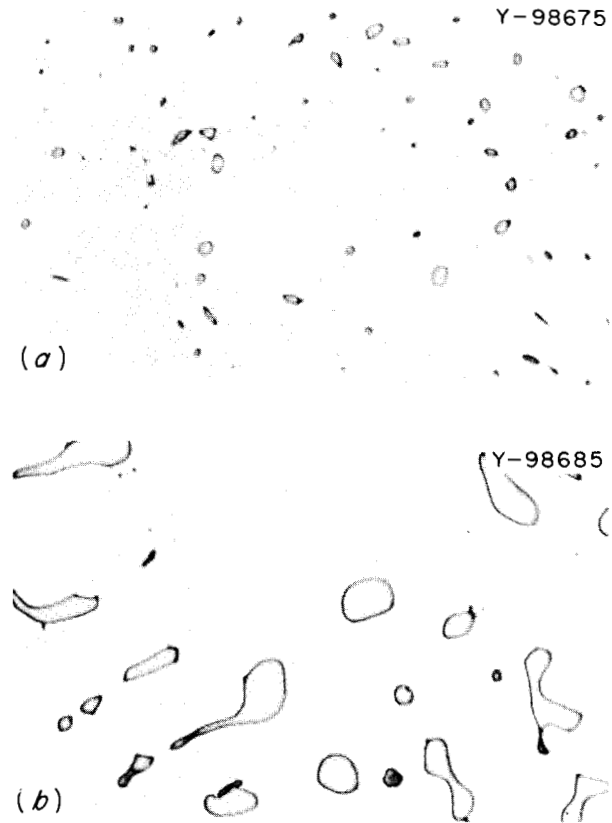


Fig. 32.6. Photomicrographs of (a) Alloy 5410 (10% Ni, 19% Cr) and (b) 5419 (14% Ni, 24% Cr). Both alloys were designed to provide microstructures that would contain 10% ferrite. Etched with Murakami's reagent.

## 33. Nondestructive Test Development

W. O. Harms      R. W. McClung

This program is designed to develop new and improved methods of examining reactor materials and components. To achieve this we study the pertinent physical phenomena, develop instrumentation and other equipment, devise application techniques, and design and fabricate reference standards. Among the subjects being actively pursued are electromagnetics (with major emphasis on eddy currents), ultrasonics, and penetrating radiation.

### ELECTROMAGNETIC INSPECTION METHODS (EDDY CURRENTS)

C. V. Dodd              W. E. Deeds<sup>1</sup>  
W. A. Simpson, Jr.      J. W. Luquire<sup>1</sup>  
C. C. Cheng<sup>2</sup>

We have continued to develop new eddy-current theory, to program the equations for numerical solution on a computer, to run the programs for both general and particular cases, and to build and test inspection systems.

#### Theoretical Solutions

We have solved the following problems for various coil and conductor configurations:

1. a finite cross-section coil near a clad conducting sphere,<sup>3</sup>
2. a finite cross-section coil with three planar conductors above and three planar conductors below the coil,<sup>4</sup>
3. a finite cross-section coil with an arbitrary number of planar conductors above and below the coil,<sup>5</sup>
4. a new reciprocity theorem for defects.

#### Development of Computer Programs

We are programming the more important theoretical solutions for numerical evaluation on a computer.<sup>6</sup> In addition we have revised and expanded some of our earlier programs to make them more usable. We wrote programs to perform the following calculations:

1. impedance of a coil above three planar conductors,
2. impedance change due to a defect in one of the planar conductors,
3. phase and amplitude of the voltage induced in a reflection-type coil above three planar conductors,
4. change in the phase and amplitude of the voltage induced in a reflection-type coil due to a defect in one of the three planar conductors,
5. magnitude and phase of a test coil in an impedance bridge eddy-current instrument,
6. magnitude and phase of signals with reflection or through-transmission coils in the phase-sensitive eddy-current instrument,
7. inductance, resistance, and winding information for a coil in air.

#### Application of Computer Programs

We applied our computer programs to calculate the optimum parameters for maximum sensitivity to de-

---

<sup>1</sup>Consultant, University of Tennessee.

<sup>2</sup>Consultant, Northwestern College, Orange City, Iowa.

<sup>3</sup>J. W. Luquire, W. E. Deeds, and C. V. Dodd, "Axially Symmetric Eddy Currents in a Spherical Conductor," to be published in *Journal of Applied Physics*.

<sup>4</sup>J. W. Luquire, W. E. Deeds, and C. V. Dodd, "An Alternating Current Distribution Between Planar Conductors," to be published in *Journal of Applied Physics*.

---

<sup>5</sup>C. C. Cheng, C. V. Dodd, and W. E. Deeds, "Matrix Method for Multiplane Boundary-Value Problems," in preparation.

<sup>6</sup>J. W. Luquire, C. V. Dodd, W. E. Deeds, and W. G. Spoeri, *Computer Programs for Some Eddy Current Problems*, ORNL-TM-2501 (August 1969).

fects for a single coil above a single conducting plate, a differential coil encircling a tube, and a differential coil inside a tube.<sup>7</sup> We determined the optimum coil shape to measure conductivity for reflection coils.

### Development of Inspection Systems

We improved the range, sensitivity, and stability of the phase-sensitive eddy-current instrument. In addition we constructed a phase-shifting network to calibrate the instrument. The instrument has a short-term stability of  $\pm 0.01^\circ$ , which corresponds to an error of  $\pm 0.05\%$  in the measurement of conductivity. We have redesigned the instrument in modular form to improve its versatility.

### ULTRASONIC TEST METHODS

K. V. Cook H. L. Whaley, Jr.  
Laszlo Adler<sup>1</sup>

#### Fabrication of Reference Standards

We are continuing our electrical discharge machining to establish realistic reference discontinuities.<sup>8</sup> We added to our machining and calibration capabilities for new materials and configurations. For instance, we increased our ability to machine transverse notches as much as 7 in. inside the bore of 0.200-in.-ID tubes.<sup>9</sup> We established a method and calibration curves for machining small cylindrical discontinuities ranging from 0.004 to 0.045 in. in diameter.<sup>10</sup> In addition, we prepared and collected all the parts for a system that will allow ED machining at both elevated and reduced temperatures<sup>8</sup> to study the effect of temperature on EDM-induced microcracking in certain alloys.

#### Optical Visualization of Ultrasound

We made several improvements in the optical system to allow us to apply the schlieren technique more effectively. A method was devised for simultaneously

mounting two pulsed light sources on the optical bench, allowing us to select the better source for a given application. A long-persistence picture tube was installed in the television monitor for use with the low-repetition-rate source. We investigated a new method of blocking the zeroth-order light with overlapping Polaroid filters.

We successfully recorded (on both video tape and motion picture film) visual sequences illustrating the interaction of ultrasonic pulses with machined grooves in an Inconel plate.

### Frequency Analysis

We are continuing our use of ultrasonic frequency analysis<sup>11</sup> to study the frequency dependence of important ultrasonic inspection variables. Our current activities are directed toward increasing our ability to characterize (determine the size, shape, and orientation of) defects detected by ultrasonic testing. The basis of the approach is a spectral analysis of a broad-banded ultrasonic pulse that has interacted with the discontinuity. This technique was far superior to the usual amplitude-based technique for this purpose. The experimental approach to the problem has been a series of experiments with various types of reflectors. These experiments and results are described in detail in a paper,<sup>12</sup> with the following abstract:

We have developed a new method for the characterization (determination of the size and orientation) of a reflector by ultrasonic spectral analysis. The nondestructive testing application of this technique is the determination of the nature of flaws ultrasonically located in a material. Feasibility by this method has been shown for the characterization of a flaw in spite of its composition (i.e., crack, void, or inclusion) or shape and without the need for a calibration standard. This technique is free of several inherent limitations of amplitude-based techniques. The results are based on a series of reflection experiments using as reflectors the ends of solid rods immersed in water and machined discontinuities in metal samples. Broad-banded ultrasonic pulses are analyzed after reflection from the interface of interest. We developed a physical and analytical model based on an interference mechanism resulting from the superposition of spherical wavelets emitted from opposing extremes of the reflector. This model predicts very well the experimentally observed spectral variations in terms of size, three-dimensional angular orientation, and distance for a flat reflector located in the far field of the transducer.

<sup>7</sup>C. V. Dodd, W. E. Deeds, and W. G. Spoeri, "Optimizing Defect Detection in Eddy Current Testing," presented at the 6th International Conference on Nondestructive Testing, Hannover, Germany (June 1970).

<sup>8</sup>K. V. Cook and H. L. Whaley, *Metals and Ceramics Div. Ann. Progr. Rept. June 30, 1969*, ORNL-4470, p. 119.

<sup>9</sup>H. L. Whaley, Jr., and K. V. Cook, *Fuels and Materials Development Program Quart. Progr. Rept. Sept. 30, 1969*, ORNL-4480, p. 269.

<sup>10</sup>K. V. Cook and H. L. Whaley, *Fuels and Materials Development Program Quart. Progr. Rept. March 31, 1970*, ORNL-4560, pp. 258-59.

<sup>11</sup>H. L. Whaley and K. V. Cook, "Ultrasonic Frequency Analysis," *Mater. Evaluation* 28, 61-66 (March 1970).

<sup>12</sup>H. L. Whaley and L. Adler, "Flaw Characterization by Ultrasonic Frequency Analysis," to be presented at the 30th Annual ASNT Conference, Oct. 19-22, 1970, and to be submitted to *Materials Evaluation*.

Consideration is given to the feasibility and practicality of applying the technique in testing various materials and in automated systems.

We developed an analytical model<sup>13</sup> which accounts for the experimental results by interference considerations. The model was extended to the general case of a randomly oriented flat reflector with successful prediction of the experimental observations. A conceptual procedure was developed (and outlined in another report)<sup>14</sup> for the steps necessary to characterize a randomly oriented natural flaw in a material.

### PENETRATING RADIATION INSPECTION METHODS

B. E. Foster S. D. Snyder

#### Radiation Attenuation

During the past several years we successfully used penetrating radiation for determining the homogeneity of reactor fuels and other materials with high atomic numbers and for determining the thickness of coatings of carbon on microspheres of nuclear fuels. We have extended the use of penetrating radiation to determine the homogeneity of graphite, a material with low atomic number.<sup>15,16</sup> This study has shown that a sensitivity of about 0.5% to changes in thickness over a range from 0.1 to 6 in. or to changes in density over a range from 1.2 to 1.8 g/cm<sup>3</sup> is readily obtained.

We began experimenting with the use of a closed-circuit television system as a rapid densitometer for reading radiographs.<sup>17</sup> We observed a 5-V/step change in video signal from a standard radiographic density step wedge with step increments of 0.2 density units.

#### Radiation Scattering

Our studies have continued on the use of scattered and fluorescent radiation for measuring the thickness of coatings or claddings on reactor components.<sup>15-18</sup> Good sensitivity to changes in aluminum thickness from 0.0003 to 0.042 in. placed over a uranium substrate were obtained when we monitored the relative changes in intensity of the fluorescent x ray emitted from the

uranium energized by the 38-keV x ray emitted from our <sup>147</sup>Pm source.

### INFRARED HOLOGRAPHIC INSPECTION

W. E. Deeds<sup>1</sup> W. A. Simpson, Jr.  
R. A. Sentell<sup>19</sup>

The first real-time holograms have been obtained with infrared radiation from a single-mode, single-frequency carbon dioxide laser.<sup>20</sup> These were also the first continuous real-time holograms ever obtained and were produced in cholesteric liquid crystals. The holograms were instantaneously reconstructed with visible light from a helium-neon laser. This makes it possible, in principle, to obtain a real-time three-dimensional view of the interior of materials that are opaque to visible light but transparent to infrared. Development is being continued to increase the power and stability of the laser to permit viewing larger samples.

<sup>13</sup>H. L. Whaley and L. Adler, "Model for the Determination of the Size and Orientation of Reflectors from Ultrasonic Frequency Analysis," presented at 79th Meeting of Acoustical Society of America, Atlantic City, N.J., April 21-24, 1970.

<sup>14</sup>H. L. Whaley and L. Adler, *A New Technique for Ultrasonic Flaw Determination by Spectral Analysis*, report in preparation.

<sup>15</sup>B. E. Foster and S. D. Snyder, *Fuels and Materials Development Program Quart. Progr. Rept. Sept. 30, 1969*, ORNL-4480, pp. 270-73.

<sup>16</sup>B. E. Foster and S. D. Snyder, *Fuels and Materials Development Program Quart. Progr. Rept. Dec. 31, 1969*, ORNL-4520, pp. 313-14.

<sup>17</sup>B. E. Foster and S. D. Snyder, "Closed-Circuit Television for Radiographic Evaluation," *Fuels and Materials Development Program Quart. Progr. Rept. June 30, 1970*, ORNL-4600, in preparation.

<sup>18</sup>B. E. Foster and S. D. Snyder, *Fuels and Materials Development Program Quart. Progr. Rept. March 31, 1970*, ORNL-4560, pp. 259-60.

<sup>19</sup>Graduate student, University of Tennessee.

<sup>20</sup>W. A. Simpson and W. E. Deeds, "Real-Time Visual Reconstruction of Infrared Holograms," *Appl. Optics* 9, 499-501 (1970).

# Part V. Reactor Development Support

## 34. Aluminum Irradiation Damage

R. T. King

Aluminum is widely used as a structural and cladding material in water-cooled reactors, including the High Flux Isotope Reactor (HFIR) and the Oak Ridge Research Reactor (ORR). Earlier investigations into dimensional distortions of ORR aluminum components<sup>1</sup> and failure of the HFIR target rod aluminum cladding<sup>2</sup> identified several important irradiation-induced structural and property changes in aluminum over the service application temperature range of 50 to 200°C. Vacancies and interstitial atoms produced in displacement cascades interact to form voids and loops, which cause swelling (density changes) and strengthening of the material. Transmutation-produced silicon, helium, and hydrogen appear to strongly influence the nucleation and stability of defect clusters; our work in this area is reported in four sections of Chapter 5. In addition to these changes, the ductility of aluminum alloys is seriously reduced by neutron irradiation, as the in-reactor HFIR target rod failures and postirradiation tests demonstrate.<sup>1,3</sup>

To determine the susceptibility to irradiation damage of various aluminum alloys that are either in service or are candidates for reactor applications, several irradiation

damage experiments and investigations of reactor components are in progress. Irradiation variables under study include the temperature, neutron flux and fluence, and environment. The results presented in this chapter indicate that void formation and swelling may be controlled by proper selection of alloy composition and structure. Useful reactor structural materials should be sufficiently ductile to withstand slow creep strains as well as rapid stress changes that result from normal and abnormal changes in operating power levels.

The ductility of irradiated aluminum is sensitive to both testing temperature and deformation rate.

### IRRADIATION-INDUCED SWELLING OF ALUMINUM ALLOYS

E. L. Long, Jr.   N. H. Packan   R. T. King

Several investigations of the rate at which voids form and swelling occurs during neutron irradiation of aluminum at about 60°C have shown that variations in alloy composition and structure have a strong effect upon the postirradiation density of aluminum alloys. Typical results that support this conclusion have been obtained for annealed high-purity (99.9999%) aluminum irradiated in the HFIR hydraulic tube, the 30% cold-worked X8001 aluminum HFIR hex can (target shroud tube), the 1100 aluminum ORR  $N_f$  tray, and the 6061 aluminum HFIR target holder. (See Fig. 34.1.)

Void nucleation and growth occurred at fluences as low as  $10^{19}$  neutrons/cm<sup>2</sup> in the high-purity aluminum, and an immersion density decrease of 7% was observed after irradiation to  $1 \times 10^{22}$  neutrons/cm<sup>2</sup>.

<sup>1</sup>J. E. Cunningham, *Severe Radiation Damage to Aluminum Alloys*, ORNL-TM-2138 (March 1968).

<sup>2</sup>E. J. Manthos, R. E. Adams, R. T. King, E. L. Long, Jr., J. E. Van Cleve, Jr., and A. L. Lotts, "Postirradiation Examination of Failed HFIR Target Elements" (Summary), *Trans. Am. Nucl. Soc.* 10(2), 480-81 (November 1967).

<sup>3</sup>R. T. King, E. L. Long, Jr., J. O. Stiegler, and K. Farrell, "High-Neutron-Fluence Damage in an Aluminum Alloy," *J. Nucl. Mater.* 35, 231-43 (1970).

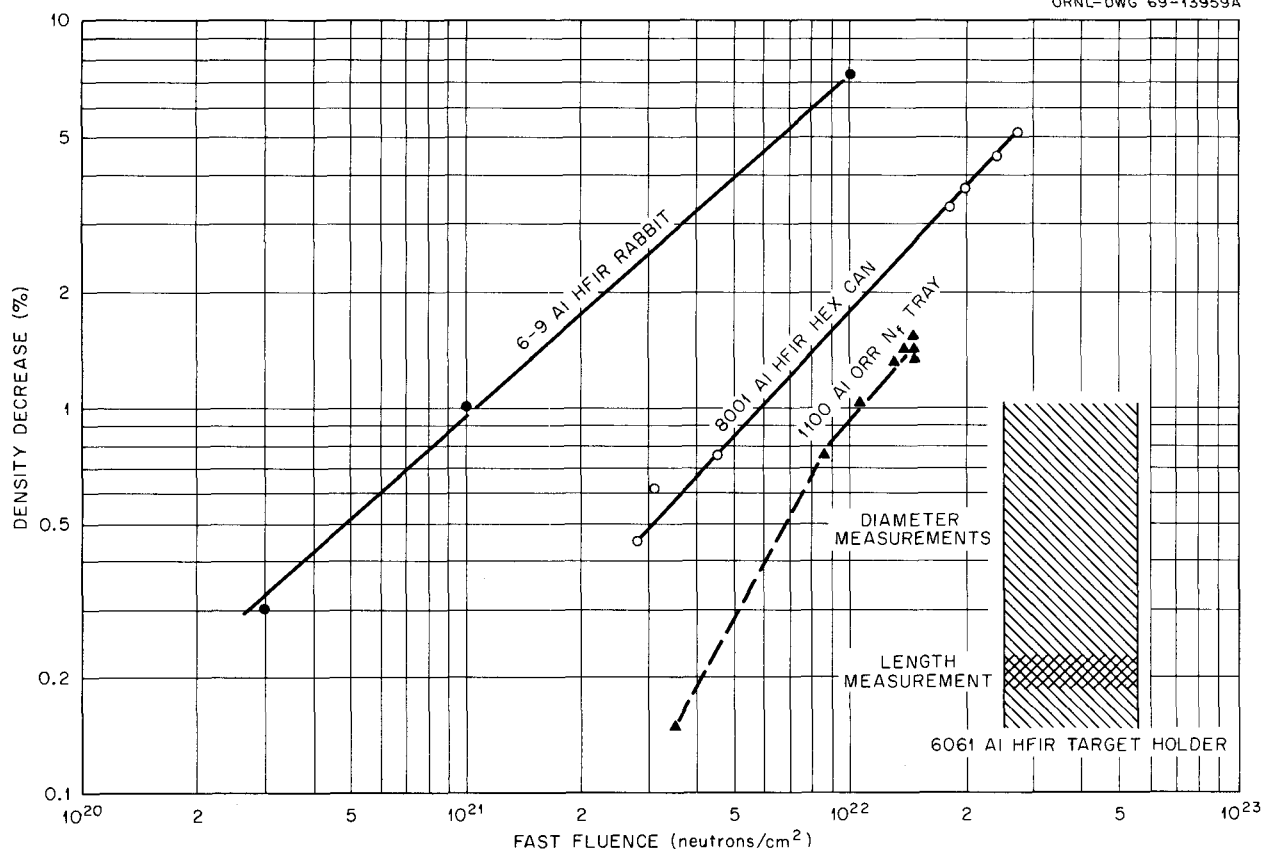


Fig. 34.1. Density Changes in Irradiated Aluminum Alloys.

In the commercially pure 1100 aluminum alloy (99% Al) and the X8001 aluminum alloy (similar to 1100 aluminum, but containing 1% Ni for corrosion resistance), the immersion density decrease at any fluence was about one tenth that in high-purity aluminum. The alloying elements in both the commercial alloys are primarily in solid solution, although some solid second phases are formed from the less soluble alloying elements.

Density changes of the 6061 aluminum HFIR target holder were calculated from measured changes in length and diameter of the component after irradiation; the uncertainties in fluence arise because of flux variations along the component, while the experimental uncertainties in the lineal measurements cause uncertainty in the calculated density change. The alloy contains a high number density of Mg<sub>2</sub>Si precipitate particles, in contrast to the relatively low density of second phase particles found in the 1100 and X8001 alloys.

Since the formation of voids is due to a complex series of interactions between irradiation-produced

vacancies, interstitial atoms, defect sinks, and impurities such as gases that affect nucleation, the differences in the swelling behavior of these alloys may have several causes. Short distances between sinks (dislocations and grain boundaries) should decrease the supersaturation of vacancies available for void nucleation and increase the competition with voids during the growth process. Both the sinks and precipitate interfaces may adsorb impurities that assist in void nucleation; this reasoning may explain the superior resistance of the 6061 alloy to void formation and swelling.

#### THE EFFECT OF HIGH FAST NEUTRON FLUENCES ON 6061 ALUMINUM

R. T. King

The 6061 aluminum HFIR target holder achieved a maximum fluence of  $5.4 \times 10^{22}$  neutrons/cm<sup>2</sup> (>0.821 MeV) at about 55°C. Since this was the most heavily irradiated aluminum available for investigation,

tensile specimens were prepared and tested over a range of temperatures (25 to 200°C) and deformation rates. Standard specimen shapes could not be prepared from this perforated cylinder, so zero-gage-length dogbone-shaped specimens whose edges were defined by the holes in the cylinder were used. (See Fig. 34.2.) Therefore, the relative ductility of specimens was determined by the crosshead separation of the testing machine before failure at separation speeds from 0.2 to 0.0002 in./min; yield strengths and ultimate tensile strengths were recorded.

The target holder was not heat treated to optimize dispersion strengthening before irradiation, but it was slightly overaged. Irradiation-induced strengthening was observed at the lower test temperatures and increased with increasing neutron fluence. At the higher test temperatures and lower deformation rates, overaging and damage recovery occurred during testing; in fact, no measurable increase in the ultimate tensile strength occurred at 200°C and 0.0002 in./min deformation rate. Under all test conditions except low strain rates and high temperatures, the ductility decreased gradually with increasing fluence. However, specimens irradiated to above  $4 \times 10^{22}$  neutrons/cm<sup>2</sup> and tested at low deformation rate at both 150 and 200°C showed a marked reduction of ductility. The mechanism responsible for this loss of ductility is not yet known.

This investigation of this irradiated HFIR component thus provided the first evidence that the ductility of irradiated aluminum is sensitive to deformation rate. Creep tests on conventionally shaped specimens are in progress to investigate this effect more thoroughly and determine which alloys are suitable for particular reactor applications.

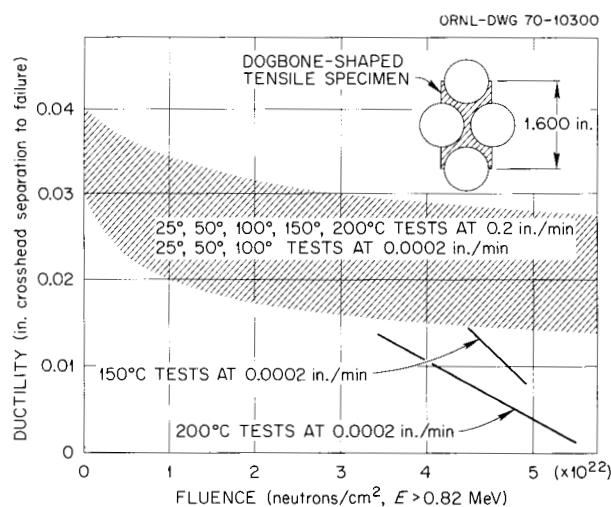


Fig. 34.2. HFIR Target Basket Dogbone Specimen Ductility.

## VOID FORMATION IN HIGH-PURITY ALUMINUM

N. H. Packan

The two most important variables influencing void formation in irradiated metals and alloys are irradiation temperature and fast neutron fluence. However, only a few controlled experiments have examined the former factor, and no published investigations have concentrated on the second. We examined voids produced in high-purity (99.9999%) aluminum irradiated at  $55 \pm 5^\circ\text{C}$  in the HFIR at fluences ranging from  $10^{17}$  to  $10^{22}$  neutrons/cm<sup>2</sup> ( $>0.82$  MeV). Void formation was observed commencing at  $10^{19}$  neutrons/cm<sup>2</sup>, and representative examples of the voids found are shown at the same magnification in Fig. 34.3.

Measurements of void concentrations and sizes were obtained by using stereographic pairs of electron micrographs to determine the foil thickness values and a Zeiss particle-size analyzer to obtain data for void size distributions; the latter results are shown in Fig. 34.4. It is evident that both the average and the maximum void sizes increased continuously as this fluence increased; the radius is proportional to the  $1/6$  power of time. This behavior is not followed in type 304 stainless steel, in which the maximum void size soon reaches a limiting value.<sup>4</sup>

Unlike the void sizes, the void number density did not increase at a constant rate with increasing neutron fluence; this indicates either a reduction in the nucleation rate of voids during irradiation or interaction of submicroscopic voids with sinks and other defects preventing voids formed late in the irradiation from growing to an observable size. Combining both size and number density data, the aggregate void volume  $\Delta V/V$  was found to obey a power law with an exponent that decreased with increasing fluence:

$$\Delta V/V \propto (\phi t)^b, \quad 0.5 < b < 2.5.$$

In a separate experiment, a specimen already irradiated to  $3 \times 10^{20}$  neutrons/cm<sup>2</sup> was annealed to remove all structural damage visible in the electron microscope and then reirradiated to the same fluence. Voids in the reirradiated material were smaller (especially in maximum size) and over twice as numerous as those produced by the original irradiation; their size distribution is shown in Fig. 34.4. These results are

<sup>4</sup>E. E. Bloom and J. O. Stiegler, *J. Nucl. Mater.* 35, 244-46 (1970).

explained qualitatively by postulating that submicroscopic remnants of the original voids (possibly tiny gas bubbles or dissolved gas atoms) survived the anneal and nucleated voids in the reirradiation. Further nuclei would have been generated during the reirradiation, and the void sizes would have therefore been restricted by increased competition for the irradiation-produced

vacancies. The experiment lends support to the recent suggestion<sup>5</sup> that impurities, especially helium, may be instrumental in causing void nucleation.

<sup>5</sup>E. E. Bloom and J. O. Stiegler, "Effect of Helium Formation on Void Formation in Irradiated Stainless Steel," to be published in *Journal of Nuclear Materials*.

PHOTO 98079

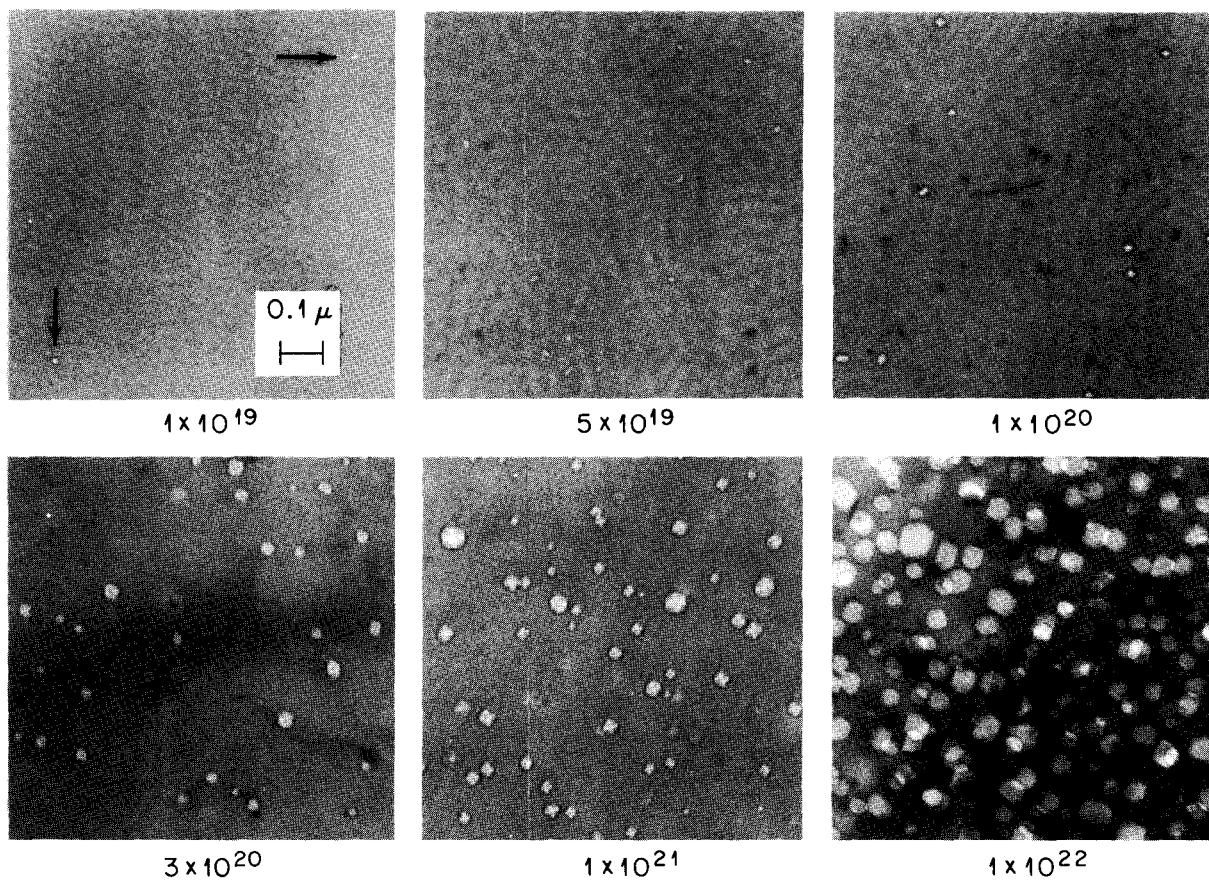


Fig. 34.3. Void Microstructure in High-Purity Aluminum Irradiated at 55°C in the HFIR to the Indicated Fluences.

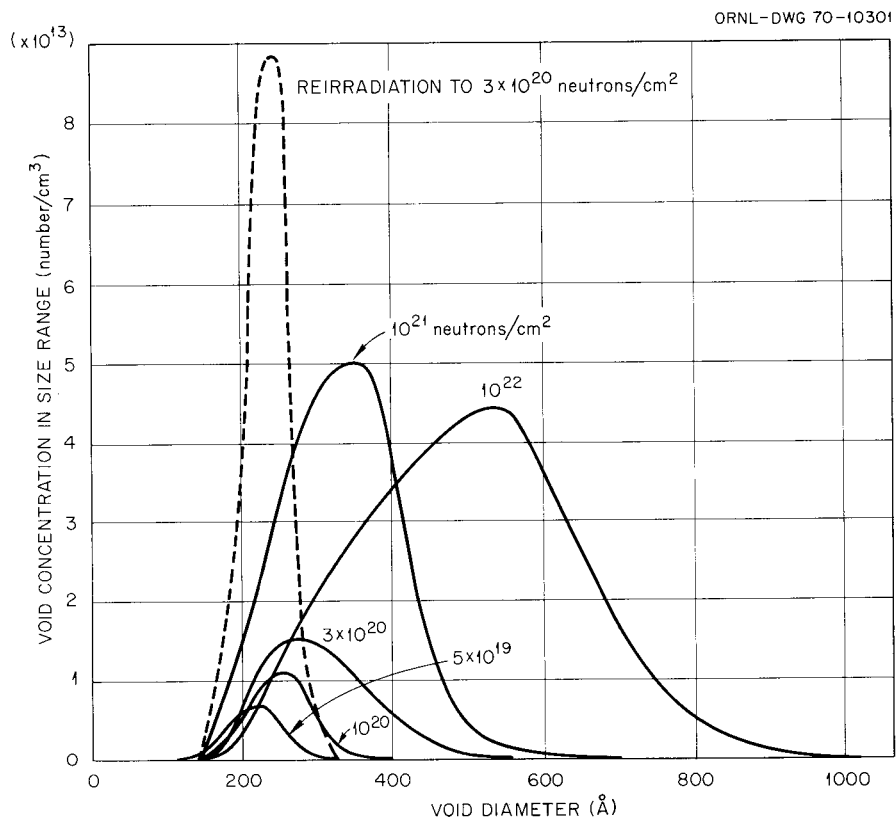


Fig. 34.4. Void Size Distribution in Irradiated High-Purity Aluminum.

## 35. Desalination

G. M. Slaughter

Metallurgical assistance for the desalination program involved exploratory investigations to determine the feasibility of various methods of fuel element fabrication for the Unclad Metal Breeder Reactor (UMBR). The UMBR has been proposed as a low-cost source of heat for seawater distillation and power generation.<sup>1</sup> The reactor consists of an unclad alloy fuel in a sodium coolant. The alloy proposed for initial use is Th-20 wt % U.

We previously surveyed the literature on thorium-uranium alloys with regard to expected irradiation performance and possible fabrication techniques.<sup>2</sup> The survey indicated that the expected irradiation performance was sufficient for the design life of the fuel element and that several techniques may be practicable for fabricating the fuel element. Our experimental work this year has been to complete studies concerning the basic feasibility of several of these fabrication techniques.

We also examined specimens of thorium and Th-20 wt % U taken from a loop operated 2000 hr at 800°F to study the compatibility of these materials with sodium in type 304 stainless steel. Our work is reported in more detail elsewhere.<sup>3</sup>

### EXPERIMENTAL FABRICATION OF Th-20% U ALLOY FOR THE UNCLAD METAL BREEDER REACTOR FUEL ELEMENT

G. L. Copeland

The reference Unclad Metal Breeder Reactor (UMBR) fuel element contains hexagonal coolant channels in a hexagonal sheath.<sup>1</sup> Our literature survey<sup>2</sup> indicated that several production techniques may be practicable for fabricating the fuel element. We have completed experiments that demonstrate the basic feasibility of (1) casting to shape, (2) casting a billet, and (3) forming from a billet component shapes of which the fuel element can be assembled.

We investment cast samples of the configuration shown in Fig. 35.1, which may be assembled to form the fuel element. Sections of stainless steel up to 10 in. long were successfully cast in air. Only the one short piece was cast of the Th-20% U alloy because of limited facilities for pouring castings in vacuum. A zircon-base investment shell mold was used and, as shown in Fig. 35.1, there was no significant reaction between the metal and the mold. The mold was cold in this experiment; reaction may be a problem if preheated molds are used to obtain better flow. The microstructure is essentially the same as that previously observed<sup>4</sup> after casting in water-cooled copper molds.

We cast the 4.5-kg Th-20% U billet shown in Fig. 35.2 by double consumable electrode arc-melting. Thorium and uranium electrodes were simultaneously melted into a water-cooled copper mold. This ingot was then hot extruded to produce a 4:1 reduction in area, and the extrusion was used as the electrode for a second melting. The structure is uniform across the billet.

A 1-in.-thick slab of the 4.5-kg billet was hot rolled, hot forged, and then cold rolled to 0.054-in.-thick sheet. Pieces of this sheet were then cold formed into halves of hexagonal tubes. No problems were encountered in rolling or forming. The microstructure consists of very fine stringers of the uranium phase and oxide particles in a thorium-rich matrix. The steps that would be involved in producing fuel elements by this technique are illustrated in Fig. 35.3.

<sup>1</sup>R. P. Hammond *et al.*, *Unclad-Metal Breeder Reactor (UMBR) for Desalting or Power*, ORNL-4202 (January 1969).

<sup>2</sup>G. L. Copeland, *Evaluation of Thorium-Uranium Alloys for the Unclad Metal Breeder Reactor*, ORNL-4557 (June 1970).

<sup>3</sup>R. P. Hammond *et al.*, *Nuclear Desalination Annual Progress Report on Activities Sponsored by the Atomic Energy Commission for Period Ending October 31, 1969*, ORNL-4538, pp. 16-19.

<sup>4</sup>G. L. Copeland, *Metals and Ceramics Div. Ann. Progr. Rept. June 30, 1969*, ORNL-4470, pp. 145-46.

PHOTO 100406

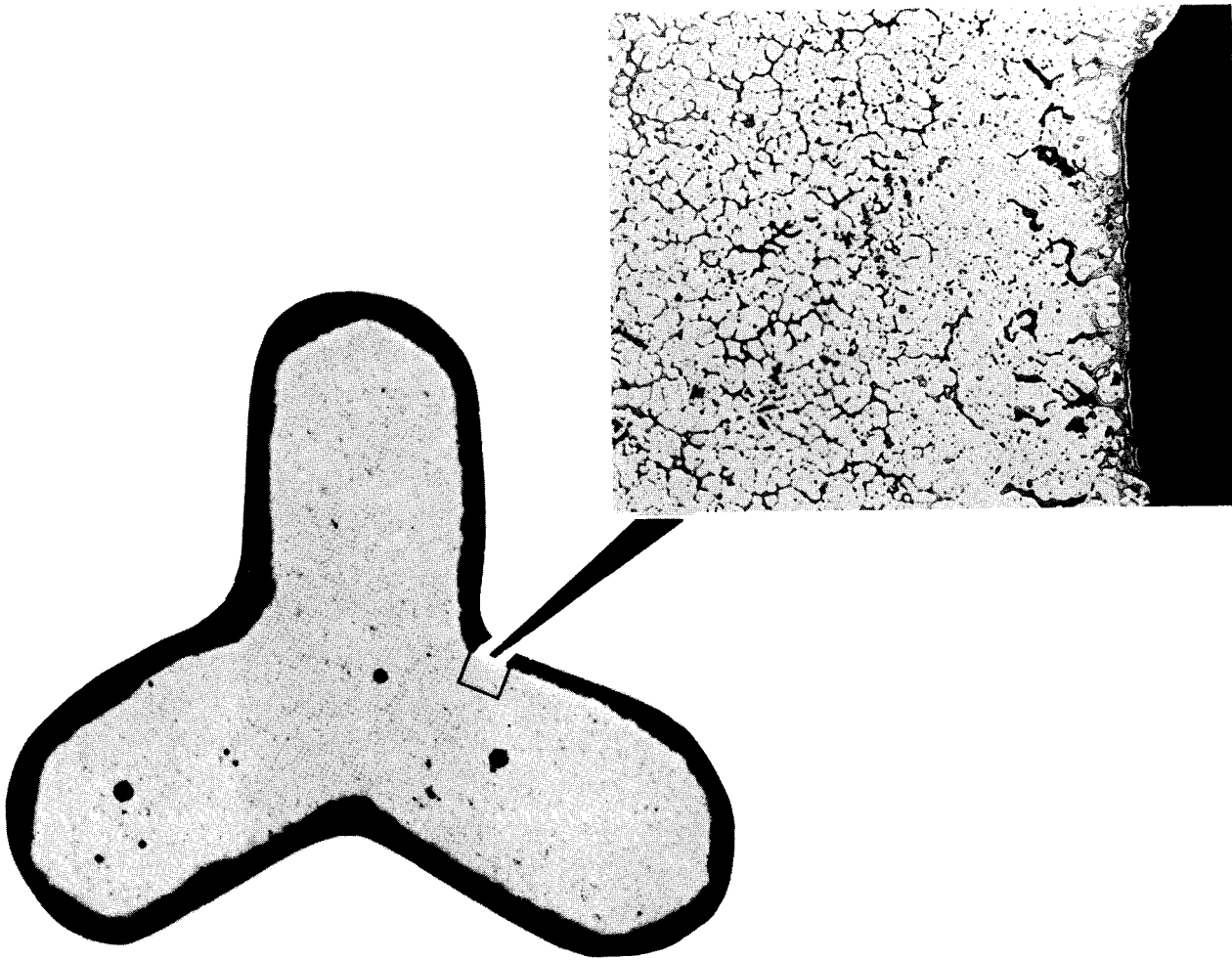


Fig. 35.1. Cross-Section of an Investment Cast Th-20 wt % U Component of Reference Design UMBR Fuel Element. Left: entire section, 13X. Right: microstructure of indicated region, 200X. Reduced 23.5%.

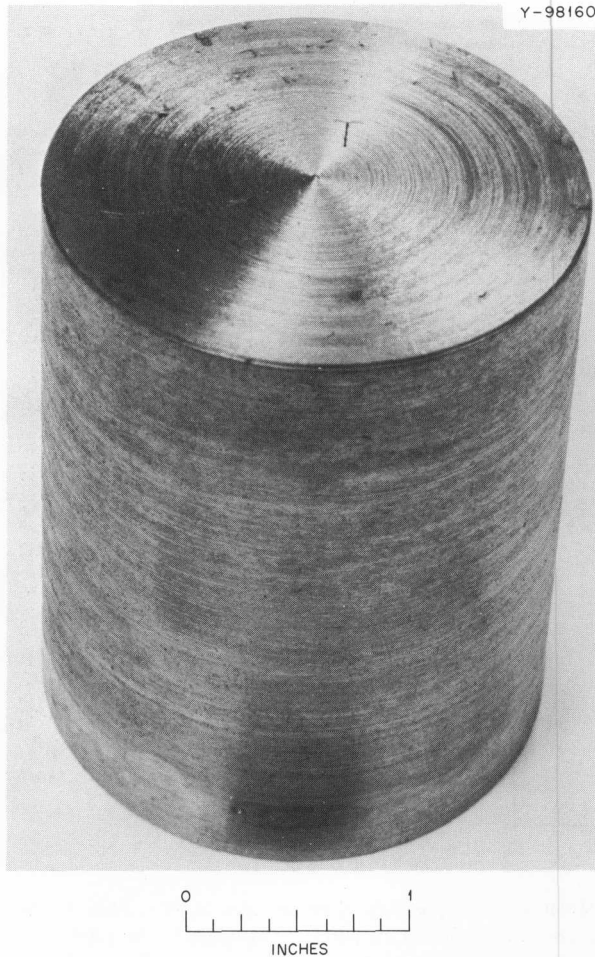


Fig. 35.2. A 4.5-kg Th-20 wt % U Billet Made by Double Consumable Electrode Arc Melting.

We are compiling a report discussing the overall feasibility of each method of fuel element manufacture. The most attractive method for economical production of fuel elements for the UMBR now appears to consist

of some combination of rolling and forming component pieces from an ingot. The ingot may be produced by consumable electrode arc-melting or possibly from alloyed or elemental powders by compaction and extrusion.

## CORROSION STUDIES

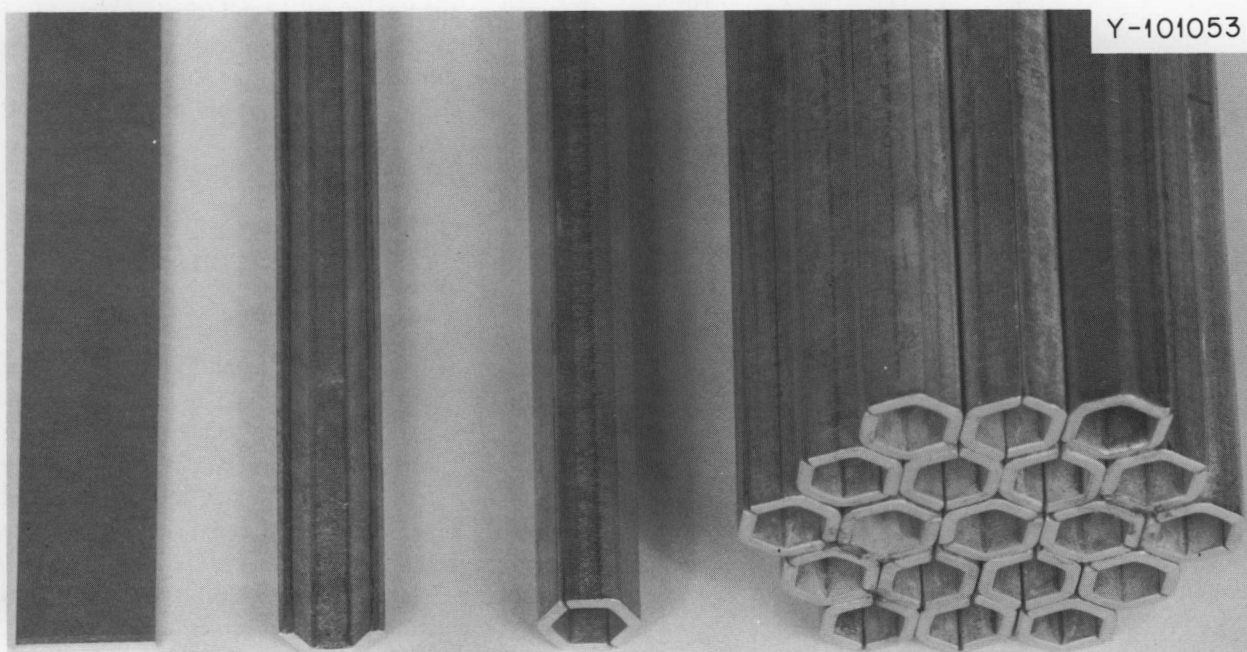
B. Fleischer

We examined specimens of Th and Th-20 wt % U for compatibility with sodium at 425°C (800°F). Specimens were exposed 500, 1000, and 2000 hr in a test loop operated to determine this compatibility in a type 304 stainless steel system. Sodium velocity past the specimens was 15 fps and the oxygen level in the sodium remained below 10 ppm.

Examination revealed no physical evidence of corrosion. The reaction product film was less than 0.1 mil. The weight gains accounted for by interstitial element changes exceeded the net weight gain of the specimens, thus indicating some very small metal loss. This was substantiated by electron microprobe analysis, which showed a slight increase of uranium at the surface of the thorium specimens. There was no apparent time effect, nor was there any notable difference between the two types of specimen. The average weight change for 2000 hr was less than 0.1 mg/cm<sup>2</sup>.

Metallographic examinations were made on test specimens exposed 500 and 2000 hr and on specimens representing before-test material and specimens exposed to simulated cleaning operations. The examination showed that a thin (<0.1 mil) reaction product layer had formed on the exposed specimens. (Again there was no detectable difference between the 500- and 2000-hr specimens.) The examination showed that there had been no intergranular corrosion.

Y-101053



A

B

C

D



INCHES

**Fig. 35.3. Typical Steps Involved in Producing Fuel Elements by Metalworking Operations from an Alloy Ingot or Slab. A, plate rolled to final thickness and trimmed. B, cold formed tube half. C, tube from two halves. D, fuel element assembled from tubes.**

## 36. Gas-Cooled Reactor Program

J. H. Coobs    J. L. Scott

Our materials effort in support of the Gas-Cooled Reactor Program is directed primarily toward the development of unclad ceramic fuel elements for high-temperature gas-cooled converter reactors (HTGR's) such as the Fort St. Vrain Reactor being constructed by Gulf General Atomic for Public Services Corporation of Colorado. The reference fuel elements consist of hexagonal graphite blocks containing coated (Th,U)O<sub>2</sub> or (Th,U)C<sub>2</sub> microspheres and are designed to retain most of the fission-product activity within the fuel element to simplify maintenance.

Our program consists principally of developing techniques for bonding coated particles into fuel elements and preparing, characterizing, and irradiation testing pyrolytic carbon coatings, coated particles, and simulated bonded fuel elements. A new phase of the program concerns the preparation and testing of coated fuel particles derived from ion-exchange resin particles. Irradiation testing is now done principally in HFIR target and reflector positions, but a few tests have been run in the Dounreay Fast Reactor (DFR). Bonded-bed specimens have been irradiated to fast-neutron exposures approaching the peak HTGR fluence of  $8 \times 10^{21}$  neutrons/cm<sup>2</sup> (>0.18 MeV), and coating materials have been tested at twice this exposure. Temperatures have spanned the range experienced in an HTGR, 600 to 1250°C.

A significant part of our program now involves participation with Gulf General Atomic in a cooperative effort to develop fuel elements for a Gas-Cooled Fast Breeder Reactor (GCFR). We are examining the compatibility problems between (U,Pu)O<sub>2</sub> fuel and metal cladding at the high temperatures (650 to 800°C) proposed for GCFR's. We are also participating in the examination and interpretation of irradiation experiments on sealed fuel pins, and we prepared the fuel and fuel pins for a set of eight pins to be tested in EBR-II and for a new experiment in the ORR to test the manifolded-vented fuel pin concept.

### COATED PARTICLES FROM ION EXCHANGE RESINS

J. L. Scott    J. M. Leitnaker    C. B. Pollock

We are loading ion exchange resins with heavy metal ions such as UO<sub>2</sub><sup>2+</sup> or Th<sup>4+</sup> by exposure to aqueous nitrate solutions of the heavy metal for a predetermined time. The metal-loaded ion exchange resin may then be carbonized at low temperature to form a fueled microsphere consisting of metal oxide or oxysulfide dispersed in a carbon matrix.

Advantages of the process are several. First of all, the raw material is cheap (about \$40/ft<sup>3</sup>). Furthermore, many processing steps could be achieved before loading. For example, the resin could be sized by screening and checked for shape uniformity before any processing other than simple drying. Quality control could be excellent, and the finished product would be uniform in size, shape, and metal distribution.

#### Fuel Loading

Cation exchange resins are loaded with fissile or fertile materials by contacting them with solutions of uranyl nitrate or thorium nitrate. Both strong and weak acid resins have been used successfully, and the resin loading procedure is well known.<sup>1</sup> Concentrations of uranium within the resins can be controlled by two methods: (1) heavy metal concentration, or (2) acid concentration of the contacting solution. Strelow *et al.*<sup>2</sup> have prepared an extensive table of conditions for loading resins.

<sup>1</sup> See, for example, *Duolite Ion-Exchange Manual*, Chemical Process Co., Redwood City, Calif., 1960.

<sup>2</sup> F. W. E. Strelow, Ruthild Rethemeyer, and C. J. C. Bothma, "Ion Exchange Selectivity Scales for Cations in Nitric Acid and Sulfuric Acid Media with a Sulfonated Polystyrene Resin," *Anal. Chem.* 37, 106-11 (1965).

We performed exploratory experiments on both weak- and strong-acid resins. Weak-acid resins from two manufacturers and strong-acid resins with three different degrees of cross linkage made by a single manufacturer were tested. Other factors varied were the concentrations of both uranium and acid as well as the time and temperature of contact between resins and solutions. We determined the heavy metal content of the resins by weighing dried samples or analyzing carbonized samples. We obtained widely different loadings on weak-acid resins, varying from 70 wt % U in the carbonized sphere from Amberlite IRC-50 down to about 30 wt % U from C-275 resin (Ionac Chemical Corporation). Uranium absorption in strong-acid resin spheres could be increased from 4 mg/g of dry resin to about 7.5 mg/g by increasing the concentration of uranium in solutions. In these experiments acid concentrations up to 2.7 M had little effect on uranium absorption, but higher concentrations of acid (>4 M) reduced the uranium loadings markedly.

#### Carbonization and Coating

Ion exchange resins and other organic materials that form highly cross-linked structures can be carbonized at low temperatures to form a hard glossy carbon that is nongraphitizable.<sup>3-6</sup> We determined that ion exchange resins loaded with uranium can be carbonized in the same manner. The carbonization process releases a number of gaseous by-products such as water, SO<sub>2</sub>, H<sub>2</sub>SO<sub>3</sub>, H<sub>2</sub>, and CH<sub>4</sub>, and to accommodate these volatiles the heating rate is critical (<200°C/hr initially). We have been carbonizing sulfonic and carboxylic resins that have been loaded with uranium in order to produce an oxide fuel that is contained in a carbon matrix. The fuel can be in the form of an oxide or an oxysulfide, depending upon the type of resin used. The carbon matrix provides a strong, hard kernel with 20 to 50% closed porosity.

The carbonized fuel particles are coated with conventional low-temperature high-density isotropic pyrolytic carbon coatings to prepare them for use as HTGR fuel. Fuel particles prepared and coated as described above were irradiated in the HFIR to fast-neutron (>0.18

MeV) doses of about  $8 \times 10^{21}$  neutrons/cm<sup>2</sup> at design temperatures of 750 and 1050°C and achieved maximum calculated burnup of 8 at. % of heavy metal. One sample that had a high-density two-layer carbon coating survived, while samples with monolayer coatings had high rates of failure. The surviving sample is being examined metallographically.

#### DENSITY AND DIMENSIONAL CHANGES IN METHANE- AND PROPYLENE-DERIVED PYROLYTIC CARBONS IRRADIATED TO $2 \times 10^{22}$ NEUTRONS/cm<sup>2</sup> AT 715°C (REF. 7)

D. M. Hewette II

We irradiated several pyrolytic carbon structures, which had been derived from either methane or propylene in a fluidized bed, to fast-neutron fluences as high as  $2 \times 10^{22}$  neutrons/cm<sup>2</sup> (>50 keV) at 715°C. Almost all the methane-derived coatings first densified and then swelled appreciably, as shown in Fig. 36.1(a). In contrast, propylene-derived coatings demonstrated a high degree of stability with (little or no) swelling, as seen in Fig. 36.1(b). Only very small dimensional changes occurred with the propylene-derived coatings; on the other hand, isotropic methane-derived samples exhibited appreciable dilations, as shown in Fig. 36.2. These results show that under fast-neutron irradiation propylene-derived coatings are exceptionally stable and that methane-derived coatings are significantly less so. This stability plus the economic advantages of depositing propylene-derived coatings at lower temperatures and higher deposition rates makes them quite attractive for use in coated-particle fuels for HTGR's.

#### COATED-PARTICLE BONDING DEVELOPMENT FOR HTGR FUELS

J M Robbins

Our goal in the development of bonded coated-particle beds is to furnish techniques for the fabrication of fuel sticks for high-temperature gas-cooled converter reactors such as the Fort St. Vrain Reactor being constructed by Gulf General Atomic for Public Services Corporation of Colorado. Our program consists principally of developing techniques for bonding coated particles into fuel elements and preparing and characterizing bonded specimens for irradiation testing.

<sup>3</sup>R. E. Franklin, *Proc. Roy. Soc. (London) Ser. A* **209**, 196 (1951).

<sup>4</sup>F. H. Winslow *et al.*, *J. Polymer Sci.* **16**, 101 (1955).

<sup>5</sup>J. A. Coffman *et al.*, *Carbonization of Plastics and Refractory Material Research*, WADD-TR-60-646 (Pt. II) (AD-297946) (August 1961).

<sup>6</sup>R. O. Grisdale, *J. Appl. Phys.* **24**, 1082 (1953).

<sup>7</sup>Abstract of paper presented at Annual Meeting of American Ceramic Society, Philadelphia, May 4-7, 1970.

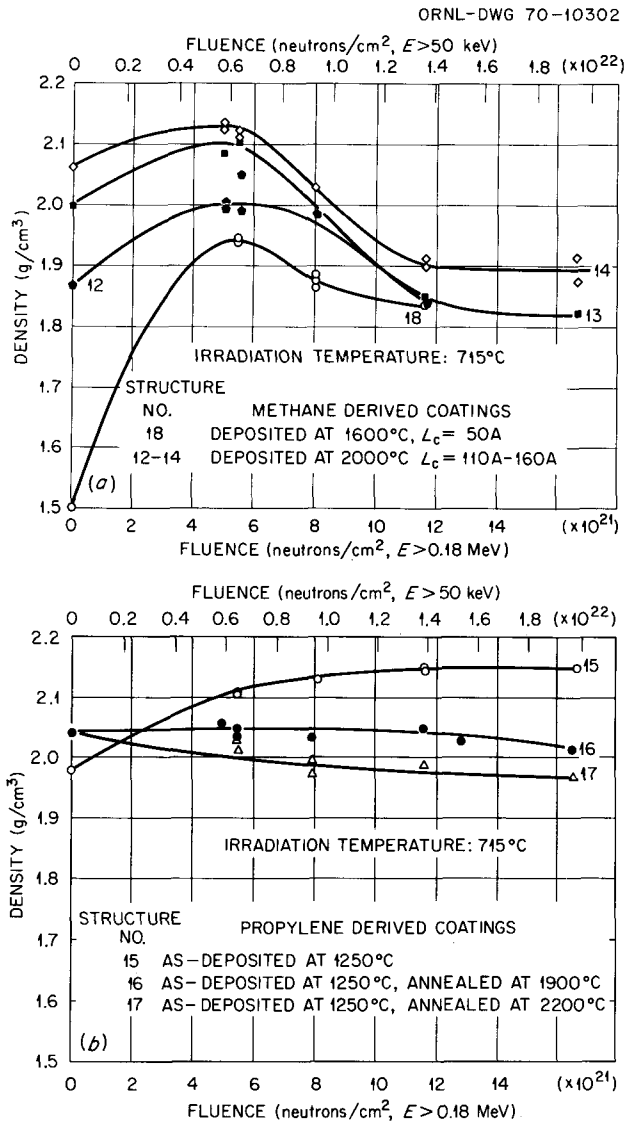


Fig. 36.1. Densification of Pyrolytic Carbon Coatings Induced by Fast Neutrons. (a) Methane-derived coatings. (b) Propylene-derived coatings.

Because of the relative ease of fabrication, most bonded beds have been prepared with thermosetting binders. However, a thermoplastic binder that yields a graphitizable carbon would, perhaps, result in a more irradiation-resistant matrix. Therefore, we developed techniques for fabricating fuel sticks by hot injection bonding using coal tar pitch<sup>8</sup> as the binder. Specimens that contained large amounts of filler material in pitch

<sup>8</sup>Grade 15V pitch from Allied Chemical Co.

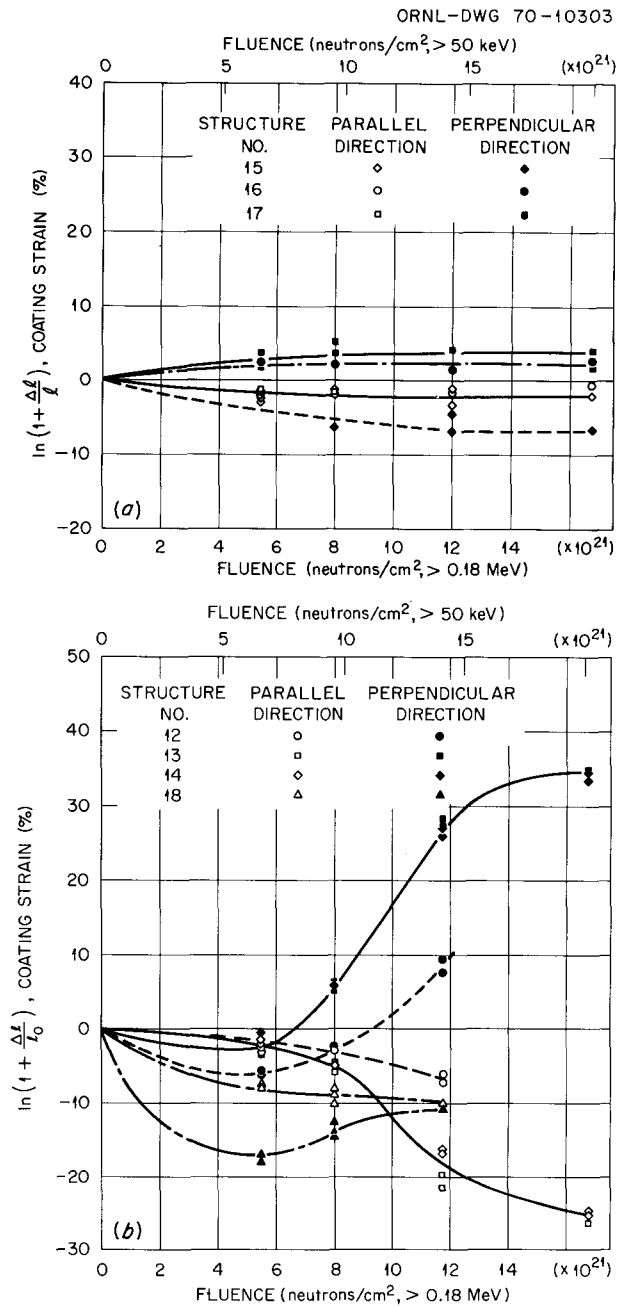


Fig. 36.2. Effect of Fast Neutron Exposure at 715°C on Dimensional Changes in Pyrolytic Carbon Coatings. (a) Propylene-derived coatings. (b) Methane-derived coatings.

or furfuryl alcohol binders all survived irradiation to the full fast neutron exposure anticipated for HTGR's, as explained in the following section of this chapter.

This and other successful irradiation experience on fuel sticks led to the adoption of bonded fuel as the

reference for large HTGR'S. As a result, bonded fuel sticks were specified for a large part of the fuel to be tested in the Recycle Test Elements (RTE's) in the Peach Bottom Reactor. For these eight test elements, ORNL was requested to prepare fuel sticks consisting of blends of fissile, recycle, or fertile particles. About 200 stacks 12.8 in. long  $\times$   $0.490 \pm 0.002$  in. in diameter were needed. Several experiments established that a mixture of 40 wt % Poco graphite in either pitch or furfuryl alcohol could be injected at least 2 in. into a bed of particles of uniform size. We therefore specified a fuel stick length of 2.14 in., which meant that about 1200 individual fuel sticks would be required for the program. The specifications for the RTE fuel permitted either pitch or Varcum (furfuryl alcohol) as binder, but in preproduction runs we observed unacceptable variations in the diameter of Varcum-bonded sticks but acceptable size control and uniformity of pitch-bonded sticks. Therefore, all RTE fuel sticks were prepared with 15V pitch as the binder.

Two problems that were encountered and solved during early production runs concerned bonding material composition and particle blending. One of the four types of fuel sticks consists of a blend of small fissile particles nominally  $400 \mu\text{m}$  in diameter and large fertile ( $\text{ThO}_2$ ) particles with diameters ranging from 600 to  $1000 \mu\text{m}$ . Whereas the particle volume loading in fuel sticks using particles of one nominal size is about 62 to 65 vol %, with this blend we obtained volume loadings as high as 70 vol %. We could not inject the binder containing 40 wt % Poco graphite flour through such a dense bed of particles, but a binder containing 35 wt % of the graphite flour could be used and was adopted as the standard for the RTE's.

The large difference in size and density of the two types of particles in this same type of fuel stick gave rise to a severe blending problem, which was solved by loading the molds by coincident feeding from vibrating trays through a two-funnel blending system. With these techniques and this bonding material composition, the required fuel sticks were produced and delivered to Gulf General Atomic for loading into the RTE's. These elements are described further in Chapter 41.

We started to study alternate grades of graphite for use as filler materials in the binder. The fuel sticks for the RTE's as well as those that survived in the earlier irradiation experiments were prepared with an expensive special graphite (Poco) in the pitch binder, whereas certain inexpensive commercial grades of graphite flour may be acceptable. We investigated the fabrication techniques and properties of materials such as Robinson, JOZ, Santa Maria, and natural flake graphites

**Table 36.1. Binder Formulations Developed for Experimental Pitch-Bonded Specimens Being Tested in RTE Spine Sampler**

Filler Material	Concentration (wt %)	Maximum Particle Size ( $\mu\text{m}$ )
Poco <sup>a</sup>	35	27
Thermax <sup>b</sup>	50	
Santa Maria <sup>c</sup>	40	40
Robinson <sup>d</sup>	40	27
JOZ <sup>e</sup>	35	40
Asbury <sup>f</sup>	35	40

<sup>a</sup>An isotropic graphite flour from Poco Graphite, Inc.

<sup>b</sup>A soft, submicron size, spherical carbon black from R. T. Vanderbilt Co.

<sup>c</sup>Graphite flour from Collier Carbon and Chemical Co.

<sup>d</sup>An air-blown graphite flour from Carbon Products Division, Union Carbide Corp.

<sup>e</sup>Graphite flour from Great Lakes Carbon Corp.

<sup>f</sup>Natural flake graphite from Asbury Graphite, Inc.

and Thermax carbon black, all mixed with grade 15V pitch. The compositions shown in Table 36.1 were used to bond special spine samples for irradiation testing in the RTE's. These and similar compositions are being used to prepare specimens for irradiation testing in the HFIR facilities.

#### DEVELOPMENT OF BONDED COATED-PARTICLE BEDS FOR HTGR FUEL ELEMENTS<sup>9</sup>

J. L. Scott      J. M. Robbins  
J. H. Coobs     D. M. Hewette II

Fuel elements proposed for advanced HTGR's consist of hexagonal blocks of graphite with parallel fuel and coolant channels. The fuel channels are loaded with pyrolytic-carbon-coated particles of fuel and fertile materials. We developed and demonstrated a method of bonding the coated particles into "fuel sticks" that will keep the fuel bed from falling apart during handling or during accidents that might damage the graphite core blocks. The bonded fuel sticks also facilitate inspection of the fuel loading and enhance the transfer of heat from the fuel to the coolant.

Several problems were overcome in developing a satisfactory binder. When a bed of particles was

<sup>9</sup>Abstract of paper presented at Gas-Cooled Reactor Information Meeting, ORNL, April 27-30, 1970, and to be published in the proceedings, CONF-700401.

impregnated with phenolic resin binder and then heated to carbonize the resin, shrinkage broke coatings on some particles. Modified coatings that survived carbonization produced weak fuel sticks that disintegrated during irradiation to HTGR fast-neutron fluences.<sup>10</sup> By using high concentrations of filler material in the binder (40 wt % Poco graphite powder in pitch or 29 wt % Poco graphite plus 29% Thermax carbon black in either pitch or resin)<sup>11</sup> we produced fuel sticks that remained intact throughout irradiation to a fast-neutron ( $>0.18$  MeV) fluence of  $7.5 \times 10^{21}$  neutrons/cm<sup>2</sup> at 1060°C. Several fuel stick specimens after irradiation are shown in Fig. 36.3, and polished sections of irradiated and unirradiated specimens bonded with pitch containing 29 wt % Poco graphite and 29 wt % Thermax are illustrated in Fig. 36.4. Only one damaged coating was found among 2000 particles examined in irradiated sticks prepared with these binders.

#### GAS-COOLED FAST BREEDER REACTOR FUEL ELEMENT DEVELOPMENT

C. M. Cox    R. B. Fitts    A. L. Lotts

Most of the effort to develop a fast breeder reactor is being applied to the sodium-cooled LMFBR concepts. There is, however, much interest in the development of the gas-cooled fast breeder reactor (GCBR) as an alternate. It has the potential of lower cost power

production and would avoid the sodium void coefficient problem and maintenance difficulties that are peculiar to liquid-metal-cooled systems.<sup>12</sup>

Our GCBR fuel element development work is done on two closely related but separate programs. One is a cooperative program with Gulf General Atomic in which several GGA fuel rod design concepts have been irradiation tested by ORNL. The other is an independent fuel element development effort. This work is closely coordinated with the GGA GCFR Core Development Program and with the GCBR core design and safety studies under way at ORNL.

The initiation of the ORNL program for the development of a fuel pin for the GCBR was described in the last report in this series.<sup>13</sup> Because of a severely curtailed funding level, work in this area has been combined with the cooperative program described below.

<sup>10</sup>S. C. Weaver, *Metals and Ceramics Div. Ann. Progr. Rept. June 30, 1969*, ORNL-4470, pp. 149–50.

<sup>11</sup>J. M. Robbins, *Metals and Ceramics Div. Ann. Progr. Rept. June 30, 1969*, ORNL-4470, pp. 148–49.

<sup>12</sup>*An Evaluation of Alternate Coolant Fast Breeder Reactors*, WASH-1090 (April 1969).

<sup>13</sup>R. B. Fitts, E. L. Long, Jr., and A. W. Longest, *Metals and Ceramics Div. Ann. Progr. Rept. June 30, 1969*, ORNL-4470, pp. 157–59.

R-50105A

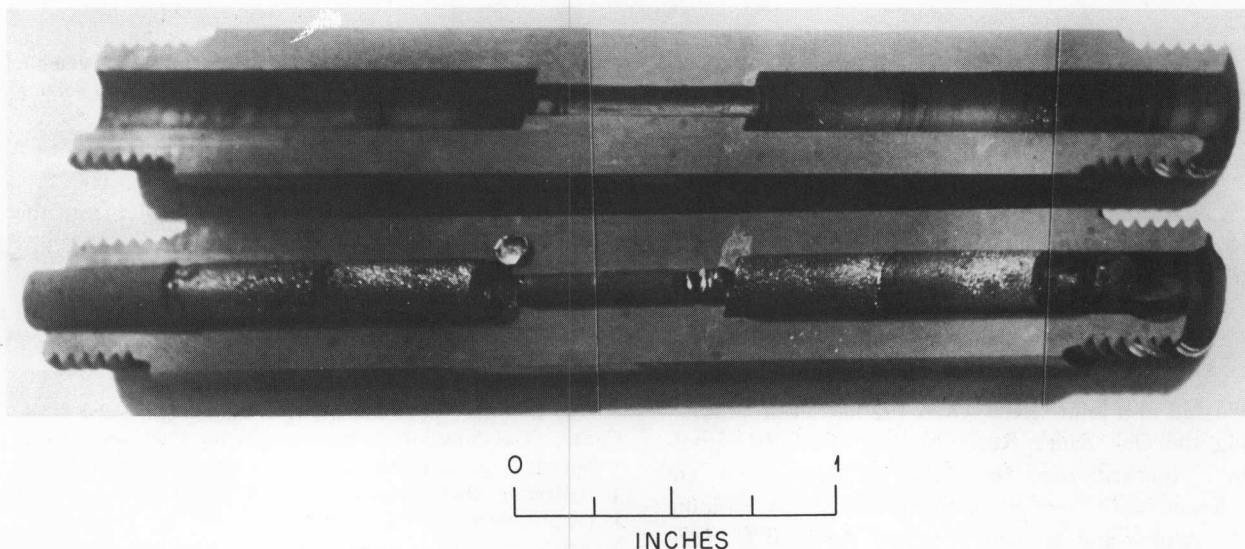


Fig. 36.3. Appearance of Bonded Beds of Coated Particles After Irradiation to  $6 \times 10^{21}$  neutrons/cm<sup>2</sup> at 800°C.

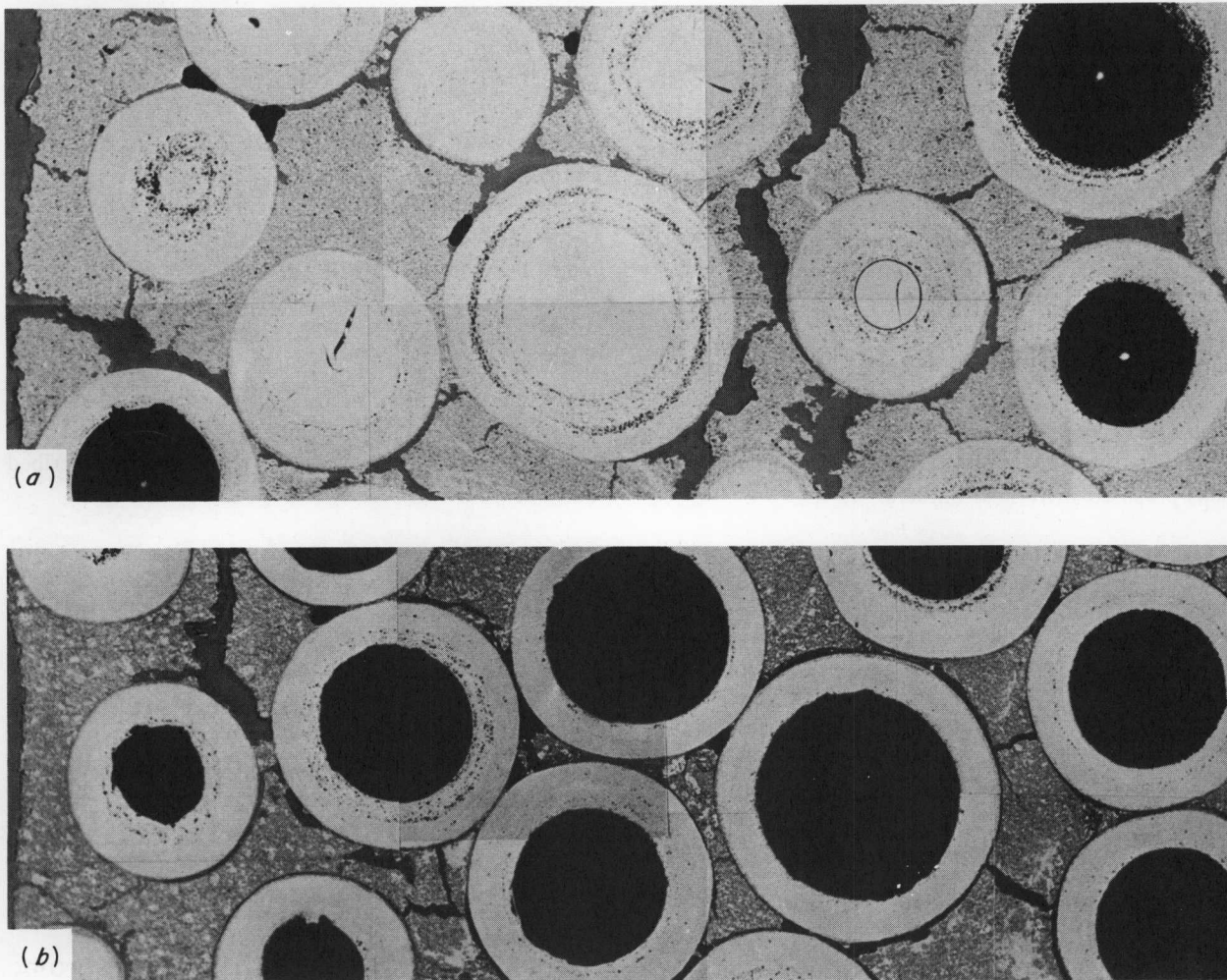


Fig. 36.4. Microstructures of Bonded Beds with Pitch Binder Tested in HFIR. The filler consists of 29 wt % Poco AXM graphite flour and 29 wt % Thermax carbon black. The particles are 220- $\mu\text{m}$ -diam carbon microspheres with a 75- $\mu\text{m}$ -thick monolayer coating. (a) Unirradiated, and (b) irradiated at 1050°C to  $8 \times 10^{21}$  neutrons/cm<sup>2</sup>. As polished, 100X. Reduced 13.5%.

#### Cooperative Irradiation Test Capsules

R. B. Fitts      A. W. Longest<sup>14</sup>  
 E. L. Long, Jr.    J. D. Sease  
 T. N. Washburn

Various fuel pin designs for use in GCBR's are being evaluated in a joint ORNL-GGA irradiation program<sup>15</sup> using the Oak Ridge Research Reactor (ORR) pool-side<sup>16</sup> thermal flux test facility. These tests are concerned with fuel pin performance at the cladding temperatures and coolant pressures that will be associated with the GCBR environment. Two basic design approaches being evaluated are (1) a sealed fuel pin and

(2) a manifolded-vented fuel pin. The results from the irradiation of the first 16 fuel pins in this series, all of which were of the sealed pin design, have been

<sup>14</sup>Reactor Division.

<sup>15</sup>R. B. Fitts, E. L. Long, Jr., J. R. Lindgren, and D. R. Cuneo, "Gas-Cooled Fast Breeder Reactor Fuel-Element Development," paper presented at Gas-Cooled Reactor Information Meeting, ORNL, April 27-30, 1970, and to be published in the proceedings, CONF-700401.

<sup>16</sup>D. B. Trauger, *Some Major Fuel Irradiation Test Facilities of the Oak Ridge National Laboratory*, ORNL-3574 (April 1964).

reported<sup>17</sup> and were summarized in the last annual report.<sup>13</sup> During the past year the operation and examination of the capsule containing the next three sealed fuel pins were successfully completed, a manifolded-vented fuel pin test was initiated in the ORR, and a set of eight GCBR-type fuel pins was fabricated and delivered to the EBR-II for fast flux irradiation testing.

Fuel fabrication for these experiments is reported in Chapter 15. The following sections give further information on the irradiation.

### Experiments in the Oak Ridge Research Reactor

R. B. Fitts E. L. Long, Jr. A. W. Longest<sup>14</sup>

The fuel pin design and operating conditions for the last sealed pin capsule, O4-P8, are given in Table 36.2. The fuel pins were immersed along with thermocouples in a NaK bath that was held under 1000 psi pressure. The wall thickness of the cladding was varied to provide comparable resistance to creep deformation for the two materials. Two variations of the design were employed — the upper two pins were fabricated with an initial internal pressure of 1 atm at room temperature, and the lower pin was prepressurized to about 17 atm. The internal volumes were adjusted to provide the same end-of-life internal pressure.

The fuel pins operated to their full design burnup. No fuel-cladding mechanical interactions were observed. The chemical reaction between fuel and cladding resulted in a uniform 0.001-in.-thick layer, Fig. 36.5,

which produced no measurable reduction in cladding thickness. A slight amount of ovality (<1% diameter change) developed in the middle fuel pin. These results indicate that these fuel pins had a cladding thickness close to the optimum, verifying the design approach,<sup>18</sup> in which the results of previous tests are combined with creep properties. We believe that these tests have demonstrated that the sealed fuel pin design is a viable approach, lacking only testing in a fast flux to assess the influence of fast neutron damage on the cladding stability of the pin under high external pressure.<sup>19</sup>

Because of its potential for successful operation at higher cladding temperatures, and because of its greater similarity with LMFBR technology, the manifolded-vented design has been chosen as the reference for the GCBR, and the fuel-cladding-interacting design was relegated to backup status. The first irradiation test of an instrumented (U,Pu)O<sub>2</sub> fueled manifolded pin was started in the ORR in March 1970 toward a burnup goal of greater than 50 GWd/metric ton at a linear heat generation rate of 525 W/cm. The cladding outer surface temperature is 700°C; the pressure outside the fuel cladding is 1000 psi, while the internal pressure is 25 psi higher.

The design of the fuel pin and capsule is shown in Fig. 36.6. The fuel pin is a shortened version of a GCBR manifolded fuel pin and has a 10-in. fuel column, UO<sub>2</sub> blanket pellets at the ends of the fuel column, and an internal charcoal trap. The charcoal trap is maintained at 300°C to simulate the GCBR coolant inlet tempera-

<sup>17</sup>E. L. Long, Jr. *et al.*, "Irradiation Testing of Fuel Rods Containing UO<sub>2</sub> and (U,Pu)O<sub>2</sub> for GCFR," pp. 179–84 in *Ceramic Nuclear Fuels, Proceedings of the International Symposium, Spec. Publ. 2*, ed. by O. L. Kruger and A. I. Kaznoff, American Ceramic Society, Columbus, Ohio, 1969.

<sup>18</sup>Gulf General Atomic, Inc., *Gas-Cooled Fast Breeder Reactor, Annual Progr. Rept. July 31, 1967*, GA-8107 (July 25, 1968).

<sup>19</sup>R. B. Fitts, E. L. Long, Jr., D. R. Cuneo, and J. R. Lindgren, "Performance of Three Sealed (U,Pu)O<sub>2</sub> GCFR Fuel Pins," *Trans. Am. Nucl. Soc.* 13(1), 34–35 (1970).

Table 36.2. Description of Fuel Pins<sup>a</sup>

Pin	Cladding			Initial Design Internal Pressure <sup>b</sup> (psia)	Heat Generation (W/cm)	Burnup (% FIMA) <sup>c</sup>	Cladding Outside Temperature (°C)
	Material	Outside Diameter (in.)	Wall (in.)				
Top	Type 316 stainless steel	0.355	0.024	30	340–400 <sup>d</sup>	4.3–5.1 <sup>d</sup>	500–600 <sup>d</sup>
Middle	Hastelloy X	0.344	0.015	30	500	6.3	685
Bottom	Hastelloy X	0.344	0.015	500	500	6.3	685

<sup>a</sup>Fueled with 0.310 ± 0.005-in.-OD × 0.058-in.-ID 90%-dense (U–12% Pu)O<sub>1.98</sub> pellets.

<sup>b</sup>Operating temperature. Final pressure 1000 psia.

<sup>c</sup>Fissions per initial metal atom, peak.

<sup>d</sup>These are average values for the cold and hot ends of this fuel pin. The heat generations were about 10% and the temperatures 50–60°C below these values at the start of each reactor fuel cycle and about the same amount above at the end of each cycle.

R-49609A

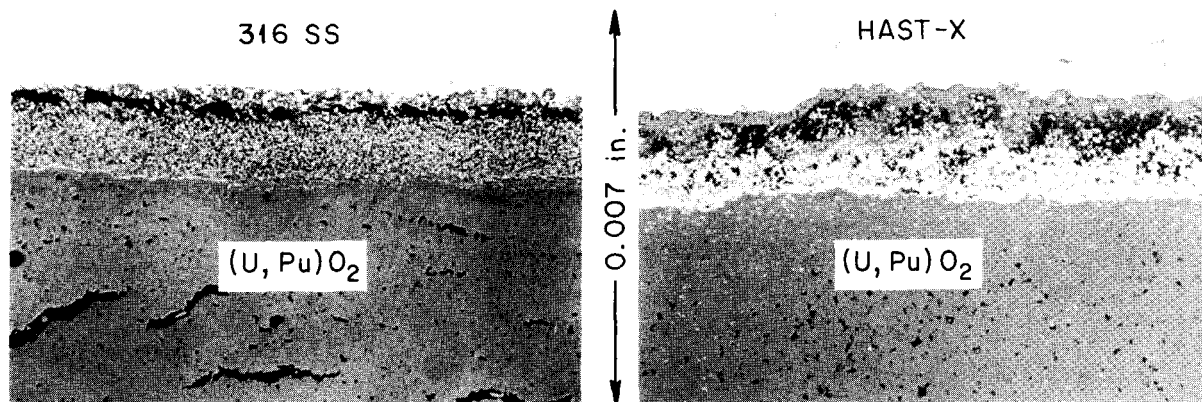


Fig. 36.5. Comparison of Fuel-Cladding Interactions in Top and Middle Pins of Capsule O4-P8. Left: top pin with type 316 stainless steel cladding with an inner surface temperature of  $580 \pm 50^\circ\text{C}$ . Right: middle pin with Hastelloy X at  $710^\circ\text{C}$ .

tures. The gas lines running into the top and bottom of the trap are used to collect samples of the fission gases that leave the fuel and blanket region, into and through the charcoal trap. These lines also permit the maintenance of a dynamic balance between the coolant overpressure and the fuel pin internal pressure. Thermocouples are distributed along the fuel pin and in the charcoal trap region.

A preliminary analysis of the results to date from this capsule indicates very satisfactory performance of the fission product trap. Measurements under steady-state operating conditions show that the short-lived gaseous fission products decay in the trap and are not released in significant quantity from the fuel pin. As was expected, the very long-lived gases are not affected by the trap. Future measurements of trap performance will include both steady-state and pressure transient conditions.

#### Fabrication of Capsules for EBR-II

R. A. Bradley      W. H. Pechin  
M. K. Preston<sup>20</sup>    J. D. Sease  
T. N. Washburn

As part of the cooperative program with Gulf General Atomic, we constructed a set of eight GCBR fuel pins to be irradiated in EBR-II. These will simulate the manifolded design in that the pressure differential

across the cladding will be low and a large fission gas plenum and charcoal trap are included to prevent the buildup of high fuel pin internal pressures. Seven of these pins will be included in the first irradiation assembly, and the eighth will replace a pin to be removed after low burnup. One pin will be operated to 50 GWd/metric ton with the cladding at  $600^\circ\text{C}$  to provide a common point for comparison of results with those from the LMFBR program. Three pins with a cladding outside temperature of  $700^\circ\text{C}$  will permit a direct comparison with the manifolded fuel pin in our current thermal reactor test. These pins will be destructively examined after 25, 50, and 100 GWd/metric ton. Pins will operate to 50 GWd/metric ton with cladding at 750 and  $800^\circ\text{C}$  to examine the effect of cladding temperature. The pins will attain cladding fast fluences up to  $6 \times 10^{22}$  neutrons/cm<sup>2</sup> at the maximum design burnup of 100 GWd/metric ton. These cladding fluences, although less than those attained at full burnup in a GCBR, will produce significant fast neutron damage to the cladding and should answer some of the questions about the influence of this damage on the performance of GCBR fuel pins. The postirradiation analysis of charcoal fission product traps included in these pins will provide information on the ability of hot charcoal to remove condensable fission products and to delay short-lived gaseous products in the fast flux environment. Additional small, sealed containers of charcoal are included to study the effects of the environment on charcoal sorption properties.

<sup>20</sup>On loan from General Engineering Division.

ORNL - DWG 69-11719

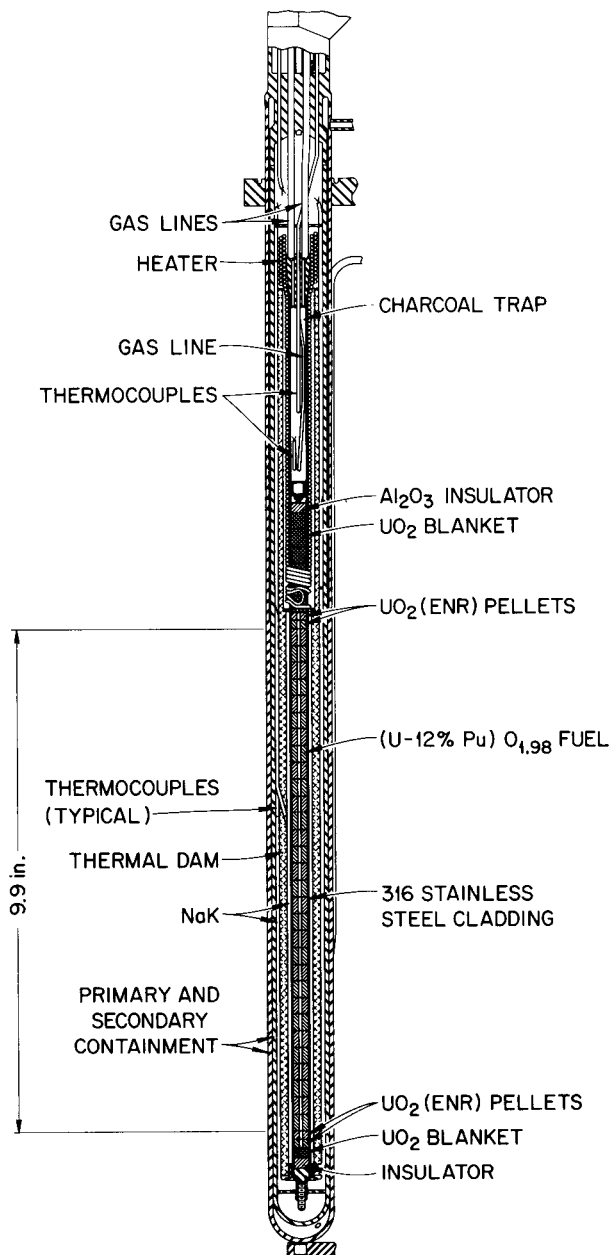


Fig. 36.6. Design of Capsule for Irradiation Testing of Manifolded-Vented Fuel Pins.

## 37. Heavy Section Steel Technology

D. A. Canonico

The Heavy Section Steel Technology Program is an engineering effort to determine the structural behavior of the thick plates and pressure vessels needed for large light water nuclear reactors. The overall program emphasizes the effects of flaws, discontinuities, and inhomogeneities on the integrity of the reactor vessel during both shutdown and operation. Extensive testing programs are being conducted on weldments and plates. These include the determination of strength and classical fracture toughness properties as well as the development and application of fracture mechanics for those steels currently being used in the fabrication of light-water nuclear pressure vessels.

We participate as both consultants and experimentalists. First, we serve on the staff of the Program Office as metallurgical consultants and are expected to contribute to decisions that require metallurgical knowledge. In addition, we are involved experimentally in those tasks that require the facilities and expertise available within the Division.

### CHARACTERIZATION OF HEAVY SECTION STEEL PLATE

R. G. Berggren

Three 12-in.-thick plates of ASTM A533, grade B, class 1 steel, quenched, tempered, and stress relieved, were characterized as to chemical composition, metallurgical structure, and mechanical properties. The mechanical properties were determined by tensile tests, Charpy V-notch impact tests, and drop weight tests as functions of orientation, distance from the surfaces, and location in the plates.

The mechanical properties of the three plates were very similar and met the specification. Tests of specimens from several regions of one plate indicated that strengths near the bottom ingot end are about 10% lower than in other regions but still within the specification. The differences in carbon and nickel

content explain the strength differences. The nil ductility temperature and transition temperatures did not vary over the plate area. Tensile strengths were higher and transition temperatures were lower for material within 1.5 in. of the plate surface than for interior material because the cooling rates are higher near the surfaces during quenching. The central 8 in. of the 12-in. thickness were very uniform in properties. Variations in properties with specimen orientation were relatively small, as would be expected for plates of this relatively low rolling reduction and cross rolling ratio.

Numerous Charpy V-notch impact specimens are in operating power reactors as part of pressure vessel surveillance programs, and it is desirable to obtain the greatest possible information from these specimens. To further this goal, we are obtaining load-deflection records during impact and slow bend tests of both standard Charpy V-notch and fatigue-precracked specimens. Strain rate effects are shown in Fig. 37.1 in which yield and fracture parameters of Charpy V-notch specimens are compared for impact and slow bend tests. The effects of notch sharpness are shown in Fig. 37.2, in which the fracture parameters of blunt flaw (Charpy V-notch) and sharp flaw (fatigue cracked) specimens are compared. Analyses of these types of data should enable us to determine fracture toughness for both static ( $K_{Ic}$ ) and dynamic ( $K_{Ia}$ ) conditions at the lower temperatures where cleavage fracture predominates. A method of analysis of flaw-initiated failure for "ductile" and transition temperature behavior is being developed and a preliminary formulation has been presented.<sup>1</sup> Development of this fracture analysis method has required testing a variety of sizes and

---

<sup>1</sup>F. J. Witt and R. G. Berggren, "Size Effects and Energy Disposition in Impact Specimen Testing of ASTM A533 Grade B Steel," Paper 1674 presented at 1970 Society for Experimental Stress Analysis Spring Meeting, Huntsville, Ala. (to be published).

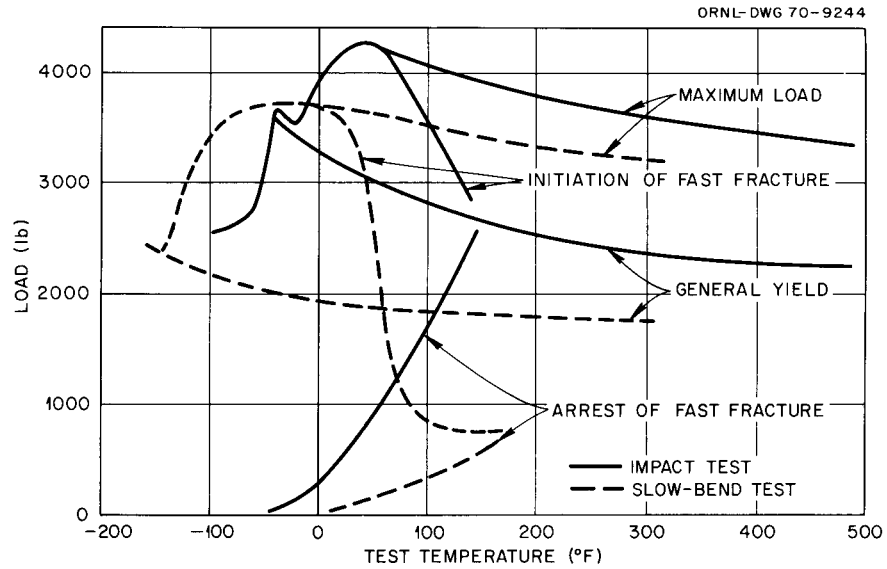


Fig. 37.1. Effect of Temperature on Various Fracture Parameters as Determined by Instrumented Charpy Tests and Slow Bend Tests on ASTM A533-B1 Steel.

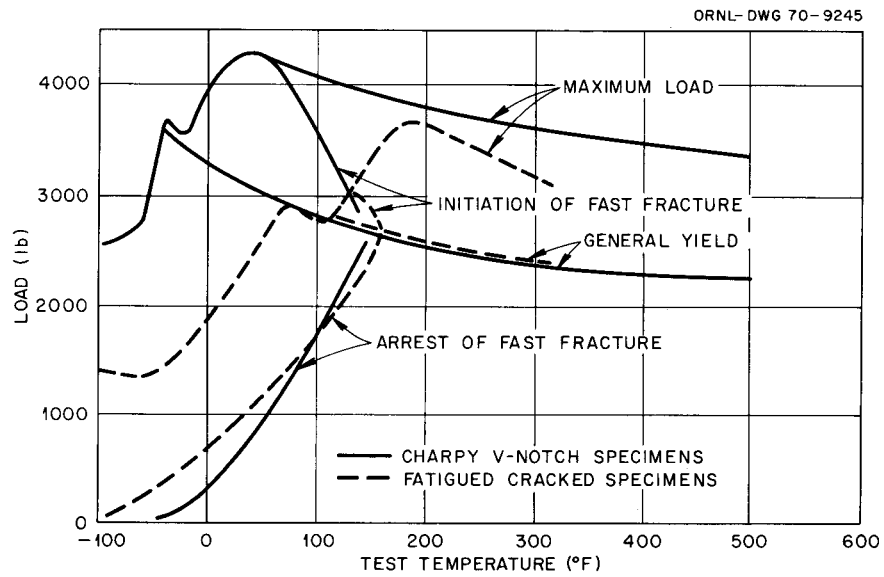


Fig. 37.2. Effect of Temperature on Fracture Parameters as Determined by Instrumented Charpy Tests on V-Notch and Fatigue-Notch Charpy Specimens of ASTM A533-B1 Steel.

configurations of specimens, some of which were prepared and tested in the Division and some at other installations.

## CHARACTERIZATION OF HEAVY SECTION STEEL WELDMENTS

D. A. Canonico

Three weldments, two in 12-in.-thick plate and one in 6 $\frac{1}{8}$ -in.-thick plate, have been procured and are under investigation. The plate used is ASTM A533, grade B, class 1. The submerged-arc and shielded metal-arc welds were made in 12-in.-thick quenched, tempered, and stress-relieved plate. They were welded by a multipass technique and then stress relieved. The electroslag weld was made in 6 $\frac{1}{8}$ -in.-thick plate that had been given the equivalent of a normalized heat treatment. The entire weldment was austenitized and quenched twice, tempered, and stress relieved.

Previously, we reported<sup>2</sup> that the 30 ft-lb Charpy V-notch ( $C_V$ ) temperature for submerged-arc weld metal was  $-60^\circ\text{F}$ . Through-the-thickness  $C_V$  studies at  $-60^\circ\text{F}$  showed that the weld metal toughness was uniform, and the scatter in energy observed is typical for the  $C_V$  test. The shelf energy of the submerged-arc weld metal is about 115 ft-lb. Our studies on the electroslag weld metal have shown that at the quarter-thickness location the 30 ft-lb temperature is  $-20^\circ\text{F}$  and that the surface and midthickness  $C_V$  properties are similar. This was unexpected in view of the postweld quench-and-temper treatment. The effectiveness of the heat treatment was established by base-metal  $C_V$  studies wherein the surface properties are shown to be considerably better than the quarter-thickness and midthickness properties. Figure 37.3 contains the results of the  $C_V$  studies on electroslag weld metal and base metal.

We have investigated the  $C_V$  properties of the electroslag welds as a function of location in the weld metal and the heat-affected zone (HAZ). Both surface and midthickness locations were investigated. Specimens were tested at  $-100$ ,  $-20$ ,  $0$ , and  $200^\circ\text{F}$ . Studies at  $0$  and  $+200^\circ\text{F}$  concentrated on the weld metal. The HAZ's were emphasized at the lower temperatures. Figure 37.4 shows the results from the  $C_V$  tests of the surface material. The photographic strips indicate the locations from which the various test specimens were

taken. The  $C_V$  results for the base metal and weld metal are included. It can be seen that the  $C_V$  results obtained in this study fall between the two curves. Similar results were obtained from the midthickness study.

In summary, the midthickness weld metal is the least tough region of an electroslag weldment. Other regions within the weld metal and the HAZ are superior to the midthickness weld metal but poorer than the base metal.

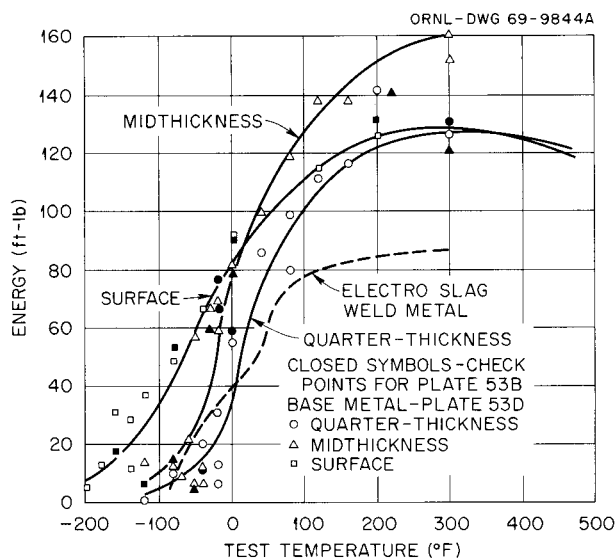


Fig. 37.3. Charpy V-Notch Tests on Electroslag Weld and Associated Base Metal.

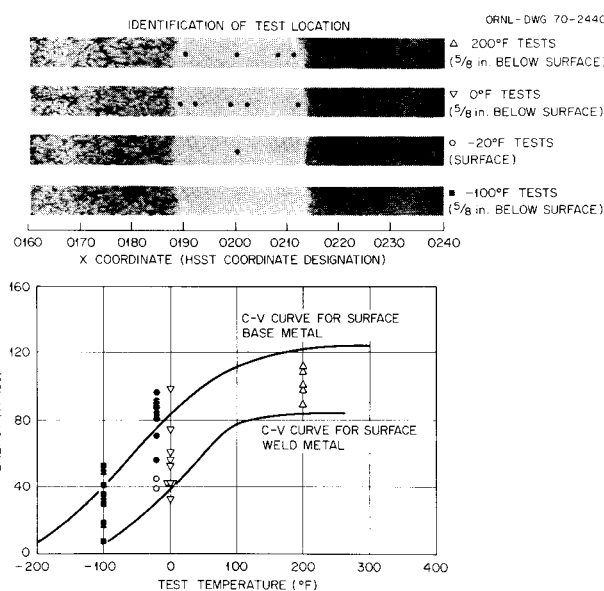


Fig. 37.4. Charpy V-Notch Results for Surface Location Electroslag Weld Investigation. HSST plate 53.

<sup>2</sup>D. A. Canonico, *Metals and Ceramics Div. Ann. Progr. Rept. June 30, 1969*, ORNL-4470, pp. 160-61.

## RADIATION STUDIES ON HSST PLATES AND WELDS

R. G. Berggren

Radiation-induced changes in tensile and Charpy V-notch impact properties of two HSST plates and one HSST submerged-arc weldment have been determined as a function of depth and orientation in the plate, irradiation temperature, and fast neutron fluence (3 to  $13 \times 10^{18}$  neutrons/cm<sup>2</sup>, >1 MeV). Some of the results are summarized in Table 37.1 as the coefficient  $A$  in the expression:

$$\text{property change} = A(\Phi/10^{18})^{1/2}.$$

The coefficient  $A$  is an index of the "radiation sensitivity" at a given irradiation temperature. The ameliorating effects of elevated irradiation temperatures are apparent. The differences for the various depths and the one different orientation in the plates are probably not significant. The square root relationship is not adequate for higher neutron fluences due to "saturation" effects.

The fracture analysis methods discussed briefly in the section on "Characterization of Heavy Section Steel Plate" are being applied to load-deflection records from instrumented notch-impact tests of irradiated specimens. This study is presently limited to impact tests of standard Charpy V-notch specimens. Fracture param-

eters for control specimens (unirradiated) and specimens irradiated at 550°F, Fig. 37.5, are typical of the data obtained. The fracture analysis procedures now being developed, when applied to data from irradiated specimens, should obtain more useful information from power reactor surveillance programs.

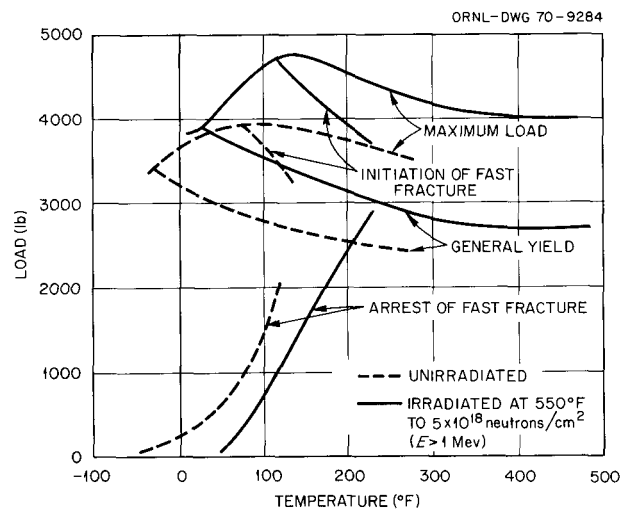


Fig. 37.5. Effect of Irradiation and Test Temperature on Fracture Parameters as Determined by Instrumented Charpy Tests on ASTM A533-B1 Steel.

Table 37.1. Effects of Radiation on 12-in.-Thick A533, Grade B, Class 1 Steel and Matching Submerged-Arc Weldment<sup>a</sup>

HSST Plate	Depth in Plate	Orientation	$\Delta DBTT$ Index, $A_{CV}^b$				$\Delta \sigma_{LY}$ Index, $A_{LY}^c$			
			Irradiation Temperature (°F)				Irradiation Temperature (°F)			
			150	450	550	650	150	450	550	650
01	Surface	Longitudinal	76	66	32	17	11.4	8.8	6.6	2.5
01	Quarter	Longitudinal	72	66	34	10	12.3	8.7	5.0	2.4
01	Quarter	Transverse	62	50			11.6	8.9		
02	$\frac{3}{8} T$	Longitudinal	60	57	22		12.3		6.0	
Weld metal	$\frac{3}{8} T$	Across weld	76	95			12.8	13.8		

<sup>a</sup>Fluence range in this study was 3 to  $13.5 \times 10^{18}$  neutrons/cm<sup>2</sup> (>1 MeV). Irradiation temperatures are  $\pm 10^\circ\text{F}$ .

<sup>b</sup>From the equation for the change in the ductile-to-brittle transition temperature:  $\Delta DBTT = A_{CV} (\Phi/10^{18})^{1/2}$ ;  $\Phi$  in neutrons/cm<sup>2</sup> (>1 MeV).

<sup>c</sup>From the equation for the change in lower yield strength:  $\Delta \sigma_{LY} = A_{LY} (\Phi/10^{18})^{1/2}$ ;  $\Phi$  in neutrons/cm<sup>2</sup> (>1 MeV).

## 38. Military Reactor Fuel Element Procurement Assistance

R. J. Beaver      W. J. Leonard

This task includes standardization of specifications, review of technical requirements for procurement packages, and participation in fuel procurement as well as quality control audits of fuel fabricators.

The second of the two PM type-4 cores for the Navy's reactor in Antarctica was procured by the AEC New York Operations Office with our assistance and surveillance. This delivery was made possible by our review and concurrence in a weld-design change of the control rod assemblies and the necessary inspections.

Procurement of 32  $\text{UO}_2$  pellet-stainless steel tubular fuel element assemblies for the MH-1A floating nuclear power plant, the "Sturgis," by the AEC New York Operations Office has progressed steadily to the point of initiation of assembling work by the Kerr-McGee Corporation. The first 16 assemblies are scheduled for completion by September 1970.

A longer life Type II core for this MH-1A reactor has been designed and we have been assigned the responsibility for preparing the fuel element assembly procurement specifications. A rough draft was prepared and completion of this task is anticipated early in the next fiscal year. We also reviewed control rod assembly procurement specifications prepared by the Army: one, the boron-stainless steel plate type assembly for the Type I core; the other, the packed  $\text{B}_4\text{C}$ -stainless steel tubular assembly proposed for the Type II core.

Procurement of 116 ETR-type, aluminum-base, plate-type fuel elements for the Air Force Nuclear Engineering Test Reactor (AFNETR) at Wright-Patterson Air Force Base by the AEC New York Operations Office was successfully completed on schedule with our assistance in inspection and surveillance. This procurement was stimulated by the design of unique functional fit gages by the vendor, United Nuclear Corporation, with our encouragement, review, and concurrence.

## 39. Molten-Salt Reactor Program

J. R. Weir, Jr. H. E. McCoy, Jr.

This program has involved us with the operation of an 8-MW (thermal) experimental reactor (Molten-Salt Reactor Experiment, MSRE) and with the materials problems associated with the future construction of a molten-salt breeder reactor. Operation of the MSRE was terminated on December 12, 1969, after it successfully completed its mission. We have examined graphite and Hastelloy N specimens from the Reactor. The work in support of an advanced reactor involves (1) development of modified Hastelloy N with improved resistance to irradiation damage,<sup>1,2</sup> (2) development of a graphite with improved dimensional stability under irradiation,<sup>2</sup> (3) development of a method for reducing the surface permeability of graphite to gaseous fission products,<sup>2</sup> (4) determination of the corrosion rate of Hastelloy N in a new coolant salt, sodium fluoroborate,<sup>2</sup> and (5) development of a technology for fabricating small processing plants for removing fission products by contacting the fertile-fissile salt with bismuth.

### MATERIALS WORK IN SUPPORT OF THE MSRE

H. E. McCoy, Jr. W. H. Cook

The MSRE is a converter reactor that produces 8 MW of thermal energy and is fueled with a mixture of U, <sup>7</sup>Li, Be, and Zr fluorides. Criticality is obtained in a small volume where the salt flows through passages in a graphite moderator. The sole metallic structural material is Hastelloy N. The Reactor went critical in 1965 and operated through several sustained periods without serious difficulty. The second phase of operation began in August 1968 when a small processing facility

<sup>1</sup>H. E. McCoy, "The INOR-8 Story," *ORNL Review* 3(2) 35-49 (Fall 1969).

<sup>2</sup>H. E. McCoy, Jr., R. L. Beatty, W. H. Cook, R. E. Gehlbach, C. R. Kennedy, J. W. Koger, A. P. Litman, C. E. Sessions, and J. R. Weir, "New Developments in Materials for Molten-Salt Reactors," *Nucl. Appl. Technol.* 8, 156-69 (1970).

attached to the reactor was used to remove the original uranium. A charge of <sup>233</sup>U was added to the salt, and on October 2 criticality was attained. On December 12, 1969, the Reactor was shut down partially because it had accomplished its intended purpose and partially because additional funds were needed for the development work on an advanced breeder.

We maintained surveillance facilities where graphite and Hastelloy N samples were exposed to the Reactor environment and then removed for examination.

Graphite and Hastelloy N specimens have been removed from the core of the MSRE after exposure to fuel salt for 22,533 hr at 650°C. These materials received fluences of  $1.5 \times 10^{21}$  neutrons/cm<sup>2</sup> (thermal) and  $1.1 \times 10^{21}$  neutrons/cm<sup>2</sup> (fast, >50 keV). As reported previously<sup>3</sup> the graphite and metal samples were in excellent mechanical condition and appeared unaffected by the exposure except for a slight darkening of the metal samples. All tests on the graphite showed that it had excellent compatibility with the fuel salt.

The details of the mechanical property tests and metallographic examination of the standard and modified Hastelloy N specimens have been reported.<sup>4-7</sup> The following significant observations were made.

<sup>3</sup>W. H. Cook and H. E. McCoy, *Metals and Ceramics Div. Ann. Progr. Rept. June 30, 1969*, ORNL-4470, pp. 182-84.

<sup>4</sup>H. E. McCoy, Jr., *An Evaluation of the Molten-Salt Reactor Experiment Hastelloy N Surveillance Specimens - First Group*, ORNL-TM-1997 (November 1967).

<sup>5</sup>H. E. McCoy, Jr., *An Evaluation of the Molten-Salt Reactor Experiment Hastelloy N Surveillance Specimens - Second Group*, ORNL-TM-2359 (February 1969).

<sup>6</sup>H. E. McCoy, Jr., *An Evaluation of the Molten-Salt Reactor Experiment Hastelloy N Surveillance Specimens - Third Group*, ORNL-TM-2647 (January 1970).

<sup>7</sup>H. E. McCoy, Jr., *An Evaluation of the Molten-Salt Reactor Experiment Hastelloy N Surveillance Specimens - Fourth Group*, ORNL-TM-3063 (to be published).

1. The mechanical properties of the standard Hastelloy N, particularly the fracture strain, deteriorated rapidly with increasing fluence.

2. Modified alloys containing nominal additions of 0.5% Ti and Hf had much better postirradiation mechanical properties.

3. The standard Hastelloy N was depleted in chromium near the surface to a depth of 2.5 mils. This profile is in excellent agreement with that predicted from the measured diffusion rate of chromium in Hastelloy N.

4. The standard Hastelloy N samples exhibited edge cracking to a depth of about 4 mils when deformed at 25°C. We have not determined whether this is due to loss of chromium or infusion of some fission product.

5. The modified alloys all showed excellent resistance to corrosion by the salt.

### HASTELLOY N DEVELOPMENT

H. E. McCoy, Jr.

#### Development of a Modified Hastelloy N

H. E. McCoy, Jr.

Hastelloy N has performed very well in the MSRE except that the fracture strain was reduced by irradiation. The material will not be exposed to fast fluences greater than  $1 \times 10^{21}$  neutrons/cm<sup>2</sup> in an advanced system, so the cause of embrittlement will continue to be the production of helium from the  $^{10}\text{B}(n,\alpha)^7\text{Li}$  transmutation. The amounts of helium necessary to cause embrittlement are so small that it is impossible to solve the problem by reducing the boron level. In an alternate approach we have added strong carbide-forming elements such as Ti, Hf, Zr, and Nb. These elements in the proper concentrations produce a fine carbide dispersion along the grain boundaries and throughout the matrix. Some boron is associated with the precipitate, so the net effects are (1) to disperse the boron (and hence the produced helium) uniformly rather than allowing it to accumulate at the grain boundaries and (2) to make the grain boundaries more resistant to fracture.

We discussed the details of this alloy modification program in Chapter 31 and will discuss here some of the scale-up work on 50- and 100-lb heats and compatibility studies.

#### Mechanical Properties of Commercial Heats of Modified Hastelloy N

H. E. McCoy, Jr.

From the results presented in Chapter 31 for laboratory melts we conclude that alloys with reasonably

good postirradiation properties result from singular additions of 1 to 2% Ti or 0.5 to 1% Hf and multiple additions of smaller concentrations of Ti, Hf, and Nb. The alloy base was modified from 16 to 12% Mo and the silicon was reduced below 0.1%. Although zirconium resulted in good postirradiation properties, it made the alloy very susceptible to cracking during welding.<sup>8</sup> Thus the desirable alloy for extended application at 700 to 760°C seems to be Ni-12% Mo-7% Cr-0 to 4% Fe-0.2 to 0.5% Mn-0.04 to 0.08% C-<0.1% Si and additions of Ti, Nb, and Hf. We have attempted to minimize the concentration of hafnium because of its high cost (about \$100/lb) and because it carries with it 2 to 5% Zr, which can cause weld cracking.

We have obtained about 25 commercial melts weighing 50 to 100 lb with additions up to 2.1% Ti and a single 5000-lb melt containing 0.5% Ti. About ten commercial melts weighing 50 to 100 lb with combined additions of Ti, Nb, and Hf have been procured. All alloys showed excellent fabricability at a breakdown temperature of 1177°C. Most of the alloys have been irradiated and generally show the same postirradiation properties as those noted in Chapter 31 for the laboratory melts. However, in a few cases the microstructures are different and the properties are less desirable for the commercial melts. We have not determined whether this is due to the presence of some impurity in the commercial melts or due to different fabrication practices.

#### Welding of Modified Hastelloy N

B. McNabb H. E. McCoy, Jr.

Several commercial alloys in the form of 1/2-in.-thick plate have been welded. Filler metal was prepared from the same alloys by swaging. A standard "V" weld groove was prepared and the plates were restrained by welding them to a 3-in.-thick steel plate. The multipass welds were made with complete recording of welding parameters and interpass inspection. All alloys except a single 5000-lb melt containing 0.5% Ti and a small 100-lb melt containing 0.3% Zr were welded satisfactorily under these conditions.

The welds were evaluated by cold side bends and tensile tests at 650°C. The materials passed the bend tests adequately. The tensile tests showed that welding increased the yield stress and decreased the fracture strain. Postweld anneals of 8 hr at 871°C (normal

<sup>8</sup>H. E. McCoy and R. E. Gehlbach, "Influence of Zirconium Additions on the Mechanical Properties of Modified Hastelloy N," to be submitted to *Journal of Nuclear Materials*.

treatment for Hastelloy N) partially recovered the properties. However, some heats required postweld heat treatments as high as 1177°C to restore the properties to those of the base metal. Even in these cases the fractures occurred in the weld metal.

### Corrosion Studies

J. W. Koger

Temperature, the impurity content of the salt, and the type of container material are principal variables that affect corrosion by molten fluoride salts. We are studying the effect of these variables on corrosion and mass transfer in experimental systems (capsules, thermal convection loops, and pumped loops) that are based on design parameters for future molten salt reactors. The alloys under investigation are Hastelloy N, Hastelloy N modified for improved radiation properties, type 304L stainless steel, and maraging steel. Salt mixtures of interest include the proposed MSBR coolant salt, a eutectic mixture of NaBF<sub>4</sub>-8 mole % NaF, and various mixtures in the LiF-BeF<sub>2</sub> system. Within the latter group are fuel salts (UF<sub>4</sub> added), blanket salts (ThF<sub>4</sub> added), and fertile-fissile salts (both UF<sub>4</sub> and ThF<sub>4</sub> added). The following significant observations were made this year.

**Fuel, Blanket, and Fertile-Fissile Salts.** — 1. A thermal convection loop of Hastelloy N with 2% Nb has circulated a simulated MSRE fuel salt with 1 mole % ThF<sub>4</sub> over 8.2 years at a maximum temperature of 705°C with no evidence of plugging.<sup>9,10</sup>

2. A type 304L stainless steel thermal convection loop with the same salt as above has operated for 7 years at a maximum temperature of 688°C. The removable specimen at the highest temperature lost 60.0 mg/cm<sup>2</sup> in 23,800 hr, equivalent to about 1.1 mils/year uniform corrosion. Although this weight loss is relatively large, flow conditions have not deteriorated. Table 39.1 compares the weight losses and corrosion rates of Hastelloy N, type 304L stainless steel, and a maraging steel (Fe-12% Ni-5% Cr-3% Mo) under similar exposure conditions. As expected because of the lower chromium content, the maraging steel shows better corrosion resistance than type 304L stainless steel, but both are still inferior to Hastelloy N.<sup>9,10</sup>

3. Removable specimens in Hastelloy N thermal convection loops containing fuel, blanket, and fertile-

**Table 39.1. Comparison of Weight Losses of Alloys at About 663°C After 3730 hr Exposure to LiF-23 mole % BeF<sub>2</sub>-5 mole % ZrF<sub>4</sub>-1 mole % UF<sub>4</sub>-1 mole % ThF<sub>4</sub> in a Temperature Gradient System**

Alloy	Weight Loss (mg/cm <sup>2</sup> )	Average Corrosion Rate (mils/year)
Maraging steel	4.8	0.55
Type 304 stainless steel	10.0	1.1
Hastelloy N	0.6	0.06

fissile salts operating at a maximum temperature of 700°C have lost no more than 1.0 mg/cm<sup>2</sup> in 10,000 hr; if the corrosion were uniform this would be equivalent to 0.04 mil/year. Modified Hastelloy N alloys, which are alloyed with 0.2 to 2.5% Ti and contain no iron, have generally shown better corrosion resistance than the unmodified Hastelloy N. The corrosion reactions in the fertile-fissile systems involve primarily the oxidation of chromium by both FeF<sub>2</sub> and UF<sub>4</sub>. Thus, the overall process is controlled by solid-state diffusion of chromium in the alloy.<sup>9-12</sup>

4. Compatibility of TZM with the fertile-fissile salt at 1100°C was excellent.<sup>13</sup>

**Coolant Salt.** — 1. Corrosion of Hastelloy N in the NaBF<sub>4</sub>-8 mole % NaF coolant salt is largely dependent on the concentration of water and oxygen-containing impurities in the salt. Twice inadvertent air leaks in a Hastelloy N thermal convection loop were indicated by abrupt increases in the corrosion rate of removable test specimens. The rates returned to a relatively low value once the leaks were corrected. At the maximum temperature position (605°C), the corrosion rate over 20,000 hr, including the time of air inleakage, averaged 0.6 mil/year.<sup>9-12,14</sup> By comparison, a Hastelloy N loop

<sup>11</sup>J. W. Koger and A. P. Litman, "Mass Transfer of the Nickel-Base Hastelloy N Alloy in a Flowing Fused Fluoride Salt System," presented at Fall Meeting of the Metallurgical Society of AIME at Philadelphia, Oct. 13-16, 1969.

<sup>12</sup>J. W. Koger and A. P. Litman, "Corrosion Mechanisms in Fused Fluoride Systems," presented at N.A.C.E. Annual Conference in Philadelphia, March 2-6, 1970.

<sup>13</sup>J. W. Koger and A. P. Litman, *Compatibility of Molybdenum-Base Alloy TZM with LiF-BeF<sub>2</sub>-ThF<sub>4</sub>-UF<sub>4</sub> (68-20-11.7-0.3 mole %) at 1100°C*. ORNL-TM-2724 (December 1969).

<sup>14</sup>J. W. Koger and A. P. Litman, "Effect of Impurities on the Corrosion Rate of Hastelloy N Exposed to Fluoride Salts at Elevated Temperatures," presented at Spring Meeting of the Metallurgical Society of AIME in Las Vegas, Nev., May 11-14, 1970.

<sup>9</sup>J. W. Koger and A. P. Litman, *MSR Program Semiann. Progr. Rept. Aug. 31, 1969*, ORNL-4449, pp. 195-208.

<sup>10</sup>J. W. Koger, *MSR Program Semiann. Progr. Rept. Feb. 28, 1970*, ORNL-4548, pp. 240-47.

with high-purity fluoroborate salt (<500 ppm H<sub>2</sub>O or O) has experienced<sup>10</sup> a loss equivalent to 0.16 mil/year over a 3800-hr period at a maximum temperature of 687°C.

2. Steam was injected into a Hastelloy N thermal convection loop system containing sodium fluoroborate and resulted in a corrosion rate of 19.5 mils/year at 607°C. However, the corrosion rate decreased<sup>9,10,12,13</sup> to approximately 3.0 mils/year in 3000 hr. About 2 mils of deposited material was found on specimens in the cold leg, but the loop has continued to operate without a significant change in flow rate.

3. A Hastelloy N pumped loop containing NaBF<sub>4</sub>-NaF has operated for 9500 hr at a maximum salt temperature of 587°C. The average weight loss at 587°C during this period was 24.0 mg/cm<sup>2</sup> (equivalent to 0.9 mil/year, assuming uniform loss). The salt initially contained about 1000 ppm each of water and oxygen, and the corrosion rate was higher than in a thermal convection loop with salt of a similar impurity content and comparable temperature conditions. This suggests that the impurity-controlled corrosion reactions are controlled by rate of solution and dependent on velocity.<sup>9,10,12,14</sup>

4. Capsule experiments were conducted to determine the uptake of chromium from Hastelloy N into NaBF<sub>4</sub>-8 mole % NaF containing approximately 400 ppm each oxygen and water. Tests at 427, 538, 649, and 760°C showed that the removal of the chromium was controlled by solid-state diffusion of chromium to the capsule walls and increased with temperature and impurity content of the salt.<sup>9,10,14</sup>

5. Purging with a mixture of BF<sub>3</sub>, He, and HF was found<sup>10</sup> to lower the water content of NaBF<sub>4</sub>-8 mole % NaF from 2000 to 300 ppm.

**Status of Fused Fluoride Salt Corrosion.** — The results support our previous findings that the temperature-gradient mass-transfer corrosion mechanism in fluoride salts with a low fluoride ion potential involves the formation of the most stable structural metal fluoride (usually chromium) in a hot section, followed by deposition as reduced metal in a cool region. The presence of impurities in the salt may cause oxidation of still other constituents of the container alloy.

The corrosion rates for Hastelloy N in fuel, blanket, and fertile-fissile salts have been extremely low and acceptable for indefinite operation. Corrosion rates have been considerably higher in the sodium fluoroborate salt mixtures and we have traced the cause to the characteristically high concentration of water and oxygen in this salt.

## Corrosion of Hastelloy N in Steam

B. McNabb H. E. McCoy, Jr.

The excellent compatibility of Hastelloy N with fluoride salts has been demonstrated<sup>15</sup> by the operation of the MSRE. We would like to use this same alloy in the steam generators for future power reactors, but the compatibility with steam must be demonstrated. A facility to test the compatibility of Hastelloy N with a supercritical steam environment at 538°C has been reported.<sup>16</sup> Additionally, a facility at the Bartow Plant of the Florida Power Corporation that operates at 593°C has been utilized. (See Chapter 29.)

Figure 39.1 compares the weight change with time for Hastelloy N (both air melted and vacuum melted) at 538 and 593°C and a 2¼%-Cr Croloy at 538°C. Metal removal rates of 0.25, 0.5, and 1 mil/year uniform attack are plotted for comparison, showing the very low corrosion rates of Hastelloy N at both temperatures.

A specimen of Hastelloy N heat 2477 that had been exposed for 4000 hr to 900 psi steam at 538°C at the Bartow Plant had blisters aligned on scratches and machining marks. Microprobe scans of the surfaces of some of these blisters showed that these areas were rich in iron and depleted in nickel, molybdenum, and chromium. We presently think that very fine iron oxide particles in the steam may have stuck on the specimens and reacted in some way to cause the observed blisters. Specimens containing no iron have blistered the same way, and the blisters contained iron. Work is continuing to determine what reactions are occurring.

## Coated Bearing Specimens

W. H. Cook

Large power reactors will likely need small auxiliary pumps and valves made of materials that will resist solid-phase bonding (galling, self-welding) and wear up to 700°C in molten fluoride salts. Metal-bonded carbides offer the best potential for such operating conditions. The least expensive and complicated approach is to apply such hard-surface coatings in thin layers on Hastelloy N bearings or valve faces and grind them to the required surface finishes. We have concluded a small program on four compositions.

<sup>15</sup>H. E. McCoy, Jr., R. L. Beatty, W. H. Cook, R. E. Gehlbach, C. R. Kennedy, J. W. Koger, A. P. Litman, C. E. Sessions, and J. R. Weir, "New Developments in Materials for Molten-Salt Reactors," *Nucl. Appl. Technol.* 8, 156-69 (1970).

<sup>16</sup>B. McNabb and H. E. McCoy, *MSR Program Semiann. Progr. Rept. Aug. 31, 1969*, ORNL-4449, pp. 205-9.

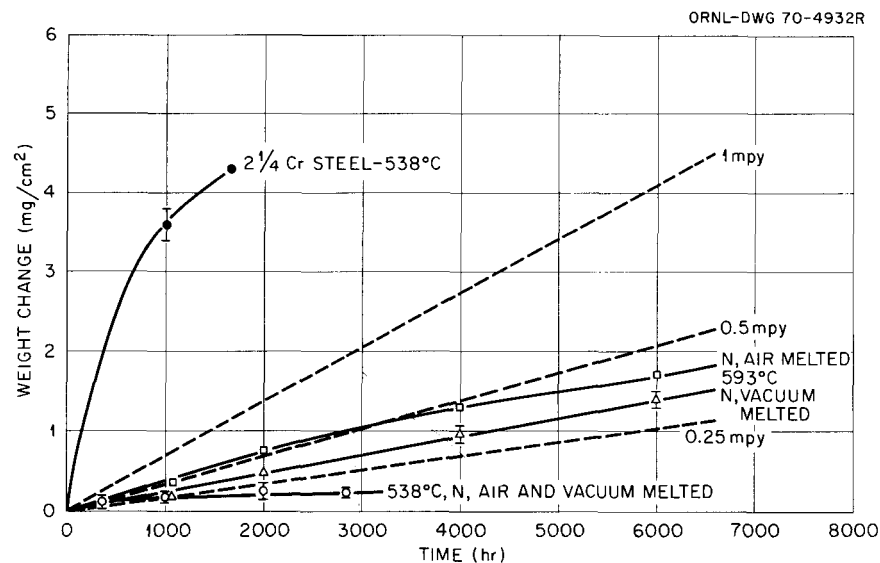


Fig. 39.1. Comparison of the Corrosion Rates of Hastelloy N and Chromium Steel in Steam.

Four 3-mil-thick hard-surface coatings on Hastelloy N survived<sup>17</sup> 100 thermal cycles between 100 and 700°C. In decreasing order of quality of appearance after treatment, these were (1) Linde LW-5, 25% tungsten carbide and the balance mixed tungsten-chromium carbides cemented with 7% Ni; (2) Linde LW-1, tungsten carbide cemented with 7 to 10% Co; (3) Metco 81NS, 75% chromium carbides with 25% nickel-chromium alloy; and (4) MTI, 84% tungsten carbide cemented with 10% Mo-6% Co. As-received (control) and selected thermally cycled specimens have been examined metallographically.<sup>18</sup> Oxygen contamination and porosity increased in the same order as the coatings listed above. The characteristics of these coatings are encouraging.

### GRAPHITE STUDIES

H. E. McCoy, Jr. W. P. Eatherly

The graphite program is aimed at providing graphite for a breeder reactor that might be built in the near future and also at developing a material for more advanced reactors with improved resistance to irradiation damage. First we are studying materials provided by commercial vendors to understand the factors that

<sup>17</sup>W. H. Cook and L. R. Trotter, *MSR Program Semiann. Progr. Rept. Feb. 28, 1969*, ORNL-4396, pp. 267-68.

<sup>18</sup>W. H. Cook, *MSR Program Semiann. Progr. Rept. Feb. 28, 1970*, ORNL-4548, pp. 271-76.

control the dimensional changes during irradiation. Our knowledge is made available to the commercial vendors with the hope that they will use it to produce improved materials. We also have a small fabrication development effort.

We evaluate graphites by several tests on unirradiated samples and then irradiation to high fast fluences and measurement of the dimensional changes. Other postirradiation measurements are also valuable in understanding the damage mechanisms.

To reduce fission product absorption, we must provide graphite with a low-permeability surface layer. Although several techniques can provide such a layer, relative dimensional changes of the layer and substrate during irradiation may increase the permeability. Several sealed samples are being irradiated to determine the extent of this problem.

### Types of Graphite Being Studied

W. H. Cook

One of the initial objectives of our irradiation studies was to obtain types of graphite that were typical of all variations in nuclear graphite technology. To a large extent we have accomplished this, and our rate of procurement has slowed. Our current procurement is directed toward (1) the acquisition of additional stock for more detailed investigation of the few grades that have shown the most resistance to fast neutron damage near 700°C, and (2) obtaining special grades that are of value in obtaining a more complete picture of irradiation

tion damage in graphite. The latter group of materials represents a variety of starting materials and fabrication processes.

Four nearly isotropic commercial grades, AXF-5Q,<sup>19</sup> AXF-5QBG,<sup>19</sup> AXM-5Q,<sup>19</sup> and H337,<sup>20</sup> have shown superior resistance to fast neutron damage at 715°C and are being studied more extensively.<sup>21</sup> The irradiation damage resistance of these are described under "Irradiation Damage in Graphite."

Grades AXF-5Q and H337 are of most interest as solid shapes. Grade AXF-5Q is a proprietary material, and grade H337 is a "raw coke"<sup>22</sup> type of graphite. Grade AXM-5Q graphite is of interest because we have crushed it into a powder and used it as the filler for making reconstituted bodies and for research with newly developed binders.<sup>23,24</sup> We are determining the potential of other special, newly developed grades of graphite obtained from commercial manufacturers<sup>25</sup> and the Materials Engineering Development Department of the Oak Ridge Y-12 Plant.

<sup>19</sup>Manufactured by Poco Graphite, Inc.

<sup>20</sup>Manufactured by the Great Lakes Carbon Corporation.

<sup>21</sup>C. R. Kennedy, *MSR Program Semiann. Progr. Rept. Feb. 28, 1970*, ORNL-4548, pp. 213-16.

<sup>22</sup>The major portion, the filler, is calcined before fabrication near 1400°C, which is less than the conventional calcining temperatures.

<sup>23</sup>W. H. Cook, *MSR Program Semiann. Progr. Rept. Feb. 28, 1969*, ORNL-4396, pp. 217-19.

<sup>24</sup>L. G. Overholser, *MSR Program Semiann. Progr. Rept. Feb. 28, 1969*, ORNL-4396, pp. 216-17.

<sup>25</sup>W. H. Cook, *MSR Program Semiann. Progr. Rept. Feb. 28, 1970*, ORNL-4548, p.201.

## Graphite Fabrication

R. L. Hamner

We began to develop high-density, isotropic bodies for molten-salt reactor applications. We fabricated bodies by warm, uniaxial pressing and by isostatic pressing; these were then impregnated to increase the density.

Three grades of graphite fillers were used, all of which indicated promise in fabricating isotropic bodies: (1) JOZ (Great Lakes Carbon Corporation), (2) Robinson (Carbon Products Division, Union Carbide Corporation), and (3) Santa Maria (Collier Carbon and Chemical Corporation). In addition, we studied the effects of Thermax (R. T. Vanderbilt Company, Inc.), a spherical carbon black, which is used frequently to enhance the packing characteristics of graphite particles. As a binder and impregnant, we used a low-melting coal tar pitch (Allied Chemical Company).

The technique of warm, uniaxial pressing was selected for first studies since it yields a product similar to extruded bodies in crystallographic orientation but requires less time and material for fabrication. Nominally 3-in. cylindrical billets were formed in a graphite die at 1600 psi and about 1100°C; these were then graphitized at 2800°C (unpressurized), impregnated with the pitch at 160°C and 500 psi, and graphitized at 2800°C to achieve ultimate bulk density.

Table 39.2 shows the characteristics of some of the billets before and after impregnation. The increase in bulk density by Thermax addition is apparent. The Robinson and JOZ bodies with Thermax additions were the densest materials both before and after impregnation. The Robinson bodies were the most isotropic, probably because of the absence of needle-coke particles in the starting material. Specimens from the

Table 39.2. Fabrication Conditions and Results for Warm-Pressed Graphite Billets<sup>a</sup>

	Valves for Various Billets					
	SM-1	SM-4	ROB-1	ROB-5	JOZ-2	JOZ-4
Graphite Powder (%)	100	85	100	85	100	85
Thermax (%)	0	15	0	15	0	15
Binder Level (ppm)	20	20	20	20	31	20
Bulk Density <sup>b</sup> (g/cm <sup>3</sup> )	1.56	1.66	1.57	1.77	1.63	1.78
Bulk Density <sup>c</sup> (g/cm <sup>3</sup> )	1.85	1.87	1.84	1.96	1.89	1.96
Crystalline Anisotropy Ratio	1.09	1.085	1.00	1.0	1.34	1.22

<sup>a</sup>Hot pressed 1080°C, 1600 psi – graphitized at 2800°C, unpressurized.

<sup>b</sup>As determined by dimensional measurements and weights, as fabricated.

<sup>c</sup>As determined by dimensional measurements and weights after four impregnations.

Robinson body with Thermax (ROB-5) are being irradiated in the HFIR.

Carbon yields from the pitch impregnant increased with successive impregnation, suggesting that as the pores become smaller, volatile species become entrapped in the matrix and are decomposed before they can escape.

The JOZ and Santa Maria materials were selected for isostatic molding because the warm-pressed bodies fabricated from these materials were too anisotropic. These bodies have not been completely evaluated, but in all cases, even after successive impregnations, the bulk densities were lower than for the same body composition that had been warm pressed and impregnated.

Our fabrication efforts led to several conclusions.

1. Isotropic bodies can be fabricated by techniques that tend to orient the filler particles, with the degree of isotropy depending upon the characteristics of the filler particles.

2. The addition of Thermax definitely increases bulk densities of graphite bodies.

3. High bulk densities can be attained by impregnating low-density bodies.

4. Carbon yields from binder or impregnant materials are variable and need extensive exploration. In general, as the bulk density for a given billet increases with successive impregnations, the carbon yield from the impregnant increases.

### X-Ray Studies

O. B. Cavin J. E. Spruiell<sup>26</sup>

Previous results<sup>27</sup> showed that the most stable graphites in a fast neutron environment near 700°C are isotropic. Thus we have continued to determine the preirradiation crystalline anisotropy of the graphites of interest to the Molten-Salt Reactor Program. We have also used crystalline anisotropy parameters to measure the effects of fabrication variables and filler particles of experimental graphites being fabricated<sup>28</sup> at the Y-12 installation. For example, we showed that a material that had been hot pressed at 2200°C and 2400 psi became more isotropic during subsequent thermal treatment at 2800°C.

<sup>26</sup>Consultant, University of Tennessee, Knoxville, Tennessee.

<sup>27</sup>O. B. Cavin, *Metals and Ceramics Div. Ann. Progr. Rept. June 30, 1969*, ORNL-4470, pp. 192-93.

<sup>28</sup>L. G. Overholser, Chemical Engineering Dept., Development Div., Y-12 Plant.

Table 39.3. Lattice Parameters ( $c_0$ ) Calculated from Centers of Gravity (cg) and Peak Positions, and Crystallite Sizes ( $L_c$ )

Grade	$c_0$ (Å), (002) <sup>a</sup>		$c_0$ (Å), (004) <sup>a</sup>		$L_c$ (Å)
	cg	Peak	cg	Peak	
AXF	6.779	6.764	6.776	6.763	230
AXF (3000°C)	6.758	6.752	6.751	6.738	330
AXF-5 ABG	6.761	6.752	6.755	6.750	280
AXF-5 ABG (3000°C)	6.754	6.740	6.757	6.737	380
H364	6.737	6.725	6.742	6.723	430
H337	6.737	6.725	6.744	6.721	440

<sup>a</sup>Diffracting planes.

In cooperation with another program, we programmed a PDP8/I computer to simultaneously control two x-ray diffraction experiments. With this programmed control we can collect step-scan data punched onto paper tape from as many as four x-ray diffraction line profiles without any operator interaction. Computer programs have been written that will correct the data and then calculate corrected lattice parameters and average crystallite sizes. Corrections are made for background scatter, Lorentz polarization, structure, temperature, and sample transparency factors. Typical results<sup>29</sup> shown in Table 39.3 demonstrate a linear relationship between the crystallite size ( $L_c$ ) and lattice parameter ( $c_0$ ) (Fig. 39.2).

### Irradiation Damage in Graphite

C. R. Kennedy

The displacement damage in graphite causes an expansion in the  $c$ -direction due to interstitial clustering and a contraction in the  $a$ -direction due to the collapse of vacancy clusters. The main concern is the structural degradation caused by the anisotropic growth shearing the boundaries between regions of dissimilar orientation. The ability of the boundaries to accommodate this shear determines the lifetime expectancy of the graphite under irradiation.

Basically three ways might be used to improve the lifetime expectancy. These are: (1) reduce the growth rates due to displacement damage, (2) improve the binder system to raise the integrity of the boundary under stress, and (3) reduce or eliminate the shear on boundaries of low integrity. To find the feasibility of these techniques, we irradiated over 30 different com-

<sup>29</sup>O. B. Cavin and J. E. Spruiell, *MSR Program Semiann. Progr. Rept. Feb. 28, 1970*, ORNL-4548, pp. 207-8.

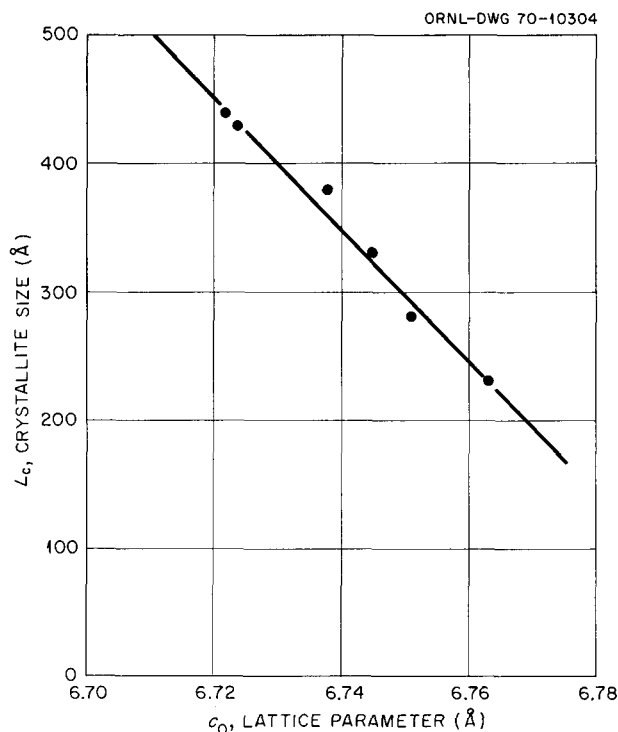


Fig. 39.2. Plot of Crystallite Size ( $L_c$ ) Against Lattice Parameter  $c_0$ .

mercial and experimental graphites at  $715^\circ\text{C}$  to fluences greater than  $1 \times 10^{22}$  neutrons/cm<sup>2</sup> ( $>50$  keV) in the HFIR.

Previously<sup>30</sup> growth rates were related to crystallite size or the degree of crystallographic perfection. We confirmed these results with polycrystalline graphites, as shown in Fig. 39.3. The problem is to fabricate an isotropic graphite with large crystallite size. To date the only materials with a large crystallite size are made with needle or acicular coke graphites. The morphology of these cokes makes it almost impossible to fabricate an isotropic graphite with the required binder or boundary integrity.

The deterioration of the structure is very clearly in the binder region. This is graphically illustrated in Fig. 39.4. The lack of structural integrity in the binder region is a result of its severe shrinkage during fabrication.

<sup>30</sup>J. C. Bokros and R. J. Price, "Dimensional Changes Induced in Pyrolytic Carbon by High-Temperature Fast Neutron Irradiation," *Carbon* 5, 301 (1967).

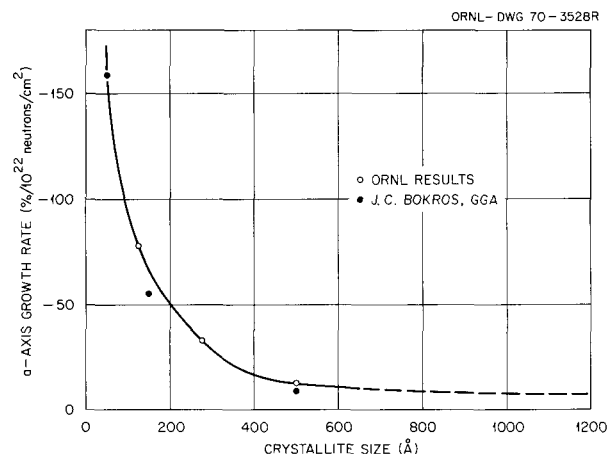


Fig. 39.3. Irradiation Growth Rate in the  $a$  Direction at  $715^\circ\text{C}$  as a Function of Crystallite Size.

To reduce these shrinkage cracks we use thermal setting resins as the binder or impregnant. The carbon residues from these binders generally have a very low density, about  $1.5 \text{ g/cm}^3$ , and are not very graphitic. Under irradiation these low-density regions densify to about  $2.1 \text{ g/cm}^3$ , as deduced from helium density measurements, and voids that reduce the integrity of the binder are created. The magnitude of this type of behavior is illustrated in Fig. 39.5. The bulk density change of the irradiated graphite is only 1.8%; however, the void volume has increased by over 9%. To date, we have not observed an increase in lifetime due to improved binding when conventional calcined cokes or graphite flours are used as filler material.

The only graphites to demonstrate an increased life have structures that reduce the shear on the weak particle-to-particle boundaries. These graphites are all highly isotropic as a result of fabrication from isotropic particles. The high-angle boundaries within the particle apparently have a much higher structural integrity and can accommodate and absorb the shear and thus reduce the forces on the weak interparticle boundaries. This results in the characteristic delay in the densification as shown by these grades.<sup>21</sup> Also, the internal absorption of the anisotropic growth results in smaller particle shape changes in isotropic cokes for the same volume reduction. This is demonstrated in Fig. 39.6, which compares the behavior of isotropic coke grades and anisotropic needle and acicular coke graphites. As shown earlier, these isotropic grades have a higher growth rate, and only the structural arrangement increases the life. The importance of boundary integrity is emphasized by the stability demonstrated for

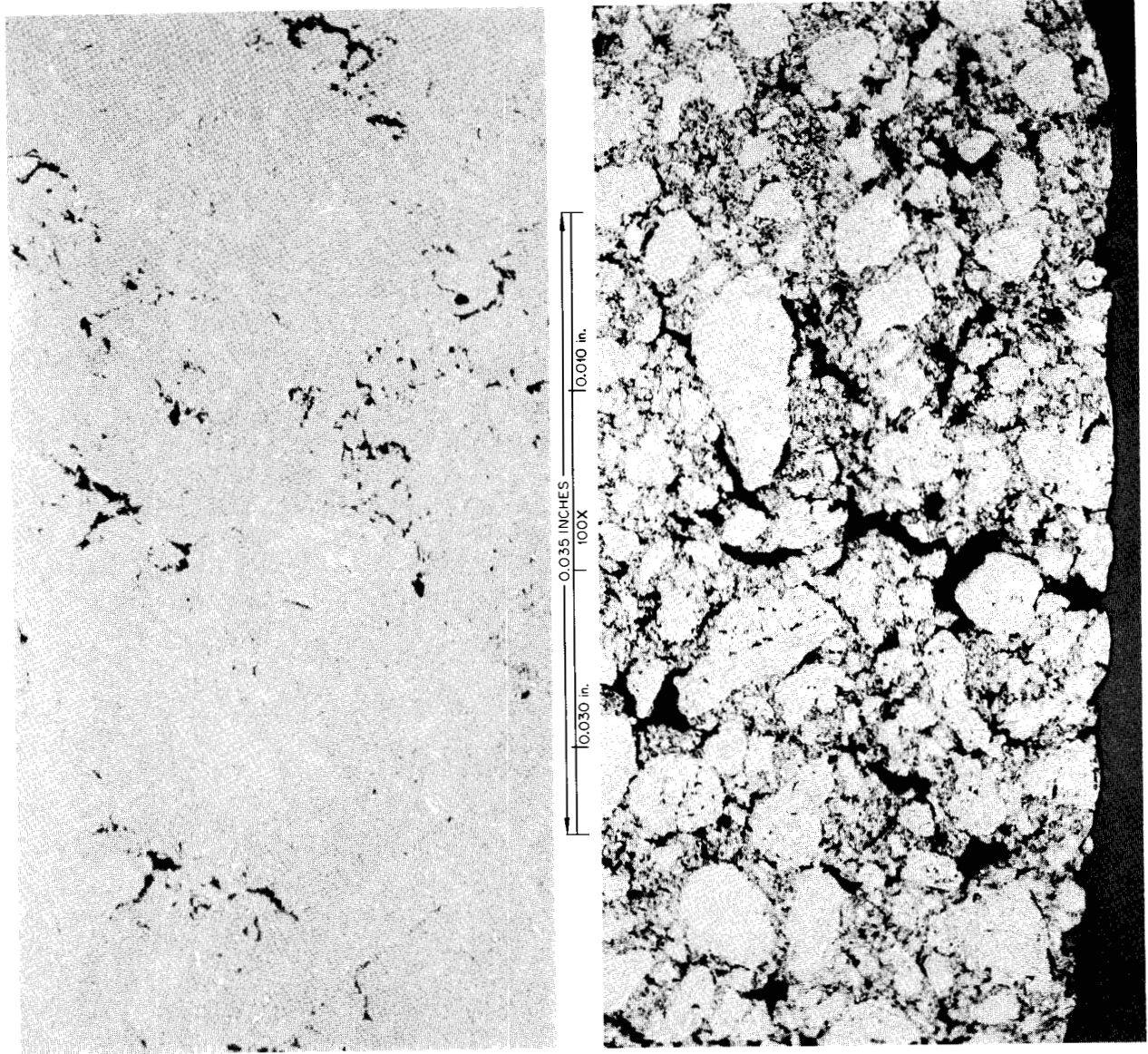


Fig. 39.4. Effect of Irradiation on the Microstructure of an Experimental Graphite. The graphite was made by the Y-12 Plant with a filler of 85% GLCC 1008 and 15% Thermax and a binder of polymerized furfuryl alcohol resin. (a) Unirradiated. (b) Irradiated to  $2.5 \times 10^{22}$  neutrons/cm<sup>2</sup>.

propylene-derived pyrocarbons.<sup>31</sup> Although these pyrocarbons have an initial growth rate at least 20 times that of the best graphite, their dimensional stability under irradiation to  $2 \times 10^{22}$  neutrons/cm<sup>2</sup> is unequalled.

#### Graphite Impregnation

C. B. Pollock R. L. Beatty<sup>32</sup>

We developed<sup>33</sup> a technique by which commercially available graphite can be sealed with pyrolytic carbon

to helium permeabilities less than  $10^{-8}$  cm<sup>2</sup>/sec. A heated piece of graphite is exposed to a gaseous hydrocarbon (1,3-butadiene) between vacuum cycles.

<sup>31</sup>D. M. Hewette II and C. R. Kennedy, *MSR Program Semiann. Progr. Rept. Feb. 28, 1970*, ORNL-4548, pp. 215-18.

<sup>32</sup>Present address: 317 Northeast 47th Street, Seattle, Wash.

<sup>33</sup>D. V. Kiplinger and R. L. Beatty, *MSR Program Semiann. Progr. Rept. Aug. 31, 1968*, ORNL-4344, pp. 230-32.

The pyrolytic carbon coats the walls of exposed pores and thus seals the surface.

During the past year we investigated using a steady flow gas impregnation system rather than the gas-pulse system. Sealing Poco graphite to helium permeabilities of less than  $10^{-8}$  cm<sup>2</sup>/sec required three to five times as long as by the vacuum-pulse technique. However, such a system could be designed to handle several graphite specimens at once and would be simpler and cheaper to scale up.

We are also considering pyrolytic carbon coatings as a sealing material in view of the recent development of a very stable pyrolytic carbon coating material. Consequently, we have coated a number of graphite specimens with pyrolytic carbon in a fluidized bed furnace and are studying ways to scale up the coating process.

We also continued to study scaling up the vacuum-pulse gas impregnation system. One significant problem has been the extremely poor efficiency of gas utiliza-

Y- 97047A

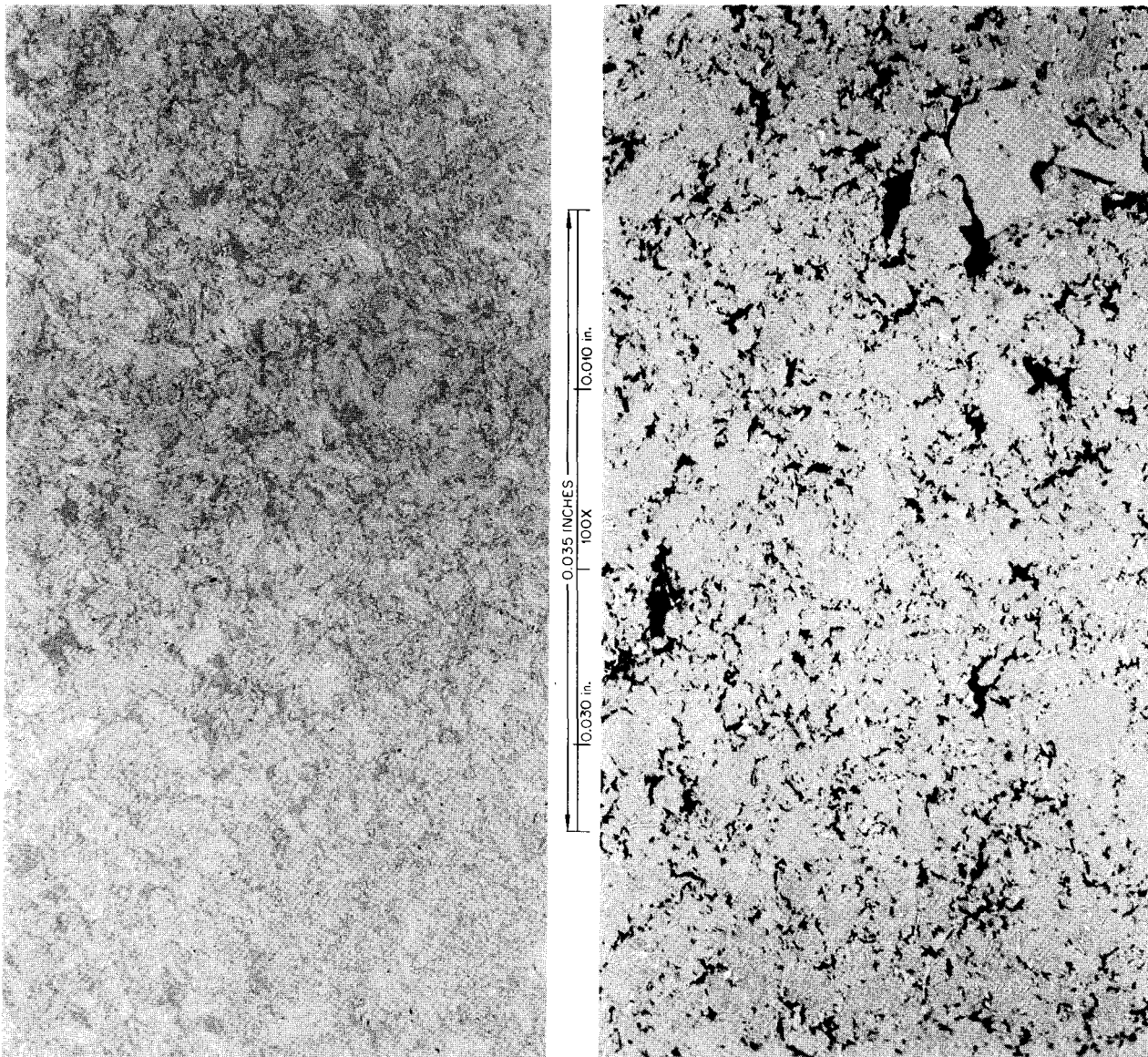


Fig. 39.5. Effect of Irradiation on Microstructure of Graphite Grade 1425, Made by Union Carbide Corporation from Needle Coke and Impregnated. (a) Unirradiated. Dark regions are partially graphitized impregnant. (b) Irradiated to  $2.4 \times 10^{22}$  neutrons/cm<sup>2</sup>. Dark regions are voids.

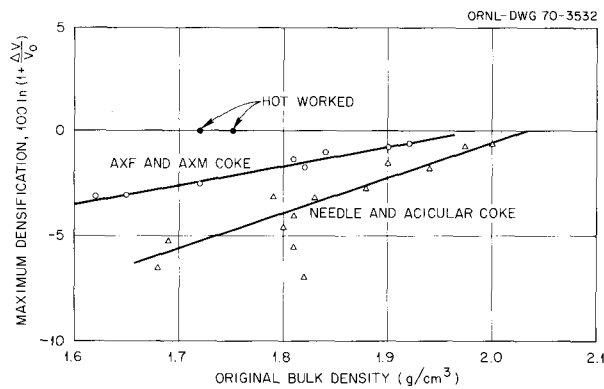


Fig. 39.6. Comparison of Maximum Densification as a Function of Original Density for Isotropic and Anisotropic Graphites Irradiated at 715°C.

tion. The present system deposits carbon only from the portion of the hydrocarbon that is in close proximity to the workpiece, wasting the remainder of the hydrocarbon and the liberated hydrogen. We designed a system that demonstrated the feasibility of collecting the excess hydrocarbon from the waste gas and recycling it through the system. The gas utilization efficiency was increased from less than 5% to greater than 90%.

We completed the third irradiation test of graphite specimens sealed by the vacuum-pulse technique. Specimens were irradiated to fast-neutron fluences of up to  $1.4 \times 10^{22}$  neutrons/cm<sup>2</sup> (>50 keV) at a temperature of 700°C. Increases in helium permeability of up to 1000-fold were observed in some of the specimens at a fluence of approximately  $1 \times 10^{22}$  neutrons/cm<sup>2</sup> (>50 keV) but with virtually no dimensional changes. The important variables appear to be the type of graphite and the fast-neutron fluence. Figure 39.7 illustrates the observed change in helium permeability as a function of fluence. A number of carbon-impregnated graphite specimens from the third irradiation test are being exposed to higher fluences to determine whether the helium permeability continues to increase with fluence.

In the same irradiation experiment we are testing a number of specimens that are coated with pyrolytic carbon. That pyrolytic carbon coatings derived from propylene are dimensionally stable at molten-salt reactor fluences and temperatures was recently demonstrated.<sup>31</sup> Furthermore, since the properties of the coatings and the graphite base stock are similar, we believe that coatings are potentially useful as a sealing material.

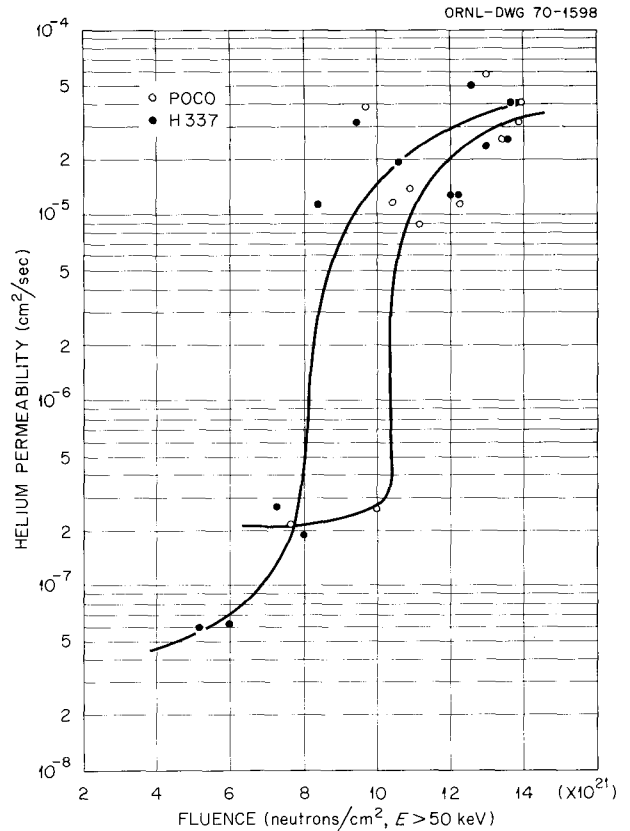


Fig. 39.7. The Change in Helium Permeability of Carbon-Impregnated Graphite Induced by Fast Neutrons at 700°C.

### Thermal Conductivity Apparatus for Graphite

J. P. Moore D. L. McElroy

We constructed a guarded linear heat flow apparatus for measuring the thermal conductivity,  $\lambda$ , electrical resistivity,  $\rho$ , and thermopower of graphite rods from 25 to 700°C. The effects of irradiation will be determined by pre- and postirradiation measurements on samples of H337 and Poco AXF graphite that have been irradiated in HFIR to various fluences from 550 to 750°C.

Figure 39.8 is a schematic drawing of the apparatus showing the placement of the specimen, thermal guards, and thermocouples. This device operates in a variable-pressure inert gas and uses a sample with three measuring sections. Table 39.4 compares the results from 50 to 480°C for an Armco iron thermal conductivity standard as deviations between the measured

ORNL DWG 70-1944

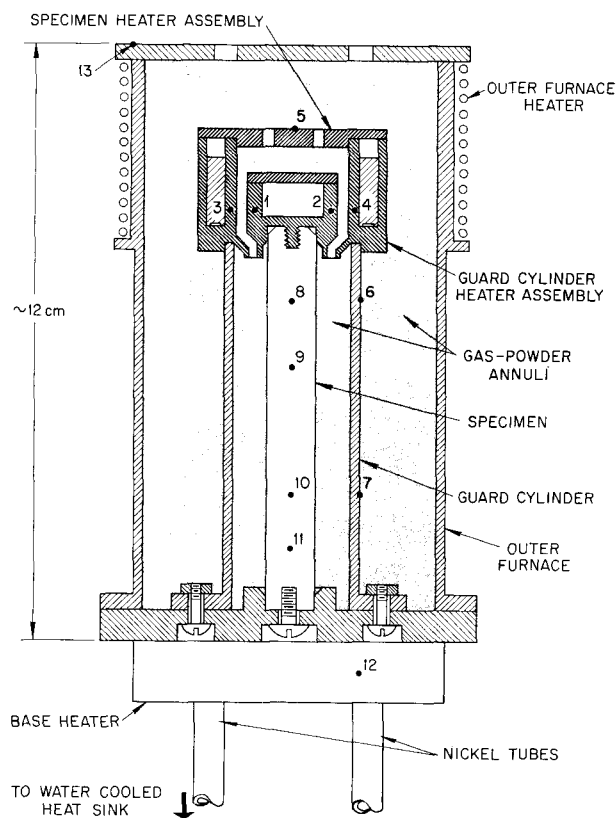


Fig. 39.8. Schematic Drawing of Guarded Linear Heat Flow Apparatus. The numbers designate thermocouple locations.

values of  $\lambda$  and values calculated from the specimen resistivity.<sup>34</sup>

### Electron Microscopy of Graphite

C. S. Yust C. S. Morgan

The structures of both polycrystalline and single-crystal graphites have been examined by transmission electron microscopy. We examined<sup>35</sup> approximately 15 polycrystalline graphite types that were prepared by a mechanical specimen thinning technique developed at ORNL. Regions of common alignment of basal planes, or domains, are observed in the polycrystals, as are cracks and voids. However, the structure is sufficiently

<sup>34</sup>W. Fulkerson, J. P. Moore, and D. L. McElroy, *J. Appl. Phys.* 37, 2639-53 (1966).

<sup>35</sup>C. S. Yust, C. S. Morgan, and H. R. Gaddis, "Transmission Electron Microscopy of Polycrystalline Graphite," to be published in *Carbon*.

complex to mask the details of irradiation damage. To simplify the structure, samples of hot pressed pyrolytic graphite have been studied. A specimen examined had been irradiated to a fluence of  $1.1 \times 10^{22}$  neutrons/cm<sup>2</sup>. Thin flakes obtained by successive cleavage steps were found to be hardened and more rigid after irradiation. Examination in the electron microscope did not reveal dislocation loops such as have previously been reported for irradiated graphite, but did reveal many small features, which appear to be voids, scattered throughout the matrix. These features also tend to gather in linear arrays, apparently delineating regions of slight lattice misorientation. An example of the void-like features is shown in Fig. 39.9. Annealing of the specimen for as long as 6 hr at 1400°C did not appreciably affect the appearance of the structure.

Table 39.4. Performance of Guarded Linear Apparatus Measuring Thermal Conductivity of Armco Iron

Temperature (°C)	Deviation of Average Value from Calculated Value (%)	Spread Between Three Sections (%)
57	+0.5	±1.6
180	+1.4	±1.0
320	+0.9	±0.4
480	+2.1	±0.1

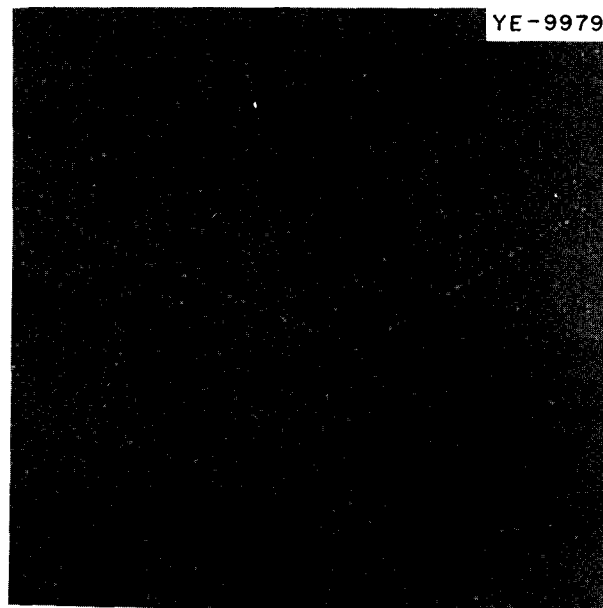


Fig. 39.9. Voidlike Features Observed in Hot-Pressed Pyrolytic Graphite Irradiated to  $1.1 \times 10^{22}$  neutrons/cm<sup>2</sup>. 62,500X.

## CHEMICAL PROCESSING MATERIALS

J. R. DiStefano

The feasibility of a molten salt breeder reactor depends upon extracting protactinium and uranium selectively from a salt that also contains thorium. One technique being investigated is a reductive extraction method in which the salt is contacted with bismuth containing lithium and thorium. Since this requires the containment at 500 to 700°C of both a molten salt fuel and bismuth in a single system, we have begun to investigate the properties of promising materials. Previous results showed that iron- and nickel-base alloys are not suitable because they are too soluble in bismuth. The most corrosion-resistant materials appear to be Mo, W, Re, Ta, and graphite. From comparison of the relative mechanical and oxidation properties of these materials we feel that molybdenum is most promising and we are concentrating on it. We are continuing to study the compatibility of some of the above materials in bismuth and salt environments, studying ways of depositing tungsten and molybdenum onto conventional alloy substrates, and beginning construction of molybdenum test equipment for chemical processing studies.

### Corrosion of Structural Materials in Bismuth

O. B. Cavin J. W. Koger L. R. Trotter

The compatibility of several potential container materials with bismuth was investigated in capsule tests at 600°C for 600 hr and in quartz thermal convection loops operated at a maximum temperature of 700°C with a temperature difference of about 100°C.

We found no measurable attack of Mo, TZM, or Mo-0.5% Ti after exposure to bismuth in the capsule tests and no evidence of mass transfer of molybdenum or TZM specimens from the hot and cold legs of a loop after 3000 hr. Greater than 50 ppm Nb was found in the bismuth from a capsule test containing Nb-1% Zr samples, and mass transfer of niobium plugged a loop containing niobium and Nb-1% Zr in only 115 hr. Bismuth tested with low-carbon steel picked up about 70 ppm Fe, but bismuth exposed to Fe-3% Mo, Fe-5% Mo, and Fe-8% Mo showed no detectable increase in iron in capsule tests. However, metallographic evidence showed attack of the iron-molybdenum alloy samples. Tantalum and graphite are being tested in pure bismuth and molybdenum is being exposed to bismuth containing 100 ppm Li in quartz thermal convection loops.

## Coatings for Corrosion Resistance

J. I. Federer L. E. Poteat

An alternative to the use of difficult-to-fabricate alloys for MSBR reprocessing equipment is to deposit a corrosion-resistant coating, such as tungsten or molybdenum, onto iron- or nickel-base alloys. We are applying tungsten and molybdenum coatings 0.005 to 0.010 in. thick to such materials by hydrogen reduction of  $WF_6$  at 550 to 660°C and  $MoF_6$  at 800 to 900°C.

Tungsten coatings were adherent to nickel, nickel-base alloys, and iron-nickel alloys containing 35 to 50% Ni but not to steels and stainless steels. This is because iron and chromium reduce  $WF_6$  to form nonadherent by-product fluorides at the coating temperature, but nickel does not. However, adherent tungsten coatings were obtained on steels and stainless steels by first electrodepositing a thin nickel coating. The adherence of tungsten coatings to Inconel 600, Hastelloy C, and types 304 and 430 stainless steel was thoroughly investigated, with the following results:

1. Coatings were adherent after 25 cycles between 25 and 600°C.
2. No separation of the coating occurred when coated specimens were bent to a radius of about 1 in.
3. The coatings withstood tensile stresses of 10,000 to 30,000 psi.

We prepared a tungsten-coated vessel for a test with liquid bismuth. We showed that uniform coatings in a complicated substrate could be obtained by pulsing the hydrogen flow, a technique that allows shadowed areas and closed-end tubes to be coated. We coated the inner wall of 0.5-in.-OD tubing with uniformly thick (0.005 in.) tungsten over a length of 4 ft, using a technique that would be applicable to tubing lengths of 20 ft or more.

Our results indicate that tungsten coatings can be applied and are adherent to a variety of iron- and nickel-base alloys. We expect similar results for molybdenum coatings when the coating process is better developed.

### Construction of a Molybdenum Reductive Extraction Test Stand

J. R. DiStefano

In conjunction with the Chemical Technology Division, a molybdenum test stand was designed for studying a continuous method of purifying molten salt mixtures. This first molybdenum loop will countercurrently circulate bismuth and a nonfertile molten-salt mixture through a Raschig-ring-packed column to obtain hydro-

dynamic data relating to column performance. In addition, we shall obtain compatibility data on molybdenum under a variety of experimental conditions.

The overall height of the loop is 15 ft, and it will fit inside a 16-in.-OD stainless steel container. The column will consist of a 1 1/4-in.-OD  $\times$  5-ft-long contacting section and upper and lower liquid disengagement pots 3 7/8 in.  $\times$  1 1/2 to 2 ft. Gas lift pumps will circulate bismuth and salt through the column, and two 3 7/8-in.-OD  $\times$  8-in.-long head pots containing flow metering orifices will be used to control the flow rate. The system will be connected by 1/4-, 3/8-, and 1/2-in.-diam tubing. The following sections describe the fabrication and joining studies relating to the construction of this test stand.

### Fabrication Development of Molybdenum Components

R. E. McDonald A. C. Schaffhauser

We are developing processes to fabricate large-diameter molybdenum closed-end vessels and pipe. These components are not commercially available except by very expensive machining from solid bar stock generally having poor mechanical properties.

To fabricate closed-end vessels we developed a technique in which metal flows into a die and extrudes back over an advancing plunger. A cross section of the back extrusion tooling and its placement in the existing container sleeve of our extrusion press are shown in Fig. 39.10. The tool steel die and plunger are coated with plasma-sprayed  $ZrO_2$ . The advantages of this process are that a simple cylindrical starting blank is used, the vessel geometry can be changed by relatively simple changes in die and plunger design, and a piece can be deformed below the recrystallization temperature to produce a wrought structure having good mechanical properties.

Using our smaller experimental tooling, we fabricated five molybdenum vessels 2.5 in. OD  $\times$  0.25 in. wall thickness, with hemispherical ends having a 3/8-in.-diam boss. The back extrusions were accomplished at 1200 and 1300°C with a stem load of 150 to 300 tons. A wrought microstructure was produced and the metal flow pattern was excellent.

We have used the tooling design shown in Fig. 39.10 to fabricate 4-in.-OD vessels with multiple bosses on the ends to provide support for inlet and exit vessel tubes. A stem load of 750 tons was not sufficient to produce a complete back extrusion over the 8-in.-long plunger for

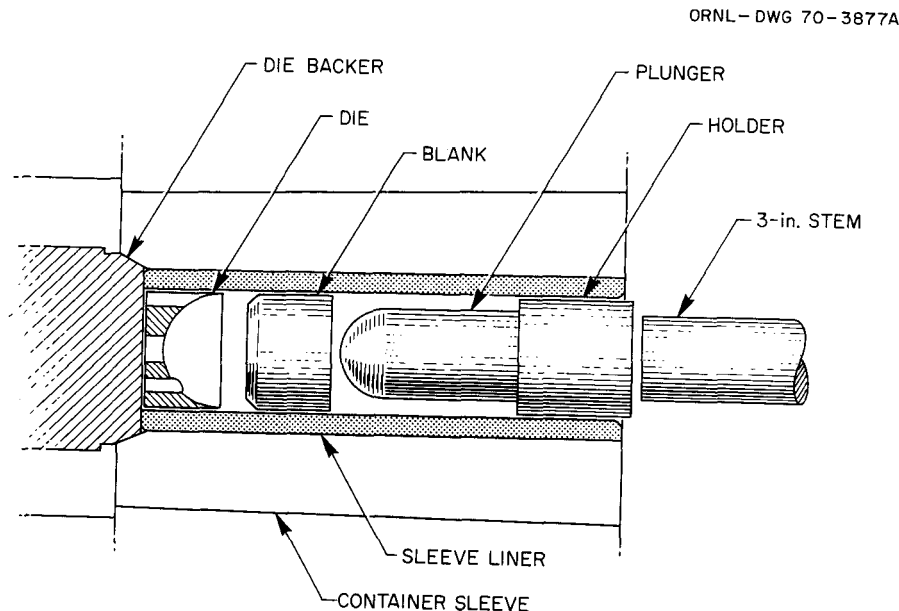


Fig. 39.10. Schematic Presentation of Fabrication by Back Extrusion. The advantages of this process are (1) the final diameter is as large as or larger than the starting blank, (2) the geometry of the final product can be changed by relatively simple changes in die and plunger design, and (3) deformation can be accomplished at temperatures low enough to obtain a wrought structure with most materials.

a blank preheat temperature of 1400°C. However, we can reheat and re-extrude these parts to produce the required vessel length.

The floating-mandrel extrusion technique, which we developed for fabricating refractory metal tubing,<sup>36</sup> is being used to produce 1- to 2-in.-OD molybdenum pipe. Extruded pipes, 1¼ in. OD × ⅛ in. wall thickness × 5 ft long, were successfully fabricated at 1350°C for studying weldability and tube drawing.

### Molybdenum Welding Development

A. J. Moorhead    T. R. Housley

Both tube-to-tube and tube-to-header welds will be required in fabricating the molybdenum test stand. We are developing welding procedures for manual gas tungsten-arc welding, and we began a study using automatic orbiting tungsten-arc equipment for the tube-to-tube butt welds. The orbiting-arc method appears advantageous, both for welding within a welding chamber, where it eliminates the difficulties of multiple-position manual welds, and for field assembly of components because it provides joint alignment and its own inert-gas environment.

The fabrication of molybdenum vessels with hemispherical ends has allowed us to consider both butt and edge joints for the tube-to-header welds. We have successfully welded low-carbon, low-oxygen molybdenum mockup samples using the edge joint by both the gas tungsten-arc (GTA) and electron-beam (EB) processes. Although both techniques produced welds that were helium leaktight, the EB process appears most promising for several reasons: (1) the confining space within the heads makes observation difficult during arc welding, and (2) the relatively low total energy input of the EB process minimizes grain growth, which generally causes a decrease in ductility in the base metal. The edge joint has the advantage (over the butt joint) of providing mechanical support for the tube.

Both ¼-in. and ⅝-in.-OD tubes have been successfully electron-beam welded to ½-in.-thick flat plates simulating the hemispherical end. All welds had helium leak rates below  $1 \times 10^{-9}$  atm cm<sup>3</sup> sec<sup>-1</sup>.

One of the electron-beam-welded tube-to-header joints was back-brazed at 1100°C in vacuum with an iron-base filler metal (Fe-15% Mo-5% Ge-4% C-1%

B) under development at ORNL. This assembly had a helium leak rate below  $1 \times 10^{-9}$  atm cm<sup>3</sup> sec<sup>-1</sup> both after brazing and after two 60-min cycles at 700°C in vacuum.

### Development of Bismuth-Resistant Filler Metals for Brazing Molybdenum

N. C. Cole    J. W. Koger    R. W. Gunkel<sup>37</sup>

Brazing also provides an attractive means for fabricating certain portions of the molybdenum test stand, and we are developing and evaluating brazing alloys to meet the stringent requirements for this application. Many commercially available brazing filler metals have been used to join molybdenum; however, none are compatible with both bismuth and fluoride salts. Although the primary requirement of a braze alloy is corrosion resistance, we are also concerned with developing an alloy that will melt at a temperature at or below the recrystallization temperature of molybdenum to avoid impairing the ductility of the joint.

We have devised several iron-base alloys that effectively braze molybdenum and its alloys in the desired range of 1050 to 1350°C. The three most promising brazing alloy systems are Fe-C-B, Fe-Mo-C-B, and Fe-Mo-Ge-C-B, and alloys from each system were tested in molten bismuth at 600°C for approximately 700 hr. Braze alloys from the Fe-C-B system suffered varying amounts of attack depending on the test conditions and joint design. However, the regions within each braze next to the molybdenum base metal were corrosion resistant because molybdenum dissolved into the braze.<sup>38,39</sup> To determine the effect of adding molybdenum to the Fe-C-B system, two brazes from an Fe-Mo-C-B system were also tested in bismuth as described above. The addition of molybdenum definitely improved the corrosion resistance, and one of these brazes is shown in Fig. 39.11. There appears to be very little attack of the brazed joint, but chemical analysis of the bismuth<sup>40</sup> showed 50 ppm Fe.

<sup>37</sup>Present address, Cabot Corp., Kokomo, Ind.

<sup>38</sup>R. W. Gunkel, N. C. Cole, and J. W. Koger, *MSR Program Semiann. Progr. Rept. Aug. 31, 1969*, ORNL-4449, pp. 211-12.

<sup>39</sup>N. C. Cole, J. W. Koger, and R. W. Gunkel, *MSR Program Semiann. Progr. Rept. Feb. 28, 1970*, ORNL-4548, pp. 255-58.

<sup>40</sup>N. C. Cole, R. W. Gunkel, and G. M. Slaughter, "Joining of Molybdenum and Its Alloys," presented at Spring Meeting of the Metallurgical Society of AIME, Las Vegas, Nev., May 11-14, 1970.

<sup>36</sup>R. E. McDonald and G. A. Reimann, *Floating-Mandrel Extrusion of Tungsten and Tungsten-Alloy Tubing*, ORNL-4210 (February 1968).

An experimental composition in the Fe-Mo-Ge-C-B system appears to show the most promise for our application. Not only does it wet the molybdenum, but it flows at the lowest temperature (1100°C) and also

appears to be the most corrosion resistant (Fig. 39.12). There was no metallographic evidence of attack, and chemical analysis of the bismuth after test showed only 10 ppm Fe and less than 3 ppm Ge.

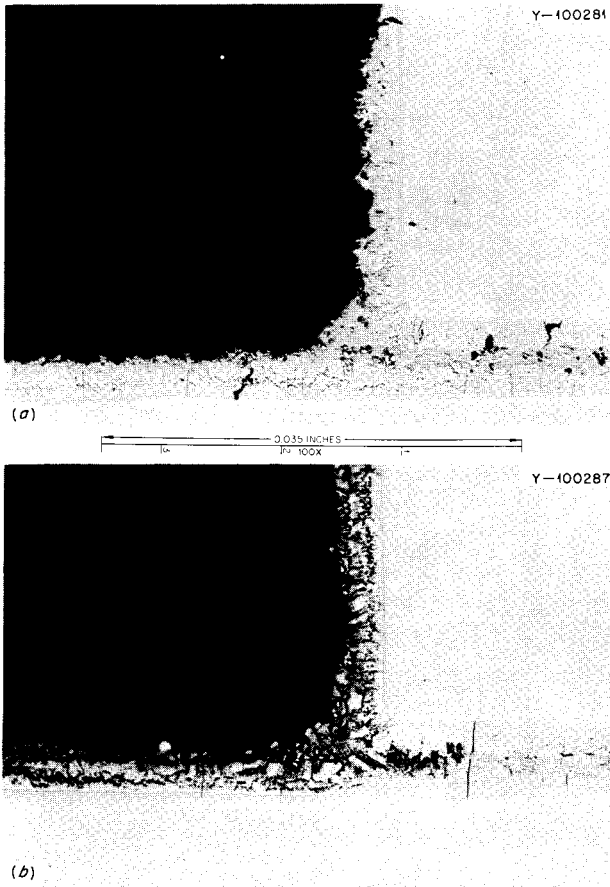


Fig. 39.11. Molybdenum Brazed with Fe-Mo-C-B Braze Alloy. (a) As brazed. (b) After testing in bismuth at 600°C for 644 hr. As polished.

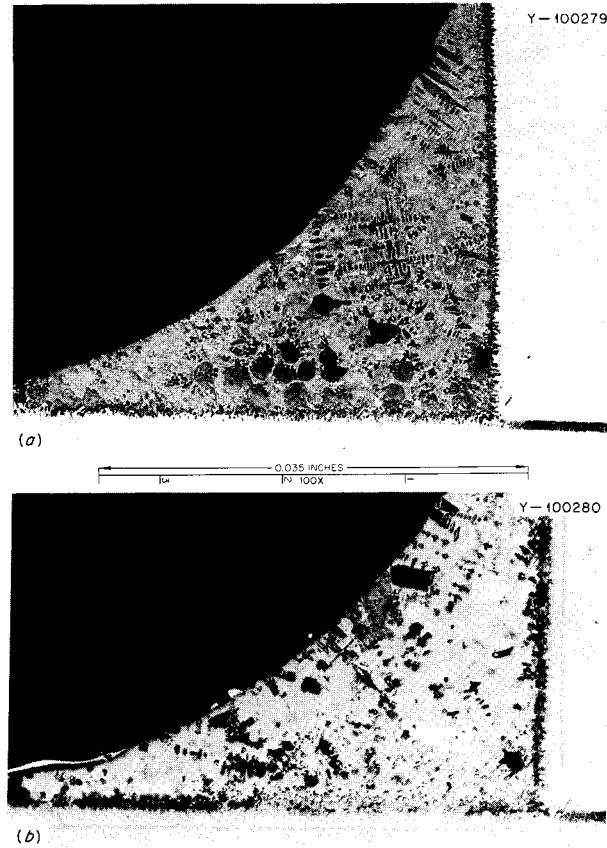


Fig. 39.12. Molybdenum Brazed with Fe-Mo-Ge-C-B Filler Metal. (a) As brazed. (b) After testing in bismuth at 600°C for 644 hr. As polished.

## 40. Reactor Evaluation

A. L. Lotts

Our purposes are to derive and maintain up-to-date methods for predicting the performance, capabilities, and cost of fuel fabrication for fuel elements of various designs and to evaluate reactor concepts of current interest. The fuel element performance and cost are significant factors in the economic production of power by nuclear reactors and must be examined in detail to assess the potential of any reactor concept. Thus, we contribute to reactor evaluation by assessing fuel cycle costs and determining the performance limits of the fuels that are envisioned by the reactor designer. The engineer is able to incorporate the assessment into his overall evaluation.

This year we continued effort to improve the computer programs for cost analysis, performed a number of cost analyses on reactor fuel elements and on various fuel element fabrication processes, investigated the release of fission gases from mixed oxide  $[(U,Pu)O_2]$  fuels, accumulated data on the physical and tensile properties of type 316 stainless steel, and assessed the nuclear performance feasibility of molybdenum fuel cladding in an LMFBR.

### COMPUTER PROGRAM DEVELOPMENT FOR COST ANALYSIS

F. J. Homan    C. R. Reese

Fuel fabrication cost is estimated by use of computer programs to ensure consistency in estimating practice for the different types of fuel elements and different times for which the estimates are made. During the past year two modifications were made to the basic computer code<sup>1</sup> for fabrication cost analysis. The pelletization subroutine was rewritten with revised cost informa-

<sup>1</sup>For a description of the basic code, see A. L. Lotts, T. N. Washburn, and F. J. Homan, *FABCOST 9, A Computer Code for Estimating Fabrication Costs for Rod-Bundle Fuel Elements*, ORNL-4287 (August 1968).

tion. Before the revision, pelletization costs were based on a 1962 study<sup>2</sup> and all pelletizing costs were lumped together, making it difficult to separate costs and manpower requirements for individual steps within the pelletization process. The revised analysis includes a breakdown of the equipment costs and manpower requirements for each step on the flowsheet, making the cost estimates for pelletization compatible in format with the other processes considered in the code. The revised subroutine results in somewhat lower cost estimates.

The other modification to the code involves estimates for fuel element hardware costs. Previously, only stainless steel, Zircaloy, and aluminum could be considered as cladding and structural materials. But additional data have been added so that costs with Haynes alloy No. 25, Nb-1% Zr, and molybdenum cladding and structures can now be estimated.

### FUEL FABRICATION COST ANALYSIS

A. L. Lotts

As a part of the overall approach to reducing power costs, we evaluate fuel fabrication costs as they relate to the fuel cycle component of total power costs. Fabrication procedures and flowsheets are selected and analyzed for capital and operating increments at each point in the processes, and the results are stored in the computer program along with estimated hardware costs for a wide range of production rates. The input parameters for the computer code for each concept to be estimated are based upon the specific design, the fabrication process desired, and the financial data and requirements and ground rules for the particular study.

During the past year we conducted a number of studies aimed at optimizing the cores of the gas-cooled

<sup>2</sup>Kaiser Engineers, *Guide to Nuclear Power Cost Evaluation, Vol. 4 (Fuel Cycle Costs)*, TID-7024 (March 1962).

fast reactor and the LMFBR. In addition, we cooperated with the AEC Systems Analysis Task Force (SATF) in evaluating several other reactor designs. We also assisted in defining proper practice for the conversion processes for LMFBR fuel materials, and we participated in the revisions to the report to be issued by the AEC Fuel Recycle Task Force (FRTF). Further, a cost comparison of four alternate routes for fabricating  $(U,Pu)O_2$  fuel for LMFBR's was completed.

#### Parametric Study of GCFR Fuel Fabrication Costs

F. J. Homan

An extensive parametric study considering a variety of fuel pin outside diameters, array sizes, and core lengths was performed for GCFR core optimization. We ran 90 separate cases for core and blanket to provide fabrication cost coefficients for the evaluation of a large gas-cooled fast reactor.

#### Alternate Cladding Fabrication Analysis

F. J. Homan    C. R. Reese  
A. L. Lotts

A study to determine the fuel fabrication costs associated with the use of alternate materials<sup>3</sup> for fuel pin cladding and structural hardware in an LMFBR was performed for the Studies and Evaluation Group. Cost coefficients were provided for use in their overall analysis.

#### Systems Analysis Study

F. J. Homan

Fabrication cost estimates were made as part of the AEC SATF comparative evaluation of several competing reactor concepts. Included in the study were the  $UO_2$ -fueled PWR, the plutonium recycle PWR, the advanced oxide LMFBR, the HTGR, and the GEAP-5678 oxide LMFBR. Fabrication cost parameters were provided the SATF.

#### Fuel Recycle Task Force

A. L. Lotts

We have continued to participate in the AEC FRTF activities as a part of their contribution toward updating *Civilian Nuclear Power, A Report to the President* —

<sup>3</sup>The primary cladding and fuel element hardware material is type 316 stainless steel. The alternate materials are Haynes alloy No. 25, Nb-1% Zr, and molybdenum.

1962. Previously, we had developed fuel fabrication cost estimates for approximately 40 reactor concepts considered in the FRTF study. These concepts were for a wide range of reactor designs. The primary effort this year has been to continue to check the calculated results against available data and to revise the manuscript according to the comments submitted by members of the FRTF. The report<sup>4</sup> is now in the final stage of publication.

#### LMFBR Fuel Material Conversion Process

W. H. Pechin    C. R. Reese

A joint program with the Chemical Technology Division was undertaken to study the economic and safety aspects of transporting various fuel forms between an LMFBR fuel reprocessing plant and a refabrication plant. A report has been prepared and will be issued soon.<sup>5</sup> Our contribution details the fuel refabrication process. Considered in this chapter were fuel materials specifications, receiving and unpackaging considerations, and the effects of scrap recycle.

#### Cost Comparison of Four Alternate Routes for Fabricating $(U,Pu)O_2$ Fuel for LMFBR's

F. E. Harrington<sup>6</sup>    R. B. Pratt<sup>7</sup>  
J. D. Sease

Four conversion-fabrication plants were investigated to determine the source and magnitude of cost differences in some of the more promising approaches to closing the  $(U,Pu)O_2$  fuel cycle. These were: mechanical blend pellet, coprecipitation pellet, sol-gel pellet, and sol-gel U-Fine Sphere-Pac. Each plant started with  $UF_6$  from diffusion plant tails and plutonium nitrate solution from reprocessing to produce LMFBR oxide core fuel elements. The plants were assumed to produce 500 kg of heavy metal core material in finished elements for 260 days each year.

The estimated cost of finished fuel elements resulted in a saving of about \$23/kg heavy metal for the Sphere-Pac plant over the three pellet plants. This savings resulted primarily from lower losses and scrap recovery requirements (\$12.42/kg) and lower capital

<sup>4</sup>*Reactor Fuel Cycle Costs for Nuclear Power Evaluation*, WASH-1099 (to be published).

<sup>5</sup>Paul A. Haas, *LMFBR Fuel Materials Conversion Development: A Partial Technical Evaluation*, ORNL-TM-3071 (to be published).

<sup>6</sup>Chemical Technology Division.

<sup>7</sup>Present address: Autoclave Engineers, Inc., Erie, Pa. 16512.

charges (\$2.45/kg). The above totals include an estimated \$2.89/kg higher cost for the pin loading step by U-Fine Sphere-Pac over the conventional route. This economic study is described in detail elsewhere.<sup>8</sup>

### FUEL PERFORMANCE ANALYSIS

C. M. Cox

Last year we reported in this chapter the preliminary work of fuel performance modeling, which is aimed at the development of a comprehensive model to enable the systematic, rapid, and accurate analysis of fuel element designs. This year the fuel performance modeling work is reported in Chapter 17.

The principal activities under reactor evaluation have involved the collection of data on fission gas release from mixed oxide fuels and on the mechanical properties of type 316 stainless steel and an analysis of the feasibility of using molybdenum fuel cladding in an LMFBR.

#### The Release of Fission Gases from Mixed Oxide Fuels

W. H. Bridges

The survey of fission gas release from mixed oxide fuels<sup>9</sup> is being continued and extended. The data developed will aid in the extension of the fuel modeling concepts currently under consideration. To examine the validity of probable release values with experimentally observed release, the PRØFIL program<sup>10</sup> has been modified to determine the release from the fuel pin regions at various temperatures and densification factors. The results so obtained will be statistically compared with the observed values to converge on the most significant fabrication and operation values.

#### The Physical and Tensile Properties of Type 316 Stainless Steel

W. H. Bridges

Available data on the physical and tensile properties of type 316 stainless steel were compiled.<sup>11</sup> The physical properties cover the density, melting range, specific heat, thermal expansion, thermal conductivity, thermal diffusivity, emissivity, and electric resistivity. The tensile properties include the room- and elevated-temperature tensile and yield strengths, Poisson's ratio, modulus of elasticity, and ductility. The available information has been developed in the light of effects of influencing factors — such as cold work, sodium and gas environments, and, in particular, irradiation — on the various properties.

A continuation of this effort will include the creep and stress-rupture properties, fatigue, and other mechanical properties of value in reactor design and modeling studies.

### Nuclear Performance Feasibility of Molybdenum Fuel Cladding in an LMFBR

C. M. Cox

The literature was reviewed to make a preliminary evaluation of the nuclear characteristics of an LMFBR, using molybdenum rather than stainless steel cladding. This work was part of a more comprehensive analysis<sup>12</sup> of the potential of using molybdenum as structural material in an LMFBR. Due to the larger molybdenum capture cross sections (typically 12 times that of type 316 stainless steel on an equal volume basis), the fuel requires a higher fissile enrichment to operate at the same power density, and the neutron energy spectrum is harder. The consequences are a lower breeding ratio, lower specific power, and less favorable reactivity coefficients.

We concluded from this preliminary review that the nuclear characteristics of an LMFBR with molybdenum cladding indicated questionable economic feasibility although an optimized reactor design might prove feasible.

A more detailed study, including fuel cycle calculations, was recommended to reevaluate this feasibility with the constraint that the sodium void and Doppler reactivity coefficients must be conservative. The latter requirements may lead to a pancake or modular geometry core with adverse economic effects.

### Metals and Ceramics Division Information Activities

W. H. Bridges    Meredith R. Hill

The Division's bibliography for the calendar year 1969 has been completed. The subject indexing has

<sup>8</sup>F. E. Harrington, R. W. Horton, R. B. Pratt, and J. D. Sease, *Cost Study of Four Alternate Routes for LMFBR Fuel Material Preparation and Element Fabrication*, ORNL-TM-2813 (February 1970).

<sup>9</sup>C. M. Cox, "The Irradiation Performance of Uranium-Plutonium Oxide Fuel Pins," *Nucl. Safety* 10, 380-91 (1969).

<sup>10</sup>C. M. Cox and F. J. Homan, *PRØFIL - A One-Dimensional FØRTRAN IV Program for Computing Steady-State Temperature Distributions in Cylindrical Ceramic Fuels*, ORNL-TM-2443 (March 1969); ORNL-TM-2443, Addendum (August 1969).

<sup>11</sup>W. H. Bridges, *The Physical and Tensile Properties of Type 316 Stainless Steel*, ORNL-TM-3037 (in press).

<sup>12</sup>W. R. Martin *et al.*, *Molybdenum for LMFBR Cladding - Technical Review and Evaluation*, ORNL report in preparation.

been done by a modified computer program developed by the Information Systems Group at the Computer Technology Center for the subject indexing of Nuclear Science Abstracts. The revised bibliography through 1968 was issued.<sup>13</sup>

An agreement with the Technical Information Division at the Laboratory for the procurement of exter-

nally originated bibliographic information computer tapes has been made. During the initial phase, tapes from Metals Abstracts, as issued by the American Society for Metals, will be scanned on a regular basis and fitted to interest profiles developed for individuals and groups in the Metals and Ceramics Division. Search and retrieval codes are being programmed by the Information Systems Group. If the test phase meets with success and acceptance, tapes from other outside organizations will be obtained and other Laboratory divisions included in the search program.

---

<sup>13</sup>*Bibliography of the Technical Literature of the Metals and Ceramics Division for the Period 1948 Through 1968*, ORNL-4270, Vol. 1, Rev. (November 1969).

## 41. Thorium Utilization

A. L. Lotts

The objective of the Thorium Utilization Program currently in progress in the Chemical Technology and Metals and Ceramics Divisions is to provide the necessary development for the Th-<sup>233</sup>U fuel cycle for the High-Temperature Gas-Cooled Reactor. The ultimate aim of the program is to demonstrate economic fuel recycle techniques for this reactor in a pilot-scale facility, the Thorium-Uranium Recycle Facility at ORNL. The program in the Metals and Ceramics Division consists of refabrication process development on an engineering scale, development of remote pilot-scale equipment that can be used in the TURF, and irradiation of fuels produced in engineering-scale equipment. The program utilizes extensively technology developed in the Gas-Cooled Reactor Program, the progress for which is reported in Chapter 36.

Equipment and processes are being developed to enable us to fabricate 10 kg/day of oxide fuel into the prismatic graphite fuel blocks used in the HTGR. During the past year we again concentrated on handling particulate fuels, coating the fuel particles, and bonding these particles into fuel sticks. A large number of particles and fuel sticks were fabricated for irradiation of Recycle Test Elements in the Peach Bottom Reactor. In addition, other irradiation tests were designed for the fuels fabricated in the pilot-scale equipment. Funding limitations have limited the level of effort that has been given to the engineering and construction of equipment. The primary emphasis in our process development has been to use existing equipment.

### THORIUM-URANIUM RECYCLE FACILITY

J. M. Chandler<sup>1</sup> J. D. Sease

The Thorium-Uranium Recycle Facility was constructed to enable processing of thorium fuels con-

taining, as an impurity, high quantities of <sup>232</sup>U, a material necessitating heavy shielding. The facility is of sufficient size that a number of processes can be developed and evaluated simultaneously at pilot-scale level. During the past year we emphasized maintaining the operational readiness of the TURF and decontaminating the cell that had been used for preparation of <sup>233</sup>U-bearing salt for the Molten-Salt Reactor Experiment.

### Status of TURF

J. M. Chandler<sup>1</sup>

We maintained the TURF equipment in operational readiness in support of the heavily shielded cell bank designed for the remote maintenance and operation of the in-cell process equipment. To do this we altered or replaced some faulty electrical motors, revised some ventilation control instrumentation, and added some equipment to better fit the expected needs. All changes were based on the results of tests made of the existing equipment pieces, individually or in functional groups. For example, the emergency power supply was revised to provide power to the large 75-hp air compressor because the small air compressor, originally connected to the emergency diesel electric generator output, will not produce the air flow needed.

Cell B outlet filters were replaced to permit a test of a "MICRETAIN" filter of the same quality as, but less costly than, the filters originally installed. One MICRETAIN filter was installed in cell B adjacent to two Cambridge Company filters of the original type so performance could be compared under the same service conditions.

The filters that were removed from cell B after about one year service contained a total of 14.8 lb of dirt, about 5 lb per filter. There was no evidence of a decrease in the effectiveness of these filters, but there was a 10% increase in pressure drop across the dirty filters.

<sup>1</sup>On loan from Chemical Technology Division.

The cell G pump room has been altered to provide work space and off-gas and waste handling equipment for a glove box installation there.

The Pyrex glass Raschig ring monitoring string in the waste tank C-6-T was removed for annual inspection. We saw no deterioration of the glass rings from one year's exposure to various acid and basic solutions and no evidence of breakage. However, redesign of the method for removal of the monitoring strings is necessary if they are to be removed safely after becoming highly contaminated. This was done and the new withdrawal system was installed. We will demonstrate its effectiveness when we next check safety of the rings.

The in-cell television camera and out-of-cell monitor were tested. A clear image was displayed on the monitor. However, two motor clutches inside the camera failed. This camera had not been used before; it is now being repaired. The solids sampler system serving cells C and D was tested and found ready for service. This system pneumatically propels a sample container (rabbit) from an in-cell sample transfer station (ball valve) to a shielded work station atop the cell.

Cell G, which was used for the  $^{233}\text{UF}_4\text{-}^7\text{LiF}$  (MSRE) fuel preparation, became contaminated; it was cleaned and decontaminated after the  $^{233}\text{U}$  product was removed from the cell. All the surplus LiF-27 mole %  $\text{UF}_4$  product was stored in Building 3019. The cell was cleaned preparatory to installation of equipment for isolating isotopically pure  $^{248}\text{Cm}$  separated from the  $^{252}\text{Cf}$  precursor. The cell was cleaned in three phases according to detailed written procedures. Successful completion without spread of contamination outside the highly contaminated cell is an example of the effectiveness of written operation procedures for such work.

Cell G was smeared in January 1970 to measure the transferable radioactivity present on the internal surfaces. The smears ranged from 40 to 500 dis/min and averaged about 300 dis/min, which is in good agreement with earlier smear results and well below the  $10^6$  dis/min found at the completion of the MSRE fuel preparation program. These low levels of contamination avoided remote installation of new process equipment.

The efforts to place the in-cell  $\text{CO}_2$  fire protection system in condition for acceptancy test by the Factory Mutual Company continued. This is a rather extensive job, requiring modification to the  $\text{CO}_2$  piping, to some structural parts in cell A, and to the ventilation control system of cells A and E. The system is unique in that gaseous rather than liquid  $\text{CO}_2$  is supplied to the cell on

fire. This type system places added burden on the cell ventilation flow and pressure control equipment. The cell  $\text{CO}_2$  fire protection system was altered after an unsuccessful attempt in September 1969 to get acceptance for preferred risk protection. Recent tests have been successful, and we plan to present our data to Factory Mutual. Our data, along with on-site spot checks of the TURF  $\text{CO}_2$  fire protection system, will be used as the basis for acceptance for preferred protection by Factory Mutual.

### Initiation of HTGR Recycle Operations

F. J. Furman

To plan the development of advanced power reactor fuel cycles, we must set goals that are consistent with the needs of the power industry. Last year we described how to estimate the economically optimum time to start fuel recycle operations in a growing high-temperature gas-cooled reactor industry.<sup>2,3</sup> We will use this information to schedule the development of processes and equipment for a demonstration of HTGR recycle in TURF before the availability of large-scale commercial HTGR recycle facilities.

Additional growth cases have been calculated and confirm the previous results. Absolute values of fuel cycle costs obtained agree with recently published values.<sup>4</sup> If the first of a series of large [approximately 1000 Mw(electric)] HTGR's is completed in 1976, the recycle of fuel would most profitably start in 1983.

### FUELED-GRAPHITE DEVELOPMENT

F. J. Furman J. D. Sease

Our objective is to perform the development necessary to design and operate the remote refabrication line to be installed in TURF to demonstrate the recycle of HTGR fuel. This year our major effort was in testing the prototype remote coating furnace and in coating particles for the Recycle Test Elements (RTE's) for irradiation testing in the Peach Bottom Reactor. Other development areas are particle handling, particle in-

<sup>2</sup>F. J. Furman, *Metals and Ceramics Div. Ann. Progr. Rept. June 30, 1969*, ORNL-4470, p. 200.

<sup>3</sup>F. J. Furman, R. B. Pratt, and A. L. Lotts, *Prediction of the Economically Optimum Time to Initiate Recycle for the High-Temperature Gas-Cooled Reactor Industry Using Computer Program DELAY*, ORNL-TM-2704 (December 1969).

<sup>4</sup>*An Evaluation of High-Temperature Gas-Cooled Reactors*, WASH-1085 (December 1969).

spection, and fuel particle bonding. A general review of our fueled-graphite development has been presented.<sup>5</sup>

### Particle Handling

In TURF over 10 kg/day of particles will have to be remotely sized, shape separated, sampled, and transferred. Devices for most of these operations have been described in detail,<sup>6</sup> and recent work has been directed toward perfecting the devices described. In addition, a particle sampling device and pneumatic particle transfer using an air pulsing technique were developed.<sup>7</sup>

### Particle Coating

Deposition of pyrolytic carbon on fuel particles is a key operation in fabrication of HTGR fuel elements. The 5-in.-diam prototype remote coating system<sup>8</sup> was placed into operation. The initial shakedown was extremely smooth for a device with such complexity. Only minor modifications were necessary to coat the material for the RTE's. The coating parameters for the prototype furnace correlated well with those found for our laboratory 5-in.-diam coater.<sup>9</sup> The coating of the RTE's is described later in this chapter.

### Particle Inspection

A production facility, such as we are planning for HTGR recycle fuel, must have immediate inspection of its product to minimize scrap production. In TURF the particles will be sampled both before and after each coating operation. The sample will be pneumatically transferred to a glove box where it will be immediately inspected by the light-blockage particle-size analyzer,<sup>8</sup> which we are currently developing. We have come closer to our goal of rapidly determining the mean diameter of batches of microspheres with an accuracy at 1%. We

<sup>5</sup>F. J. Furman, J. D. Sease, and A. L. Lotts, "Economics and Technology of High Temperature Gas-Cooled Reactor Fuel Refabrication," pp. 281-308 in *Proceedings of Symposium on Sol-Gel Processes and Reactor Fuel Cycles, Gatlinburg, Tennessee, May 4-7, 1970*, CONF-700502.

<sup>6</sup>F. J. Furman, J. T. Meador, and J. D. Sease, *Microsphere Handling Techniques*, ORNL-TM-2782 (March 1970).

<sup>7</sup>F. J. Furman, "Particle Handling," *Status and Progress Report for Thorium Fuel Cycle Development Jan. 1, 1969-March 31, 1970*, in preparation.

<sup>8</sup>F. J. Furman and J. D. Sease, *Metals and Ceramics Div. Ann. Progr. Rept. June 30, 1969*, ORNL-4470, pp. 205-6.

<sup>9</sup>R. B. Pratt, J. D. Sease, W. H. Pechin, and A. L. Lotts, "Pyrolytic Carbon Coating in an Engineering-Scale System," *Nucl. Appl.* 6, 241-55 (1969).

eliminated drift of the critical voltage supplies in the instrumentation to enable us to operate for extended periods without recalibrating.

### Bonding of Fuel Particles

The reference HTGR fuel consists of the coated fuel particles bonded into sticks. This design allows the fuel to be inspected for homogeneity before insertion into the graphite blocks and prevents the particles from spilling if the block should break. The particles are currently bonded with coal tar pitch filled with carbon flour.

To make acceptable fuel sticks, the recycle particles must be accurately blended with fertile ( $\text{ThC}_2$ ) particles. Since the particles differ in size and density, this step is extremely difficult. To facilitate this operation, we have designed and are now fabricating a loader-blender, a device for concurrently blending two or more types of particles while loading a fuel stick mold. The particles pour out of hoppers with orifices adjusted by stepping motors, which permit the particle flow rate to be accurately set remotely.

### FABRICATION OF RECYCLE TEST ELEMENTS

F. J. Furman    J. D. Sease    W. H. Pechin

A program was initiated cooperatively by Gulf General Atomic (GGA) and ORNL to irradiate prototype Recycle Test Elements (RTE) in the Peach Bottom Reactor. During this year we fabricated, coated, and bonded a number of different types of fuel particles for the RTE program, described later in this chapter.

### Coating of Recycle Test Element Fuel

F. J. Furman    W. H. Pechin

We have coated approximately 13 kg of reference HTGR recycle fuel particles. The noteworthy features of this fuel are that, besides being of the reference recycle design, it was coated in the prototype<sup>8</sup> of the furnace to be used in TURF and the quantity is sufficient to supply the needs of the reprocessing studies on irradiated fuels. The reference recycle coatings are of the "BISO" or two-layer type as shown in Fig. 41.1. For the RTE's we produced the reference particle except for the substitution of  $^{235}\text{U}$  for the  $^{233}\text{U}$ . We applied the inner coating by the thermal decomposition of acetylene diluted with helium and the outer coating by the decomposition of propylene. In addition, quantities of  $\text{ThO}_2$  were produced with reference coatings to be used as fertile particles.

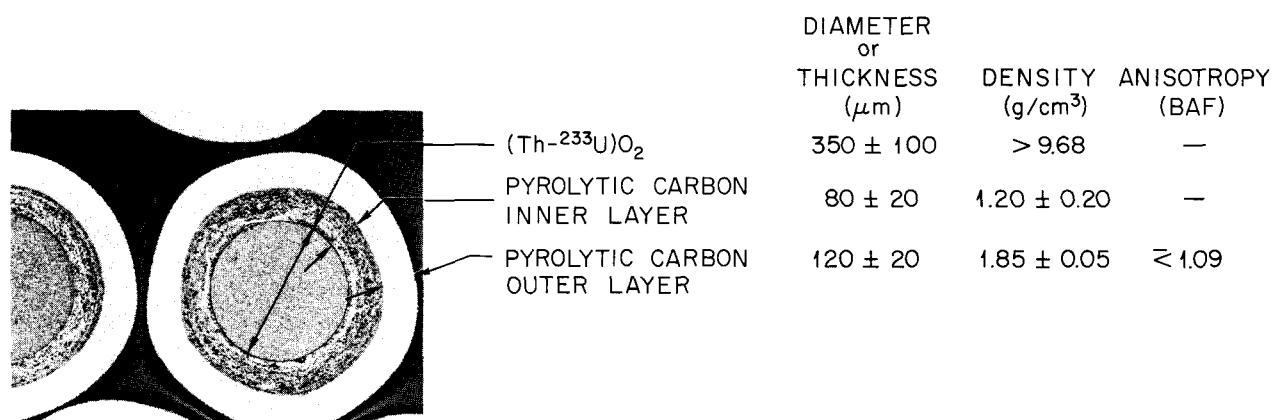


Fig. 41.1. Reference Recycle Particle.

### Bonding of Recycle Test Element Fuel

J M Robbins    D. M. Hewette II    J. H. Coobs

We supplied a portion of the RTE's to be operated in the Peach Bottom Reactor starting in July 1970. Our part was fabricated by bonding the beds of mixed coated particles with 30 to 40 wt % Poco graphite flour in 15V pitch. Particle beds are blended by coincident feeding of weighed charges. The requirement of RTE's from ORNL is shown in Table 41.1. All uranium-bearing particles are 93%-enriched in <sup>235</sup>U.

### HTGR RECYCLE FUELS IRRADIATION

T. N. Washburn    R. B. Fitts    A. R. Olsen

The irradiation tests on the HTGR recycle program have two main objectives: (1) to provide irradiated fuel for head-end process studies, and (2) to provide irradiation proof tests of the products of coated particle process development for the Thorium-Uranium Recycle

Table 41.1. Fuel Stick Fabrication Requirements for Recycle Test Elements

Type Particles	Number of 2.14-in.-long Sticks		
	1st Group	2nd Group	Total
(Th-20% U)O <sub>2</sub>	72	96	168
(Th-33% U)O <sub>2</sub> + ThO <sub>2</sub>	72	96	168
(Th-33% U)O <sub>2</sub> + ThC <sub>2</sub>	168	144	312
UO <sub>2</sub> + ThO <sub>2</sub>	120	96	216
Total	432	432	864

Facility. The test conditions of interest include fuel temperatures between 600 and 1300°C, burnup to 20% FIMA in the (Th,U)O<sub>2</sub> particles, and fast fluence exposures up to  $8 \times 10^{21}$  neutrons/cm<sup>2</sup>.

The first two stages in this program were implemented this year. They are: (1) the start of accelerated-burnup capsule irradiations, and (2) fabrication of eight test fuel elements to be irradiated in the Peach Bottom Reactor.

### Capsule Irradiations

A. R. Olsen

The fuel performance in an HTGR is a complex interaction of fuel burnup and fast neutron irradiation damage to the pyrolytic carbon coatings on the fuel and to the carbonaceous bonding material. The relative proportions of burnup effects and fast neutron damage are determined by the time and temperature of irradiation and the neutron energy spectrum. In a commercial HTGR the spectrum is such that the thermal and fast (>1 MeV) neutron fluxes are essentially equal. In the available positions in thermal flux test reactors such as the ORR, ATR, and ETR, the thermal flux is normally 4 to 12 times the fast flux. Therefore, we designed a capsule in which thermal neutron filter shrouds reduce the thermal-to-fast flux ratio by a factor of 2.6 to more nearly simulate the HTGR conditions. These shrouds<sup>10</sup> are fabricated from material obtained

<sup>10</sup>Richard M. Lieberman, "A System for Calculation of Fission Power in Irradiation Tests," pp. 473-90 in *National Symposium on Developments in Irradiation Testing Technology*, CONF-690910 (1969).

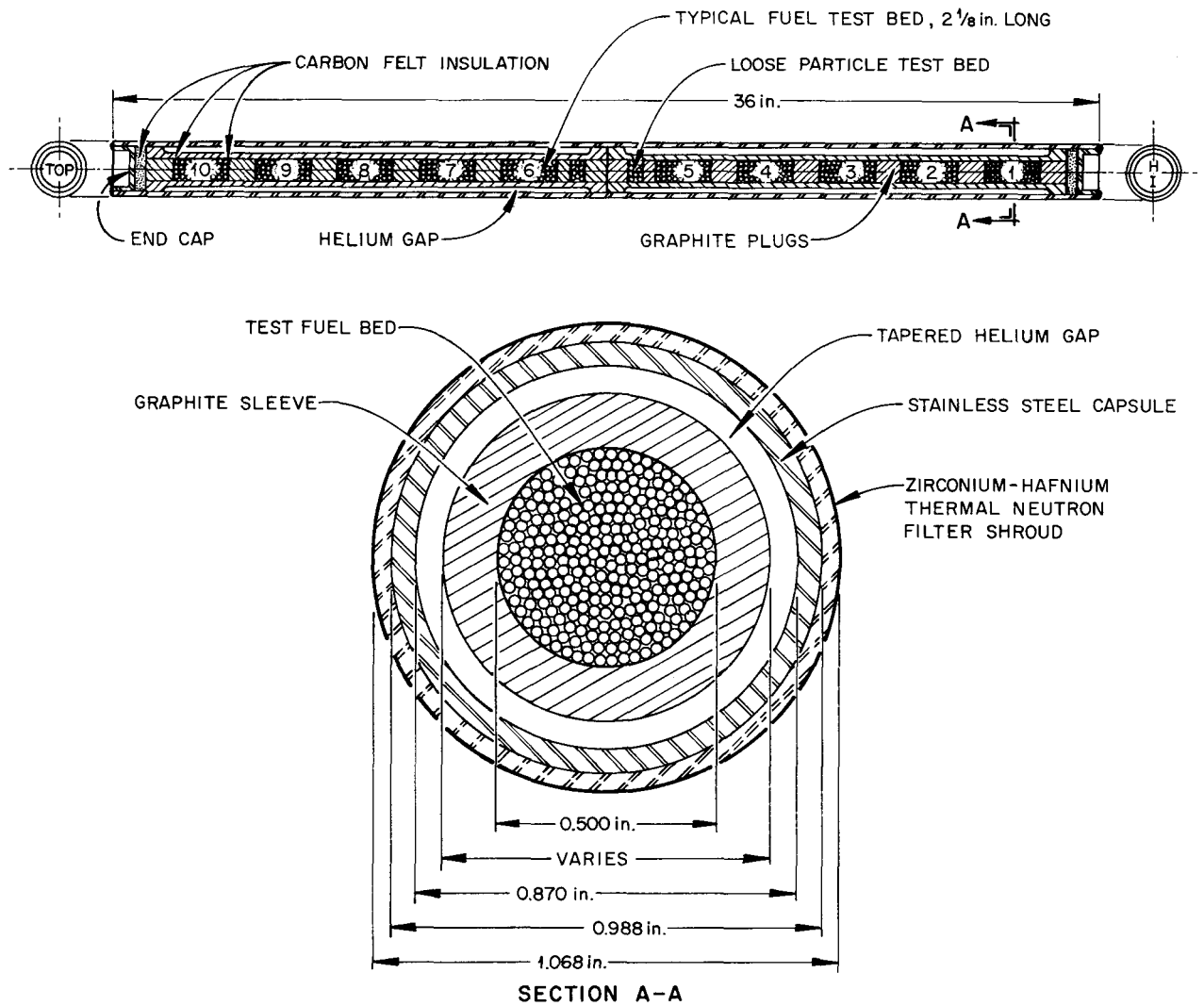


Fig. 41.2. Schematic of HTGR Recycle Irradiation Capsule.

from the Bettis Atomic Power Laboratory. The capsule design is shown schematically in Fig. 41.2. Two capsules are being fabricated for irradiation in the ETR. Four fissile-fertile particle combinations will be irradiated at 750, 950, 1050, and 1300°C to fast fluence levels between  $6$  and  $8 \times 10^{21}$  neutrons/cm<sup>2</sup>.

These capsules will provide small quantities of irradiated fuels for chemical reprocessing studies in advance of the material from the Peach Bottom Reactor irradiations and samples for evaluation of the irradiation performance characteristics. Additional capsule tests will be made only as the remote reprocessing and fuel fabrication reach critical stages of development, such as testing of the remote coating furnace product.

### Large-Scale Irradiation

R. B. Fitts

The cooperative irradiation program with GGA has three main objectives: (1) to provide gram quantities of irradiated HTGR fuel for head-end reprocessing studies, (2) to provide irradiated fuel blocks for testing engineering-scale reprocessing equipment, and (3) to provide irradiation proof tests of recycle fuel particles prepared in prototype equipment using the processes to be used in the Thorium-Uranium Recycle Facility. To achieve these objectives, eight RTE's are being operated in the Peach Bottom Reactor starting in June 1970. The fuels tested include all those presently known to be of

prime interest for large HTGR systems. The test conditions cover the range from 540 to 1260°C, burnups to 20% FIMA<sup>11</sup> in the (Th,U)O<sub>2</sub> particles, and fast fluence exposures up to  $4.2 \times 10^{21}$  neutrons/cm<sup>2</sup>.

The fuel has been fabricated at ORNL (sol-gel oxides) and at GGA (carbides). Coated particle and fuel stick preparation at ORNL are reported earlier in this chapter. The fuel elements were assembled at GGA and shipped to the Peach Bottom Reactor.

The RTE is made up of six fuel bodies stacked within a standard Peach Bottom graphite fuel element sleeve. Each fuel body is a graphite cylinder 15.5 in. long  $\times$  2.739 in. in diameter. Eight 0.500-in.-diam fuel holes surround a 1.1-in.-diam central hole, which prevents the development of pressure stresses on the outer sleeve if a fuel body cracks. This hole normally contains a loosely fitting graphite spine, although some small, self-contained test samples can be irradiated in this position.

The coated particle fuels tested in the RTE's, along with their projected HTGR uses, are listed in Table 41.2. These particles are to be mixed for testing in nine different two-particle combinations, each of which has application to large HTGR's, either as reference fuel or as a primary alternate fuel.

The reference fuel design employs these coated particles bonded into fuel sticks with a carbonaceous matrix. Most of the fuel in these tests is in these sticks. However, a few packed beds of loose particles are

<sup>11</sup>Fissions per Initial Metal Atom.

Table 41.2. Particles of Interest to the HTGR Recycle Program

Particle	Coating <sup>a</sup>	Possible Uses
(Th-20% U)O <sub>2</sub>	BISO	Reference recycle fissile particle
(Th-33% U)O <sub>2</sub>	BISO	Stand-in to provide faster burnup
UO <sub>2</sub> (buffer diluted)	BISO	Alternate recycle fissile particle
ThO <sub>2</sub>	BISO	Alternate recycle fertile particle
UC <sub>2</sub>	TRISO	Alternate makeup fissile particle
UC <sub>2</sub>	BISO	Alternate makeup fissile particle
ThC <sub>2</sub>	BISO	Reference recycle fertile particle
ThC <sub>2</sub>	TRISO	Reference makeup fertile particle
ThC <sub>2</sub>	TRISO	Alternate fertile particle

<sup>a</sup>The details of the BISO (2-layer pyrolytic carbon) and TRISO (3-layer pyrolytic carbon plus a SiC layer) coatings are given in GGA Specifications RF-1-1, 1002-4040-2, and 1002-4040-3.

included to study their performance and to assist in determining the effect of bonding on the performance of the particles in the bonded sticks.

The discharge of these test elements after one, two, and three years of irradiation will provide a series of samples with increasing burnup and fast neutron exposure. This series will permit the investigation of HTGR fuel performance and reprocessing processes as a function of progressive exposure of the fuel under prototypic HTGR conditions.

## THORIUM CERAMICS DATA COMPILATION

Sigfred Peterson

Data on the physical, mechanical, and chemical properties of ceramic compounds of thorium are being compiled from the literature. The collection has been completed<sup>12</sup> on oxides through October 1969 and nitrides through January 1970. That on carbides has been drafted, and information is being collected on other systems (borides, sulfides, etc.) and on the completed parts for future extensions and revisions. The collection is being issued in loose-leaf form so additions and revisions can be easily incorporated.

"Volumes" on the different systems contain major divisions on the useful compounds; divisions so far are on ThO<sub>2</sub>, ThN, Th<sub>3</sub>N<sub>4</sub>, ThC, and ThC<sub>2</sub>. Under each are "Parts" dealing with the compound, its binaries with uranium, with plutonium, and with other elements, more complex systems, and in some cases with other negative elements. The parts contain sections on composition, preparation, crystal properties, thermodynamic properties, change of state, electrical and magnetic properties, heat and mass transport, mechanical properties, chemical properties, and surface properties.

Volume I cites 256 references but defers systems with a second negative element (such as oxysulfides) to later volumes. Volume II cites 35 references and includes information on systems with added negative elements, such as carbonitrides. Many gaps exist in the characterization of the thorium nitrides. The most serious deficiencies in the carbides are the lack of reliable thermodynamic properties of ThC and the sparsity of mechanical and transport property data for both carbides.

<sup>12</sup>S. Peterson and C. E. Curtis, *Thorium Ceramics Data Manual Vol. I, Oxides and Vol. II, Nitrides*, ORNL-4503, Vols. I, II, in press.

## 42. Transuranium Program

A. L. Lotts

The Transuranium Project is producing quantities of the heavier transuranium elements for research by successive neutron captures in  $^{239}\text{Pu}$ . The program at ORNL started with primarily  $^{242}\text{Pu}$ ,  $^{243}\text{Am}$ , and  $^{244}\text{Cm}$ . Target elements containing principally these three isotopes are fabricated at ORNL and irradiated in the High Flux Isotope Reactor at a flux of approximately  $3 \times 10^{15}$  neutrons  $\text{cm}^{-2} \text{sec}^{-1}$ . In addition, special target elements of higher isotopes are fabricated occasionally and irradiated in HFIR. The target elements are removed periodically from the HFIR and reprocessed in the Transuranium Processing Facility (TRU). At TRU the product actinides are separated and the target actinides are recovered and fabricated into recycle target elements. In addition, special targets for irradiation in the HFIR Hydraulic Rabbit Facility are fabricated and special encapsulations are made of the product actinides.

The program at TRU is carried out jointly by the Chemical Technology, Metals and Ceramics, and Analytical Chemistry Divisions. Our present tasks in the program include the fabrication of targets in TRU for HFIR, the fabrication of HFIR rabbits, the fabrication of special encapsulations for neutron and gamma sources, the evaluation of the performance of the target elements, the improvement of the target element design, and the improvement of the processing equipment in TRU.

### TARGET FABRICATION

L. C. Williams      J. E. Van Cleve

The target fabrication production line, used to fabricate target rods containing either  $^{242}\text{PuO}_2$  or  $(\text{Am,Cm})\text{O}_2$  as the starting material, has operated as the feed was available. The remote target fabrication equipment was used during the past year with minimum trouble. Difficulty in making the final closure weld on the targets has apparently arisen largely from deterioration of the remote portion of the equipment. We are

replacing the major portion of the remote welding equipment; this should alleviate the problem. The targets fabricated during this reporting period are listed in Table 42.1.

Small amounts of isotopes of special interest are most efficiently produced by exposing the starting material in the HFIR Hydraulic Rabbit Facility. The standard rabbit design was developed last year<sup>1</sup> and has not been changed. The rabbits fabricated during this year are listed in Table 42.2.

Seven neutron sources and one gamma source were assembled. The configurations were all of the same type

<sup>1</sup>A. L. Lotts, J. E. Van Cleve, Jr., E. J. Manthos, R. T. King, and E. L. Long, Jr., *Metals and Ceramics Div. Ann. Progr. Rept. June 30, 1969*, ORNL-4470, pp. 163-67.

Table 42.1. Targets Fabricated at TRU in FY 1970 in Order of Completion Date

Target	Oxide Form	Isotope	Actinide Weight (g)	Oxide Weight (g)	Pellet Length Standard Deviation (in.)
					$\times 10^{-3}$
D71	Shards	$^{242}\text{Pu}$	9.04	10.56	28.1
K27	Microspheres	$^{244}\text{Cm}$	7.24	11.15	9.7
K29	Microspheres	$^{244}\text{Cm}$	7.42	11.43	11.5
K30	Microspheres	$^{244}\text{Cm}$	7.42	11.43	14.4
K31	Microspheres	$^{244}\text{Cm}$	7.31	11.26	42.6
K33	Microspheres	$^{244}\text{Cm}$	7.33	11.27	41.9
K34	Microspheres	$^{244}\text{Cm}$	7.46	11.13	1.08
K15	Microspheres	$^{244}\text{Cm}$	7.46	11.13	8.97
K18	Microspheres	$^{244}\text{Cm}$	8.37	10.15	20.2
K22	Microspheres	$^{244}\text{Cm}$	9.44	11.09	23.6
K28	Microspheres	$^{244}\text{Cm}$	9.44	11.09	29.7
K40	Microspheres	$^{244}\text{Cm}$	8.04	10.00	21.2
K36	Microspheres	$^{244}\text{Cm}$	8.04	10.00	19.9
K39	Microspheres	$^{244}\text{Cm}$	8.04	10.00	23.2
K46	Microspheres	$^{244}\text{Cm}$	8.04	10.00	13.8

Table 42.2. Rabbits Fabricated in FY 1970

Identification	Major Isotope	Actinide Weight ( $\mu\text{g}$ )
1-70-21	$^{244}\text{Pu}$	1000
3-70-2	$^{253}\text{Es}$	1.0
4-70-4	$^{249}\text{Bk}$	5.0
4-70-5	$^{249}\text{Bk}$	5.0
5-70-1	$^{253}\text{Es}$	2.0
5-70-2	$^{244}\text{Pu}$	1100
5-70-12	$^{249}\text{Bk}$	1200
6-70-1	$^{253}\text{Es}$	2.0
6-70-5	$^{253}\text{Es}$	5.0

as presented previously.<sup>1</sup> The neutron sources contained from 0.1 to 2.0 mg  $^{252}\text{Cf}$ . The encapsulation materials include types 304 and 405 stainless steel as well as X8001 aluminum. The single gamma source contained 1 mg of  $^{244}\text{Cm}$  oxide mixed with  $^{13}\text{C}$ . It was fabricated by standard procedures.

### HFIR TARGET PERFORMANCE

J. E. Van Cleve

#### Status of the Targets Exposed in HFIR

Table 42.3 lists the categories of targets exposed in HFIR during the year. Although not immediately seen, the table shows the status of three different type targets. These are the original HFIR loading, which contained 8 g of  $^{242}\text{PuO}_2$  per target with the pellets containing 10% void volume; targets that contain 11 g of  $^{242}\text{PuO}_2$  per target with the pellets containing 20% void volume; and the recycle targets, which contain 11 g of mixed ( $^{243}\text{Am}, ^{244}\text{Cm}$ ) $\text{O}_2$  with the pellets containing 20% void volume. The second and third types were fabricated remotely in the TRU.

#### Analysis of Target Performance

Three groups of targets were removed from the HFIR and chemically processed to recover the contained transplutonium elements. One group consisted of 15 of the "virgin" plutonium targets that had been irradiated in HFIR only. Five had developed cracks in the target cladding of the same type as previously shown.<sup>2,3</sup> These failures are the first seen in the virgin targets.

According to the updated failure model,<sup>4</sup> these targets may be expected to fail between 58 and 68% FIMA. The spread in the predicted failure point is due to the selection of pellet parameters. The five failures

were between 56.8 and 63.2% FIMA, about in the predicted range. One target, D12, had experienced 75.8% FIMA when it was removed. The longevity of this particular target may be explained as follows. Swelling under long-term irradiation is very sensitive to the void volume initially in the pellet — that is, it swells much less when the initial void volume is high. Second, the FIMA values reported are the maximum for each target; the center section will fission faster than the ends due to the neutron flux distribution along the target. Apparently, the pellets in the center section of D12 were of higher average quality than those in the targets that failed. Target rod D12 was removed because of demand for the transplutonium isotopes it contained as well as the fact that it had absorbed more neutrons than planned for any subsequent target of the same type.

The second type targets removed were experimental and built to demonstrate that the presence of greater void volume initially in the pellets would materially extend the life of the target. The pellets in these targets were pressed so that four targets had pellets with 20% void volume and two had 25%. The targets had been in the reactor for 31 fuel cycles, about two years. These targets had been exposed to the highest fluence and attained the highest burnup of any targets ever placed in the reactor; yet none showed any indication of failure. The targets were visually inspected upon their receipt at TRU, and no sign of failure was noted. They were normal in appearance and covered with a light-colored oxide deposit. A section of the cover can was obtained. The trouble-free irradiation of these targets further confirms the validity of the failure model.

The last group of targets comprises recycle targets fabricated in the TRU plant. These targets are loaded with a mixture of americium and curium oxides, and the pellets in them had been pressed to contain 20% void volume. Most of these targets are being irradiated; however, three have been removed on schedule. These targets were also visually examined upon receipt at TRU and found to be normal.

As of June 1970, we have experienced no unexpected target element failures. The targets that developed cracks in the cladding were at or near the point in their

<sup>2</sup>A. L. Lotts, J. E. Van Cleve, E. J. Manthos, R. T. King, and E. L. Long, Jr., *Metals and Ceramics Div. Ann. Progr. Rept. June 30, 1968*, ORNL-4370, pp. 193–97.

<sup>3</sup>A. L. Lotts, E. J. Manthos, J. E. Van Cleve, E. L. Long, Jr., J. R. Weir, and R. E. Adams, *Metals and Ceramics Div. Ann. Progr. Rept. June 30, 1967*, ORNL-4170, pp. 187–91.

<sup>4</sup>R. E. Adams, *Trans. Am. Nucl. Soc.* 12(2), 560–61 (1969).

Table 42.3. HFIR Target Element Performance as of June 13, 1970

Actinide Oxide Loading (g)	Pellet Void Volume (%)	Number of Targets	Present Status	Range of Burnup (% FIMA)	Range of Fluence (neutrons/cm <sup>2</sup> )	
					<0.41 eV	>0.81 MeV
					× 10 <sup>21</sup>	× 10 <sup>21</sup>
8	10	5	Failed	56.8–63.2	11.14–12.52	3.92–4.22
8	10	16	Scheduled removal	60.3–82.0	11.77–18.31	3.59–5.45
8	10	3	In HFIR	57.4–61.0	11.52–12.40	3.76–3.97
11	20	3	Scheduled removal	24.0–58.2	2.59–7.93	0.88–2.70
11	20	23	In HFIR	5.7–44.3	0.57–5.41	0.16–1.81

irradiation where the failure model predicted possible failure. The experience with the six experimental targets confirms the validity of the failure model, and all targets are now loaded with pellets pressed to contain 20% void volume. The failure model was developed and applied to targets loaded with plutonium oxide. A similar analysis is being performed on the curium targets, but the final results are not yet available.

#### HFIR Target Rod Irradiation Damage

R. T. King

Improving the life expectancy of the HFIR target element cladding, in which transplutonium elements are generated, is the goal of the Aluminum Irradiation Damage Program. In addition to the experiments described below, investigations of the nature of and solutions to irradiation damage problems in aluminum are reported in Chapters 5 and 34.

We are investigating the properties of aluminum irradiated near the maximum service temperature (up to about 150°C) of the target rod cladding. In addition to the currently used X8001 aluminum alloy, other potential candidate alloys for this application, such as 1100 and 6061 aluminum, are under study. Two experiments containing both creep-rupture and electron microscopy specimens have been irradiated for five and ten cycles in HFIR to maximum fluences of approximately 0.8 and 1.6 × 10<sup>22</sup> neutrons/cm<sup>2</sup>, respectively.

Early results from the creep-rupture testing of specimens irradiated and tested near 100°C indicate that the postirradiation creep strength, as measured by strain rate at a given stress, and rupture life are increased for all alloys mentioned above. However, irradiation causes a marked reduction in ductility under these conditions. Tensile results on irradiated 6061 HFIR components (see Chapter 34) indicate that the ductility of this alloy is sensitive to deformation strain rate, decreasing with decreasing strain rate at high temperatures. This result supports the need for further creep-rupture tests under a variety of stress conditions.

The results of this investigation will be used to optimize the selection of alloy and metallurgical condition for the fabrication of future HFIR targets.

#### PREPARATION OF PLATINUM FILTERS FOR A CALIFORNIUM ION EXCHANGE ASSEMBLY

M. M. Martin R. W. Knight R. G. Donnelly

Californium-bearing solutions have been contaminated with undesirable reaction products resulting from the interaction of the stainless steel with the ion exchange resin used in the purification of <sup>252</sup>Cf. The resin is contained in stainless steel tubes plugged at both ends with stainless steel filters. To overcome the contamination problem, an all-platinum tube and filter assembly has been proposed.

We investigated the preparation<sup>5</sup> of platinum filters and manufactured an ion exchange assembly (tube plus two filters). Rather than use an all-platinum tube, we electroplated a 0.35-in.-ID × 1.3-in.-long stainless steel tube with a 0.0002-in.-thick layer of platinum. Before plating, a recess was machined into the inside surface near the end of the tube to position the filler. The rim of the tube was then roll-swaged to lock the filler in place.

The method of preparing the porous metal filter consists of adding a pore-forming additive of -80 +230-mesh NH<sub>4</sub>HCO<sub>3</sub> to -400-mesh Pt powder. The ammonium bicarbonate decomposes rapidly above 120°C. The two powders are blended at room temperature, pressed in a die at 50 tsi, and then sintered at 1460°C for 4 hr at less than 5 × 10<sup>-5</sup> torr. Figure 42.1 presents the structure of a specimen prepared with 40 vol % Pt, 50 vol % NH<sub>4</sub>HCO<sub>3</sub> and 10% voids. Upon sintering, similar filters contain 60 vol % total porosity.

After testing the assembly for flow and corrosion resistance it was used successfully in the preparation of a high-purity <sup>252</sup>Cf solution.

<sup>5</sup>P. Duwez and E. Martens, *Trans. AIME* 70, 848 (1948).

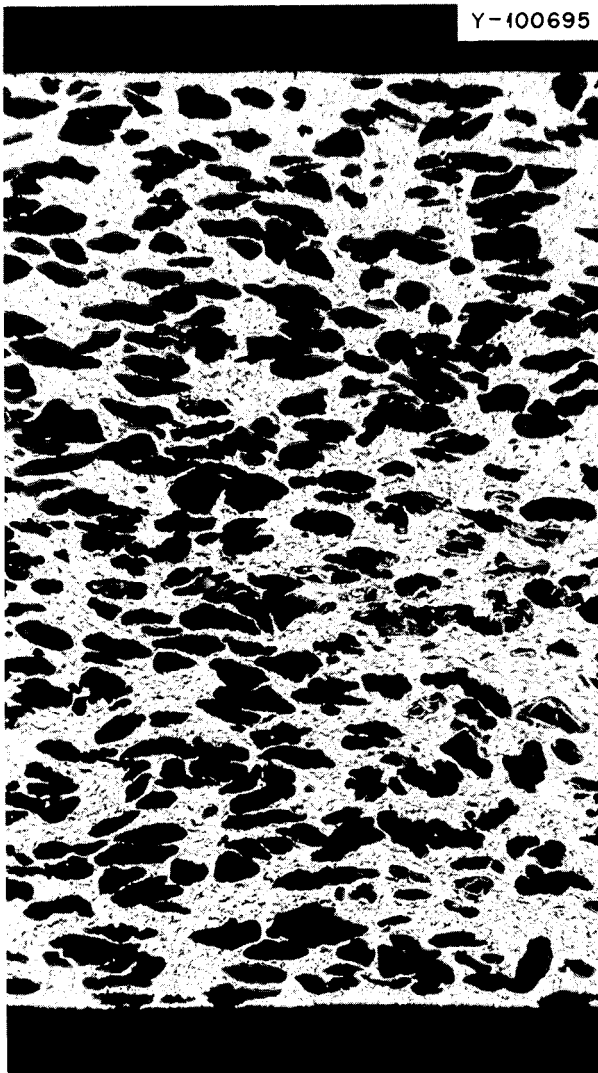


Fig. 42.1. Cross Section of Plutonium Frit Showing the Porous Structure Produced by Use of the  $\text{NH}_4\text{HNO}_3$  Additive. 35X.

## 43. Water Reactor Safety

P. L. Rittenhouse

The  $\text{UO}_2$  fuel of a modern light-water reactor (LWR) is contained in zirconium alloy tubes (Zircaloy) nominally 12 ft long  $\times$  0.5 in. in diameter. Radioactive fission products generated during the operation of these reactors are retained either within the body of the fuel or inside the fuel cladding gap and plenum. Further protection against release of fission products to the environment is provided by the primary system and the containment vessel. However, one can postulate accidents that will compromise the integrity of one or more of the barriers mentioned above. In one such incident, the loss-of-coolant accident (LOCA), the primary system coolant and pressure are assumed to be lost because of a rupture in the system piping. The fuel cladding would undergo a severe thermal transient during this accident. The initial driving force for the transient would result from redistribution of the heat stored in the fuel, but heat produced by decay of fission products and the exothermic reaction of zirconium with residual steam would predominate at later times and higher temperatures, respectively. Were this transient allowed to progress unhindered, it would result in gross damage to the reactor core.

Even though an LOCA is considered highly unlikely, its consequences would be severe, and emergency core cooling systems (ECCS) are therefore provided in LWR's to terminate the postulated transient. However, should an accident occur, portions of the core may reach temperatures sufficient to cause rupture of the fuel rod cladding even with the ECCS performing as designed. This rupture occurs when the hoop stress provided by fission gas pressure exceeds the ultimate strength of the cladding. Considerable swelling (plastic deformation) of the rods may occur before rupture and reduce the passageway for flow of the emergency coolant through portions of the core. At some critical but unknown degree of flow restriction transient termination may be seriously delayed. This will increase the probability of cladding embrittlement and sub-

sequent disintegration or melting of the cladding and fuel.

Because of these possibilities, a concerted effort is under way to (1) assess the modes of failure of the fuel rod cladding in terms of accident conditions and reactor operating history, and (2) determine to what extent deformation and rupture may affect emergency cooling capability. In addition, it is necessary to determine the margins of safety relative to the above. The work reported here is sponsored by the U.S. Atomic Energy Commission (USAEC), but related efforts are under way in the LWR industry.

### PROGRAM COORDINATION

P. L. Rittenhouse

We coordinate the USAEC-sponsored work on the failure modes of Zircaloy-clad LWR fuel rods during an LOCA and the effect of this on emergency cooling behavior. We are also performing several studies on the high-temperature deformation and other behavior of Zircaloy cladding. Other USAEC-sponsored research on fuel rod failure is being performed at Idaho Nuclear Corporation (Idaho Falls, Idaho), at Battelle Memorial Institute (Columbus, Ohio), and in the Reactor and Reactor Chemistry Divisions at ORNL. Related activities conducted by the LWR manufacturers are factored into the direction and scope of the USAEC studies to obtain a balanced and timely approach to the questions on fuel rod failure and its effects.

In addition to monitoring and coordinating the studies mentioned above, ORNL has the responsibility for preparing program documents covering these areas of work. The most recent<sup>1</sup> of these is the work plan for

---

<sup>1</sup>P. L. Rittenhouse, *Failure Modes of Zircaloy-Clad Fuel Rods, Part 3: Description of the ORNL Program*, ORNL-TM-2742 (January 1970).

ORNL. Communication and coordination among the sites mentioned above have been effected by scheduled Fuel Rod Failure Program meetings, other informal meetings, interchange of progress reports, and correspondence.

### BASE-LINE DATA FROM TRANSIENT TEMPERATURE RUPTURE TESTS OF ZIRCALOY TUBING

D. O. Hobson

Transient rupture tests of Zircaloy cladding performed by several installations in the past have shown considerable variation in results. This has made a base-line study of rupture behavior under closely controlled test conditions imperative. We studied boiling water reactor (BWR) -size tubing (0.563 in. OD  $\times$  0.032 in. wall, nominal). A workable framework of parameters was achieved by limiting the test to two controlled independent variables (internal pressure and heating rate) and one monitored variable (wall thickness). The dependent variables were rupture temperature, time to rupture, circumferential strain, maximum internal pressure, and the physical appearance of the ruptured tubing. The specimens were heated internally by tungsten resistance heaters and were contained in a highly reflective furnace. The surroundings of the specimen were thereby maintained at the same instantaneous temperature as the specimen surface throughout the temperature transient. This duplicates the thermal environment of a fuel rod during the LOCA.

The test conditions and the appearance of the tubes are shown in Fig. 43.1, a montage of photographs of the rupture sections of the tubing. Minimum circumferential strains occurred in the tests at intermediate pressure. Initial pressures of 50, 100, and (in two tests) 200 psig were low enough to cause the specimens before rupture to reach temperatures that produced the body-centered cubic or  $\beta$  phase. Higher pressures, 200 to 700 psig, caused rupture at lower temperatures, generally in the two-phase  $\alpha + \beta$  region. The diffusionless  $\alpha$ -to- $\beta$  transformation occurs by a shear-type diffusionless mechanism, which provides a "free," stress-directed deformation mechanism and probably nullifies any work hardening ability the tubing might have while in the two-phase region. This would result in nonuniform expansion of the tubing and rupture at low strain levels at the weakest place in the tube wall, exactly the behavior observed in these particular tests.

Figure 43.2 shows the effect of maximum internal pressure on circumferential strain. It contains test

points characterized by heating rate and rupture temperature. The strain minimum at intermediate pressures is obvious.

Wall thickness variation was also found to be an important factor in the rupture behavior of the tubing. Figure 43.3 shows the decrease in circumferential strain with increasing wall thickness variation for duplicate or triplicate tests run under several conditions of pressure and heating rate.

This series of transient rupture tests has demonstrated that internal pressure — and, therefore, rupture temperature — has the maximum effect on the strain produced in the tubing. Maximum strain occurred in the two single-phase regions; the  $\beta$ -region corresponding to high-temperature rupture associated with low pressures and the  $\alpha$ -region corresponding to low temperatures associated with high pressures. Rupture in the two-phase  $\alpha + \beta$  region resulted in low strain values. Heating rate apparently has a much smaller effect on the rupture behavior of the tubing. In general, the strain observed was decreased by the presence of wall thickness variations in all tubes tested. These variations ranged from 0.0007 to 0.0040 in.

### MULTIROD TRANSIENT BURST EXPERIMENTS

R. D. Waddell, Jr.

The deformation and failure behavior of Zircaloy fuel rod cladding may, in the event of an LOCA, cause coolant channel blockage of such magnitude as to impair emergency core cooling. Because of this, a series of multirod transient tube burst tests is being conducted to study the interaction of simultaneously deforming Zircaloy tubes and to measure the resulting coolant channel blockage.

Tests have been conducted on bundles of 13 Zircaloy tubes of BWR size and are planned with bundles containing 32 tubes of pressurized water reactor (PWR) size. In both cases the bundles are 2 ft long, and each tube contains a 16-in. 3200-W, quartz-encapsulated tungsten heater. Rod spacings typical of LWR's are used in all bundles, and tubes representative of each position within the bundle are monitored for both temperature and pressure.

After assembly the bundle is placed in a combination heater-containment vessel, enveloped in argon, and heated to the nominal in-reactor operating temperature of the cladding. The tubes are pressurized with argon to a preselected level, and the transient is initiated and continued until all tubes fail. The range of pressures (100 to 2000 psi) and heating rates (10 to 100°F/sec)

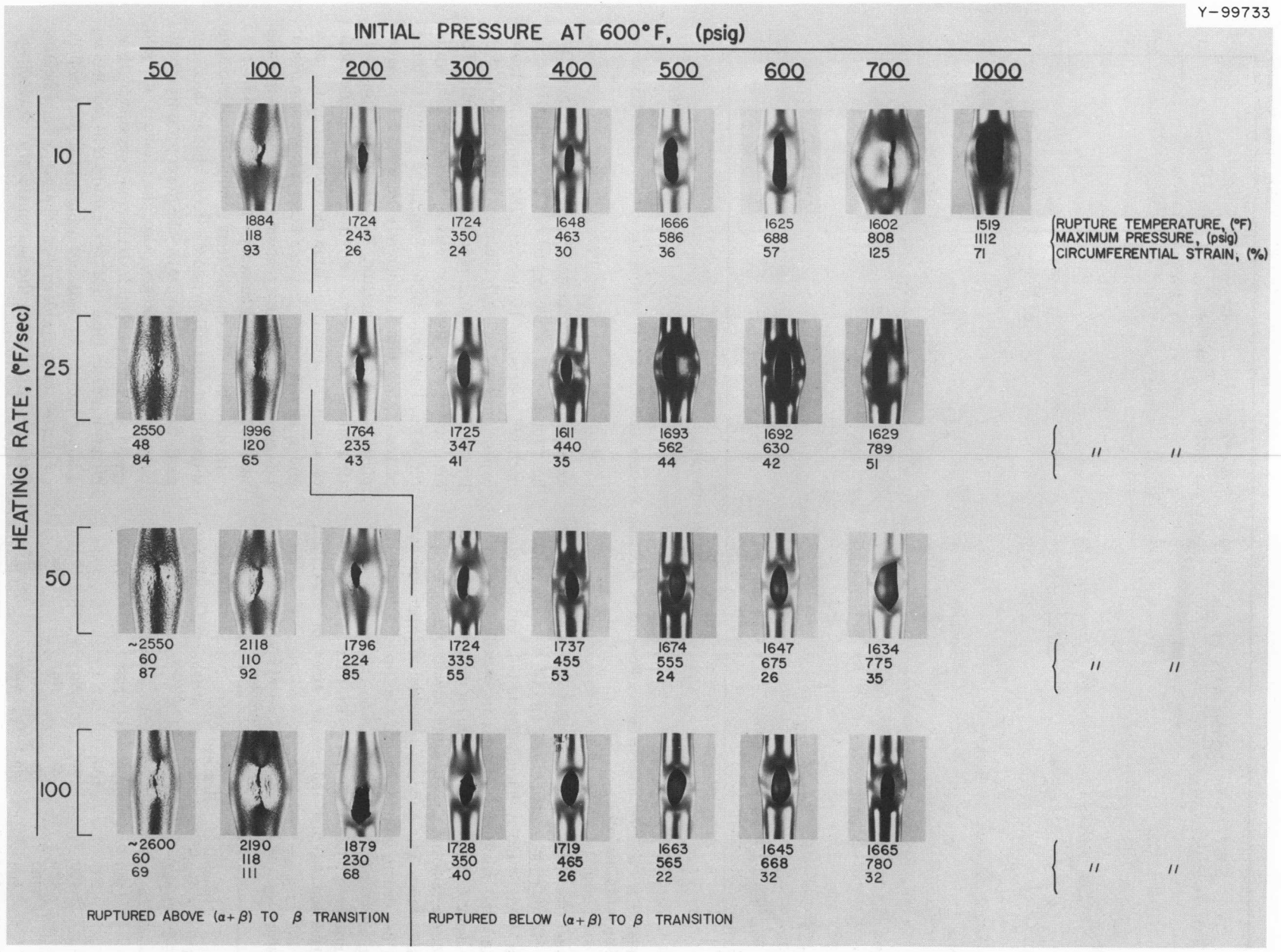


Fig. 43.1. Test Conditions and Rupture Areas.

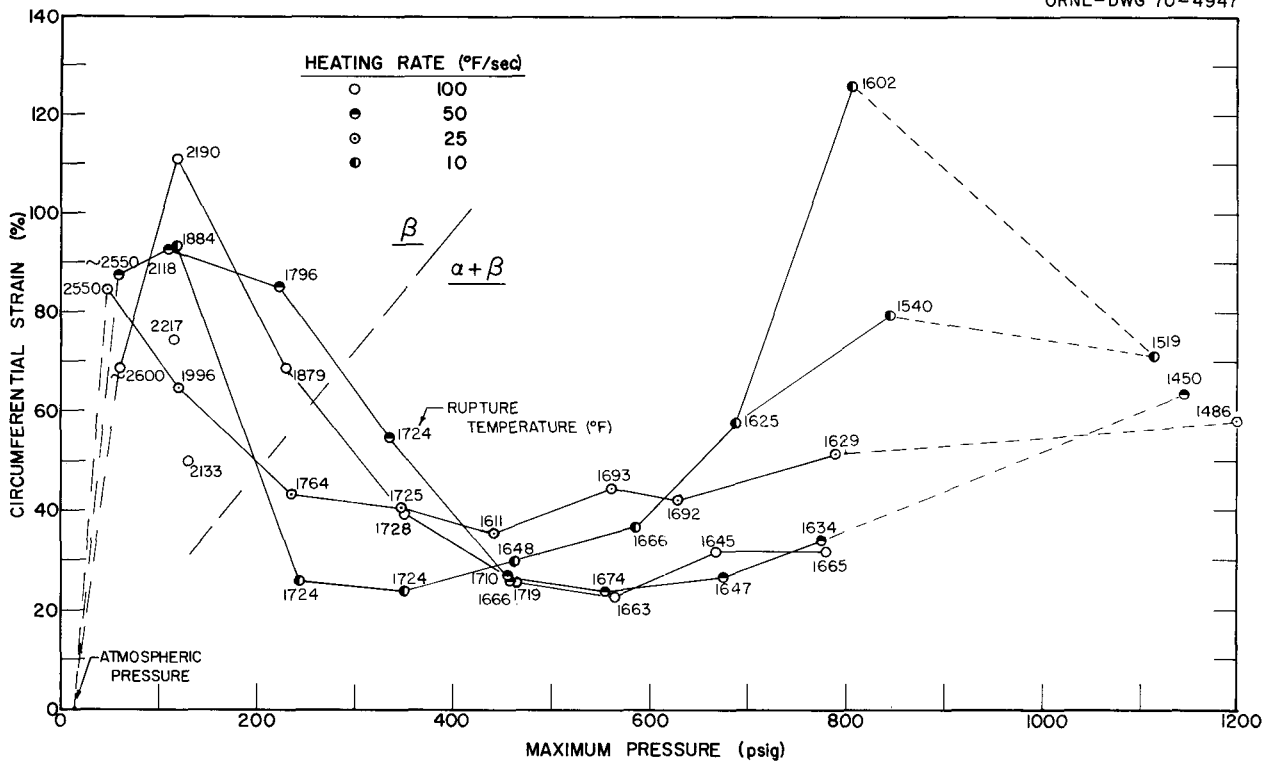


Fig. 43.2. Circumferential Strain as a Function of Maximum Pressure. Base-line data illustrating the strain minimum that occurs at intermediate pressures.

planned for these tests encompass the range of values that will be encountered during a LOCA.

Six BWR bundles have been tested, and the conditions and resulting blockages are seen in Table 43.1. The largest coolant channel reductions shown in the table are associated with the lowest pressures and heating rates. The effect of pressure on expansion can also be seen by comparing cross sections of bundles 2 (Fig. 43.4) and 3 (Fig. 43.5).

Another point of interest in these tests is the distribution of the failures or areas of maximum

expansion along the heated length of the bundle. We have found that, while expansions of around 10% have occurred over some 10 in. along the bundle, maximum expansions have generally occurred within a 3- to 4-in. length near the axial midpoint of the bundle. The distribution of failures for tests 2, 4, and 5 is shown in Fig. 43.6. The results of test 1 are quite similar to those of test 2, but test 3, apparently because of the higher pressure and faster heating, had expansions from 6 to 12% along the center 8 in. of the bundle with essentially no points of large expansion. The use of a grid spacer in test 6 prevents this type of comparison; however, our preliminary observations suggest that the spacers may reduce axial randomness (see Fig. 43.7).

In summary, the bundle tests conducted to date have shown that internal pressure affects channel blockage more than does heating rate. The lower pressures result in large channel blockages. Also, the presence of a grid spacer appears to reduce axial randomness, which, in effect, increases local blockage. Future tests, containing a larger number of rods and using grid spacers, will be conducted over a wider range of pressures and heating rates to further aid in the assessment of core blockage.

Table 43.1. Test Parameters and Coolant Channel Blockage for BWR Test Bundles

Test	Internal Pressure (psig)	Heating Rate (°F/sec)	Grid Sleeve	Typical Coolant Area Reduction (%)
1	300	100	No	42
2	200	100	No	50
3	400	100	No	18
4	400	25	No	25
5	200	25	No	34
6	100	50	Yes	76

## METALLURGICAL SUPPORT

D. O. Hobson

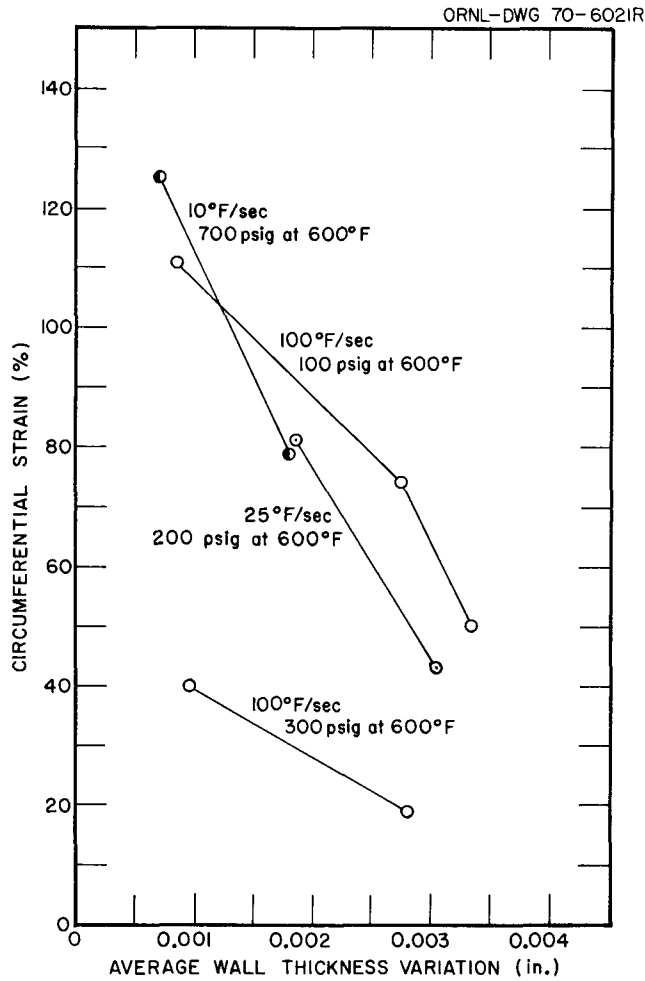
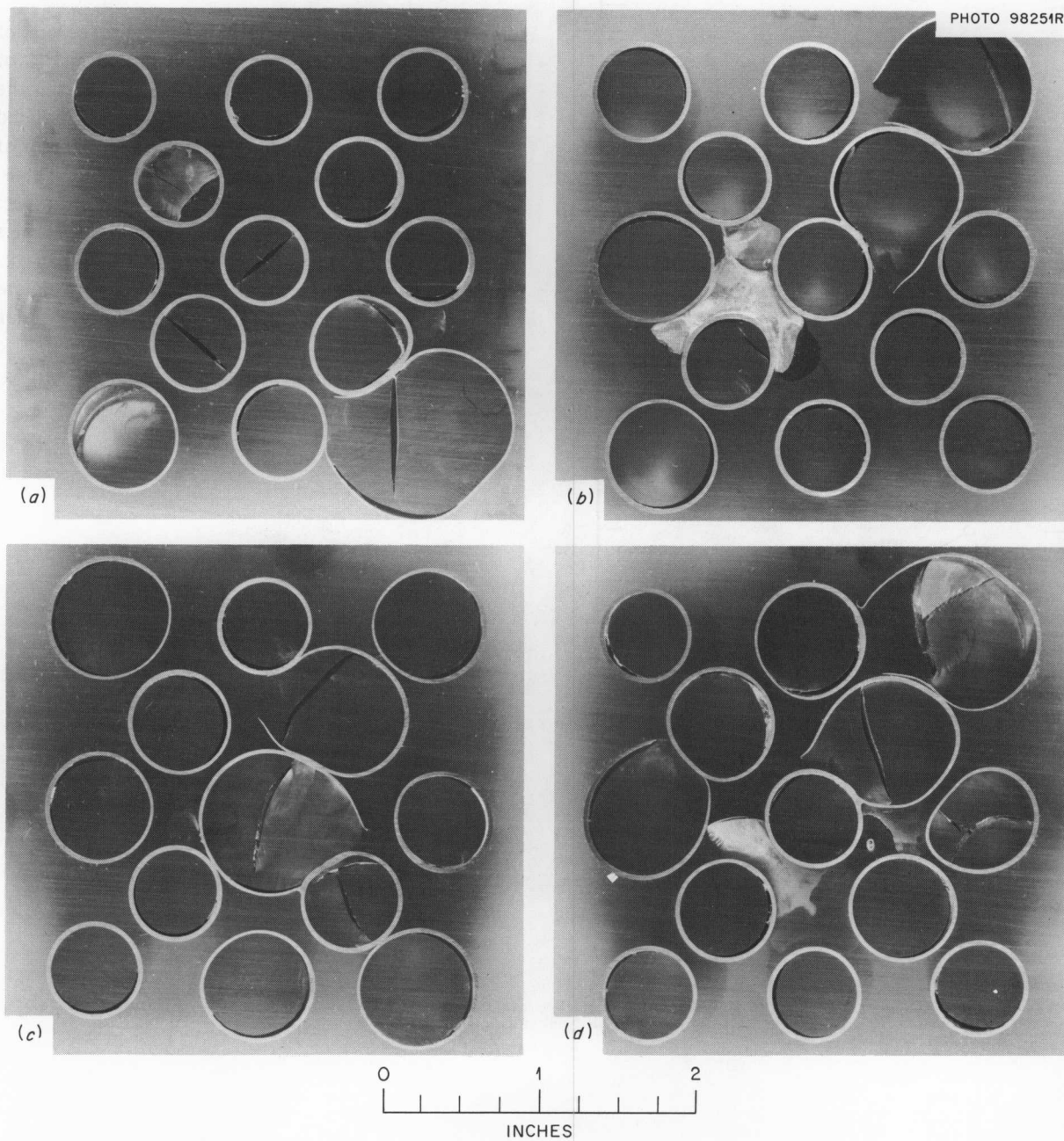


Fig. 43.3. Effect of Average Wall Thickness Variation on Circumferential Strain. These curves illustrate the large decrease in strain caused by the variations in wall thickness.

Metallurgical support has been provided for several of the tasks in the ORNL program on failure modes of Zircaloy cladding. Included in this effort has been the examination of fuel rods heated through a simulated LOCA temperature transient in the TREAT reactor at the National Reactor Testing Station (Idaho Falls, Idaho). These rods were examined to assess the effect of the transient on microstructure, hardness, hardness profiles, and the amount of oxidation that had occurred. In support of another task, cladding specimens exposed to steam at high temperature and then quenched are being examined to determine and to correlate oxygen content with hardness and ductility at room and elevated temperatures.



**Fig. 43.4. Cross Sectional Views of Test Bundle 2.** Pressurized to 200 psig at 575°F and heated at 100°F/sec to failure at 1850°F and 205 psig. (a) 4.75 in. below center, 37% blockage. (b) 3.15 in. below center, 42% blockage. (c) Axial center, 56% blockage. (d) 1.50 in. below center, 57% blockage.

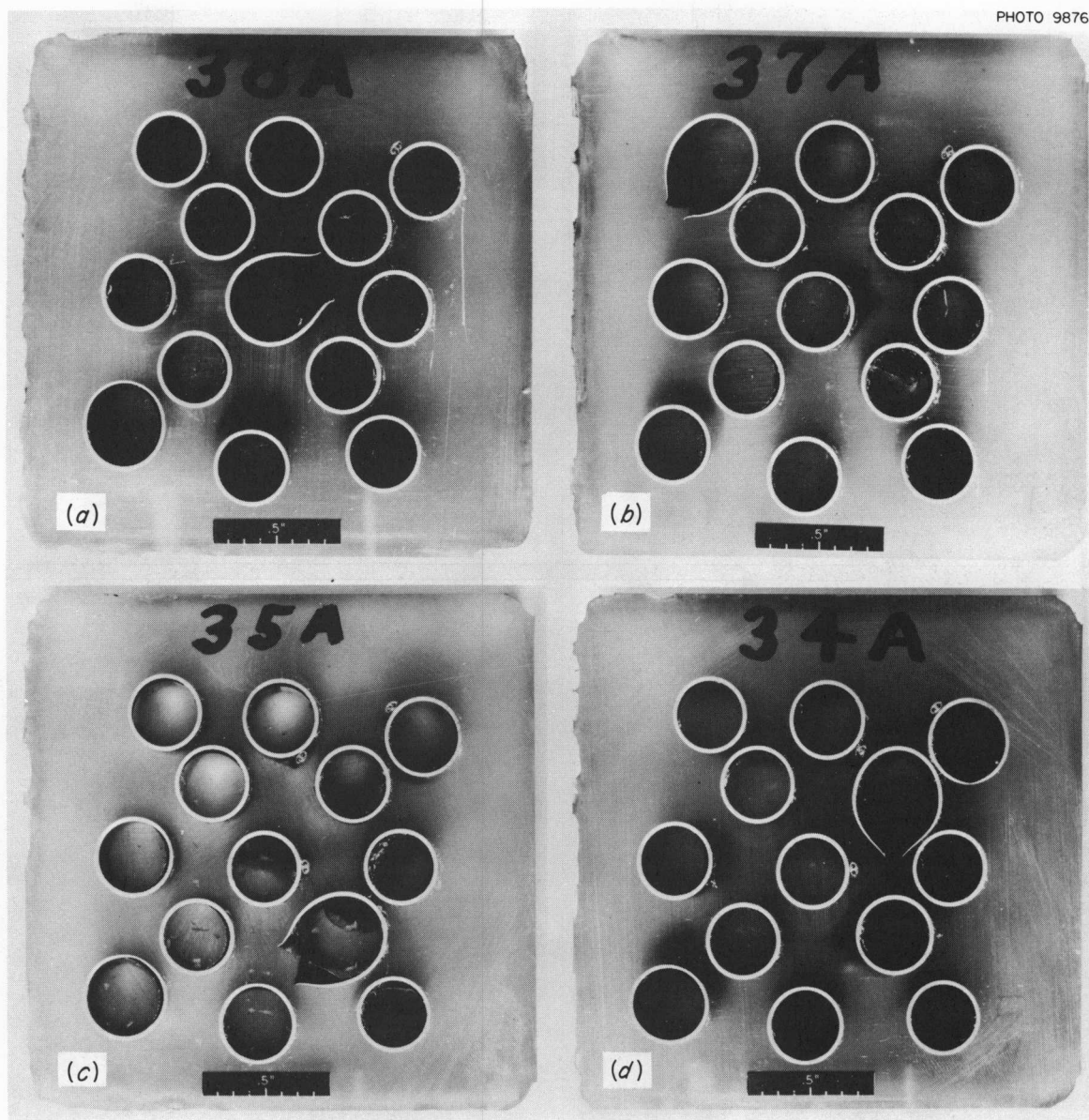


Fig. 43.5. Cross Sectional Views of Test Bundle 3. Pressurized to 400 psig at 575°F and heated at 100°F/sec to failure at 1715°F and 430 psig. (a) 1.75 in. above center, 17% blockage. (b) 0.31 in. above center, 22% blockage. (c) 0.75 in. below center, 19% blockage. (d) 1.75 in. below center, 19% blockage.

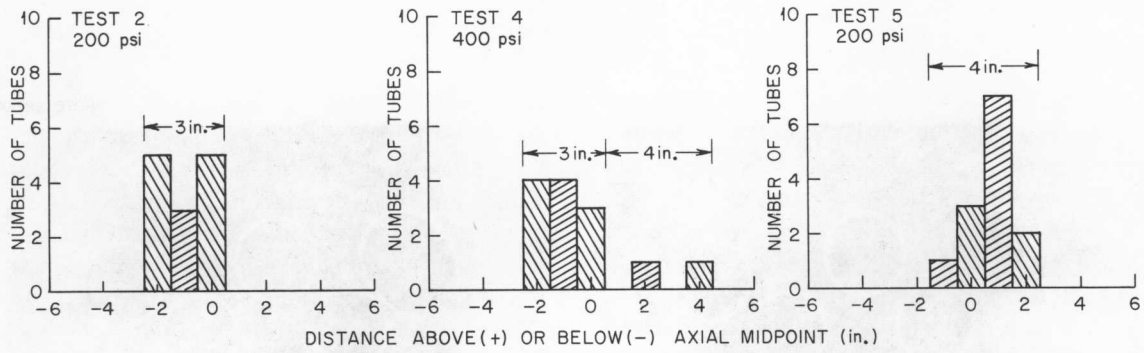


Fig. 43.6. Distance over which Maximum Expansion Occurred for Tubes in Tests 2, 4, and 5.

PHOTO 99458

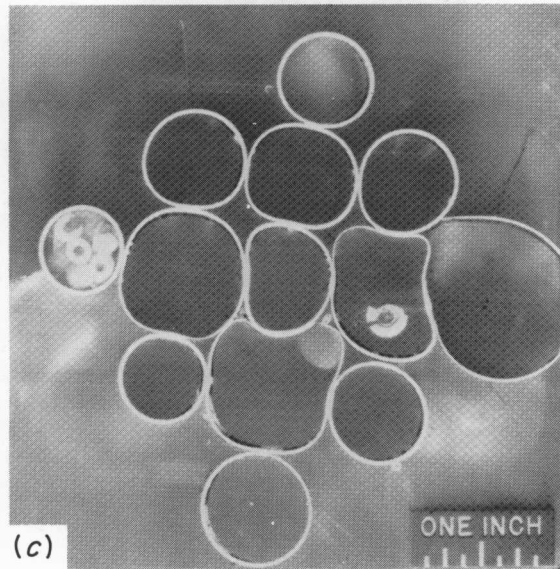
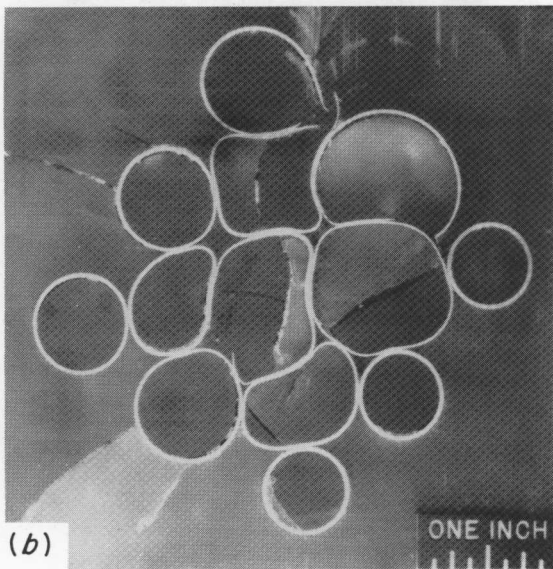
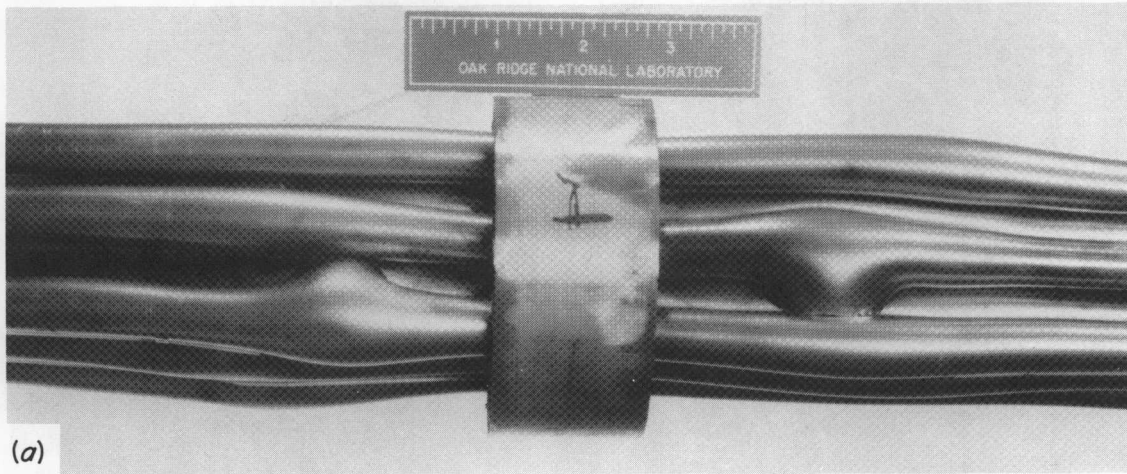


Fig. 43.7. Post-test Photographs of Test Bundle 6. (a) Overall view showing deformed regions and grid spacer. Bundle was pressurized to 100 psig at 575°F and heated at 50°F/sec to failure at 2460°F and 105 psig. (b) Section 4.37 in. below axial center, 78% blockage. (c) Section 2.75 in. above axial center, 75% blockage.

## Part VI. Other Program Activities

### 44. Absorber Materials for Sulfur Dioxide from Flue Gas

W. S. Ernst, Jr. T. G. Godfrey

Various methods of removing SO<sub>2</sub> from flue gas of coal-fired plants are being evaluated by the National Air Pollution Control Administration of HEW. We have studied one candidate material, a synthetic sodium aluminate mineral called dawsonite, which, when heated, reacts with SO<sub>2</sub> to form Na<sub>2</sub>SO<sub>4</sub> and Al<sub>2</sub>O<sub>3</sub>. Regeneration in hydrogen produces H<sub>2</sub>S and permits recycle of the fresh dawsonite. Early pilot plant runs in fluidized beds or falling-particle contactors showed that attrition losses were excessive for the small manufactured spheres. In addition to the impact loading, other factors such as the crystallographic changes might contribute to the observed attrition.

#### BEHAVIOR OF DAWSONITE IN SORPTION-REGENERATION CYCLES

W. S. Ernst, Jr. T. G. Godfrey

Our studies involved static-bed sorption-regeneration cycles of high sulfur loadings and showed that the cyclic process *per se* apparently does not contribute to the physical degradation of the dawsonite, although some sintering of the highly porous particles does occur and reduces the sorption capacity. The starting material contains a significant quantity of water and carbon dioxide and must be activated at about 660°C in dry gases before being used. During the cycling tests, the dawsonite is extremely hygroscopic if exposed to the atmosphere and is considerably weakened by water adsorption. In this condition, the material is subject to

attrition by steam explosion if it is suddenly heated. A significant factor in the poor attrition resistance is the presence of gross cracks and voids in almost all of the fabricated spheres. Using microradiography, we selected essentially sound particles and found that their crushing strength was essentially constant for at least four cycles.

#### A HIGH TEMPERATURE X-RAY AND THERMAL ANALYSIS STUDY OF SYNTHETIC DAWSONITE

L. A. Harris V. J. Tennery

The decomposition of synthetic dawsonite [NaAlCO<sub>3</sub>(OH)<sub>2</sub>] was studied by DTA, TGA, and x-ray techniques and found to be considerably more complex than indicated by earlier work. In DTA, a broad asymmetrical endothermic peak started at about 250°C and ended at about 450°C, with a bulge at 325°C. This suggests that two separate reactions may be occurring, an initial loss of water and the subsequent loss of carbon dioxide. A previously unreported exothermic peak was observed at about 650°C followed by a shallow endotherm at about 670°C. X-ray diffraction at high temperatures showed that the dawsonite structure collapsed at about 200°C, and sodium aluminate (NaAlO<sub>2</sub>) is well crystallized at 500°C. In the interval 200 to 500°C, the material appears to be noncrystalline by x-ray techniques. The TGA results corroborated the DTA, and the temperature differences between the dynamic (DTA and TGA) and static (x-ray) experiments are reasonable and explicable.

## 45. Alloy Development for Army Pulsed Radiation Facility Reactor

A. P. Litman<sup>1</sup>

The Army Pulsed Radiation Facility Reactor (APRFR) is the most recent among first-generation, fast-burst reactors for which gamma-stabilized alloys based on U-10% Mo are used for core and control-element components. Fast-burst reactors operate with prompt neutrons and are designed to simulate the radiation environment of an atomic weapon explosion. Their primary usefulness is to study the effects of radiation on nuclear fuels under transient conditions. Reactors of this type, including the APRFR, are used in basic studies of the fission process, radiation dosimetry, shielding studies, calibration of radiation alarms for criticality accidents, and radiobiology.

Last year<sup>2</sup> we embarked upon a core-alloy development program to select an alloy better than U-10% Mo for pulsed reactor fuel. Some of the results of this program are reported here. This work is sponsored by the U.S. Army Ballistic Research Laboratories through interagency agreement with the USAEC.<sup>3</sup>

### CORE ALLOY DEVELOPMENT AND EVALUATION

C. W. Dean<sup>4</sup> A. P. Litman<sup>1</sup>

Service conditions for fast-burst reactors demand that the core material withstand unusually high stress levels resulting from rapid thermal expansion and inertia loads. As an example, rapid additions of reactivity above prompt criticality during the APRFR core test program have resulted in temperature increases as large as 880°C in a fraction of a millisecond.<sup>5</sup> Using the criterion that toughness (the ability to resist brittle fracture), rather than strength alone, is the controlling mechanical property for a pulsed-reactor fuel, we investigated the notch-toughness properties of U-10%

Mo alloys containing 0.25% Al, 0.3% Cr, 0.3% Ti, 1% Ta, and 2% Nb plus 1.0% Ti.

Ingots of these compositions were vacuum induction melted, cast, heated in vacuum at 900°C for 16 hr, and water quenched. Metallographic examination showed that the ingots were homogeneous and, with the possible exception of the U-10% Mo-1% Ta alloy, contained only a single phase. The castings were then machined into standard Charpy V-notch impact specimens and aged at 475°C – the estimated maximum embrittlement temperature – for times to 64 hr. All specimens were then impact tested at 200°C in air. The notch toughness of the alloy containing 0.3% Ti was clearly superior, and the impact behavior of the U-10% Mo-1% Ta alloy, while inferior to that of the alloy containing 0.3% Ti, was relatively independent of aging time.

Eight U-10% Mo ingots containing 0.1, 0.2, 0.5, and 1.0% Ti, and 0.1, 0.2, 0.5, and 0.75% Ta were cast and homogenized by the procedure described above. By metallographic examination, all of these alloys were single-phased except for those containing 0.5 and 0.75% Ta, which contained two phases. Charpy impact tests of these alloys are in progress.

---

<sup>1</sup>Now with the USAEC, Washington, D.C.

<sup>2</sup>A. P. Litman, *Metals and Ceramics Div. Ann. Progr. Rept. June 30, 1969*, ORNL-4470, p. 212.

<sup>3</sup>M. I. Lundin, Reactor Division, served as Program Director at ORNL.

<sup>4</sup>Metallurgical Development Department, Y-12 Plant, Oak Ridge, Tenn.

<sup>5</sup>J. T. Mihalcz, *Static and Dynamic Measurements with the Army Pulse Radiation Facility Reactor*, ORNL-TM-2330 (June 1969).

## 46. Metallography

R. J. Gray

The Metallography Groups provide technical services to the various laboratories and programs of the Metals and Ceramics Division and to other divisions of this Laboratory. Three metallographic facilities are used in this function. Highly radioactive materials are remotely processed in the heavily shielded cells of the High Radiation Level Examination Laboratory. Alpha radioactive materials are processed in a glove box facility, and nonradioactive materials are processed in a conventional metallography laboratory. Since metallography is both an art and a science, we aim to maintain a high level of service, improve on existing techniques, endeavor to develop new methods of investigation, and keep aware of the state of the overall field.

---

<sup>1</sup>R. S. Crouse and H. V. Mateer, *Metals and Ceramics Div. Ann. Progr. Rept. June 30, 1969*, ORNL-4470, pp. 213-16.

### ELECTRON MICROPROBE ANALYSIS

R. S. Crouse    T. J. Henson  
H. V. Mateer    J. L. Miller, Jr.,

The conversion<sup>1</sup> of the MAC model 400 microprobe to model 400S has enabled us to do beam scanning in four modes: x-ray, sample current, backscattered electrons, and secondary electrons. The scanning modes are so efficient that they are used to display the sample surface and to locate with good precision the spot to be probed with a static beam. For example, the light optics are used only to locate the area of interest, and the cathode-ray tube display of backscattered electrons enables us to electronically deflect the probe beam and position it exactly on the target area.

Figure 46.1 illustrates the use of a backscattered electron image and an x-ray display to characterize an

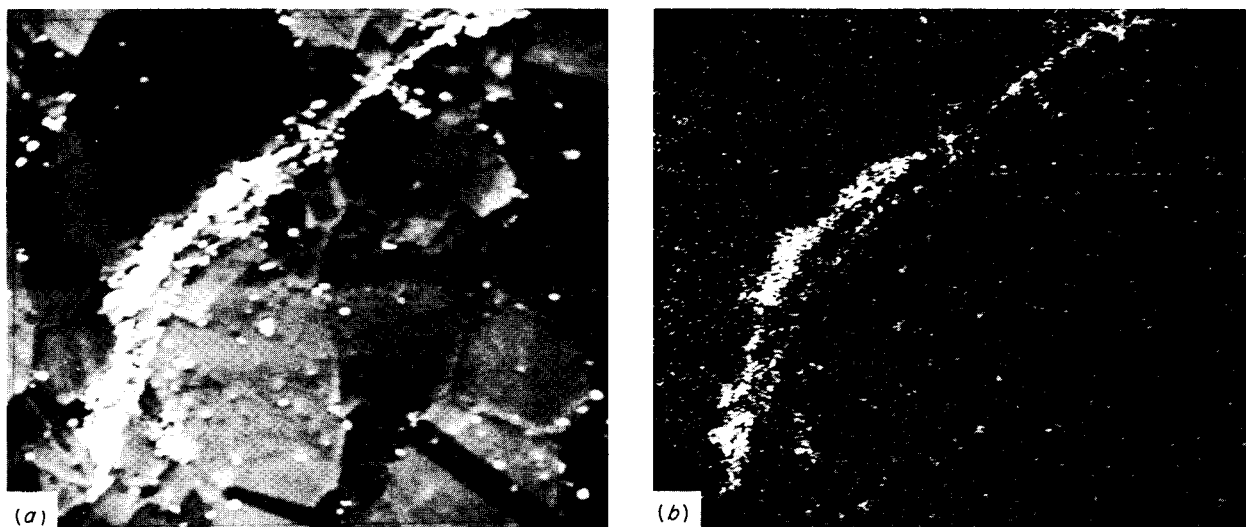


Fig. 46.1. Cathode-Ray Tube Displays of Hafnium Oxide Inclusion in Hastelloy N. (a) Backscattered electrons. (b) Hafnium  $L\alpha$  x rays. 375X.

unknown inclusion in Hastelloy N. The inclusion was identified as hafnium oxide by x-ray display. Since the average atomic weight of hafnium oxide is greater than that of Hastelloy N, the oxide appears white in the backscatter mode.

In the air oxidation of uranium-niobium-zirconium alloys, a two-layer oxide is produced. Figure 46.2 shows a typical microstructure. A microprobe step scan across the layers from metal to oxide-air interface produced

the profiles shown in Fig. 46.3. It is interesting to note that the zirconium decreases only slightly in the oxides, but the niobium drops markedly in the inner zone and returns in the outer zone almost to the level found in the alloy. This is not readily explainable. The uranium profile indicates that there are two distinctly different uranium oxides formed. Apparently the inner oxide has low niobium solubility but does not bar the migration of niobium to the outer oxide. This work was in

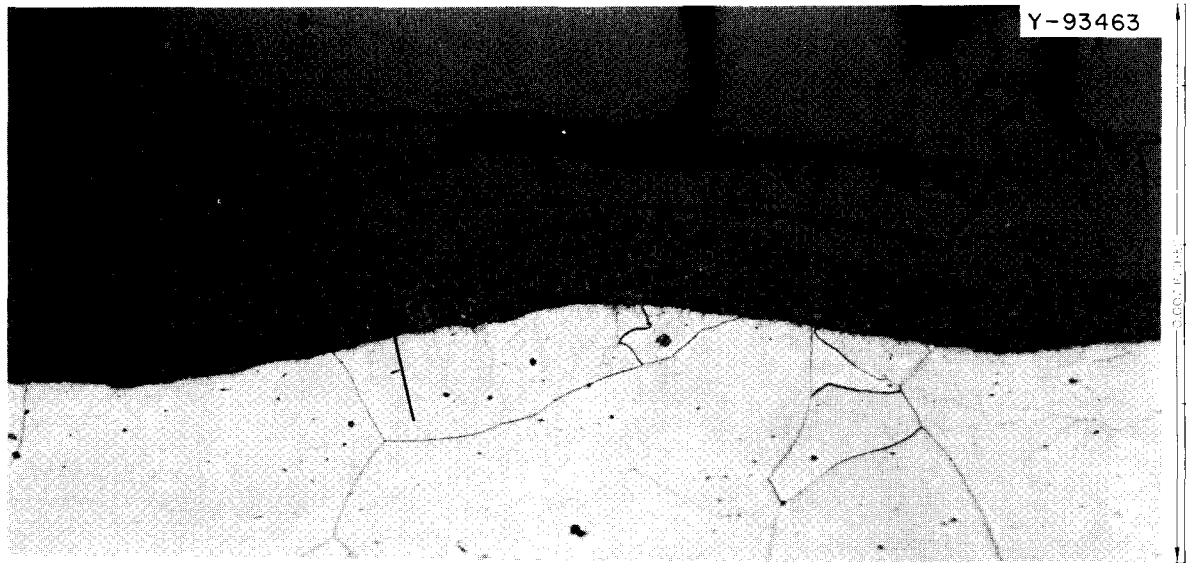


Fig. 46.2. Oxidized Uranium-Niobium-Zirconium Alloy Showing the Two Oxide Layers. Arrow indicates the direction of microprobe traverse, 400X.

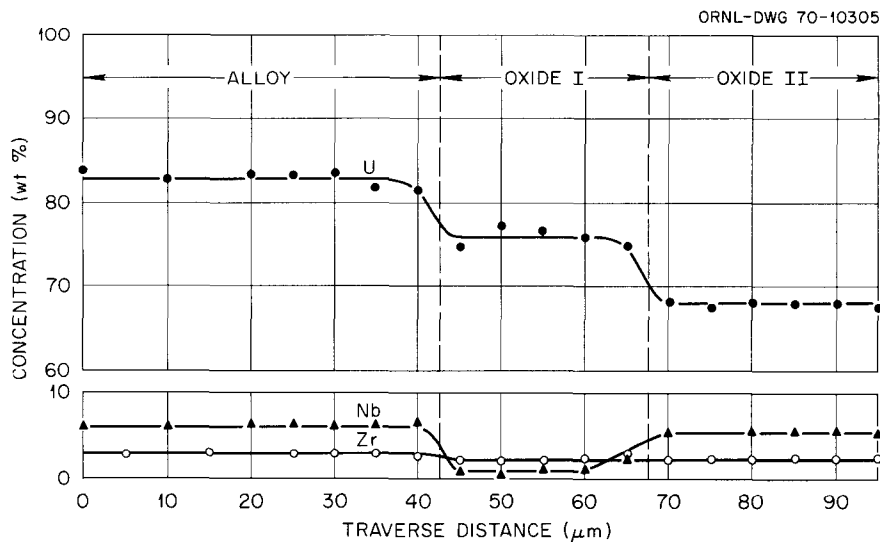


Fig. 46.3. Microprobe Analysis Through Oxide Film on Uranium-Niobium-Zirconium Alloy. Scan traverses the metal phase and two oxide layers as indicated in Fig. 46.2.

support of a program described in Chapter 12 of this report.

The analytical versatility of the electron microprobe has been shown on some human tissue for the Biology Division. This was our first venture into the microprobe analysis of soft tissue and has opened the way for more such work with this instrument. Specimens of human testes tissue were examined for signs of malacoplakia, a disease that results in small ( $<7\text{-}\mu\text{m-diam}$ ) crystal bodies in the testes. Samples were taken from tissue that had given a positive histochemical test for the disease and from tissue suspected of having the disease without the positive histochemical test. Figure 46.4 shows a secondary electron display of the known affected tissue and x-ray displays of Ca, P, and Fe. Figure 46.5 shows

similar displays of the suspected tissue and reveals it to have essentially the same elements present in similar areas. One concludes that malacoplakia is indeed present in the suspect tissue.

Some new techniques for data reduction and presentation have been employed in microprobe analysis this year. As has been shown above, cathode-ray tube x-ray displays are used to demonstrate the presence and location of elements in a microstructure. Normally, this requires one picture per element, but by using color photography, we can present all the same information in a single picture. One method of making an x-ray display in color is to rephotograph black and white displays through color filters, assign a different color to

Y-97355

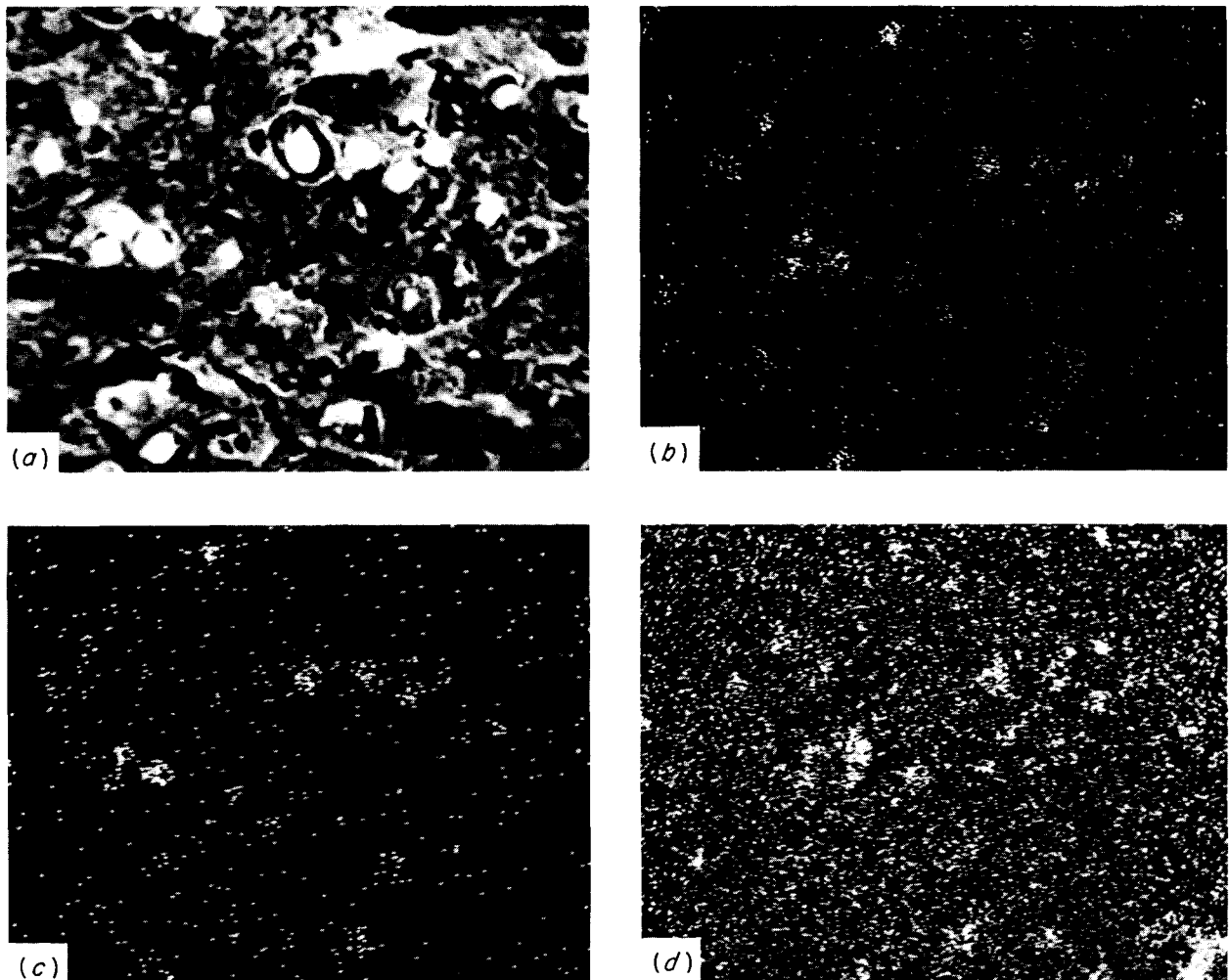


Fig. 46.4. Cathode-Ray Tube Display of Tissue Known to Be Affected by Malacoplakia. (a) Secondary electrons. (b) Calcium K $\alpha$  x rays. (c) Phosphorous K $\alpha$  x rays. (d) Iron K $\alpha$  x rays.

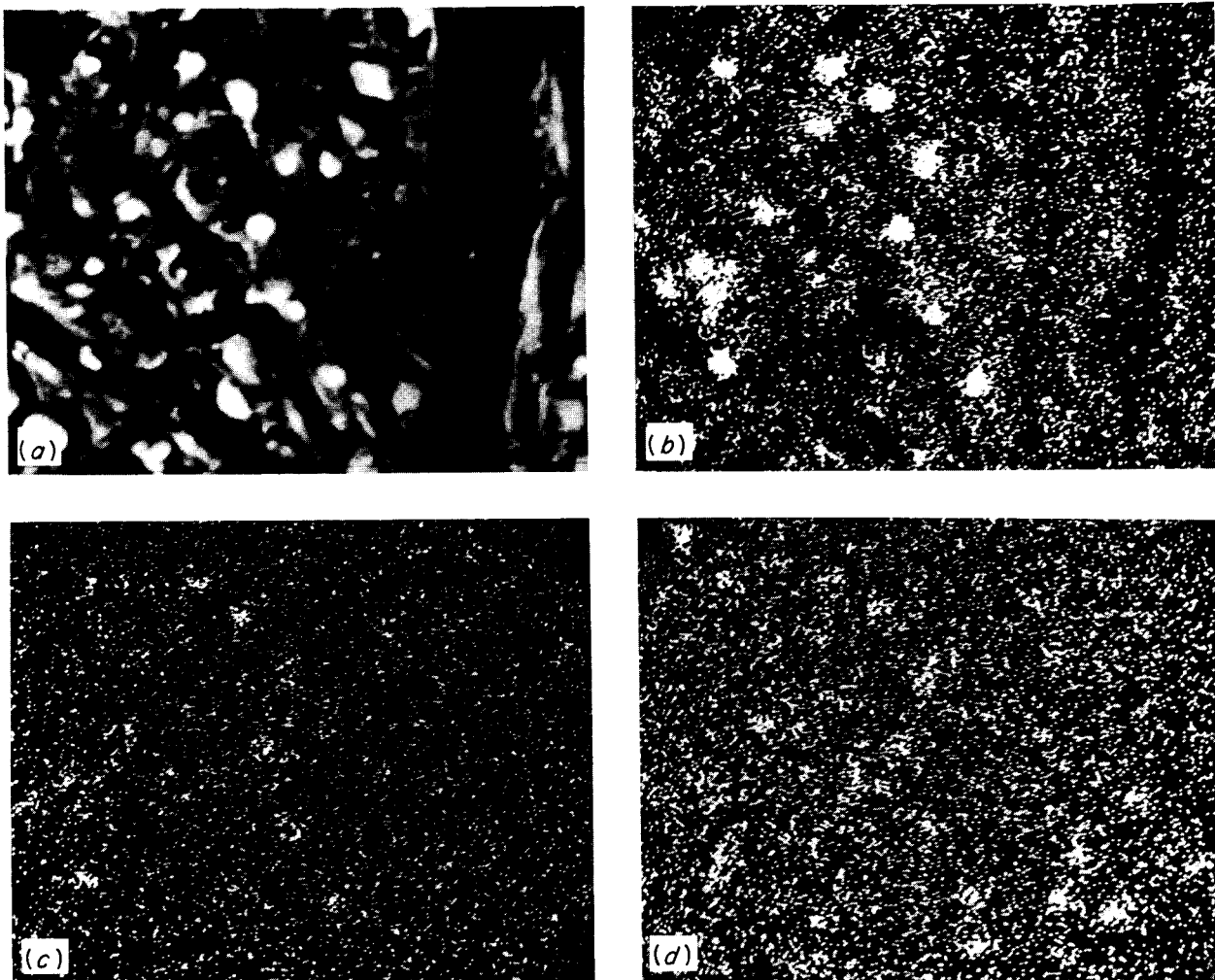


Fig. 46.5. Cathode-Ray Tube Display of Tissue Suspected of Being Affected by Malacoplakia. (a) Secondary electrons. (b) Calcium  $K\alpha$  x rays. (c) Phosphorous  $K\alpha$  x rays. (d) Iron  $K\alpha$  x rays.

each element, and superimpose the images on a single piece of color film.

A computer program was developed and installed in an ORNL computer for reducing x-ray intensities to numerical values and producing a computer-plotted graph. The program is designed specifically for plotting concentration gradients from a linear step scan across a specimen. An application of this program is illustrated in Fig. 46.6. A cross section of a human tooth containing fillings of silver-tin amalgam and a 100X photomicrograph of the amalgam-tooth interface where the traverse was made are shown with the tin concentration as plotted by the computer.

A Materials Analysis Company<sup>2</sup> (MAC) shielded electron microprobe has been installed at the hot cells

in HRLEL and was activated for radioactive samples in November 1969. Figure 46.7 shows the installation on the second floor of Bldg. 3525. A more detailed description of the installation of the shielded microprobe and its relationship to the hot cell facility has been reported.<sup>3</sup> Some of the results obtained have been reported in the General Fuels and Materials Research Section.

<sup>2</sup>Model 450, Materials Analysis Company, Palo Alto, Calif.

<sup>3</sup>E. L. Long, Jr., J. L. Miller, Jr., and R. J. Gray, *Metals and Ceramics Div. Ann. Progr. Rept. June 30, 1969*, ORNL-4470, p. 216.

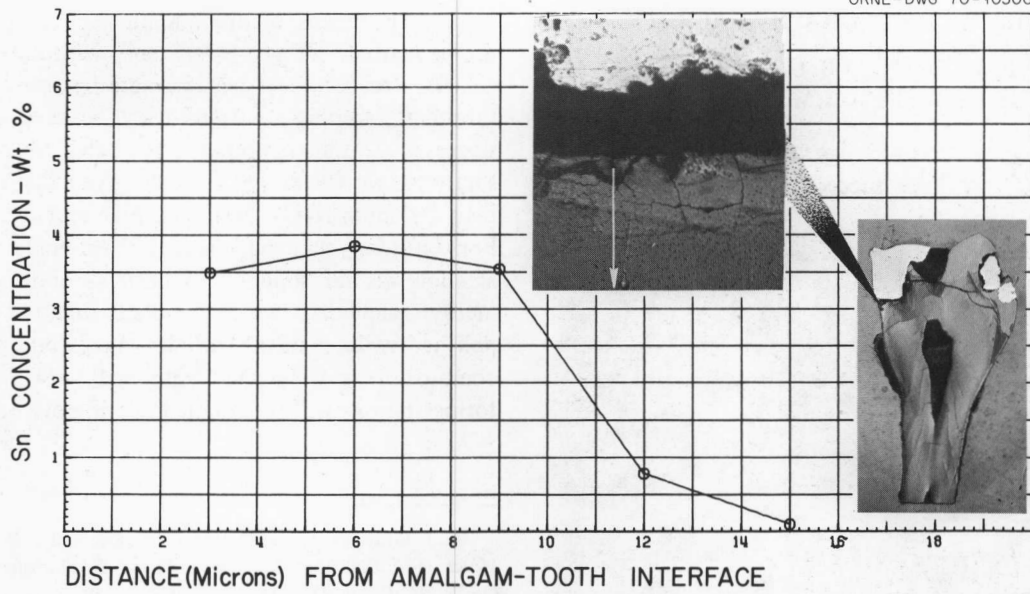


Fig. 46.6. Computer Plot Showing Penetration of Tooth by Silver-Tin Amalgam Filling. Insets show location of microprobe scan.

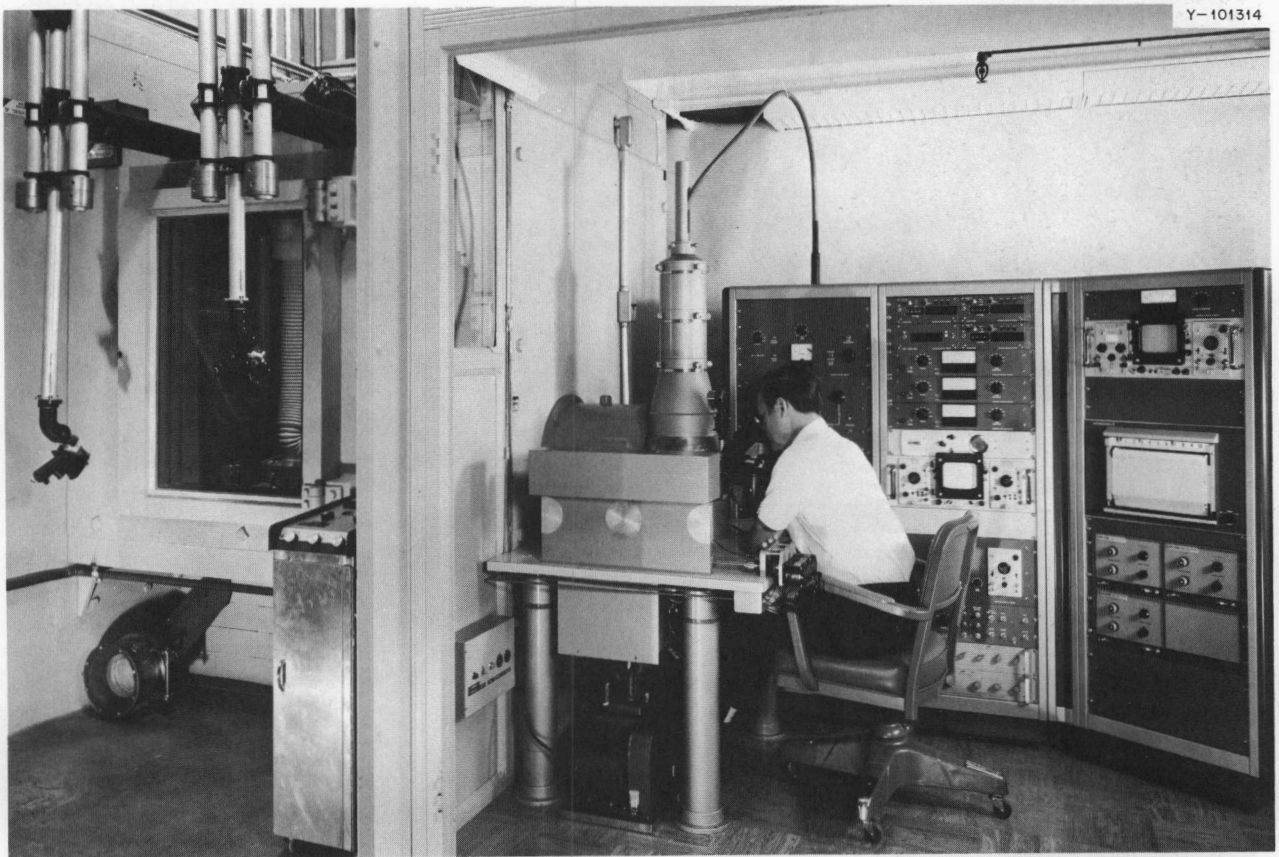


Fig. 46.7. Shielded Electron Microprobe Analyzer. Specimen is transferred from the metallography cell through the cell wall to the steel cubicle (left). A second transfer is made to the shielded microprobe or to a shielded x-ray diffraction unit behind the steel cubicle.

## ALPHA METALLOGRAPHY FACILITY

R. J. Gray      B. C. Leslie  
H. R. Gaddis    J. W. Chumley

Since our glove box line has been equipped for argon atmosphere,<sup>4</sup> we have successfully prepared metallo-

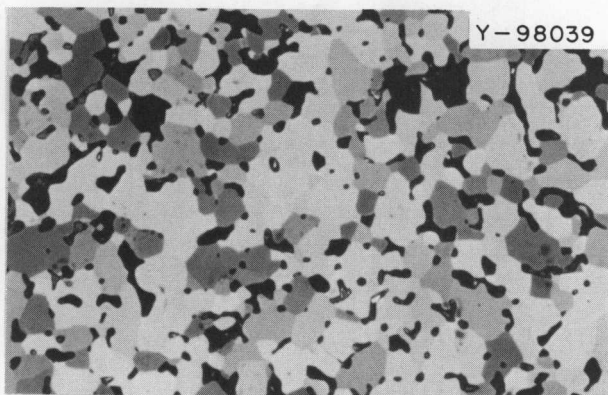


Fig. 46.8. Uranium-Plutonium Nitride. Etchant: lactic, nitric, and hydrofluoric acids. 200X.

graphic specimens of uranium-plutonium nitride (Fig. 46.8), carbide (Fig. 46.9), and carbonitride (Fig. 46.10). Because these materials are hygroscopic, moisture-free polishing solutions must be used during all stages of specimen preparation. After testing several solutions, we found that ethylene glycol distilled to less than 600 ppm H<sub>2</sub>O was an acceptable abrasive vehicle. For cleaning the specimens reagent-grade isopropyl alcohol was far superior to both absolute ethyl and methyl alcohols, which reacted slightly with the polished surfaces of the carbides. As a safety measure, a combustible gas detector equipped with four monitoring stations will be installed in our glove boxes soon.

<sup>4</sup>R. J. Gray, H. R. Gaddis, B. C. Leslie, and J. W. Chumley, *Metals and Ceramics Div. Ann. Progr. Rept. June 30, 1969*, ORNL-4470, pp. 213-15.

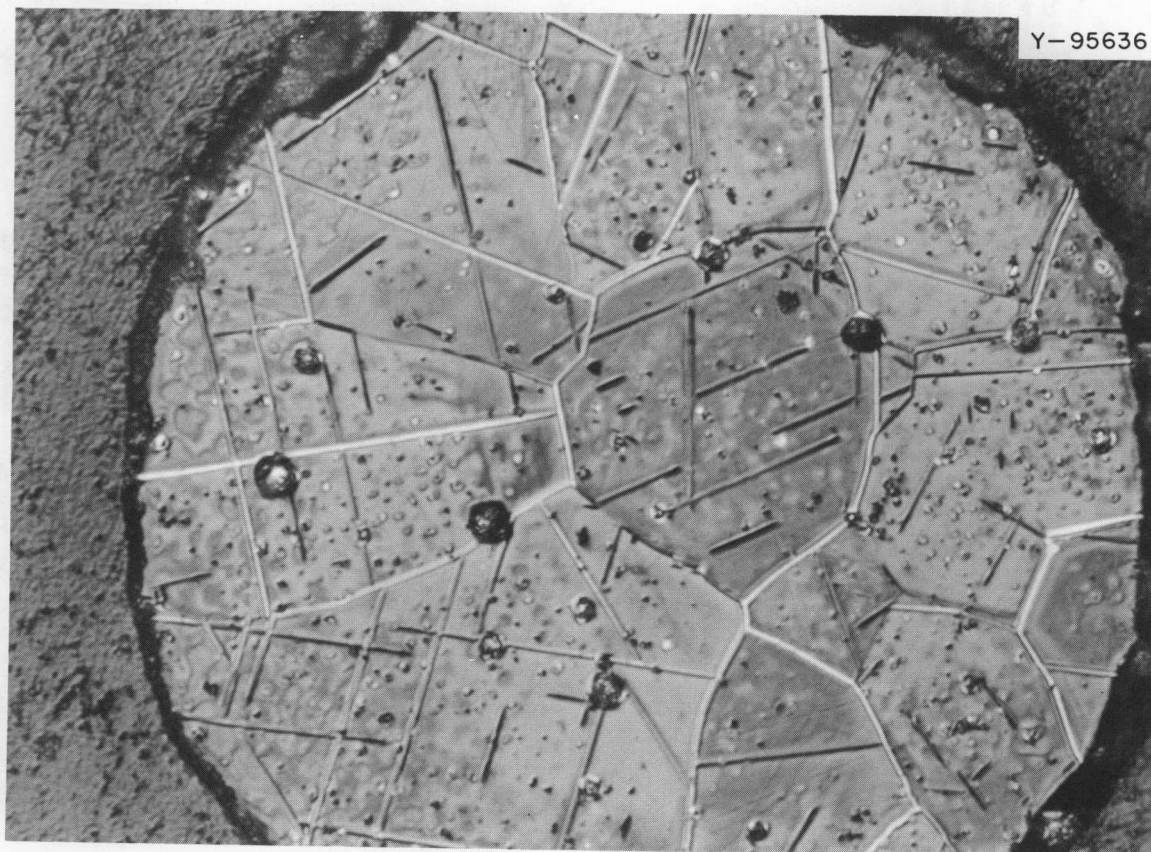


Fig. 46.9. Uranium-Plutonium Carbide Microsphere. Note the presence of (U, Pu)C<sub>2</sub> (light phase) in the etched microstructure. 1000X.

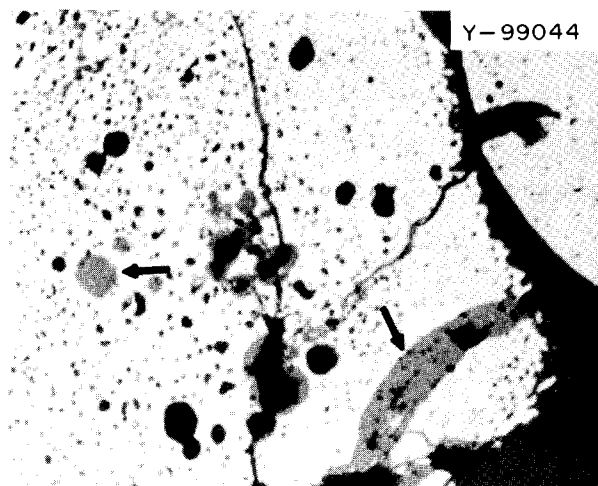


Fig. 46.10. Unetched Microstructure of Pu-U Carbonitride Prepared from Oxide by High-Temperature Conversion. Arrows point to unreacted oxide.

#### METALLOGRAPHY OF RADIOACTIVE MATERIALS AT OAK RIDGE NATIONAL LABORATORY

R. J. Gray E. L. Long, Jr. A. E. Richt

A general description of radiation metallography in the Metallography Groups of the Metals and Ceramics Division has been reported.<sup>5</sup> Both specifically designed and modified commercial metallographic equipment are described, and microstructural alterations of structural and fuel materials after exposure in a nuclear reactor are presented.

#### ALPHA AUTORADIOGRAPHY

T. M. Kegley, Jr.

Alpha autoradiography has proven to be a very useful adjunct to the metallography of nuclear materials.<sup>6-8</sup> Since uranium and plutonium are excellent alpha

<sup>5</sup> Abstracted from paper in *Applications of Modern Metallographic Techniques, Spec. Tech. Publ. 480*, American Society for Testing and Materials, Philadelphia, 1970, in press.

<sup>6</sup> J. H. Davies and R. W. Darmitzel, "Alpha Autoradiographic Technique for Irradiated Fuel," *Nucleonics* 23(7), 86-87 (July 1965).

<sup>7</sup> J. L. Hascall, *Alpha Autoradiography of Irradiated Materials*, BNWL-324 (October 1966).

<sup>8</sup> W. J. Gruber, "Autoradiography of Irradiated Ceramic Fuels," pp. 21-25 in *Proceedings of the 17th Conference on Remote Systems Technology, 1969*, American Nuclear Society, Hinsdale, Ill., 1969.

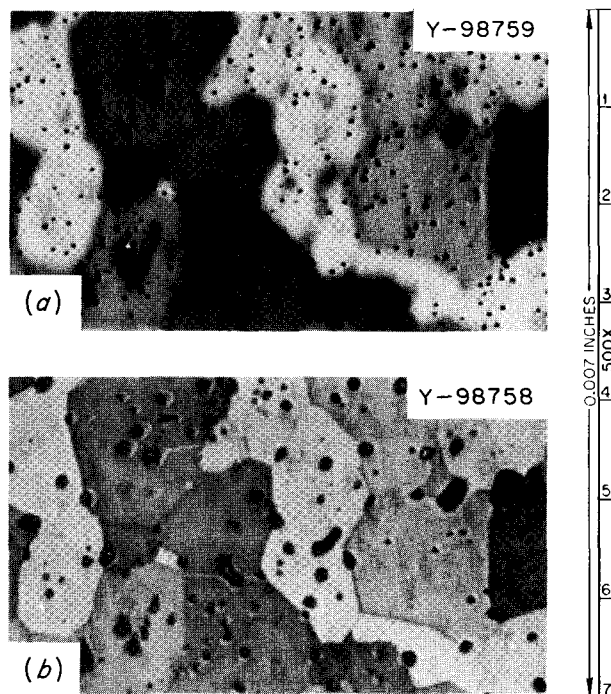


Fig. 46.11. Specimen-Supported Alpha Autoradiograph of Enriched Uranium Nitride Specimen. Cellulose nitrate film previously stripped from a glass plate was wetted to surface with acetone. (a) Alpha particle tracks at surface in focus. (b) Specimen surface in focus.

emitters, materials containing these elements can be autoradiographed advantageously. Although specimens can be autoradiographed by use of photographic silver emulsions, we employed cellulose nitrate since it is simpler to develop and does not require dark room facilities. While using cellulose nitrate we have tried to develop and extend our technique. As ordinarily used, cellulose nitrate is supported by a plastic film or a glass plate. This means that before development in sodium hydroxide the specimen must be removed from the cellulose nitrate and only a contact autoradiograph is obtained. If the cellulose is supported directly by the specimen being autoradiographed, then the cellulose nitrate film can be developed *in situ*. Figure 46.11 shows a specimen-supported alpha autoradiograph of an enriched uranium nitride specimen. The alpha autoradiograph was made by fixing a cellulose nitrate disk 13 mm in diameter  $\times$  10 to 20  $\mu$ m thick to the surface by wetting the disk with a drop of acetone. The cellulose nitrate film was exposed 16 hr to alpha particles emitted from the specimen before developing 22 min in 6 N NaOH at 24°C.

## SHATTERPROOF COATINGS FOR GLASS<sup>9</sup>

R. J. Gray

The shatterproofing of glass with Silastic coatings, which can be applied in the laboratory, was investigated. The items tested were light bulbs, Pyrex tubing, Dewar flasks, and capillary tubes. Two commercial products definitely improved the impact resistance of the glass and greatly reduced shattering of the sharp particles. The primary purpose was to minimize the hazard of glass containers used in glove boxes.

## IMPROVED METALLOGRAPH ILLUMINATION SYSTEM

R. J. Gray B. C. Leslie

Carbon-arc illumination systems have been used for metallographs for many years. Although this light source is intense, it is unstable and nonuniform, so its use in photomicrography can present problems. We installed commercially available xenon arc lamps,<sup>10</sup> and they decidedly improved the performance of our older metallographs. Our experience with this new product, including information on installation, performance, and, particularly, its application in color metallography, has been reported.<sup>11</sup>

## QUANTITATIVE TELEVISION MICROSCOPY

T. M. Kegley, Jr.

Area measurements made with the Quantimet image analyzing computer are very dependent on a proper

setting of the threshold control, which determines the threshold of detection relative to the optical intensity of the detected feature. Figure 46.12 compares threshold-area curves for a nickel-bakelite compact, whose nickel content was 20.02 vol % as found by immersion density measurement. As the objective magnification increases, the curve becomes flatter in the region of the correct area measurement. The increasing flatness of the curve with increasing magnification is related to a decrease in the number of features in the blank frame. This is directly analogous to the previous results,<sup>12</sup> where the threshold-area curve for the sample containing a single large feature exhibited a vertical plateau at the correct area reading, while the curve for the sample containing many small features exhibited no such plateau. These results point out the necessity for using sufficient magnification for proper detection of microstructures containing many small features.

<sup>9</sup>Abstracted from ORNL-4521 (March 1970).

<sup>10</sup>Ionics Inc., Electronics Division, Watertown, Mass.

<sup>11</sup>R. J. Gray and B. C. Leslie, "High-Intensity Xenon Arc Lamp for Older Research Metallographs," pp. 121-38 in *Proceedings of Second Annual Technical Meeting, International Metallographic Society, Sept. 8-10, 1969, San Francisco, Calif.*, International Metallographic Society, Los Alamos, N.M., 1970.

<sup>12</sup>T. M. Kegley, Jr., "Quantimet Area Measurement Problems," pp. 163-69 in *Proceedings of Second Annual Technical Meeting, International Metallographic Society, Sept. 8-10, 1969, San Francisco, Calif.*, International Metallographic Society, Los Alamos, N.M., 1970.

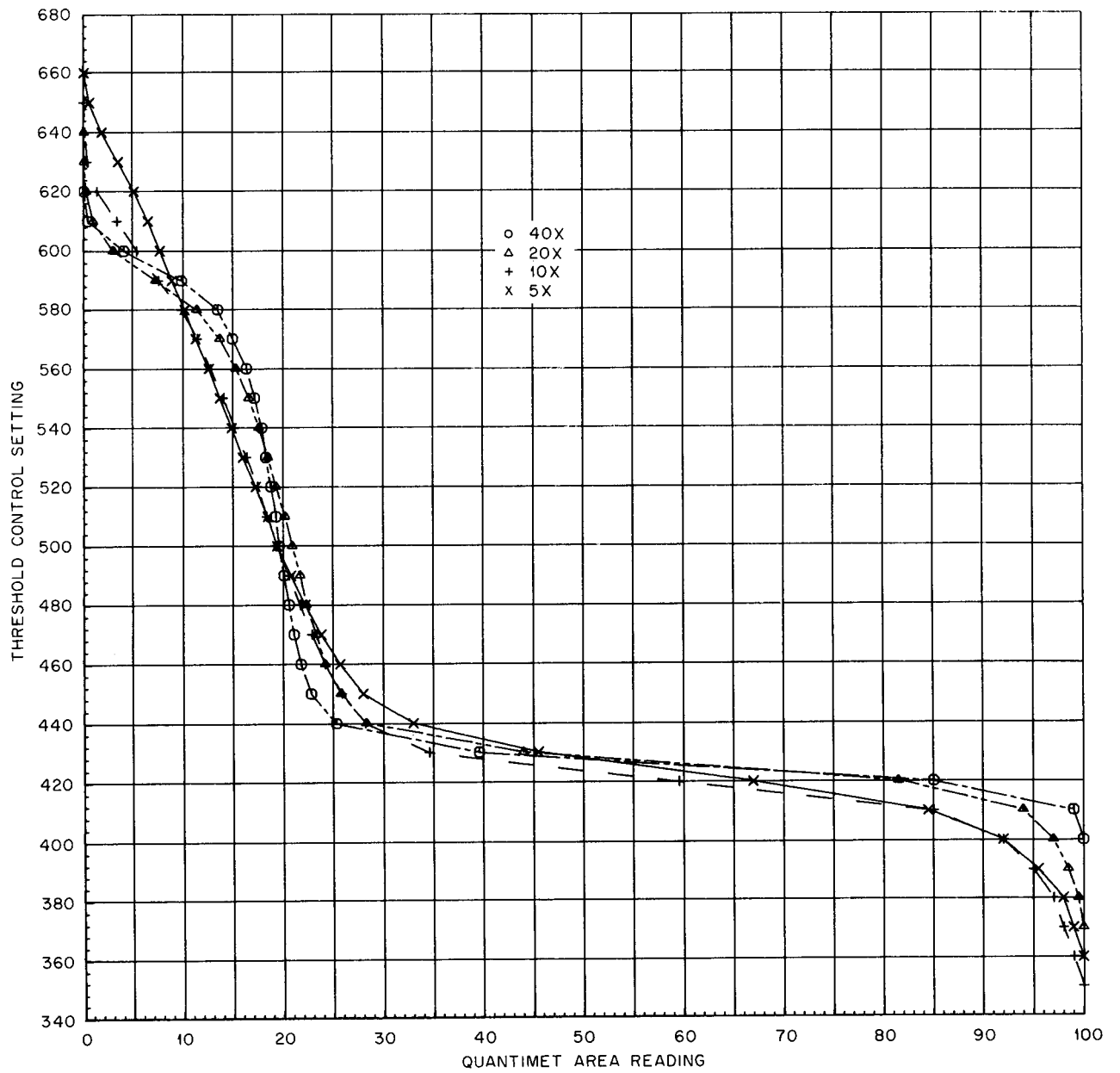


Fig. 46.12. Threshold-Area Curves Obtained for Nickel-Bakelite Compact, with Different Objective Magnifications.

## 47. NERVA Program Metallurgical Support

R. E. Clausing

We continue to provide support for the Materials and Structures Branch of the AEC-NASA Space Nuclear Propulsion Office on the NERVA Program.<sup>1,2</sup> We provide technical consultation for NASA and some of its contractors and also perform experimental work including developing special nondestructive testing techniques and studying outgassing characteristics of NERVA fuel elements, adhesion of NERVA materials in simulated space environments, and selected physical properties of NERVA materials. Previous work on thermal fatigue testing of nozzle tube configurations<sup>3,4</sup> has led to additional mechanical properties measurements.

### EFFECTS OF SPACE ENVIRONMENT ON NERVA MATERIALS

R. E. Clausing

Exposure of the NERVA engine to the environment of space may produce materials problems not encountered in ground tests. A committee composed of representatives from the NASA Space Nuclear Propulsion Office at Cleveland, Aerojet General Corporation, Westinghouse Astronuclear Laboratory, Oak Ridge National Laboratory, and TRW, Inc., attempts to define such problem areas and to ensure that the NERVA design and fabrication are consistent with reliable operation in the space environment.

The tendency of atomically clean surfaces to adhere is one of the important space-related phenomena. Adhesion and friction of clean surfaces are not well

understood, but the presence or absence of adsorbed gases on otherwise atomically clean surfaces is known to alter adhesional and frictional properties of both pure materials and engineering alloys. To assess the importance of these effects on the materials in the NERVA system we need to know (1) the specific environment at the location of particular components in the engine and (2) how this environment will influence adhesion and friction. We are providing information on both of these subjects through the two experimental studies described briefly below.

### Outgassing of NERVA Fuel Elements

R. E. Clausing D. S. Easton

The gaseous atmosphere at any point in the NERVA engine will depend upon the temperature and history of the entire engine system; in the present design it will be determined primarily by the outgassing of the graphite reactor components. This outgassing cannot be accurately estimated because of the special nature of the core material, its configuration, and its coating. Experimental data must be sought for the prototype core elements at temperatures and pressures similar to those expected in space operation.

A facility to provide such information has been designed, built, tested, and put into operation.<sup>1,2</sup> This apparatus measures the type, quantity, and outgassing rates of gases released at various temperatures from graphite fuel elements held in vacuum. Semiautomatic data readout from a quadrupole residual gas analyzer and nude Bayard-Alpert ion gages permits rapid analysis of data for as many as 12 gases simultaneously. The data are processed by an IBM 360/91 computer, and the results are available in tabular and graphical form. The computer program calculates the partial pressure for each gas, tabulates the outgassing rates for each sampling time, and plots outgassing rate as a function of time and/or temperature. In addition, the outgassing

<sup>1</sup>R. E. Clausing *et al.*, *Metals and Ceramics Div. Ann. Progr. Rept. June 30, 1968*, ORNL-4370, pp. 235-37.

<sup>2</sup>R. E. Clausing *et al.*, *Metals and Ceramics Div. Ann. Progr. Rept. June 30, 1969*, ORNL-4470, pp. 218-21.

<sup>3</sup>D. G. Harman, *Thermal Fatigue of Rocket Nozzle Cooling Tubes*, ORNL-TM-2089 (February 1969).

<sup>4</sup>D. G. Harman, "Thermal Fatigue of Rocket Nozzle Cooling Tubes," to be submitted for publication.

data are reduced to analytical form and extrapolated to yield estimates of outgassing rates after very long periods.

We are presently using this apparatus to collect outgassing data on XE-II fuel elements. Quarter-length single elements, full-length single elements, and quarter-length clusters of seven elements are to be tested in the present series. Quarter-length elements have been tested in the as-received condition and after having been heated to 2200°C in hydrogen and transferred to the outgassing apparatus without exposure to air.

Isothermal outgassing rates for 13 gases ( $H_2$ , He,  $CH_4$ ,  $H_2O$ ,  $N_2$ , CO,  $O_2$ , Ar,  $CO_2$ ,  $C_2H_4$ ,  $C_2H_6$ ,  $C_3H_8$ , and higher hydrocarbons) were measured at five temperatures between 50 and 870°C for these elements. The data in all cases can be described by the relationship  $q = A(t/t_0)^B$ , where  $q$  is the rate of outgassing,  $t$  is the time of outgassing, and  $A$ ,  $B$ , and  $t_0$  are constants. The values found for  $B$  ranged from  $-0.3$  to  $-2.3$  and were sensitive both to temperature and to the pretreatment given the fuel elements.

We also measured outgassing rates with the temperature increasing linearly with time. Figure 47.1 shows data from a run in which the temperature was increased from 50 to 870°C at a rate of 220°C/hr. Note especially that there are several temperatures at which one or more gases begin to be evolved quite rapidly. These temperatures can be used to estimate activation energies for desorption or chemical reaction. They may also reflect changes in chemical equilibrium constants or in the structure of the fuel element.

Because these data are preliminary and because the system is chemically complex, no interpretations are offered at this time. Work will continue, however, in order that we may determine whether it is practical to extrapolate and interpolate our results in temperature as well as time. We also intend to examine systematically the effect of manufacturing storage and handling variables on outgassing behavior.

### Adhesion of NERVA Materials

R. E. Clausing

This program was conducted through an ORNL subcontract with Syracuse University Research Corporation. R. G. Aldrich is the principal investigator, and R. E. Clausing of the ORNL Metals and Ceramics Division is the project monitor. Special emphasis has been placed on determining the roles of surface contamination and shear motion in the adhesion of engineering materials of interest to NERVA. The

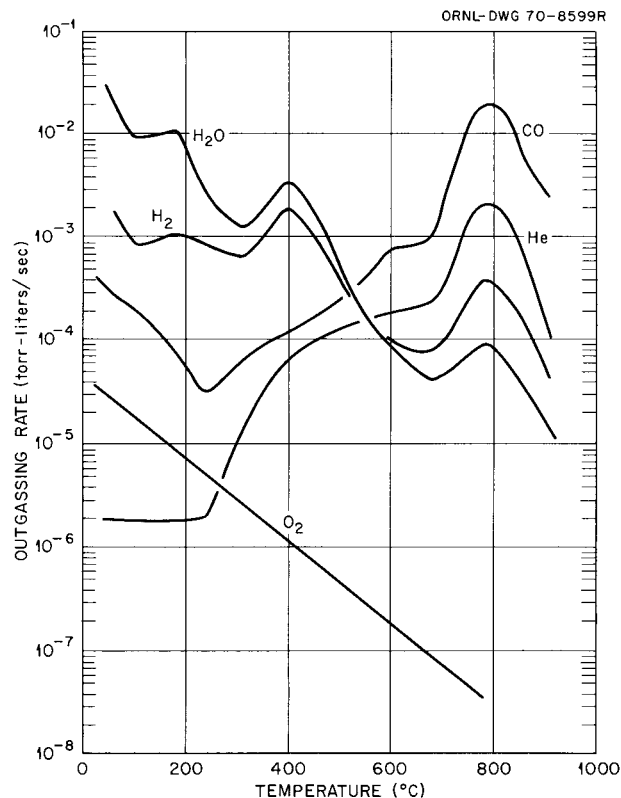


Fig. 47.1. Outgassing Rate as a Function of Temperature. The sample temperature was increased from 50 to 870°C at a rate of 220°C/hr.

experiment is providing both a preliminary evaluation of possible adhesion problems with NERVA materials and a guide for the design of future materials and component qualification tests.<sup>5</sup> Several surface cleaning methods were used, and various gases were permitted to contaminate the cleaned surfaces before and during the adhesion testing. Adhesion was obtained for these engineering materials only after severe cleaning and high, normal-force loading or surface shearing motions. The results of the first portion of these tests, which emphasized normal-force loading, have been reported.<sup>2,6</sup>

Materials that exhibit no significant tendency to cold weld under static loads may do so rather abruptly under rubbing conditions. This has been investigated for the following adhesion couples: (1) type 440C stainless steel versus itself, (2) pyrolytic graphite versus ZTA

<sup>5</sup>K. I. Johnson and D. V. Keller, *J. Appl. Phys.* 38, 1896-904 (1967).

<sup>6</sup>R. G. Aldrich, *Ultra High Vacuum Adhesion Testing of NERVA Engine Materials*, TID-25088 (July 1968).

graphite, (3) NbC on graphite versus itself, (4) electrolyzed Inconel 718 versus gold-plated type 302 stainless steel. In all cases rubbing caused a gradual increase in the coefficient of friction and promoted adhesion by either disrupting contaminant films, by mechanical contact area growth, or a combination of both.

### NONDESTRUCTIVE INSPECTION OF COOLANT CHANNELS IN BERYLLIUM REFLECTOR COMPONENTS

C. V. Dodd R. W. McClung

We are continuing the development of nondestructive test methods for the detection of ferromagnetic inclusions in the coolant channels of a beryllium reflector component.<sup>7</sup>

A Hall test probe, consisting of a 0.180-in.-diam  $\times$  1-in.-long permanent magnet with a Hall device on each end, was designed and built. The device measures the magnitude of the magnetic field, which is changed by the presence of small ferromagnetic objects. The difference in magnetic fields detected by the two Hall devices is amplified and recorded; thus, a double pulse is produced as the probe is moved past a ferromagnetic inclusion. For calibration we scanned inside a 0.255-in.-OD aluminum tube with a 0.035-in.-thick wall. A 0.032-in.-diam ferromagnetic wire was looped around the outside of the tube, and another 0.030 in. long was placed in a hole in the wall. Both wires were detected, although the signal was only slightly greater than the background noise. We scanned 24 holes in the beryllium sector and found no ferromagnetic inclusions as large as the standards.

As a result of this investigation and some computer calculations on eddy current techniques, we concluded that a more sensitive test for ferromagnetic inclusions could be made using a low-frequency eddy-current bridge instrument. The measurement errors that would be caused by a drift in bridge components have been calculated and components with the desired stability obtained. The instrument is now under construction.

### THERMAL FATIGUE OF NOZZLE TUBES

D. G. Harman

The cooling tubes that line the inner surface of the nozzle are subjected to temperatures ranging from that

of liquid hydrogen to possibly as high as 2000°F (1090°C). Since the tubes are brazed to a nozzle jacket that remains at a relatively low temperature throughout the operating cycle, thermal stresses of some consequence are generated within them.

We conducted tensile tests on 0.016-in.-thick sheet material from three separate heats of type 347 stainless steel. At each of six test temperatures we conducted 12 repetitive tests for each heat both parallel and transverse to the rolling direction of the sheet. These test results are being statistically analyzed by Aerojet General personnel.

### PHYSICAL PROPERTIES OF SELECTED NERVA MATERIALS

J. P. Moore R. S. Graves  
D. L. McElroy W. P. Murray

#### Beryllium

Since any beryllium body is likely to be anisotropic, rod samples of Brush beryllium 200 were tested in two conditions: with the rod axis parallel and perpendicular to the pressing direction. The samples were characterized with respect to immersion density, metallographic features, hardness, orientation factor, and resistivity ratio. This material had a preferred positioning of *c*-axes parallel to the pressing direction and was a relatively impure beryllium.

Table 47.1 lists smoothed thermal conductivity,  $\lambda$ , and electrical resistivity,  $\rho$ , values obtained from tests on three parallel rods and one perpendicular rod in a guarded longitudinal heat flow apparatus.<sup>8</sup> Our raw data for parallel rods were within  $\pm 0.5\%$  of these smoothed values. These  $\lambda$  results agree with those of Powell *et al.*<sup>9</sup> at low temperatures and those of Tye<sup>10</sup> at high temperatures. Generally  $\lambda$  is no more than 2% greater perpendicular than parallel, but the perpendicular  $\rho$  is 4 to 8% less than the parallel. These data yield Wiedemann-Franz Lorenz values significantly above the high-temperature Sommerfeld limit  $L_0$  of  $2.443 \times 10^{-8} \text{ V}^2/(\text{°K})^2$ , indicating the contribution of a large lattice component to  $\lambda$ . Both W-F-L ratios exhibit minima near 140°K. A simple "alloy separa-

<sup>8</sup>J. P. Moore, D. L. McElroy, and R. S. Graves, *Can. J. Phys.* 45, 3849-65 (1967).

<sup>9</sup>R. L. Powell, J. L. Harden, and E. F. Gibson, *J. Appl. Phys.* 31, 1221 (1960).

<sup>10</sup>R. P. Tye, *Thermophysical Properties of Hot Pressed Beryllium*, Dynatech Corp., Cambridge, Mass., July 1, 1968.

<sup>7</sup>C. V. Dodd and R. W. McClung, *Metals and Ceramics Div. Ann. Progr. Rept.* June 30, 1969, ORNL-4470, pp. 218-19.

Table 47.1. Smoothed Thermal Conductivity and Electrical Resistivity Values for Brush Beryllium 200 Parallel and Perpendicular to the Pressing Direction

Temperature (°K)	Parallel			Perpendicular		
	Thermal Conductivity [W cm <sup>-1</sup> (°K) <sup>-1</sup> ]	Electrical Resistivity (μΩ-cm)	W-F-L <sup>a</sup> [V <sup>2</sup> /(°K) <sup>2</sup> ]	Thermal Conductivity [W cm <sup>-1</sup> (°K) <sup>-1</sup> ]	Electrical Resistivity (μΩ-cm)	W-F-L <sup>a</sup> [V <sup>2</sup> /(°K) <sup>2</sup> ]
			× 10 <sup>-8</sup>			× 10 <sup>-8</sup>
80	2.973	0.761	2.83	3.04	0.701	2.66
100	3.269	0.827	2.70	3.36	0.785	2.64
200	2.634	2.098	2.76	2.65	1.97	2.61
300	1.961	4.602	3.00	1.96	4.42	2.89
400	1.602	7.655	3.07	1.61	7.33	2.95

<sup>a</sup>Wiedemann-Franz Lorenz ratio.

tion" of the lattice and electronic  $\lambda$  components using our perpendicular data and that of Hust *et al.*<sup>11</sup> showed the lattice component to rise from 0.6 W cm<sup>-1</sup> (°K)<sup>-1</sup> at 80°K to 1.2 at 300°K, while the Lorenz number was virtually temperature independent at about 0.5  $L_0$ . A large uncertainty exists in this analysis because the alloy differences were not as large as desired.

### Graphites

Thermal conductivity was measured in a comparative heat flow apparatus in the range 30 to 120°C on several orientations of Carbitex-700 and PO-3 graphite. We also measured  $\rho$  at room temperature on these materials. Results on these pitch-bonded graphites fit to at least 10% the empirical room-temperature correlation  $\lambda =$

0.0013/ $\rho$  suggested by Currie, Hamister, and MacPherson.<sup>12</sup>

Measurements of  $\lambda$  and  $\rho$  in the low-temperature apparatus<sup>8</sup> were completed from 80 to 400°K on one PO-3 graphite with an axial orientation. The  $\lambda$  values increased from 80 to 300°K and appear to reach a broad maximum near 340°K. Our  $\lambda$  results are 3% below those of Hust *et al.*,<sup>11</sup> and our  $\rho$  values are about 1% higher than theirs.

<sup>11</sup>J. G. Hust, R. L. Powell, and D. H. Weizel, *Thermal Conductivity, Electrical Resistivity, and Thermopower of Aerospace Alloys from 4 to 300 K*, NBS-9732 (June 1969).

<sup>12</sup>L. M. Currie, V. C. Hamister, and H. G. MacPherson, Vol. 8, pp. 451-73 in *Proc. Intern. Conf. Peaceful Uses At. Energy, Geneva, 1955*, United Nations, New York, 1956.

# Papers and Publications

## Papers and Oral Presentations

Compiled by Frances A. Scarboro

Gordon Research Conference on Corrosion, New London, N.H., July 21–25, 1969

J. V. Cathcart,\* “Oxidation of a U–7.5% Nb–2.5% Zr Alloy”

J. E. Epperson,\* “X-Ray Diffraction Analysis of the Structure of Thin Oxide Films Grown on Copper Single Crystals”

International Conference Quantitative Relation Between Properties and Microstructure, Haifa, Israel, July 24–Aug. 1, 1969

R. A. Vandermeer,\* “The Recrystallization Characteristics of Moderately Deformed Aluminum”

Conference on Crystal Growth, National Bureau of Standards, Washington, D.C., Aug. 11–13, 1969

A. T. Chapman, G. W. Clark,\* and D. E. Hendrix, “Unidirectional Solidification of Tungsten Rods and Plates from the UO<sub>2</sub>-W System”

8th International Congress on Crystallography, Stony Brook, N.Y., Aug. 12–24, 1969

B. Borie,\* “Basic Theory for Thermal Diffuse Scattering at the Bragg Angle”

H. L. Yakel,\* “Crystal Structures of Transition Phases Formed in U–16.60 at. % Nb–5.64 at. % Zr Alloys”

International Round Table Meeting on Sintering, Hercig-Novi, Yugoslavia, Aug. 14–24, 1969

C. S. Morgan\* and C. J. McHargue, “Some Aspects of Initial Densification Kinetics During Sintering”

Gordon Research Conference, Meriden, N.H., Aug. 24–29, 1969

C. R. Boston,\* L. F. Grantham, and S. J. Yosim, “Electrical Conductivities of Molten Aluminum Halide–Alkali Halide Mixtures”

J. Brynestad,\* “Acid-Base Chemistry of Nickel(II) in Molten Cesium Tetrachloroaluminate”

158th National Meeting of the American Chemical Society, New York, Sept. 7–12, 1969

K. E. Spear\* and J. M. Leitnaker, “Preparation and Crystal Structures of UVC<sub>2</sub> and UVN<sub>2</sub>”

International Conference on Heterogeneous Kinetics at Elevated Temperatures, Philadelphia, Sept. 8–10, 1969

T. B. Lindemer,\* J. M. Leitnaker, and K. E. Spear, “The Role of Carbon in Reactions in the U-C-O-N System”

2nd International Metallography Conference, San Francisco, Sept. 8–10, 1969

R. E. Gehlbach,\* C. E. Sessions, and S. W. Cook, “Effect of Alloying Additions on Precipitation in a Ni-Mo-Cr Alloy”

---

\*Speaker.

- R. J. Gray\* and B. C. Leslie, "High Intensity Xenon Arc Lamp for Older Research Metallographs"  
T. M. Kegley, Jr., "Quantimet Area Fraction Problems" (presented by R. J. Gray)
- National Symposium on Developments in Irradiation Testing Technology, Sandusky, Ohio, Sept. 9–11, 1969  
A. R. Olsen,\* R. B. Fitts, and C. M. Cox, Jr., "Analysis of the Validity of Fast Reactor Fuel Tests in Existing Test Reactors"
- AEC Metallography Group Meeting, San Francisco, Sept. 11–12, 1969  
R. E. Gehlbach,\* J. O. Stiegler, and K. Farrell, "Direct Observation and Identification of Transmutation Induced Silicon in a Neutron Irradiated Aluminum Alloy"  
E. L. Long, Jr., J. L. Miller, Jr., and R. J. Gray,\* "The Shielded Electron Microprobe Analyzer at Oak Ridge National Laboratory"
- Libby-Cockcroft Exchange Meeting on In-Pile Measurements and Capsule Technology, BMI, Columbus, Ohio, Sept. 15–17, 1969  
E. E. Bloom, J. W. Woods,\* and A. F. Zulliger, "Measurements of Nuclear Heating Rates in EBR-II and HFIR"  
C. M. Cox,\* J. A. Conlin, R. L. Senn, and S. C. Weaver, "Review of Selected ORNL Fuel Irradiation Capsules – Instrumented and Uninstrumented Capsules for the High Flux Isotope Reactor"  
C. M. Cox,\* V. A. DeCarlo, K. R. Thoms, R. B. Fitts, S. C. Weaver, and T. N. Washburn, "Review of Selected ORNL Fuel Irradiation Capsules – An Instrumented Oak Ridge Research Reactor Fuel Irradiation Capsule for Operation with Continuously Controlled Heat Rates up to 20 kw/ft with High Pressures and High Cladding Temperature"  
J. W. Woods,\* E. E. Bloom, and A. F. Zulliger, "Design of Experiments for Irradiation of Mechanical Property Test Specimens in Experimental Breeder Reactor-II and High Flux Isotope Reactor"
- US/UK Libby-Cockcroft Information Exchange Meeting on Corrosion in Reactor Coolants, Harwell, England, Sept. 15–17, 1969  
J. H. DeVan,\* "Corrosion Studies of Advanced LMFBR Fuel Cladding Materials in Sodium"  
J. H. DeVan,\* "Analysis of Oxygen in Sodium by Galvanic Cell Techniques" (based on studies performed by Atomic Power Development Associates, United Nuclear Corp., Brookhaven National Laboratory, and General Electric Breeder Reactors Development Operation)
- International Conference on the Use of Cyclotrons in Chemistry, Metallurgy, and Biology, St. Catherine's College, Oxford, England, Sept. 22–23, 1969  
R. T. King,\* "Cyclotron Simulation of Neutron Transmutation Produced Gases in Reactor Cladding and Structures"
- 13th Conference on Analytical Chemistry in Nuclear Technology, Gatlinburg, Tenn., Sept. 30–Oct. 2, 1969  
W. O. Harms,\* "The Role of Analytical Chemistry in the Development and Operation of Liquid-Metal Fast Breeder Reactors"
- American Nuclear Society Reactor Operations Division Biannual Conference on Reactor Operating Experience, San Juan, Puerto Rico, Oct. 1–3, 1969  
W. R. Martin,\* G. M. Adamson, Jr., and J. E. Cunningham, "Recent Developments in Materials Research"
- 9th Thermal Conductivity Conference, Ames Laboratory, Ames, Iowa, Oct. 6–8, 1969  
J. P. Moore,\* T. G. Kollie, and R. S. Graves, "The Physical Properties of Ni<sub>3</sub>Fe from 80 to 400 K"  
P. Spindler,\* J. P. Moore, and R. S. Graves, "The Thermal Conductivity of LiF from 80 to 1100 K"
- American Welding Society National Fall Meeting, New Orleans, Oct. 6–9, 1969  
C. D. Lundin\* and K. Farrell, "Distribution and Effects of Porosity in Welds in CVD Tungsten"  
C. D. Lundin\* and G. M. Slaughter, "Weld Ripples – Clues to Weld Behavior"

American Society for Metals—American Society for Testing and Materials 1969 Materials Engineering Congress, Applications of Modern Metallographic Techniques Session, Philadelphia, Oct. 13, 1969

R. J. Gray,\* E. L. Long, Jr., and A. E. Richt, "Metallography of Radioactive Materials"

29th National Convention of the American Society for Nondestructive Testing, Philadelphia, Oct. 13–16, 1969

B. E. Foster and S. D. Snyder,\* "Measurement of Carbon Coating Thickness on Microspheres of Nuclear Fuels"

1969 Fall Meeting of the Metallurgical Society of AIME, Philadelphia, Oct. 13–16, 1969

E. E. Bloom and J. O. Stiegler,\* "Recent Observations on Irradiation Induced Void Formation in Austenitic Stainless Steels" (Technical Session of the Refractory Metals Committee)

D. T. Bourgette,\* "Effect of High Vacuum and Specimen Thickness on the Creep Behavior of Haynes Alloy No. 25"

D. A. Canonico, N. C. Cole,\* and G. M. Slaughter, "Direct Brazing of Refractory Metals, Ceramics and Graphite"

N. C. Cole,\* R. G. Gilliland, and G. M. Slaughter, "Weldability of Tungsten and Tungsten Alloys"

K. Farrell,\* "Gas Porosity and Hot Cracking in Fusion Welds in Tungsten"

J. S. Faulkner,\* "The Electronic States in Copper and Aluminum"

J. I. Federer,\* "Chemical Vapor Deposition of Vanadium"

D. G. Harman,\* "Effects of Irradiation Temperature on the Properties of Several Compositions of Incoloy 800"

H. Inouye,\* "The Effect of Low Pressure Oxygen on the Creep Properties of Tungsten and a Tungsten-Molybdenum Alloy (50–50 wt %)"

Roy T. King,\* "Production of Displacement Damage by Light Ions"

R. L. Klueh,\* "Penetration of Refractory Metals by Alkali Metals"

C. C. Koch,\* "Solid Solution Intra Rare Earth Alloys"

J. W. Koger\* and A. P. Litman, "Mass Transfer of the Nickel-Base Hastelloy N Alloy in a Flowing Fused Fluoride Salt System"

D. K. Reimann and T. S. Lundy, "Cation Self-Diffusion in  $UN_{1+x}$ " (presented by D. M. Kroeger)

R. L. Stephenson,\* "Comparative Creep-Rupture Properties of W–25% Re Consolidated by Arc Melting and Powder Metallurgy Techniques"

R. L. Stephenson\* and R. G. Donnelly, "Creep-Rupture Properties of D-43 and FS-85 Welds"

J. O. Stiegler,\* K. Farrell, and B. T. M. Loh, "The Influence of Impurities on Radiation Damage in Aluminum"

R. A. Vandermeer\* and J. C. Ogle, "Texture Development in a Columbium–40 Pct Vanadium Alloy"

R. O. Williams,\* "An Analysis of the Effect of Deformation on Non-Random Solid Solutions"

R. L. Wagner,\* "Sublimation of W–25% Re Between 1650 and 1950°C in Low-Pressure Oxygen"

A. Wolfenden,\* "The Energy Relations in the Room Temperature Deformation of Aluminum Single Crystals"

M. H. Yoo\* and B. T. M. Loh, "Characteristics of Stress and Dilatation Fields of Straight Dislocations in Anisotropic Crystals"

29th National Conference of the American Society for Nondestructive Testing, Philadelphia, Oct. 13–16, 1969

H. L. Whaley\* and K. V. Cook, "Ultrasonic Frequency Analysis"

Joint Meeting of the Nuclear Division of the American Ceramic Society and the Pacific Coast Regional Meeting, Seattle, Wash., Oct. 15–17, 1969

R. A. Bradley\* and J. D. Sease, "Fabrication of (Pu,U)O<sub>2</sub> Pellets by the Sol-Gel Process"

D. M. Hewette II, "Irradiation of Pyrolytic-Carbon-Coated ThO<sub>2</sub> Particles to Significant HTGR Fast Fluences" (presented by T. B. Lindemer)

T. B. Lindemer\* and J. M. Leitnaker, "Kinetics of the UC<sub>2</sub>-N<sub>2</sub> Reaction from 1500 to 1700°C"

Contribution to Tenth General Meeting, Irradiation Effects on Reactor Structural Materials, Idaho Falls, Idaho, Oct. 21–23, 1969

E. E. Bloom\* (compiler), "Irradiation Effects on Reactor Structural Materials"

1969 Thermionic Conversion Specialist Conference, Carmel, Calif., Oct. 21–23, 1969

H. Inouye,\* "The Effect of Low-Pressure Oxygen on the Creep Properties of Tungsten and a Tungsten-Molybdenum Alloy"

R. L. Stephenson,\* "Structural Material Selection for Isotopic Capsules"

R. L. Wagner,\* "Sublimation of W–0.25% Re Between 1650 and 1950°C in Low-Pressure Oxygen"

16th National Vacuum Symposium, Seattle, Wash., Oct. 28–31, 1969

R. E. Clausing,\* A. Catlin, and K. R. Lawless, "Electron Bombardment Induced Desorption of Carbon Monoxide from Polycrystalline Tungsten"

R. L. Wagner\* and H. Inouye, "Ultrahigh Vacuum Techniques for Measuring the Solubility and Diffusivity of Gases in Metals with Application to Nitrogen in Tungsten and Nb–0.1% Zr"

Electron Density of States Symposium, National Bureau of Standards, Washington, D.C., Nov. 3–6, 1969

R. W. Williams\* and H. L. Davis, "Adjustment of Calculated Band Structures for Calcium by Use of Low-Temperature Specific Heat Data"

American Chemical Society Regional Meeting, Richmond, Va., Nov. 5–8, 1969

C. R. Boston,\* "Spectra of Dilute Solutions of Bismuth Metal in Molten Bismuth Tribromide"

G. P. Smith\* and T. W. Couch, "Phonon Modes in Electronically Excited States of  $\text{NiCl}_4^{2-}$  in Crystals and Glasses"

K. E. Spear,\* J. M. Leitnaker, and T. B. Lindemer, "Thermodynamic Properties of the Ternary Uranium-Vanadium Carbide Phase"

American Society of Mechanical Engineers Meeting, Los Angeles, Nov. 16–21, 1969

G. M. Slaughter,\* "Welded and Back-Brazed Tube Attachments for Heat Exchangers"

Joint Meeting of the California Sections of the American Society for Nondestructive Testing, Anaheim, Calif., Nov. 18, 1969

R. W. McClung,\* "A New Look at Nondestructive Testing"

American Nuclear Society Winter Meeting, San Francisco, Nov. 30–Dec. 4, 1969

R. E. Adams,\* "Failure Model for HFIR Target Rods"

E. E. Bloom,\* "Review of Evidence for Irradiation Damage from Neutron-Charged Particle Reactions in Metals"

E. E. Bloom\* and J. O. Stiegler, "Recent Observations of Irradiation Induced Void Formation in Austenitic Stainless Steels"

G. L. Copeland\* and W. R. Martin, "Fabrication of Thorium-Uranium Alloy for the UMBR Fuel Element"

C. M. Cox\* and F. J. Homan, "Analysis of Mixed Oxide Fuel Pin Performance Using the FMØDEL Computer Code"

D. R. Cuneo, E. L. Long, Jr., J. H. Coobs, J. A. Conlin, and A. W. Longest, "Performance of Pyrolytic-Carbon Coated  $\text{UO}_2$  and  $\text{UC}_2$  Microspheres at High Burnup" (presented by J. L. Scott)

W. Fulkerson,\* "Fundamental Properties of UN"

David O. Hobson, "Texture Control in Zircaloy Tubing" (presented by P. L. Rittenhouse)

R. T. King, "Evaluation of Accelerator Radiation Experiments for Reactor Damage Problems" (presented by J. R. Weir, Jr.)

T. B. Lindemer\* and J. M. Leitnaker, "Kinetics of the  $UC_2-N_2$  Reaction from 1500 to 1700°C"

A. R. Olsen, C. M. Cox,\* and R. B. Fitts, "Low Burnup Irradiation Tests of Sphere-Pac Sol-Gel (U,Pu)O<sub>2</sub> Fuels"

J. M. Leitnaker, T. B. Lindemer, K. E. Spear II, and K. J. Notz, "Producing Advanced Fuels for LMFBR's" (presented by W. Fulkerson)

G. A. Reimann\* and W. R. Martin, "Improved Processes for the Fabrication of 316 Stainless Steel Tubing"

C. E. Sessions,\* S. W. Cook, R. E. Gehlbach, and H. E. McCoy, "Correlation of the Creep Behavior of a Nickel Alloy with Precipitate Distribution"

K. E. Spear and J. M. Leitnaker, "Chemical Effects of Nuclear Burnup on Fast-Reactor Fuels" (presented by W. Fulkerson)

S. C. Weaver,\* K. R. Thoms, and V. A. DeCarlo, "Irradiation Testing of Uranium Nitride in ORR"

J. R. Weir, Jr.,\* "A Review of Fast Neutron Radiation Damage Problems in Reactor Materials"

R. T. King, "Evaluation of Accelerator Irradiation Experiments for Reactor Problems" (presented by J. R. Weir, Jr.)

29th High-Temperature Fuels Committee Meeting, Sunnyvale, Calif., Dec. 8–10, 1969

R. B. Fitts, D. R. Cuneo, E. L. Long, Jr., and A. W. Longest, "GCFR Fuels Irradiation Tests on the Cooperative GGA-ORNL Program" (presented by A. L. Lotts)

T. N. Washburn (compiler), "Summaries of Recent ORNL Work on Fuels and Cladding Materials" (presented by A. L. Lotts and J. L. Scott)

15th AEC Coated Particle Fuels Working Group Meeting, Los Alamos, N.M., Dec. 10–11, 1969

J. H. Coobs\* and O. Sisman, "Coated Particle Fuels Development at Oak Ridge National Laboratory"

American Mathematical Society & Mathematical Association of America, Miami, Fla., Jan. 22–26, 1970

Lida K. Barrett\* and C. S. Yust, "Topological Sintering Models"

American Physical Society Meeting, Chicago, Ill., Jan. 26–29, 1970

W. Glaeser,\* G. Czjzek, J. E. Tansil, and F. E. Obenshain, "Mössbauer Measurements with  $^{61}Ni$  in Ni-Pd Alloys"

26th Annual Conference of the National Association of Corrosion Engineers, Philadelphia, Mar. 2–6, 1970

J. W. Koger\* and A. P. Litman, "Corrosion Mechanisms in Fused Fluoride Systems"

Joseph P. Hammond,\* P. Patriarca, G. M. Slaughter, and W. A. Maxwell, "Corrosion of Advanced Steam Generator Alloy Weldments in 1100 and 1200°F (595 and 650°C) Steam"

American Physical Society Meeting, Dallas, Tex., Mar. 23–26, 1970

J. S. Faulkner,\* "Two Particle Scattering Terms in Perturbation Theory of Electronic States in Disordered Systems"

Thirtieth Annual Conference on Physical Electronics (A Topical Conference of the American Physical Society, Division of Electron and Atomic Physics), University of Wisconsin, Milwaukee, Mar. 30–Apr. 1, 1970

R. E. Clausing,\* "Measurement of the Desorption of Neutral Gases from Metal Surfaces by Electron Bombardment"

Heavy Section Steel Technology Program 4th Annual Information Meeting, Oak Ridge National Laboratory, Mar. 31–Apr. 1, 1970

R. G. Berggren\* and T. N. Jones, "Characterization of HSST Plates"

R. G. Berggren,\* W. J. Stelzman, and T. N. Jones, "Radiation Studies on HSST Plate and Welds"

D. A. Canonico,\* "Through Thickness Transition Temperature of Irradiated Thick-Wall Nuclear Pressure Vessels"

D. A. Canonico,\* W. J. Stelzman, and R. G. Berggren, "Mechanical Properties of Thick-Section Weldments"

American Society for Metals Metallography Symposium, Cleveland, Ohio, April 2–3, 1970

R. J. Gray,\* “Color Metallography”

R. J. Gray,\* E. L. Long, Jr., and A. E. Richt, “Metallography of Radioactive Materials”

8th Rare Earth Research Conference, Reno, Nev., Apr. 19–22, 1970

C. C. Koch, P. G. Mardon, and C. J. McHargue,\* “An Elevated Temperature X-Ray Diffraction and an Electron Microscopy Study of the Transformations to the Samarium-Type Structure in Gadolinium-Cerium Alloys”

79th Meeting of the Acoustical Society of America, Atlantic City, N.J., Apr. 21–24, 1970

H. L. Whaley and L. Adler,\* “A Model for the Determination of the Size and Orientation of Reflectors from Ultrasonic Frequency Analysis”

Gas-Cooled Reactor Program Semiannual Information Meeting, Oak Ridge National Laboratory, Apr. 27–29, 1970

J. L. Scott,\* J. A. Conlin, J. H. Coobs, D. M. Hewette II, J M Robbins, and R. L. Senn, “Development of Bonded Beds of Coated Particles for HTGR Fuel Elements”

R. B. Fitts,\* J. R. Lindgren, E. L. Long, Jr., and D. R. Cuneo, “Gas-Cooled Fast Breeder Reactor Fuel-Element Development”

Symposium on Nondestructive Testing in the Nuclear Field, Battelle Northwest Laboratory, Richland, Wash., Apr. 28–30, 1970

R. W. McClung,\* “Nondestructive Test Development at Oak Ridge National Laboratory – 1970”

72nd Annual Meeting of the American Ceramic Society, Philadelphia, May 2–7, 1970

D. M. Hewette II,\* “Density and Dimensional Changes in Methane and Propylene Derived Pyrolytic Carbons Irradiated to  $2 \times 10^{22}$  neutrons/cm<sup>2</sup> at 715°C”

V. J. Tennery,\* R. A. Potter, and T. G. Godfrey, “Synthesis and Characterization of Uranium Nitride”

Sol-Gel Processes and Reactor Fuel Cycles Symposium, Gatlinburg, Tenn., May 4–7, 1970

J. H. Coobs,\* J. L. Scott, A. R. Olsen, D. M. Hewette II, and E. L. Long, Jr., “Irradiation Performance of (U,Th)O<sub>2</sub> Coated Fuels for HTGR’s”

C. M. Cox,\* A. R. Olsen, R. B. Fitts, and A. L. Lotts, “Irradiation Performance of Sol-Gel (U,Pu)O<sub>2</sub> Fuels for Breeder Reactors”

F. J. Furman, Jr.,\* J. D. Sease, and A. L. Lotts, “Economics and Technology of High-Temperature Gas-Cooled Reactor Fuel Refabrication”

T. B. Lindemer,\* “Factors That Control the Carbothermic Synthesis of Advanced Fuels”

J. D. Sease,\* R. A. Bradley, C. R. Reese, W. H. Pechin, and A. L. Lotts, “Sphere-Pac and Pelletization of (U,Pu)O<sub>2</sub>”

Second International Conference on Chemical Vapor Deposition, Los Angeles, May 10–15, 1970

K. Farrell, J. I. Federer,\* A. C. Schaffhauser, and W. C. Robinson, Jr., “Gas Bubble Formation in Metal Deposits”

J. E. Spruiell, “Chemical Vapor Deposition of Silicon Carbide from Silicon Tetrachloride-Methane-Hydrogen Mixtures” (presented by J. I. Federer)

Spring Meeting of the Metallurgical Society of the American Institute of Mining, Metallurgical and Petroleum Engineers, Las Vegas, Nevada, May 11–14, 1970

D. T. Bourgette,\* “Evaporation of Cobalt- and Nickel-Base Alloys”

R. W. Carpenter,\* “Phase Transformations in Niobium-Hafnium and Tantalum-Hafnium Alloys”

W. A. Coghlan\* and W. D. Nix, “Contributions to the Theory of Jogged Screw Dislocation Glide”

W. A. Coghlan\* and W. D. Nix, “A Study of High Temperature Glide in LiF Single Crystals”

- N. C. Cole,\* G. M. Goodwin, and G. M. Slaughter, "Joining of Chemical Vapor Deposited Tungsten"
- N. C. Cole,\* G. M. Goodwin, and G. M. Slaughter, "Recent Studies of Ferrite in Stainless Steel Welds"
- N. C. Cole,\* R. W. Gunkel, and G. M. Slaughter, "Joining of Molybdenum and Its Alloys"
- G. L. Copeland,\* R. S. Mateer, and W. R. Martin, "Void Formation During Heat Treating of Boron Carbide"
- D. S. Easton\* and J. O. Betterton, "The Equilibrium Diagram of the Zirconium-Gallium System"
- K. Farrell, R. T. King, and A. Wolfenden,\* "Effect of Preinjected Gases on Irradiation-Produced Voids in Aluminum"
- R. E. Gehlbach,\* C. E. Sessions, H. E. McCoy, Jr., and S. W. Cook, "Effect of Molybdenum, Titanium, Silicon, and Carbon on Carbide Precipitation in a Nickel-Base Alloy"
- J. W. Koger\* and A. P. Litman, "Effect of Impurities on the Corrosion Rate of Hastelloy N Exposed to Fluoride Salts at Elevated Temperatures"
- C. T. Liu\* and B. T. M. Loh, "Quasichemical Models and Cahn's Spinodal Decomposition"
- G. R. Love,\* "Losses Due to Moving Fluxoids in Superconductors"
- Jack C. Ogle,\* "Rolling Textures in Ordered and Disordered Copper-25 at. pct Gold Alloy"
- R. L. Stephenson,\* "Creep-Rupture Properties of SU-16 and Their Response to Heat Treatment"
- R. A. Vandermeer,\* "Impurities and the Relationship Between Grain-Boundary Velocity and Driving Force: A Rationalization of Power Law Behavior"
- A. Wolfenden,\* "An Inverse Strain Rate Effect During the Deformation of Gold-Silver Alloys"
- A. Wolfenden,\* "Effects of Pre-Quench Proton and Alpha Particle Bombardment on Void Formation in Quenched Aluminum"

Conference on Computational Methods on Band Theory, IBM Thomas J. Watson Research Center, Yorktown Heights, N.J., May 14-15, 1970

- G. S. Painter,\* "Discrete Variational Method for the Energy Band Problem with LCAO Basis and Non-spherical Local Potential"

Air Force Materials Symposium, Miami, Fla., May 18, 1970

- R. W. McClung,\* "Major Technical Problems in Nondestructive Testing"

30th Meeting of the High Temperature Fuels Committee, USAEC Headquarters, Germantown, Md., May 18-20, 1970

- T. N. Washburn (compiler), "Summaries of Recent ORNL Work on Fuels and Cladding Materials" (presented by T. N. Washburn and J. L. Scott)

Hauptversammlung der Deutschen Gesellschaft für Metallkunde, Aachen, West Germany, Mai 19-22, 1970

- E. Tenckhoff\* and P. L. Rittenhouse, "Textur und Texturgradienten in Zircaloy Rohren"

Annual Meeting of the Institute of Nuclear Materials Management, Gatlinburg, Tenn., May 25-27, 1970

- J. C. Gower, R. G. Cardwell,\* and B. E. Foster, "An Integrated System of Nuclear Materials Control at Oak Ridge National Laboratory"

Sixth International Conference on Nondestructive Testing, Hannover, Germany, June 1-5, 1970

- C. V. Dodd, W. E. Deeds, and W. G. Spoeri, "Optimizing Defect Detection in Eddy Current Testing" (presented by R. W. McClung)

- R. W. McClung,\* "Developments for More Quantitative Nondestructive Testing"

51st Annual Meeting of the American Welding Society, Cleveland, Ohio, June 8-12, 1970

- E. A. Franco-Ferreira and L. C. Williams,\* "Fabrication of Instrumented Fuel Elements and In-Pile Capsules"

G. M. Goodwin,\* N. C. Cole, and G. M. Slaughter, "A Study of Ferrite Morphology in Austenitic Stainless Steel Weldments"

R. W. Gunkel,\* H. E. McCoy, and G. M. Slaughter, "Welding of Neutron Irradiated Hastelloy N"

Joseph P. Hammond\* and G. M. Slaughter, "Bonding Graphite to Metals by Transition Piece Concept"

Carl D. Lundin,\* "Microprobe and Scanning Electron Microscope Team Up to Solve Welding Cracking Problem"

Carl D. Lundin\* and R. W. Gunkel, "Cold Cracking Linked to Hot Cracking"

A. J. Moorhead,\* "Laser Welding and Drilling Applications"

Second Symposium on the Thermal Expansion of Solids, Joint Sponsorship, University of Illinois and Sandia Laboratories, Santa Fe, N.M., June 10–12, 1970

O. B. Cavin\* and J. L. Cook, "Correlation of Thermal Expansion Anisotropy and Texture of Carbon-Carbon Composites"

International Conference of the Vacuum Metallurgy Division of the American Vacuum Society, Anaheim, Calif., June 15–19, 1970

R. E. Clausing,\* "Application of Auger Electron Spectroscopy to Reactor Materials Research"

D. S. Easton\* and R. E. Clausing, "Outgassing of Nuclear Rocket Fuel Elements"

R. L. Stephenson,\* "Creep-Rupture Properties of C-129Y"

ASTM, 73rd Annual Meeting, North American Materials Exposition, Toronto, Canada, June 21–26, 1970

K. Farrell\* and J. O. Stiegler, "Application of Electron Fractography to the Study of High-Temperature Processes," presented at the Symposium on Applications of Electron Microfractography

C. R. Kennedy,\* W. P. Eatherly, and J. W. Prados, "Radiation-Induced Stresses in Graphite Cylinders," presented at the Symposium on Stress Relaxation Testing and Its Applications

R. L. Klueh\* and J. H. DeVan, "Liquid Metal Corrosion Test Procedures," presented at the Symposium on State of the Art in Corrosion Testing

ASTM Symposium on Effects of Radiation on Structural Metals, Niagara Falls, Canada, June 29–July 1, 1970

R. G. Berggren,\* "Radiation Embrittlement of ASTM A-533, Grade B Steel Plate"

E. E. Bloom\* and J. O. Stiegler, "The Effect of Fast Neutron Irradiation on the Structure and Properties of Type 304 Stainless Steel"

J. R. Weir (rapporteur) "Swelling of Austenitic Stainless Steel in Fast Reactors — Experimental Evidence and Design Considerations"

4th Libby Cockcroft Exchange Meeting on the Effects of Irradiation on Structural Materials, AEC Headquarters, Germantown, Md., June 23–25, 1970

E. E. Bloom,\* C. E. Sessions, D. G. Harman, H. E. McCoy, and J. R. Weir, Jr., "Elevated-Temperature Embrittlement of Reactor Cladding and Structural Materials"

E. E. Bloom\* and J. O. Stiegler, "Radiation-Induced Void Formation and Swelling in Austenitic Stainless Steels"

K. Farrell, R. T. King, A. Wolfenden, and J. T. Houston, "Void Formation in Stainless Steels" (presented by E. E. Bloom)

R. T. King, "Effect of Cyclotron-Injected Helium on Type 304 and 0.2% Ti Type 304L Stainless Steels" (presented by E. E. Bloom)

F. W. Wiffen, "Irradiation Damage to Vanadium and Refractory Metals" (presented by E. E. Bloom)

16th Annual Meeting of the American Nuclear Society, Los Angeles, June 28–July 2, 1970

D. A. Canonico,\* "Transition Temperature Considerations for Thick-Wall Nuclear Pressure Vessels"

- G. L. Copeland,\* R. S. Mateer, and W. R. Martin, "Characterization of Boron Carbide for Fast Reactor Absorbers"
- R. B. Fitts,\* E. L. Long, Jr., D. R. Cuneo, and J. R. Lindgren, "Performance of Three Sealed (U,Pu)O<sub>2</sub> GCFR Fuel Pins"
- K. W. Haff, J. I. Federer,\* W. R. Martin, and D. W. Ramey, "Chemical-Vapor-Deposited Tungsten Capsules for Radioisotope Sources"
- D. O. Hobson,\* M. F. Osborne, and G. W. Parker, "Comparison of Rupture Data from Irradiated Fuel Rods and Unirradiated Cladding"
- W. R. Huntley,\* D. L. Clark, and B. Fleischer, "Design and Operation of a 1370°C Forced-Convection Lithium Corrosion Test Loop"
- H. Inouye\* and C. T. Liu, "New Platinum-Base Capsule Alloys for Space Isotopic Heat Sources"
- R. T. King\* and G. A. Reimann, "Effect of Fabrication Variables on the Biaxial Creep-Rupture Properties of Stainless Steel Tubing"
- R. L. Klueh,\* "The Effect of Oxygen on the Compatibility of Tantalum and Potassium"
- R. A. Lorenz,\* D. O. Hobson, and G. W. Parker, "Fuel Rod Failure Under Loss-of-Coolant Conditions in TREAT"
- W. R. Martin, A. E. Richt, and M. M. Martin,\* "Postirradiation Examination and Evaluation of Tungsten-Urania Cermets"
- R. E. McDonald, R. G. Donnelly, and A. C. Schaffhauser,\* "Extrusion of Refractory Metals for Isotope Fuel Capsules"
- A. R. Olsen,\* "Intermediate-Burnup Irradiation Tests of Sphere-Pac Sol-Gel Fuels"
- L. E. Poteat\* and J. I. Federer, "Corrosion-Resistant Coatings for MSBR Reprocessing Equipment"
- J. L. Scott, J. H. Coobs, D. M. Hewette II, J M Robbins, R. L. Senn, and J. A. Conlin, "Development of Bonded Beds of Coated Particles for HTGR Fuel Elements" (presented by R. B. Fitts)
- G. M. Slaughter and G. M. Goodwin,\* "Welding Procedures for LMFBR Vessels"
- R. D. Waddell,\* "Measurement of LWR Coolant Channel Reduction Arising from Cladding Deformation During a Loss-of-Coolant Accident"
- T. N. Washburn,\* K. R. Thoms, S. C. Weaver, D. R. Cuneo, and E. L. Long, Jr., "Examination of UN Fueled Pins Irradiated at 1400°C Cladding Temperature"

## Publications

Compiled by Meredith R. Hill

- Abraham, M. M., C. B. Finch, R. W. Reynolds, and H. Zeldes, "Electron Spin Resonance Spectrum of Divalent Europium in Thorium Dioxide," *Phys. Rev.* **187**(2), 451–55 (November 1969).
- Adams, R. E., "Failure Model for HFIR Target Rods," (Summary) *Trans. Am. Nucl. Soc.* **12**(2), 560–61 (November 1969).
- Anderegg, J. W., P. G. Mardon, and R. W. Hendricks, *An Alignment Procedure for the Kratky Small-Angle X-Ray Camera*, ORNL-4476 (February 1970).
- Angelini, P., R. E. McHenry, J. L. Scott, W. S. Ernst, Jr., and J. W. Prados, "Helium Release in  $^{238}\text{PuO}_2$ ," (Summary) *Trans. Am. Nucl. Soc.* **12**(2), 477–78 (November 1969).
- Angelini, Peter, R. E. McHenry, J. L. Scott, W. S. Ernst, Jr., and J. W. Prados, *Helium Release from  $^{238}\text{PuO}_2$  Microspheres*, ORNL-4507 (March 1970).
- Bannister, M. J., "The Surface Enthalpy of Thoria Gel," *J. Am. Ceram. Soc.* **52**(12), 675–76 (December 1969).
- Barrett, Lida K., and C. S. Yust, "Some Fundamental Ideas in Topology and Their Application to Problems in Metallurgy," (Summary) *Scripta Met.* **3**(7), 461–64 (July 1969).
- Barrett, Lida K., and C. S. Yust, "Some Fundamental Ideas in Topology and Their Application to Problems in Metallography," *Metallography* **3**(1), 1–33 (March 1970).
- Beatty, R. L., J. L. Scott, and D. V. Kiplinger, *Minimizing Thermal Effects in Fluidized-Bed Deposition of Dense, Isotropic Pyrolytic Carbon*, ORNL-4531 (April 1970).
- Beatty, R. L., and D. V. Kiplinger, "Gas Pulse Impregnation of Graphite with Carbon," *Nucl. Appl. Technol.* **8**(6), 488–95 (June 1970).
- Bloom, E. E., "Review of Evidence for Irradiation Damage from Neutron-Charged Particle Reactions in Metals," (Summary) *Trans. Am. Nucl. Soc.* **12**(2), 701 (November 1969).
- Bloom, E. E., and J. O. Stiegler, "Recent Observations of Irradiation-Induced Void Formation in Austenitic Stainless Steels," (Summary) *Trans. Am. Nucl. Soc.* **12**(2), 589 (November 1969).
- Bloom, E. E., and J. R. Weir, "Development of Austenitic Stainless Steels with Improved Resistance to Elevated-Temperature Irradiation Embrittlement," pp. 261–89 in *Irradiation Effects in Structural Alloys for Thermal and Fast Reactors, Spec. Tech. Publ. 457*, American Society for Testing and Materials, Philadelphia, 1969.
- Bloom, E. E., and J. O. Stiegler, "A Comparison of Irradiation-Induced Swelling and Void Formation in Two Austenitic Stainless Steels," *J. Nucl. Mater.* **35**(2), 244–46 (May 1970).
- Bode, K.-H., "Possibilities to Determine Thermal Conductivity Using New Solutions for Current-Carrying Conductors," pp. 201–21 in *Europäische Konferenz über thermophysikalische Eigenschaften von festen Stoffen bei hohen Temperaturen vom 11. bis 13. November 1968 in Baden-Baden*, Bundesministerium für Bildung und Wissenschaft, Forschungsbericht K70-01 (February 1970).
- Boston, C. R., S. J. Yosim, and L. F. Grantham, "The Electrical Conductivity of Aluminum Chloride Liquid and Supercritical Vapor," *J. Chem. Phys.* **51**(4), 1669–71 (August 1969).

- Boston, C. R., L. F. Grantham, and S. J. Yosim, "Electrical Conductivities of Molten Aluminum Chloride-Potassium Chloride Mixtures," *J. Electrochem. Soc.* **117**(1), 28-31 (January 1970).
- Boston, C. R., "Spectra of Dilute Solutions of Bismuth Metal in Molten Bismuth Trihalides. III. The Bismuth-Bismuth Tribromide System," *Inorg. Chem.* **9**(2), 389-90 (February 1970).
- Bowman, R. A., *Formation of ThO<sub>2</sub> Microspheres by a Freeze-Form Vacuum-Dry Technique*, ORNL-TM-2872 (April 1970).
- Braski, D. N., and N. H. Packan, "Annealing of Irradiation-Produced Voids in X8001 Alloy," (Summary) pp. 188-89 in *Proceedings, Twenty-Seventh Annual Meeting, Electron Microscopy Society of America, St. Paul, Minnesota, August 26, 27, 28, and 29, 1969*, ed. by C. J. Arceneaux, Claitor's Publishing Division, Baton Rouge, Louisiana, 1969.
- Bridges, W. H., and R. W. McClung, "Computerized Information Retrieval for Nondestructive Testers - A Nondestructive Memory," *Mater. Evaluation* **27**(9), 199-204 (September 1969).
- Brynestad, Jorulf, H. L. Yakel, and G. P. Smith, "Nickel(II) Tetrachloroaluminate," *Inorg. Chem.* **9**(3), 986 (March 1970).
- Brynestad, J., and G. P. Smith, "Evidence of a Three-Coordinate Complex of Nickel(II)," *J. Am. Chem. Soc.* **92**(10), 3198-99 (May 1970).
- Buhr, J. B., T. M. Kegley, Jr., and R. J. Gray, "Potentiostatic Metallographic Etching Experiments," pp. 38-67 in *Technical Papers of the 21st Metallographic Group Meeting, Held May 10-12, 1967, Brookhaven National Laboratory, Upton, New York*, CONF-670533.
- Canonico, D. A., W. F. Savage, W. J. Werner, and G. M. Goodwin, "Effects of Minor Additions on Weldability of Incoloy 800," pp. 68-92 in *Effects of Minor Elements on the Weldability of High-Nickel Alloys* (Proceedings of a Symposium), The Welding Research Council, New York, July 1969.
- Canonico, D. A., "Transition Temperature Considerations for Thick-Wall Nuclear Pressure Vessels," (Summary) *Trans. Am. Nucl. Soc.* **13**(1), 168-69 (June 1970).
- Carden, A. E., and T. B. Slade, "High-Temperature Low-Cycle Fatigue Experiments on Hastelloy X," pp. 111-29 in *Fatigue at High Temperature, Spec. Tech. Publ. 459*, American Society for Testing and Materials, Philadelphia, 1969.
- Cardwell, R. G., *Cost Distribution - A Method of Direct Costing in a Research Installation*, ORNL-TM-2921 (May 1970).
- Cavin, O. B., "Anisotropy Determinations of Potential Nuclear Graphites," (Summary) pp. 94-95 in *Summary of Papers, Bien. Conf. Carbon, 9th, 1969*, Defense Ceramic Information Center, Battelle Memorial Institute, Columbus, Ohio, 1969.
- Chakraborty, A. K., R. S. Crouse, and W. R. Martin, *Factors Affecting the Swelling During Degassing of Compacts Containing Uranium-Aluminum Intermetallics Dispersed in Aluminum*, ORNL-TM-2800 (March 1970).
- Chapman, A. T., G. W. Clark, and D. E. Hendrix, "UO<sub>2</sub>-W Cermets Produced by Unidirectional Solidification," *J. Am. Ceram. Soc.* **49**(1), 49-50 (January 1970).
- Chapman, A. T., G. W. Clark, D. E. Hendrix, C. S. Yust, and O. B. Cavin, "Substructure and Perfection in UO<sub>2</sub> Single Crystals," *J. Am. Ceram. Soc.* **53**(1), 46-51 (January 1970).
- Chandler, J. M., and R. B. Lindauer, "Preparation and Processing of MSRE Fuel," pp. 97-122 in *Symposium on Reprocessing of Nuclear Fuels, Nucl. Met.* **15**, ed. by P. Chiotti, American Institute of Mining, Metallurgical and Petroleum Engineers, New York, 1969.
- Conlin, J. A., D. R. Cuneo, E. L. Long, Jr., and C. L. Segasser, "Compatibility of (U,Th)O<sub>2</sub> with Graphite During Irradiation," *Nucl. Appl. Technol.* **8**(6), 507-15 (June 1970).
- Coobs, J. H., J. L. Scott, A. R. Olsen, D. M. Hewette II, and E. L. Long, Jr., "Irradiation Performance of (U,Th)O<sub>2</sub> Coated Fuels for HTGR's," pp. 567-84 in *Symposium on Sol-Gel Processes and Reactor Fuel Cycles, Gatlinburg, Tennessee, May 4-7, 1970*, CONF-700502.

- Cook, K. V., "Remote Ultrasonic Examination of Closure Welds on Isotope Capsules," pp. 210–18 in *Proceedings of the Seventh Symposium on Nondestructive Evaluation of Components and Materials in Aerospace, Weapons Systems and Nuclear Applications, April 23–25, 1969, San Antonio, Texas*, South Texas Section, American Society for Nondestructive Testing and Southwest Research Institute, Printed in Los Angeles, California, July 1969.
- Copeland, G. L., R. S. Mateer, and W. R. Martin, "Characterization of Boron Carbide for Fast Reactor Absorbers," (Summary) *Trans. Am. Nucl. Soc.* **13**(1), 100–1 (June 1970).
- Copeland, G. L., M. M. Martin, D. G. Harman, and W. R. Martin, "The Effect of Powder and Process Variables on the Properties of Sintered Aluminum Products," *Powder Technol.* **3**, 136–52 (1969/70).
- Copeland, G. L., *Evaluation of Thorium-Uranium Alloys for the Unclad-Metal Breeder Reactor*, ORNL-4557 (June 1970).
- Cox, C. M., and F. J. Homan, *PRØFIL – A One-Dimensional FØRTRAN IV Program for Computing Steady-State Temperature Distributions in Cylindrical Ceramic Fuels*, ORNL-TM-2443, Addendum (August 1969).
- Cox, C. M., "The Irradiation Performance of Uranium-Plutonium Mixed Oxide Fuel Pins," *Nucl. Safety* **10**(5), 380–91 (September–October 1969).
- Cox, C. M., and F. J. Homan, "Analysis of Mixed Oxide Fuel Pin Performance Using the FMØDEL Computer Code," (Summary) *Trans. Am. Nucl. Soc.* **12**(2), 536–37 (November 1969).
- Cox, C. M., A. R. Olsen, R. B. Fitts, and A. L. Lotts, "Irradiation Performance of Sol-Gel (U,Pu)O<sub>2</sub> Fuels for Breeder Reactors," pp. 359–73 in *Symposium on Sol-Gel Processes and Reactor Fuel Cycles, Gatlinburg, Tennessee, May 4–7, 1970*, CONF-700502.
- Cuneo, D. R., E. L. Long, Jr., J. H. Coobs, J. A. Conlin, and A. W. Longest, "Performance of Pyrolytic-Carbon-Coated UO<sub>2</sub> and UC<sub>2</sub> Microspheres at High Burnup," (Summary) *Trans. Am. Nucl. Soc.* **12**(2), 548–49 (November 1969).
- Czjzek, G., and W. G. Berger, "Hyperfine Interactions at the Final Positions of <sup>56</sup>Fe(*n*, $\gamma$ )<sup>57</sup>Fe Recoil Nuclei in bcc Iron-Aluminum Alloys," *Phys. Rev. B* **1**(3), 957–73 (February 1970).
- DiStefano, J. R., and J. H. DeVan, "Refluxing Capsule Experiments with Refractory Metals in Boiling Alkali Metals," *Nucl. Appl. Technol.* **8**(1), 29–44 (January 1970).
- DiStefano, J. R., "Compatibility of Strontium and Curium Fuels with Capsule Materials," *Symposium on Materials for Radioisotope Heat Sources*, TID-25358, pp. 90–111 (April 1970). CLASSIFIED.
- Dodd, C. V., W. E. Deeds, J. W. Luquire, and W. G. Spoeri, "Analysis of Eddy-Current Problems with a Time-Sharing Computer," *Mater. Evaluation* **27**(7), 165–68 (July 1969).
- DuBose, C. K. H., and C. Jones, "The Preparation of Transmission Electron Microscopy Specimens from Tubing," *Metallography* **2**(2–3), 31–39 (September 1969).
- Farrell, K., "Cathodic Hydrogen Absorption and Severe Embrittlement in a High Strength Steel," *Corrosion* **26**(3), 105–10 (March 1970).
- Farrell, K., J. T. Houston, and J. W. Chumley, "Hot Cracking in Fusion Welds in Tungsten," *Welding J. (N.Y.)* **49**(3), 132-s–37-s (March 1970).
- Faulkner, J. S., "Electronic States of a Liquid Metal from the Coherent Potential Approximation," *Phys. Rev.* **1**(2), 934–36 (January 1970).
- Faulkner, J. S., "KKR Structure Constants for Complex Crystals," *Phys. Letters* **31A**(5), 227–28 (March 1970).
- Federer, J. I., *Chemical Vapor Deposition of Vanadium and Vanadium Alloys – A Feasibility Study*, ORNL-TM-2923 (May 1970).
- Finch, C. B., and G. W. Clark, "High-Temperature Solution Growth of Single-Crystal Neptunium Dioxide," *J. Cryst. Growth* **6**(3), 245–48 (March–April 1970).
- Fitts, R. B., E. L. Long, Jr., D. R. Cuneo, and J. R. Lindgren, "Performance of Three Sealed (U,Pu)O<sub>2</sub> GCFR Fuel Pins," (Summary) *Trans. Am. Nucl. Soc.* **13**(1), 34–35 (June 1970).

- Foster, B. E., and S. D. Snyder, "An X-Ray Technique for Measuring Thickness of Tungsten on Copper," pp. 337–42 in *Proceedings of the Seventh Symposium on Nondestructive Evaluation of Components and Materials in Aerospace, Weapons Systems and Nuclear Applications, April 23–25, 1969, San Antonio, Texas*, South Texas Section, American Society for Nondestructive Testing and Southwest Research Institute, Printed in Los Angeles, California, July 1969.
- Foster, B. E., and S. D. Snyder, *Measurement of Carbon Coating Thickness on Microspheres of Nuclear Fuels*, ORNL-TM-2683 (October 1969); also *Mater. Evaluation* 28(1), 13–16 (January 1970).
- Frye, J. H., Jr., J. E. Cunningham, and staff, *Metals and Ceramics Div. Ann. Progr. Rept. June 30, 1969*, ORNL-4470 (October 1969).
- Frye, J. H., Jr., "Technology Forecast – Surveying the 70's," *Metal Progr.* 97(1), 25, 26, 29 (January 1970).
- Fulkerson, W., "Fundamental Properties of UN," (Summary) *Trans. Am. Nucl. Soc.* 12(2), 591 (November 1969).
- Furman, F. J., R. B. Pratt, and A. L. Lotts, *Prediction of the Economically Optimum Time to Initiate Recycle for the High-Temperature Gas-Cooled Reactor Industry Using Computer Program DELAY*, ORNL-TM-2704 (December 1969).
- Furman, F. J., J. T. Meador, and J. D. Sease, *Microsphere Handling Techniques*, ORNL-TM-2782 (March 1970).
- Furman, F. J., Jr., J. D. Sease, and A. L. Lotts, "Economics and Technology of High-Temperature Gas-Cooled Reactor Fuel Refabrication," pp. 281–308 in *Symposium on Sol-Gel Processes and Reactor Fuel Cycles, Gatlinburg, Tennessee, May 4–7, 1970*, CONF-700502.
- Gehlbach, R. E., and J. T. Houston, "Application of Electron Metallography to Precipitation Studies of Hastelloy N," pp. 206–15 in *Technical Papers of the 21st Metallographic Group Meeting, Held May 10–12, 1967, Brookhaven National Laboratory, Upton, New York*, CONF-670533.
- Gehlbach, R. E., T. J. Henson, B. C. Leslie, and Helen Mateer, *Evaluation of a TZM Isotopic Heat Source Fire Test Capsule*, ORNL-TM-2776 (January 1970).
- Gerdes, R. J., A. T. Chapman, and G. W. Clark, "Refractory Oxide–Metal Composites: Scanning Electron Microscopy and X-Ray Diffraction of Uranium Dioxide–Tungsten," *Science* 167(3920), 979–80 (February 1970).
- Gilliland, R. G., and G. M. Slaughter, "The Development of Brazing Filler Metals for High Temperature Service," *Welding J. (N.Y.)* 48(10), 463-s–68-s (October 1969).
- Gilmore, F. C., *Optical Spectra of the Cobalt(II) Ion at Sites of Approximately Octahedral Symmetry in Several Chloride Crystals*, ORNL-TM-2507 (July 1969). Ph.D. Thesis, the University of Tennessee, March 1969.
- Gittus, John, *A Theory of Crack Propagation During Tension-Tension Fatigue in a Material Exhibiting Time-Dependent Plasticity*, ORNL-TM-2857 (March 1970).
- Goode, J. H., and C. M. Cox, *The Distribution of Fission Product Tritium in a Zircaloy-Clad UO<sub>2</sub> Blanket Rod for PWR-1*, ORNL-TM-2994 (June 1970).
- Gray, R. J., *Shatterproof Coatings for Glass*, ORNL-4521 (March 1970).
- Gray, R. J., and B. C. Leslie, "High-Intensity Xenon Arc Lamp for Older Research Metallographs," pp. 121–38 in *Proc. 2nd Ann. Tech. Meet. Int. Metallographic Soc. Sept. 8–10, 1969*, International Metallographic Society, Los Alamos, New Mexico, 1970.
- Gray, R. J., and B. C. Leslie, "Metallographic Applications of Xenon Illumination Systems," *Metallography* 3(2), 135–45 (June 1970).
- Gunkel, R. W., R. G. Donnelly, and G. M. Slaughter, "Electron-Beam Welding of Strontium-Fueled Capsules," *Welding J. (N.Y.)* 48(12), 950–55 (December 1969).
- Gyorffy, B. L., "Electronic States in Liquid Metals: A Generalization of the Coherent-Potential Approximation for a System with Short-Range Order," *Phys. Rev. B* 1(8), 3290–99 (April 1970).
- Haff, K. W., J. I. Federer, W. R. Martin, and D. W. Ramey, "Chemical-Vapor-Deposited Tungsten Capsules for Radioisotope Sources," (Summary) *Trans. Am. Nucl. Soc.* 13(1), 85–86 (June 1970).

- Hallerman, G., and M. L. Picklesimer, "The Influence of the Preparation of Metal Specimens on the Precision of Electron Probe Microanalysis," pp. 197–225 in Suppl. 6, "Advances in Electronics and Electron Physics," *Electron Probe Microanalysis*, ed. by A. J. Tousimis and L. Martin, Academic Press, New York, 1969.
- Harman, D. G., and T. A. Nolan, "Fracture Initiation in XAP-001 Dispersion Strengthened Aluminum Alloy," *J. Nucl. Mater.* **34**(3), 290–98 (March 1970).
- Harrington, F. E., R. W. Horton, R. B. Pratt, and J. D. Sease, *Cost Study of Four Alternate Routes for LMFBR Fuel Material Preparation and Element Fabrication*, ORNL-TM-2813 (February 1970).
- Harris, L. A., and H. L. Yakel, "The Crystal Structure of  $\text{SrBe}_3\text{O}_4$ ," *Acta Cryst.* **B25**(Part 8), 1647–51 (August 1969).
- Harris, L. A., and H. L. Yakel, "Synthesis and X-Ray Study of Single-Crystal  $3\text{Al}_2\text{O}_3 \cdot \text{BeO}$ ," *J. Am. Ceram. Soc.* **53**(6), 359 (June 1970).
- Hendricks, R. W., "Space Charge Effects in Proportional Counters," *Rev. Sci. Instr.* **40**(9), 1216–23 (September 1969).
- Hobson, D. O., "Texture Control in Zircaloy Tubing," (Summary) *Trans. Am. Nucl. Soc.* **12**(2), 571–72 (November 1969).
- Hobson, D. O., "Texture Changes Produced During Zircaloy-4 Tubing Fabrication: From Forged Billet to Finished Tubing," pp. 37–49 in *Applications-Related Phenomena for Zirconium and Its Alloys*, Spec. Tech. Publ. 458, American Society for Testing and Materials, Philadelphia, 1969.
- Hobson, D. O., M. F. Osborne, and G. W. Parker, "Comparison of Rupture Data from Irradiated Fuel Rods and Unirradiated Cladding," (Summary) *Trans. Am. Nucl. Soc.* **13**(1), 150 (June 1970).
- Homan, F. J., and T. N. Washburn, "Capacity Expansion Optimization in a Growing Nuclear Fuel Fabrication Industry," *Nucl. Appl. Technol.* **8**(4), 384–94 (April 1970).
- Houston, J. T., and K. Farrell, "Recrystallization of Nickel-270," *Metallography* **2**(2–3), 239–46 (September 1969).
- Huntley, W. R., D. L. Clark, and B. Fleischer, "Design and Operation of a 1370°C Forced-Convection Lithium Corrosion Test Loop," (Summary) *Trans. Am. Nucl. Soc.* **13**(1), 6–7 (June 1970).
- Inouye, H., and A. C. Schaffhauser, *Low-Temperature Ductility and Hydrogen Embrittlement of Uranium – A Literature Review*, ORNL-TM-2563 (July 1969).
- Inouye, H., "The Effect of Low-Pressure Oxygen on the Creep Properties of Tungsten and a Tungsten-Molybdenum Alloy," pp. 425–33 in *IEEE Conference Record of 1969 Thermionic Conversion Specialist Conference, October 21–23, 1969*, The Institute of Electrical and Electronics Engineers, Inc., New York, (69 C 51-ED); also pp. 91–112 in *Trans. Vac. Met. Conf. 1969*, ed. by D. T. Bourgette and A. Simkovich, American Vacuum Society, New York, 1969.
- Inouye, H., and C. T. Liu, "New Platinum-Base Capsule Alloys for Space Isotopic Heat Sources," (Summary) *Trans. Am. Nucl. Soc.* **13**(1), 84 (June 1970).
- Kasten, P. R., E. S. Bettis, W. H. Cook, W. P. Eatherly, D. K. Holmes, R. J. Kedl, C. R. Kennedy, S. S. Kirslis, H. E. McCoy, A. M. Perry, R. C. Robertson, D. Scott, and R. A. Strehlow, "Graphite Behavior and Its Effects on MSBR Performance," *Nucl. Eng. Des.* **9**(2), 157–95 (February 1969).
- Kegley, T. M., Jr., and R. J. Gray, "Metallographic Preparation of Cerium Carbides," pp. 23–37 in *Technical Papers of the 21st Metallographic Group Meeting, Held May 10–12, 1967, Brookhaven National Laboratory, Upton, New York*, CONF-670533.
- Kegley, T. M., Jr., "Quantimet Area Measurement Problems," pp. 163–69 in *Proc. 2nd Ann. Tech. Meet. Int. Metallographic Soc. Sept. 8–10, 1969*, International Metallographic Society, Los Alamos, New Mexico, 1970.
- Kennedy, C. R., "The Irradiation of Graphite in HFIR," (Summary) pp. 86–88 in *Summary of Papers, Bien. Conf. Carbon, 9th, 1969*, Defense Ceramic Information Center, Battelle Memorial Institute, Columbus, Ohio, 1969.

- King, R. T., "Evaluation of Accelerator Radiation Experiments for Reactor Damage Problems," (Summary) *Trans. Am. Nucl. Soc.* **12**(2), 699–700 (November 1969).
- King, R. T., E. M. Thomas, and H. E. McCoy, "The Computer – An Aid for Analyzing and Processing Creep-Rupture Data," *J. Metals* **21**(11), 62–68 (November 1969).
- King, R. T., E. L. Long, Jr., J. O. Stiegler, and K. Farrell, "High-Neutron-Fluence Damage in an Aluminum Alloy," *J. Nucl. Mater.* **35**(2), 231–43 (May 1970).
- King, R. T., and G. A. Reimann, "Effect of Fabrication Variables on the Biaxial Creep-Rupture Properties of Stainless Steel Tubing," (Summary) *Trans. Am. Nucl. Soc.* **13**(1), 143 (June 1970).
- Klindt, K. K., and D. A. Canonico, "Evaluation of Discontinuities in HSST Twelve Inch Thick Plate," pp. 194–209 in *Proceedings of the Seventh Symposium on Nondestructive Evaluation of Components and Materials in Aerospace, Weapons Systems and Nuclear Applications, April 23–25, 1969, San Antonio, Texas*, South Texas Section, American Society for Nondestructive Testing and Southwest Research Institute, Printed in Los Angeles, California, July 1969.
- Klueh, R. L., "The Effect of Oxygen on the Compatibility of Niobium with Potassium," *Corrosion* **25**(10), 416–22 (October 1969).
- Klueh, R. L., and J. H. DeVan, *The Oxidation of Vanadium and Vanadium Alloys in Sodium*, ORNL-TM-2827 (March 1970).
- Klueh, R. L., *Penetration of Refractory Metals by Alkali Metals*, ORNL-TM-2836 (April 1970).
- Klueh, R. L., "The Effect of Oxygen on the Compatibility of Tantalum and Potassium," (Summary) *Trans. Am. Nucl. Soc.* **13**(1), 162 (June 1970).
- Klueh, R. L., "Penetration of Refractory Metals by Alkali Metals," pp. 177–96 in *Corrosion by Liquid Metals*, ed. by J. E. Draley and J. R. Weeks, Plenum Press, New York, 1970.
- Koch, C. C., and G. R. Love, "Superconductivity in Niobium Containing Ferromagnetic Gadolinium or Paramagnetic Yttrium Dispersions," *J. Appl. Phys.* **40**(9), 3582–87 (August 1969).
- Koch, C. C., and G. R. Love, "The Influence of Precipitation on the Superconducting Properties of a Tc-30 Pct V Alloy," *Trans. Met. Soc. AIME* **245**(9), 1957–62 (September 1969).
- Koger, J. W., and A. P. Litman, *Compatibility of Molybdenum-Base Alloy TZM with LiF-BeF<sub>2</sub>-ThF<sub>4</sub>-UF<sub>4</sub> (68-20-11.7-0.3 mole %) at 1100°C*, ORNL-TM-2724 (December 1969).
- Koger, J. W., and A. P. Litman, *Catastrophic Corrosion of Type 304 Stainless Steel in a System Circulating Fused Sodium Fluoroborate*, ORNL-TM-2741 (January 1970).
- Koger, J. W., and A. P. Litman, *Compatibility of Fused Sodium Fluoroborates and BF<sub>3</sub> Gas with Hastelloy N Alloys*, ORNL-TM-2978 (June 1970).
- Kollie, T. G., *Contributions to the Specific Heat Capacity of Nickel, Iron, and the Alloy Ni<sub>3</sub>Fe*, ORNL-TM-2649 (December 1969). Ph.D. Thesis, the University of Tennessee, August 1969.
- Kollie, T. G., M. Barisoni, D. L. McElroy, and C. R. Brooks, "Pulse Calorimetry Using a Digital Voltmeter for Transient Data Acquisition," *High Temperatures – High Pressures* **1**(2), 167–84 (1969); also pp. 490–530 in *Europäische Konferenz über thermophysikalische Eigenschaften von festen Stoffen bei hohen Temperaturen vom 11. bis 13. November 1968 in Baden-Baden*, Bundesministerium für Bildung und Wissenschaft, Forschungsbericht K70-01 (February 1970).
- Kroeger, D. M., "A Peak Effect in Critical Current with Respect to Temperature and Field in a Type-II Superconductor," *Solid State Commun.* **7**(11), 843–47 (November 1969).
- Kuhlmann-Wilsdorf, D., and A. Wolfenden, "Comments on 'Remarks on the Stored Energy in FCC Metals'," *Scripta Met.* **3**(7), 503–6 (July 1969).
- Kuhlmann-Wilsdorf, D., and A. Wolfenden, "Further Comments on the Stored Energy in F.C.C. Metals," *Scripta Met.* **4**(1), 3–4 (January 1970).

- Larson, L. T., "Equipment for the Quantitative Photometric Measurement of Reflectivity by Polarized Light Microscopy," *Rev. Sci. Instr.* **40**(8), 1088–92 (August 1969).
- Larson, L. T., "Reflectivity Measurements on Zirconium," *Trans. Met. Soc. AIME* **245**(9), 2047–50 (September 1969).
- Leitnaker, J. M., T. B. Lindemer, K. E. Spear, and K. J. Notz, "Producing Advanced Fuels for LMFBR's," (Summary) *Trans. Am. Nucl. Soc.* **12**(2), 579–80 (November 1969).
- Leitnaker, J. M., R. A. Potter, K. E. Spear, and W. R. Laing, "The Lattice Parameter of U(C,N) as a Function of Composition," *High Temp. Sci.* **1**(4), 389–400 (December 1969).
- Lieto, L. R., *A New Method for the Calculation of Successive Stability Constants*, ORNL-TM-2714 (November 1969). Ph.D. Thesis, Arizona State University, August 1969.
- Lindemer, T. B., J. M. Leitnaker, and K. E. Spear, *The Role of Carbon in Reactions in the U-C-O-N System*, ORNL-TM-2715 (November 1969).
- Lindemer, T. B., "Factors that Control the Carbothermic Synthesis of Advanced Fuels," pp. 423–33 in *Symposium on Sol-Gel Processes and Reactor Fuel Cycles, Gatlinburg, Tennessee, May 4–7, 1970*, CONF-700502.
- Loh, B. T. M., "Orientation Determination from Dodecahedral Etch Pits," *Metallography* **2**(1), 79–88 (March 1969).
- Loh, B. T. M., "Stress Concentration and Cavity Growth," *Scripta Met.* **4**(4), 299–303 (April 1970).
- Long, E. L., Jr., F. R. McQuilkin, D. R. Cuneo, J. R. Lindgren, and J. N. Siltanen, "Irradiation Tests of Fuel Rods Containing  $\text{UO}_2$  and  $(\text{U,Pu})\text{O}_2$  for GCFR," pp. 179–84 in *Ceramic Nuclear Fuels, Proceedings of the International Symposium, Spec. Publ. 2*, ed. by O. L. Kruger and A. I. Kaznoff, American Ceramic Society, Columbus, Ohio, 1969.
- Lorenz, R. A., G. W. Parker, and D. O. Hobson, *Preliminary Evaluation of the First Fuel Rod Failure Transient Test of a Zircaloy-Clad Fuel Rod Cluster in TREAT*, ORNL-TM-2774 (November 1969).
- Lorenz, R. A., D. O. Hobson, and G. W. Parker, "Fuel Rod Failure Under Loss-of-Coolant Conditions in TREAT," (Summary) *Trans. Am. Nucl. Soc.* **13**(1), 152 (June 1970).
- Love, G. R., C. C. Koch, J. M. Victor, G. A. Persyn, and W. L. Rollwitz, "High Q resonators in higher d c magnetic fields," *Cryogenics* **9**(5), 392 (October 1969).
- Love, G. R., C. C. Koch, H. L. Whaley, and Z. R. McNutt, "Elastic Moduli and Debye Temperature of Polycrystalline Technetium by Ultrasonic Velocity Measurements," *J. Less-Common Metals* **20**(1), 73–75 (January 1970).
- Love, G. R., "The Critical State in Hysteretic Superconductors," *Phil. Mag.* **21**(173), 1003–26 (May 1970).
- Lubell, M. S., and D. M. Kroeger, "Flux-Flow Studies and Stability Criteria of Nb–Ti Strips," pp. 123–32 in *Advan. Cryog. Eng.* **14**, Plenum Press, New York, 1969.
- Luquire, J. W., W. E. Deeds, C. V. Dodd, and W. G. Spoeri, *Computer Programs for Some Eddy Current Problems*, ORNL-TM-2501 (August 1969).
- Luquire, J. W., III, *Theoretical Analyses of Selected Electromagnetic Induction Problems*, ORNL-TM-2633 (September 1969). Ph.D. Thesis, the University of Tennessee, August 1969.
- Mardon, P. G., and C. C. Koch, "Structural Changes in Samarium Metal at Elevated Temperatures," *Scripta Met.* **4**(6), 477–84 (June 1970).
- Martin, W. R., G. M. Adamson, Jr., and J. E. Cunningham, "Recent Developments in Materials Research," (Summary) pp. 41–42 in *Conf. Reactor Operating Experience, Oct. 1–3, 1969, San Juan, Puerto Rico*, Supplement to *Trans. Am. Nucl. Soc.* **12** (1969).
- Martin, W. R., A. E. Richt, and M. M. Martin, "Postirradiation Examination and Evaluation of Tungsten-Urania Cermet," (Summary) *Trans. Am. Nucl. Soc.* **13**(1), 2 (June 1970).
- McClung, R. W., "A Personal Challenge," *Mater. Eval.* **27**(11), 10A (November 1969).
- McClung, R. W., "NDT with Direct Feedback to Expand," *Qual. Assurance* **9**(1), 51 (January 1970).

- McCoy, H. E., and J. R. Weir, "Development of a Titanium-Modified Hastelloy N with Improved Resistance to Radiation Damage," pp. 290–311 in *Irradiation Effects in Structural Alloys for Thermal and Fast Reactors, Spec. Tech. Publ. 457*, American Society for Testing and Materials, Philadelphia, 1969.
- McCoy, H. E., "The INOR-8 Story," *ORNL Review* 3(2), 35–49 (Fall 1969).
- McCoy, H. E., *An Evaluation of the Molten-Salt Reactor Experiment Hastelloy N Surveillance Specimens – Third Group*, ORNL-TM-2647 (January 1970).
- McCoy, H. E., R. L. Beatty, W. H. Cook, R. E. Gehlbach, C. R. Kennedy, J. W. Koger, A. P. Litman, C. E. Sessions, and J. R. Weir, "New Developments in Materials for Molten-Salt Reactors," *Nucl. Appl. Technol.* 8(2), 156–69 (February 1970).
- McCoy, H. E., R. W. Gunkel, and G. M. Slaughter, *Tensile Properties of Hastelloy N Welded After Irradiation*, ORNL-TM-2858 (April 1970).
- McDonald, R. E., R. G. Donnelly, and A. C. Schaffhauser, "Extrusion of Refractory Metals for Isotope Fuel Capsules," (Summary) *Trans. Am. Nucl. Soc.* 13(1), 84–85 (June 1970).
- McElroy, D. L., and J. P. Moore, "Radial Heat Flow Methods for the Measurement of the Thermal Conductivity of Solids," pp. 185–239 in *Thermal Conductivity*, Vol. 1, ed. by R. P. Tye, Academic Press, London, 1969.
- Moore, J. P., R. S. Graves, J. G. Stradley, J. H. Hannah, and D. L. McElroy, *Some Thermal Transport Properties of a Limestone Concrete*, ORNL-TM-2644 (August 1969).
- Moore, J. P., W. Fulkerson, and D. L. McElroy, "Thermal Conductivity, Electrical Resistivity, and Seebeck Coefficient of Uranium Mononitride," *J. Am. Ceram. Soc.* 53(2), 76–82 (February 1970).
- Moore, J. P., R. K. Williams, and D. L. McElroy, "Comments on 'Lorenz-Function Enhancement Due to Inelastic Processes Near the Néel Point of Chromium'," *Phys. Rev. Letters* 24(11), 587–88 (March 1970).
- Moorhead, A. J., and P. W. Turner, "Welding a Thermocouple Gauge to Apollo Lunar Sample Return Containers," *Welding J. (N.Y.)* 49(1), 15–21 (January 1970).
- Morgan, C. S., "Activation Energy in Sintering," *J. Am. Ceram. Soc.* 52(8), 453–54 (August 1969).
- Morgan, C. S., and C. J. McHargue, "Analogies Between Densification Kinetics in Sintering and Dislocation Motion," *Phys. Sintering* 2(2), 55–70 (May 1970).
- Morgan, M. T., E. L. Long, Jr., D. M. Hewette, and O. Sisman, *Fuel Migration in Pyrocarbon-Coated Particles*, ORNL-TM-2717 (November 1969).
- Nilsson, T. M., and P. L. Rittenhouse, *Experimental Fabrication of Zircaloy-4 Tubing*, ORNL-TM-2576 (August 1969).
- Nilsson, T. M., *Textures of Drawn and Planetary Swaged Tubes of 0.2% Ti Type 304L Stainless Steel*, ORNL-TM-2682 (October 1969).
- Nilsson, T. M., "Effect of Working Direction on the Microstructure and High-Temperature Mechanical Properties of an Extruded SAP Alloy," *Intern. J. Powder Met.* 5(4), 43–56 (October 1969).
- Obenshain, F. E., J. C. Love, and G. Czjzek, "Mössbauer Measurements with Nickel-61 in Third Transition Metal Alloys," pp. 532–35 in *Proceedings of Eleventh International Conference on Low Temperature Physics*, Vol. 1, ed. by J. F. Allen, D. M. Finlayson, and D. M. McCall, University of St. Andrews Printing Department, St. Andrews, Scotland, 1968.
- Olsen, A. R., R. B. Fitts, and C. M. Cox, *Analysis of the Validity of Fast Reactor Fuel Tests in Existing Test Reactors*, ORNL-TM-2716 (October 1969); also pp. 127–50 in *National Symposium on Development in Irradiation Testing Technology held at Sandusky, Ohio, September 9–11, 1969*, CONF-690910.
- Olsen, A. R., C. M. Cox, and R. B. Fitts, "Low Burnup Irradiation Tests of Sphere-Pac Sol-Gel (U,Pu)O<sub>2</sub> Fuels," (Summary) *Trans. Am. Nucl. Soc.* 12(2), 605–6 (November 1969).
- Olsen, A. R., *Experiment Description and Hazards Evaluation for the Series I ORNL Oxide Fuels Irradiation in EBR-II*, ORNL-TN-2635 (April 1970).

- Olsen, A. R., "Intermediate-Burnup Irradiation Tests of Sphere-Pac Sol-Gel Fuels," (Summary) *Trans. Am. Nucl. Soc.* **13**(1), 32–33 (June 1970).
- Packan, N. H., and D. N. Braski, *Electron Microscope in Situ Annealing Study of Voids Induced by Irradiation in Aluminum*, ORNL-TM-2645 (August 1969); also *J. Nucl. Mater.* **34**(3), 290–98 (March 1970).
- Packan, N. H., *Voids in Re-Irradiated Aluminum*, ORNL-TM-2976 (June 1970).
- Painter, G. S., and D. E. Ellis, "Electronic Band Structure and Optical Properties of Graphite from a Variational Approach," *Phys. Rev. B* **1**(12), 4747–52 (June 1970).
- Patriarca, P., "Introduction," pp. 1–5 in *Effects of Minor Elements on the Weldability of High-Nickel Alloys*, Welding Research Council, New York, July 1969.
- Patriarca, P., *Fuels and Materials Development Program Quart. Progr. Rept. June 30, 1969*, ORNL-4440.
- Patriarca, P., *Fuels and Materials Development Program Quart. Progr. Rept. Sept. 30, 1969*, ORNL-4480.
- Patriarca, P., *Fuels and Materials Development Program Quart. Progr. Rept. Dec. 31, 1969*, ORNL-4520.
- Patriarca, P., *Fuels and Materials Development Program Quart. Progr. Rept. Mar. 31, 1970*, ORNL-4560.
- Pawel, R. E., and T. S. Lundy, "Tracer Diffusion in Tungsten," *Acta Met.* **17**(8), 979–88 (August 1969).
- Pawel, R. E., "The Estimation of Bending Stresses from Flexure Measurements," *J. Electrochem. Soc.* **116**(8), 1144–46 (August 1969).
- Pollock, C. B., R. L. Beatty, and J. L. Scott, "Inert Dimensionally Stable Microspheres for Coated-Particle Irradiation Testing," *J. Am. Ceram. Soc.* **53**(6), 358 (June 1970).
- Poteat, L. E., and J. I. Federer, "Corrosion-Resistant Coatings for MSBR Reprocessing Equipment," (Summary) *Trans. Am. Nucl. Soc.* **13**(1), 164–65 (June 1970).
- Reagan, P. E., E. L. Long, Jr., J. G. Morgan, and J. H. Coobs, "Irradiation Performance of Pyrolytic Carbon and Silicon Carbide Coated Fuel Particles," *Nucl. Appl. Technol.* **8**(5), 417–31 (May 1970).
- Reimann, D. K., and T. S. Lundy, "Diffusion of  $^{233}\text{U}$  in  $\text{UO}_2$ ," *J. Am. Ceram. Soc.* **52**(9), 511–12 (September 1969).
- Reimann, D. K., and J. P. Stark, "Oxidation Kinetics and Its Influence on the Near-Surface Effect of Diffusion," *Acta Met.* **18**(1), 63–70 (January 1970).
- Reimann, G. A., *Feasibility Study on Redrawing to Produce Usable Tantalum Tubing*, ORNL-TM-2694 (October 1969).
- Reimann, G. A., and W. R. Martin, "Improved Processes for the Fabrication of 316 Stainless Steel Tubing," (Summary) *Trans. Am. Nucl. Soc.* **12**(2), 569–70 (November 1969).
- Reimann, G. A., *Development of An Ultrafine Grain Size Type 316 Stainless Steel Cladding*, ORNL-TM-2937 (May 1970).
- Richt, A. E., and V. O. Haynes, *Postirradiation Nondestructive Examination of the SM-2B Fuel Element from the Army SM-1 Power Reactor*, ORNL-TM-2673 (January 1970).
- Richt, A. E., M. M. Martin, and W. R. Martin, *Postirradiation Examination and Evaluation of Tungsten-Urania Cermets*, ORNL-4569 (June 1970).
- Rittenhouse, P. L., "The Effect of Texture on the Torsional Yielding of Zircaloy Tubing," pp. 241–51 in *Applications-Related Phenomena for Zirconium and Its Alloys*, Spec. Tech. Publ. 458, American Society for Testing and Materials, Philadelphia, 1969.
- Robbins, J M, and J. G. Stradley, *Fabrication of Sol-Gel-Derived Thoria-Urania by Cold Pressing and Sintering*, ORNL-4426 (July 1969).
- Scott, J. L., J. A. Conlin, J. H. Coobs, D. M. Hewette II, J M Robbins, and R. L. Senn, "Development of Bonded Beds of Coated Particles for HTGR Fuel Elements," (Summary) *Trans. Am. Nucl. Soc.* **13**(1), 134–35 (June 1970).

- Sease, J. D., R. A. Bradley, C. R. Reese, W. H. Pechin, and A. L. Lotts, "Sphere-Pac and Pelletization of (U,Pu)O<sub>2</sub>," pp. 323–41 in *Symposium on Sol-Gel Processes and Reactor Fuel Cycles, Gatlinburg, Tennessee, May 4–7, 1970*, CONF-700502.
- Sessions, C. E., and T. S. Lundy, "Diffusion of Titanium in Modified Hastelloy N," *J. Nucl. Mater.* **31**(3), 316–22 (July 1969).
- Sessions, C. E., R. E. Gehlbach, S. W. Cook, and H. E. McCoy, "Correlation of the Creep Behavior of a Nickel Alloy with Precipitate Distribution," (Summary) *Trans. Am. Nucl. Soc.* **12**(2), 570–71 (November 1969).
- Shankle, G. E., *The Electronic Structure of the Nickel(II) Ion in Doped LiCl Crystals*, ORNL-TM-2514 (July 1969). Ph.D. Thesis, the University of Tennessee, March 1969.
- Simpson, W. A., and W. E. Deeds, "Real-Time Visual Reconstruction of Infrared Holograms," *Appl. Opt.* **9**(2), 499–501 (February 1970).
- Slaughter, G. M., and G. M. Goodwin, "Welding Procedures for LMFBR Vessels," (Summary) *Trans. Am. Nucl. Soc.* **13**(1), 117 and 120 (June 1970).
- Smith, G. P., J. Brynestad, C. R. Boston, and W. E. Smith, "Coordination Equilibria of Nickel(II) in Molten Chloride Salts," pp. 143–68 in *Molten Salts, Characterization and Analysis*, ed. by Gleb Mamantov, Marcel Dekker, Inc., New York, 1969.
- Smith, W. E., J. Brynestad, and G. P. Smith, "Spectroscopic Behavior and Coordination of Nickel(II) in Liquid Mixtures of Zinc and Cesium Chlorides," *J. Chem. Phys.* **52**(8), 3890–3903 (April 1970).
- Sparks, C. J., and Ernest Epperson, "Thermal Motion in Highly Oriented Graphite," (Summary) p. 195 in *Summary of Papers, Bien. Conf. Carbon, 9th 1969*, Defense Ceramic Information Center, Battelle Memorial Institute, Columbus, Ohio, 1969.
- Spear, K. E., and J. M. Leitnaker, "Chemical Effects of Nuclear Burnup on Fast-Reactor Fuels," (Summary) *Trans. Am. Nucl. Soc.* **12**(2), 593–94 (November 1969).
- Spear, K. E., and J. M. Leitnaker, "Equilibrium Investigations of Carbon-Rich V(C,N) Solutions," *High Temp. Sci.* **1**(4), 401–11 (December 1969).
- Spear, K. E., J. M. Leitnaker, and T. B. Lindemer, "Phase Behavior of the U-V-C System and the Thermodynamic Properties and Crystal Structure of UVC<sub>2</sub>," *High Temp. Sci.* **2**(2), 176–97 (June 1970).
- Starke, E. A., Jr., J. C. Ogle, and C. J. Sparks, Jr., "Deformation Textures of Ordered and Disordered Cu<sub>3</sub>Au," pp. 372–90 in *Advances in X-Ray Analysis*, Vol. 12, ed. by C. S. Barrett, J. B. Newkirk, and G. R. Mallett, Plenum Press, New York, 1969.
- Stark, J. P., "Combined Surface and Grain-Boundary Diffusion," *J. Appl. Phys.* **40**(8), 3101–4 (July 1969).
- Stephenson, R. L., *Comparative Creep-Rupture Properties of W-25% Re Consolidated by Arc Melting and Powder Metallurgy Techniques*, ORNL-TM-2651 (September 1969).
- Stephenson, R. L., and R. W. Swindeman, "Prediction of Failure Times for Decay-Heated Capsules Containing Alpha-Emitting Isotopes," *Nucl. Appl. Technol.* **7**(6), 572–75 (December 1969).
- Stephenson, R. L., "Evaluation of the High-Temperature Creep Properties of Refractory Metal Alloys in Vacuum," pp. 15–27 in *Trans. Vac. Met. Conf. 1968*, ed. by R. B. Barrow and A. Simkovich, American Vacuum Society, New York, 1968.
- Stephenson, R. L., *Creep-Rupture Properties of SU-16 and Their Response to Heat Treatment*, ORNL-TM-2835 (March 1970).
- Stephenson, R. L., "Material Selections for Thermionic Capsules," pp. 404–10 in *IEEE Conference Record of 1969 Thermionic Conversion Specialist Conference, October 21–23, 1969*, The Institute of Electrical and Electronics Engineers, Inc., New York, (69 C 51-ED).
- Stiegler, J. O., and E. E. Bloom, "The Effects of Large Fast-Neutron Fluences on the Structure of Stainless Steel," *J. Nucl. Mater.* **33**(2), 173–85 (November 1969).

- Stiegler, J. O., K. Farrell, C. K. H. DuBose, and R. T. King, "High-Fluence Neutron-Irradiation Damage in Aluminum," pp. 215–32 in *Radiation Damage in Reactor Materials Vol. II* (Proceedings of a Symposium, Vienna, 2–6 June 1969), International Atomic Energy Agency, Vienna, 1969.
- Swindeman, R. W., "Low-Cycle Fatigue Study on Columbium Alloy D-43," pp. 34–41 in *Fatigue at High Temperature, Spec. Tech. Publ. 459*, American Society for Testing and Materials, Philadelphia, 1969.
- Swindeman, R. W., *Predicting the Performance of Arc-Cast Tungsten Capsules Containing Alpha-Emitting Isotopes at Thermionic Temperatures*, ORNL-TM-2809 (February 1970).
- Tenckhoff, E., and P. L. Rittenhouse, "Texture Development and Texture Gradients in Zircaloy Tubing," pp. 50–67 in *Applications-Related Phenomena for Zirconium and Its Alloys, Spec. Tech. Publ. 458*, American Society for Testing and Materials, Philadelphia, 1969.
- Tenckhoff, E., "Der Einfluss der Reduktionswerte Auf die Entwicklung von Textur und Texturgradienten in Zircaloy Rohren (The Influence of the Reduction Ratio on the Development of Texture and Texture Gradients in Zircaloy Tubes)," *Z. Metallk.* 61(1), 64–71 (January 1970).
- Tenckhoff, E., and P. L. Rittenhouse, "Annealing Textures in Zircaloy Tubing," *J. Nucl. Mater.* 35(1), 14–23 (April 1970).
- Toth, L. M., J. P. Young, and G. P. Smith, "Diamond-Windowed Cell for Spectrophotometry of Molten Fluoride Salts," *Anal. Chem.* 41(4), 683–85 (April 1969).
- Toth, L. M., G. D. Brunton, and G. P. Smith, "The Structure and Spectrum of Potassium Hexafluoromolybdate(III)," *Inorg. Chem.* 8(12), 2694–97 (December 1969).
- Vandermeer, R. A., and J. C. Ogle, "Texture Inhomogeneities in Cold-Rolled Niobium (Columbium)," *Trans. Met. Soc. AIME* 245(7), 1511–18 (July 1969).
- Vandermeer, R. A., "The Recrystallization Characteristics of Moderately Deformed Aluminum," *Met. Trans.* 1(4), 819–26 (April 1970).
- Vandermeer, R. A., and J. C. Ogle, "The Development of Rolling Texture in a Nb(Cb)-40 Pct V Alloy," *Met. Trans.* 1(5), 1461–63 (May 1970).
- Waddell, R. D., "Measurement of LWR Coolant Channel Reduction Arising from Cladding Deformation During a Loss-of-Coolant Accident," (Summary) *Trans. Am. Nucl. Soc.* 13(1), 150–51 (June 1970).
- Wagner, R. L., *A Technique for Measuring the Diffusivity and Solubility of Gases in Metals with Application to Nitrogen in Tungsten*, ORNL-TM-2584 (July 1969). M.S. Thesis, the University of Tennessee, June 1969.
- Wagner, R. L., "Sublimation of Tungsten–25% Rhenium Between 1650 and 1950°C in Low-Pressure Oxygen," pp. 411–16 in *IEEE Conference Record of 1969 Thermionic Conversion Specialist Conference, October 21–23, 1969*, The Institute of Electrical and Electronics Engineers, Inc., New York, (69 C 51-ED).
- Washburn, T. N., "Porous UO<sub>2</sub> Bodies Produced by Reduction of U<sub>3</sub>O<sub>8</sub>," *Nucl. Appl. Technol.* 8(1), 23–28 (January 1970).
- Washburn, T. N., K. R. Thoms, S. C. Weaver, D. R. Cuneo, and E. L. Long, Jr., "Examination of UN Fueled Pins Irradiated at 1400°C Cladding Temperature," (Summary) *Trans. Am. Nucl. Soc.* 13(1), 101–2 (June 1970).
- Weaver, S. C., R. L. Senn, J. L. Scott, and B. H. Montgomery, *Effects of Irradiation on Uranium Nitride Under Space-Reactor Conditions*, ORNL-4461 (October 1969). CLASSIFIED.
- Weaver, S. C., K. R. Thoms, and V. A. DeCarlo, "Irradiation Testing of UN in ORR," (Summary) *Trans. Am. Nucl. Soc.* 12(2), 547 (November 1969).
- Weir, J. R., Jr., "A Review of Fast Neutron Radiation Damage Problems in Reactor Materials," (Summary) *Trans. Am. Nucl. Soc.* 12(2), 699 (November 1969).
- Werner, W. J., *An Investigation of the Effect of Certain Minor Elements on the Elevated Temperature Ductility of Incoloy 800*, ORNL-4504 (March 1970).
- Whaley, H. L., W. Fulkerson, and R. A. Potter, "Elastic Moduli and Debye Temperature of Polycrystalline Uranium Nitride by Ultrasonic Velocity Measurements," *J. Nucl. Mater.* 31(3), 345–50 (July 1969).

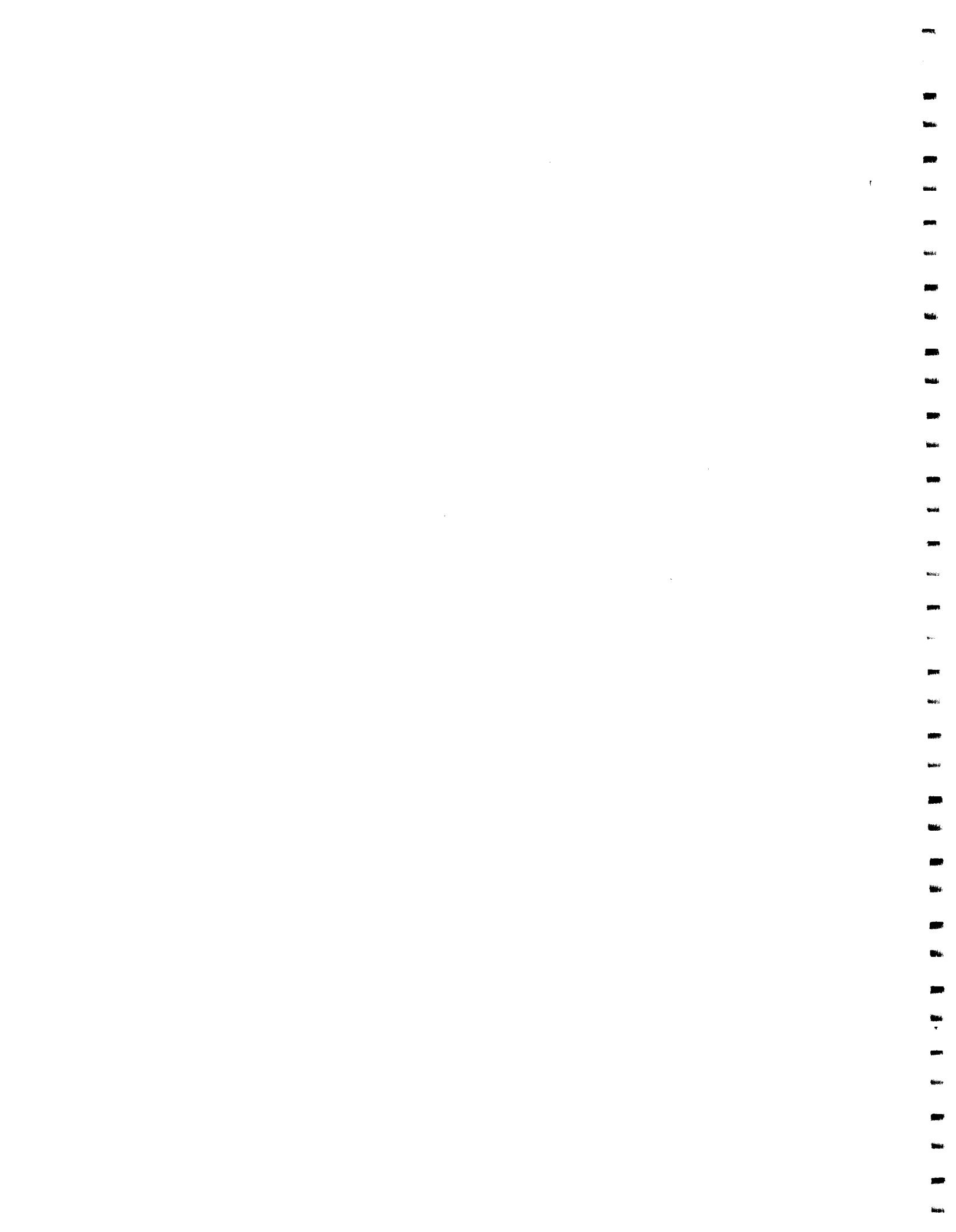
- Whaley, H. L., and K. V. Cook, *Ultrasonic Frequency Analysis*, ORNL-TM-2655 (September 1969); also *Mater. Evaluation* 28(3), 61–66 (March 1970).
- Williams, R. O., "Series Representation of Thermodynamic Functions of Binary Solutions," *Trans. Met. Soc. AIME* 245(12), 2565–70 (December 1969).
- Williams, R. O., *Computer Program for Calculating the Configurational Changes in Nonrandom Alloys Due to Deformation*, ORNL-TM-2855 (February 1970).
- Williams, R. O., *A Computer Program for the Simulation of Solid Solutions from X-Ray Data*, ORNL-TM-2866 (March 1970).
- Williams, R. O., "Calculation of Configurational Changes in Nonrandom Solid Solutions Due to Deformation," *Acta Met.* 18(4), 457–61 (April 1970).
- Wolfenden, A., "The Energy Stored in a Gold-Silver Alloy," *Scripta Met.* 3(7), 429–34 (July 1969).
- Wolfenden, A., "The Energy Relations in the Room-Temperature Deformation of Aluminum Single Crystals," *Scripta Met.* 3(10), 709–14 (October 1969).
- Wolfenden, A., "The Ratio of Stored to Expended Energy During the Room-Temperature Deformation of Copper Single Crystals," *Scripta Met.* 4(5), 327–32 (May 1970).
- Wymer, R. G., and A. L. Lotts, *Status and Progress Report for Thorium Fuel Cycle Development for 1967 and 1968*, ORNL-4429 (August 1969).
- Yakel, H. L., "Crystal Structures of Transition Phases Formed in U–16.60 at. % Nb–5.64 at. % Zr Alloys," *J. Nucl. Mater.* 33(3), 286–95 (December 1969).
- Yoo, M. H., "Interaction of Slip Dislocations with Twins in Hcp Metals," *Trans. Met. Soc. AIME* 245(9), 2051–60 (September 1969).
- Yoo, M. H., "Reply to 'Zonal Dislocations and Dislocation Reactions with Twins in Hexagonal-Close-Packed Metals'," *Scripta Met.* 4(1), 9–11 (January 1970).
- Yoo, M. H., and B. T. M. Loh, "Characteristics of Stress and Dilatation Fields of Straight Dislocations in Anisotropic Crystals," *J. Appl. Phys.* 41(7), 2805–14 (June 1970).
- Yust, C. S., and C. J. McHargue, "Comments on the 'Dependence of Flow Stress on Nonstoichiometry in Oxygen-Rich Uranium Dioxide,'" *J. Am. Ceram. Soc.* 52(10), 568–69 (October 1969).
- Bibliography of the Technical Literature of the Metals and Ceramics Division for the Period 1948 Through 1968*, ORNL-4270, Vol. 1, Rev. (November 1969).

## Author Index

- Abraham, M. M., 3  
Adams, R. E., 58  
Adamson, G. M., Jr., 127, 128  
Adler, Laszlo, 150  
Arakawa, E. T., 21
- Barrett, C. R., 8  
Barrett, Lida K., 25  
Beatty, R. L., 183  
Beaver, R. J., 174  
Begun, G. M., 33  
Berggren, R. G., 170, 173  
Binkley, N. C., 88  
Bloom, E. E., 76  
Bomar, E. S., 63, 64  
Bopp, C. D., 95  
Borie, Bernard, 44  
Boston, C. R., 32, 33  
Bourgette, D. T., 108  
Bradley, R. A., 48, 49, 50, 51, 168  
Braski, D. N., 99  
Bridges, W. H., 70, 193  
Brynstad, J., 31, 32
- Canonico, D. A., 114, 143, 145, 147, 170, 172  
Carpenter, R. W., 10  
Cathcart, J. V., 37  
Cavin, O. B., 1, 181, 187  
Chandler, E. W., 14  
Chandler, J. M., 195  
Chapman, A. T., 1, 2  
Cheng, C. C., 149  
Chumley, J. W., 220  
Clark, G. W., 1, 2  
Clausing, R. E., 224, 225  
Coghlan, W. A., 8, 9  
Cole, N. C., 88, 120, 189  
Coobs, J. H., 161, 164, 198  
Cook, K. V., 87, 95, 107, 111, 150  
Cook, S. W., 136  
Cook, W. H., 175, 178, 179
- Copeland, G. L., 98, 99, 101, 102, 157  
Couch, T. W., 34  
Cox, C. M., 53, 58, 68, 70, 165, 193  
Crouse, R. S., 215  
Cuneo, D. R., 53, 56, 58, 116  
Czjzek, Gordon, 23
- Davis, H. L., 20, 41  
Dean, C. W., 214  
DeCarlo, V. A., 56  
Deeds, W. E., 149, 151  
DeLuca, J. P., 64, 65, 67  
DeVan, J. H., 92, 95, 103  
Dewey, B. R., 73  
DiStefano, J. R., 107, 111, 187  
Dodd, C. V., 96, 97, 149, 226  
Donnelly, R. G., 106, 112, 127, 130, 203  
DuBose, C. K. H., 99
- Easton, D. S., 224  
Eatherly, W. P., 179  
Ellis, D. E., 42  
Epperson, J. E., 44  
Ernst, W. S., Jr., 213  
Erwin, J. H., 130, 132  
Ewing, W. M., 33
- Farrell, K., 16, 17, 18, 19, 113  
Faulkner, J. S., 40, 41  
Federer, J. I., 108, 118, 187  
Finch, C. B., 2, 3  
Fitts, R. B., 56, 60, 165, 166, 167, 198, 199  
Fleischer, B., 103, 159  
Folzer, C., 46  
Foster, B. E., 133, 151  
Fulkerson, W., 20, 21, 24  
Furman, F. J., 196, 197
- Gaddis, H. R., 220  
Gehlbach, R. E., 17, 136, 138  
Gerdes, R. J., 1

- Glaeser, W., 23  
 Godfrey, T. G., 116, 213  
 Goodwin, G. M., 88, 106, 111, 114  
 Grantham, L. F., 22  
 Graves, R. S., 29, 134, 226  
 Gray, R. J., 215, 220, 221, 222  
 Gunkel, R. W., 189  
 Guthrie, P. V., 7  
 Gyorffy, B. L., 41  
  
 Haff, K. W., 108  
 Hall, L. L., 25  
 Hamner, R. L., 180  
 Hammond, J. P., 124  
 Harman, D. G., 82, 88, 226  
 Harms, W. O., 92, 96, 103, 149  
 Harrington, F. E., 192  
 Harris, L. A., 4, 44, 45, 99, 213  
 Hendricks, R. W., 45, 46  
 Hendrix, D. E., 1, 2  
 Henson, T. J., 215  
 Hewette, D. M. II, 162, 164, 198  
 Hill, Meredith R., 192, 237  
 Hobson, D. O., 206, 209  
 Homan, F. J., 68, 70, 71, 73, 75, 191, 192  
 Housley, R. T., 189  
 Houston, J. T., 16  
  
 Inouye, H., 93, 109, 110, 112, 123  
  
 Jansen, D. H., 93  
 Jenkins, J. D., 60  
 Jordan, R. G., 41  
  
 Keilholtz, G. W., 102  
 Kegley, T. M., Jr., 221, 222  
 Kelly, O. A., 14  
 Kennedy, C. R., 45, 181  
 King, R. T., 16, 81, 86, 152, 153, 203  
 Klueh, R. L., 92, 104  
 Knight, R. W., 128, 130, 203  
 Koch, C. C., 35, 36, 45  
 Koger, J. W., 177, 187, 189  
 Kollie, T. G., 29  
 Kopp, O. C., 4  
 Kroeger, D. M., 13, 14, 36  
 Kuhlmann-Wilsdorf, D., 18  
  
 Lackey, W. J., 50, 51, 60, 68  
 Laing, W. R., 66  
 Leitnaker, J. M., 65, 66, 67, 161  
 Leonard, W. J., 49, 174  
  
 Leslie, B. C., 220, 222  
 Lin, Wen, 45  
 Lindemer, T. B., 64, 66  
 Litman, A. P., 214  
 Liu, C. T., 10, 109, 110, 112  
 Loh, B. T. M., 11, 18, 112  
 Long, E. L., Jr., 116, 152, 166, 167, 221  
 Longest, A. W., 166, 167  
 Lotts, A. L., 47, 165, 191, 192, 195, 201  
 Love, G. R., 35, 36  
 Lundy, T. S., 13, 14  
 Luquire, J. W., 149  
  
 Manley, L. C., Jr., 14  
 Manthos, E. J., 58  
 Mardon, P. G., 10, 36, 44  
 Martin, M. M., 127, 128, 131, 132, 203  
 Martin, W. R., 85, 98, 108, 127, 128, 130  
 Mateer, H. V., 215  
 Mateer, R. S., 98, 99  
 McClung, R. W., 87, 96, 149, 226  
 McCorkle, K. H., 26  
 McCoy, H. E., Jr., 76, 86, 113, 120, 136, 138, 140, 175,  
 176, 178, 179  
 McDonald, R. E., 106, 110, 118, 188  
 McElroy, D. L., 21, 27, 28, 29, 52, 111, 115, 134, 185,  
 226  
 McHargue, C. J., 23, 36  
 McNabb, B., 176, 178  
 Meyer, A., 43  
 Miller, J. L., Jr., 60, 215  
 Moore, J. P., 21, 28, 29, 52, 115, 134, 185, 226  
 Moorhead, A. J., 147, 189  
 Morgan, C. S., 24, 25, 26  
 Morgan, J. G., 60, 186  
 Murray, W. P., 226  
  
 Narten, A. H., 46  
 Nix, W. D., 8, 9  
  
 Obenshain, F. E., 23  
 Ogle, J. C., 6  
 Oliver, B. F., 2  
 Olsen, A. R., 53, 57, 60, 198  
  
 Packan, N. H., 152, 154  
 Padgett, R. A., 14  
 Painter, G. S., 42, 43  
 Patriarca, P., 62, 106, 112, 116, 118, 124  
 Pawel, R. E., 37, 38  
 Pechin, W. H., 50, 168, 192, 197  
 Persyn, G. A., 35

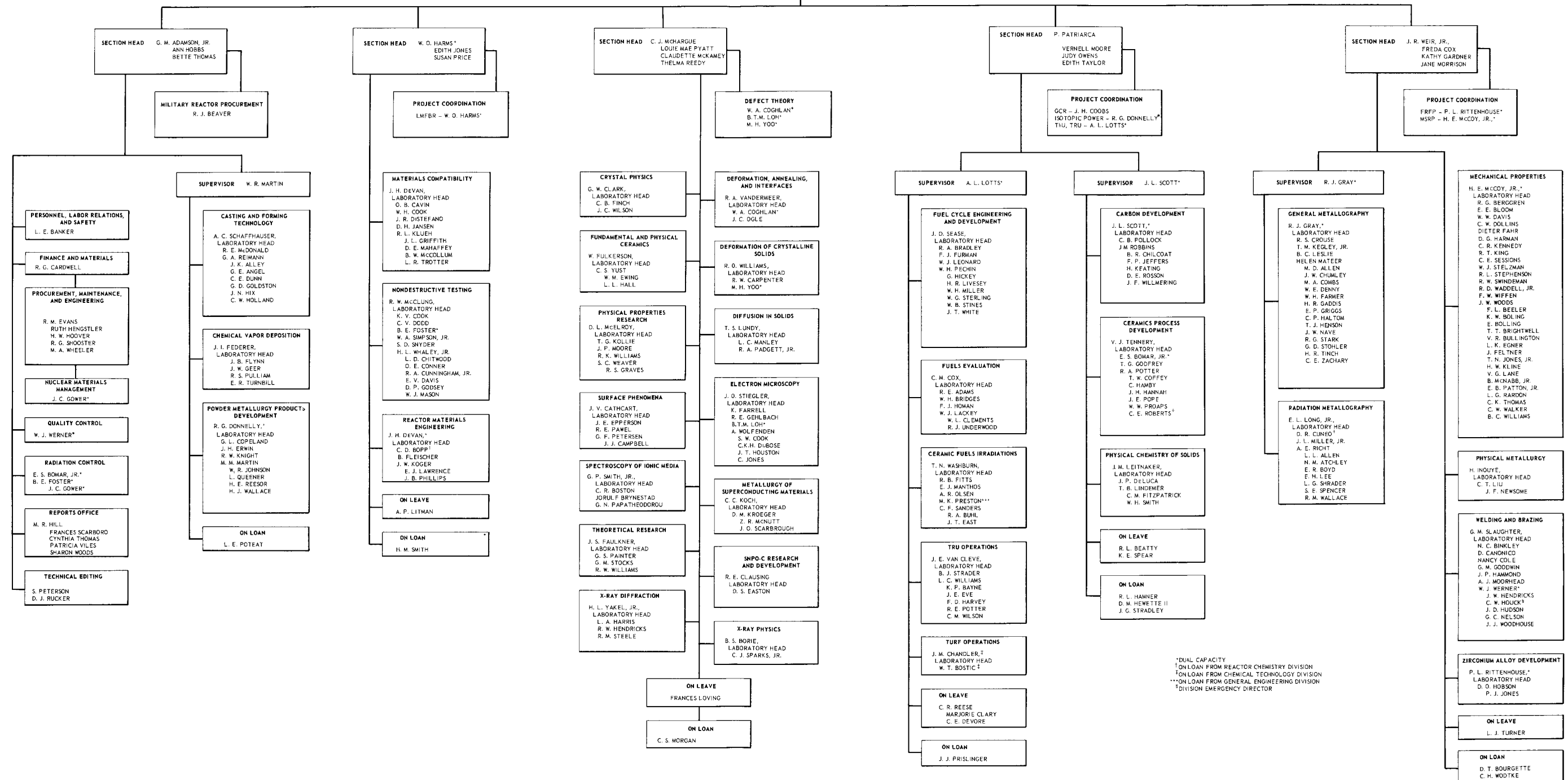
- Petersen, G. F., 37  
 Peterson, Sigfred, 200  
 Pollock, C. B., 161, 183  
 Poole, C. P., Jr., 42  
 Poteat, L. E., 187  
 Potter, R. A., 66, 116  
 Pratt, R. B., 49, 192  
 Preston, M. K., 49, 168
- Ramey, D. W., 108  
 Reese, C. R., 47, 191, 192  
 Reimann, D. K., 13  
 Reimann, G. A., 85, 86, 87  
 Richt, A. E., 127, 128, 221  
 Rittenhouse, P. L., 205  
 Robbins, J. M., 162, 164, 198  
 Rollwitz, W. L., 35
- Sanders, C. F., 56  
 Scarboro, Frances A., 228  
 Scarbrough, J. O., 22, 29  
 Schaffhauser, A. C., 106, 110, 118, 188  
 Scott, J. L., 62, 116, 161, 164  
 Sease, J. D., 47, 50, 166, 168, 195, 196, 197  
 Senn, R. L., 60  
 Sentell, R. A., 151  
 Sessions, C. E., 139, 140  
 Simpson, W. A., Jr., 97, 149, 151  
 Slaughter, G. M., 88, 120, 124, 134, 143, 157  
 Smith, G. P., 31, 32, 33, 34  
 Smith, W. E., 31  
 Snyder, S. D., 151  
 Sparks, Cullie J., Jr., 44, 45  
 Spear, K. E., 65, 66, 67  
 Spedding, F. H., 41  
 Spindler, P. H., 29, 52  
 Spruiell, J. E., 181  
 Staats, P. A., 4  
 Stark, J. P., 13
- Steele, R. M., 44  
 Stephenson, R. L., 120, 122  
 Stiegler, J. O., 16, 17, 18, 76, 123  
 Stillman, W. E., 73  
 Stocks, G. M., 43  
 Swindeman, R. W., 71
- Tansil, J. E., 23  
 Tennery, V. J., 63, 64, 99, 116, 213  
 Thoms, K. R., 116  
 Trotter, L. R., 187
- Van Cleve, J. E., 201, 202  
 Vandermeer, R. A., 5  
 Victor, J. M., 35  
 von Winbush, S., 32
- Waddell, R. D., Jr., 206  
 Wagner, R. L., 93  
 Washburn, T. N., 62, 116, 166, 168, 198  
 Weaver, S. C., 29, 116  
 Weir, J. R., Jr., 76, 136  
 Werner, W. J., 134, 143  
 Whaley, H. L., 96, 150  
 Wiffen, F. W., 84  
 Williams, L. C., 201  
 Williams, M. W., 21  
 Williams, R. K., 28, 67, 115  
 Williams, R. O., 10, 12  
 Williams, R. W., 41  
 Wilson, J. C., 2  
 Wolfenden, A., 16, 17, 18
- Yakel, H. L., 32, 33, 44, 45, 99  
 Yoo, M. H., 11  
 Yosim, S. J., 32  
 Young, W. H., 43  
 Yust, C. S., 1, 24, 25, 186



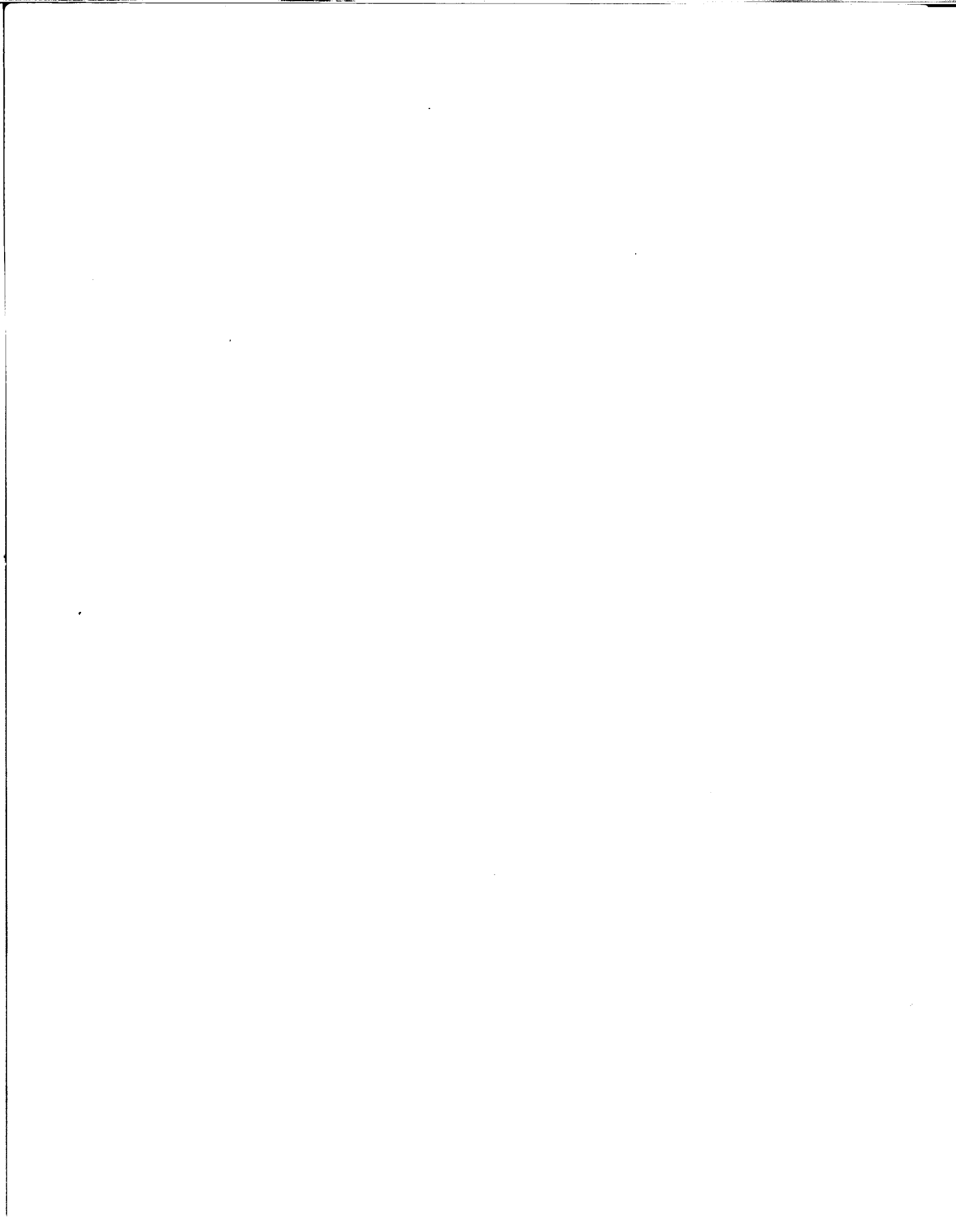
METALS AND CERAMICS DIVISION

JUNE 30, 1970

DIRECTOR J. H. FRYE, JR.
BERTIE BYRUM
ASSOCIATE DIRECTOR J. E. CUNNINGHAM
MARGE WHITE



\*DUAL CAPACITY
†ON LOAN FROM REACTOR CHEMISTRY DIVISION
‡ON LOAN FROM CHEMICAL TECHNOLOGY DIVISION
§ON LOAN FROM GENERAL ENGINEERING DIVISION
|| DIVISION EMERGENCY DIRECTOR



## INTERNAL DISTRIBUTION

- 1–3. Central Research Library
- 4–5. ORNL – Y-12 Technical Library,  
Document Reference Section
- 6–60. Laboratory Records Department
61. Laboratory Records, ORNL R. C.
62. MIT Practice School
63. ORNL Patent Office
64. Laboratory Shift Supervisor
65. G. M. Adamson, Jr.
66. S. E. Beall
67. R. J. Beaver
68. M. Bender
69. D. S. Billington
70. A. L. Boch
71. E. S. Bomar
72. B. S. Borie
73. R. B. Briggs
74. F. R. Bruce
75. J. V. Cathcart
76. J. M. Chandler
77. G. W. Clark
78. R. E. Clausing
79. W. A. Coghlan
80. W. C. Colwell
81. J. H. Coobs
82. W. B. Cottrell
83. C. M. Cox
84. J. A. Cox
85. F. L. Culler
86. J. E. Cunningham
87. J. H. DeVan
88. R. G. Donnelly
89. J. S. Faulkner
90. J. I. Federer
91. D. E. Ferguson
92. B. E. Foster
93. A. P. Fraas
94. J. H. Frye, Jr.
95. W. Fulkerson
96. J. H. Gillette
97. R. J. Gray
98. J. L. Gregg (Y-12)
99. W. R. Grimes
100. J. P. Hammond
101. W. O. Harms
102. C. S. Harrill
103. R. F. Hibbs
- 104–118. M. R. Hill
119. A. P. Huber (K-25)
120. H. Inouye
121. R. G. Jordan (K-25)
122. P. R. Kasten
123. S. I. Kaplan
124. M. T. Kelley
125. E. M. King
126. C. C. Koch
127. J. A. Lane
128. J. M. Leitnaker
129. A. L. Lotts
130. E. L. Long, Jr.
131. T. S. Lundy
132. W. R. Martin
133. R. W. McClung
134. H. E. McCoy
135. H. C. McCurdy
136. D. L. McElroy
137. C. J. McHargue
138. A. J. Miller
139. E. C. Miller
140. C. S. Morgan
141. A. R. Olsen
- 142–143. R. B. Parker
144. P. Patriarca
145. S. Peterson
146. J. W. Prados
147. P. L. Rittenhouse
148. M. W. Rosenthal
149. A. W. Savolainen
150. A. C. Schaffhauser
151. J. L. Scott
152. H. E. Seagren
153. J. D. Sease
154. G. M. Slaughter
155. G. P. Smith, Jr.
156. J. O. Stiegler
157. D. A. Sundberg
158. V. J. Tennery
159. D. B. Trauger
160. J. E. Van Cleve, Jr.
161. R. A. Vandermeer
162. T. N. Washburn
163. A. M. Weinberg

- |                      |                                       |
|----------------------|---------------------------------------|
| 164. J. R. Weir, Jr. | 169. Clyde M. Adams, Jr. (consultant) |
| 165. W. J. Werner    | 170. Leo Brewer (consultant)          |
| 166. G. D. Whitman   | 171. L. S. Darken (consultant)        |
| 167. R. O. Williams  | 172. Jan Korringa (consultant)        |
| 168. H. L. Yakel     | 173. Sidney Siegel (consultant)       |

*EXTERNAL DISTRIBUTION*

- 174–175. D. F. Cope, RDT, SSR, AEC, Oak Ridge National Laboratory
176. E. C. Creutz, National Scientific Foundation, Washington, D.C.
177. G. W. Cunningham, AEC, Washington, D.C.
178. Morgan Dubrow, AEC, Washington, D.C.
179. R. L. Ednic, AEC, Washington, D.C.
180. N. Engel, Georgia Institute of Technology, Atlanta, Georgia
181. E. E. Fowler, AEC, Washington, D.C.
182. V. D. Frechette, Alfred University, Alfred, N.Y.
183. Angelo Giambusso, AEC, Washington, D.C.
184. W. W. Grigorieff, Assistant to the Executive Director, Oak Ridge Associated Universities
185. R. F. Hehemann, Case Western Reserve University
186. P. A. Halpine, AEC, Washington, D.C.
187. J. R. Hunter, AEC, Washington, D.C.
188. L. C. Ianniello, AEC, Washington, D.C.
189. O. C. Kopp, University of Tennessee, Knoxville, Tennessee
190. G. Kavanagh, , AEC, Washington, D.C.
191. E. E. Kintner, AEC, Washington, D.C.
192. R. E. Kirkpatrick, AEC, Washington, D.C.
193. M. Klein, AEC, Washington, D.C.
194. Walter Kohn, University of California, San Diego, California
195. W. H. Layman, AEC, Washington, D.C.
196. A. P. Litman, AEC, Washington, D.C.
197. J. J. Lombardo, NASA, Lewis Research Center
198. W. D. Manly, Stellite Division, Cabot Corp., Kokomo, Indiana
199. C. L. Matthews, RDT, AEC, Oak Ridge National Laboratory
200. P. W. McDaniel, AEC, Washington, D.C.
201. T. W. McIntosh, AEC, Washington, D.C.
202. W. H. McVey, AEC, Washington, D.C.
203. J. J. Morabito, AEC, Washington, D.C.
204. R. R. Nash, NASA, Washington, D.C.
205. R. E. Pahler, AEC, Washington, D.C.
206. A. J. Pressesky, AEC, Washington, D.C.
207. F. N. Rhines, University of Florida, Gainesville, Florida
208. D. R. Riley, AEC, Washington, D.C.
209. M. A. Rosen, AEC, Washington, D.C.
210. M. Shaw, AEC, Washington, D.C.
211. F. C. Schwenk, AEC, Washington, D.C.
212. J. M. Simmons, AEC, Washington, D.C.
213. E. E. Sinclair, AEC, Washington, D.C.
214. B. Singer, AEC, Washington, D.C.
215. L. M. Slifkin, University of North Carolina, Chapel Hill, N.C.
216. E. E. Stansbury, University of Tennessee, Knoxville, Tennessee

217. D. K. Stevens, AEC, Washington, D.C.
218. Dorothy Smith, AEC, Washington, D.C.
219. J. A. Swartout, Union Carbide Corporation, New York, N.Y.
220. R. F. Sweek, AEC, Washington, D.C.
221. A. N. Tardiff, AEC, Washington, D.C.
222. A. Van Echo, AEC, Washington, D.C.
223. C. E. Weber, AEC, Washington, D.C.
224. J. Weertman, Northwestern University, Evanston, Illinois
225. G. W. Wench, AEC, Washington, D.C.
226. M. J. Whitman, AEC, Washington, D.C.
227. C. H. T. Wilkins, University of Alabama, University, Alabama
228. Laboratory and University Division, AEC, ORO
229. Patent Office, AEC, ORO
- 230-428. Given distribution as shown in TID-4500 under Metals, Ceramics, and Materials category (25 copies - CFSTI)